POLITECHNIKA GDAŃSKA

Imię i nazwisko autora rozprawy: Bartosz Nowosielski
Dyscyplina naukowa: Nauki Chemiczne

ROZPRAWA DOKTORSKA

Tytuł rozprawy w języku polskim: Ciecze głęboko eutektyczne – właściwości i zastosowanie w separacji ditlenku węgla

Tytuł rozprawy w języku angielskim: Deep eutectic solvents – properties and application in carbon dioxide separation

Promotor *podpis*	Promotor pomocniczy *podpis*
dr hab. inż. Dorota Warmińska, prof. uczelni	dr inż. Iwona Cichowska-Kopczyńska

Gdańsk, rok 2024

POLITECHNIKA GDAŃSKA

OŚWIADCZENIE

Autor rozprawy doktorskiej: Bartosz Nowosielski

Ja, niżej podpisany(a), oświadczam, iż jestem świadomy(a), że zgodnie z przepisem art. 27 ust. 1 i 2 ustawy z dnia 4 lutego 1994 r. o prawie autorskim i prawach pokrewnych (t.j. Dz.U. z 2021 poz. 1062), uczelnia może korzystać z mojej rozprawy doktorskiej zatytułowanej:
Ciecze głęboko eutektyczne – właściwości i zastosowanie w separacji ditlenku węgla

do prowadzenia badań naukowych lub w celach dydaktycznych.[1]

Świadomy(a) odpowiedzialności karnej z tytułu naruszenia przepisów ustawy z dnia 4 lutego 1994 r. o prawie autorskim i prawach pokrewnych i konsekwencji dyscyplinarnych określonych w ustawie Prawo o szkolnictwie wyższym i nauce (Dz.U.2021.478 t.j.), a także odpowiedzialności cywilno-prawnej oświadczam, że przedkładana rozprawa doktorska została napisana przeze mnie samodzielnie.

Oświadczam, że treść rozprawy opracowana została na podstawie wyników badań prowadzonych pod kierunkiem i w ścisłej współpracy z promotorem dr hab. inż. Dorotą Warmińską, prof. uczelni, promotorem pomocniczym dr inż. Iwoną Cichowską-Kopczyńską *.

Niniejsza rozprawa doktorska nie była wcześniej podstawą żadnej innej urzędowej procedury związanej z nadaniem stopnia doktora.

Wszystkie informacje umieszczone w ww. rozprawie uzyskane ze źródeł pisanych i elektronicznych, zostały udokumentowane w wykazie literatury odpowiednimi odnośnikami, zgodnie z przepisem art. 34 ustawy o prawie autorskim i prawach pokrewnych.

Potwierdzam zgodność niniejszej wersji pracy doktorskiej z załączoną wersją elektroniczną.

Gdańsk, dnia ....

podpis doktoranta

Ja, niżej podpisany(a), wyrażam zgodę/nie wyrażam zgody* na umieszczenie ww. rozprawy doktorskiej w wersji elektronicznej w otwartym, cyfrowym repozytorium instytucjonalnym Politechniki Gdańskiej.

Gdańsk, dnia ....

podpis doktoranta

**niepotrzebne usunąć*

---

[1] Art. 27. 1. Instytucje oświatowe oraz podmioty, o których mowa w art. 7 ust. 1 pkt 1, 2 i 4–8 ustawy z dnia 20 lipca 2018 r. – Prawo o szkolnictwie wyższym i nauce, mogą na potrzeby zilustrowania treści przekazywanych w celach dydaktycznych lub w celu prowadzenia działalności naukowej korzystać z rozpowszechnionych utworów w oryginale i w tłumaczeniu oraz zwielokrotniać w tym celu rozpowszechnione drobne utwory lub fragmenty większych utworów.

2. W przypadku publicznego udostępniania utworów w taki sposób, aby każdy mógł mieć do nich dostęp w miejscu i czasie przez siebie wybranym korzystanie,o którym mowa w ust. 1, jest dozwolone wyłącznie dla ograniczonego kręgu osób uczących się, nauczających lub prowadzących badania naukowe, zidentyfikowanych przez podmioty wymienione w ust. 1.

POLITECHNIKA GDAŃSKA

OPIS ROZPRAWY DOKTORSKIEJ

Autor rozprawy doktorskiej: Bartosz Nowosielski

Tytuł rozprawy doktorskiej w języku polskim: Ciecze głęboko eutektyczne – właściwości i zastosowanie w separacji ditlenku węgla

Tytuł rozprawy w języku angielskim: Deep eutectic solvents – properties and application in carbon dioxide separation

Język rozprawy doktorskiej: Polski

Promotor rozprawy doktorskiej: dr hab. inż. Dorota Warmińska, prof. uczelni

Drugi promotor rozprawy doktorskiej*:

Promotor pomocniczy rozprawy doktorskiej*: dr inż. Iwona Cichowska-Kopczyńska

Kopromotor rozprawy doktorskiej*:

Data obrony:

Słowa kluczowe rozprawy doktorskiej w języku polskim: ciecze głęboko eutektyczne, właściwości fizyczne, struktura, absorpcja CO_2, unieruchomione membrany ciekłe

Słowa kluczowe rozprawy doktorskiej w języku angielskim: deep eutectic solvents, physical properties, structure, CO_2 absorption, supported liquid membranes

Streszczenie rozprawy w języku polskim: Tematyka i cel badawczy niniejszej rozprawy doktorskiej dotyczą charakterystyki cieczy głęboko eutektycznych (DES) opartych na aminoalkoholach (3-aminopropan-1-olu, 2-(metyloamino)etanolu i 2-(butyloamino)etanolu) i glikolach propylenowych (propano-1,2-diolu i propano-1,3-diolu) oraz oceny możliwości ich zastosowania do wychwytu ditlenku węgla ze strumieni gazowych. Ponadto, celem pracy było określenie wpływu wody na strukturę i zdolności sorpcyjne badanych mieszanin. Wyniki przeprowadzonych badań, poza wynikami dotyczącymi symulacji dynamiki molekularnej (MD), zostały opublikowane w siedmiu artykułach naukowych i stanowią podstawę niniejszej rozprawy. Część teoretyczna dysertacji obejmuje przegląd aktualnego stanu wiedzy na temat właściwości fizycznych DES, ich struktury oraz zdolności do pochłaniania ditlenku węgla. Ponadto, zawarto w niej podstawy teoretyczne symulacji MD oraz separacji gazów z użyciem membran ciekłych. W części poświęconej badaniom własnym omówiono wpływ akceptora i donora wiązania wodorowego DES na właściwości termiczne i fizyczne otrzymanych mieszanin. Opisano strukturę cieczy opartych na aminoalkoholach, uwzględniając przy tym wpływ obecności wody i powiązano ją ze zdolnością DES do absorpcji ditlenku węgla. Omówiono efektywność separacji CO_2 przy użyciu unieruchomionych membran ciekłych opartych na DES zawierających glikole propylenowe. Analizę oparto na modelu rozpuszczalnościowo-dyfuzyjnym przenikania masy. W efekcie wskazano najbardziej efektywne układy spośród badanych oraz zaproponowano dalsze kierunki badań nad cieczami głęboko eutektycznymi i ich zastosowaniem w separacji gazów.

POLITECHNIKA GDAŃSKA

Streszczenie rozprawy w języku angielskim: The topic and research objective of this doctoral thesis is focused on the characterisation of deep eutectic solvents (DES) based on aminoalcohols (3-aminopropan-1-ol, 2-(methylamino)ethanol and 2-(butylamino)ethanol) and propylene glycols (propane-1,2-diol and propane-1,3-diol) and the evaluation of their applicability for carbon dioxide capture from gaseous streams. Additionally, the aim of the study was to determine the effect of water on the structure and sorption capacity of the studied mixtures. The results of the conducted research, except for the results of molecular dynamics (MD) simulations, have been published in seven scientific articles serving as a basis of this thesis. The theoretical part of the dissertation includes a review of the current state of knowledge on the physical properties of DES, their structure and ability to interact with carbon dioxide. In addition, it includes the theoretical background of MD simulations and gas separation using liquid membranes. In the research section, the effect of the hydrogen bond acceptor and donor of DES on the thermal and physical properties of the mixtures is discussed. The structure of aminoalcohol-based liquids is described, taking into account the effect of the presence of water, and correlated with the ability of DES to absorb carbon dioxide. The efficiency of CO_2 separation using DES-based supported liquid membranes containing propylene glycols is discussed. The analysis was based on a solution-diffusion model of mass transfer. As a result, the most efficient systems among those studied were identified and further research directions for deep eutectic liquids and their application in gas separation were proposed.

Streszczenie rozprawy w języku, w którym została napisana**:

Słowa kluczowe rozprawy doktorskiej w języku, w którym została napisana**:

** niepotrzebne skreślić*

*** dotyczy rozpraw doktorskich napisanych w innych językach, niż polski lub angielski*

Spis treści

Wykaz skrótów

%ARD	średnie odchylenie względne
[bmim][BF_4]	tetrafluoroboran 1-butylo-3-metyloimidazoliowy
[bmim][Tf_2N]	bis(trifluorometylosulfonylo)imidek 1-butylo-3-metyloimidazoliowy
[bmim][PF_6]	heksafluorofosforan 1-butylo-3-metyloimidazoliowy
[hemim][Tf_2N]	bis(trifluorometylosulfonylo)imidek 1-(2-hydroksyetylo)-3-metyloimidazoliowy
[hemim][OTf]	trifluorometanosulfonian 1-(2-hydroksyetylo)-3-metyloimidazoliowy
[hemim][PF_6]	heksafluorofosforan 1-(2-hydroksyetylo)-3-metyloimidazoliowy
[$MeBu_3N$][Tf_2N]	bis(trifluorometylosulfonylo)imidek metylotributyloamoniowy
[MeBuPyrr][Tf_2N]	bis(trifluorometylosulfonylo)imidek 1-butylo-1-metylopirolidynowy
[$N_{(10)113}$][Tf_2N]	bis(trifluorometylosulfonylo)imidek decylodimetylopropyloamoniowy
[$N_{(4)113}$][Tf_2N]	bis(trifluorometylosulfonylo)imidek butylodimetylopropyloamoniowy
[$N_{(6)113}$][Tf_2N]	bis(trifluorometylosulfonylo)imidek heksylodimetylopropyloamoniowy
[N_{2222}][Im]	imidazolan tetraetyloamoniowy
AC	metody udziałów atomowych
AChCl	chlorek acetylocholiny
AP	3-aminopropan-1-ol
AQM	addytywne wielkości molowe
ATMAC	chlorek allilotrimetyloamoniowy
BAE	2-(butyloamino)etanol
Bet	betaina
BGI	bonding-group interaction contribution
BLM	membrany ciekłe grubowarstwowe
BTEAC	chlorek benzylotrietyloamoniowy
ChCl	chlorek choliny
DES	ciecz głęboko eutektyczna
DSC	skaningowa kalorymetria różnicowa
EDA	etanodiamina
EG	glikol etylenowy
ELM	emulsyjne membrany ciekłe
FTIR	spektroskopia fourierowska w zakresie podczerwieni
GC	metody udziałów grupowych
HBA	akceptor wiązania wodorowego
HBD	donor wiązania wodorowego
HDES	hydrofobowe ciecze głęboko eutektyczne
IL	ciecz jonowa
LoMMS	mieszanina eutektyczna o niskiej temperaturze topnienia

LZO	lotne związki organiczne
FA	kwas mrówkowy
MA	kwas jabłkowy
MAE	2-(metyloamino)etanol
MCI	mass connectivity index
MD	dynamika molekularna
MDES	magnetyczne ciecze głęboko eutektyczne
MEA	monoetanoloamina
MEACl	chlorowodorek monoetanoloaminy
NADES	naturalne ciecze głęboko eutektyczne
NMTU	*N*-metylotiomocznik
NPT	układ izotermiczno-izobaryczny
OPLS/AA	giętkie pole siłowe ogólnego przeznaczenia w wersji ze wszystkimi atomami ujętymi w sposób jawny
OxaA	kwas szczawiowy
PDES	polimerowe ciecze głęboko eutektyczne
PFP	równanie Prigogine'a–Flory'ego–Patterson'a
PG	glikol propylenowy
PTFE	politetrafluoroetylen
PVDF-co-PTFE	poli(fluorek winylidenu)-ko-poli(tetrafluoroetylenu)
RDF	funkcja rozkładu radialnego
SDT	mechanizm rozpuszczalnościowo-dyfuzyjny
SLM	unieruchomione membrany ciekłe
SUPRADES	ciecze głęboko eutektyczne oparte na cyklodekstrynach
TA	kwas winowy
TBAB	bromek tetrabutyloamoniowy
TBAC	chlorek tetrabutyloamoniowy
TEAC	chlorek tetraetyloamoniowy
TGA	analiza termograwimetryczna
THADES	terapeutyczne ciecze głęboko eutektyczne
TMAC	chlorek tetrametyloamoniowy
U	mocznik
VFT	równanie Vogel'a-Fulcher'a-Tamman'a

Wykaz symboli

α_{ij}	selektywność
ø	kąt torsyjny
A	powierzchnia membrany
D	współczynnik dyfuzji
$dn_B(r)$	liczba cząsteczek B w położonych w odległości (r, $r + dr$) od A
dV(r)	objętość powłoki sferycznej zawartej pomiędzy tymi promieniami
E_{ab}	energia oddziaływania pomiędzy cząsteczkami A i B
g_e	nadmiarowa molowa energia Gibbsa
J	strumień molowy
K_r	stała sprężystości
K_θ	stała siłowa
l	grubość membrany
n	współczynnik załamania światła
P	przenikalność
$p_{i(f,p)}$	ciśnienie składnika i w fazie zasilającej / permeatu
q_i, q_j	ładunki cząstkowe na atomach
r	długość wiązania
R	stała gazowa
r_{eq}	równowagowa długość wiązania
S	współczynnik rozpuszczalności
t	czas
$V_{1\text{-}3}$	stałe szeregu Fouriera
V_n	objętość gazu w warunkach standardowych
ΔH_m	ciepło topnienia
Δp	różnica ciśnienia
η	lepkość
η_0, b, i T_o	optymalizowane parametry w równaniu VFT
η_∞, E_a	optymalizowane parametry w równaniu Arrheniusa
θ	wielkość kąta między wiązaniami
θ_{eq}	równowagowa wartość kąta wiązania
ρ	gęstość
$\rho_B(r)$	średnia gęstość atomów B w odległości r od wybranego atomu A
ρ_B^0	średnia gęstość atomów B w układzie
$\sigma_{i,j}$, $\varepsilon_{i,j}$	parametry studni potencjału dla oddziaływania dyspersyjnego

Chciałbym serdecznie podziękować:

Pani dr hab. Inż. Dorocie Warmińskiej, prof. uczelni

za pomoc udzieloną w trakcie prowadzonych badań oraz przygotowywania rozprawy doktorskiej, opiekę naukową i merytoryczne wskazówki

Pani dr inż. Iwonie Cichowskiej-Kopczyńskiej

za nieocenioną pomoc, poświęcony czas oraz cenne rady

Pani dr hab. inż. n. farm. Marzenie Jamrógiewicz oraz

Panu dr hab. inż. Maciejowi Śmiechowskiemu, prof. uczelni

za pomoc i umożliwienie prowadzenia badań stanowiących ważną część mojej pracy

Pracownikom i Doktorantom Katedry Chemii Fizycznej

za stworzenie wspaniałej atmosfery, która towarzyszyła mi każdego dnia

Margaricie

za wieloletnią przyjaźń, wsparcie i dodawanie sił do działania

Mamie, Pawłowi, Michalinie

za podnoszenie na duchu, nawet w najgorszych chwilach i wiarę we mnie

Oldze, Asi i Malwinie

za wspólne przeżycie tej przygody

Oli

za codzienną dawkę pozytywnej energii

1. Wprowadzenie

Obecnie, jednym z wiodących kierunków światowych badań jest opracowanie metod mających na celu redukcję emisji ditlenku węgla, głównego czynnika odpowiadającego za występowanie efektu cieplarnianego. Gaz ten jest emitowany do atmosfery w procesach produkcji energii elektrycznej i cieplnej, opartych na spalaniu paliw. W elektrowniach, ze względu na niskie (bliskie atmosferycznemu) ciśnienie gazów spalinowych, jedną z najczęściej stosowanych technologii usuwania CO_2 jest absorpcja chemiczna z wykorzystaniem wodnych roztworów amin. Jednak korozyjny charakter środowiska reakcji, energochłonna regeneracja oraz utrata rozpuszczalnika, wynikająca z jego lotności, wymuszają konieczność poszukiwania alternatywnych absorbentów ditlenku węgla.

W ostatnich latach podjęto próby zastosowania cieczy głęboko eutektycznych (DES- ang. -„*Deep Eutectic Solvents*") jako potencjalnych zamienników roztworów amin w procesach usuwania CO_2. Podobnie jak w przypadku cieczy jonowych (IL - ang. -„*Ionic Liquids*"), rozpuszczalniki te zaliczane są do „rozpuszczalników projektowalnych" (ang. -„*designer solvents*"), co oznacza możliwość zaprojektowania DES o pożądanych właściwościach fizykochemicznych. Do zalet cieczy głęboko eutektycznych należy również zaliczyć ich niską lotność, stosunkowo niski koszt produkcji oraz niepalność, niską toksyczność i często biodegradowalność.

Większość dotychczasowych badań nad cieczami głęboko eutektycznymi jako potencjalnymi rozpuszczalnikami CO_2 dotyczy mieszanin, które wykazują zdolność fizycznej absorpcji ditlenku węgla. W przypadku cieczy głęboko eutektycznych, które wiążą CO_2 w sposób chemiczny, liczba prac jest zdecydowanie mniejsza. Jeszcze bardziej ograniczona jest liczba doniesień na temat zastosowania cieczy głęboko eutektycznych jako fazy membranowej w unieruchomionych membranach ciekłych (SLM - ang. -„*Supported Liquid Membranes*"), stosowanych do selektywnej separacji ditlenku węgla z mieszanin gazowych. Analiza danych literaturowych wskazuje, że ciecze głęboko eutektyczne mogą absorbować ditlenek węgla lepiej niż ciecze jonowe, a przy odpowiednim doborze składników DES można uzyskać mieszaniny, które są nawet bardziej efektywne od najczęściej stosowanego 30% roztworu wodnego monoetanoloaminy (MEA).

Niezależnie od metody usuwania CO_2, tj. absorpcji w rozpuszczalniku lub za pomocą SLM, efektywność separacji zależy przede wszystkim od budowy DES, która decyduje nie tylko o charakterze chemicznym rozpuszczalnika (możliwości chemisorpcji lub jej braku), ale także o jego właściwościach fizycznych. Dodatkowo, strukturę i właściwości fizyczne mieszanin eutektycznych można modyfikować poprzez celowe dodanie wody, która w pewnych ilościach jest praktycznie zawsze obecna w tych rozpuszczalnikach ze względu na ich silnie higroskopijny charakter.

Przedmiotem niniejszej pracy jest otrzymywanie i charakterystyka nowych cieczy głęboko eutektycznych na bazie aminoalkoholi (3-aminopropan-1-olu (AP), 2-(metyloamino)etanolu

(MAE) i 2-(butyloamino)etanolu (BAE)) i ich wodnych roztworów oraz ocena możliwości ich zastosowania do absorpcji ditlenku węgla ze strumieni gazowych o jego stosunkowo niskim ciśnieniu cząstkowym. Ponadto, celem pracy jest porównanie efektywności DES opartych na glikolach propylenowych (propano-1,2-diolu i propano-1,3-diolu) w procesie membranowej separacji CO_2.

Rozprawa doktorska została napisana w oparciu o jedną publikację przeglądową oraz sześć prac badawczych, stanowiących załącznik A do niniejszej pracy:

A1 - I. Cichowska-Kopczyńska, **B. Nowosielski**, D. Warmińska, Deep Eutectic Solvents: Properties and Applications in CO_2 Separation, Molecules 28 (2023) 5293. https://doi.org/10.3390/molecules28145293. **IF_{2023}: 4,2, $MNSW_{2023}$: 140**

A2 - **B. Nowosielski,** M. Jamrógiewicz, J. Łuczak, M. Śmiechowski, D. Warmińska, Experimental and predicted physicochemical properties of monopropanolamine-based deep eutectic solvents, J. Mol. Liq. 309 (2020) 113110. https://doi.org/10.1016/j.molliq.2020.113110. **IF_{2020}: 6,16, $MNSW_{2020}$: 100**

A3 - **B. Nowosielski,** M. Jamrógiewicz, J. Łuczak, A. Tercjak, D. Warmińska, Effect of temperature and composition on physical properties of deep eutectic solvents based on 2-(methylamino)ethanol – measurement and prediction, J. Mol. Liq. 371 (2023) 121069. https://doi.org/10.1016/j.molliq.2022.121069. **IF_{2023}: 5,3, $MNSW_{2023}$: 100**

A4 - **B. Nowosielski,** M. Jamrógiewicz, I. Cichowska-Kopczyńska, D. Warmińska, Comprehensive evaluation of physical properties and carbon dioxide capacities of new 2-(butylamino)ethanol-based deep eutectic solvents, Pure Appl. Chem. 96 (2024) 1733–1749. https://doi.org/10.1515/pac-2024-0228. **IF_{2023}: 1,8, $MNSW_{2023}$: 140**

A5 - **B. Nowosielski,** M. Jamrógiewicz, J. Łuczak, D. Warmińska, Novel Binary Mixtures of Alkanolamine Based Deep Eutectic Solvents with Water—Thermodynamic Calculation and Correlation of Crucial Physicochemical Properties, Molecules 27 (2022) 788. https://doi.org/10.3390/molecules27030788. **IF_{2022}: 4,6, $MNSW_{2022}$: 140**

A6 - I. Cichowska-Kopczyńska, D. Warmińska, **B. Nowosielski,** Solubility of carbon dioxide in deep eutectic solvents based on 3-amino-1-propanol and tetraalkylammonium salts at low pressure, Materials 14 (2021) 1–14. https://doi.org/10.3390/ma14030594. **IF_{2021}: 3,75, $MNSW_{2021}$: 140**

A7 - **B. Nowosielski,** D. Warmińska, I. Cichowska-Kopczyńska, CO_2 Separation Using Supported Deep Eutectic Liquid Membranes Based on 1,2-propanediol, ACS Sustain. Chem. Eng. 11 (2023) 4093–4105. https://doi.org/10.1021/acssuschemeng.2c06278. **IF_{2023}: 7,1, $MNSW_{2023}$: 140**

2. Przegląd literaturowy dotyczący tematyki rozprawy doktorskiej

2.1. Ciecze głęboko eutektyczne – definicja, typy, metody syntezy i właściwości

W literaturze termin "ciecz głęboko eutektyczna" (DES) odnosi się najczęściej do mieszaniny eutektycznej, czyli mieszaniny dwóch lub więcej substancji mieszających się bez ograniczeń w fazie ciekłej oraz wykazujących częściowy lub całkowity brak mieszalności w fazie stałej. Pyykkö oraz Martins i in. zaproponowali jednak, aby zawęzić stosowalność nazwy ciecz głęboko eutektyczna do takiej mieszaniny eutektycznej, której temperatura topnienia jest niższa niż temperatura obliczona za pomocą równania van Laara-Hildebranda, przy założeniu jej doskonałości (Rysunek 1):

$$T = \frac{T_i}{\left[1 - \frac{RT_i}{\Delta H_m} \ln(x_i)\right]} \quad (1)$$

gdzie x_i, T_i i ΔH_m to ułamek molowy, temperatura topnienia oraz ciepło topnienia składnika i (pełniącego rolę rozpuszczalnika w mieszaninie) oraz T to temperatura topnienia mieszaniny [1,2].

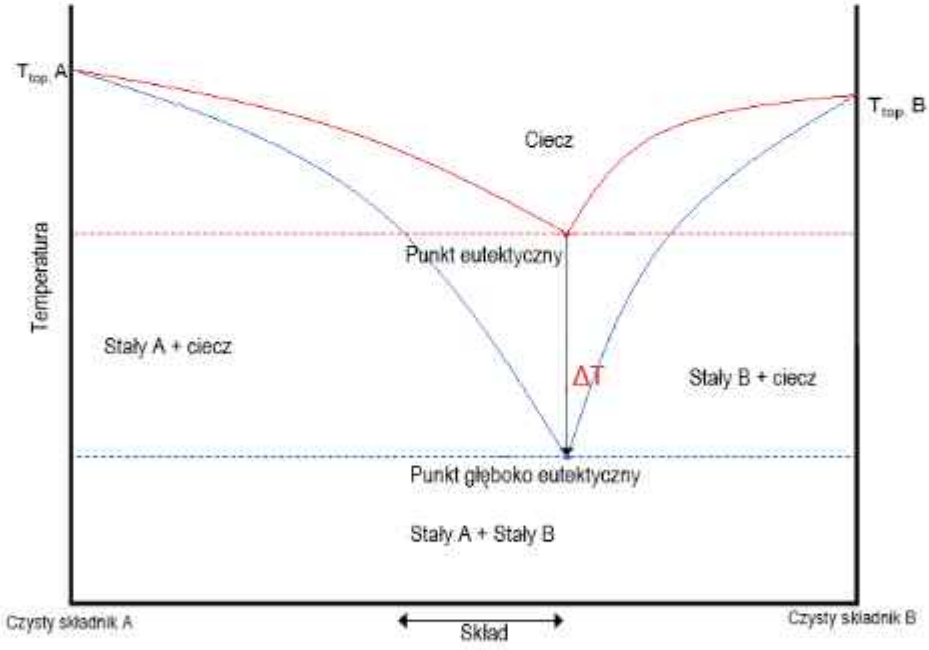

Rysunek 1 Porównanie diagramu fazowego dwuskładnikowego układu eutektycznego prostego, otrzymanego przy założeniu doskonałości mieszaniny (czerwona linia) oraz diagramu fazowego dla składników tworzących ciecz głęboko eutektyczną (niebieska linia).

Ponadto, według autorów stosowalności nazwy ciecz głęboko eutektyczna nie należy ograniczać tylko do mieszanin o składzie eutektycznym, ale należy ją rozszerzyć do mieszanin

o dowolnych składach tworzących układ eutektyczny prosty. Oczywiście, warunek o ujemnym odchyleniu temperatury topnienia od temperatury obliczonej w oparciu o założenie doskonałości mieszaniny eutektycznej powinien być zachowany. Zmiana ilości składników mieszaniny głęboko eutektycznej stanowi bowiem prosty sposób uzyskania jej pożądanych właściwości fizykochemicznych w wybranym zastosowaniu. Na ogół jednak, najprostszym sposobem sterowania właściwościami fizykochemicznymi DES jest użycie różnych składników w mieszaninie.

Dyskusja nad przynależnością danej mieszaniny eutektycznej do cieczy głęboko eutektycznych jest wciąż otwarta, czego dowodem jest publikacja Like i in. z 2023 roku. W swojej pracy autorzy podali nowe, bezwymiarowe i ilościowe kryterium, jakim jest wartość nadmiarowej molowej energii Gibbsa, znormalizowanej przez iloczyn stałej gazowej oraz temperatury eutektycznej mniejsza od -1/3 ($\frac{g_e}{RT_E} < -\frac{1}{3}$) [3]. Zgodnie z tym warunkiem, na przykład mieszanina chlorku choliny z glikolem etylenowym, od lat uważana za ciecz głęboko eutektyczną, nie powinna być zaliczana do tego rodzaju rozpuszczalników. Dlatego też, żeby uniknąć nieścisłości w terminologii, Chen i You zaproponowali wprowadzenie bardziej ogólnej nazwy w stosunku do terminu "ciecz głęboko eutektyczna" na mieszaninę eutektyczną o niskiej temperaturze topnienia, mianowicie "low-melting mixture solvent (LoMMS)" [4]. Jak wynika z Bazy Scopus, taka nazwa zaczyna coraz częściej się pojawiać w publikacjach i być może w przyszłości zastąpi stosowaną do tej pory.

Ze względu na rodzaj składników tworzących ciecze głęboko eutektyczne dzieli się te rozpuszczalniki na 5 podstawowych typów [5]:

Typ I, składający się z czwartorzędowych soli amoniowych i chlorków metali,

Typ II, składający się z czwartorzędowych soli amoniowych i hydratów chlorków metali,

Typ III, składający się z czwartorzędowych soli amoniowych (akceptorów wiązania wodorowego HBA – ang. – *„hydrogen bond acceptor"*) i donorów wiązania wodorowego (HBD – ang. – *„hydrogen bond donor"*),

Typ IV, składający się z hydratów chlorków metali i HBD,

Typ V, składający się z niejonowych HBA i HBD.

W literaturze można też znaleźć inne rodzaje DES, takie jak: naturalne (NADES), terapeutyczne (THADES), magnetyczne (MDES), hydrofobowe (HDES), polimerowe (PQES), oparte na cyklodekstrynach (SUPRADES) [5]. Przynależność do danej klasy cieczy głęboko eutektycznych zależy od charakteru składników mieszanin.

Jak do tej pory, do najbardziej popularnych należą ciecze głęboko eutektyczne typu trzeciego, w których za obniżenie temperatury topnienia głównie odpowiada utworzenie wiązań wodorowych pomiędzy składnikami rozpuszczalnika. Najwięcej publikacji poświęconych jest właściwościom, strukturze i zastosowaniom mieszanin opartych na chlorku choliny (ChCl) pełniącym rolę akceptora wiązania wodorowego oraz na kwasach i glikolach jako donorach wiązania wodorowego. Według danych z Bazy *Scopus* z czerwca 2024 roku tylko 176 artykułów spośród 12451 poświęconych cieczom głęboko eutektycznym dotyczy DES opartych na aminoalkoholach. Pięć głównych dziedzin w jakich były publikowane prace to: chemia, inżyniera

chemiczna, inżyniera materiałowa, nauki o środowisku, fizyka i astronomia, z czego najwięcej artykułów pojawiło się do tej pory w dziedzinie chemii (Rysunek 2).

Rysunek 2 Dziedziny w jakich publikowane były artykuły ze słowem kluczowym „deep eutectic solvents" (*Scopus*).

Ciecze głęboko eutektyczne zaliczane są do nowej klasy „zielonych rozpuszczalników", które obok cieczy nadkrytycznych i cieczy jonowych stanowią alternatywę dla organicznych, lotnych rozpuszczalników mających negatywny wpływ na środowisko. Podobnie jak ciecze jonowe są one praktycznie nielotne, niepalne oraz posiadają wysoką stabilność termiczną i elektrochemiczną, ale koszt ich wytwarzania jest znacząco niższy, są mniej toksyczne i często biodegradowalne [6]. Ich właściwości fizyczne i chemiczne mogą być w prosty sposób modyfikowane poprzez wprowadzenie grup funkcyjnych czy też zmianę proporcji składników tworzących DES [7]. Dlatego też rozpuszczalniki te mogą znaleźć zastosowanie w przetwarzaniu biomasy [8], w ekstrakcji m.in. kwasów tłuszczowych [9], biocząsteczek [10], jonów metali grup przejściowych [11] i pestycydów [12] oraz jako środowisko reakcji chemicznych np. w enancjoselektywnej krzyżowej reakcji aldolowej [13], stereoselektywnej addycji Michael'a [14], reakcjach cyklokondensacji [15] i wielu innych [16]. Trwają prace nad zastosowaniem DES jako katalizatorów w syntezie organicznej [17–19], w odsiarczaniu paliw [20,21], produkcji biopaliw [22] i chemicznym recyklingu polimerów [23]. Podejmuje się również próby wykorzystania DES do separacji gazów, takich jak CH_4, H_2S, NO_2, SO_2 [24].

Ciecze głęboko eutektyczne mogą być otrzymywane przy pomocy kilku technik. Do najczęściej stosowanych należą: metoda podgrzewania, synteza wspomagana ultradźwiękami oraz synteza wspomagana mikrofalami. Okazuje się, że pomiędzy

właściwościami fizycznymi cieczy głęboko eutektycznych otrzymanych przy pomocy tych metod syntezy, nie ma znaczących statystycznie różnic [25]. Rzadziej stosowane metody syntezy DES to metoda odparowywania pod zmniejszonym ciśnieniem, gdzie składniki rozpuszczone są w wodzie, która następnie jest usuwana przy pomocy wyparki obrotowej, oraz technika liofilizacji, w której składniki są rozpuszczane tworząc około 5% roztwór wodny, następnie jest on zamrażany i liofilizowany aż do uzyskania klarownego roztworu. Jednakże, wadą tych metod jest duża zawartość wody w otrzymywanej cieczy głęboko eutektycznej, co przekłada się na ich właściwości fizykochemiczne [26].

Pełny przegląd literaturowy właściwości fizykochemicznych cieczy głęboko eutektycznych został dokonany przeze mnie w pracy **A1**. Zawiera on nie tylko dane dotyczące parametrów fizycznych szczególnie istotnych z punktu widzenia zastosowania DES w procesach usuwania ditlenku węgla z gazów przemysłowych, tj. gęstości, lepkości i współczynnika załamania światła. Przedstawione zostały w nim również inne właściwości, które uzupełniają charakterystykę tych rozpuszczalników, ważne w kontekście innych zastosowań.

Z analizy danych literaturowych wynika, że większość przebadanych do tej pory cieczy głęboko eutektycznych w temperaturze pokojowej posiada gęstość w granicach od 1,0 do 1,35 $g \cdot cm^{-3}$ [8]. Wyjątek stanowią rozpuszczalniki zawierające sole metali, takie jak $ZnCl_2$, mające gęstość w zakresie 1,3–1,6 $g \cdot cm^{-3}$ oraz hydrofobowe DES o gęstości niższej od gęstości wody [27–29]. Współczynniki załamania światła cieczy głęboko eutektycznych są zbliżone do cieczy jonowych i wyższe niż dla klasycznych rozpuszczalników, takich jak etanol lub aceton [30]. Generalnie, ciecze głęboko eutektyczne odznaczają się wysoką lepkością, w szczególności te oparte na cukrach i na aminokwasach [31,32]. Najniższe lepkości (<100 $mPa \cdot s$) wykazują DES zawierające glicerol, glikol, aminoalkohole, aminy, niektóre kwasy karboksylowe i alkohole [33–35]. Wzrost temperatury powoduje spadek gęstości, współczynnika załamania światła i lepkości cieczy głęboko eutektycznych, przy czym zależność temperaturowa gęstości i współczynnika załamania światła ma charakter liniowy, a spadek lepkości ze wzrostem temperatury opisywany jest równaniami o charakterze wykładniczym [35].

Tak jak w przypadku innych rozpuszczalników, o gęstości i współczynniku załamania światła cieczy głęboko eutektycznych decyduje "objętość swobodna" (ang. - *„free volume"*) mieszanin. Wzrostowi "objętości swobodnej", prowadzącemu do niższych wartości gęstości i współczynnika załamania światła, sprzyja wzrost długości i symetrii łańcucha alkilowego w cząsteczce akceptora lub donora wiązania wodorowego DES oraz wzrost rozmiaru anionu HBA [36–41]. Natomiast obecność grup hydroksylowych czy aminowych w składnikach cieczy głęboko eutektycznych, prowadząca do bardziej zwartej struktury rozpuszczalnika, skutkuje wzrostem wartości ρ i n [36,42,43].

W przypadku lepkości na jej wartość wpływa rozmiar cząsteczek rozpuszczalnika oraz oddziaływania międzycząsteczkowe, takie jak wodorowe czy van der Waalsa. Dlatego też wzrostowi lepkości DES sprzyja zarówno obecność w składnikach cieczy głęboko eutektycznych grup hydroksylowych, aminowych, karboksylowych i acetylowych [34,41,44,45], jak i obecność długiego łańcucha alkilowego [46,47].

Jak wynika z literatury, w przypadku większości DES, wraz ze wzrostem stosunku molowego HBA do HBD ich gęstość, współczynnik załamania światła i lepkość maleje [40,45,48,49]. Wynika to ze wzrostu "objętości swobodnej", powiązanego z osłabieniem wiązań wodorowych. Wyjątek stanowią ciecze głęboko eutektyczne, w których występuje silna asocjacja pomiędzy cząsteczkami HBD [50].

Tabela 1 Zebrane właściwości fizyczne DES opartych o aminoalkohole [51].

HBA	HBD	stosunek molowy	ρ / kg m^{-3}	n	η / mPa s
chlorek choliny	monoetanoloamina	1:5	1076,7	1,4849	48,5
chlorek choliny	monoetanoloamina	1:6	1069,0	1,4821	36,7
chlorek choliny	monoetanoloamina	1:7	1065,0	1,4791	37,7
chlorek choliny	monoetanoloamina	1:8	1064,0	1,4777	31,9
chlorek choliny	trietanoloamina	1:2	1330,0	-	838,8
bromek tetrabutyloamoniowy	monoetanoloamina	1:3	1061,6	1,4920	35,97
bromek tetrabutyloamoniowy	monoetanoloamina	1:4	1054,7	1,4881	-
bromek tetrabutyloamoniowy	monoetanoloamina	1:6	1032,2	-	41,67
bromek tetrabutyloamoniowy	monoetanoloamina	1:7	-	-	51,76
bromek tetrabutyloamoniowy	dietanoloamina	1:6	1077,7	-	390
bromek tetrabutyloamoniowy	trietanoloamina	1:7	1091,2	-	556
bromek metylotrifenylofosfoniowy	monoetanoloamina	1:5	1195,8	1,5664	-
bromek metylotrifenylofosfoniowy	monoetanoloamina	1:6	1120,4	-	38,3
bromek metylotrifenylofosfoniowy	monoetanoloamina	1:7	1109,2	-	35,6
bromek metylotrifenylofosfoniowy	monoetanoloamina	1:8	1099,5	1,5024	31,5
2-metoksyfenol	monoetanoloamina	1:1	1137,8	-	531,4
3-metoksyfenol	monoetanoloamina	1:1	1128,3	-	232,8
4-metoksyfenol	monoetanoloamina	1:1	1119,6	-	100,2
2-metoksyfenol	dietanoloamina	1:1	1140,2	-	941,9
3-metoksyfenol	dietanoloamina	1:1	1144,0	-	1198,3
4-metoksyfenol	dietanoloamina	1:1	1136,6	-	566,3
2-metoksyfenol	trietanoloamina	1:1	1133,1	-	440,9
3-metoksyfenol	trietanoloamina	1:1	1131,4	-	631,1
4-metoksyfenol	trietanoloamina	1:1	1131,6	-	421,0

Należy zauważyć, że przestawiona w pracy **A1** analiza wpływu budowy cieczy głęboko eutektycznych na ich właściwości fizykochemiczne opiera się w głównej mierze na DES zawierających HBD inne niż aminoalkohole. Wynika to z małej liczby publikacji poświęconych

właściwościom fizykochemicznym cieczy głęboko eutektycznych zawierających te związki. Doskonale obrazuje to artykuł przeglądowy, który zbiera właściwości fizyczne DES opublikowane w latach 2003-2021 [51]. Na około 1540 DES indeksowanych w tej publikacji, tylko 24 jest opartych o aminoalkohole jako HBD, z czego 15 dotyczy mieszanin zawierających monoetanoloaminę [51]. Ponadto, jak wynika z Tabeli 1, zebrane przez Omara i Sedehdiego dane literaturowe dotyczą głównie cieczy głęboko eutektycznych opartych o HBA inne niż sole tetraalkiloamoniowe. W przypadku DES zawierających sole tetraalkiloamoniowe, właściwości fizyczne zostały wyznaczone tylko dla układów opartych o bromek tetrabutyloamoniowy i etanoloaminę, dietanoloaminę lub trietanoloaminę. Potwierdza to przeglądowa praca Song i in., opublikowana w 2023 roku, poświęcona wyłącznie cieczom głęboko eutektycznym zawierającym aminoalkohole [52]. Autorzy podkreślają w niej, że lepkość tego rodzaju rozpuszczalników jest niższa w porównaniu z DES opartymi na innych HBD, co może prowadzić do obniżenia kosztów ich wykorzystania.

Do najprostszych i najczęściej stosowanych technik modelowania właściwości fizycznych cieczy głęboko eutektycznych należą korelacje, opierające się na empirycznych, liniowych i nieliniowych modelach regresyjnych. Zostały one z powodzeniem zastosowane do powiązania wielu właściwości fizycznych DES z temperaturą, takich jak gęstość [53–56], współczynnik załamania światła [53,55] i prędkość rozchodzenia dźwięku [55,57]. Ponadto, zależność lepkości DES od temperatury najczęściej modelowana jest przy pomocy empirycznego równania Arrheniusa (2) bądź Vogela-Fulchera-Tammana (VFT) (3):

$$\eta = \eta_{\infty} exp^{\frac{E_a}{RT}} \tag{2}$$

$$\eta = \eta_0 exp^{\frac{b}{T-T_0}} \tag{3}$$

gdzie η_{∞}, E_a, η_0, b, i T_0 są optymalizowanymi parametrami, R to stała gazowa, a T to temperatura w Kelvinach.

Pomimo prostoty metod korelacyjnych ich zastosowanie w projektowaniu procesów na skalę przemysłową jest ograniczone tylko do zakresu temperatur i DES użytych przy opracowywaniu modelu. Z tego powodu częściej używane są inne, bardziej ogólne techniki m. in. metody udziałów grupowych (GC- ang. – *„Group contribution methods"*). Ich podstawą jest podział cząsteczki związku chemicznego na podstawowe grupy charakteryzujące się addytywnymi wielkościami molowymi (AQM- ang. – *„additive molar quantities"*). Wartości AQM dla określonych grup znajduje się na podstawie danych eksperymentalnych dla znanych związków chemicznych i są one wykorzystywane do określenia właściwości fizykochemicznych nieznanej substancji, takiej jak na przykład ciecz głęboko eutektyczna, oczywiście przy pomocy odpowiednich reguł mieszania. Metody udziałów grupowych używane w literaturze do przewidywania gęstości, lepkości i współczynnika załamania światła cieczy głęboko eutektycznych opisałem w pracach **A2 i A3.** Zostały one opracowane na podstawie dostępnych danych dla DES opartych głównie o alkohole, cukry, kwasy organiczne i aminokwasy. Początkowo używano ich do przewidywania wartości parametrów krytycznych oraz współczynnika acentrycznego DES [58,59]. Oszacowane parametry krytyczne wykorzystywano następnie

do prognozowania wartości gęstości, lepkości i współczynnika załamania światła rozpuszczalników [60–64]. Z czasem metody udziałów grupowych zastosowano do bezpośredniego przewidywania gęstości, współczynnika załamania światła, pojemności cieplnych, prędkości rozchodzenia dźwięku i napięcia powierzchniowe różnych rodzajów DES [60–70].

2.2. Struktura DES – przewidywanie przy pomocy symulacji MD

Dynamika molekularna (MD - ang. - *Molecular Dynamics*) stanowi obecnie najczęściej stosowane narzędzie umożliwiające głębsze zrozumienie struktury cieczy głęboko eutektycznych na poziomie atomowym [71]. Symulacje MD pozwalają bowiem nie tylko na śledzenie ruchu atomów w czasie, ale również na ilościowe określenie odległości między nimi, co umożliwia dokładną analizę geometrii układu, rozmieszczenia wiązań wodorowych oraz innych oddziaływań międzycząsteczkowych.

Pole siłowe jest kluczowym elementem symulacji metodą dynamiki molekularnej, umożliwiając realistyczne odwzorowanie struktury i właściwości układów chemicznych na poziomie atomowym. Jest ono matematycznym opisem definiującym sposób, w jaki atomy oddziałują ze sobą w układzie molekularnym. Pole siłowe opiera się na energii potencjalnej, która jest zazwyczaj reprezentowana w postaci sumy łatwo interpretowalnych i weryfikowalnych eksperymentalnie członów takich jak energia deformacji wiązań, deformacji kątów między wiązaniami, obrotów wokół wiązań oraz energia oddziaływań elektrostatycznych i van der Waalsa. Funkcja energii potencjalnej może mieć dodatkowe człony, które dokładniej opisują pewne właściwości molekuły np. oddziaływanie pochodzące od wiązań wodorowych.

Giętkie pole siłowe ogólnego przeznaczenia OPLS/AA (OPLS - ang. - „*optimized potentials for liquid simula*tions") w wersji ze wszystkimi atomami ujętymi w sposób jawny (AA – ang. -„*all-atom*"), jest często stosowane w symulowaniu zachowania cieczy organicznych i ich mieszanin z wodą [72,73]. W polu siłowym OPLS/AA oddziaływania międzycząsteczkowe niewiążące opisane są poprzez połączenie energii oddziaływań elektrostatycznych i potencjału Lennarda-Jonesa w następujący sposób:

$$E_{ab} = \sum_i^a \sum_j^b \left[\frac{q_i q_j e^2}{r_{ij}} + 4\varepsilon_{ij} \left(\frac{\sigma_{ij}^{12}}{r_{ij}^{12}} - \frac{\sigma_{ij}^{6}}{r_{ij}^{6}} \right) \right] f_{ij} \qquad (4)$$

gdzie, E_{ab} - energia oddziaływania pomiędzy cząsteczkami a i b, q_i,q_j - ładunki cząstkowe na atomach, σ_{ij}, ε_{ij} - parametry studni potencjału dla oddziaływania dyspersyjnego.

Energia oddziaływań wewnątrzcząsteczkowych obliczana jest jako łączna energia potencjalna wiązań (wkłady 2-atomowe), kątów (wkłady 3-atomowe) i kątów torsyjnych (wkłady 4-atomowe). Wiązania i kąty modelowane są jako oscylatory harmoniczne, zaś kąty torsyjne jako funkcje periodyczne kąta.

Energia związana z rozciąganiem wiązań i deformacjami kątów wyrażone są jako:

$$E_{wiązanie} = \sum_{wiązania} K_r \left(r - r_{eq} \right)^2 \qquad (5)$$

$$E_{kąty} = \sum_{kąty} K_\theta \left(\theta - \theta_{eq}\right)^2 \quad (6)$$

gdzie, K_r i K_θ - stałe sprężystości i siłowa, r - długość wiązania, r_{eq} - równowagowa długość wiązania, θ - wielkość kąta między wiązaniami, θ_{eq} - równowagowa wartość kąta wiązania.

Ostatni człon energetyczny w polu siłowym OPLS/AA opisuje energię torsyjną (rotacji wokół pojedynczych wiązań):

$$E_{torsyjna} = \sum_i \frac{V_1^i}{2}[1 + cos\,(\emptyset_i)] + \frac{V_2^i}{2}[1 + cos\,(2\emptyset_i)] + \frac{V_3^i}{2}[1 + cos\,(3\emptyset_i)] \quad (7)$$

gdzie, ø - kąt torsyjny, $V_{1\text{-}3}$ - stałe szeregu Fouriera [72].

Kluczowym narzędziem stosowanym w analizie wyników symulacji metodą dynamiki molekularnej, pozwalającym na badanie lokalnej struktury oraz oddziaływań międzycząsteczkowych jest funkcja rozkładu radialnego (RDF – ang. *„radial distribution function"*). Wskazuje ona prawdopodobieństwo znalezienia się cząsteczek lub atomów B w odległości *r* od wybranej cząsteczki odniesienia A (w szczególnym przypadku A jest tożsame z B). Formalnie jest ona definiowana jako:

$$g_{AB}(r) = \frac{\rho_B(r)}{\rho_B^0} \quad (8)$$

gdzie, $\rho_B(r)$ - średnia gęstość atomów B w odległości r od wybranego atomu A, ρ_B^0 - średnia gęstość atomów B w układzie.

W sposób jawny jej wartość obliczana jest w następujący sposób:

$$g_{AB}(r) = \frac{dn_B(r)}{dV(r)\rho} \approx \frac{dn_B(r)}{4\pi r^2 dr \rho_B^0} \quad (9)$$

gdzie, $dn_B(r)$ - liczba cząsteczek B w położonych w odległości (r, r + dr) od A, dV(r) - objętość powłoki sferycznej zawartej pomiędzy tymi promieniami [74].

Pierwsze prace, w których użyto metody dynamiki molekularnej w odniesieniu do cieczy głęboko eutektycznych poświęcone były mechanizmowi powstawania DES złożonego z chlorku choliny i mocznika (U). Sun i in. badając energię oddziaływań w szerokim zakresie składu mieszaniny, wykazali, że przy składzie 1:2 oddziaływania pomiędzy kationem i anionem soli, kationem soli i mocznikiem oraz pomiędzy anionem soli i mocznikiem pozostają w równowadze [75]. Według Celebi i in., prowadzi to do największego obniżenia temperatury topnienia, a efekt ten maleje wraz ze wzrostem zawartości mocznika w mieszaninie na skutek wzrostu mocy oddziaływań pomiędzy cząsteczkami mocznika i osłabienia oddziaływań pomiędzy mocznikiem i chlorkiem choliny [76]. Osłabienie sieci wiązań wodorowych pomiędzy jonami soli i cząsteczkami donora wiązania wodorowego w mieszaninach o większej zawartości HBD, prowadzące do wyższej temperatury topnienia DES, potwierdzają również obliczenia przeprowadzone przez Pour i in. dla mieszanin złożonych z chlorku choliny i glukozy [77]. Naik i in. fakt powstania cieczy głęboko eutektycznej również przypisują tworzeniu wiązań wodorowych pomiędzy anionem HBA a HBD oraz osłabieniu oddziaływań typu HBD-HBD i kation-anion HBA [78]. Pozostaje to w zgodzie z symulacjami MD przeprowadzonymi przez Shokri i in. pokazującymi, że na oddziaływania pomiędzy HBA i HBD wpływa moc oddziaływań elektrostatycznych pomiędzy jonami soli. Zgodnie z wynikami autorów spośród trzech mieszanin zawierających N-metylotiomocznik (NMTU) jako donor wiązania wodorowego oraz różne akceptory wiązania

wodorowego – chlorek choliny, chlorek allilotrimetyloamoniowy (ATMAC) i chlorek benzylotrietyloamoniowy (BTEAC) najsilniejsze oddziaływania pomiędzy jonami soli, prowadzące do najsłabszych oddziaływań pomiędzy HBA i HBD, występują pomiędzy anionem chlorkowym a kationem cholinowym [79].

Z przeprowadzonych dotąd obliczeń metodą MD wynika też, że nie bez znaczenia dla oddziaływań wodorowych pozostaje obecność, typ i położenie grup funkcyjnych w składnikach cieczy głęboko eutektycznych. Z pracy Migliorati i in., dotyczącej struktury DES opartych na chlorku choliny lub chlorku benzylotrimetyloamoniowym, wynika, że obecność grupy hydroksylowej w ChCl powoduje powstanie swoistej dla tej cieczy głęboko eutektycznej trójwymiarowej sieci wiązań wodorowych, w której uczestniczą zarówno kation i anion soli, jak i mocznik. W przypadku DES opartego o chlorek benzylotrimetyloamoniowy, ze względu na brak grupy hydroksylowej, wiązanie wodorowe powstaje tylko pomiędzy anionem soli a mocznikiem i według autorów prowadzi to do obniżenia temperatury topnienia w mniejszym stopniu niż dla ChCl/U [80]. Z analizy funkcji rozkładu radialnego dla cieczy głęboko eutektycznej złożonej z chlorku choliny i kwasu askorbinowego, przeprowadzonej przez Cheng i in., wynika, że oddziaływania wodorowe pomiędzy anionem soli a grupami hydroksylowymi HBD są preferowane, gdy grupy te są połączone z pierścieniem laktonowym kwasu a nie z jego łańcuchem alkilowym [81]. W przypadku DES zawierających kwasy karboksylowe w większości wiązań wodorowych pomiędzy HBA i HBD uczestniczą terminalne grupy –OH pochodzące od grupy karboksylowej. Dowodzą tego obliczenia Rozas i in. dotyczące mieszanin złożonych z 1,8-cyneolu oraz kwasu jabłkowego lub kwasu mlekowego [82]. W cieczach głęboko eutektycznych opartych o glikole o takiej samej długości łańcucha alkilowego, ale o różnym położeniu grupy hydroksylowych, jak to ma miejsce w przypadku mieszanin chlorku choliny z propano-1,2-diolem oraz z propano-1,3-diolem, silniejsze oddziaływania wodorowe pomiędzy anionem chlorkowym chlorku choliny a HBD zaobserwowano dla glikolu propano-1,2-diolowego [83]. Według autorów pracy oddalenie grup -OH w propano-1,3-diolu zwiększa liczbę oddziaływań typu glikol-glikol, które mogą konkurować z oddziaływaniami pomiędzy anionem chlorkowym a cząsteczkami glikolu i w efekcie powstają słabsze wiązania wodorowe między Cl^- a grupami -OH glikolu. Osłabieniu wiązań wodorowych pomiędzy HBA i HBD sprzyja również zamiana grupy hydroksylowej na aminową. Wykazali to Kussainowa i in. w swojej pracy dotyczącej cieczy głęboko eutektycznej składającej się z bromku metylotrifenylofosfoniowego i monoetanoloaminy, która przynajmniej według mojej wiedzy, stanowi jedyną pozycję przedstawiającą symulacje MD dla DES opartych na aminoalkoholach i halogenkach kationów czwartorzędowych. Zgodnie z obliczeniami autorów, oddziaływanie między anionem bromkowym a grupą hydroksylową monoetanoloaminy jest prawie pięciokrotnie silniejsze niż oddziaływanie między Br^- a grupą aminową [84]. Badania przeprowadzone przez Ferreira i in., oparte na analizie funkcji rozkładu radialnego dla cieczy głęboko eutektycznych złożonych z chlorku choliny oraz glikolu etylenowego (EG) lub glikolu propylenowego (PG), wskazują na istotny wpływ długości łańcucha alkilowego HBD na strukturę tych cieczy [83,85]. Z badań wynika, że w mieszaninie ChCl/PG dominują wiązania wodorowe między anionem chlorkowym a cząsteczką glikolu propylenowego.

Natomiast w przypadku mieszaniny ChCl/EG, ilość oddziaływań wodorowych pomiędzy anionem chlorkowym a glikolem etylenowym oraz wiązań typu EG-EG jest bardziej zrównoważona. To zróżnicowanie w strukturze wiązań wodorowych wynika z różnic w długości łańcucha alkilowego HBD – dłuższy łańcuch w przypadku glikolu propylenowego sprzyja powstawaniu silniejszych oddziaływań między anionem Cl^- a glikolem, podczas gdy krótszy łańcuch glikolu etylenowego prowadzi do bardziej zrównoważonych oddziaływań w mieszaninie [83,85].

2.2.1.Wpływ wody na właściwości i strukturę DES

Ze względu na swoje silnie higroskopijne właściwości, ciecze głęboko eutektyczne zostają zanieczyszczone śladowymi ilościami wody już w procesie ich syntezy [86]. Ponadto rozpuszczalniki te mogą ulegać dalszemu zawodnieniu w trakcie użytkowania. Czasami woda może być jednak celowo dodawana do DES w celu poprawy ich właściwości fizykochemicznych, zwłaszcza tych odpowiedzialnych za transport masy jak np. lepkość.

Większość prac eksperymentalnych dedykowanych wodnym roztworom cieczy głęboko eutektycznych dotyczy właściwości termodynamicznych roztworów DES zawierających chlorek choliny. Przede wszystkim są to prace oparte na pomiarach gęstości przeprowadzone dla rozpuszczalników, w skład których wchodzi mocznik, ale są też dedykowane DES, w których rolę HBD pełni glikol etylenowy, glikol propylenowy, kwas malonowy i mlekowy czy też cukry [87,88]. W literaturze znajduje się zdecydowanie mniej prac dotyczących charakterystyki wodnych roztworów DES uzyskanej przy pomocy pomiarów lepkości czy współczynnika załamania światła, a jeszcze mniej doniesień literaturowych poświęconych jest pomiarom prędkości dźwięku [87]. Dla wszystkich zbadanych dotąd układów binarnych wody z cieczą głęboko eutektyczną opartą o chlorek choliny uzyskano dodatnie odchylenia współczynnika załamania światła i odchylenia lepkości [89] oraz ujemne nadmiarowe objętości molowe [90], nadmiarowe adiabatyczne ściśliwości molowe i odchylenia ściśliwości adiabatycznej [91,92]. Uzyskane wyniki dowodzą więc, że pomiędzy wodą a cząsteczkami DES powstają silne oddziaływania wodorowe, które w połączeniu z efektem upakowania cząsteczek wody w strukturze DES prowadzą do zmniejszenia "objętości swobodnej" mieszaniny i w konsekwencji do spadku objętości i ściśliwości oraz do wzrostu współczynnika załamania światła i lepkości w całym zakresie składów [90,93–95]. W przypadku wodnych roztworów DES opartych o bromek tetrabutyloamoniowy oraz kwas mrówkowy (FA) uzyskana przez Zuo i in. [96] sinusoidalna zależność nadmiarowych objętości molowych od składu mieszaniny wskazuje na nieco inne zachowanie. Dodatnie wartości nadmiarowych objętości molowych, obserwowane przy niskiej zawartości wody wskazują, że wprowadzenie wody do TBAB/FA powoduje wzrost objętości roztworu, co jest najprawdopodobniej spowodowane rozrywaniem silniejszych wiązań wodorowych pomiędzy cząsteczkami DES i powstawaniem w ich miejsce słabszych wiązań pomiędzy DES a wodą, co prowadzi do rozluźnienia struktury mieszaniny. Ujemne wartości nadmiarowych objętości molowych przy wyższych stężeniach wody sugerują z kolei, że wiązania

wodorowe pomiędzy cząsteczkami wody są słabsze niż wiązania wodorowe tworzone pomiędzy cząsteczkami TBAB/FA i wodą.

Jako że nadmiarowe wielkości termodynamiczne pozwalają na ocenę oddziaływań obecnych w układzie jedynie w skali makroskopowej, w celu głębszego zrozumienia oddziaływań cieczy głęboko eutektycznych z wodą na poziomie mikroskopowym, podjęto w przeszłości próby określenia struktury wodnych roztworów DES między innymi za pomocą dynamiki molekularnej. Zdecydowana większość symulacji dotyczyła wpływu wody na strukturę cieczy głęboko eutektycznych opartych na chlorku choliny.

W swojej pracy, poświęconej oddziaływaniom w wodnym roztworze ChCl/U (1:2), Shah i in. podzielili wpływ wody na strukturę DES w zależności od ułamka masowego H_2O na trzy zakresy [97]. Według autorów, przy niskiej zawartości wody (w_{H2O}< 5%) woda wzmacnia wiązania wodorowe pomiędzy cząsteczkami mocznika, w zakresie od 5% do 25% ułamka masowego H_2O tworzy wiązania wodorowe ze składnikami DES, ale wciąż zachowana jest jego struktura, a powyżej 25% ułamka masowego H_2O woda burzy strukturę DES. Skokowe zniszczenie struktury ChCl/U przy dużej zawartości wody potwierdzają wyniki innych niezależnych grup badawczych Fetisov i in. oraz Sapir i Harries (50% ułamka masowego H_2O), Zhekenov i in. (30% ułamka masowego H_2O) oraz Kumari i in. (41% ułamka masowego H_2O) [98–101]. Wszyscy autorzy za główną przyczynę zmian strukturalnych DES w obecności wody zgodnie podają preferencyjną hydratację jonu chlorkowego. Fakt nagłego zniszczenia struktury DES przy konkretnej zwartości wody zakwestionowała natomiast praca Monteiro i in., w której autorzy postulują stopniową zmianę hydratacji składników DES z płynnym przejściem między strukturami „woda-w-DES" i „DES-w-wodzie" [102]. Symulacje MD przeprowadzone przez Gao i in. dla wodnych roztworów ChCl/U wykazały, że nawet dla wysokich ułamków molowych wody (x_{H2O}=0,9), jony chlorkowe są tylko częściowo uwodnione [103].

Jedna z nielicznych prac poświęconych DES opartych na innych HBA niż chlorek choliny dotyczyła wodnych roztworów hydrofobowych DES opartych o chlorki tetraalkiloamoniowe jako HBA i kwas kaprylowy jako HBD. Obliczenia przeprowadzone przez Pour i in. dla tych mieszanin potwierdziły efekt obserwowany dla DES opartych o ChCl, a mianowicie to, że niezależnie od układu, dodatek wody powoduje osłabianie oddziaływań pomiędzy HBA a HBD poprzez preferencyjną hydratację jonu chlorkowego soli [104].

2.3. Wykorzystanie DES w procesie usuwania CO_2

Pierwszy artykuł dotyczący wykorzystania DES w procesie absorpcji ditlenku węgla pojawił się w literaturze w 2008 roku i dotyczył mieszaniny złożonej z chlorku choliny i mocznika w stosunku molowym 1:2 [105]. Od tego czasu zainteresowanie tym tematem znacznie wzrosło. Przegląd literatury dotyczącej absorpcji ditlenku węgla w cieczach głęboko eutektycznych został przeze mnie szeroko opisany w pracy **A1**, obejmującej sposoby pomiaru rozpuszczalności ditlenku węgla oraz wpływ budowy składników tworzących DES na jej zdolności sorpcyjne.

Najczęściej stosowane metody badań przydatności DES w separacji gazów opierają się na pomiarze rozpuszczalności ditlenku węgla metodą wagową oraz izochoryczną równowagową. Pierwsza wymieniona metoda polega na pomiarze zmian masy próbki medium sorpcyjnego wysycanego gazem aż do osiągnięcia stałej wartości w ustalonych warunkach ciśnienia i temperatury, natomiast metoda izochoryczna równowagowa opiera się na pomiarze zmian ciśnienia gazu nad rozpuszczalnikiem aż do uzyskania stanu równowagi. Zgodnie z literaturą, metoda izochoryczna równowagowa jest odpowiednia do pomiarów pojemności sorpcyjnej w warunkach wysokiego ciśnienia, natomiast metoda wagowa sprawdza się lepiej przy pomiarach w warunkach ciśnienia atmosferycznego [52].

Największy wpływ na pojemność sorpcyjną ditlenku węgla mają grupy funkcyjne obecne zarówno w cząsteczce akceptora, jak i donora wiązania wodorowego. Obecność grupy aminowej w HBD lub HBA decyduje o chemicznym charakterze procesu sorpcji, co prowadzi do wyższych wartości rozpuszczalności CO_2. Z nielicznych doniesień literaturowych dotyczących cieczy głęboko eutektycznych opartych na aminach, wynika, że mieszaniny, w których zachodzi zarówno fizyczna, jak i chemiczna absorpcja ditlenku węgla, często wykazują wyższą pojemność sorpcyjną w stosunku do tego gazu niż powszechnie stosowany wodny 30% wag. roztwór monoetanoloaminy. Przykładem takiego rozpuszczalnika jest mieszanina chlorku tetraetyloammoniowego i monoetanoloaminy w stosunku molowym HBA do HBD 1:5, w której rozpuszczalność CO_2 w temperaturze 303 K i ciśnieniu 1 atm wynosi 0,1628 g/g, podczas gdy w wodnym roztworze MEA wynosi ona w tych samych warunkach 0,118 g/g [52].

Przeprowadzone dotąd badania wskazują też, że ciecze głęboko eutektyczne zawierające pierwszorzędowe aminy charakteryzują się wyższą pojemnością sorpcyjną ditlenku węgla w porównaniu do mieszanin zawierających aminy drugo- czy trzeciorzędowe [106]. Ponadto, według Haidera i Kumara DES oparte na drugorzędowych aminach wykazują odmienną zależność między długością łańcucha alkilowego a zdolnościami sorpcyjnymi niż te z pierwszorzędowymi aminami, tzn. ich zdolności sorpcyjne obniżają się wraz ze wzrostem długości łańcucha alkilowego HBD, co wynika ze zwiększonej zawady sterycznej [107]. Co więcej, trzeciorzędowe aminy nie tworzą z CO_2 kwasu karbaminowego, a sorpcja wynika z oddziaływań fizycznych, co w konsekwencji skutkuje niższą rozpuszczalnością ditlenku węgla [106,108].

Grupy funkcyjne o wyższym powinowactwie do CO_2 zapewniają wyższą rozpuszczalność i zgodnie z tym kryterium można by je uszeregować według następującej kolejności: grupa amidowa > grupa karbonylowa > wiązanie eterowe > grupa hydroksylowa [49,109,110]. Nie bez znaczenia pozostaje też sama liczba i położenie grup funkcyjnych w składnikach DES. Chen i in. zaobserwowali wyższą rozpuszczalność CO_2 w mieszaninach, w których grupy –OH w glikolach były położone blisko siebie [111]. Z kolei Pishro i in. wykazali, że rozpuszczalniki zawierające większą liczbę grup aminowych charakteryzują się wyższą pojemnością sorpcyjną CO_2 [112]. Według Sarmada i in. mieszaniny oparte o związki, które zawierają grupy funkcyjne mogące tworzyć wewnątrzcząsteczkowe wiązania wodorowe słabiej oddziałują z ditlenkiem węgla i w rezultacie słabiej go absorbują [34].

Istotnym czynnikiem wpływającym na pojemność sorpcyjną DES jest stosunek molowy HBA do HBD. Jak wynika z doniesień literaturowych, optymalny stosunek może różnić się w zależności od zastosowanych składników mieszaniny. W przypadku cieczy głęboko eutektycznych absorbujących CO_2 w sposób fizyczny, najczęściej obserwuje się obniżenie rozpuszczalności wraz ze wzrostem zawartości HBD, spowodowane spadkiem "objętości swobodnej" [108,109,111,113]. Z kolei w przypadku DES tworzących z ditlenkiem węgla wiązania chemiczne wraz ze wzrostem stosunku molowego HBA do HBD rozpuszczalność CO_2 przeważnie rośnie. Wynika to ze zwiększonej liczby cząsteczek mogących z nim reagować [106,112]. Znane są jednak wyjątki, w których efekt związany z obniżeniem "objętości swobodnej" rozpuszczalnika przeważa i ostatecznie rozpuszczalność CO_2 maleje wraz ze wzrostem ilości HBD, mimo zachodzącej reakcji. Zjawisko to zaobserwowali Ali i in. dla cieczy złożonych z bromku metylotrifenylofosfoniowego i monoetanoloaminy [114]. W przypadku cieczy absorbujących CO_2 w sposób fizyczny, wzrostowi rozpuszczalności sprzyja wzrost długości łańcuchów alkilowych i ich symetrii oraz wielkości anionu, zarówno w cząsteczce HBA jak i HBD [34,108,115,116].

Wpływ zawartości wody na rozpuszczalność ditlenku węgla w cieczach głęboko eutektycznych został opisany tylko w kilku pracach. W przypadku mieszanin wykazujących fizyczny mechanizm sorpcji CO_2 zwiększenie zawartości wody prowadzi do obniżenia rozpuszczalności gazu, natomiast w przypadku DES zawierających aminy, niewielki dodatek wody może mieć korzystny wpływ na wielkość pojemności sorpcyjnej ditlenku węgla [117,118]. Wskazują na to badania Trivedi i in. przeprowadzone dla wodnych roztworów DES złożonej z chlorowodorku monoetanoloaminy i etanodiaminy MEACl/EDA (1:3). Według autorów, dodatek niewielkiej ilości wody do MEACl/EDA (do 10%) powoduje wzrost pojemności sorpcyjnej CO_2, ale przekroczenie granicznej wartości prowadzi do jej spadku [119]. Podobny spadek rozpuszczalności ditlenku węgla przy większej ilości wody zaobserwowali Li i in. w przypadku mieszanin złożonych z monoetanoloaminy i chlorków tetrametyloamoniowego i tetraetyloamoniowego TMAC/MEA i TEAC/MEA. Warto jednak zaznaczyć, że ci sami autorzy wykazali, że dla mieszaniny ChCl/MEA dodatek wody w zakresie 15-20 % masowych nie wpływa znacząco na rozpuszczalność CO_2 w DES [106].

Mechanizm wpływu wody na rozpuszczalność CO_2 w cieczach głęboko eutektycznych nie jest w pełni poznany. Su i in. w badaniach nad DES wykazującymi fizyczny mechanizm sorpcji sugerują, że zmniejszenie rozpuszczalności wraz ze wzrostem zawartości wody jest wynikiem obniżenia stężenia składników mieszaniny, co prowadzi do redukcji liczby grup funkcyjnych oddziałujących z CO_2 [117]. Podobne wnioski przedstawiają Shukla i in. na podstawie badań wodnych roztworów cieczy głęboko eutektycznych opartych na aminach, zawierających ponad 10% wag. H_2O [120]. Jest to uzasadnione biorąc pod uwagę różnicę w rozpuszczalności CO_2 w DES i w wodzie, mogącą sięgać dwóch rzędów wielkości [121]. Z kolei wzrost rozpuszczalności ditlenku węgla po dodaniu niewielkiej ilości wody do DES absorbujących CO_2 w sposób chemiczny tłumaczony jest osłabieniem oddziaływań międzycząsteczkowych w mieszaninie, wynikającym z występowania nowych oddziaływań z H_2O [106,119]. Według badaczy, proces ten

prowadzi zarówno do zwiększenia "objętości swobodnej" DES jak i do ułatwionego tworzenia oddziaływań CO_2 ze składnikami DES, co ostatecznie skutkuje wzrostem absorpcji.

Jak dotąd, techniki absorpcyjne są najczęściej stosowanymi w praktyce metodami separacji ditlenku węgla ze strumieni gazowych. Ze względu jednak na liczne wady tych metod, proponowane są nowe rozwiązania, które wykorzystują mniejsze ilości bardziej przyjaznych środowisku odczynników oraz cechują się łatwością i niskimi kosztami wdrażania i eksploatacji. Obok procesów adsorpcyjnych, kriogenicznych i elektrochemicznych należą do nich metody membranowe, charakteryzujące się niewielkim kosztem inwestycyjnym, łatwością zwiększania skali oraz niskim zużyciem energii. Membrany ciekłe można podzielić na:

- Membrany ciekłe grubowarstwowe (BLM - ang. - *„Bulk Liquid Membrane"*)
- Emulsyjne membrany ciekłe (ELM - ang. - *„Emulsion Liquid Membrane"*)
- Unieruchomione membrany ciekłe (SLM – ang. - *„Supported Liquid Membrane"*)

Zastosowanie unieruchomionych membran ciekłych do usuwania CO_2 pozwala na maksymalne obniżenie zużycia rozpuszczalnika przy jednoczesnym zachowaniu zadowalającej efektywności. SLM składają się z porowatego nośnika i ciekłej fazy membranowej. Najczęściej fazę membranową tworzy ciecz organiczna, która jest utrzymywana w porach nośnika przez siły kapilarne. Przekrój SLM został przedstawiony na Rysunku 3.

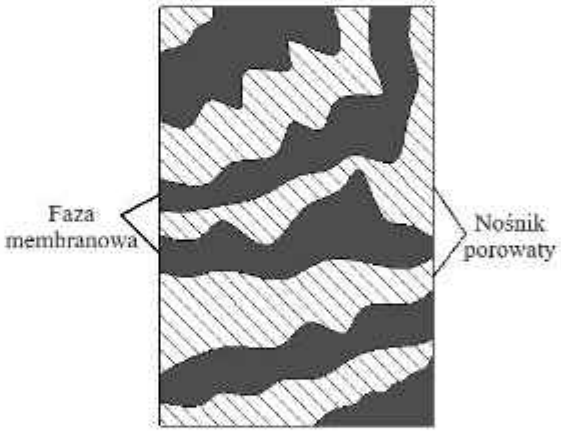

Rysunek 3 Przekrój unieruchomionej membrany ciekłej

Proces rozdzielania mieszanin w układzie SLM zachodzi na podstawie mechanizmu rozpuszczalnościowo-dyfuzjnego (SDT – ang. *„solution-diffusion theory"*). Zgodnie z tym modelem, transport gazu można opisać w siedmiu etapach (Rysunek 4):

1. dyfuzja substancji S przez warstwę graniczną w fazie zasilającej (donorowej),
2. ekstrakcja (sorpcja) substancji na granicy faz donorowej i membranowej,
3. dyfuzja przez warstwę graniczną po stronie zasilającej (donorowej),
4. transport konwekcyjny w fazie membranowej,
5. dyfuzja przez warstwę graniczną w fazie permeatu (akceptorowej),
6. ponowna ekstrakcja (desorpcja) na granicy faz membranowej i permeatu,
7. dyfuzja przez warstwę graniczną w fazie permeatu (akceptora).

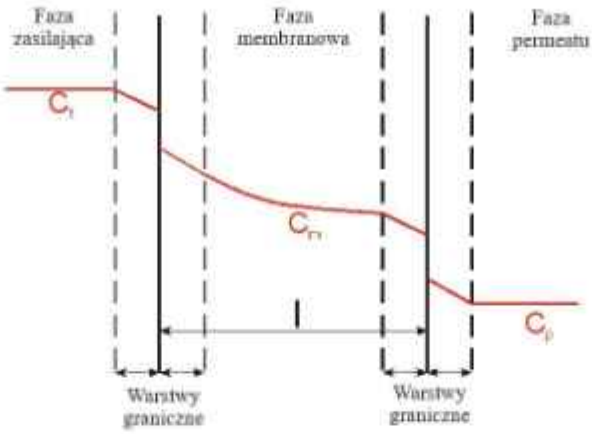

Rysunek 4 Schematyczny rysunek mechanizmu rozpuszczalnościowo-dyfuzjnego.

Strumień molowy może być wyrażony jako:

$$J = \frac{DS\Delta p}{l} = \frac{P\Delta p}{l} \tag{10}$$

gdzie;

J – strumień molowy [mol·m^{-2}·s^{-1}],

S – współczynnik rozpuszczalności [mol·m^{-3}·Pa],

P – przenikalność [mol·m^{-1}·s^{-1}·Pa^{-1}],

D - współczynnik dyfuzji [m^2·s^{-1}],

Δp –różnica ciśnienia [Pa],

l –grubość membrany [m].

Siłą napędową procesu jest gradient potencjału chemicznego substancji pomiędzy obiema stronami membrany. Ponieważ w SDT zakłada się, że ciśnienie wewnątrz membrany jest jednakowe, potencjał chemiczny jest reprezentowany przez stężenie substancji w poszczególnych fazach. Przez to, w układzie statycznym, wydajność separacji maleje z czasem z powodu zmniejszenia różnicy stężeń po obu stronach membrany [122].

Przenikalność może być obliczona przy pomocy równania (11) i wówczas wyrażona jest w barrerach:

$$P = 10^{-10}\frac{V_n l}{At(p_{i,f} - p_{i,p})} \tag{11}$$

gdzie;

A – powierzchnia membrany [cm^2],

t – czas [s],

P – przenikalność [barrer]

V_n– objętość gazu w warunkach standardowych [cm$^3_{STP}$]

$p_{i(f,p)}$ – ciśnienie składnika i w fazie zasilającej/permeatu [cmHg].

Przenikalność może być również wyrażona w jednostce GPU (1 GPU jest równy 10^{-4} barrera).

Proces przenikania masy przez SLM zależny jest, jak wynika to z mechanizmu SDT, zarówno od oporów dyfuzji (lepkości cieczy), jak i rozpuszczalności gazu w fazie membranowej. Zbyt niska lepkość cieczy może prowadzić do niestabilności membrany, natomiast zbyt wysoka powoduje duże opory dyfuzji. Niska rozpuszczalność składnika separowanego z kolei obniża efektywność procesu rozdziału.

Na stabilność SLM wpływa wiele czynników, a do najczęstszych przyczyn jej obniżenia należą: 1) utrata rozpuszczalnika wskutek różnicy ciśnień między stronami membrany lub w wyniku odparowania z porów, 2) blokowanie porów przez wytrącanie się fazy stałej, 3) degradacja mechaniczna w wyniku zerwania ciągłości nośnika i 4) pęcznienie membrany spowodowane oddziaływaniem nośnika z fazą membranową [123,124]. W celu minimalizacji tych efektów kluczowy jest dobór rozpuszczalnika, który nie reaguje z nośnikiem, charakteryzuje się niską lotnością oraz stabilnie utrzymuje się w porach membrany. Sam nośnik natomiast powinien wykazywać odporność chemiczną, termiczną i mechaniczną (w warunkach prowadzenia procesu), a także odpowiednią hydrofilowość/hydrofobowość, dopasowaną do właściwości fazy membranowej. Z punktu widzenia procesu korzystna jest również jak najmniejsza krętość porów, co pozwala na maksymalne skrócenie drogi dyfuzji separowanego składnika [125].

Podstawowym parametrem określającym efektywność działania membrany jest jej selektywność (α_{ij}) w danym układzie. Idealną selektywność można zdefiniować jako stosunek przenikalności dwóch czystych gazów przez membranę, natomiast selektywność rzeczywista mierzona jest na podstawie przenikalności poszczególnych składników dla całej mieszaniny gazów.

W początkowych badaniach nad SLM jako fazę membranową najczęściej stosowano lotne związki organiczne (LZO). Ze względu jednak na ich toksyczność oraz wysokie koszty operacyjne związane z utratą rozpuszczalnika (spowodowaną dużą lotnością), zaczęto poszukiwać nowych mediów separacyjnych o niższej lotności, takich jak ciecze jonowe [126,127]. Jak wynika z literatury, SLM oparte o IL wykazują często zadowalające wyniki w selektywnej separacji dwutlenku węgla z fazy gazowej [128,129]. Niestety, ich wysoka lepkość, niska biodegradowalność, wysokie koszty syntezy oraz toksyczność znacząco ograniczają ich zastosowanie w przemyśle [130].

Pierwsze doniesienie o próbie wykorzystania cieczy głęboko eutektycznych w unieruchomionych membranach ciekłych pojawiło się w 2018 roku [39]. Amira i in. przygotowali wówczas SLM na bazie poli(fluorku winylidenu)-ko-poli(tetrafluoroetylenu) (PVDF-co-PTFE) oraz mieszaniny ChCl/EG (1:3), pokrytą z dwóch stron poli(dimetylosiloksanem) i zastosowali ją do separacji CO_2. W porównaniu z membraną niezawierającą DES, SLM oparte o mieszaniny eutektyczne wykazywały wyższą przenikalność ditlenku węgla ($25{,}5 \cdot 10^3$ GPU w porównaniu z $12 \cdot 10^3$ GPU) oraz niższą przenikalność azotu ($12{,}7 \cdot 10^3$ GPU w porównaniu z $17 \cdot 10^3$ GPU), co w konsekwencji przełożyło się na poprawę selektywności (2,7 krotnie).

Kolejne badania nad zastosowaniem cieczy głęboko eutektycznych w unieruchomionych membranach ciekłych do separacji ditlenku węgla dotyczyły DES opartych na ChCl lub betainie jako HBA i kwasach karboksylowych [131,132], moczniku, glikolu etylenowym, glicerolu [133–135], monoetanoloaminie, dietanoloaminie, trietanoloaminie [136] lub poliakrylamidzie [137] jako HBD. Badania te udowodniły, że skuteczność SLM opartych na DES może być konkurencyjna w stosunku do membran opartych na imidazolowych cieczach jonowych [138]. Warto jednak pokreślić, że takich prac jest niewiele i w większości dotyczą one SLM zawierających poli(fluorek winylidenu) jako nośnik polimerowy. Saeed i in. badając SLM, które zawierały DES złożone z betainy (Bet) oraz ChCl jako HBA oraz kwasów jabłkowego (MA), kwasu winowego (TA) oraz kwasu szczawiowego (OxaA) jako HBD odnotowali, że niezależnie od rodzaju soli przenikalność CO_2 spada w zależności od użytego kwasu w DES w kolejności OxaA > MA > TA [132,138]. Najniższą rozpuszczalność, najniższy współczynnik dyfuzji, a co za tym idzie najniższą przenikalność CO_2 w SLM opartych na Bet/TA autorzy tłumaczyli bardziej stabilną siecią wiązań wodorowych, tworzoną przez większą liczbę grup –OH obecnych w cząsteczce TA w stosunku do MA i OxaA [132,138]. W swojej pracy, autorzy pokazali wpływ temperatury na efektywność separacji. Podkreślili, że ponieważ temperatura ma silny wpływ zarówno na opory dyfuzji w membranie ciekłej, wynikające z lepkości cieczy, jak i na rozpuszczalność gazów, kluczowe jest określenie optimum dla danego układu. Dla wszystkich układów obserwowali wzrost przenikalności oraz spadek rozpuszczalności CO_2 na skutek wzrostu temperatury. Efekt ten szczególnie był widoczny przypadku dla układu ChCl/TA DES-SLM, dla którego zmiana temperatury z 298 K do 338 K spowodowała wzrost wartości przenikalności z 30 do 47 barrerów. Podobną zależność temperaturową przenikalności i selektywności obserwowali Ishaq i in. dla SLM opartej na DES złożonym z chlorku choliny i mocznika oraz Shamair i in. dla SLM opartych o IL [134,139].

Craveiro i in. opisali SLM złożone z nośnika politetrafluoroetylenowego (PTFE) i DES opartych na ChCl i kwasie szczawiowym, moczniku, glikolu etylenowym lub glicerolu. Spośród zbadanych układów, najwyższą przenikalność CO_2 uzyskali dla ChCl/U, ale najwyższą selektywność CO_2/N_2 dla DES złożonego z chlorku choliny i glicerolu [133].

Jak dotąd, powstały tylko dwie prace dotyczące wpływu stosunku molowego HBA:HBD oraz zawartości wody w DES na efektywność SLM. Są to prace Ishaq i in. oraz Castro i in. [131,134]. W pierwszej z nich, dotyczącej SLM opartych na ChCl/U, autorzy wykazali, że wraz ze wzrostem zawartości ChCl w DES wzrasta przenikalność CO_2, podczas gdy przenikalność N_2 jest praktycznie stała [134]. W drugiej zaś, Castro i in. przygotowali membrany na bazie PTFE wypełnione DES złożonym z chlorku choliny i kwasu lewulinowego (1:2) i udowodnili, że wraz ze wzrostem zawartości wody obniża się zarówno przenikalność, jak i selektywność CO_2/N_2 [131].

3. Cel i zakres pracy

Dokonany przez mnie przegląd literatury pokazał, że większość badań nad cieczami głęboko eutektycznymi jako potencjalnymi absorbentami CO_2 dotyczyła DES, które oddziałują fizycznie z ditlenkiem węgla. Znacznie mniej uwagi poświęcono cieczom głęboko eutektycznym absorbującym CO_2 chemicznie. Dotychczasowe badania ograniczały się do kilku DES opartych aminoalkoholach, tj. na monoetanoloaminie [48,140,141], dietanoloaminie [108,114,142], trietanoloaminie [114] i metylodietanoloamnie [108,140,141].

Podjęto też tylko kilka nowatorskich prób użycia cieczy głęboko eutektycznych jako fazy membranowej w unieruchomionych membranach ciekłych (SLM) w celu oceny ich przydatności do usuwania ditlenku węgla ze strumieni gazowych powstałych w procesach przemysłowych. W swoich pracach autorzy podkreślali, że zastosowanie SLM na bazie cieczy głęboko eutektycznych, które absorbują ditlenek węgla w sposób fizyczny, ma przewagę nad DES na bazie amin, w szczególności ze względu na niższy koszt procesu [131,132,134].

Generalnie jednak, powstałe dotychczas prace dotyczące cieczy głęboko eutektycznych jako potencjalnych mediów do usuwania ditlenku węgla miały charakter typowo aplikacyjny. Wyraźnie brakowało kompleksowych badań, które pozwoliłyby na powiązanie rozpuszczalności CO_2 z właściwościami fizycznymi, budową i strukturą cieczy głęboko eutektycznych, w szczególności tych opartych na aminoalkoholach.

Przegląd literatury pozwolił na wytypowanie najważniejszych czynników, które należałoby w tym kontekście rozważyć. Należą do nich:

a) obecność i położenie grup aminowych, karboksylowych i hydroksylowych w składnikach DES,
b) symetria i długość łańcuchów alkilowych w HBA i HBD,
c) siła oddziaływań wodorowych pomiędzy składnikami DES,
d) wpływ zawartości wody.

Biorąc pod uwagę te czynniki do badań wybrałem nowe ciecze głęboko eutektyczne na bazie aminoalkoholi (tj. 3-aminopropan-1-olu, 2-(metyloamino)etanolu i 2-(butyloamino)etanolu) oraz mieszaniny zawierające glikole propylenowe (propano-1,2-diol i propano1,3-diol). W przypadku DES opartych na aminoalkoholach jako akceptor wiązania wodorowego wykorzystałem bromek tetrabutyloamoniowy, chlorek tetrabutyloamoniowy i chlorek tetraetyloamoniowy. W DES zawierających glikole propylenowe jako soli użyłem chlorku tetrabutyloamoniowego, chlorku choliny oraz chlorku acetylocholiny.

Taki dobór składników DES pozwolił mi na realizację następujących celów badawczych:

1) dokonanie analizy wpływu długości łańcuchów alkilowych w cząsteczkach HBA i HBD, rodzaju anionu soli oraz rzędowości aminy na oddziaływania w mieszaninach opartych na aminoalkoholach;
2) powiązanie struktury DES opartych na aminoalkoholach z ich właściwościami fizycznymi oraz zdolnością do absorpcji ditlenku węgla;

3) określenie wpływu wody na strukturę cieczy głęboko eutektycznych zawierających aminoalkohole oraz bromek tetrabutyloamoniowy i ich zdolności sorpcyjne w stosunku do CO_2;
4) ocenę wpływu położenia grupy hydroksylowej HBD oraz obecności grupy estrowej i symetrii HBA na efektywność separacji ditlenku węgla z użyciem SLM opartych o DES zawierających glikole propylenowe.

4. Omówienie wyników badań

4.1. Charakterystyka badanych cieczy głęboko eutektycznych

4.1.1. Otrzymywanie i charakterystyka termiczna

Zestawienie cieczy głęboko eutektycznych użytych w niniejszej pracy znajduje się w Tabeli 2 oraz Tabeli 3. Skład DES dobrałem tak, aby dla rozpuszczalników opartych na tym samym aminoalkoholu najniższy stosunek HBA do HBD odpowiadał najmniejszej zawartości AP, MAE lub BAE, dla którego otrzymałem stabilną ciecz w temperaturze pokojowej oraz żeby umożliwić porównywanie wpływu rodzaju składników DES na właściwości fizyczne i separacyjne ditlenku węgla. W przypadku cieczy głęboko eutektycznych opartych na izomerach propanodiolu badania przeprowadziłem głównie dla DES o składzie 1:3. Tylko w przypadku DES zawierających chlorek choliny rozszerzyłem skład DES do stosunku 1:4. Miało to na celu, podobnie jak w przypadku DES opartych o aminoalkohole, określenie wpływu stosunku molowego HBA do HBD na właściwości separacyjne ditlenku węgla ze strumieni gazowych o jego stosunkowo niskim ciśnieniu cząstkowym.

Sposób sporządzania cieczy głęboko eutektycznych oraz metodykę pomiarów właściwości fizycznych i ich wodnych roztworów szczegółowo opisałem w publikacjach **A2**-**A7.** Specyfikacja cieczy głęboko eutektycznych opartych o propano-1,3-diol znajduje się w Tabeli B1. Powyższe prace nie obejmują metodyki obliczeń metodą dynamiki molekularnej, które wykonałem w celu określenia struktury DES zawierających sole TBAB, TEAC, TBAC oraz aminoalkohole o stosunkach molowych HBA do HBD 1:4, 1:6, 1:8 dla cieczy zawierających AP oraz 1:6, 1:8, 1:10 dla cieczy zawierających MAE lub BAE. Dodatkowo, dla wodnych roztworów DES TBAB/AP 1:6, TBAB/MAE 1:6 i TBAB/BAE 1:6 przeprowadziłem symulacje w zakresie ułamka molowego H_2O od 0,1 do 0,9. Obliczenia wykonałem przy użyciu pakietu Gromacs (wersja 2018.5) [143]. Zastosowałem giętkie pole siłowe ogólnego przeznaczenia OPLS/AA, które jest skuteczne w odtwarzaniu właściwości termodynamicznych i strukturalnych cieczy organicznych i ich mieszanin z wodą [72,73]. Pudło symulacyjne zawierało łącznie 945 cząsteczek dla układów DES i 1000 cząsteczek dla układów DES + woda, początkowo upakowanych zgodnie z gęstością eksperymentalną. Liczba cząsteczek znajdujących się w pudle symulacyjnym dla poszczególnych układów została podana w Tabeli 4. Oddziaływania elektrostatyczne wyznaczyłem za pomocą metody sum Ewalda z promieniem odcięcia 1,2 nm i gęstości siatki 0,1 nm [144]. Oddziaływania van der Waals'a były w sposób ciągły skalowane do zera pomiędzy 1,0 a 1,2 nm.

Tabela 2 Zestawienie użytych w pracy cieczy głęboko eutektycznych absorbujących CO_2 w sposób chemiczny.

HBA / HBD	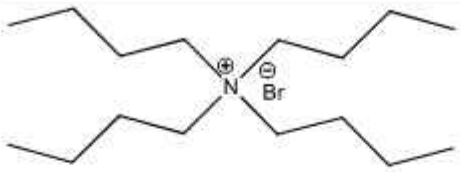 bromek tetrabutyloamoniowy (TBAB)	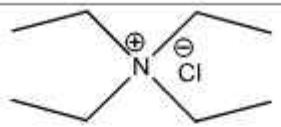 chlorek tetraetyloamoniowy (TEAC)	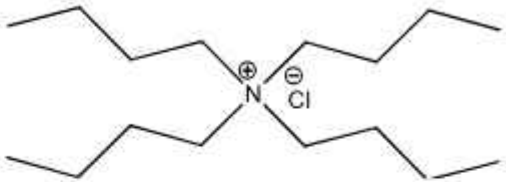 chlorek tetrabutyloamoniowy (TBAC)
 3-aminopropan-1-ol (AP)	DES1 (1:4)	DES4 (1:4)	DES7 (1:4)
	DES2 (1:6)	DES5 (1:6)	DES8 (1:6)
	DES3 (1:8)	DES6 (1:8)	DES9 (1:8)
 2-(metyloamino)etanol (MAE)	DES10 (1:6)	DES13 (1:6)	DES16 (1:6)
	DES11 (1:8)	DES14 (1:8)	DES17 (1:8)
	DES12 (1:10)	DES15 (1:10)	DES18 (1:10)
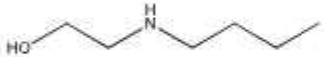 2-(butyloamino)etanol (BAE)	DES19 (1:6)	DES22 (1:6)	DES25 (1:6)
	DES20 (1:8)	DES23 (1:8)	DES26 (1:8)
	DES21 (1:10)	DES24 (1:10)	DES27 (1:10)

Tabela 3 Zestawienie użytych w pracy cieczy głęboko eutektycznych absorbujących CO_2 w sposób fizyczny.

HBA / HBD	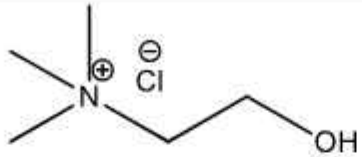 chlorek choliny (ChCl)	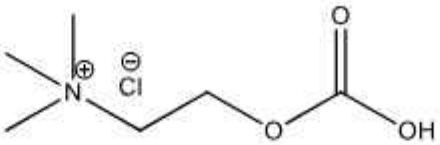 chlorek acetylocholiny (AChCl)	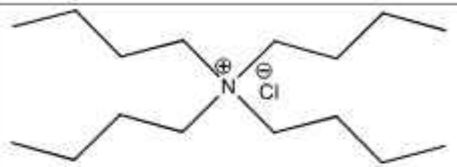 chlorek tetrabutyloammoniowy (TBAC)
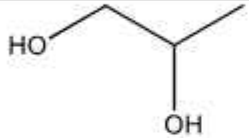 propano-1,2-diol	DES28 (1:3) DES29 (1:4)	DES30 (1:3)	DES31 (1:3)
 propano-1,3-diol	DES32 (1:3) DES33 (1:4)	DES34 (1:3)	DES35 (1:3)

Po wstępnej minimalizacji energii, każdy układ był równoważony przez 5 ns w układzie izotermiczno-izobarycznym (NPT), po czym do trajektorii produkcyjnej wykorzystano kolejny cykl NPT o długości 50 ns, podczas którego zbierano dane do analizy w odstępie czasowym 0,1 ps. Zastosowany krok czasowy wynosił 0,5 fs. Temperaturę utrzymywano na poziomie 298 K za pomocą kanonicznego termostatu przeskalowującego prędkość [145], podczas gdy ciśnienie stabilizowano na poziomie 1 bara za pomocą barostatu Parrinello-Rahmana [146]. Stałe czasowe termostatu i barostatu ustalono na odpowiednio 1 ps i 5 ps. Analizę wyników przeprowadziłem przy użyciu pakietu narzędzi Gromacs.

Tabela 4 Liczba cząsteczek w pudle symulacyjnym dla poszczególnych układów badanych przy pomocy MD.

	TBA^+/TEA^+	Br^-/Cl^-	AP/MAE/BAE	H_2O
DES 1:4	189	189	756	-
DES 1:6	135	135	810	-
DES 1:8	105	105	840	-
DES 1:10	86	86	860	-
wodne roztwory DES oparte o TBAB i AP/MAE/BAE w stosunku molowym 1:6				
x_{H2O}=0,1	129	129	771	100
x_{H2O}=0,2	114	114	686	200
x_{H2O}=0,3	100	100	600	300
x_{H2O}=0,4	86	86	514	400
x_{H2O}=0,5	71	71	429	500
x_{H2O}=0,6	57	57	343	600
x_{H2O}=0,7	43	43	257	700
x_{H2O}=0,8	29	29	171	800
x_{H2O}=0,9	14	14	86	900

Preparatyki DES dokonałem metodą podgrzewania, a otrzymanie mieszaniny eutektycznej potwierdziłem za pomocą spektroskopii fourierowskiej w podczerwieni (FTIR). Otrzymane widma FTIR dla DES zawierających aminoalkohole oraz ich czystych składników zostały zaprezentowane i szczegółowo omówione w pracach **A2**-**A4**. Wyraźnie wskazują one na występowanie wiązań wodorowych pomiędzy składnikami cieczy głęboko eutektycznych, przy jednoczesnym braku reakcji chemicznych. Nie zaobserwowałem żadnych nowych pasm w stosunku do czystych składników, a pasma drgań rozciągających v(OH)/v(NH) aminoalkoholi przesunęły się w kierunku wyższych liczb falowych. Przykładowo, dla DES zawierających MAE w stosunku molowym HBA do HBD wynoszącym 1:10, pasmo drgania v(OH)/v(NH) zmieniło swoje położenie z 3309 cm^{-1} dla aminoalkoholu na 3378, 3392 i 3404 cm^{-1} dla TEAC/MAE, TBAB/MAE i TBAC/MAE. Odpowiada to wzrostowi energii, wynikającemu z tworzenia nowych wiązań wodorowych między cząsteczkami aminoalkoholu i halogenku tetraalkiloamoniowego, a tym samym potwierdza fakt powstania DES. Analogiczne przesunięcie pasma drgań

rozciągających ν(OH) zaobserwowałem w przypadku cieczy głęboko eutektycznych opartych na glikolach propylenowych (**A7** oraz Rysunek B1).

W celu potwierdzenia, że badane mieszaniny to ciecze głęboko eutektyczne zmierzyłem ich temperatury topnienia i porównałem je z temperaturami topnienia obliczonymi przy założeniu doskonałości fazy ciekłej z równania van Laara-Hildebrandta (Równanie 1). Pomiarów dokonałem przy pomocy skaningowej kalorymetrii różnicowej (DSC), a uzyskane wartości temperatur topnienia mieszanin zostały zebrane w pracach **A2**-**A4**. Dla wszystkich układów temperatury topnienia są niższe niż dla czystych składników, a obniżenie eksperymentalnej temperatury topnienia w odniesieniu do teoretycznej uzyskane dla DES złożonych z TBAB i AP, mieszczące się w zakresie 2-12 K dowiodło, że kryterium stawiane DES przez Martinsa i in. [2] jest spełnione i mieszany te rzeczywiście mogą być uznane za ciecze głęboko eutektyczne. Tym niemniej należy zauważyć, że obniżenie temperatury topnienia badanych mieszanin w stosunku do temperatury topnienia odpowiednich aminoalkoholi jest stosunkowo niskie, co jest szczególnie widoczne w przypadku cieczy zawierających BAE. Dlatego też, biorąc pod uwagę kryterium stawiane przez część autorów mieszaninom głęboko eutektycznym, jako duże obniżenie temperatury topnienia mieszanin względem czystych składników, można by rozważyć opcję nazywania badanych cieczy niskotopliwymi mieszaninami eutektycznymi (LoMMS) zamiast cieczami głęboko eutektycznymi.

Generalnie, temperatura topnienia cieczy głęboko eutektycznych zależy od czynników, takich jak siła oddziaływań pomiędzy składnikami DES, zmiana entropii podczas procesu topnienia oraz energia sieci krystalicznej i rozmiar jonów akceptora wiązania wodorowego [147,148]. Analiza danych z publikacji **A2**-**A4** może prowadzić do wniosku, że temperatura topnienia badanych DES zależy głównie od użytego donora wiązania wodorowego i układa się w sposób zgodny z temperaturą topnienia aminoalkoholu: AP > BAE > MAE. Wpływ soli na ten parametr jest bardziej skomplikowany i jest uzależniony od użytego donora wiązania wodorowego.

Dla wszystkich badanych cieczy głęboko eutektycznych wykonałem pomiary za pomocą techniki analizy termograwimetrycznej (TGA) celem oznaczenia ich trwałości termicznej. Temperatura rozkładu jest bowiem podstawowym parametrem określającym zakres temperatur, w których dany rozpuszczalnik może być stosowany bez jego strat i degradacji. Szczegółowe wyniki analizy termograwimetrycznej dla cieczy opartych o MAE, BAE i propano-1,2-diolu przedstawiłem w publikacjach **A3, A4 i A7**. W przypadku cieczy opartych na AP i propano-1,3-diolu najważniejsze parametry, tj. temperatury rozkładu przy 10% ($T_{10\%}$) i 90% ($T_{90\%}$) utracie masy umieściłem w Tabeli B2 oraz Tabeli B3 załącznika B niniejszej rozprawy.

Analiza otrzymanych termogramów potwierdza doniesienia literaturowe, mówiące o tym, że temperatura rozkładu cieczy głęboko eutektycznych typu III-ego mieści się pomiędzy temperaturami rozkładu soli i donora wiązania wodorowego oraz maleje wraz ze wzrostem udziału HBD w cieczy. Efekt ten niewątpliwie jest spowodowany większą trwałością termiczną halogenków tetraalkiloamoniowych w porównaniu do trwałości typowych donorów wiązania wodorowego, czyli alkoholi, kwasów czy glikoli [149]. W przypadku badanych DES reguła ta jest również spełniona. Wyjątek stanowią mieszaniny złożone z TEAC i BAE, dla których stabilność

termiczna wzrasta wraz ze wzrostem zawartości BAE. Najbardziej prawdopodobnym wytłumaczeniem tego zjawiska wydaje się być fakt, że rozkład TEAC rozpoczyna się szybciej niż rozkład BAE, co uwidaczniają termogramy zamieszczone w publikacji **A3**.

Trwałość termiczna cieczy głęboko eutektycznych wzrasta wraz z mocą oddziaływań wodorowych pomiędzy składnikami DES oraz wraz z wydłużaniem się łańcucha alkilowego zarówno soli, jak i HBD [149]. Tłumaczy to największą trwałość DES opartych na AP, który może tworzyć największą ilość wiązań wodorowych w porównaniu z pozostałymi aminoalkoholami. Wpływ długości łańcucha alkilowego soli na temperaturę rozkładu uwidaczniają wyniki dla cieczy opartych o TBAC i TEAC oraz dla cieczy zawierających BAE oraz MAE. Na przykład, w przypadku DES zawierających AP, $T_{10\%}$ dla TBAC/AP 1:4 i TEAC/AP 1:4 wynosi odpowiednio 396,7 K oraz 381,0 K, a w przypadku cieczy zawierających TBAB, $T_{10\%}$ dla TBAB/MAE 1:6 i TBAB/BAE 1:6 wynosi odpowiednio 333,9 K oraz 372,0 K. Co więcej, otrzymane wyniki wskazują na przewagę wpływu mocy oddziaływań wodorowych nad wpływem długości łańcucha alkilowego składników cieczy na stabilność badanych DES. Wystarczy porównać $T_{10\%}$ dla TBAC/BAE 1:6 i TBAC/MAE 1:6 czy TEAC/MAE 1:6 i TBAB/MAE 1:6, które wynoszą odpowiednio 363,3 K i 376,8 K oraz 341,1 K i 333,9 K, a więc nie spełniają reguły: im dłuższy łańcuch alkilowy tym wyższa temperatura rozkładu. Wyższa trwałość termiczna TBAC/MAE 1:6 oraz TEAC/MAE 1:6 musi więc wynikać z silniejszych wiązań wodorowych pomiędzy składnikami tych DES w porównaniu z TBAC/BAE 1:6 czy TBAB/MAE 1:6.

Na trwałość termiczną DES wpływa również symetria łańcuchów alkilowych HBA oraz położenie grup funkcyjnych w HBD. Większa symetria łańcucha soli prowadzi do wyższej trwałości termicznej, co doskonale widać na przykładzie DES składających się z glikoli propylenowych, dla których najwyższe temperatury rozkładu zaobserwowałem w przypadku cieczy zawierających TBAC w stosunku do cieczy opartych o ChCl czy AChCl. Porównanie $T_{10\%}$ DES opartych na propano-1,2-diolu i propano-1,3-diolu wskazuje, że wyższą trwałość termiczną mają ciecze zawierające propano-1,3-diol, w którym grupy hydroksylowe są bardziej oddalone od siebie niż w przypadku propano-1,2-diolu.

Generalnie jednak należy podkreślić stosunkowo niską trwałość termiczną cieczy głęboko eutektycznych, szczególnie w porównaniu z cieczami jonowymi. Ogranicza to możliwość wykorzystania badanych DES tylko do procesów, które nie wymagają wysokich temperatur.

4.1.2. Właściwości fizyczne mieszanin eutektycznych – wartości eksperymentalne i ich modelowanie

Do podstawowych właściwości fizycznych cieczy głęboko eutektycznych, decydujących o procesie absorpcji i separacji ditlenku węgla, należą gęstość oraz lepkość. Dla wszystkich badanych cieczy wielkości te wyznaczyłem w szerokim zakresie temperatur. Ponadto, dla pełniejszej charakterystyki rozpuszczalników, w tych samych zakresach temperatur wyznaczyłem współczynnik załamania światła, który wraz z gęstością umożliwia obliczenie „objętości

swobodnej" w strukturze rozpuszczalnika, której wartość wiąże się z efektywnością absorpcji fizycznej ditlenku węgla.

Liczbowe wartości właściwości fizycznych DES badanych w ramach niniejszej pracy znajdują się w publikacjach **A2-A4 i A7** oraz w Tabeli B4.

Gęstość i współczynnik załamania światła zmniejszają się liniowo wraz ze wzrostem temperatury. Lepkość spada wykładniczo, co najlepiej opisuje równanie Vogela-Fulchera-Tammana (VFT).

Rysunek 5 przedstawia wpływ donora wiązania wodorowego na właściwości fizyczne DES opartych o TBAC, przy czym stosunek molowy akceptora do donora wiązania wodorowego w przypadku cieczy opartych o aminoalkohole wynosi 1 do 6, a w przypadku cieczy opartych o glikole propylenowe jest równy 1:3. Podobne zależności można zaobserwować dla badanych cieczy zawierających pozostałe sole.

Jak można zauważyć, niezależnie od użytego akceptora wiązania wodorowego, gęstości oraz współczynniki załamania światła DES opartych o aminoalkohole (o tym samym stosunku HBA do HBD) układają się w szereg AP > MAE > BAE. Najniższe wartości obserwowane dla DES opartych o BAE są spowodowane najdłuższymi łańcuchami alkilowymi aminoalkoholu, które prowadzą do zwiększenia „objętości swobodnej" cieczy. Z kolei wyższe wartości gęstości i współczynników załamania światła cieczy zawierających AP w porównaniu do cieczy opartych o MAE wynikają z różnych rzędowości aminoalkoholi. Pierwszorzędowy 3-aminopropan-1-ol tworzy większą ilość wiązań wodorowych niż drugorzędowy 2-(metyloamino)etanol o tej samej długości łańcucha alkilowego. Prowadzi to do bardziej uporządkowanej struktury DES opartych o AP i w konsekwencji do większej wartości gęstości i współczynnika załamania światła. Silniejsze wiązania wodorowe w DES opartych o 3-aminopropan-1-ol są również odpowiedzialne za największą lepkość tych cieczy. O najmniejszej lepkości DES zawierających MAE decyduje natomiast najmniejszy rozmiar tego aminoalkoholu, który powoduje najmniejsze opory przepływu cieczy.

Rozpatrując właściwości fizyczne DES opartych o glikole propylenowe wyraźnie widoczny jest wpływ położenia grup hydroksylowych w cząsteczkach HBD. Wyższe wartości gęstości, współczynnika załamania światła i lepkości DES zawierających liniowy propano-1,3-diol wynikają najprawdopodobniej z silniejszych wiązań wodorowych oraz większego upakowania, co prowadzi do bardziej zwartej struktury cieczy.

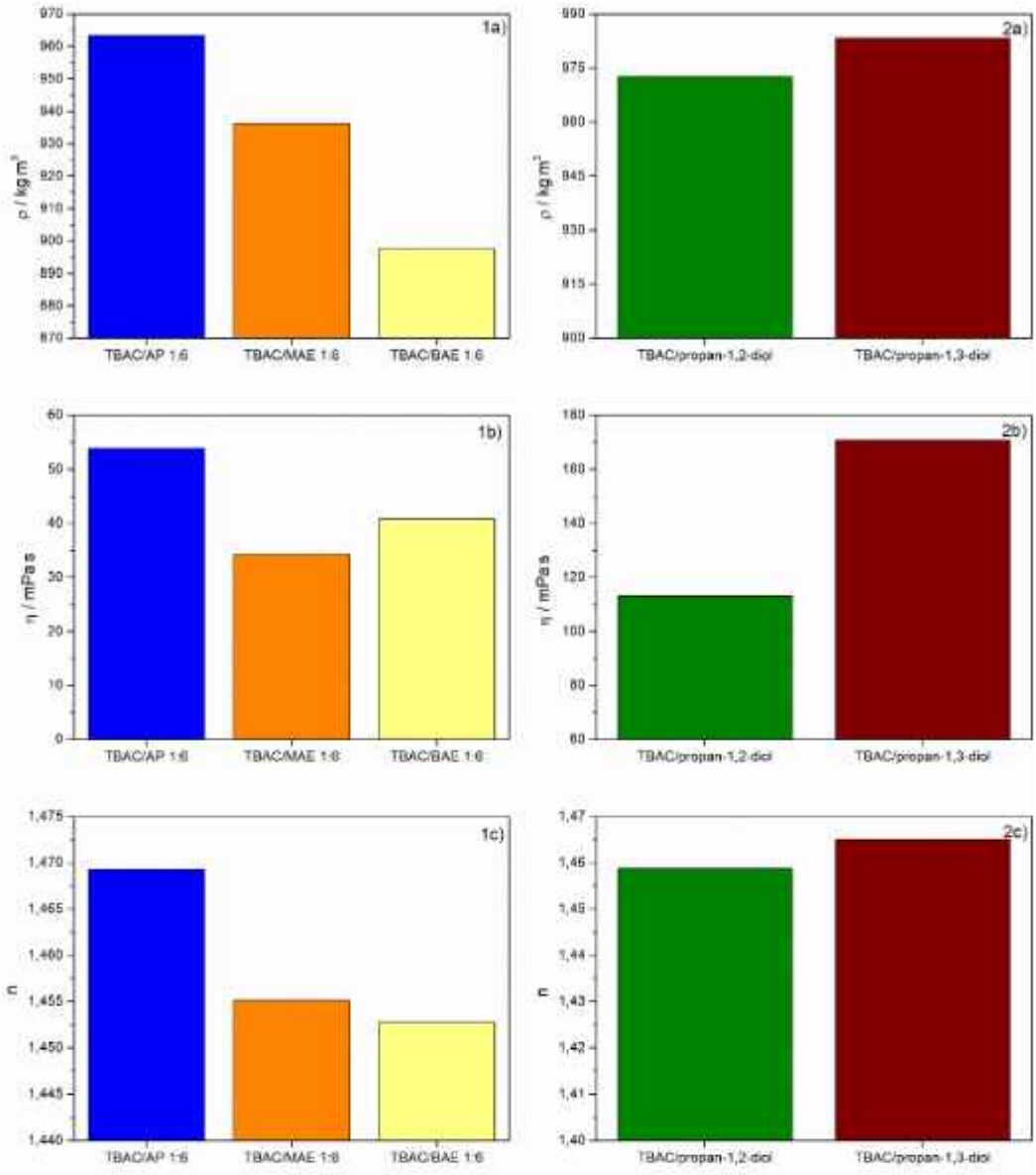

Rysunek 5 Właściwości fizyczne wybranych DES w temperaturze 298,15 K, pokazujące wpływ donora wiązania wodorowego na a) gęstość b) lepkość c) współczynnik załamania światła

Rysunek 6 1a-1c przedstawia wpływ akceptora wiązania wodorowego na właściwości fizyczne DES opartych o 3-aminopropan-1-ol, w których stosunek molowy HBA do HBD wynosi 1 do 6. Podobne zależności można zaobserwować dla cieczy zawierających inne aminoalkohole. Rysunek 6 2a-2b przedstawia natomiast wpływ akceptora wiązania wodorowego na właściwości fizyczne DES opartych o glikole propylenowe, w których stosunek molowy HBA do HBD wynosi 1 do 3. W przypadku DES opartych na aminoalkoholach, niezależnie od użytego HBD, najwyższe wartości gęstości, współczynnika załamania światła i lepkości mają DES zawierające TBAB. Jest to zgodne z literaturą, według której im większy i cięższy anion w HBA tym większa ρ, η i n DES. Wpływ długości łańcucha alkilowego soli jest widoczny, kiedy porówna się wyniki dla cieczy zawierających TBAC i TEAC. Krótsze łańcuchy alkilowe w TEAC umożliwiają większe upakowanie i przez to zmniejszenie „objętości swobodnej" DES. Prowadzi to do wyższych wartości gęstości i współczynnika załamania światła. Z kolei większy rozmiar TBAC powoduje,

że lepkość cieczy zawierających tę sól jest wyższa niż dla cieczy opartych o TEAC. W wynikach uzyskanych dla DES opartych o glikole propylenowe uwidacznia się nie tylko wpływ rozmiaru, ale również symetrii oraz obecności dodatkowych grup funkcyjnych w HBA. Zarówno dla cieczy opartych o propano-1,2-diol, jak i o propano-1,3-diol (o tym samym stosunku HBA do HBD), lepkości układają się w szereg ChCl < AcChCl < TBAC, co jest zgodne ze wzrastającym rozmiarem HBA. Gęstość i współczynnik załamania światła zmieniają się natomiast odpowiednio w kolejności ChCl < AcChCl > TBAC oraz ChCl > AcChCl < TBAC. Czynnikiem decydującym o gęstości badanych mieszanin wydaje się być więc "objętość swobodna", która rośnie z symetrią i długością łańcucha alkilowego w HBA. W przypadku współczynnika załamania światła, jego niższe wartości obserwowane dla DES zawierającego AcChCl w porównaniu do mieszanin zawierających ChCl czy TBAC mogą wynikać z innych czynników, takich jak specyficzne oddziaływania międzycząsteczkowe, a nie bezpośrednio z obecności grupy karboksylowej, która sama w sobie zwiększa polaryzowalność elektronową i prowadzi do większych wartości n.

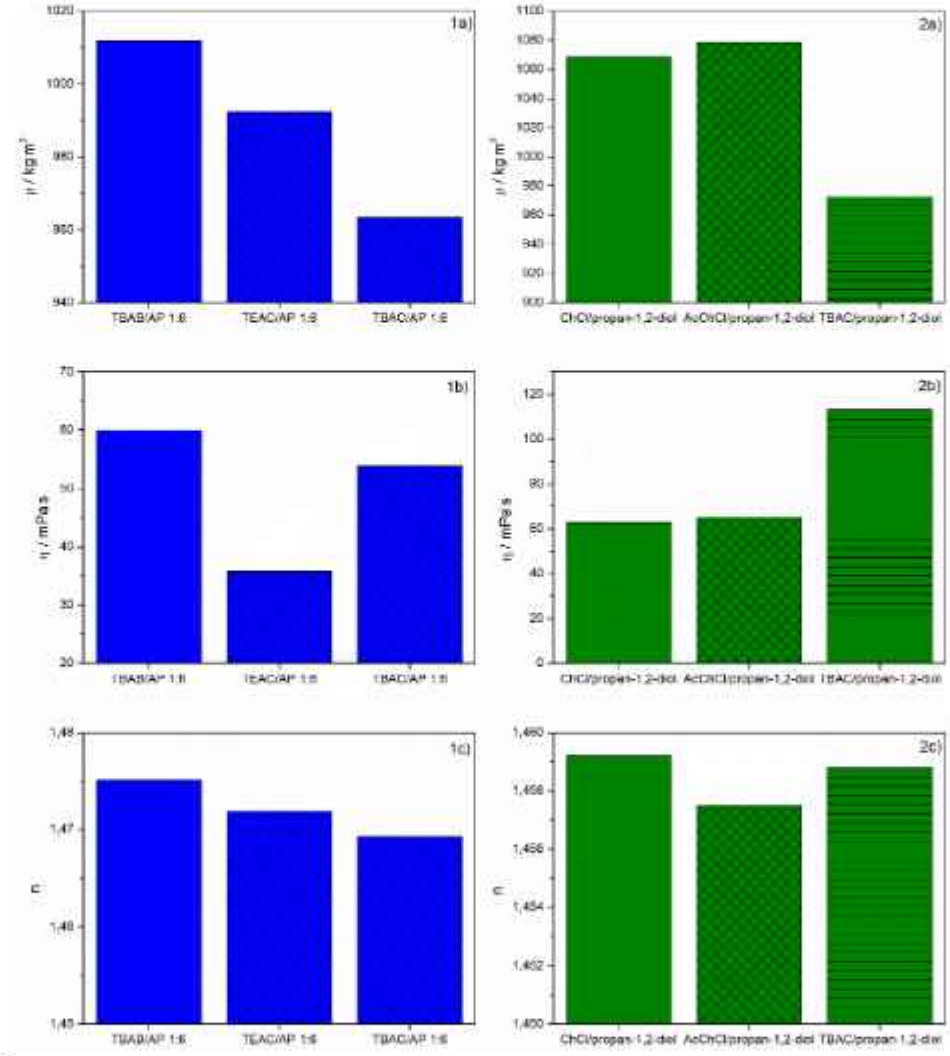

Rysunek 6 Właściwości fizyczne wybranych DES w temperaturze 298,15 K, pokazujące wpływ akceptora wiązania wodorowego na a) gęstość b) lepkość c) współczynnik załamania światła

Na właściwości fizyczne cieczy głęboko eutektycznych wpływa również stosunek molowy HBA do HBD. Ich wartości spadają wraz ze wzrostem zawartości donora wiązania wodorowego w DES. Spowodowane jest to niewątpliwie przez wzrost "objętości swobodnej" DES oraz spadek siły oddziaływań pomiędzy składnikami DES [45]. Wyjątkiem od tej reguły jest zależność gęstości cieczy głęboko eutektycznych zawierających TBAC od stosunku HBA:HBD (Rysunek 7). Gęstość DES złożonych z TBAC i BAE spada wraz ze wzrostem stosunku molowego HBA do HBD, w przypadku TBAC/AP wzrasta wraz ze wzrostem zawartości AP, a dla TBAC/MAE stosunek molowy HBA:HBD ma znikomy wpływ na gęstość. Najprawdopodobniej wynika to ze wzajemnej relacji gęstości DES z gęstością czystego aminoalkoholu. Gęstości TBAC/AP są niższe niż czystego AP, TBAC/MAE są podobne do czystego MAE, a dla TBAC/BAE są wyższe niż czystego BAE.

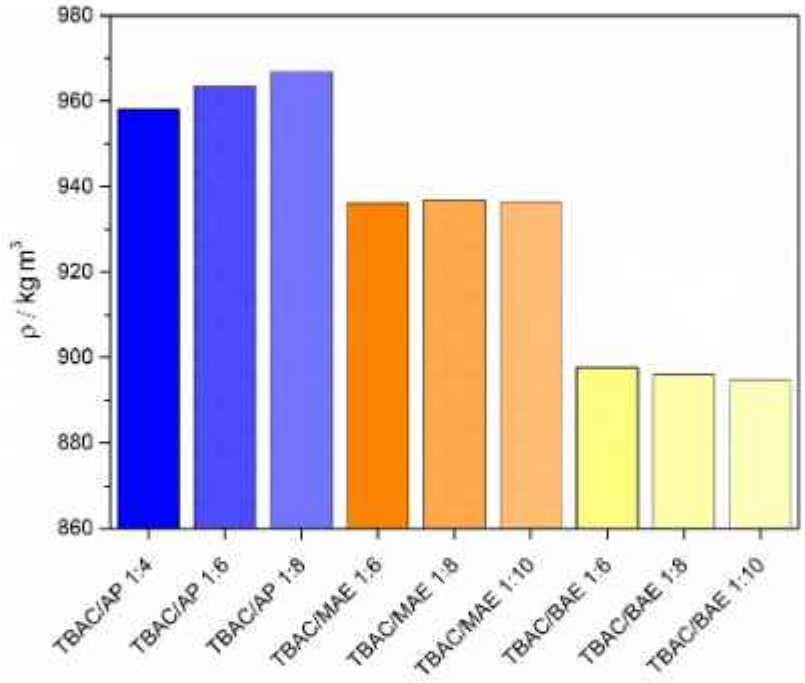

Rysunek 7 Wpływ stosunku molowego HBA/HBD na gęstość badanych DES zawierających TBAC w temperaturze 298,15 K.

Modelowanie właściwości fizycznych cieczy głęboko eutektycznych opartych na MAE i AP przedstawiłem w pracach **A2** i **A3.** Ponieważ w pracy **A2** znajduje się ocena tylko kilku modeli predykcyjnych, tj. Racketta i MCI (ang. - „*mass connectivity index*") dla gęstości oraz udziałów atomowych dla współczynnika załamania światła, wartości liczbowe średniego odchylenia względnego (%ARD - ang. – „*absolute relative deviation percent*") dla pozostałych modeli i DES opartych o BAE i glikoli propylenowych znajdują się w załączniku B (Tabele B5-B7) niniejszej pracy.

Do przewidywania wartości liczbowych gęstości DES użyłem 7 półempirycznych modeli dostępnych w literaturze: 1- metodę opartą na równaniu Racketta zmodyfikowanego przez Spencera i Dannera [62], 2- metodę opartą na równaniu Racketta zmodyfikowanego przez Mjalli [63], 3- metodę wykorzystującą właściwości krytyczne opracowana przez Haghbakhsha i in. [64], 4- metodę opartą na BGI (ang. - *„bonding-group interaction contribution"*) [69], 5- metodę opartą na MCI [70], 6- metodę udziałów grupowych GC (ang - *„group contribution"*) [66], 7- metodę udziałów atomowych AC (ang. - *„atomic contribution"*) [66]. Uśrednione wartości %ARD uwzgledniające wszystkie ciecze dla każdej metody zostały przedstawione na Rysunku 8.

Jak widać, metody 1, 2 i 5 charakteryzują się niskimi wartościami liczbowymi %ARD, a co za tym idzie satysfakcjonującą zdolnością przewidywania gęstości badanych DES. Niestety, dużą wadą tych modeli jest konieczność użycia eksperymentalnej wartości liczbowej gęstości w jednej temperaturze, więc nie spełniają one wszystkich wymagań stawianych metodom predykcyjnym.

Model oparty na BGI i metoda oparta na udziałach grupowych, tj. metody 4 i 6, odznaczają się stosunkowo niskimi %ARD. Dużą zaletą wymienionych modeli jest całkowita niezależność od danych eksperymentalnych.

Największe %ARD otrzymałem dla modelu wykorzystującego właściwości krytyczne i modelu opartego na udziałach atomowych, tj. metod 3 i 7. W przypadku tych modeli, dla większości badanych cieczy, wartości liczbowe %ARD przekraczają 10%, co wyklucza właściwie te metody do predykcji gęstości.

Analizując uzyskane wyniki (prace **A2** i **A3**), można stwierdzić, że większość wyżej wymienionych modeli dobrze przewiduje zmiany gęstości wraz ze wzrostem stosunku molowego HBA:HBD. Wyjątek stanowią modele oparte na udziałach grupowych i atomowych, zaproponowane przez Haghbakhsha i in.. Przy użyciu model BGI udało się wychwycić różnice w nietypowej zmianie gęstości wraz ze wzrostem zawartości HBD w DES opartych o TBAC (opisywanej powyżej).

Do przewidywania wartości liczbowych lepkości DES użyłem tylko jednego modelu dostępnego w literaturze. Jest to model oparty na właściwościach krytycznych zaproponowany przez Bakhtyariego i in. [61]. Dla wszystkich badanych układów uzyskałem wartości %ARD powyżej 5%, a ponieważ model wymaga znajomości danych eksperymentalnych lepkości w jednej temperaturze, wydaje się on być mało przydatny przy przewidywaniu lepkości cieczy głęboko eutektycznych.

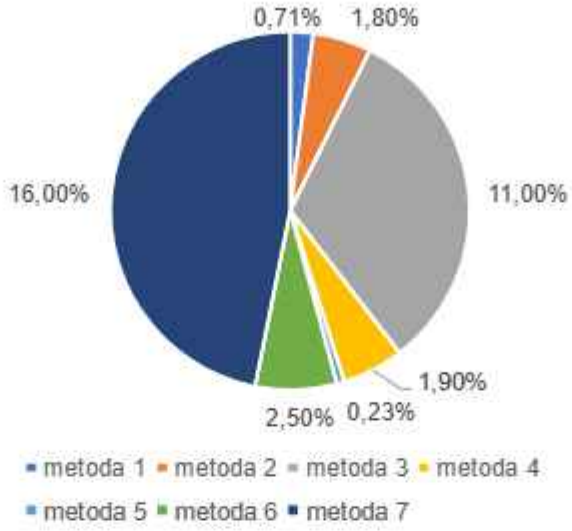

Rysunek 8 Uśrednione %ARD dla modeli półempirycznych zastosowanych do przewidywania gęstości DES; metoda 1 oparta na równaniu Racketta zmodyfikowanego przez Spencera i Dannera [62], metoda 2 oparta na równaniu Racketta zmodyfikowanego przez Mjalli [63], metoda 3 oparta na właściwościach krytycznych opracowana przez Haghbakhsh i in. [64], metoda 4 oparta na BGI [69], metoda 5 oparta na MCI [70], metoda 6 oparta na GC opracowana przez Haghbakhsha i in. [66], metoda 7 oparta na AC opracowana przez Haghbakhsha i in. [66].

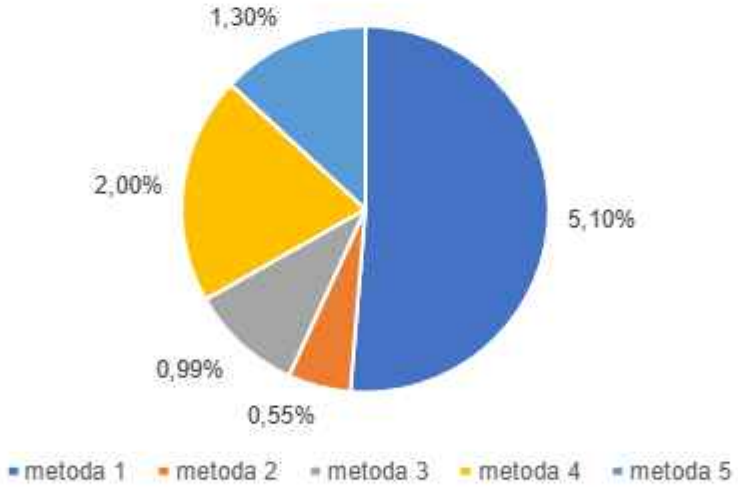

Rysunek 9 Uśrednione %ARD dla modeli półempirycznych zastosowanych do przewidywania współczynnika załamania światła DES; metoda 1 oparta na refrakcji molowej opracowana przez Shabaza i in. [67], metoda 2 oparta na właściwościach krytycznych opracowana przez Taherzadeha i in. [60], metoda 3 oparta na GC opracowana przez Khajeha i in. [68], metoda 4 oparta na GC opracowana przez Haghbakhsha i in. [66], metoda 5 oparta na AC opracowana przez Haghbakhsh i in.[66].

Do przewidywania wartości liczbowych współczynnika załamania światła DES użyłem 5 modeli półempirycznych: 1- metodę opartą na refrakcji molowej opracowaną przez Shabaza i in. [67], 2- metodę opartą na właściwościach krytycznych opracowaną przez Taherzadeha i in. [60], 3- metodę opartą na GC opracowaną przez Khajeh'a i in. [68], 4- metodę opartą na GC opracowaną przez Haghbakhsha i in. [66], 5- metodę opartą na AC opracowaną przez Haghbakhsha i in. [66]. Rysunek 9 przedstawia uśrednione wartości %ARD uwzgledniające wszystkie badane ciecze. Jak widać, największym %ARD charakteryzuje się metoda oparta na refrakcji molowej. Jednocześnie należy zwrócić uwagę, że dla DES opartych o AP i MAE maksymalne %ARD są zdecydowanie mniejsze, odpowiednio 2,3% i 0,29% (Tabela B7). Niemniej wadą tego modelu jest konieczność użycia danych eksperymentalnych dotyczących gęstości. Metody 2, 3 i 5 charakteryzują się niskimi %ARD dla wszystkich badanych DES, a przy tym nie wymagają żadnych danych eksperymentalnych. Niestety, model zaproponowany przez Khajeha nie umożliwia zastosowania go do przewidywania współczynnika załamania światła dla DES zawierających anion bromkowy w swojej strukturze. Metoda oparta na udziałach grupowych opracowana przez Haghbakhsh i in. odznacza się stosunkowo wysokimi wartościami %ARD, przez co jest mniej użyteczna przy przewidywaniu wartości współczynnika załamania światła dla badanych DES.

Podsumowując ocenę użyteczności opisanych modeli do predykcji gęstości, współczynnika załamania światła i lepkości badanych DES należy podkreślić fakt, że podczas tworzenia tych modeli praktycznie nie brano pod uwagę właściwości fizycznych cieczy głęboko eutektycznych opartych o aminoalkohole. Spowodowane było to w głównej mierze brakiem dostępnych danych w literaturze. Dlatego też, niezmiernie istotnym jest poszerzanie baz danych oraz tworzenie nowych modeli predykcyjnych dedykowanych DES opartym o aminoalkohole lub najlepiej modeli o charakterze jak najbardziej ogólnym, obejmującym cały przekrój cieczy eutektycznych. Warto podkreślić, że niższe %ARD uzyskane dla DES zawierających glikole propylenowe wynikają w dużej mierze z tworzenia opisywanych modeli przy pomocy cieczy głęboko eutektycznych o podobnej budowie.

4.2. Struktura cieczy głęboko eutektycznych i jej wpływ na właściwości fizyczne DES

Znajomość struktury cieczy głęboko eutektycznych, wynikającej w głównej mierze z obecności wiązań wodorowych pomiędzy składnikami DES, jest istotna w ocenie wpływu stosunku molowego HBA do HBD, jak i budowy samych składników, na właściwości fizykochemiczne cieczy głęboko eutektycznych oraz ich zdolności absorpcyjne względem ditlenku węgla. Dlatego też, w ramach niniejszej pracy, przeprowadziłem obliczenia metodą dynamiki molekularnej i uzyskałem funkcje rozkładu radialnego RDF dla wszystkich badanych DES opartych na aminoalkoholach. Rysunek 10 przedstawia funkcje rozkładu radialnego dla DES zawierających TBAB w różnych stosunkach molowych soli do aminoalkoholu, przy czym Rysunek 10-1a,2a,3a ilustruje wpływ stosunku molowego HBA do HBD na oddziaływanie Br^-···H-N, a Rysunek 10-1b,2b,3b prezentuje wpływ stosunku molowego HBA do HBD na oddziaływanie Br^-···H-O. Na wykresach RDF DES opartych na AP, ze względu na obecność grupy $-NH_2$ w cząsteczce tego aminoalkoholu, występują dwa piki obrazujące oddziaływanie Br^-···H-N w pierwszej sferze koordynacyjnej jonu bromkowego, podczas gdy w przypadku DES opartych na MAE lub BAE występuje tylko jeden pik odpowiadający temu oddziaływaniu, którego maksimum przypada na 0,244 nm.

Dla DES opartych o TBAC i TEAC uzyskałem podobne zależności, jak dla cieczy zawierających TBAB, i są one przedstawione na Rysunkach B2 i B3. Szczegółowe dane liczbowe dotyczące wszystkich układów, to jest pików obrazujących oddziaływania anionu soli danego DES z jej kationem oraz z grupą aminową lub hydroksylową aminoalkoholu, a także liczby koordynacyjne jonu halogenkowego (biorąc pod uwagę pierwszą sferę koordynacyjną) zebrałem w Tabeli B8.

Jak łatwo zauważyć, dla wszystkich rozpatrywanych cieczy, intensywność pików odpowiadających oddziaływaniu X^-···H-N w pierwszej sferze koordynacyjnej jonu halogenkowego maleje wraz ze wzrostem zawartości HBD w DES (Rysunki 10-1a,2a,3a, B2-1a,2a,3a oraz B3-1a,2a,3a), a liczba koordynacyjna X^- wzrasta (Tabela B8). Wraz ze wzrostem zawartości aminoalkoholu powstaje więc większa ilość wiązań wodorowych, ale są one słabsze.

Analiza wykresów RDF obrazujących oddziaływania X^-···H-O prowadzi do analogicznych wniosków (Rysunki 10-1b,2b,3bB2-1b,2b,3b oraz B3-1b,2b,3b). Wyjątek stanowią DES zawierające BAE, dla których intensywność piku odpowiadającego za oddziaływania X^-···H-O w pierwszej sferze koordynacyjnej jonu halogenkowego jest największa przy stosunku molowym HBA do HBD wynoszącym 1:10. Generalnie jednak wydaje się być uzasadnionym stwierdzenie, że wraz ze wzrostem stosunku molowego soli do aminoalkoholu oddziaływania wodorowe pomiędzy HBA i HBD stają się mniej preferowane. Potwierdza to również analiza piku odpowiadającego oddziaływaniu X^-···H-O, który obrazuje dalsze otoczenie jonu halogenkowego (drugi pik w okolicy 0,46 nm na Rysunkach 10-1b,2b,3bB2-1b,2b,3b oraz B3-1b,2b,3b). Intensywność tego piku wzrasta wraz ze wzrostem zawartości AP lub MAE w DES, co przy jednoczesnym spadku intensywności piku odpowiadającego za pierwszą sferę koordynacyjną może świadczyć o przemieszczaniu się cząsteczek aminoalkoholu z pierwszej do drugiej sfery

koordynacyjnej i w rezultacie o osłabieniu siły wiązań wodorowych pomiędzy solą a aminoalkoholem. Dla DES opartych o BAE takiego efektu się nie obserwuje. Osłabienie oddziaływań wodorowych pomiędzy składnikami DES wraz ze wzrostem ilości HBD w DES obserwowano wcześniej dla TBAB/EG, gdzie dodanie glikolu etylenowego prowadziło do zmniejszenia piku $Br^{-}\cdots EG$ na wykresie RDF [150]. Autorzy publikacji powiązali to z większą liczbą oddziaływań pomiędzy cząsteczkami EG, które są konkurencyjne w stosunku do oddziaływań między anionem bromkowym a glikolem etylenowym.

Na tworzenie silniejszych wiązań wodorowych pomiędzy cząsteczkami aminoalkoholu oraz słabszych pomiędzy cząsteczkami HBA i HBD na skutek wzrostu zawartości aminoalkoholu w mieszaninie wskazuje również wzrost intensywności piku $N^{+}\cdots X^{-}$ (Rysunki 10-1c,2c,3c, B2-1c,2c,3c oraz B3-1c,2c,3c) na wykresie RDF. Spadek liczby koordynacyjnej jonu halogenkowego w soli (uzyskany poprzez scałkowanie powierzchni piku $N^{+}\cdots X^{-}$) obserwowany przy wzroście zawartości aminoalkoholu w DES może być powiązany ze zmniejszeniem stężenia soli oraz słabszą tendencją do tworzenia par jonowych przy większym rozcieńczeniu.

Rysunek 11 przedstawia wpływ akceptora wiązania donorowego na strukturę DES opartych na badanych aminoalkoholach o jednakowym stosunku molowym HBA do HBD, wynoszącym 1 do 6. Porównując RDF mieszanin zawierających TBAC (zielona linia) oraz mieszanin opartych na TBAB (czerwona linia), zarówno prezentujące oddziaływanie anionu soli z grupą -NH (Rysunek 11-1) jak i grupą -OH (Rysunek 11-2) aminoalkoholu, piki o większej intensywności obserwuje się dla DES opartych o TBAC. Dzieje się tak niezależnie od zastosowanego aminoalkoholu, ponadto maksima tych pików znajdują się przy mniejszych odległościach. Można więc stwierdzić, że każdy z badanych aminoalkoholi tworzy silniejsze wiązania wodorowe z TBAC niż z TBAB, ale generalnie jest ich mniej, na co wskazują otrzymane wartości liczb koordynacyjnych przedstawione w Tabeli B8. Podobne rezultaty uzyskali Migliorati i D'Angelo dla DES złożonych z mocznika i chlorku choliny oraz mocznika i fluorku choliny [151]. W swojej pracy autorzy większe intensywności pików odpowiadających oddziaływaniu $F^{-}\cdots H\text{-}N$ uzasadniali niższą masą molową anionu fluorkowego w porównaniu do masy anionu chlorkowego. Analizując uzyskane wyniki, warto jednak zauważyć, że obserwowana różnica w sile oddziaływań tworzonych przez badane aminoalkohole oraz TBAB czy TBAC jest stosunkowo niewielka, szczególnie w przypadku cieczy opartych o AP i BAE. Fakt ten tłumaczy eksperymentalne wartości liczbowe lepkości DES, które są nieznacznie większe dla cieczy zawierających TBAB. Biorąc pod uwagę tylko siłę oddziaływań wodorowych pomiędzy HBA i HBD, lepkości powinny być większe w przypadku cieczy zawierających TBAC. Ponieważ tak się nie dzieje, należy uznać, że w przypadku badanych DES, które charakteryzują się niewielką różnicą oddziaływań pomiędzy HBA i HBD, to masa molowa i promień jonowy anionu mają decydujący wpływ na lepkość DES. Masa molowa anionu soli wchodzącej w skład DES decyduje również o gęstości i współczynniku załamania światła cieczy. Wniosek ten potwierdza analiza RDF opisujących oddziaływanie pomiędzy kationem a anionem soli, zilustrowane na Rysunku 11-3.

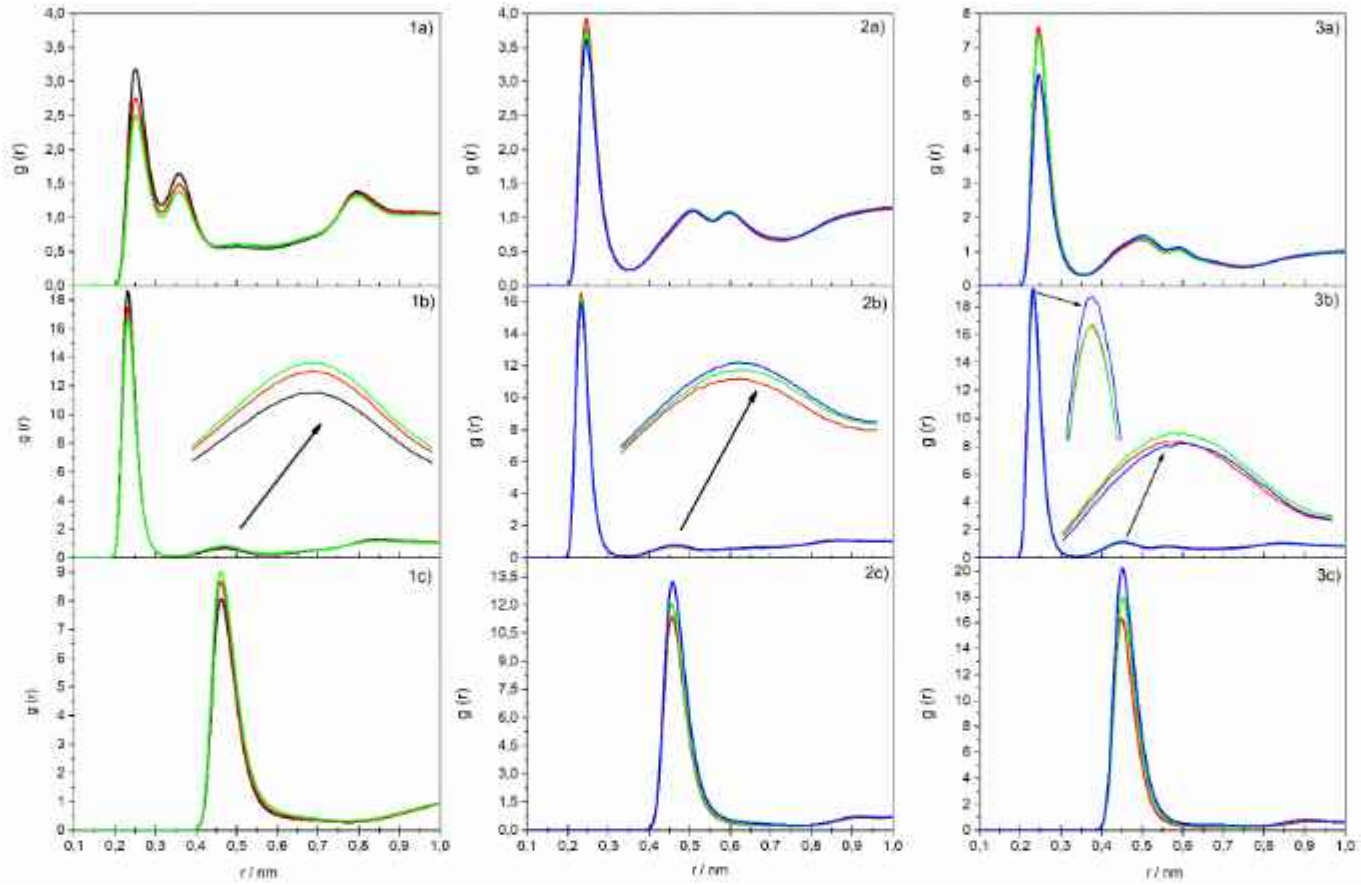

Rysunek 10 Funkcje rozkładu radialnego oparte o odległości międzyatomowe a) Br⁻···H-N; b) Br⁻···H-O; c) N⁺···Br⁻ dla DES-ów opartych o TBAB zawierających 1) AP; 2) MAE; 3) BAE przy stosunku molowym HBD do HBA; czarna linia – 1:4; czerwona linia – 1:6; zielona linia 1:8; niebieska linia - 1:10

Generalnie, dla wszystkich cieczy piki odpowiadające oddziaływaniu $N^+\cdots X^-$ są szersze w przypadku cieczy zawierających TBAB, a ich maksima znajdują się w większych odległościach niż dla cieczy opartych na TBAC. Świadczy to o tym, że w badanych DES powstaje większa liczba oddziaływań $N^+\cdots Br^-$ niż oddziaływań $N^+\cdots Cl^-$ (Tabela B8), ale są one słabsze. Dlatego też w przypadku DES opartych na TBAC, biorąc pod uwagę również nieco silniejsze oddziaływania pomiędzy solą i aminoalkoholem opisywane powyżej, dochodzi do większego uporządkowania struktury. Mimo to, ze względu na wyższą masę jonu Br^-, wyższe wartości liczbowe gęstości i współczynników załamania światła obserwuje się dla DES zawierających TBAB.

Dalsza analiza Rysunku 11, przedstawiającego funkcje rozkładu radialnego dla DES na bazie TBAC (zielona linia) lub TEAC (niebieska linia), pozwala na określenie wpływu długości łańcucha alkilowego w cząsteczce HBA na strukturę DES. Niezależnie od użytego aminoalkoholu i rozpatrywanego oddziaływania, maksima pików na wykresach RDF znajdują się w tych samych odległościach, ale sygnały są niższe i bardziej rozmyte dla DES opartych na TEAC. W rezultacie, liczby koordynacyjne jonów chlorkowych dla DES opartych na TEAC są większe w stosunku do DES zawierających TBAC (Tabela B6). Można więc przyjąć, że mniejszy rozmiar kationu TEA^+ w porównaniu do kationu TBA^+ pozwala na tworzenie większej liczby wiązań wodorowych między anionem chlorkowym a cząsteczkami alkanoloaminy, a także liczniejszych oddziaływań elektrostatycznych między anionem chlorkowym a kationem. Struktura DES opartych o TEAC, czyli HBA o krótszym łańcuchu alkilowym, jest bardziej uporządkowana, co znajduje swoje odzwierciedlenie w eksperymentalnych wartościach właściwości fizycznych DES. Zarówno gęstość jak i współczynnik załamania światła cieczy głęboko eutektycznych opartych o TEAC są większe niż dla cieczy zawierających TBAC. Wyższa lepkość DES opartych na TBAC, obserwowana mimo mniej uporządkowanej struktury, jest wynikiem większych oporów związanych z poruszaniem się większego jonu tetrabutyloamoniowego w porównaniu z mniejszym kationem tetraetyloamoniowym. Podobne wyniki uzyskali Salehi i in. [152] dla DES zawierających chlorek tetrabutyloamoniowy, chlorek tetraheptyloamoniowy i chlorek tetraoktyloamoniowy.

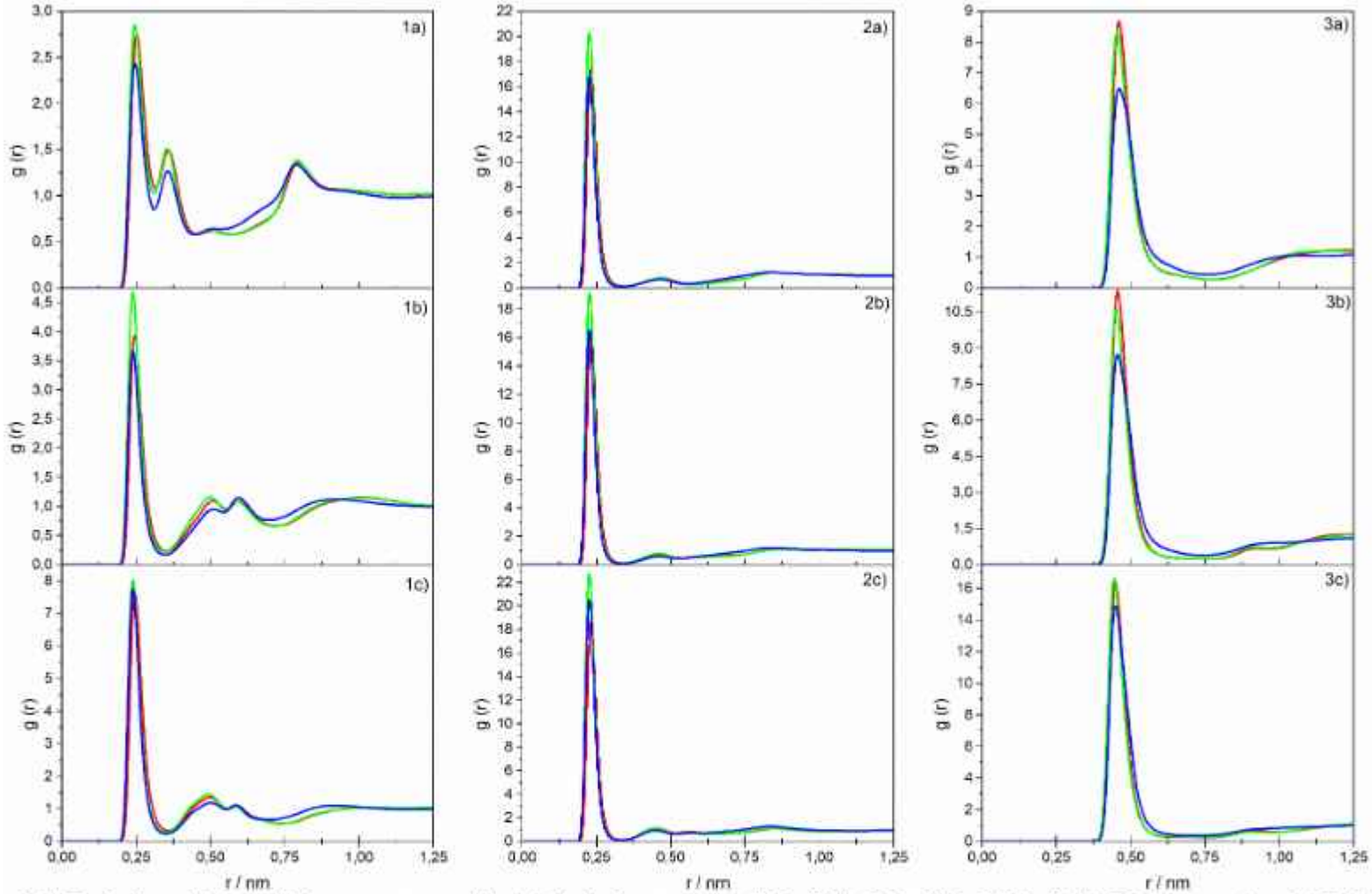

Rysunek 11 Funkcje rozkładu radialnego oparte o odległości międzyatomowe 1) $X^{-}\cdots H\text{-}N$; 2) $X^{-}\cdots H\text{-}O$; 3) $N^{+}\cdots X^{-}$ dla DES opartych o a) AP; b) MAE; c) BAE zawierających; czerwona linia – TBAB; zielona linia -TBAC; niebieska linia - TEAC przy stosunku molowym HBD do HBA wynoszącym 1:6

Zgodnie z przeprowadzonymi obliczeniami, największy wpływ na właściwości strukturalne, a w konsekwencji na właściwości fizykochemiczne cieczy głęboko eutektycznych ma donor wiązania wodorowego. Obrazuje to Rysunek 12, który przedstawia RDF otrzymane dla DES zawierających badane sole w stosunku molowym HBA do HBD wynoszącym 1:6. Największe różnice można zauważyć w oddziaływaniach pomiędzy jonem X^- soli a grupą –NH aminoalkoholu (Rysunek 12-a,b,c). Jak pisałem już wcześniej, w przypadku cieczy głęboko eutektycznych opartych o 3-amino-propan-1-ol oddziaływaniu X^-···H-N odpowiadają dwa piki. Jest to związane z preferencją do tworzenia wiązania wodorowego przez jeden z dwóch atomów wodoru pierwszorzędowej grupy aminowej AP. Oczywiście, takiej sytuacji nie obserwuje się w przypadku DES zawierających drugorzędowe aminoalkohole, tj. 2-(metyloamino)etanol MAE lub 2-(butyloamino)etanol. Jak widać, wysokość pików układa się zgodnie z szeregiem AP < MAE < BAE. Oznacza to, że najsilniejsze oddziaływania występują pomiędzy solą a BAE, a najsłabsze obserwowane są dla cieczy opartych o AP. Taką gradację siły oddziaływań potwierdza odległość pomiędzy X^-···H-N, która jest najkrótsza dla DES opartych na MAE i BAE i dłuższa dla DES zawierających AP. Najwyższe wartości liczb koordynacyjnych dla DES opartych o AP (Tabela B8) wskazują jednak na to, że chociaż 3-aminopropan-1-ol tworzy z rozpatrywanymi solami słabsze wiązania wodorowe niż 2-(metyloamino)etanol czy 2-(butyloamino)etanol, są one bardziej liczne i kompleksowe. Znalazło to odbicie w eksperymentalnych wartościach liczbowych lepkości - największych dla cieczy opartych o AP, a najniższych dla DES zawierających MAE, dla których obserwowano też najmniejsze liczby koordynacyjne. Rysunek 12-2a,b,c pokazuje wpływ HBD na oddziaływanie X^-···H-O. Generalnie, piki odpowiadające temu oddziaływaniu są wyższe od pików obrazujących oddziaływanie X^-···H-N, przez co można wnioskować, że wiązania wodorowe tworzone przez grupą alkoholową aminoalkoholu są silniejsze niż te tworzone przez grupę aminową. Ponadto, wyższe piki odpowiadające oddziaływaniu X^-···H-O odnotowano dla DES opartych na BAE w stosunku do praktycznie jednakowych dla DES zawierających MAE lub AP. Jednocześnie, liczby koordynacyjne dla DES opartych na BAE były najniższe. Może to oznaczać, że DES zawierające BAE mają jednak najmniej zwartą strukturę. Fakt ten może być spowodowany przeszkodami sterycznymi występującymi w tych mieszaninach, co związane jest z występowaniem najdłuższych łańcuchów alkilowych w aminoalkoholu. Potwierdza to również największa odległość między X^-···H-O oraz największa wysokość pików obrazujących oddziaływania X^-···N^+ (Rysunek 12-3a,b,c) dla DES opartych o BAE. Nie pozostaje to bez znaczenia dla eksperymentalnych wartości liczbowych gęstości. Ze względu na najmniej zwartą strukturę, gęstości cieczy zawierających BAE są najniższe.

Warto zauważyć, że na wykresach RDF widoczna jest również druga powłoka solwatacyjna dla wszystkich badanych przeze mnie DES. W przypadku DES opartych na MAE lub BAE znajduje się ona w odległości około 0,5 nm, zaś dla DES zawierających AP około 0,75 nm. Ta różnica odległości może być spowodowana większą liczbą cząsteczek AP w pierwszej powłoce solwatacyjnej w porównaniu z MAE lub BAE, co skutkuje przesunięciem drugiej powłoki solwatacyjnej na dalszą odległość.

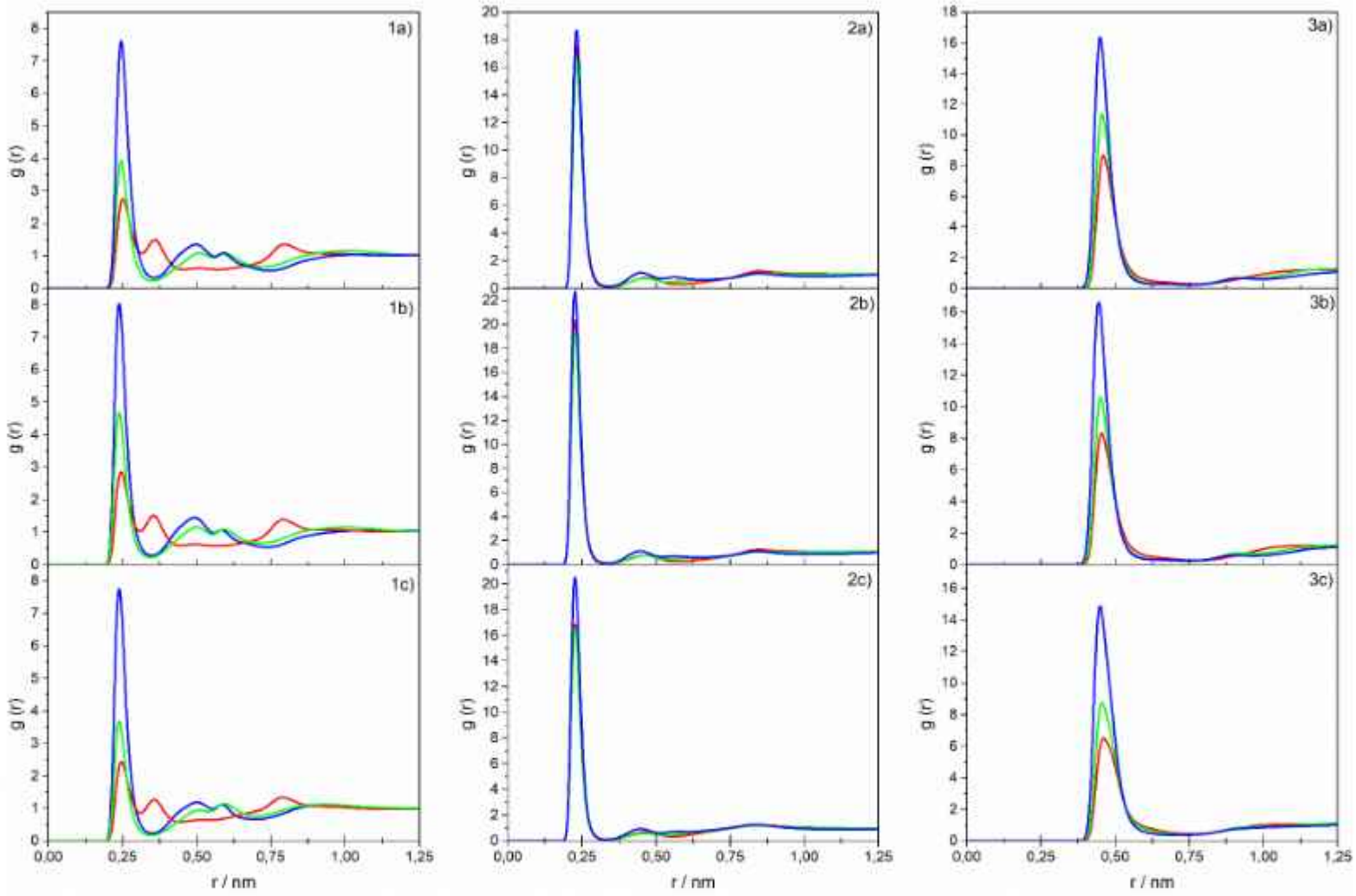

Rysunek 12 Funkcje rozkładu radialnego oparte o odległości międzyatomowe 1) $X^{-}\cdots H\text{-}N$; 2) $X^{-}\cdots H\text{-}O$; 3) $N^{+}\cdots X$ dla DES opartych o a) TBAB; b) TBAC; c) TEAC zawierających; czerwona linia – AP; zielona linia - MAE; niebieska linia - BAE przy stosunku molowym HBA do HBD wynoszącym 1:6

4.2.1. Wpływ wody na strukturę cieczy głęboko eutektycznych

Zgodnie z analizą literatury, woda często stanowi celowy dodatek do cieczy głęboko eutektycznych mający polepszyć jej właściwości, przede wszystkim zmniejszyć lepkość oraz gęstość mieszaniny. Dlatego też realizując jeden z celów pracy, a mianowicie określenie wpływu wody na właściwości fizyczne DES wykonałem pomiary gęstości, lepkości, współczynnika załamania światła i prędkości rozchodzenia się dźwięku dla wodnych roztworów DES złożonych z TBAB oraz badanych aminoalkoholi: TBAB/AP, TBAB/MAE oraz TBAB/BAE (jako przykładowych), w jednakowym stosunku molowym HBA do HBD 1:6. Wyniki tych pomiarów szczegółowo opisałem w pracy **A5,** a ponieważ wszystkie właściwości fizyczne zmieniają się nieliniowo wraz z rosnącą zawartością wody w DES, otrzymane wyniki prowadzą do prostego wniosku, że wodne roztwory DES należą do roztworów niedoskonałych. Obliczone nadmiarowe objętości molowe, mające najbardziej ujemne wartości dla TBAB/MAE, dowodzą, że właśnie w przypadku mieszaniny tej cieczy z wodą dochodzi do najsilniejszych oddziaływań pomiędzy cząsteczkami DES i wody (w porównaniu do oddziaływań pomiędzy cząsteczkami DES czy wody). Co więcej, efekt ten jest silniejszy niż efekt upakowania, na co wskazują dalsze obliczenia wykonane przy użyciu teorii Prigogine'a–Floryeg'o–Patterson'a (PFP). Do podobnych wniosków prowadzą wartości innych wielkości obliczone z gęstości tzn. nadmiarowe rozszerzalności cieplne i objętości cząstkowe, oraz wielkości otrzymane przy użyciu prędkości rozchodzenia się dźwięku, współczynnika załamania światła oraz lepkości, tj. nadmiarowe ściśliwości adiabatyczne, odchylenia współczynnika załamania światła i odchylenia lepkości.

W celu dokładniejszej oceny wpływu wody na ciecze głęboko eutektyczne wykonałem obliczenia metodą dynamiki molekularnej dla wodnych roztworów DES TBAB/AP 1:6, TBAB/MAE 1:6 i TBAB/BAE 1:6 w zakresie ułamka molowego H_2O od 0,1 do 0,9. Pozwoliło mi to na określenie zmian struktury DES, zachodzących na skutek dodatku wody. Wpływ wody na strukturę DES na bazie TBAB przedstawia Rysunek 13. Zawiera on RDF odpowiadające oddziaływaniom $Br^-\cdots H\text{-}N$, $Br^-\cdots H\text{-}O$, $Br^-\cdots H\text{-}O_{H2O}$ oraz $N^+\cdots Br^-$ w wodnych roztworach DES opartych o AP, MAE oraz BAE w stosunku molowym HBA do HBD 1:6 o różnej zawartości wody. Rysunek 13-1a,b,c przedstawia wykresy funkcji rozkładu radialnego dla oddziaływań $Br^-\cdots H\text{-}N$. Jak widać, w przypadku cieczy opartych o AP nadal obserwuje się rozszczepienie piku, czyli wiązanie przez jeden atom wodoru jest nadal bardziej preferowane, ale intensywność obu pików maleje wraz ze wzrostem zawartości wody, co prowadzi do spadku liczb koordynacyjnych (Tabela B9). Ponadto, pozycje maksimów pierwszych pików wraz z dodatkiem wody przesuwają się w kierunku krótszych odległości, podczas gdy maksima drugich pików przesuwają się w kierunku dłuższych odległości i prawie zanikają przy $x_{DES}<0,2$. Podobny spadek intensywności piku, odpowiedzialnego za oddziaływania pomiędzy anionem bromkowym soli a grupą –NH aminoalkoholu, następujący na skutek dodatku wody, obserwuje się dla DES zawierających BAE lub MAE. Generalnie, w przypadku DES opartych na MAE lub BAE maksima pików przesuwają się ku większym odległościom, a liczby koordynacyjne maleją. Tylko w przypadku wodnego roztworu cieczy głęboko eutektycznej opartej na MAE, dla której ułamek molowy DES wynosi 0,9,

intensywność piku Br^-···H-N jest wyższa niż dla czystego DES, a liczba koordynacyjna większa. Można więc stwierdzić, że na skutek dodania wody do DES zawierających AP lub BAE oddziaływania pomiędzy HBA i HBD maleją. W przypadku TBAB/MAE analiza oddziaływania Br^-···H-N prowadzi do wniosku, że dodatek niewielkiej ilości wody wzmacnia strukturę DES, ale jej dalszy wzrost zawartości powoduje spadek oddziaływań pomiędzy składnikami mieszaniny. Analizując oddziaływania Br^-···H-O i Br^-···N^+ (Rysunki 13-2a,b,c i 13-4a,b,c), niezależnie od badanego DES, obserwuje się wzrastające wraz z dodatkiem wody osłabienie oddziaływań między składnikami DES, które objawia się zmniejszeniem intensywności piku i przesunięciem położeń w kierunku większych odległości. Takie rozluźnienie struktury DES w wyniku wprowadzenia cząsteczek wody zostało potwierdzone przez badania przeprowadzone przez Fetisova i in. dla cieczy głęboko eutektycznych złożonych z chlorku choliny i mocznika [153]. Ponadto, największy spadek intensywności pików Br^-···N^+, liczb koordynacyjnych oraz największe przejście ku dłuższym odległościom, zaobserwowano dla cieczy głęboko eutektycznej TBAB/MAE 1:6 przy przejściu z czystego DES do roztworu wodnego o x_{DES}=0,9. Spowodowane jest to odsuwaniem się anionu bromkowego od kationu TBA^+ w wyniku działania wody, czego efektem jest łatwiejszy dostęp cząsteczki MAE do Br^-. Dowodem na to jest podwyższenie piku na wykresie oddziaływania Br^-···H-N dla roztworu wodnego o x_{DES}=0,9 w stosunku do czystego DES.

Oddziaływania pomiędzy jonem Br- i grupą hydroksylową wody zobrazowałem na Rysunku 13-3a,b,c. Jak widać, w przypadku wodnych roztworów wszystkich badanych DES, na wykresach RDF występują dwa piki wskazujące na tworzenie się dwóch powłok hydratacyjnych. Ponadto intensywności pików Br^-···H-O_{H2O} są zdecydowanie wyższe niż pików obrazujących oddziaływania pomiędzy składnikami danego DES. Wskazuje to na najsilniejsze oddziaływania pomiędzy cząsteczkami DES i wody i pozostaje to w zgodzie z wnioskami uzyskanymi za pomocą nadmiarowych wielkości termodynamicznych.

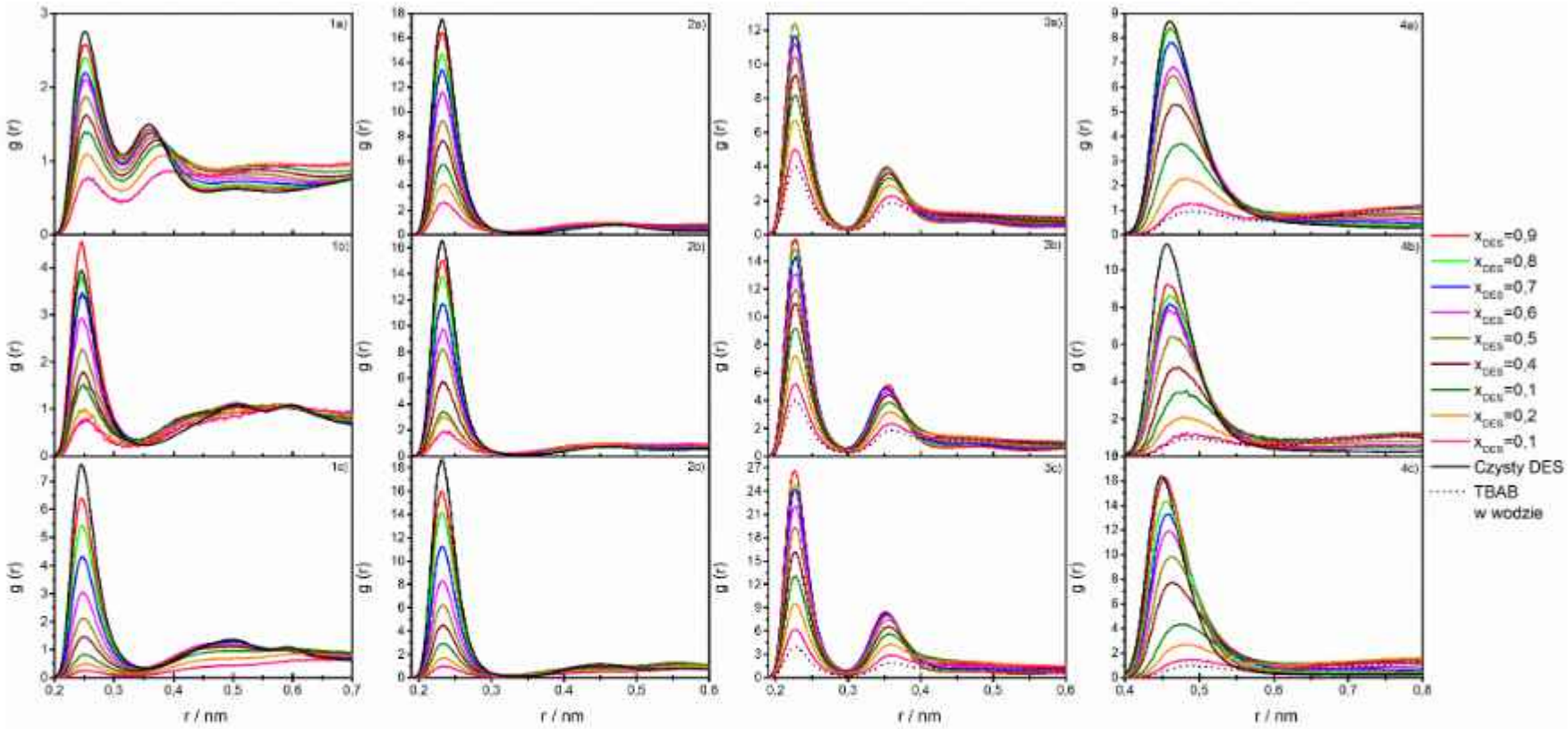

Rysunek 13 Funkcje rozkładu radialnego oparte o odległości międzyatomowe 1) Br^-···H-N; 2) Br^-···H-O; 3) Br^-···H-O_{H2O} 4) N^+···Br^- dla wodnych roztworów DES opartych o a) AP; b) MAE; c) BAE przy stosunku molowym HBA do HBD wynoszącym 1:6.

4.3. Absorpcja ditlenku węgla w DES i ich roztworach wodnych

Wyniki pomiarów rozpuszczalności ditlenku węgla w badanych przeze mnie cieczach głęboko eutektycznych, zawierających aminoalkohole, uzyskane za pomocą metody grawimetrycznej, zostały szerzej opisane w publikacji **A4**. Ponadto, dla wybranych DES opartych o AP, rozpuszczalność CO_2 zmierzyłem równowagową metodą izochoryczną przy różnych ciśnieniach gazu, a wyniki pomiarów przedstawiłem w pracy **A5**. Tej samej metody, tj. izochorycznej metody równowagowej, użyłem do wyznaczenia rozpuszczalności CO_2 w DES opartych o glikole propylenowe.

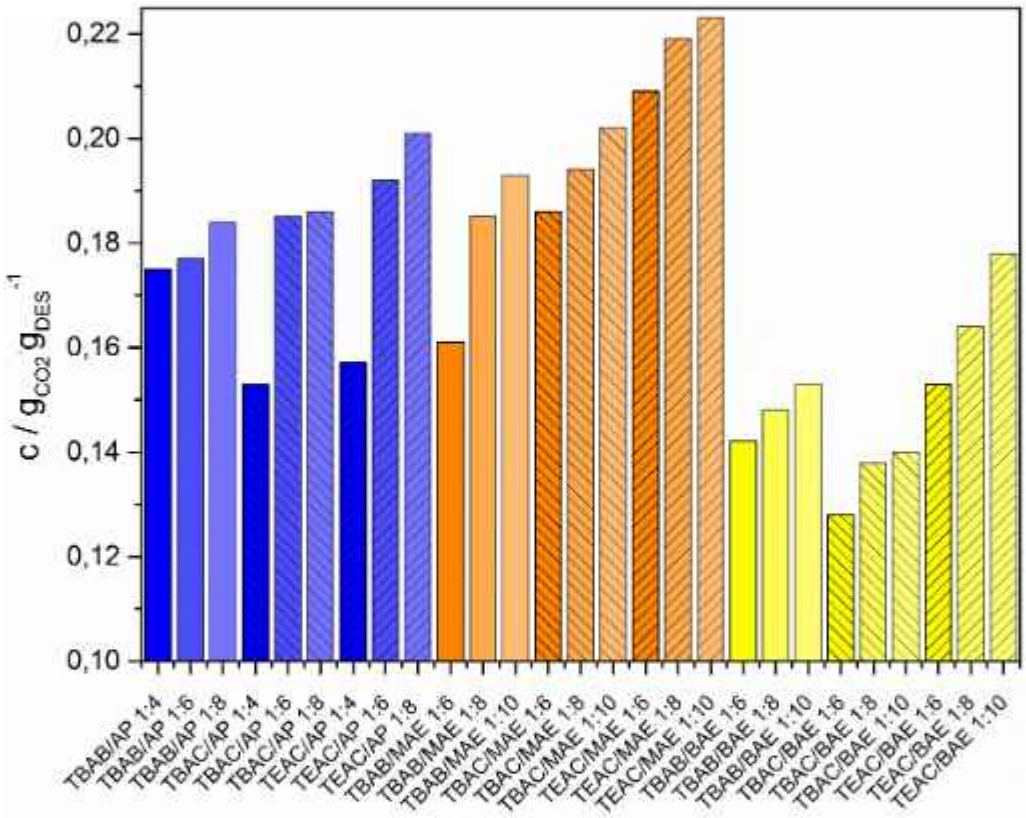

Rysunek 14 Rozpuszczalność CO_2 w badanych DES pod ciśnieniem atmosferycznym, w temperaturze 298,15 K.

Wartości rozpuszczalności dla DES opartych na aminoalkoholach pod ciśnieniem atmosferycznym i temperaturze 298,15 K przedstawia Rysunek 14. Mieszczą się one w zakresie od 0,128 do 0,223 g_{CO2}/g_{DES}, co pozwala na stwierdzenie, że badane DES zawierające aminoalkohole mogą lepiej absorbwać ditlenek węgla niż ciecze jonowe i niektóre ciecze głęboko eutektyczne, przedstawione w Tabeli 5. Mieszaniny TEAC/AP 1:8, TBAC/MAE 1:10 i TEAC/MAE 1:10 wykazują wyższą pojemność sorpcyjną w stosunku CO_2 niż TBAB/MEA 1:5, ale żadna z badanych cieczy nie osiąga pojemności [MEACl]/AP 1:4.

Tabela 5 Porównanie rozpuszczalności CO_2 w wybranych IL i DES pod ciśnieniem atmosferycznym w temperaturze 298,15 K.

ciecz	rozpuszczalność $g_{CO2}/g_{rozp.}$	odnośnik
TBAB/AP 1:8	0,184	badania własne
TBAC/AP 1:8	0,186	badania własne
TEAC/AP 1:8	0,201	badania własne
TBAB/MAE 1:10	0,193	badania własne
TBAC/MAE 1:10	0,202	badania własne
TEAC/MAE 1:10	0,223	badania własne
TBAB/BAE 1:10	0,153	badania własne
TBAC/BAE 1:10	0,140	badania własne
TEAC/BAE 1:10	0,178	badania własne
[hemim][PF_6]	0,0021[a]	[154]
[hemim][OTf]	0,0027[a]	[154]
[hemim][NTf_2]	0,0024[a]	[154]
[bmim][PF_6]	0,0026	[155]
[bmim][Tf_2N]	0,0033	[155]
[bmim][BF_4]	0,0032	[155]
[$MeBu_3N$][Tf_2N]	0,0021	[155]
[MeBuPyrr][Tf_2N]	0,0025	[155]
[$N_{(4)113}$][Tf_2N]	0,0017	[156]
[$N_{(6)113}$][Tf_2N]	0,0019	[156]
[$N_{(10)113}$][Tf_2N]	0,0022	[156]
[MEACl]/AP 1:4	0,263	[120]
TBAB/MEA 1:5	0,197	[142]
[N_{2222}][Im]/EG 1:2	0,114	[157]
TBAB/TEA 1:2	0,025	[142]
ChCl/butan-1,4-diol 1:4	0,0001	[111]

[a] T = 303,15 K

Z analizy Rysunku 14 wynika, że największy wpływ na rozpuszczalność CO_2 w badanych mieszaninach eutektycznych ma rodzaj zastosowanego aminoalkoholu. Rozpatrując ciecze bazujące na tej samej soli i jednakowym stosunku molowym HBA do HBD, rozpuszczalność maleje w kolejności MAE > AP > BAE, co wynika ze struktury mieszanin, decydującej o zdolnościach absorpcyjnych DES. Najniższa rozpuszczalność obserwowana dla cieczy opartych na BAE wynika z najsilniejszych oddziaływań wodorowych pomiędzy między grupą aminową tego aminoalkoholu a anionem soli (strona 49), co osłabia oddziaływania DES z CO_2. Efekt ten dominuje nad efektem „objętości swobodnej", która z uwagi na najdłuższy łańcuch alkilowy w cząsteczce BAE jest największa w porównaniu z DES zawierającymi AP czy MAE. Silna sieć wiązań wodorowych powstająca w DES zawierającej AP odpowiada również za niższą rozpuszczalność CO_2 w porównaniu do mieszanin zawierających MAE. Potwierdzają to wyniki symulacji MD, zgodnie z którymi średnia liczba cząsteczek aminoalkoholu w otoczeniu anionu soli jest zdecydowanie większa w przypadku DES zawierającego AP niż dla DES zawierającego MAE. Większy udział grup aminowych AP w tworzeniu wiązań wodorowych z anionem chlorkowym lub bromkowym sprawia, że są one słabiej dostępne w reakcji z CO_2 niż grupy aminowe w MAE, co w rezultacie prowadzi to do niższej rozpuszczalności.

Analizując wyniki pomiarów rozpuszczalności ditlenku węgla w cieczach głęboko eutektycznych opartych na TBAC i TBAB można stwierdzić, że wpływ anionu HBA na rozpuszczalność jest stosunkowo niewielki. Niemniej jednak, mieszaniny zawierające AP lub MAE mają wyższe powinowactwo do CO_2, gdy rolę HBA pełni TBAC (wyjątek stanowi TBAC/AP 1:4), natomiast DES oparte na BAE lepiej absorbują CO_2, gdy w ich skład wchodzi TBAB.

Wynika to z siły oddziaływań między kationem a anionem soli wchodzącej w skład DES - im jest większa, tym słabsze jest oddziaływanie mieszaniny z ditlenkiem węgla. Z uzyskanych funkcji rozkładu radialnego (Rysunek 11) wynika, że dla DES opartych na BAE, silniejsze oddziaływania występują pomiędzy TBA^+ i Cl^-, natomiast dla mieszanin zawierających AP lub MAE – pomiędzy TBA^+ i Br^-. W rezultacie rozpuszczalność CO_2 w TBAB/BAE jest wyższa niż w TBAC/BAE, a w mieszaninach zawierających AP i MAE zależność jest odwrotna. Wyjątek stanowią mieszaniny o składzie 1:4 zawierające AP, w których rozpuszczalność CO_2 układa się w szeregu TBAB/AP > TBAC/AP. Wynik ten potwierdziłem za pomocą izochorycznej metody równowagowej (**A5**). Siła oddziaływań pomiędzy TBA^+ a Br^- lub Cl^- jest zbliżona przy takim składzie mieszaniny (Rysunek B4), co może prowadzić do odwrócenia trendu w rozpuszczalności dla cieczy TBAB/AP i TBAC/AP.

Niezależnie od użytego donora wiązania wodorowego rozpuszczalność CO_2 w DES (o tych samych stosunkach molowych HBA do HBD) zawierających TBAC jest niższa niż w DES zawierających TEAC. Wynika to ze słabszych oddziaływań pomiędzy składnikami w mieszaninie zawierającej sól o krótszym łańcuchu alkilowym (Rysunek 11), co skutkuje wyższą dostępnością i prawdopodobieństwem zajścia reakcji grupy aminowej z CO_2.

Rozpuszczalność ditlenku węgla rośnie również wraz ze wzrostem zawartości donora wiązania wodorowego. Spowodowane jest to głównie zwiększaniem się stężenia aminoalkoholu, który jest odpowiedzialny za reakcję chemiczną DES z CO_2. Ponadto, zwiększenie jego ilości powoduje osłabienie wiązań wodorowych pomiędzy składnikami tworzącymi DES, co umożliwia oddziaływanie grupy aminowej z ditlenkiem węgla. W tym miejscu należy zaznaczyć, że wyniki uzyskane z użyciem izochorycznej metody równowagowej, które uzyskałem dla cieczy głęboko eutektycznych opartych na AP wykazały odwrotną zależność rozpuszczalności ditlenku węgla od stosunku molowego HBA do HBD. W pomiarach tych założono, że stan równowagi został osiągnięty, gdy zmiana ciśnienia nad powierzchnią cieczy była mniejsza niż 0,5 kPa w ciągu 24 h. Jednakże, wraz ze wzrostem zawartości CO_2 rozpuszczonego w mieszaninie wzrasta jej lepkość, co prowadzi do powstania znacznych oporów dyfuzji w warstwie powierzchniowej. W efekcie, pomimo zastosowania w badaniu niewielkiej grubości warstwy, ciecz może pozostawać niejednolicie wysycona, a rzeczywisty stan równowagi może nie zostać osiągnięty przy ustalonych założeniach. Czas niezbędny do osiągnięcia stanu równowagi może znacząco przekraczać ten zgodny z przyjętymi kryteriami. Szczegółowe dane o kinetyce absorbcji CO_2 przedstawiłem w publikacji **A5**. Wzrost lepkości i temperatury towarzyszący absorpcji ditlenku węgla w mieszaninach opartych o aminoalkohole wykluczył również ten typ DES z dalszych badań z użyciem SLM. Duże opory dyfuzji i efekty cieplne towarzyszące rozpuszczaniu CO_2 w mieszaninie, mogłyby się bowiem przyczyniać do wzmożonego pęcznienia, zmiany krętości porów i degradacji nośników.

W publikacji **A4** opisałem problem wpływu obecności wody na rozpuszczalność ditlenku węgla w badanych cieczach głęboko eutektycznych. Analizę przeprowadziłem na podstawie badań rozpuszczalności CO_2 w mieszaninach złożonych z TBAB i AP, MAE lub BAE w stosunku molowym HBA do HBD 1:6, które zawierały odpowiednio 0,5%, 1% i 5% wag. H_2O.

Uzyskane wyniki (Rysunek 15) wskazują na obniżenie rozpuszczalności gazu w TBAB/AP i TBAB/BAE z dodatkiem wody, i to niezależnie od jej ilości. Natomiast w przypadku TBAB/MAE, woda w ilości 0,5% i 1% wag. spowodowała wzrost rozpuszczalności, ale przy stężeniu 5% wag. rozpuszczalność CO_2 była już niższa niż dla czystego DES. Zaobserwowane zależności pozostają w zgodzie zarówno z wynikami symulacji MD, jak i z wynikami badań densymetrycznych i akustycznych. Jak opisywałem w poprzednim rozdziale, obecność wody w cieczy głęboko eutektycznej prowadzi do powstania silnych oddziaływań wodorowych pomiędzy cząsteczkami H_2O a cząsteczkami DES (osłabiają się przy tym oddziaływania pomiędzy hydratowanymi składnikami mieszaniny) i znajduje to swoje odzwierciedlenie w niższej rozpuszczalności CO_2. Jak wynika z symulacji MD, tylko w przypadku TBAB/MAE dodatek niewielkiej ilości wody (około 1,9%) wzmacnia strukturę DES (oddziaływania z wodą są słabsze), co skutkuje zwiększeniem reaktywności z ditlenkiem węgla. Dalszy wzrost zawartości wody powoduje osłabienie oddziaływań pomiędzy hydratowanymi składnikami mieszaniny i co za tym idzie spadek rozpuszczalności.

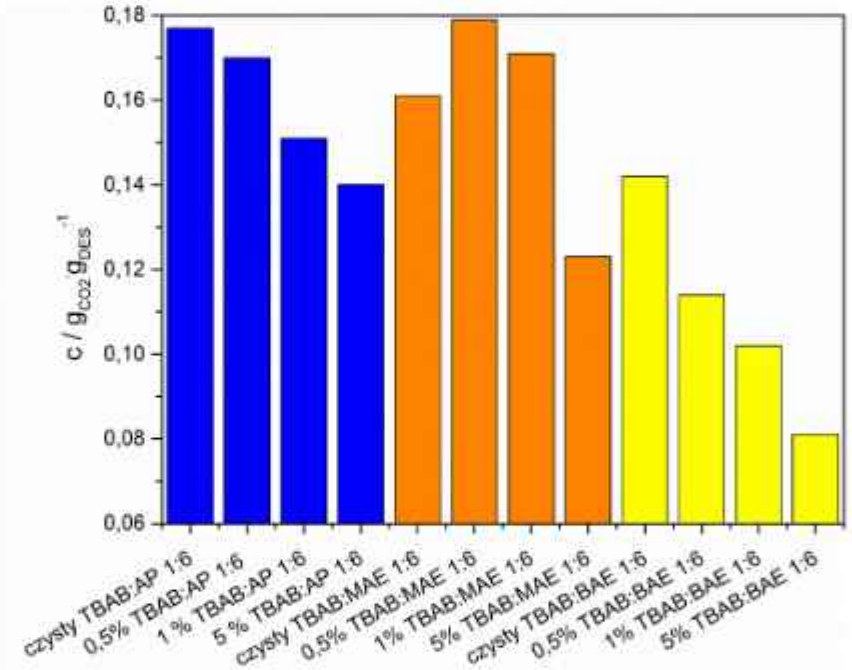

Rysunek 15 Wpływ wody na rozpuszczalność ditlenku węgla na przykładzie wybranych DES.

Jak wcześniej wspominałem, rozpuszczalność ditlenku węgla w DES opartych o glikole propylenowe wyznaczyłem przy użyciu metody równowagowej. Metoda ta dobrze sprawdza się w wyznaczaniu pojemności sorpcyjnych DES absorbujących CO_2 w sposób fizyczny, ze względu na szybki czas ustalenia równowagi i niewielki wzrost lepkości po procesie absorpcji. Wyniki otrzymane dla DES opartych o propan-1,2-diol znajdują się w pracy **A7**, natomiast dla cieczy opartych o propan-1,3-diol zostały umieszczone w Tabeli B10. Rysunek 16 przedstawia przykładowe izotermy absorpcji w temperaturze 298,15 K.

W celu porównania rozpuszczalności ditlenku węgla w DES, które absorbują CO_2 w sposób fizyczny, obliczyłem stałe Henry'ego. Jak widać z Tabeli 6, niezależnie od temperatury

i HBA wchodzącego w skład DES, mieszaniny oparte na propano-1,2-diolu w porównaniu do DES zawierających propano-1,3-diol charakteryzują się niższymi wartościami H_x, a więc wyższą rozpuszczalnością CO_2. Oznacza to, że bliższe położenie grup hydroksylowych w łańcuchu węglowym zwiększa rozpuszczalność ditlenku węgla. Do podobnych wniosków doszli Chen i in. dla cieczy głęboko eutektycznych opartych o butan-1,4-diol i butan-2,3-diol [111].

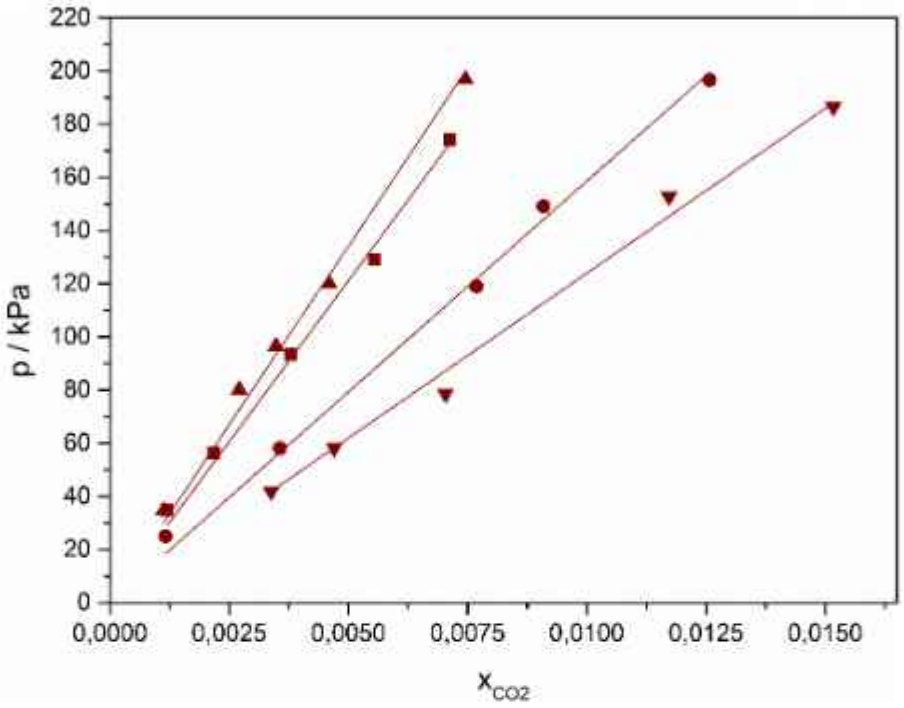

Rysunek 16 Izotermy absorbcji CO_2 w DES opartych o propan-1,3-diol w temperaturze 298,15 K: ● - ChCl/propano-1,3-diol 1:3, ■ - ChCl/propano-1,3-diol 1:4, ▲ - AcChCl/propano-1,3-diol 1:3, ▼ - TBAC/propano-1,3-diol 1:3

Z kolei porównanie rozpuszczalności w grupach DES zawierających propanodiol danego typu prowadzi do wniosku, że najwyższą pojemność sorpcyjną CO_2 wykazują DES oparte na TBAC jako HBA. Wynika to z najdłuższych łańcuchów alkilowych oraz najwyższej symetrii tej soli, co daje jej największą "objętością swobodną" spośród badanych DES.

Co ciekawe, dla cieczy głęboko eutektycznych opartych na propano-1,2-diolu zaobserwowałem niższe wartości H_x dla DES zawierających AcChCl, podczas gdy w przypadku DES z propano-1,3-diolem niższe wartości wykazywały mieszaniny oparte na ChCl. Generalnie, grupa karboksylowa obecna w cząsteczce AcChCl ma wyższe powinowactwo do CO_2, przez co ditlenek węgla wykazuje wyższą rozpuszczalność w cieczach zawierających chlorek acetylocholiny. Uzyskane wyniki wskazują więc, że również inne czynniki, takie jak: "objętość swobodna", oddziaływania między HBA a HBD oraz zawada steryczna, mają znaczący wpływ na ostateczną wartość liczbową stałej Henry'ego.

Tabela 6 Stałe Henry'ego (H_x) w układach CO_2 /DES opartych o glikole propylenowe

T / K	H_x / MPa	T / K	H_x / MPa
ChCl/propano-1,2-diol 1:3		ChCl/propano-1,3-diol 1:3	
293,15	10,8 ± 0,36	293,15	14,9 ± 0,13
298,15	11,2 ± 0,39	298,15	15,9 ± 0,25
303,15	11,8 ± 0,44	303,15	17,0 ± 0,40
308,15	12,3 ± 0,51	308,15	18,2 ± 0,58
313,15	13,2 ± 0,58	313,15	19,4 ± 0,85
ChCl/propano-1,2-diol 1:4		ChCl/propano-1,3-diol 1:4	
293,15	10,7 ± 0,54	293,15	22,4 ± 0,24
298,15	11,1 ± 0,55	298,15	24,2 ± 0,40
303,15	11,9 ± 0,57	303,15	26,5 ± 0,90
308,15	12,8 ± 0,57	308,15	29,7 ± 1,27
313,15	13,4 ± 0,59	313,15	33,1 ± 2,10
AcChCl/propano-1,2-diol 1:3		AcChCl/propano-1,3-diol 1:3	
293,15	10,2 ± 0,40	293,15	25,4 ± 0,27
298,15	10,7 ± 0,40	298,15	26,8 ± 0,56
303,15	11,2 ± 0,42	303,15	29,1 ± 0,74
308,15	11,9 ±0,43	308,15	31,3 ±1,26
313,15	12,7 ± 0,48	313,15	33,1 ± 1,76
TBAC/propano-1,2-diol 1:3		TBAC/propano-1,3-diol 1:3	
293,15	7,8 ± 0,21	293,15	11,6 ± 0,28
298,15	8,3 ± 0,18	298,15	12,7 ± 0,27
303,15	8,8 ± 0,26	303,15	13,6 ± 0,28
308,15	9,6 ± 0,35	308,15	14,8 ± 0,40
313,15	10,4 ± 0.51	313,15	15,4± 0,55

W przeciwieństwie do DES opartych na aminoalkoholach, dla których wraz ze wzrostem zawartości HBD obserwowałem wzrost rozpuszczalności CO_2, w przypadku DES zawierających propanodiole rozpuszczalność ditlenku węgla malała wraz z rosnącą zawartością HBD w mieszaninie. Wynika to ze zmniejszenia "objętości swobodnej" rozpuszczalnika, która jest kluczowym parametrem decydującym o jego pojemności sorpcyjnej, podczas gdy dla DES tworzących z CO_2 oddziaływania chemiczne, o rozpuszczalności decyduje ilość aminoalkoholu wchodzącego w reakcję chemiczną z CO_2.

4.4. Unieruchomione membrany ciekłe oparte na cieczach głęboko eutektycznych

Wyniki badań nad wykorzystaniem unieruchomionych membran ciekłych opartych na cieczach głęboko eutektycznych zawierających propano-1,2-diol do separacji ditlenku węgla zostały opublikowane i szczegółowo opisane w pracy **A7**. W niniejszym rozdziale przedstawiłem również nieopublikowane dotąd wyniki dla SLM opartych o DES zawierające propano-1,3-diol.

Zgodnie z mechanizmem rozpuszczalnościowo-dyfuzjnym przenikalność gazów przez SLM zależy od ich rozpuszczalności oraz od parametrów dyfuzji przez ciecz tworzącą membranę. Dla badanych układów ilustruje to Rysunek 17. Ponadto, Tabela 7 zawiera uzyskane wartości przenikalności CO_2 i N_2 oraz idealną selektywność. Dla wszystkich układów przenikalność azotu jest zbliżona i niewielka, co wynika z niskiej rozpuszczalności tego gazu w DES. Jak widać z Tabeli 7, przenikalność azotu wykazuje niewielkie zmiany w funkcji temperatury i dopiero w wyższych temperaturach, na skutek wzrostu „objętości swobodnej", który prowadzi do spadku lepkości, zaczyna wyraźnie wzrastać.

Przenikalność ditlenku węgla przez unieruchomione membrany ciekłe oparte na DES jest zdecydowanie większa niż przenikalność azotu, co wynika ze zdecydowanie większej rozpuszczalności CO_2 niż N_2. Z tego też względu przenikalność ditlenku węgla przez SLM zależy zarówno od lepkości, jak i rozpuszczalności CO_2. W przypadku SLM zawierających mieszaniny oparte na tym samym HBA, ale różnych glikolach, które zdecydowanie różnią się lepkością, większa przenikalność ditlenku węgla jest obserwowana dla SLM opartych na DES o mniejszej lepkości, i to niezależnie od wzajemnej relacji rozpuszczalności. Wystarczy porównać przenikalności dla SLM zawierających DES oparte na ChCl lub TBAC. Niezależnie od temperatury, SLM oparte na ChCl/propano-1,3-diolu i TBAC/propano-1,2-diolu wykazują wyższe wartości przenikalności CO_2 w porównaniu do SLM zawierających odpowiednio ChCl/propano-1,2-diol i TBAC/propano-1,3-diol. W przypadkach, gdy lepkości DES są zbliżone, tak jak to ma miejsce w przypadku mieszanin opartych o AChCl, o przenikalności CO_2 decyduje rozpuszczalność. Dlatego też, w każdej temperaturze, przenikalność CO_2 dla SLM opartej na AChCl/propano-1,2-diolu jest większa niż dla SLM opartej na AChCl/propano-1,3-diol. W powyższe reguły, dotyczące wpływu lepkości i rozpuszczalności na przenikalność, wpasowują się uzyskane wartości przenikalności ditlenku węgla dla SLM opartych na DES zawierających różne HBA i ten sam izomer glikolu propylenowego oraz mieszaniny zawierające ChCl i propanodiole o różnych stosunkach molowych HBA do HBD. W przypadku SLM opartych na ChCl/propano-1,2-diolu, którego lepkość wyraźnie się zmniejsza wraz ze wzrostem ilości glikolu, większą przenikalnością CO_2 charakteryzuje się SLM zawierająca ChCl/propano-1,2-diol o składzie 1:4. Natomiast dla SLM zawierających ChCl/propano-1,3-diol, którego lepkość przechodząc od składu 1:3 do 1:4 praktycznie się nie zmienia, większa przenikalność ditlenku węgla w przypadku DES o mniejszej ilości glikolu wynika z większej pojemności absorpcyjnej tej mieszaniny. Jedynie SLM oparta na TBAC/propano-1,2-diolu, mimo wyższej lepkości tego DES w porównaniu do ChCl/propano-1,2-diolu i AcChCl/propano-1,2-diolu, wykazuje większą przenikalność ditlenku węgla. Zjawisko to można przypisać najwyższej spośród badanych DES

wartości rozpuszczalności CO_2 w TBAC/propano-1,2-diolu, która odkrywa kluczową rolę, obok lepkości, w determinowaniu przenikalności ditlenku węgla.

Tabela 7 Przenikalność czystych gazów oraz idealna selektywność dla SLM opartych o DES zawierających glikole propylenowe

T / K	P / barrer		α_{CO_2/N_2}	P / barrer		α_{CO_2/N_2}
	CO_2	N_2		CO_2	N_2	
	ChCl/propano-1,2-diol 1:3			ChCl/propano-1,3-diol 1:3		
293,15	86	3	29	127	4	32
298,15	104	5	21	136	5	27
303,15	117	6	19	144	7	21
308,15	130	7	19	154	8	19
313,15	145	16	9	159	11	14
	ChCl/propano-1,2-diol 1:4			ChCl/propano-1,3-diol 1:4		
293,15	96	4	24	123	4	31
298,15	112	5	22	128	6	21
303,15	120	8	15	136	7	19
308,15	135	10	14	141	11	13
313,15	149	23	6	150	16	9
	AcChCl/propano-1,2-diol 1:3			AcChCl/propano-1,3-diol 1:3		
293,15	117	4	29	95	4	24
298,15	127	7	18	106	4	26
303,15	141	8	18	117	5	23
308,15	154	8	19	127	6	21
313,15	170	14	12	147	7	21
	TBAC/propano-1,2-diol 1:3			TBAC/propano-1,3-diol 1:3		
293,15	152	5	30	89	4	22
298,15	162	8	20	100	5	20
303,15	191	14	14	115	8	14
308,15	207	24	9	130	12	11
313,15	226	29	8	146	17	9

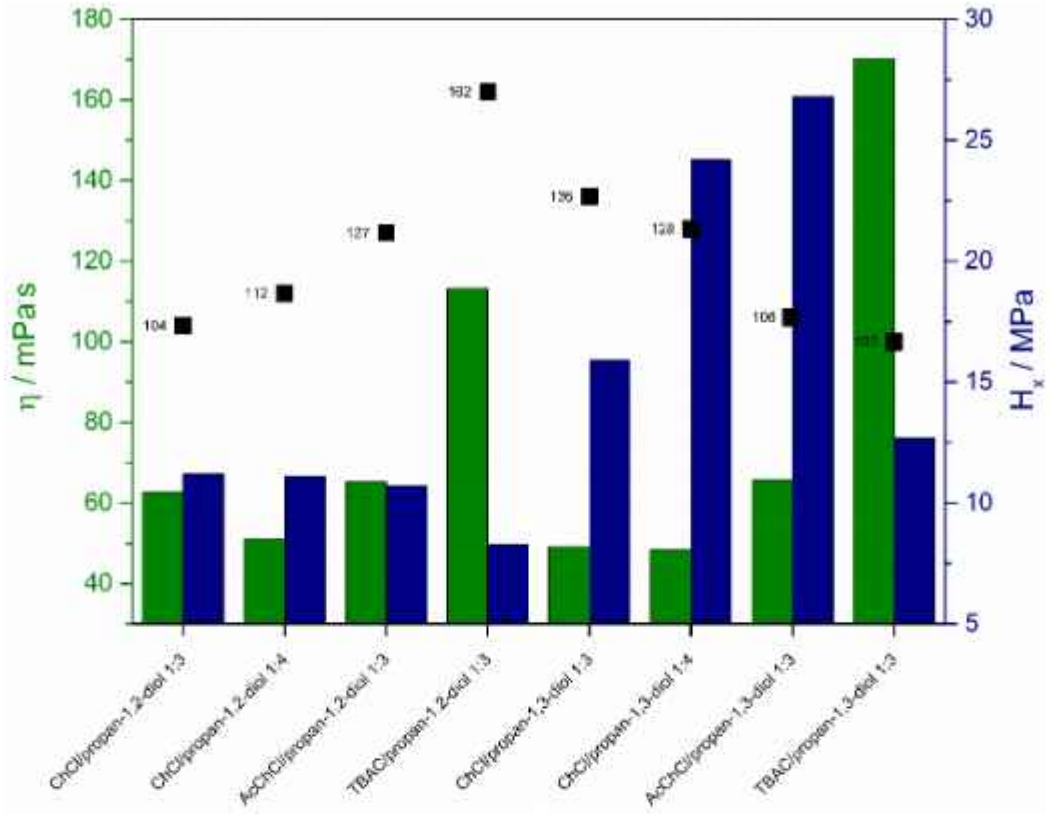

Rysunek 17 Wpływ lepkości DES i rozpuszczalności CO_2 na wartość liczbową przenikalności CO_2 przez SLM oparte na cieczach głęboko eutektycznych w temperaturze 298,15 K

Na energię aktywacji przenikalności (Tabela 8), która pokazuje wpływ temperatury na przenikalność, składa się energia aktywacji dyfuzji oraz entalpia rozpuszczania. Dla procesów sorpcji ten drugi parametr ma zazwyczaj znak ujemny, dlatego też dodatnie wartości energii aktywacji przenikalności sugerują większy wpływ temperatury na proces dyfuzji niż rozpuszczania. Najmniejszy wpływ zaobserwowałem dla ChCl/propano-1,3-diolu, dla którego spadek lepkości i wzrost przenikalności wraz ze wzrostem temperatury był najwolniejszy (Rysunek 18).

Tabela 8 Wartości energii aktywacji przenikalności dla badanych SLM.

DES	E_a / kJ·mol^{-1}
ChCl/propano-1,2-diol 1:3	18,85
ChCl/propano-1,2-diol 1:4	16,17
AcChCl/propano-1,2-diol 1:3	14,45
TBAC/propano-1,2-diol 1:3	15,78
ChCl/propano-1,3-diol 1:3	8,68
ChCl/propano-1,3-diol 1:4	7,58
AcChCl/propano-1,3-diol 1:3	16,36
TBAC/propano-1,3-diol 1:3	19,14

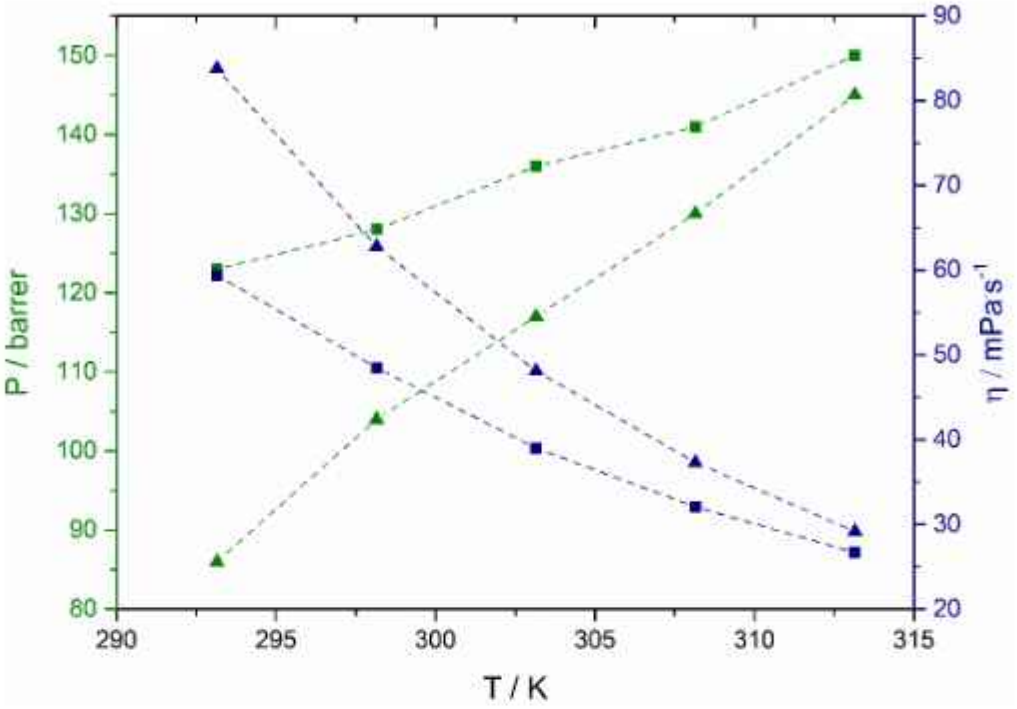

Rysunek 18 Wpływ temperatury na przenikalność CO_2 w SLM opartych o; ■ChCl/propano-1,3-diol 1:4; ▲ChCl/propano-1,2-diol 1:3

Idealna selektywność CO_2/N_2, zdefiniowana jako stosunek przenikalności ditlenku węgla do przenikalności azotu, maleje wraz ze wzrostem temperatury. W przypadku membran, w których fazę ciekłą stanowią DES oparte na ChCl i AchCl, większą selektywność wykazują SLM zawierające mieszaniny oparte na propan-1,3-diolu. Natomiast w przypadku DES zawierających TBAC, idealna selektywność CO_2/N_2 membrany praktycznie nie zależy do rodzaju glikolu wchodzącego w skład mieszaniny eutektycznej. Spośród badanych układów, w temperaturach 293,15 K i 298,15 K, największą selektywnością charakteryzuje się SLM oparta na ChCl/propano-1,3-diolu w stosunku molowym HBA do HBD 1:3. Wynika to z podobnych wartości przenikalności N_2 dla wszystkich SLM oraz relatywnie wysokich wartości przenikalności CO_2 w niskich temperaturach dla tego konkretnego układu. W wyższych temperaturach najlepszą selektywność CO_2/N_2 wykazuje membrana oparta na AcChCl/propano-1,3-diolu 1:3. Otrzymane zależności są wynikiem wpływu wielu czynników, zarówno zależnych od temperatury, jak i rodzaju DES – jego lepkości oraz zdolności sorpcyjnych względem azotu i ditlenku węgla oraz od wzajemnej relacji tych wielkości.

Otrzymane przeze mnie unieruchomione membrany ciekłe oparte o DES charakteryzowały się stabilnością. Pory użytych nośników wypełnione zostały DES w 100%, zaobserwowałem także tworzenie cienkiej warstwy cieczy na powierzchni membrany. Na podstawie obserwacji zachowania membran maksymalne ciśnienie robocze dla badanych SLM wynosi około 33 kPa. Przekroczenie tej wartości może skutkować potencjalnymi odkształceniami nośnika, które mogłyby spowodować zmiany w geometrii porów i ewentualne mechaniczne zerwanie membrany. Wstępne badania pęcznienia membran wykazały stosunkowo

niskie pęcznienie nośnika po nasyceniu DES (maks. 22% dla DES na bazie AChCl), co potwierdza stabilność badanych SLM. Dodatkowo, dostępne w literaturze [158] wartości liczbowe napięcia powierzchniowego dla DES opartych o ChCl i propano-1,2-diol lub propano-1,3-diol pozwoliły na obliczenie ciśnienia, które mogłoby doprowadzić do wypchnięcia DES z porów membrany. Obliczone wartości ciśnienia kapilarnego przekraczają wartość 3 barów, co znajduje się poza zakresem ciśnienia roboczego badanych membran.

5. Podsumowanie

Wyniki przeprowadzonych przeze mnie badań pozwoliły na sformułowanie następujących wniosków:

1. W cieczach głęboko eutektycznych opartych na aminoalkoholach największy wpływ na ilość i siłę oddziaływań wodorowych, powstających pomiędzy składnikami mieszanin, ma rzędowość aminoalkoholu. AP w porównaniu do MAE czy BAE tworzy słabsze, ale zdecydowanie bardziej liczne oddziaływania wodorowe z HBA, co znajduje odzwierciedlenie w największych wartościach gęstości, lepkości i współczynnika załamania światła DES opartych na tym HBD. DES zawierające drugorzędowe aminoalkohole, tj. MAE oraz BAE charakteryzuje różna relacja lepkości oraz gęstości i współczynnika załamania światła. Wyższa lepkość mieszanin opartych na BAE, obserwowana mimo ich mniej uporządkowanej struktury, jest wynikiem większych oporów związanych z poruszaniem się większych cząsteczek HBA/BAE w porównaniu do mniejszych HBA/MAE oraz silniejszych oddziaływań wodorowych. Większe wartości gęstości i współczynnika załamania światła mieszanin zawierających MAE wynikają z ich mniejszej „objętości swobodnej", powstającej na skutek liczniejszych oddziaływań wodorowych, prowadzących do większego upakowania DES.
2. Podobne efekty są odpowiedzialne za lepkość oraz gęstość i współczynnik załamania światła obserwowany dla DES opartych o TEAC i TBAC. DES zawierające TEAC, które tworzą silniejsze wiązania wodorowe i posiadają mniejszą „objętość swobodną" charakteryzują większe gęstości i współczynniki załamania światła. Większa lepkość mieszanin opartych na TBAC wynika z większego rozmiaru kationu TBA^+ w porównaniu do kationu TEA^+. Rodzaj anionu soli ma niewielki wpływ na strukturę DES. Mieszaniny zawierające TBAB i TBAC tworzą wiązania wodorowe z aminoalkoholami o podobnej mocy, a o większej wartości gęstości, lepkości i współczynnika załamania światła DES zawierających TBAB decyduje większa masa molowa i rozmiar anionu bromkowego.
3. Wraz ze wzrostem stężenia HBD maleje siła oddziaływań pomiędzy składnikami DES, co skutkuje spadkiem lepkości, gęstości i współczynnika załamania światła mieszanin.
4. Woda tworzy z cząsteczkami DES silne wiązania wodorowe, co prowadzi do osłabienia oddziaływań pomiędzy HBA i HBD mieszaniny. Jedynie w przypadku TBAB/MAE 1:6 dodatek niewielkiej ilości wody (do 10%mol.) wzmacnia strukturę DES. Ponadto, jak wynika, zarówno z analizy RDF uzyskanych za pomocą symulacji MD, jak i nadmiarowych objętości i ściśliwości molowych otrzymanych z pomiarów gęstości i prędkości dźwięku, oddziaływania pomiędzy cząsteczkami wody i cząsteczkami DES są mocniejsze niż pomiędzy cząsteczkami wody czy cząsteczkami DES.
5. Największy wpływ na rozpuszczalność ditlenku węgla w badanych mieszaninach eutektycznych ma rodzaj zastosowanego HBD. Rozpuszczalność CO_2 w DES opartych na aminoalkoholach jest zdecydowanie większa niż w mieszaninach zawierających glikole propylenowe, co wynika z różnego sposobu absorpcji. W DES opartych o aminoalkohole rozpuszczalność ditlenku węgla maleje w kolejności MAE > AP > BAE. Za najmniejszą

rozpuszczalność dla cieczy opartych na BAE odpowiadają najsilniejsze oddziaływania wodorowe pomiędzy między grupą aminową tego aminoalkoholu a anionem soli. Liczna sieć wiązań wodorowych powstająca w DES zawierającej AP jest również odpowiedzialna za słabszą dostępność grup aminowych w reakcji z CO_2 i w rezultacie za niższą rozpuszczalność CO_2 w porównaniu do mieszanin zawierających MAE. W przypadku DES opartych o glikole propylenowe większą rozpuszczalność ditlenku węgla wykazują mieszaniny zawierające propan-1,2-diol. Wynika to z tego, że bliższe położenie grup hydroksylowych w łańcuchu węglowym prowadzi do większej „objętości swobodnej" DES.

6. Wpływ anionu obecnego w cząsteczce HBA na rozpuszczalność CO_2 jest stosunkowo niewielki i zależy od jego oddziaływań z kationem. Im są one silniejsze tym dany DES słabiej oddziałuje z CO_2. W mieszaninach zawierających AP i MAE, TBA^+ tworzy silniejsze wiązania z Br^- niż z Cl^- i przekłada się to na niższe pojemności sorpcyjne DES zawierających TBAB w porównaniu do DES opartych na TBAC. W przypadku mieszanin zawierających BAE występuje odwrotna relacja.

Wraz z długością łańcucha alkilowego kationu HBA rosną oddziaływania pomiędzy składnikami w mieszaninie i skutkuje to niższą dostępnością oraz prawdopodobieństwem zajścia reakcji grupy aminowej z CO_2. Niezależnie od użytego donora wiązania wodorowego rozpuszczalność CO_2 w DES zawierających TBAC jest niższa niż w DES zawierających TEAC

7. W przeciwieństwie do cieczy głęboko eutektycznych absorbujących ditlenek węgla w sposób fizyczny, w DES opartych na aminoalkoholach rozpuszczalność CO_2 rośnie wraz ze wzrostem zawartości HBD. Jest to spowodowane osłabieniem wiązań pomiędzy składnikami DES, które prowadzi do większej rozpuszczalności CO_2. W przypadku cieczy głęboko eutektycznych absorbujących CO_2 w sposób fizyczny malejąca absorpcja diltenku węgla wraz ze wzrostem zawartości HBD wynika ze zmniejszenia się „objętości swobodnej". „Objętość swobodna" decyduje też o większej rozpuszczalności DES fizycznie absorbujących CO_2 zawierających HBA o dłuższych i bardziej symetrycznych łańcuchach alkilowych.

8. Ze względu na hydratację grup aminowych aminoalkoholi, nawet niewielka ilość wody w TBAB/AP 1:6 i TBAB/BAE 1:6 powoduje spadek ich zdolności sorpcyjnych. W przypadku TBAB/MAE 1:6 0,5% i 1% dodatek wody podwyższa rozpuszczalność CO_2, a spadek absorpcji gazu następuje dopiero przy zawartości H_2O równej 5%. Jest to efekt wzmacniania struktury oraz zmniejszenia oddziaływań grupy -NH tego DES z wodą, obserwowany przy niewielkich, tj. do około 1,9% ilościach wody.

9. Efektywność unieruchomionych membran ciekłych zawierających DES oparte na glikolach propylenowych zależy zarówno od lepkości, jak i zdolności sorpcyjnych mieszanin eutektycznych. Największą przenikalność CO_2 wykazała SLM oparta na TBAC/propano-1,2-diol 1:3, a najwyższą selektywność została osiągnięta dla SLM zawierającej ChCl/propano-1,3-diol. Ze względu na odwrotną zależność między lepkością a zdolnością absorpcji ditlenku węgla w tych mieszaninach można wnioskować, że niższa lepkość i większa rozpuszczalność CO_2 sprzyjają przenikalności, podczas gdy wyższa lepkość i mniejsza absorpcja gazu prowadzą do większej selektywności.

10. Uzyskane wartości rozpuszczalności ditlenku węgla w cieczach głęboko eutektycznych opartych na aminoalkoholach wskazują, że mieszaniny te mogą stanowić alternatywę dla tradycyjnie stosowanych roztworów amin. Jednak ich przydatność jako sorbentów ditlenku węgla w zastosowaniach przemysłowych wymaga dalszych badań, szczególnie w zakresie recyklingu oraz zapotrzebowania energetycznego procesu absorpcji. Z kolei badania nad zastosowaniem DES opartych na glikolach w unieruchomionych membranach ciekłych do separacji CO_2 mogłyby zostać rozszerzone o wyznaczenie rzeczywistej selektywności oraz o układy zawierające inne glikole niż propylenowe.

Spis dorobku naukowego

Publikacje

1) A. Panuszko, J. Stangret, **B. Nowosielski**, P. Bruździak, Interactions between hydration spheres of two different solutes in solution: The least squares fitting with constraints as a tool to determine water properties in ternary systems, J. Mol. Liq. 310 (2020) 113181. https://doi.org/10.1016/j.molliq.2020.11318.1 **IF_{2020}: 6,16, $MNSW_{2020}$: 100**

2) **B. Nowosielski,** M. Jamrógiewicz, J. Łuczak, M. Śmiechowski, D. Warmińska, Experimental and predicted physicochemical properties of monopropanolamine-based deep eutectic solvents, J. Mol. Liq. 309 (2020) 113110. https://doi.org/10.1016/j.molliq.2020.113110 **IF_{2020}: 6,16, $MNSW_{2020}$: 100**

3) I. Cichowska-Kopczyńska, D. Warmińska, **B. Nowosielski,** Solubility of carbon dioxide in deep eutectic solvents based on 3-amino-1-propanol and tetraalkylammonium salts at low pressure, Materials 14 (2021) 1–14. https://doi.org/10.3390/ma14030594. **IF_{2021}: 3,75, $MNSW_{2021}$: 140**

4) D. Warmińska, **B. Nowosielski**, A. Szewczyk, J. Ruszkowski, M. Prokopowicz, Effect of choline chloride based natural deep eutectic solvents on aqueous solubility and thermodynamic properties of acetaminophen, J. Mol. Liq. 323 (2021) 114834. https://doi.org/10.1016/j.molliq.2020.114834. **IF_{2020}: 6,63, $MNSW_{2020}$: 100**

5) **B. Nowosielski,** M. Jamrógiewicz, J. Łuczak, D. Warmińska, Novel Binary Mixtures of Alkanolamine Based Deep Eutectic Solvents with Water—Thermodynamic Calculation and Correlation of Crucial Physicochemical Properties, Molecules 27 (2022) 788. https://doi.org/10.3390/molecules27030788 **IF_{2022}: 4,6, $MNSW_{2022}$: 140**

6) I. Cichowska-Kopczyńska, **B. Nowosielski**, D. Warmińska, Deep Eutectic Solvents: Properties and Applications in CO_2 Separation, Molecules 28 (2023) 5293. https://doi.org/10.3390/molecules28145293. **IF_{2023}: 4,2, $MNSW_{2023}$: 140**

7) **B. Nowosielski,** M. Jamrógiewicz, J. Łuczak, A. Tercjak, D. Warmińska, Effect of temperature and composition on physical properties of deep eutectic solvents based on 2-(methylamino)ethanol – measurement and prediction, J. Mol. Liq. 371 (2023) 121069. https://doi.org/10.1016/j.molliq.2022.121069. **IF_{2023}: 5,3, $MNSW_{2023}$: 100**

8) **B. Nowosielski,** D. Warmińska, I. Cichowska-Kopczyńska, CO_2 Separation Using Supported Deep Eutectic Liquid Membranes Based on 1,2-propanediol, ACS Sustain. Chem. Eng. 11 (2023) 4093–4105. https://doi.org/10.1021/acssuschemeng.2c06278. **IF_{2023}: 7,1, $MNSW_{2023}$: 140**

9) **B. Nowosielski,** M. Jamrógiewicz, I. Cichowska-Kopczyńska, D. Warmińska, Comprehensive evaluation of physical properties and carbon dioxide capacities of new 2-(butylamino)ethanol-based deep eutectic solvents, Pure Appl. Chem. 96 (2024) 1733–1749. https://doi.org/10.1515/pac-2024-0228. **IF_{2023}: 1,8, $MNSW_{2023}$: 140**

Konferencje

1) **Nowosielski B**, Śmiechowski M, Łuczak J., Cichowska-Kopczyńska I., Warmińska D. : Ciecze głęboko eutektyczne oparte na 3-amino-1-propanolu – ich charakterystyka i zastosowanie do absorpcji CO_2 (2019), Zjazd Zimowy Sekcji Studenckiej PTChem, Gdańsk, Polska

2) **Nowosielski B**., Warmińska D. Cichowska-Kopczyńska I.: Supported Liquid Membranes Based On Deep Eutectic Solvents For Carbon Dioxide Separation (2021)// Material, Methods & Technologies, Burgas, Bułgaria

3) **Nowosielski B**, Cichowska-Kopczyńska I., Jamrógiewicz M, Łuczak J., Warmińska D. Wodne mieszaniny cieczy głęboko eutektycznych opartych o bromek tetrabutyloamoniowy – badania termodynamiczne i korelacja najważniejszych właściwości fizycznych (2021) XIV Kopernikańskie Seminarium Doktoranckie, Toruń, Polska

Pozostałe

1) Zespołowa Nagroda Naukowa Rektora (II stopnia) GUMED za lata 2022/2023 za *„Badania właściwości fizykochemicznych matryc polimerowych i łączników molekularnych z wykorzystaniem spektroskopii i technik termoanalitycznych."*

2) Członek Rady Szkoły Doktorskiej Politechniki Gdańskiej w latach 2020-2023

3) Członek Samorządu Doktorantów Politechniki Gdańskiej w latach 2020-2021

4) Stypendium *„Francium"* dla najlepszych doktorantów przyznawane przez Szkołę Doktorską Politechniki Gdańskiej 2021-2023

6. Bibliografia

[1] P. Pyykkö, Simple Estimates for Eutectic Behavior, ChemPhysChem. 20 (2019) 123–127. https://doi.org/10.1002/cphc.201800922.

[2] M.A.R. Martins, S.P. Pinho, J.A.P. Coutinho, Insights into the Nature of Eutectic and Deep Eutectic Mixtures, J. Solution Chem. 48 (2019) 962–982. https://doi.org/10.1007/s10953-018-0793-1.

[3] B.D. Like, C.E. Uhlenbrock, M.J. Panzer, A quantitative thermodynamic metric for identifying deep eutectic solvents, Phys. Chem. Chem. Phys. 25 (2023) 7946–7950. https://doi.org/10.1039/d3cp00555k.

[4] Y. Chen, Z. Yu, Low-melting mixture solvents: extension of deep eutectic solvents and ionic liquids for broadening green solvents and green chemistry, Green Chem. Eng. 5 (2024) 409–417. https://doi.org/10.1016/j.gce.2023.11.001.

[5] P.A. Shah, V. Chavda, D. Hirpara, V.S. Sharma, P.S. Shrivastav, S. Kumar, Exploring the potential of deep eutectic solvents in pharmaceuticals: Challenges and opportunities, J. Mol. Liq. 390 (2023) 123171. https://doi.org/10.1016/j.molliq.2023.123171.

[6] F.M. Perna, P. Vitale, V. Capriati, Deep eutectic solvents and their applications as green solvents, Curr. Opin. Green Sustain. Chem. 21 (2020) 27–33. https://doi.org/10.1016/j.cogsc.2019.09.004.

[7] Y. Elhamarnah, H. Qiblawey, M. Nasser, A review on Deep eutectic solvents as the emerging class of green solvents for membrane fabrication and separations, J. Mol. Liq. 398 (2024) 124250. https://doi.org/10.1016/j.molliq.2024.124250.

[8] Y. Marcus, Deep Eutectic Solvents, Springer International Publishing, 2019. https://doi.org/10.1007/978-3-030-00608-2.

[9] D.J.G.P. van Osch, L.F. Zubeir, A. van den Bruinhorst, M.A.A. Rocha, M.C. Kroon, Hydrophobic deep eutectic solvents as water-immiscible extractants, Green Chem. 17 (2015) 4518–4521. https://doi.org/10.1039/C5GC01451D.

[10] B.D. Ribeiro, C. Florindo, L.C. Iff, M.A.Z. Coelho, I.M. Marrucho, Menthol-based Eutectic Mixtures: Hydrophobic Low Viscosity Solvents, ACS Sustain. Chem. Eng. 3 (2015) 2469–2477. https://doi.org/10.1021/acssuschemeng.5b00532.

[11] S.E.E. Warrag, M.C. Kroon, Hydrophobic Deep Eutectic Solvents, in: Deep Eutectic Solvents, Wiley, 2019: pp. 83–93. https://doi.org/10.1002/9783527818488.ch5.

[12] C. Florindo, L.C. Branco, I.M. Marrucho, Development of hydrophobic deep eutectic solvents for extraction of pesticides from aqueous environments, Fluid Phase Equilib. 448 (2017) 135–142. https://doi.org/10.1016/j.fluid.2017.04.002.

[13] C.R. Müller, I. Meiners, P. Domínguez de María, Highly enantioselective tandem enzyme–organocatalyst crossed aldol reactions with acetaldehyde in deep-eutectic-solvents, RSC Adv. 4 (2014) 46097–46101. https://doi.org/10.1039/C4RA09307K.

[14] E. Massolo, S. Palmieri, M. Benaglia, V. Capriati, F.M. Perna, Stereoselective organocatalysed reactions in deep eutectic solvents: highly tunable and biorenewable reaction media for sustainable organic synthesis, Green Chem. 18 (2016) 792–797.

https://doi.org/10.1039/C5GC01855B.

[15] Z.-H. Zhang, X.-N. Zhang, L.-P. Mo, Y.-X. Li, F.-P. Ma, Catalyst-free synthesis of quinazoline derivatives using low melting sugar–urea–salt mixture as a solvent, Green Chem. 14 (2012) 1502. https://doi.org/10.1039/c2gc35258c.

[16] F.M. Perna, P. Vitale, V. Capriati, Organic Synthesis in DESs, in: Deep Eutectic Solvents, Wiley, 2019: pp. 111–134. https://doi.org/10.1002/9783527818488.ch7.

[17] N. Azizi, M. Edrisi, Deep eutectic solvent immobilized on SBA-15 as a novel separable catalyst for one-pot three-component Mannich reaction, Microporous Mesoporous Mater. 240 (2017) 130–136. https://doi.org/10.1016/j.micromeso.2016.11.009.

[18] S. Gore, S. Baskaran, B. Koenig, Efficient synthesis of 3,4-dihydropyrimidin-2-ones in low melting tartaric acid–urea mixtures, Green Chem. 13 (2011) 1009. https://doi.org/10.1039/c1gc00009h.

[19] N. Azizi, S. Dezfooli, M. Khajeh, M.M. Hashemi, Efficient deep eutectic solvents catalyzed synthesis of pyran and benzopyran derivatives, J. Mol. Liq. 186 (2013) 76–80. https://doi.org/10.1016/j.molliq.2013.05.011.

[20] J. Yin, J. Wang, Z. Li, D. Li, G. Yang, Y. Cui, A. Wang, C. Li, Deep desulfurization of fuels based on an oxidation/extraction process with acidic deep eutectic solvents, Green Chem. 17 (2015) 4552–4559. https://doi.org/10.1039/C5GC00709G.

[21] L. Hao, M. Wang, W. Shan, C. Deng, W. Ren, Z. Shi, H. Lū, L-proline-based deep eutectic solvents (DESs) for deep catalytic oxidative desulfurization (ODS) of diesel, J. Hazard. Mater. 339 (2017) 216–222. https://doi.org/10.1016/j.jhazmat.2017.06.050.

[22] A. Hayyan, M.A. Hashim, M. Hayyan, F.S. Mjalli, I.M. AlNashef, A new processing route for cleaner production of biodiesel fuel using a choline chloride based deep eutectic solvent, J. Clean. Prod. 65 (2014) 246–251. https://doi.org/10.1016/j.jclepro.2013.08.031.

[23] Q. Wang, X. Yao, Y. Geng, Q. Zhou, X. Lu, S. Zhang, Deep eutectic solvents as highly active catalysts for the fast and mild glycolysis of poly(ethylene terephthalate)(PET), Green Chem. 17 (2015) 2473–2479. https://doi.org/10.1039/C4GC02401J.

[24] A. Al-Bodour, N. Alomari, A. Gutiérrez, S. Aparicio, M. Atilhan, Exploring the thermophysical properties of natural deep eutectic solvents for gas capture applications: a comprehensive review, Green Chem. Eng. 5 (2024) 307–338. https://doi.org/10.1016/j.gce.2023.09.003.

[25] A.P.R. Santana, J.A. Mora-Vargas, T.G.S. Guimarães, C.D.B. Amaral, A. Oliveira, M.H. Gonzalez, Sustainable synthesis of natural deep eutectic solvents (NADES) by different methods, J. Mol. Liq. 293 (2019). https://doi.org/10.1016/j.molliq.2019.111452.

[26] L. Meneses, F. Santos, A.R. Gameiro, A. Paiva, A.R.C. Duarte, Preparation of binary and ternary deep eutectic systems, J. Vis. Exp. 2019 (2019). https://doi.org/10.3791/60326.

[27] Q. Zhang, K. De Oliveira Vigier, S. Royer, F. Jérôme, Deep eutectic solvents: Syntheses, properties and applications, Chem. Soc. Rev. 41 (2012) 7108–7146. https://doi.org/10.1039/c2cs35178a.

[28] K.A. Omar, R. Sadeghi, Novel Nonanol-Based deep eutectic solvents: Thermophysical

properties and their applications in Liquid-Liquid extraction and amino acid detection, J. Mol. Liq. 336 (2021) 116359. https://doi.org/10.1016/j.molliq.2021.116359.

[29] J.L. Trenzado, C. Benito, M. Atilhan, S. Aparicio, Hydrophobic Deep eutectic Solvents based on cineole and organic acids, J. Mol. Liq. 377 (2023) 121322. https://doi.org/10.1016/j.molliq.2023.121322.

[30] S. Seki, S. Tsuzuki, K. Hayamizu, Y. Umebayashi, N. Serizawa, K. Takei, H. Miyashiro, Comprehensive refractive index property for room-temperature ionic liquids, J. Chem. Eng. Data. 57 (2012) 2211–2216. https://doi.org/10.1021/je201289w.

[31] C. Florindo, M.M. Oliveira, L.C. Branco, I.M. Marrucho, Carbohydrates-based deep eutectic solvents: Thermophysical properties and rice straw dissolution, J. Mol. Liq. 247 (2017) 441–447. https://doi.org/10.1016/j.molliq.2017.09.026.

[32] F.S. Mjalli, R. Al-Hajri, A. Al-Muhtaseb, O. Ahmed, M. Nagaraju, Novel amino acid-based ionic liquid analogues: neutral hydroxylic and sulfur-containing amino acids, Asia-Pacific J. Chem. Eng. 11 (2016) 683–694. https://doi.org/10.1002/apj.1995.

[33] W.J. Jiang, F.Y. Zhong, L. Sen Zhou, H.L. Peng, J.P. Fan, K. Huang, Chemical dual-site capture of NH3 by unprecedentedly low-viscosity deep eutectic solvents, Chem. Commun. 56 (2020) 2399–2402. https://doi.org/10.1039/c9cc09043f.

[34] S. Sarmad, Y. Xie, J.P. Mikkola, X. Ji, Screening of deep eutectic solvents (DESs) as green CO2 sorbents: from solubility to viscosity, New J. Chem. 41 (2016) 290–301. https://doi.org/10.1039/c6nj03140d.

[35] B.B. Hansen, S. Spittle, B. Chen, D. Poe, Y. Zhang, J.M. Klein, A. Horton, L. Adhikari, T. Zelovich, B.W. Doherty, B. Gurkan, E.J. Maginn, A. Ragauskas, M. Dadmun, T.A. Zawodzinski, G.A. Baker, M.E. Tuckerman, R.F. Savinell, J.R. Sangoro, Deep Eutectic Solvents: A Review of Fundamentals and Applications, Chem. Rev. 121 (2021) 1232–1285. https://doi.org/10.1021/acs.chemrev.0c00385.

[36] C. Florindo, F.S. Oliveira, L.P.N.N. Rebelo, A.M. Fernandes, I.M. Marrucho, Insights into the synthesis and properties of deep eutectic solvents based on cholinium chloride and carboxylic acids, ACS Sustain. Chem. Eng. 2 (2014) 2416–2425. https://doi.org/10.1021/sc500439w.

[37] F. Yang, Q. Zheng, H. Tan, X. Wang, Insight into the role of hydrogen bond donor in deep eutectic solvents, J. Mol. Liq. 399 (2024) 124332. https://doi.org/10.1016/j.molliq.2024.124332.

[38] Y. Wang, Y. Hou, W. Wu, D. Liu, Y. Ji, S. Ren, Roles of a hydrogen bond donor and a hydrogen bond acceptor in the extraction of toluene from: N -heptane using deep eutectic solvents, Green Chem. 18 (2016) 3089–3097. https://doi.org/10.1039/c5gc02909k.

[39] M.N. Amira, M.D. Irfan Hatim, N. Jullok, M. Syahmie Rasidi, H.R. Alamery, Synthesis and Preparation of Asymmetric PVDF-co-PTFE/DES Supported Membrane for CO2/N2 Separation, IOP Conf. Ser. Mater. Sci. Eng. 429 (2018). https://doi.org/10.1088/1757-899X/429/1/012067.

[40] K. Shahbaz, S. Baroutian, F.S. Mjalli, M.A. Hashim, I.M. Alnashef, Densities of ammonium

and phosphonium based deep eutectic solvents: Prediction using artificial intelligence and group contribution techniques, Thermochim. Acta. 527 (2012) 59–66. https://doi.org/10.1016/j.tca.2011.10.010.

[41] Y. Zuo, M. Hong, R. Zhang, J. Tong, Physical properties of deep eutectic solvents with efficient nitrogen removal capability, J. Mol. Liq. 394 (2024) 123715. https://doi.org/10.1016/j.molliq.2023.123715.

[42] A. Basaiahgari, S. Panda, R.L. Gardas, Effect of Ethylene, Diethylene, and Triethylene Glycols and Glycerol on the Physicochemical Properties and Phase Behavior of Benzyltrimethyl and Benzyltributylammonium Chloride Based Deep Eutectic Solvents at 283.15-343.15 K, J. Chem. Eng. Data. 63 (2018) 2613–2627. https://doi.org/10.1021/acs.jced.8b00213.

[43] F.S. Mjalli, G. Vakili-Nezhaad, K. Shahbaz, I.M. Alnashef, Application of the Eötvos and Guggenheim empirical rules for predicting the density and surface tension of ionic liquids analogues, Thermochim. Acta. 575 (2014) 40–44. https://doi.org/10.1016/j.tca.2013.10.017.

[44] K. Singh, R.P. Shibu, S. Mehra, A. Kumar, Insights into the physicochemical properties of newly synthesized benzyl triethylammonium chloride-based deep eutectic solvents, J. Mol. Liq. 386 (2023) 122589. https://doi.org/10.1016/j.molliq.2023.122589.

[45] Y. Hou, B. Zhang, M. Gao, S. Ren, W. Wu, Densities, viscosities and specific heat capacities of deep eutectic solvents composed of ethanediol + betaine and ethanediol + L-carnitine for absorbing SO2, J. Chem. Thermodyn. 179 (2023) 106999. https://doi.org/10.1016/j.jct.2022.106999.

[46] V.P. Cotroneo-Figueroa, N.F. Gajardo-Parra, P. López-Porfiri, Á. Leiva, M. Gonzalez-Miquel, J.M. Garrido, R.I. Canales, Hydrogen bond donor and alcohol chain length effect on the physicochemical properties of choline chloride based deep eutectic solvents mixed with alcohols, J. Mol. Liq. 345 (2022) 116986. https://doi.org/10.1016/j.molliq.2021.116986.

[47] K.A. Omar, R. Sadeghi, New chloroacetic acid-based deep eutectic solvents for solubilizing metal oxides, J. Mol. Liq. 347 (2022) 118393. https://doi.org/10.1016/j.molliq.2021.118393.

[48] F.S. Mjalli, G. Murshid, S. Al-Zakwani, A. Hayyan, Monoethanolamine-based deep eutectic solvents, their synthesis and characterization, Fluid Phase Equilib. 448 (2017) 30–40. https://doi.org/10.1016/j.fluid.2017.03.008.

[49] M. Lu, G. Han, Y. Jiang, X. Zhang, D. Deng, N. Ai, Solubilities of carbon dioxide in the eutectic mixture of levulinic acid (or furfuryl alcohol) and choline chloride, J. Chem. Thermodyn. 88 (2015) 72–77. https://doi.org/10.1016/j.jct.2015.04.021.

[50] A.P. Abbott, R.C. Harris, K.S. Ryder, C. D'Agostino, L.F. Gladden, M.D. Mantle, Glycerol eutectics as sustainable solvent systems, Green Chem. 13 (2011) 82–90. https://doi.org/10.1039/c0gc00395f.

[51] K.A. Omar, R. Sadeghi, Database of deep eutectic solvents and their physical properties:

A review, J. Mol. Liq. 384 (2023) 121899. https://doi.org/10.1016/j.molliq.2023.121899.

[52] X. Song, J. Yuan, C. Yang, G. Deng, Z. Wang, J. Gao, Carbon dioxide separation performance evaluation of amine-based versus choline-based deep eutectic solvents, Renew. Sustain. Energy Rev. 184 (2023) 113499. https://doi.org/10.1016/j.rser.2023.113499.

[53] K.R. Siongco, R.B. Leron, M.-H.H. Li, Densities, refractive indices, and viscosities of N,N-diethylethanol ammonium chloride–glycerol or –ethylene glycol deep eutectic solvents and their aqueous solutions, J. Chem. Thermodyn. 65 (2013) 65–72. https://doi.org/10.1016/j.jct.2013.05.041.

[54] P.B. Sánchez, B. González, J. Salgado, J. José Parajó, Á. Domínguez, Physical properties of seven deep eutectic solvents based on L-proline or betaine, J. Chem. Thermodyn. 131 (2019) 517–523. https://doi.org/10.1016/j.jct.2018.12.017.

[55] M.A. Sedghamiz, S. Raeissi, Physical properties of deep eutectic solvents formed by the sodium halide salts and ethylene glycol, and their mixtures with water, J. Mol. Liq. 269 (2018) 694–702. https://doi.org/10.1016/j.molliq.2018.08.045.

[56] N.F. Gajardo-Parra, M.J. Lubben, J.M. Winnert, Á. Leiva, J.F. Brennecke, R.I. Canales, Physicochemical properties of choline chloride-based deep eutectic solvents and excess properties of their pseudo-binary mixtures with 1-butanol, J. Chem. Thermodyn. 133 (2019) 272–284. https://doi.org/10.1016/j.jct.2019.02.010.

[57] D. Lapeña, L. Lomba, M. Artal, C. Lafuente, B. Giner, Thermophysical characterization of the deep eutectic solvent choline chloride:ethylene glycol and one of its mixtures with water, Fluid Phase Equilib. 492 (2019) 1–9. https://doi.org/10.1016/j.fluid.2019.03.018.

[58] K. Shahbaz, F.S. Mjalli, M.A. Hashim, I.M. Alnashef, Prediction of deep eutectic solvents densities at different temperatures, Thermochim. Acta. 515 (2011) 67–72. https://doi.org/10.1016/j.tca.2010.12.022.

[59] N.R. Mirza, N.J. Nicholas, Y. Wu, S. Kentish, G.W. Stevens, Estimation of Normal Boiling Temperatures, Critical Properties, and Acentric Factors of Deep Eutectic Solvents, J. Chem. Eng. Data. 60 (2015) 1844–1854. https://doi.org/10.1021/acs.jced.5b00046.

[60] M. Taherzadeh, R. Haghbakhsh, A.R.C. Duarte, S. Raeissi, Generalized Model to Estimate the Refractive Indices of Deep Eutectic Solvents, J. Chem. Eng. Data. 65 (2020) 3965–3976. https://doi.org/10.1021/acs.jced.0c00308.

[61] A. Bakhtyari, R. Haghbakhsh, A.R.C. Duarte, S. Raeissi, A simple model for the viscosities of deep eutectic solvents, Fluid Phase Equilib. 521 (2020) 112662. https://doi.org/10.1016/j.fluid.2020.112662.

[62] C.F. Spencer, R.P. Danner, Improved Equation for Prediction of Saturated Liquid Density, J. Chem. Eng. Data. 17 (1972) 236–241. https://doi.org/10.1021/je60053a012.

[63] F.S. Mjalli, K. Shahbaz, I.M. AlNashef, Modified Rackett equation for modelling the molar volume of deep eutectic solvents, Thermochim. Acta. 614 (2015) 185–190. https://doi.org/10.1016/j.tca.2015.06.026.

[64] R. Haghbakhsh, R. Bardool, A. Bakhtyari, A.R.C. Duarte, S. Raeissi, Simple and global

correlation for the densities of deep eutectic solvents, J. Mol. Liq. 296 (2019) 111830. https://doi.org/10.1016/j.molliq.2019.111830.

[65] H.G. Rackett, Equation of State for Saturated Liquids, J. Chem. Eng. Data. 15 (1970) 514–517. https://doi.org/10.1021/je60047a012.

[66] R. Haghbakhsh, S. Raeissi, A.R.C. Duarte, Group contribution and atomic contribution models for the prediction of various physical properties of deep eutectic solvents, Sci. Rep. 11 (2021) 6684. https://doi.org/10.1038/s41598-021-85824-z.

[67] K. Shahbaz, F.S.G. Bagh, F.S. Mjalli, I.M. AlNashef, M.A. Hashim, Prediction of refractive index and density of deep eutectic solvents using atomic contributions, Fluid Phase Equilib. 354 (2013) 304–311. https://doi.org/10.1016/j.fluid.2013.06.050.

[68] A. Khajeh, K. Parvaneh, M. Shakourian-Fard, Refractive index prediction of deep eutectic solvents by molecular approaches, J. Mol. Liq. 332 (2021) 115843. https://doi.org/10.1016/j.molliq.2021.115843.

[69] X.-J. Hou, L.-Y. Yu, Y.-X. Wang, K.-J. Wu, C.-H. He, Comprehensive Prediction of Densities for Deep Eutectic Solvents: A New Bonding-Group Interaction Contribution Scheme, Ind. Eng. Chem. Res. 60 (2021) 13127–13139. https://doi.org/10.1021/acs.iecr.1c02260.

[70] F.S. Mjalli, Mass connectivity index-based density prediction of deep eutectic solvents, Fluid Phase Equilib. 409 (2016) 312–317. https://doi.org/10.1016/j.fluid.2015.09.053.

[71] C. Velez, O. Acevedo, Simulation of deep eutectic solvents: Progress to promises, WIREs Comput. Mol. Sci. 12 (2022). https://doi.org/10.1002/wcms.1598.

[72] W.L. Jorgensen, D.S. Maxwell, J. Tirado-Rives, Development and testing of the OPLS all-atom force field on conformational energetics and properties of organic liquids, J. Am. Chem. Soc. 118 (1996) 11225–11236. https://doi.org/10.1021/ja9621760.

[73] G. Kaminski, E.M. Duffy, T. Matsui, W.L. Jorgensen, Free energies of hydration and pure liquid properties of hydrocarbons from the OPLS all-atom model, J. Phys. Chem. 98 (1994) 13077–13802. https://doi.org/10.1021/j100100a043.

[74] D. Chandler, Introduction to Modern Statistical Mechanics, 1st ed., Oxford University Press, 1987.

[75] H. Sun, Y. Li, X. Wu, G. Li, Theoretical study on the structures and properties of mixtures of urea and choline chloride, J. Mol. Model. 19 (2013) 2433–2441. https://doi.org/10.1007/s00894-013-1791-2.

[76] A.T. Celebi, N. Dawass, O.A. Moultos, T.J.H. Vlugt, How sensitive are physical properties of choline chloride–urea mixtures to composition changes: Molecular dynamics simulations and Kirkwood–Buff theory, J. Chem. Phys. 154 (2021). https://doi.org/10.1063/5.0049064.

[77] S. Barani Pour, J. Jahanbin Sardroodi, A. Rastkar Ebrahimzadeh, The study of structure and interactions of glucose-based natural deep eutectic solvents by molecular dynamics simulation, J. Mol. Liq. 334 (2021) 115956. https://doi.org/10.1016/j.molliq.2021.115956.

[78] P.K. Naik, S. Paul, T. Banerjee, Physiochemical Properties and Molecular Dynamics

Simulations of Phosphonium and Ammonium Based Deep Eutectic Solvents, J. Solution Chem. 48 (2019) 1046–1065. https://doi.org/10.1007/s10953-019-00903-0.

[79] S. Shokri, N. Ebrahimi, R. Sadeghi, Theoretical and experimental study of molecular interactions between constituents of deep eutectic solvents, Fluid Phase Equilib. 583 (2024) 114121. https://doi.org/10.1016/j.fluid.2024.114121.

[80] V. Migliorati, F. Sessa, P. D'Angelo, Deep eutectic solvents: A structural point of view on the role of the cation, Chem. Phys. Lett. X. 2 (2019). https://doi.org/10.1016/j.cpletx.2018.100001.

[81] K. Cheng, X. Xu, J. Song, Y. Chen, Z. Kan, C. Li, Molecular dynamics simulations of choline chloride and ascorbic acid deep eutectic solvents: Investigation of structural and dynamics properties, J. Mol. Graph. Model. 130 (2024) 108784. https://doi.org/10.1016/j.jmgm.2024.108784.

[82] S. Rozas, N. Alomari, M. Atilhan, S. Aparicio, Theoretical insights into the cineole-based deep eutectic solvents, J. Chem. Phys. 154 (2021) 184504. https://doi.org/10.1063/5.0048369.

[83] E.S.C. Ferreira, I. V. Voroshylova, C.M. Pereira, M.N. D. S. Cordeiro, Improved Force Field Model for the Deep Eutectic Solvent Ethaline: Reliable Physicochemical Properties, J. Phys. Chem. B. 120 (2016) 10124–10137. https://doi.org/10.1021/acs.jpcb.6b07233.

[84] D. Kussainova, D. Shah, Structure of monoethanolamine based type III DESs: Insights from molecular dynamics simulations, Fluid Phase Equilib. 482 (2019) 112–117. https://doi.org/10.1016/j.fluid.2018.11.017.

[85] E.S.C. Ferreira, I. V. Voroshylova, N.M. Figueiredo, C.M. Pereira, M.N.D.S. Cordeiro, Computational and experimental study of propeline: A choline chloride based deep eutectic solvent, J. Mol. Liq. 298 (2020). https://doi.org/10.1016/j.molliq.2019.111978.

[86] G. Garcia, S. Aparicio, R. Ullah, M. Atilhan, Deep eutectic solvents: Physicochemical properties and gas separation applications, Energy and Fuels. 29 (2015) 2616–2644. https://doi.org/10.1021/ef5028873.

[87] C. Ma, A. Laaksonen, C. Liu, X. Lu, X. Ji, The peculiar effect of water on ionic liquids and deep eutectic solvents, Chem. Soc. Rev. 47 (2018) 8685–8720. https://doi.org/10.1039/c8cs00325d.

[88] J.Y. Seyf, F. Zarei, Density, Viscosity, and Refractive Index of a Choline Chloride + <scp>d</scp> -(−)-Fructose Deep Eutectic Solvent + Water Mixture at Different Temperatures: An Experimental Study and Thermodynamic Modeling, J. Chem. Eng. Data. 67 (2022) 3007–3021. https://doi.org/10.1021/acs.jced.2c00440.

[89] R.B. Leron, A.N. Soriano, M.H. Li, Densities and refractive indices of the deep eutectic solvents (choline chloride+ethylene glycol or glycerol) and their aqueous mixtures at the temperature ranging from 298.15 to 333.15K, J. Taiwan Inst. Chem. Eng. 43 (2012) 551–557. https://doi.org/10.1016/j.jtice.2012.01.007.

[90] A. Yadav, J.R. Kar, M. Verma, S. Naqvi, S. Pandey, Densities of aqueous mixtures of (choline chloride + ethylene glycol) and (choline chloride + malonic acid) deep eutectic

solvents in temperature range 283.15–363.15 K, Thermochim. Acta. 600 (2015) 95–101. https://doi.org/10.1016/j.tca.2014.11.028.

[91] H. Shekaari, M.T. Zafarani-Moattar, M. Mokhtarpour, S. Faraji, Volumetric and compressibility properties for aqueous solutions of choline chloride based deep eutectic solvents and Prigogine–Flory–Patterson theory to correlate of excess molar volumes at T = (293.15 to 308.15) K, J. Mol. Liq. 289 (2019) 111077. https://doi.org/10.1016/j.molliq.2019.111077.

[92] M. Kuddushi, G.S. Nangala, S. Rajput, S.P. Ijardar, N.I. Malek, Understanding the peculiar effect of water on the physicochemical properties of choline chloride based deep eutectic solvents theoretically and experimentally, J. Mol. Liq. 278 (2019) 607–615. https://doi.org/10.1016/j.molliq.2019.01.053.

[93] R.B. Leron, M.H. Li, High-pressure density measurements for choline chloride: Urea deep eutectic solvent and its aqueous mixtures at T = (298.15 to 323.15) K and up to 50 MPa, J. Chem. Thermodyn. 54 (2012) 293–301. https://doi.org/10.1016/j.jct.2012.05.008.

[94] A.K. Kumar, E. Shah, A. Patel, S. Sharma, G. Dixit, Physico-chemical characterization and evaluation of neat and aqueous mixtures of choline chloride + lactic acid for lignocellulosic biomass fractionation, enzymatic hydrolysis and fermentation, J. Mol. Liq. 271 (2018) 540–549. https://doi.org/10.1016/j.molliq.2018.09.032.

[95] A. Zarghampour, P. Jafari, E. Rahimpour, A. Jouyban, Thermodynamic investigation on the aqueous mixtures of choline chloride/propylene glycol deep eutectic solvent at T = (293.15 to 313.15) K, BMC Chem. 18 (2024) 51. https://doi.org/10.1186/s13065-024-01153-y.

[96] Y. Zuo, X. Chen, N. Wei, J. Tong, Effect of water or ethanol on the excess properties of deep eutectic solvents (tetrabutylammonium bromide + formic acid/propionic acid), J. Mol. Liq. 383 (2023) 122034. https://doi.org/10.1016/j.molliq.2023.122034.

[97] D. Shah, F.S. Mjalli, Effect of water on the thermo-physical properties of Reline: An experimental and molecular simulation based approach, Phys. Chem. Chem. Phys. 16 (2014) 23900–23907. https://doi.org/10.1039/c4cp02600d.

[98] E.O. Fetisov, D.B. Harwood, I.F.W. Kuo, S.E.E. Warrag, M.C. Kroon, C.J. Peters, J.I. Siepmann, First-Principles Molecular Dynamics Study of a Deep Eutectic Solvent: Choline Chloride/Urea and Its Mixture with Water, J. Phys. Chem. B. 122 (2018) 1245–1254. https://doi.org/10.1021/acs.jpcb.7b10422.

[99] T. Zhekenov, N. Toksanbayev, Z. Kazakbayeva, D. Shah, F.S. Mjalli, Formation of type III Deep Eutectic Solvents and effect of water on their intermolecular interactions, Fluid Phase Equilib. 441 (2017) 43–48. https://doi.org/10.1016/j.fluid.2017.01.022.

[100] P. Kumari, Shobhna, S. Kaur, H.K. Kashyap, Influence of Hydration on the Structure of Reline Deep Eutectic Solvent: A Molecular Dynamics Study, ACS Omega. 3 (2018) 15246–15255. https://doi.org/10.1021/acsomega.8b02447.

[101] L. Sapir, D. Harries, Restructuring a Deep Eutectic Solvent by Water: The Nanostructure of Hydrated Choline Chloride/Urea, J. Chem. Theory Comput. 16 (2020) 3335–3342.

https://doi.org/10.1021/acs.jctc.0c00120.

[102] H. Monteiro, A. Paiva, A.R.C. Duarte, N. Galamba, On the not so anomalous water-induced structural transformations of choline chloride–urea (reline) deep eutectic system, Phys. Chem. Chem. Phys. 25 (2023) 439–454. https://doi.org/10.1039/D2CP04139A.

[103] Q. Gao, Y. Zhu, X. Ji, W. Zhu, L. Lu, X. Lu, Effect of water concentration on the microstructures of choline chloride/urea (1:2) /water mixture, Fluid Phase Equilib. 470 (2018) 134–139. https://doi.org/10.1016/j.fluid.2018.01.031.

[104] S. Barani Pour, M. Dabbagh Hosseini pour, J. Jahanbin Sardroodi, A. Rastkar Ebrahimzadeh, G. Pazuki, Effect of water addition on caprylic acid: Quaternary ammonium salts (QAS) deep eutectic solvents: Characterization of their structural and dynamical properties, J. Mol. Graph. Model. 125 (2023) 108561. https://doi.org/10.1016/j.jmgm.2023.108561.

[105] X. Li, M. Hou, B. Han, X. Wang, L. Zou, Solubility of CO2 in a choline chloride + urea eutectic mixture, J. Chem. Eng. Data. 53 (2008) 548–550. https://doi.org/10.1021/je700638u.

[106] Z. Li, L. Wang, C. Li, Y. Cui, S. Li, G. Yang, Y. Shen, Absorption of Carbon Dioxide Using Ethanolamine-Based Deep Eutectic Solvents, ACS Sustain. Chem. Eng. 7 (2019) 10403–10414. https://doi.org/10.1021/acssuschemeng.9b00555.

[107] M.B. Haider, R. Kumar, Solubility of CO2 and CH4 in sterically hindered amine-based deep eutectic solvents, Sep. Purif. Technol. 248 (2020). https://doi.org/10.1016/j.seppur.2020.117055.

[108] M.B. Haider, D. Jha, B. Marriyappan Sivagnanam, R. Kumar, Thermodynamic and Kinetic Studies of CO2 Capture by Glycol and Amine-Based Deep Eutectic Solvents, J. Chem. Eng. Data. 63 (2018) 2671–2680. https://doi.org/10.1021/acs.jced.8b00015.

[109] X. Liu, B. Gao, Y. Jiang, N. Ai, D. Deng, Solubilities and Thermodynamic Properties of Carbon Dioxide in Guaiacol-Based Deep Eutectic Solvents, J. Chem. Eng. Data. 62 (2017) 1448–1455. https://doi.org/10.1021/acs.jced.6b01013.

[110] T. Altamash, M.S. Nasser, Y. Elhamarnah, M. Magzoub, R. Ullah, H. Qiblawey, S. Aparicio, M. Atilhan, Gas solubility and rheological behavior study of betaine and alanine based natural deep eutectic solvents (NADES), J. Mol. Liq. 256 (2018) 286–295. https://doi.org/10.1016/j.molliq.2018.02.049.

[111] Y. Chen, N. Ai, G. Li, H. Shan, Y. Cui, D. Deng, Solubilities of carbon dioxide in eutectic mixtures of choline chloride and dihydric alcohols, J. Chem. Eng. Data. 59 (2014) 1247–1253. https://doi.org/10.1021/je400884v.

[112] K.A. Pishro, G. Murshid, F.S. Mjalli, J. Naser, Investigation of CO2 solubility in monoethanolamine hydrochloride based deep eutectic solvents and physical properties measurements, Chinese J. Chem. Eng. 28 (2020) 2848–2856. https://doi.org/10.1016/j.cjche.2020.07.004.

[113] G. Li, D. Deng, Y. Chen, H. Shan, N. Ai, Solubilities and thermodynamic properties of CO2 in choline-chloride based deep eutectic solvents, J. Chem. Thermodyn. 75 (2014) 58–62.

https://doi.org/10.1016/j.jct.2014.04.012.

[114] E. Ali, M.K. Hadj-Kali, S. Mulyono, I. Alnashef, A. Fakeeha, F. Mjalli, A. Hayyan, Solubility of CO2 in deep eutectic solvents: Experiments and modelling using the Peng-Robinson equation of state, Chem. Eng. Res. Des. 92 (2014) 1898–1906. https://doi.org/10.1016/j.cherd.2014.02.004.

[115] D. Deng, Y. Jiang, X. Liu, Z. Zhang, N. Ai, Investigation of solubilities of carbon dioxide in five levulinic acid-based deep eutectic solvents and their thermodynamic properties, J. Chem. Thermodyn. 103 (2016) 212–217. https://doi.org/10.1016/j.jct.2016.08.015.

[116] L.F. Zubeir, D.J.G.P. Van Osch, M.A.A. Rocha, F. Banat, M.C. Kroon, Carbon Dioxide Solubilities in Decanoic Acid-Based Hydrophobic Deep Eutectic Solvents, J. Chem. Eng. Data. 63 (2018) 913–919. https://doi.org/10.1021/acs.jced.7b00534.

[117] W.C. Su, D.S.H. Wong, M.H. Li, Effect of water on solubility of carbon dioxide in (aminomethanamide + 2-hydroxy-N,N,N-trimethylethanaminium chloride), J. Chem. Eng. Data. 54 (2009) 1951–1955. https://doi.org/10.1021/je900078k.

[118] Y. Xie, H. Dong, S. Zhang, X. Lu, X. Ji, Effect of water on the density, viscosity, and CO2 solubility in choline chloride/urea, J. Chem. Eng. Data. 59 (2014) 3344–3352. https://doi.org/10.1021/je500320c.

[119] T.J. Trivedi, J.H. Lee, H.J. Lee, Y.K. Jeong, J.W. Choi, Deep eutectic solvents as attractive media for CO2 capture, Green Chem. 18 (2016) 2834–2842. https://doi.org/10.1039/c5gc02319j.

[120] S.K. Shukla, J.P. Mikkola, Intermolecular interactions upon carbon dioxide capture in deep-eutectic solvents, Phys. Chem. Chem. Phys. 20 (2018) 24591–24601. https://doi.org/10.1039/c8cp03724h.

[121] P. Scharlin, IUPAC-NIST Solubility Data Series. 62. Carbon dioxide in water and aqueous electrolyte solutions, 1996. https://iupac.github.io/SolubilityDataSeries/volumes/SDS-62.pdf.

[122] J.G.H. Wijmans, R.W. Baker, The Solution-Diffusion Model: A Unified Approach to Membrane Permeation, Mater. Sci. Membr. Gas Vap. Sep. (2006) 159–189. https://doi.org/10.1002/047002903X.ch5.

[123] M.S. Manna, P. Saha, A.K. Ghoshal, Studies on the stability of a supported liquid membrane and its cleaning protocol, RSC Adv. 5 (2015) 71999–72008. https://doi.org/10.1039/C5RA11897B.

[124] A.J.B. Kemperman*, D. Bargeman, T. Van Den Boomgaard, H. Strathmann, Stability of Supported Liquid Membranes: State of the Art, Sep. Sci. Technol. 31 (1996) 2733–2762. https://doi.org/10.1080/01496399608000824.

[125] P.K. Parhi, Supported Liquid Membrane Principle and Its Practices: A Short Review, J. Chem. 2013 (2013) 1–11. https://doi.org/10.1155/2013/618236.

[126] H. Takeuchi, K. Takahashi, W. Goto, Some observations on the stability of supported liquid membranes, J. Memb. Sci. 34 (1987) 19–31. https://doi.org/10.1016/S0376-7388(00)80018-6.

[127] L. Bao, M.C. Trachtenberg, Facilitated transport of CO2 across a liquid membrane: Comparing enzyme, amine, and alkaline, J. Memb. Sci. 280 (2006) 330–334. https://doi.org/10.1016/j.memsci.2006.01.036.

[128] H. Ohno, M. Yoshizawa-Fujita, Y. Kohno, Functional design of ionic liquids: Unprecedented liquids that contribute to energy technology, bioscience, and materials sciences, Bull. Chem. Soc. Jpn. 92 (2019) 852–868. https://doi.org/10.1246/bcsj.20180401.

[129] M.J. Trujillo-Rodríguez, H. Nan, M. Varona, M.N. Emaus, I.D. Souza, J.L. Anderson, Advances of Ionic Liquids in Analytical Chemistry, Anal. Chem. 91 (2019) 505–531. https://doi.org/10.1021/acs.analchem.8b04710.

[130] M. Taghizadeh, A. Taghizadeh, V. Vatanpour, M.R. Ganjali, M.R. Saeb, Deep eutectic solvents in membrane science and technology: Fundamental, preparation, application, and future perspective, Sep. Purif. Technol. 258 (2021). https://doi.org/10.1016/j.seppur.2020.118015.

[131] A.M. de Castro, D. Prasavath, J. V. Bevilaqua, C.A.M. Portugal, L.A. Neves, J.G. Crespo, Role of water on deep eutectic solvents (DES) properties and gas transport performance in biocatalytic supported DES membranes, Sep. Purif. Technol. 255 (2021) 117763. https://doi.org/10.1016/j.seppur.2020.117763.

[132] U. Saeed, A. Laeeq Khan, M. Amjad Gilani, M. Roil Bilad, A. Ullah Khan, Supported liquid membranes comprising of choline chloride based deep eutectic solvents for CO2 capture: Influence of organic acids as hydrogen bond donor, J. Mol. Liq. 335 (2021). https://doi.org/10.1016/j.molliq.2021.116155.

[133] R. Craveiro, L.A. Neves, A.R.C. Duarte, A. Paiva, Supported liquid membranes based on deep eutectic solvents for gas separation processes, Sep. Purif. Technol. 254 (2021). https://doi.org/10.1016/j.seppur.2020.117593.

[134] M. Ishaq, M.A. Gilani, F. Ahmad, Z.M. Afzal, I. Arshad, M.R. Bilad, K. Ayub, A.L. Khan, Theoretical and experimental investigation of CO2 capture through choline chloride based supported deep eutectic liquid membranes, J. Mol. Liq. 335 (2021). https://doi.org/10.1016/j.molliq.2021.116234.

[135] U. Saeed, A.L. Khan, M.A. Gilani, M.R. Bilad, A.U. Khan, Supported deep eutectic liquid membranes with highly selective interaction sites for efficient CO2 separation, J. Mol. Liq. 342 (2021) 117509. https://doi.org/10.1016/j.molliq.2021.117509.

[136] M. Ishaq, M.A. Gilani, M.R. Bilad, A. Faizan, A.A. Raja, Z.M. Afzal, A.L. Khan, Exploring the potential of highly selective alkanolamine containing deep eutectic solvents based supported liquid membranes for CO2 capture, J. Mol. Liq. 340 (2021) 117274. https://doi.org/10.1016/j.molliq.2021.117274.

[137] M. Ishaq, M.A. Gilani, Z.M. Afzal, M.R. Bilad, A.-S. Nizami, M. Rehan, E. Tahir, A.L. Khan, Novel Poly Deep Eutectic Solvents Based Supported Liquid Membranes for CO2 Capture, Front. Energy Res. 8 (2020). https://doi.org/10.3389/fenrg.2020.595041.

[138] U. Saeed, A.L. Khan, M.A. Gilani, M. Aslam, A.U. Khan, CO2 separation by supported

liquid membranes synthesized with natural deep eutectic solvents, Environ. Sci. Pollut. Res. 28 (2021) 33994–34008. https://doi.org/10.1007/s11356-020-10260-x.

[139] Z. Shamair, N. Habib, M.A. Gilani, A.L. Khan, Theoretical and experimental investigation of CO2 separation from CH4 and N2 through supported ionic liquid membranes, Appl. Energy. 268 (2020). https://doi.org/10.1016/j.apenergy.2020.115016.

[140] I. Adeyemi, M.R.M. Abu-Zahra, I. Alnashef, Novel Green Solvents for CO2 Capture, Energy Procedia. 114 (2017) 2552–2560. https://doi.org/10.1016/j.egypro.2017.03.1413.

[141] I. Adeyemi, M.R.M. Abu-Zahra, I.M. AlNashef, Physicochemical properties of alkanolamine-choline chloride deep eutectic solvents: Measurements, group contribution and artificial intelligence prediction techniques, J. Mol. Liq. 256 (2018) 581–590. https://doi.org/10.1016/j.molliq.2018.02.085.

[142] S.K. Shukla, D. Nikjoo, J.P. Mikkola, Is basicity the sole criterion for attaining high carbon dioxide capture in deep-eutectic solvents?, Phys. Chem. Chem. Phys. 22 (2020) 966–970. https://doi.org/10.1039/c9cp06017k.

[143] M.J. Abraham, T. Murtola, R. Schulz, S. Páll, J.C. Smith, B. Hess, E. Lindah, E. Lindahl, GROMACS: High performance molecular simulations through multi-level parallelism from laptops to supercomputers, SoftwareX. 1–2 (2015) 19–25. https://doi.org/10.1016/j.softx.2015.06.001.

[144] U. Essmann, L. Perera, M.L. Berkowitz, T. Darden, H. Lee, L.G. Pedersen, A smooth particle mesh Ewald method, J. Chem. Phys. 103 (1995) 8577–8593. https://doi.org/10.1063/1.470117.

[145] G. Bussi, D. Donadio, M. Parrinello, Canonical sampling through velocity rescaling, J. Chem. Phys. 126 (2007) 014101. https://doi.org/10.1063/1.2408420.

[146] M. Parrinello, A. Rahman, Polymorphic transitions in single crystals: A new molecular dynamics method, J. Appl. Phys. 52 (1981) 7182–7190. https://doi.org/10.1063/1.328693.

[147] A. van den Bruinhorst, L.J.B.M. Kollau, M. Vis, M.M.R.M. Hendrix, J. Meuldijk, R. Tuinier, A.C.C. Esteves, From a eutectic mixture to a deep eutectic system via anion selection: Glutaric acid + tetraethylammonium halides, J. Chem. Phys. 155 (2021) 014502. https://doi.org/10.1063/5.0050533.

[148] M.A.R. Martins, D.O. Abranches, L.P. Silva, S.P. Pinho, J.A.P. Coutinho, Insights into the Chloride versus Bromide Effect on the Formation of Urea-Quaternary Ammonium Eutectic Solvents, Ind. Eng. Chem. Res. 61 (2022) 11988–11995. https://doi.org/10.1021/acs.iecr.2c01274.

[149] H. Ghaedi, M. Ayoub, S. Sufian, B. Lal, Y. Uemura, Thermal stability and FT-IR analysis of Phosphonium-based deep eutectic solvents with different hydrogen bond donors, J. Mol. Liq. 242 (2017) 395–403. https://doi.org/10.1016/j.molliq.2017.07.016.

[150] R. Yusof, K. Jumbri, M.B. Abdul Rahman, An insight into the effects of ratios and temperatures on a tetrabutylammonium bromide and ethylene glycol deep eutectic solvent, J. Mol. Liq. 339 (2021) 116709. https://doi.org/10.1016/j.molliq.2021.116709.

[151] V. Migliorati, P. D'Angelo, Deep eutectic solvents: A structural point of view on the role of

the anion, Chem. Phys. Lett. 777 (2021) 138702. https://doi.org/10.1016/j.cplett.2021.138702.

[152] H. S. Salehi, A.T. Celebi, T.J.H. Vlugt, O.A. Moultos, Thermodynamic, transport, and structural properties of hydrophobic deep eutectic solvents composed of tetraalkylammonium chloride and decanoic acid, J. Chem. Phys. 154 (2021). https://doi.org/10.1063/5.0047369.

[153] E.O. Fetisov, D.B. Harwood, I.-F.W. Kuo, S.E.E. Warrag, M.C. Kroon, C.J. Peters, J.I. Siepmann, First-Principles Molecular Dynamics Study of a Deep Eutectic Solvent: Choline Chloride/Urea and Its Mixture with Water, J. Phys. Chem. B. 122 (2018) 1245–1254. https://doi.org/10.1021/acs.jpcb.7b10422.

[154] A.H. Jalili, A. Mehdizadeh, M. Shokouhi, H. Sakhaeinia, V. Taghikhani, Solubility of CO2 in 1-(2-hydroxyethyl)-3-methylimidazolium ionic liquids with different anions, J. Chem. Thermodyn. 42 (2010) 787–791. https://doi.org/10.1016/j.jct.2010.02.002.

[155] J.L. Anthony, J.L. Anderson, E.J. Maginn, J.F. Brennecke, Anion Effects on Gas Solubility in Ionic Liquids, J. Phys. Chem. B. 109 (2005) 6366–6374. https://doi.org/10.1021/jp046404l.

[156] P.K. Kilaru, R.A. Condemarin, P. Scovazzo, Correlations of Low-Pressure Carbon Dioxide and Hydrocarbon Solubilities in Imidazolium-, Phosphonium-, and Ammonium-Based Room-Temperature Ionic Liquids. Part 1. Using Surface Tension, Ind. Eng. Chem. Res. 47 (2008) 900–909. https://doi.org/10.1021/ie070834r.

[157] G. Cui, M. Lv, D. Yang, Efficient CO2 absorption by azolide-based deep eutectic solvents, Chem. Commun. 55 (2019) 1426–1429. https://doi.org/10.1039/c8cc10085c.

[158] P. Aravena, E. Cea-Klapp, N.F. Gajardo-Parra, A.F. Olea, H. Carrasco, J.M. Garrido, R.I. Canales, Influence of Hydrogen Bond Acceptors and Water Content on Surface Tension in Glycol-Based Eutectic Mixtures, Ind. Eng. Chem. Res. 63 (2024) 11184–11195. https://doi.org/10.1021/acs.iecr.4c01600.

[159] N.F. Gajardo-Parra, V.P. Cotroneo-Figueroa, P. Aravena, V. Vesovic, R.I. Canales, Viscosity of Choline Chloride-Based Deep Eutectic Solvents: Experiments and Modeling, J. Chem. Eng. Data. 65 (2020) 5581–5592. https://doi.org/10.1021/acs.jced.0c00715.

[160] R. Pandian, D. Kim, Y. Zhang, I. Alfurayj, D.M. Prado, E. Maginn, C. Burda, Chain length and OH-spacing effects on diol-based deep eutectic solvents, J. Mol. Liq. 393 (2024) 123534. https://doi.org/10.1016/j.molliq.2023.123534.

[161] X. Deng, X. Duan, L. Gong, D. Deng, Ammonia Solubility, Density, and Viscosity of Choline Chloride-Dihydric Alcohol Deep Eutectic Solvents, J. Chem. Eng. Data. 65 (2020) 4845–4854. https://doi.org/10.1021/acs.jced.0c00386.

Załącznik A

Załącznik A1

I. Cichowska-Kopczyńska, **B. Nowosielski**, D. Warmińska, Deep Eutectic Solvents: Properties and Applications in CO_2 Separation, Molecules 28 (2023) 5293. https://doi.org/10.3390/molecules28145293. **IF_{2023}: 4,2, $MNSW_{2023}$: 140**

molecules

MDPI

Review

Deep Eutectic Solvents: Properties and Applications in CO_2 Separation

Iwona Cichowska-Kopczyńska [1,*], Bartosz Nowosielski [2] and Dorota Warmińska [2]

[1] Department of Process Engineering and Chemical Technology, Faculty of Chemistry, Gdańsk University of Technology, 80-233 Gdańsk, Poland
[2] Department of Physical Chemistry, Faculty of Chemistry, Gdańsk University of Technology, 80-233 Gdańsk, Poland; bartosz.nowosielski@pg.edu.pl (B.N.); dorota.warminska@pg.edu.pl (D.W.)
* Correspondence: iwona.kopczynska@pg.edu.pl

Abstract: Nowadays, many researchers are focused on finding a solution to the problem of global warming. Carbon dioxide is considered to be responsible for the "greenhouse" effect. The largest global emission of industrial CO_2 comes from fossil fuel combustion, which makes power plants the perfect point source targets for immediate CO_2 emission reductions. A state-of-the-art method for capturing carbon dioxide is chemical absorption using an aqueous solution of alkanolamines, most frequently a 30% wt. solution of monoethanolamine (MEA). Unfortunately, the usage of alkanolamines has a number of drawbacks, such as the corrosive nature of the reaction environment, the loss of the solvent due to its volatility, and a high energy demand at the regeneration step. These problems have driven the search for alternatives to that method, and deep eutectic solvents (DESs) might be a very good substitute. Many types of DESs have thus far been investigated for efficient CO_2 capture, and various hydrogen bond donors and acceptors have been used. Deep eutectic solvents that are capable of absorbing carbon dioxide physically and chemically have been reported. Strategies for further CO_2 absorption improvement, such as the addition of water, other co-solvents, or metal salts, have been proposed. Within this review, the physical properties of DESs are presented, and their effects on CO_2 absorption capacity are discussed in conjunction with the types of HBAs and HBDs and their molar ratios. The practical issues of using DESs for CO_2 separation are also described.

Keywords: carbon dioxide; deep eutectic solvent; absorption; membrane; separation; solubility

Citation: Cichowska-Kopczyńska, I.; Nowosielski, B.; Warmińska, D. Deep Eutectic Solvents: Properties and Applications in CO_2 Separation. *Molecules* **2023**, *28*, 5293. https://doi.org/10.3390/molecules28145293

Academic Editor: Joaquín García Álvarez

Received: 25 May 2023
Revised: 21 June 2023
Accepted: 3 July 2023
Published: 8 July 2023

1. Introduction

One of the main objectives of current global research is to develop materials and methods aimed at reducing emissions of acid and toxic gases, especially carbon dioxide. One of the most common technologies used to remove CO_2 is its absorption with aqueous amine solutions, mainly a 30% aqueous solution of monoethanolamine (MEA). However, other amine absorbents can be considered, particularly those including hydroxyamines such as aminomethylpropanol (AMP) or 2-piperidineethanol (2-PPE) which, compared to aqueous MEA solutions, require less heat at the regeneration stage, resulting in a reduction in the process cost. However, new alternative solvents will be indispensable to make the process more efficient, still less expensive, and more environmentally friendly.

Over the last few years, a lot of attention has been paid to ionic liquids (ILs). These solvents are characterized by a low melting point, low vapor pressure, and relatively high solubility of CO_2. However, research has shown that a vast majority of ILs absorb carbon dioxide physically, which ensures relatively low costs for solvent regeneration, but at the same time limits capacity and requires high operating pressures for the removal of carbon dioxide. Serious disadvantages of ionic liquids used on a technical scale are their high price, relatively high viscosity, toxicity, and corrosivity.

An alternative to ILs is using deep eutectic solvents (DESs), which were originally introduced as systems formed from a mixture of two or more Lewis acids and bases

or Brønsted–Lowry acids and bases, and which have a lower freezing point compared to the starting constituents. In recent years, the definition of a DES was made more precise and it has been established that the term "deep eutectic solvent" can only be assigned to a eutectic mixture for which the eutectic point temperature is lower than that calculated from the Schröder–Van Laar equation valid for an ideal liquid eutectic mixture [1]. However, in practice, most researchers use the term "deep eutectic solvent" simply for the eutectic mixture. DESs are usually obtained by mixing several reagents to form a homogenous liquid. There is always a small amount of water in these solvents, which is involved in the formation of a network of hydrogen bonds. Deep eutectic solvents have similar physical properties to ionic liquids, and they are practically non-volatile and non-flammable, but additionally they are definitely cheaper and usually easier to synthesize, and they are less toxic and often biodegradable. However, compared to ILs, DESs have lower thermal stability and a lower electrochemical window [2]. The vapor pressure of eutectic liquids is higher than that of ionic liquids, but still relatively low. For an *N,N*-diethylethanolammonium chloride 1: 2 mixture with glycerol at temperatures from 343 to 393 K, the vapor pressure is from 2 to 60 Pa, and for mixtures with urea it is from 0.14 to 6.8 Pa [3]. Similar to ionic liquids, eutectic liquids' physical properties can be controlled by changing the composition and ratio of their components in order to obtain properties favorable for a specific application. These properties are affected by the chemical structure of the DESs and the resulting interactions between their components, mainly the hydrogen bonds that are responsible for the physical state of deep eutectic solvents. Examples of commonly used ingredients of DESs, i.e., hydrogen bond acceptors (HBAs) and hydrogen bond donors (HBDs), are presented in Figure 1.

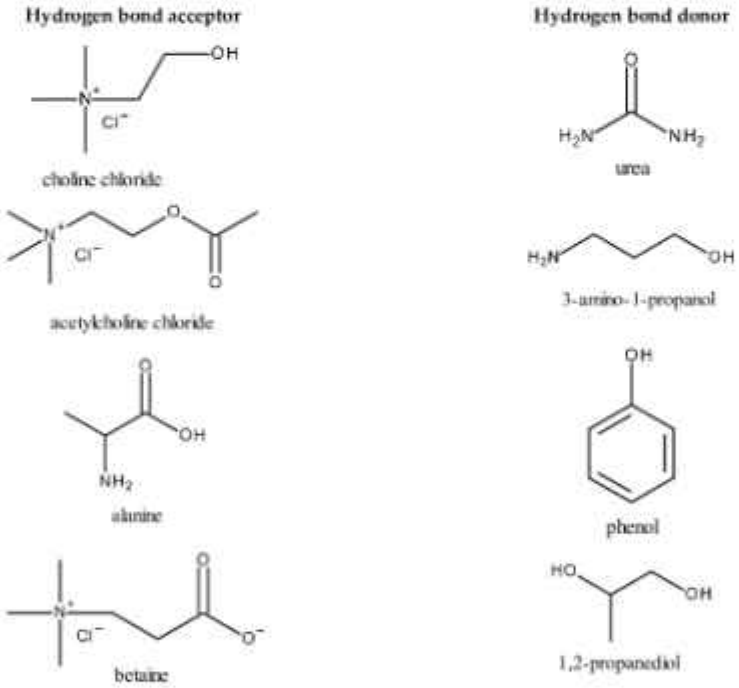

Figure 1. *Cont.*

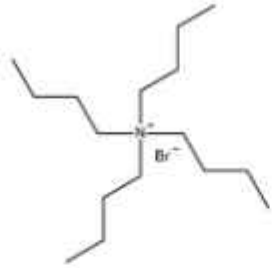

tetrabutylammonium bromide

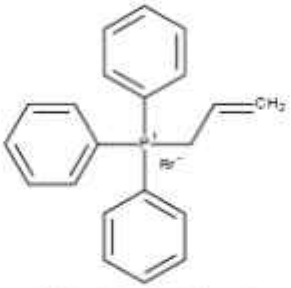

allyltriphenylphosphonium bromide

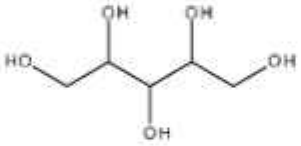

xylitol

imidazole

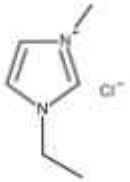

1-ethyl-3-methylimidazolium chloride

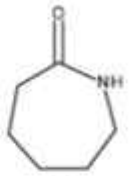

caprolactam

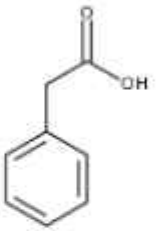

phenylacetic acid

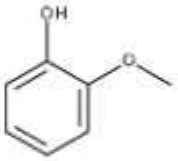

guaiacol

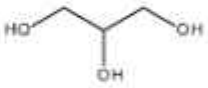

glycerol

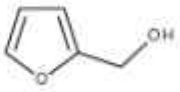

furfuryl alcohol

Figure 1. *Cont.*

Figure 1. Examples of commonly used HBAs and HBDs.

Taking into account the available research reports, it can be concluded that there are no highly accurate models able to predict the properties of DESs. Most of the currently available knowledge is focused on choline chloride-based DESs. Although this is the most widely used hydrogen bond acceptor, there is a whole range of DESs based on other compounds that have not been described in detail. DESs have found their place in several separation applications [4–6]. Hence, they are considered to be green and have been examined for the absorption and separation of carbon dioxide and other gaseous pollutants. Depending on their structure, deep eutectic mixtures can absorb carbon dioxide through physical or chemical absorption.

This present article reviews the properties that make these solvents appropriate for CO_2 separation applications, as well as their CO_2 absorption capacity.

2. Properties of Deep Eutectic Solvents

Growing interest in DESs as a new generation of solvents for various practical applications has resulted in the need for accurate and reliable knowledge about their main physical, chemical, and thermodynamic properties. Therefore, numerous scientific articles devoted to the development and characterization of DES properties have recently been added to the literature. This section describes and discusses the main physicochemical and thermodynamic properties of DESs, including those that affect their suitability for gas separation.

There are seven types of DESs that can be distinguished. The general formulas and examples of the specific types are presented in Table 1. Since most of the research carried out so far has been related to the properties and applications of mixtures of quaternary ammonium salts and HBD, this review is focused mainly on DESs of type III.

Table 1. Types of deep eutectic solvents.

Type	General Formulas	Examples
I	Cat^+X^-:metal halides	1:2 ChCl: $FeCl_3$
II	Cat^+X^-:metal halides hydrate	1:2 ChCl:$CrCl_3 \cdot 6H_2O$
III	Cat^+X^-:HBD	1:2 ChCl:H_2NCONH_2
IV	Metal chloride:HBD	1:3 $ZnCl_2$:CH_3CONH_2
V	Nonsalt HBA:HBD	1:1 Citric acid:sucrose
VI	API as HBA or HBD (THEDES)	1:1 ChCl:phenylacetic acid
VII	Amino acid as HBA or HBD (AADES)	1:1 Betaine:L-histidine

2.1. Freezing Point

As mentioned above, a DES is formed by mixing two or three components capable of forming a new liquid phase with a lower freezing point than that for the ideal eutectic mixture (Figure 2) [1]. A significant depression of the freezing point is observed mainly due to the hydrogen bond interactions between the hydrogen bond acceptor and the hydrogen bond donor. Although the number of DESs reported in the literature is huge, the number of DESs with the freezing point lower than room temperature is still limited. In general, the freezing point of a DES is influenced by the nature of its constituents and their molar ratio. However, no clear correlation between the melting points of individual components and the

freezing points of the corresponding DESs has been found. Among all the choline chloride-based DESs studied, lower melting points were obtained for DESs consisting of polyols such as glycerol or ethylene glycol [7,8]. However, Shahbaz et al. recorded a very low melting point for 2,2,2-trifluoroacetamide, which confirms a very large contribution of the HBD to lowering the melting point by forming a hydrogen bond [8]. It has been established that the nature of the HBA anion also affects the DES freezing point. For example, Abbott et al. studied DESs based on urea and they concluded that DESs consisting of urea and a choline salt have freezing points decreasing in the order $F^- > NO_3^- > Cl^- > BF_4^-$ [9]. Moreover, in their article, the HBA effect on the freezing point of the DESs was investigated. The researchers found that mixing urea with different salts in the same ratio (1:2) results in liquids that exhibit very different freezing points from −38 to 113 °C.

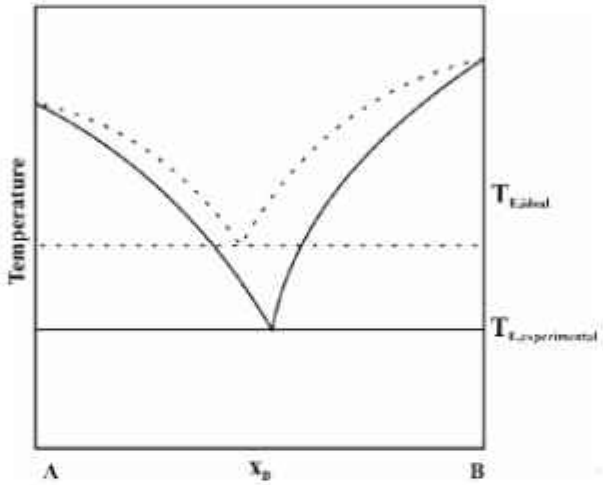

Figure 2. Phase diagram of deep eutectic solvent.

The influence of the molar ratio of HBAs and HBDs on the freezing point of a DES has been studied by many researchers and it has been demonstrated that, depending on the mixture, it can be significant. For example, when methyl triphenyl phosphonium bromide was mixed with glycerol in a molar ratio of 1:3 or 1:4, the resulting DESs exhibited freezing points of −5.5 and 15.6 °C, respectively [10].

Abbott et al. suggested that the depression of the melting point is due to the lattice energy of the DES, and the entropy changes are caused by the formation of a liquid phase and the interaction between HBAs and HBDs [11]. Based on the analysis of 13 choline chloride DESs, researchers have tried to show a correlation between the freezing point depression and the experimentally measured enthalpy of hydrogen bond formation. However, the discovered correlation was not satisfactory [12]. Marcus tried to compare the standard entropies of DES formation with the freezing point depression but did not identify any general correlation [13].

Pontes et al. used the perturbed-chain statistical associating fluid theory (PC-SAFT) for modelling the phase behavior of DES systems [14]. They observed a compatibility with the experimental data, but this method requires a number of molecules and mixing parameters fitted from experimental data. Thus, this model has a limited predictive capability for novel systems. Garcia et al. proposed a quantitative structure–activity relationship (QSAR) predictive model for choline chloride-based DESs and obtained high predictive ability as shown by the cross-validated R^2 values of 0.93 [15]. Recently, a conductor-like screening

model for realistic solvation (COSMO- RS) applying experimentally independent molecular descriptors has been proposed by Song et al. [16]. Using 35 choline chloride-based DESs, they found a reliable multilinear relationship between the freezing point depression of DESs and the molecular volume descriptor and their molecular descriptors associated with hydrogen bond interactions.

2.2. Vapor Pressure

Despite a very limited amount of data on the vapor pressure of DESs, there is general agreement that the vapor pressures of pure deep eutectic solvents at ambient temperatures are low or even negligible, but higher than those of ionic liquids. Recently, Ravula et al. studied the vapor pressure of fluids presenting low-volatility and found that they vary in the following order: short-chain PEGs > long-chain PEGs > DESs > protic ILs > polymeric ILs > aprotic ILs > dicationic ILs [17].

Experimental measurements of the vapor pressures of deep eutectic solvents have so far been taken only at 40–120 °C, considerably above ambient temperatures. Boisset et al. determined the vapor pressure at 40 °C for a DES consisting of *N*-methylacetamide and lithium bis(trifluoromethylsulfonyl)-imide to be 20 Pa [18]. Shahbaz et al. found that at 100 °C the vapor pressures of reline, glyceline, diethylethanolammonium chloride:urea, *N*,*N*-diethylethanolammonium chloride:glycerol, and methyltriphenylphosphonium bromide:glycerol are equal to 1.33, 11.6, 1.8, 16.9, and 9.9 Pa, respectively [2]. Recently, Dietz et al. measured the vapor pressures of hydrophobic DESs at 100 °C and obtained values in a range from 55.5 Pa for decanoic acid:lidocaine to 540.9 Pa for decanoic acid:menthol [19].

2.3. Density

Most DESs have a density between 1.0 and 1.35 g·cm^{-3} at 25 °C [20]. However, DESs containing metal salts, such as $ZnCl_2$, have slightly higher densities, in the range of 1.3 to 1.6 g·cm^{-3}, whereas hydrophobic DESs exhibit a density lower than that of water [21,22]. It is certain, however, that DES densities are higher than those of their individual starting components. According to the principle of the hole theory, mixing DES components reduces the average hole's radius and thus increases DES density relative to that of the individual constituents.

In general, the influence of the amount of HBDs on the density of a DES depends on the molecular characteristics of the HBD used. For most DESs, their density decreases as the amount of HBDs increases [23–27]. However, in the case of DESs, where there is a strong association between HBD molecules, an increase in DES density with the increasing amount of HBDs was observed. Abbott et al. reported the densities of DESs with different molar ratios of choline chloride to glycerol and concluded that as the ratio of HBDs decreased, DES density increased [28].

The increasing number of hydroxyl groups in HBDs, resulting in the formation of additional H-bonds and possibly reducing the available free volume, leads to the higher density of DESs. The results obtained by Basaiahgari et al. showed that ethylene glycol-based DESs have lower densities compared to glycerol-based DESs for both benzyltrimethylammonium and benzyltributylammonium chloride as HBA [29]. The same effect was observed by Mjalli et al. for similar choline chloride-based DESs [30].

According to the literature, the increase in DES density is also caused by the presence of additional carboxylic groups as well as additional ether bonds in the HBDs. For example, in the case of DESs based on choline chloride, the density of a DES consisting of oxalic acid was higher than that of a DES consisting of glycolic acid [31]. Basaiahgari et al. reported the densities of DESs consisting of ethylene, diethylene, and triethylene glycol as HBDs and benzyltrimethylammonium chloride as the HBA to be equal to 1.101, 1.110, and 1.117 g·cm^{-3} at 25 °C, respectively [29].

It has been established that the density of DESs decreases with the increasing chain length of the HBDs or HBAs. The results obtained by Florindo et al. show that DESs composed of glutaric acid or levulinic acid have lower density values compared to those ob-

served for DESs based on oxalic or glycolic acids [31]. Wang et al. reported that the density of ethylene glycol-based DESs consisting of tetraethylammonium bromide, tetrapropylammonium bromide, and tetrabutylammonium bromide were 1.1596, 1.1121, and 1.0762, respectively [32].

Another factor affecting DES density is the type of salt they consist of. Shahbaz et al. observed that ammonium-based DESs have lower densities than phosphonium-based DESs [24]. Moreover, bromide salts form denser DESs than chloride ones [23].

In general, an increase in temperature causes a linear decrease in density [33]. However, Yadav et al. found that the decrease in density with increasing temperature of a DES composed of choline chloride and glycerol in a 1:2 mole ratio follows a quadratic expression [34]. Temperature-dependent density measurements for DESs can be used to estimate their isobaric thermal expansion coefficients, which can quantify DESs' free volume [29].

Several attempts at predicting deep eutectic solvents' densities have been reported in the literature so far. Shahbaz et al. applied artificial intelligence and group contribution methods in order to predict the densities of DESs consisting of ethylene glycol and glycerol as HBDs and choline chloride, diethylethanolammonium chloride, and methyltriphenylphosphonium bromide as HBAs [24]. Mjalli introduced mass connectivity index (MCI)-based density prediction for a set of 20 deep eutectic solvent systems comprising various salts and hydrogen bond donors [35]. Nowosielski et al. used the Rackett equation modified by Spencer and Danner and the MCI-based density model to predict the density of DESs based on 3-amino-1-propanol [23]. Finally, recently, Haghbakhsh et al. presented group contribution and atomic contribution models for predicting the density of various types of DESs by simply decomposing the molecular structure into a number of predefined groups or atoms [36].

2.4. Viscosity

The viscosity of deep eutectic solvents varies significantly at room temperature. The lowest viscosity values were observed for DESs based on ethylene glycol, ethanolamine, or acetic acid [37,38]. According to Mjalli and Naser, a mixture of choline chloride and ethylene glycol in a molar ratio of 1:2 has a viscosity of 40 mPa·s at 25 °C [39]. The highest viscosities are those of DESs containing derived sugars or amino acids [40,41]. A DES consisting of sorbitol and choline chloride in a molar ratio of 1:12 has a viscosity of 19,470 mPa·s at 25 °C [42]. However, most DESs show relatively high viscosities at room temperature (>100 mPa·s) [20].

Since viscosity is related to the free volume and the probability of finding holes of suitable dimensions for solvent molecules or ions to enter, this property depends on the size of the DES constituents. The high viscosity of DESs also results from the presence of hydrogen bonds as well as electrostatic and van der Waals interactions between the individual components of the DESs. Thus, the viscosity depends on the chemical nature of the components, their molar ratio, water content, and temperature.

In general, increasing the amount of HBDs reduces the viscosity of a DES [25]. However, in the case of DESs based on hydrogen bond donors with a strong cohesive energy, due to the presence of the intermolecular hydrogen bond network, the opposite effect is observed. At 25 °C, the viscosities of choline chloride and glycerol mixtures with molar ratios of 1:4, 1:3, and 1:2 were 350, 320, and 259 mPa·s, respectively [28].

The viscosity of DESs decreases considerably with increasing temperature. For example, for choline chloride:urea (1:2) and choline chloride:glucose (2:1), the viscosity decreases from 750 to 95 mPa·s and from 7992 to 262 mPa·s, respectively, at 25 and 55 °C [43]. The dependence of DESs' viscosity on temperature is described in the literature by Arrhenius or Vogel–Fulcher–Tamman (VFT) equations [20]. Mjalli and Naser proposed a model for the viscosity of choline chloride-based DESs taking into account not only the temperature, but also the composition of the mixture. According to their results, the model based on the Arrhenius equation is more accurate for less viscous liquids, while the VFT-based viscosity

model fits experimental viscosities also for more viscous DESs in a wide temperature range [39].

It has been established that DESs' viscosity drastically decreases with the water content. This property seems to be the main reason for the differences in the literature values of viscosity for any given deep eutectic solvent, in some cases even within a factor of two. According to Florindo et al., a highly viscous DES such as choline chloride:oxalic acid (1:1) is capable of capturing water from the atmosphere up to 19.40 wt%, which reduces its viscosity from 5363 to 44.49 mPa·s [31].

In 2018, Haghbakhsh et al. modelled the viscosity of deep eutectic solvents following the free volume theory coupled with equations of state [44]. The results showed that the free volume theory with both the CPA and PC-SAFT EoSs (total AARD% of 2.7% and 2.7%, respectively) gives reliable and highly accurate results with respect to the corresponding experimental viscosity values of 27 DESs. Both models also showed good compliance with the temperature trends of viscosity for the investigated DESs. Furthermore, the effect of changing HBD ratios for a fixed HBA was correctly estimated.

More recently, Benguerba et al. proposed a new mathematical model for predicting amine-based DESs' viscosities using the quantitative structure–property relationship (QSPR) approach. To develop this model, a combination of the multilinear regression (MLR) and the artificial neural networks (ANN) methods was applied. The results show that the proposed models are able to predict DESs' viscosities with very high accuracy, i.e., with an R^2 value of 0.9975 in training and 0.9863 for validation using the ANN model, and an R^2 value of 0.9305 for the MLR model [45].

2.5. Surface Tension

The surface tension values of DESs are higher than those of most molecular solvents and exhibit a wide range of changes from 23.9 mN·m^{-1} for tetrabutylammonium bromide:1-nonanol (1:4) to 75.2 mN·m^{-1} for choline chloride: D-glucose (2.5:1) at 20 °C [22,46].

Significant roles in the surface tension values of DESs are played by the nature and length of the alkyl chain of HBAs, the molar ratio of HBA:HBD, and temperature. A cation containing a hydroxyl group leads to the formation of a DES with high surface tension. For instance, according to Omar and Sagedhi, the surface tension of choline chloride:pyrogallol (1:1) is equal to 68.0 mN·m^{-1}, while for DESs based on the same HBD but with tetrabutylammonium bromide as the HBA, the surface tension is 41.0 mN·m^{-1} at 20 °C [47]. The results obtained by the same authors further demonstrated that in the case of tetraalkylammonium-based DESs, an increase in the chain length leads to an increase in the surface tension in the following order: tetraethylammonium bromide:pyrogallol < tetrapropylammonium bromide:pyrogallol < tetrabutylammonium bromide:pyrogallol.

According to the literature, surface tension increases with a decrease in the molar fraction of the salt due to the strengthening of HBD hydrogen bonding. Thus, the surface tension of DESs consisting of choline chloride and lactic acid decreases with increasing salt concentration, due to the disturbance of the hydrogen bond network of lactic acid [48]. Hayyan et al. analyzed the effect of increasing the molar amount of choline chloride in DESs containing D-glucose. At 20 °C, with a 1:1 molar ratio of choline chloride to D-glucose, the surface tension (70.4 mN·m^{-1}) was lower compared to that for a 2.5:1 molar ratio (75.0 mN·m^{-1}) [46]. For all the studied DESs, the surface tensions showed an inversely proportional linear correlation with the temperature [39,46–49].

There are reports of successful prediction of the surface tension of DESs using the group contribution and atomic contribution models and the Guggenheim empirical equation [30,34].

2.6. Electrical Conductivity

Due to their relatively high viscosity, most DESs exhibit ionic conductivities lower than 1 mS·cm^{-1} at room temperature. The exception is a DES composed of ethylene glycol and choline chloride, the conductivity of which is equal to 7.61 mS·cm^{-1} at 20 °C [37].

The conductivity of DESs generally increases significantly as the temperature increases, and the Arrhenius-like equation or the Vogel–Fulcher–Tammann (VFT) expression can be used to predict the conductivity behavior of DESs [20].

The conductivities of DESs are dependent on both the HBD and the nature of the salt. Basaiahgari et al. showed that DESs based on benzyltrimethylammonium chloride and benzyltributylammonium chloride have conductivities relatively lower than those of their choline chloride analogues, which can be attributed to their high viscosity values [29].

Generally, an increase in the amount of salt in a DES causes an increase in its conductivity. Such a phenomenon was observed by Abbott et al. for a DES consisting of choline chloride and glycerol [28]. However, this behavior is not true for all the DESs for which the conductivity–salt concentration trend evolves through a maximum (e.g., choline chloride + ethylene glycol) or is decreasing (e.g., tetrabutylammonium chloride + ethylene glycol) [15].

The relationship between viscosity and conductivity is commonly analyzed in the literature using Walden plots, in which the molar conductivity (Λ, calculated from conductivity and density) and the fluidity (the inverse of viscosity) are plotted on log–log scales and compared with an ideal line obtained for a 0.01 M KCl aqueous solution. According to the literature data, Walden plots indicate that almost all DESs lie below the "ideal" Walden line [15]. However, Mjalli et al. observed a positive deviation for aliphatic-based DESs such as tetrabutylammonium chloride:L-isoleucine, tetrabutylammonium chloride:proline, and tetrabutylammonium chloride:L-valine, which indicates a high ionic pairing between tetrabutylammonium chloride and amino acids in these DESs [49].

Overall, the literature results show that DESs display larger deviations from the ideal reference line than most ILs, which can be explained by considering the fact that the migrating species are ions for ILs and ions + HBD complexes for DESs. Therefore, it can be concluded that the conductivity of DESs is determined not only by their viscosity, but also by the size of the ions.

The development of predictive methods for DES conductivity is very limited in the literature. Bagh et al. used the artificial neural network (ANN) approach to study the electrical conductivity of ammonium- and phosphonium-based DESs and they obtained an absolute relative deviation of 4.4%, which may be considered satisfactory [50]. The hole theory was also applied by Abbott et al. to predict DESs' conductivity, and although good results were obtained in some cases (e.g., choline chloride:ethylene glycol), poor predictions were reported for others (e.g., choline chloride:glycerol) [37].

2.7. *Solvatochromic Parameters*

Solvent polarity is commonly assessed using the polarity scale of Dimroth and Reichardt, $E_T(30)$, which is important for understanding the solubilizing power. Other parameters are the Kamlet–Taft π^*, which measures the combined polarity and polarizability of solvents, α, which measures their hydrogen bond donation ability, and β, which measures their hydrogen bond acceptance ability.

The values that have so far been reported in the literature for these solvatochromic parameters for deep eutectic solvents are generally between those of methanol and water among the common solvents and commensurate with those of ionic liquids [20]. This means that deep eutectic solvents are highly polar and polarizable, and that they have good hydrogen bond donation and acceptance abilities toward solutes.

In general, the number of publications related to DES solvatochromic parameters is limited. Abbott et al. determined the polarities of choline chloride:glycerol DESs of different molar ratios based on several parameters, revealing a linear polarity increase with increasing choline chloride concentration [28]. Pandey et al. employed solvatochromic probes to examine the polarities of four DESs based on combinations of choline chloride with glycerol, urea, malic acid, and ethylene glycol in 1:2 molar ratios [51]. They concluded that the high polarity of these DESs was significantly influenced by the HBD nature. Among the above four combinations, choline chloride:glycerol exhibited the highest $E_T(30)$ value. Moreover, Pandey et al. investigated the effect of temperature and the addition

of water on the DESs' solvatochromic parameters. These researchers demonstrated that an increase in temperature results in a reduced H-bond donor acidity for the DESs, while no temperature effect was observed for dipolarity/polarizability and H-bond accepting basicity. It was also shown that the addition of water to the DESs caused an increase in their dipolarity/polarizability and a decrease in their H-bond accepting basicity. Teles et al. determined the solvatochromic properties of DESs formed by ammonium-based salts and carboxylic acids and concluded that the studied DESs presented a greater ability to donate and accept protons compared to most ionic liquids or organic molecular solvents [52]. Moreover, according to these authors, the high acidity of the studied DESs was mainly due to the organic acid present in the mixtures, and an increase in the alkyl side chain of both the HBA and the HBD species leads to a lower ability of the solvent to donate protons. Florindo et al. determined solvatochromic properties for two different types of DESs: those based on salts, such as choline chloride and tetrabutylammonium chloride, and those based on the neutral compound DL-menthol [53]. They found high values of hydrogen-bonding acidity for all the DESs, probably due to the organic acids present in all the systems. On the other hand, hydrogen-bonding basicity of these DESs did not vary much within the same HBA, but differed slightly in the case of DESs based on choline chloride, tetrabutylammonium chloride, or DL-menthol.

2.8. Other Relevant Properties

Thermal stability. Scarce information is available in the literature on the thermal stability of DESs. Generally, the thermal stability of these solvents is determined by the nature of the hydrogen bond donor and increases with the alkyl chain length on HBDs [54]. Zhao et al. analyzed the thermal stability of DESs consisting of a choline salt (chloride or acetate form) and glycerol [55]. They showed that the studied DESs exhibit relatively high thermal resistance while being stable up to nearly 200 °C. Florindo et al. measured the decomposition temperature of choline chloride-based DESs with several carboxylic acids (levulinic, glutaric, malonic, oxalic, and glycolic) [31]. The lowest value was observed for the DES containing malonic acid (124.68 °C) and the highest was for the DES containing glutaric acid (239.05 °C). Ghaedi et al. studied DESs based on allyltriphenyl phosphoniumbromide and where the HBDs were glycerol, ethylene glycol, diethylene glycol, and triethylene glycol. They found that, among the HBDs, glycerol had the highest thermal stability, while ethylene glycol had the lowest. The DESs followed a similar trend to that of the thermal stability of the HBDs: GL > TEG > DEG > EG [54]. The studies of Delgado et al. concluded that the thermal stability of choline chloride-based DESs, which were formed using levulinic acid, malonic acid, glycerol, ethylene glycol, phenylacetic acid, phenylpropionic acid, urea, and glucose as hydrogen bond donors, increase in the following order: ChCl:EG < ChCl:MalA < ChCl:LevA < ChCl:PhenylacA < ChCl:PhenylpropA < ChCl:GL < ChCl:Urea < ChCl:Gluc [56].

Heat capacity. There are only a few studies available which present experimentally measured heat capacities for some DESs. The majority of the data was provided by Naser et al., who studied deep eutectic solvents of three salts (choline chloride, tetrabutylammonium chloride, and methyltriphenylphosphonium bromide) and several HBDs [57]. Siongco et al. determined the molar heat capacities of DESs based on *N*,*N*-diethylethanolammonium chloride and ethylene glycol or glycerol, while Zhang et al. measured the C_p of DESs consisting of ethylene glycol and betaine or L-carnitine [58,59]. They found that the molar heat capacity values of these DESs increase with temperature and they used different degrees of polynomials for the expression of the temperature dependence. Moreover, all the authors observed the linear relationship between the molar heat capacity and the molar mass of the DESs, which is similar to that of ILs.

In general, three models, based only on knowledge of the molecular structure of the DESs, are available to predict their heat capacities. Taherzadeh et al. developed a correlation to estimate the heat capacity of DESs as a function of temperature, molecular weight, critical pressure, and acentric factor with the resulting AARD% equal to 5.5% [60]. Haghbakhsh

et al. presented group contribution (GC) and atomic contribution (AC) models which can be applied to the molar heat capacities of DESs. The AARD% for the GCM and the ACM was 3.26% and 9.93%, respectively [36]. Bunquin et al. proposed a generalized model using an artificial neural network (ANN) for predicting the heat capacity of ammonium- and phosphonium-based two-component DESs [61]. The overall average absolute relative deviation of the proposed model from the data was 0.57%.

Refractive index. Despite the possibility of using the refractive index as an additional tool to demonstrate hydrogen bonding in DESs, this property has not often been studied [62]. However, the research carried out thus far has shown that the n_D values of deep eutectic solvents are higher than those of ethanol or acetone, but similar to common ILs [63]. Moreover, for all the studied DESs, a linear decrease in the refractive index with increasing temperature was observed. Murshid et al. investigated DESs based on diethanolamine as HBDs and found that the refractive index of all the systems studied decreases with the increase in the molar ratio of HBAs to HBDs from (1:4 to 1:6) [64]. This observation was in line with the results reported by other researchers, for example by Sanchez et al. for a DES composed of betaine and lactic acid, and by Mjalli et al. for a DES composed of tetrabutylammonium bromide and monethanolamine [25,65]. Ilasaiahgari et al. investigated several DESs based on benzyltrimethylammonium chloride and benzyltributylammonium chloride as HBAs, with three ethylene glycols and glycerol as HBDs, and found that the refractive index decreases in the order GLY > EG > DEG > TEG, irrespective of the HBAs [29]. A report by Su et al. investigated several DESs based on tetrabutylammonium chloride (TBAC) and varying HBDs, such as propionic acid (PA), ethylene glycol (EG), polyethylene glycol (PEG), and phenyl acetic acid (PAA) [62]. Among the tested HBDs, a DES composed of TBAC and PAA had the highest refractive index. Mjalli et al. also investigated DESs based on choline chloride as the HBA, but as HBDs they used glutamic acid, aspartic acid, and arginine, and they found that for acidic amino acids-based DESs, the refractive index values were lower than that for the corresponding basic one (arginine) [40]. Troter et al. investigated DESs based on choline chloride as HBA and obtained the following order of the refractive index: ChCl:thiourea > ChCl:urea > ChCl:ethylene glycol > ChCl:glycerol > ChCl:1,3-dimethylurea > ChCl:propylene glycol.

Speed of sound. There are only a few reports that describe the speed of sound for DESs, and the information available is mainly limited to deep eutectic solvents based on choline chloride. According to these reports, the speed of sound for DESs decreases with an increase in temperature, and in most cases linear dependence is observed [22,23]. However, in the case of DESs composed of glycerol and benzyltrimethylammonium chloride or benzyltributylammonium chloride, the temperature dependence of the speed of sound was found to be nonlinear, especially in the lower temperature region [29]. This type of behavior was also observed by Sanchez et al. for L-proline-based DESs [65].

3. Solubility of CO_2 in Deep Eutectic Solvents

3.1. Experimental Methods for Measuring the Solubility of Carbon Dioxide in DESs

Over the years, many experimental methods have been developed to measure CO_2 solubility in DESs. The most common ones are the isochoric saturation method and the gravimetric method. Additionally, the pressure drop method and the magnetic suspension balance method are used, but not as frequently. These methods enable taking measurements in a very wide range of temperatures and pressures. The majority of these methods are based on the assumption that the vapor pressure of DESs is negligible.

Isochoric saturation is the most common method used to measure the absorption of gases. In this method, a degassed DES is placed in a thermostated, well-sealed equilibrium cell at constant temperature, and then the equilibrium cell is evacuated, the gas from the thermostated reservoir is delivered to the cell, and the initial pressure is recorded. Next, the equilibrium is reached when the pressure in the system is constant [66–73].

The solubility is most often described by mole fraction and is derived by:

$$x_g = \frac{n_g}{n_g + n_{DES}} \quad (1)$$

The solubility is determined from the difference between the initial gas pressure and the equilibrium gas pressure, and it is expressed as:

$$n_g = n_0 - n_1 \quad (2)$$

where

$$n_{(0,1)} = \frac{p_{(0,1)}V}{Z_2RT} \quad (3)$$

where V is the volume of the gas phase in the cell, p_0 is the initial gas pressure, p_1 is the equilibrium gas pressure, R is the universal gas constant, T is the temperature, and Z_2 is the gas compressibility factor.

The apparatus used in the isochoric saturation method is relatively simple to design and can be used in a wide range of pressures. Unfortunately, during the absorption, the liquid volume may change. In order to overcome this obstacle, three approaches have been introduced: (a) the change in volume is assumed to be negligible, which was proven to be accurate for low gas pressures [66,74], (b) the volume expansion is measured using a cathetometer as a function of pressure [75], and (c) the percent volume expansion is correlated with the mole fraction of gas [74].

The gravimetric method is based on changes in the weight of the sample upon carbon dioxide absorption. In brief, the DES is placed in a thermostated absorption vial and then the gas is bubbled through the liquid at a known flow rate. The weight of the sample is recorded at regular time intervals. The equilibrium is obtained when the mass of the sample is constant [76–80]. This method is usually used for measurements at atmospheric pressure.

Isotherms are also measured with the magnetic suspension balance method [81,82]. This method is based on magnetic suspension coupling, which is responsible for the transmission of force from the measuring cell to the microbalance, and it allows for measurements in wide ranges of pressure and temperature.

Other methods, which are modification of those mentioned above, are also used [83].

3.1.1. Impact of the Hydrogen Bond Acceptor on CO_2 Capacity

In Table 2, the solubility of carbon dioxide in deep eutectic solvents is presented. One of the most important structural properties of a DES is the size of the cation in its salt which acts as the HBA. Deng et al. [69] examined the solubility of CO_2 in levulinic acid-based DESs. They found that the solubilities in TEAC- and TEAB-based DESs were much lower than those observed for TBAC- and TBAB-based ones, which indicates that salts with a larger cation possess higher carbon dioxide absorption capacity than those with a smaller cation. Such behavior is the effect of the higher free volume of the sorbent at longer chain lengths [84]. Additionally, the effect of the anion is modest, as exchanging the chloride anion with the bromide anion results in a slight increase in carbon dioxide solubility. These conclusions are in compliance with the results obtained for DESs based on other HBAs, such as TBAB:AC (1:2) ≈ TBAC:AC (1:2) > TEAC:AC (1:2) [38]; TOAB:DecA (1:2) ≈ TOAC:DecA (1:2) > TBAC:DecA (1:2) [85]; and TBAC:LA (1:2) > TEAC:LA (1:2) > TMAC:LA (1:2) [82]. Furthermore, the effect of the free volume can be seen in tetrabutylammonium bromide- and in choline chloride-based DESs. TBAB-based DESs have more free volume, and thus the absorption capacity is higher than that of ChCl-based DESs [86].

Another important factor is the symmetry of the salt. Sarmad et al. [38] concluded that exchanging one ethyl group in TEAC:AC (1:2) for one benzyl group in BTEA:AC (1:2) results in lower carbon dioxide absorption capacity. Furthermore, introducing methyltrioctylammonium bromide/chloride instead of tetraoctylammonium bromide/chloride in decanoic acid-based DESs leads to lower solubility of carbon dioxide [85].

The last important factor is the chemical nature of the hydrogen bond acceptor. Introducing HBAs with groups that can interact with CO_2 may improve its solubility. Liu et al. [87] proved that acetylcholine chloride-based DESs have higher carbon dioxide absorption capacity than choline chloride-based DESs, because of the ester group in ACC which has better affinity towards CO_2 than the hydroxyl group in ChCl. The results obtained by Altamash et al. [88] showed that CO_2 solubility in betaine-based DESs is higher than it is in alanine-based DESs due to the stronger interaction with the COO^- group than with the COOH.

Table 2. Solubility of carbon dioxide in deep eutectic solvents.

Ep.	HBA	HBD	Molar Ratio	T/K	P/bar	x_{CO_2}/x_{DES}	Ref.
1	[bmim][$MeSO_4$]	Urea	1:1	303.15	2.8–7.0	0.0071–0.0186	[89] [1]
2	[HDBU][Im]	Ethylene glycol	7:3	313.15	1.0	0.141	[90] [4]
3	[HDBU][Im]	Ethylene glycol	6:4	313.15	1.0	0.118	[90] [4]
4	[HDBU][Im]	Ethylene glycol	5:5	313.15	1.0	0.109	[90] [4]
5	[HDBU][Im]	Ethylene glycol	4:6	313.15	1.0	0.082	[90] [4]
6	[HDBU][Im]	Ethylene glycol	3:7	313.15	1.0	0.063	[90] [4]
7	[HDBU][Ind]	Ethylene glycol	7:3	313.15	1.0	0.117	[90] [1]
8	[HDBU][Triz]	Ethylene glycol	7:3	313.15	1.0	0.108	[90] [1]
9	[N_{2222}][Im]	Ethylene glycol	1:2	298.15	1 atm	0.114	[91] [1]
10	[N_{2222}][Triz]	Ethylene glycol	1:2	298.15	1 atm	0.111	[91] [1]
11	[P_{2222}][Im]	Ethylene glycol	1:2	298.15	1 atm	0.106	[91] [1]
12	[P_{2222}][Triz]	Ethylene glycol	1:2	298.15	1 atm	0.106	[91] [1]
13	1-Methylimidazolium hydrochloride	3-Amino-1-propanol	1:1	r.t.	1 atm	0.020	[92] [4]
14	1-Methylimidazolium hydrochloride	3-Amino-1-propanol	1:2	r.t.	1 atm	0.095	[92] [4]
15	1-Methylimidazolium hydrochloride	3-Amino-1-propanol	1:3	r.t.	1 atm	0.139	[92] [4]
16	1-Methylimidazolium hydrochloride	3-Amino-1-propanol	1:4	r.t.	1 atm	0.194	[92] [1]
17	1-Methylimidazolium hydrochloride	Diethylenetriamine	1:4	r.t.	1 atm	0.228	[92] [1]
18	1-Methylimidazolium hydrochloride	Ethylenediamine	1:1	r.t.	1 atm	0.090	[92] [1]
19	1-Methylimidazolium hydrochloride	Ethylenediamine	1:2	r.t.	1 atm	0.250	[92] [1]
20	1-Methylimidazolium hydrochloride	Ethylenediamine	1:3	r.t.	1 atm	0.267	[92] [1]
21	1-Methylimidazolium hydrochloride	Ethylenediamine	1:4	r.t.	1 atm	0.308	[92] [4]
22	1-Methylimidazolium hydrochloride	Pentaethylenehexamine	1:4	r.t.	1 atm	0.084	[92] [4]
23	1-Methylimidazolium hydrochloride	Tetraethylenepentamine	1:4	r.t.	1 atm	0.099	[92] [1]
24	Acetylcholine chloride	1,2,4-Triazole	1:1	303.15	6.4–58.8	0.0012–0.0096	[93] [1]
25	Acetylcholine chloride	Guaiacol	1:3	303.15	5.4–53.1	0.0007–0.0069	[87] [1]
26	Acetylcholine chloride	Guaiacol	1:4	303.15	5.5–55.9	0.0007–0.0076	[87] [1]
27	Acetylcholine chloride	Guaiacol	1:5	303.15	5.2–52.8	0.0008–0.0076	[87] [1]
28	Acetylcholine chloride	Imidazole	2:3	303.15	3.0–37.3	0.0003–0.0100	[93] [1]
29	Acetylcholine chloride	Imidazole	1:2	303.15	2.7–37.8	0.0008–0.0115	[93] [1]
30	Acetylcholine chloride	Imidazole	1:3	303.15	5.3–56.8	0.0012–0.0129	[93] [1]
31	Acetylcholine chloride	Levulinic acid	1:3	303.15	0.6–5.4	0.0019–0.0132	[69] [1]
32	Alanine	Lactic acid	1:1	298.15	0.06–49.9	0.0013–0.1891	[88] [2]
33	Alanine	Malic acid	1:1	298.15	0.06–49.9	0.0035–0.1823	[88] [2]
34	Allyltriphenylphosphonium bromide	Diethylene glycol	1:4	303.15	1.6–19.4	0.0100–0.3207	[94] [3]
35	Allyltriphenylphosphonium bromide	Diethylene glycol	1:10	303.15	1.6–19.5	0.0098–0.2547	[94] [3]
36	Allyltriphenylphosphonium bromide	Diethylene glycol	1:16	303.15	1.7–19.6	0.0085–0.1404	[94] [3]
37	Allyltriphenylphosphonium bromide	Phenol	1:4	313.15	2.2–13.3	0.0090–0.0786	[95] [3]
38	Allyltriphenylphosphonium bromide	Phenol	1:6	313.15	1.8–13.2	0.0082–0.0787	[95] [3]

Table 2. *Cont.*

Lp.	HBA	HBD	Molar Ratio	T/K	P/bar	g_{CO_2}/g_{IL}	Ref.
39	Allyltriphenylphosphonium bromide	Triethylene glycol	1:4	303.15	1.4–19.5	0.0084–0.2826	[94] [a]
40	Allyltriphenylphosphonium bromide	Triethylene glycol	1:10	303.15	1.5–19.5	0.0078–0.2101	[94] [a]
41	Allyltriphenylphosphonium bromide	Triethylene glycol	1:16	303.15	1.4–19.6	0.0063–0.1867	[94] [a]
42	Benzyltriethylammonium chloride	2-Ethylaminoethanol	1:4	303.15	10.2	0.090	[96] [i]
43	Benzyltriethylammonium chloride	2-Methylaminoethanol	1:4	303.15	10.1	0.100	[96] [i]
44	Benzyltriethylammonium chloride	Acetic acid	1:2	298.15	3.2–20.5	0.0056–0.0429	[36] [i]
45	Benzyltrimethylammonium chloride	Acetic acid	1:2	298.15	2.2–20.4	0.0034–0.0640	[36] [i]
46	Benzyltrimethylammonium chloride	Glycerol	1:2	298.15	3.9–20.3	0.0016–0.0114	[36] [i]
47	Benzyltrimethylammonium chloride	Glycerol–H_2O	1:2:0.05	298.15	2.1–20.2	0.0019–0.0125	[36] [i]
48	Benzyltrimethylammonium chloride	Glycerol–H_2O	1:2:0.11	298.15	2.6–20.3	0.0007–0.0143	[36] [i]
49	Benzyltriphenylphosphonium chloride	Glycerol	1:12	298.15	10.0	0.0206	[97] [i]
50	Betaine	Lactic acid	1:1	298.15	0.06–49.9	0.0022–0.1675	[98] [i]
51	Betaine	Malic acid	1:1	318.15	0.05–49.9	0.0009–0.1536	[98] [i]
52	BHDE[b]	Acetic acid	1:2	298.15	2.1–20.3	0.0028–0.0371	[36] [i]
53	BHDE[c]	Glycerol–H_2O	1:3:0.11	298.15	2.3–20.2	0.0016–0.0091	[36] [i]
54	BHDE[a]	Lactic acid	1:2	298.15	2.8–20.9	0.0007–0.0219	[36] [i]
55	Choline chloride	1,2-Propanediol	1:3	298.15	1.1–5.1	0.0001–0.0007	[68] [i]
56	Choline chloride	1,2-Propanediol	1:4	298.15	1.0–5.0	0.0001–0.0007	[68] [i]
57	Choline chloride	1,4-Butanediol	1:3	298.15	1.1–5.1	0.0001–0.0007	[68] [i]
58	Choline chloride	1,4-Butanediol	1:4	298.15	1.1–5.1	0.0001–0.0007	[68] [i]
59	Choline chloride	2,3-Butanediol	1:3	298.15	1.1–5.1	0.0001–0.0067	[68] [i]
60	Choline chloride	2,3-Butanediol	1:4	298.15	1.1–5.1	0.0002–0.0068	[68] [i]
61	Choline chloride	Cardanol	1:3	293.15	1.0	0.0037	[98] [a]
62	Choline chloride	Cardanol	1:4	293.15	1.0	0.0038	[98] [a]
63	Choline chloride	Cardanol	1:5	293.15	1.0	0.0039	[98] [a]
64	Choline chloride	Diethanol amine	1:6	303.15	5.2–9.7	0.0133–0.0396	[96] [i]
65	Choline chloride	Diethanolamine	1:6	298.15	10.0	0.0409	[97] [i]
66	Choline chloride	Diethanolamine	1:12	r.t.	1 atm	0.196	[99] [i]
67	Choline chloride	Diethylene glycol	1:3	303.15	5.6–11.1	0.0071–0.0140	[86] [i]
68	Choline chloride	Diethylene glycol	1:4	303.15	5.2–11.2	0.0067–0.0146	[86] [i]
69	Choline chloride	Diethylene glycol	1:3	298.15	11.3–51.3	0.0014–0.0074	[66] [i]
70	Choline chloride	Diethylene glycol	1:4	298.15	11.0–50.9	0.0015–0.0082	[66] [i]
71	Choline chloride	Ethanolamine	1:6	298.15	10.0	0.0749	[97] [i]
72	Choline chloride	Ethanolamine	1:7	298.15	1.8–20.2	0.0359–0.2441	[100] [i]
73	Choline chloride	Ethanolamine	1:7	298.15	1.9–20.4	0.0345–0.1577	[36] [i]
74	Choline chloride	Ethanolamine	1:6	r.t.	1 atm	0.292	[99] [a]
75	Choline chloride	Ethanolamine/aminoethylpiperazine	1:7:1	298.15	1.4–20.1	0.0256–0.2093	[100] [i]
76	Choline chloride	Ethanolamine/diethanolamine	1:7:1	298.15	1.1–20.1	0.0188–0.1708	[100] [i]
77	Choline chloride	Ethanolamine/methyldiethanolamine	1:7:1	298.15	1.8–20.1	0.0317–0.2020	[100] [i]
78	Choline chloride	Ethanolamine/methyldiethanolamine	1:7:5	298.15	1.4–20.1	0.0205–0.1629	[100] [i]
79	Choline chloride	Ethanolamine/piperazine	1:7:1	298.15	1.6–22.4	0.0409–0.3291	[100] [i]
80	Choline chloride	Ethylene glycol	1:4	298.15	10.0	0.0133	[97] [i]
81	Choline chloride	Ethylene glycol	1:8	298.15	10.0	0.0168	[97] [i]
82	Choline chloride	Ethylene glycol	1:2	303.15	6.4–12.5	0.0135–0.0274	[96] [i]
83	Choline chloride	Furfuryl alcohol	1:3	303.15	8.1–58.3	0.0012–0.0082	[27] [i]
84	Choline chloride	Furfuryl alcohol	1:4	303.15	8.2–58.2	0.0013–0.0097	[27] [i]
85	Choline chloride	Furfuryl alcohol	1:5	303.15	7.0–57.7	0.0013–0.0100	[27] [i]
86	Choline chloride	Glycerol	1:3	298.15	10.0	0.0201	[97] [i]
87	Choline chloride	Glycerol	1:8	298.15	10.0	0.0143	[97] [i]
88	Choline chloride	Glycerol/acetic acid	1:1:1	298.15	2.6–20.1	0.0023–0.0191	[36] [i]
89	Choline chloride	Glycerol/DBN	1:2:6	r.t.	1 atm	0.103	[101] [a]
90	Choline chloride	Glycerol/DBN	1:2:3	r.t.	1 atm	0.096	[101] [a]
91	Choline chloride	Glycerol/DBN	1:2:7	r.t.	1 atm	0.105	[101] [a]
92	Choline chloride	Glycerol/DBN	1:2:8	r.t.	1 atm	0.103	[101] [a]
93	Choline chloride	Glycerol/DBN	1:3:10	r.t.	1 atm	0.104	[101] [a]
94	Choline chloride	Glycerol/DBU	1:2:6	r.t.	1 atm	0.036	[101] [a]
95	Choline chloride	Glycerol/MTBD	1:2:6	r.t.	1 atm	0.100	[101] [a]
96	Choline chloride	Guaiacol	1:3	303.15	5.5–55.3	0.0007–0.0062	[87] [i]
97	Choline chloride	Guaiacol	1:4	303.15	10.0–54.9	0.0012–0.0068	[87] [i]
98	Choline chloride	Guaiacol	1:5	303.15	4.7–53.9	0.0006–0.0071	[87] [i]

Table 2. *Cont.*

Ep.	HBA	HBD	Molar Ratio	T/K	P/bar	g_{CO_2}/g_{IL}	Ref.
99	Choline chloride	Guaiacol	1:3	293.15	1.0	0.0014	[98] [a]
100	Choline chloride	Guaiacol	1:4	293.15	1.0	0.0015	[98] [a]
101	Choline chloride	Guaiacol	1:5	293.15	1.0	0.0015	[98] [a]
102	Choline chloride	Levulinic acid	1:3	303.15	7.9–57.0	0.0015–0.0112	[27] [a]
103	Choline chloride	Levulinic acid	1:4	303.15	7.2–57.5	0.0014–0.0119	[27] [a]
104	Choline chloride	Levulinic acid	1:5	303.15	7.1–56.7	0.0015–0.0126	[27] [a]
105	Choline chloride	Methyldiethanol amine	1:6	303.15	4.4–51.0	0.0428–0.0665	[86] [a]
106	Choline chloride	Methyldiethanol amine	1:7	303.15	5.9–50.3	0.0488–0.0896	[86] [a]
107	Choline chloride	Phenol	1:2	298.15	9.9–49.9	0.0015–0.0086	[66] [a]
108	Choline chloride	Phenol	1:3	298.15	10.4–50.8	0.0018–0.0090	[66] [a]
109	Choline chloride	Phenol	1:4	298.15	10.8–50.9	0.0018–0.0093	[66] [a]
110	Choline chloride	Triethanolamine	1:3	r.t.	1 atm	0.080	[99] [a]
111	Choline chloride	Triethylene glycol	1:4	298.15	10.0	0.0130	[97] [a]
112	Choline chloride	Triethylene glycol	1:3	298.15	10.9–50.4	0.0016–0.0084	[66] [a]
113	Choline chloride	Triethylene glycol	1:4	298.15	11.9–51.4	0.0018–0.0085	[66] [a]
114	Choline chloride	Urea	1:4	298.15	10.0	0.0142	[97] [a]
115	Choline chloride	Urea	1:2.5	298.15	10.0	0.0114	[97] [a]
116	Choline chloride	Urea	1:3.5	313.15	0.1–2.0	0.0003–0.0048	[70] [a]
117	Choline chloride	Urea	1:2	313.15	0.1–2.0	0.0005–0.0080	[70] [a]
118	Choline chloride	Urea	1:2.5	313.15	0.1–2.0	0.0003–0.0049	[70] [a]
119	DBN	DMLU	1:2	318.15	1.0	0.0427	[102] [a]
120	DBN	DMU	1:2	318.15	1.0	0.1734	[102] [a]
121	DBN	EU	1:2	318.15	1.0	0.2302	[102] [a]
122	DBN	EU	1:3	318.15	1.0	0.1931	[102] [a]
123	Diethylamine hydrochloride	Guaiacol	1:3	303.15	5.4–51.4	0.0009–0.0091	[87] [a]
124	Diethylamine hydrochloride	Guaiacol	1:4	303.15	6.2–52.5	0.0010–0.0086	[87] [a]
125	Diethylamine hydrochloride	Guaiacol	1:5	303.15	5.7–52.0	0.0010–0.0088	[87] [a]
126	Diethylenetriamine hydrochloride	3-Amino-1-propanol	1:4	r.t.	1 atm	0.183	[99] [a]
127	Diethylenetriamine hydrochloride	Ethylenediamine	1:4	r.t.	1 atm	0.322	[99] [a]
128	Diethylenetriamine hydrochloride	Tetraethylenepentamine	1:4	r.t.	1 atm	0.099	[99] [a]
129	Ethanolamine hydrochloride	3-Amino-1-propanol	1:1	r.t.	1 atm	0.158	[92] [a]
130	Ethanolamine hydrochloride	3-Amino-1-propanol	1:2	r.t.	1 atm	0.210	[92] [a]
131	Ethanolamine hydrochloride	3-Amino-1-propanol	1:3	r.t.	1 atm	0.243	[92] [a]
132	Ethanolamine hydrochloride	3-Amino-1-propanol	1:4	r.t.	1 atm	0.263	[92] [a]
133	Ethanolamine hydrochloride	Diethylenetriamine	1:1	313.15	8.0	0.1132	[103] [b]
134	Ethanolamine hydrochloride	Diethylenetriamine	1:3	313.15	8.0	0.1756	[103] [b]
135	Ethanolamine hydrochloride	Diethylenetriamine	1:6	313.15	8.0	0.2412	[103] [b]
136	Ethanolamine hydrochloride	Diethylenetriamine	1:9	313.15	8.0	0.2835	[103] [b]
137	Ethanolamine hydrochloride	Diethylenetriamine	1:4	r.t.	1 atm	0.255	[92] [a]
138	Ethanolamine hydrochloride	Ethylenediamine	1:1	313.15	8.0	0.1123	[103] [b]
139	Ethanolamine hydrochloride	Ethylenediamine	1:3	313.15	8.0	0.1833	[103] [b]
140	Ethanolamine hydrochloride	Ethylenediamine	1:6	313.15	8.0	0.3299	[103] [b]
141	Ethanolamine hydrochloride	Ethylenediamine	1:9	313.15	8.0	0.3458	[103] [b]
142	Ethanolamine hydrochloride	Ethylenediamine	1:1	r.t.	1 atm	0.235	[92] [a]
143	Ethanolamine hydrochloride	Ethylenediamine	1:2	r.t.	1 atm	0.309	[92] [a]
144	Ethanolamine hydrochloride	Ethylenediamine	1:3	r.t.	1 atm	0.365	[92] [a]
145	Ethanolamine hydrochloride	Ethylenediamine	1:4	r.t.	1 atm	0.390	[92] [a]
146	Ethanolamine hydrochloride	Monoethanolamine	1:1	313.15	8.0	0.0910	[103] [b]
147	Ethanolamine hydrochloride	Monoethanolamine	1:3	313.15	8.0	0.1085	[103] [b]

Table 2. *Cont.*

Lp.	HBA	HBD	Molar Ratio	T/K	P/bar	g_{CO_2}/g_{IL}	Ref.
148	Ethanolamine hydrochloride	Monoethanolamine	1:6	313.15	8.0	0.1487	[103] [3]
149	Ethanolamine hydrochloride	Monoethanolamine	1:9	313.15	8.0	0.1863	[103] [3]
150	Ethanolamine hydrochloride	Pentaethylenehexamine	1:4	r.t.	1 atm	0.127	[92] [4]
151	Ethanolamine hydrochloride	Tetraethylenepentamine	1:1	313.15	8.0	0.0835	[103] [3]
152	Ethanolamine hydrochloride	Tetraethylenepentamine	1:3	313.15	8.0	0.1011	[103] [3]
153	Ethanolamine hydrochloride	Tetraethylenepentamine	1:6	313.15	8.0	0.1484	[103] [3]
154	Ethanolamine hydrochloride	Tetraethylenepentamine	1:9	313.15	8.0	0.1715	[103] [3]
155	Ethanolamine hydrochloride	Tetraethylenepentamine	1:4	r.t.	1 atm	0.166	[92] [4]
156	Ethanolamine hydrochloride	Triethylenetetramine	1:1	313.15	8.0	0.0982	[103] [3]
157	Ethanolamine hydrochloride	Triethylenetetramine	1:3	313.15	8.0	0.1655	[103] [3]
158	Ethanolamine hydrochloride	Triethylenetetramine	1:6	313.15	8.0	0.1765	[103] [3]
159	Ethanolamine hydrochloride	Triethylenetetramine	1:9	313.15	8.0	0.2045	[103] [3]
160	Guanidinium hydrochloride	Ethanolamine	1:2	298.15	2.3–20.2	0.0135–0.0732	[98] [1]
161	L-arginine	Glycerol	1:5	353.15	1 atm	0.1677	[104] [1]
162	L-arginine	Glycerol	1:6	353.15	1 atm	0.1957	[104] [1]
163	L-arginine	Glycerol	1:7	353.15	1 atm	0.1959	[104] [1]
164	Methyltrioctylammonium bromide	Decanoic acid	1:2	298.15	0.9–19.9	0.0033–0.0783	[85] [2]
165	Methyltrioctylammonium chloride	Decanoic acid	1:2	298.15	0.9–19.9	0.0024–0.0595	[85] [2]
166	Methyltriphenylphosphonium bromide	1,2-Propanediol	1:4	298.15	2.2–20.3	0.0010–0.0242	[36] [1]
167	Methyltriphenylphosphonium bromide	Acetic acid	1:4	298.15	1.7–20.1	0.0182–0.1330	[36] [1]
168	Methyltriphenylphosphonium bromide	Ethanolamine	1:6	298.15	10.0	0.0716	[97] [1]
169	Methyltriphenylphosphonium bromide	Ethanolamine	1:7	298.15	10.0	0.0643	[97] [1]
170	Methyltriphenylphosphonium bromide	Ethanolamine	1:8	298.15	10.0	0.0632	[97] [1]
171	Methyltriphenylphosphonium bromide	Ethylene glycol	1:2	298.15	1.9–20.2	0.0020–0.0155	[36] [1]
172	Methyltriphenylphosphonium bromide	Glycerol	1:4	298.15	1.6–20.3	0.0004–0.0127	[36] [1]
173	Methyltriphenylphosphonium bromide	Levulinic acid	1:3	298.15	3.0–2.1	0.0011–0.0303	[36] [1]
174	Methyltriphenylphosphonium bromide	Levulinic acid/acetic acid	1:3:0.03	298.15	2.9–20.6	0.0077–0.0579	[36] [1]
175	Monoethanolamine hydrochloride	Ethylenediamine	1:1	r.t.	1 atm	0.205	[105] [4]
176	Monoethanolamine hydrochloride	Ethylenediamine	1:2	r.t.	1 atm	0.244	[105] [4]
177	Monoethanolamine hydrochloride	Ethylenediamine	1:3	r.t.	1 atm	0.315	[105] [4]
178	Monoethanolamine hydrochloride	Ethylenediamine	1:4	r.t.	1 atm	0.308	[105] [4]
179	n-Butyltriphenylphosphonium bromide	Ethylene glycol	1:12	298.15	10.0	0.0201	[97] [1]
180	Tetrabutylammonium bromide	2-Ethylaminoethanol	1:4	303.15	10.0	0.071	[96] [1]
181	Tetrabutylammonium bromide	2-Methylaminoethanol	1:4	303.15	10.5	0.106	[96] [1]
182	Tetrabutylammonium bromide	3-Amino-1-propanol	1:2	r.t.	1 atm	0.111	[92] [4]
183	Tetrabutylammonium bromide	3-Amino-1-propanol	1:3	r.t.	1 atm	0.156	[92] [4]
184	Tetrabutylammonium bromide	3-Amino-1-propanol	1:4	r.t.	1 atm	0.181	[92] [4]
185	Tetrabutylammonium bromide	Acetic acid	1:2	298.15	3.9–20.1	0.0060–0.0497	[36] [1]

Table 2. *Cont.*

Lp.	HBA	HBD	Molar Ratio	T/K	P/bar	g_{CO_2}/g_{mix}	Ref.
186	Tetrabutylammonium bromide	Aminomethylpropanol	1:3	r.t.	1 atm	0.105	[92] [4]
187	Tetrabutylammonium bromide	Aminomethylpropanol	1:4	r.t.	1 atm	0.122	[92] [4]
188	Tetrabutylammonium bromide	Diethanol amine	1:6	303.15	6.1–10.1	0.0157–0.0367	[86] [1]
189	Tetrabutylammonium bromide	Diethanolamine	1:6	298.15	10.0	0.0373	[97] [1]
190	Tetrabutylammonium bromide	Diethanolamine	1:2	r.t.	1 atm	0.096	[99] [4]
191	Tetrabutylammonium bromide	Diethylene glycol	1:2	303.15	7.2–13.9	0.0086–0.0272	[86] [1]
192	Tetrabutylammonium bromide	Diethylene glycol	1:3	303.15	6.9–12.0	0.0113–0.0271	[86] [1]
193	Tetrabutylammonium bromide	Diethylene glycol	1:4	303.15	5.9–10.5	0.0146–0.0290	[86] [1]
194	Tetrabutylammonium bromide	Ethanolamine	1:6	298.15	10.0	0.0591	[87] [1]
195	Tetrabutylammonium bromide	Ethanolamine	1:6	298.15	3.5–20.2	0.0193–0.1223	[38] [1]
196	Tetrabutylammonium bromide	Ethanolamine	1:7	298.15	3.8–20.4	0.0235–0.1324	[38] [1]
197	Tetrabutylammonium bromide	Ethanolamine	1:5	r.t.	1 atm	0.197	[98] [4]
198	Tetrabutylammonium bromide	Ethylene glycol	1:2	303.15	4.1–12.8	0.0045–0.0168	[86] [1]
199	Tetrabutylammonium bromide	Ethylene glycol	1:3	303.15	5.0–12.5	0.0059–0.0189	[86] [1]
200	Tetrabutylammonium bromide	Ethylene glycol	1:4	303.15	5.4–13.7	0.0074–0.0201	[86] [1]
201	Tetrabutylammonium bromide	Levulinic acid	1:3	303.15	0.7–5.7	0.0015–0.0119	[69] [1]
202	Tetrabutylammonium bromide	Methyldiethanol amine	1:3	303.15	4.2–10.0	0.0244–0.0663	[86] [1]
203	Tetrabutylammonium bromide	Methyldiethanol amine	1:4	303.15	5.0–10.2	0.0340–0.0800	[86] [1]
204	Tetrabutylammonium bromide	Triethanolamine	1:3	298.15	10.0	0.2070	[97] [1]
205	Tetrabutylammonium bromide	Triethanolamine	1:2	r.t.	1 atm	0.025	[99] [4]
206	Tetrabutylammonium chloride	Acetic acid	1:2	298.15	3.5–20.0	0.0081–0.0621	[38] [1]
207	Tetrabutylammonium chloride	Decanoic acid	1:2	298.15	0.9–19.9	0.0027–0.0668	[85] [2]
208	Tetrabutylammonium chloride	Lactic acid	1:2	308.15	0.9–19.9	0.0016–0.0420	[82] [2]
209	Tetrabutylammonium chloride	Levulinic acid	1:3	303.15	0.6–5.6	0.0015–0.0133	[69] [1]
210	Tetrabutylphosphonium bromide	Diethylene glycol	1:4	313.15	1.9–14.0	0.0070–0.0776	[95] [3]
211	Tetrabutylphosphonium bromide	Phenol	1:4	313.15	2.3–15.8	0.0092–0.0792	[95] [3]
212	Tetraethylammonium bromide	Levulinic acid	1:3	303.15	0.7–5.6	0.0018–0.0106	[69] [1]
213	Tetraethylammonium chloride	Acetic acid	1:2	298.15	2.8–20.2	0.0063–0.0518	[38] [1]
214	Tetraethylammonium chloride	Acetic acid	1:3	298.15	4.0–20.2	0.0193–0.1223	[38] [1]
215	Tetraethylammonium chloride	Lactic acid	1:2	308.15	1.0–19.9	0.0012–0.0298	[82] [2]
216	Tetraethylammonium chloride	Levulinic acid	1:3	303.15	0.7–5.6	0.0015–0.0121	[69] [1]
217	Tetraethylammonium chloride	Octanoic acid	1:3	298.15	3.5–20.2	0.0069–0.0612	[38] [1]
218	Tetramethylammonium chloride	Acetic acid	1:4	298.15	2.9–21.0	0.0053–0.0667	[38] [1]
219	Tetramethylammonium chloride	Lactic acid	1:2	308.15	1.0–19.9	0.0011–0.0282	[82] [2]
220	Tetraoctylammonium bromide	Decanoic acid	1:2	298.15	0.9–19.9	0.0023–0.0586	[85] [2]
221	Tetraoctylammonium chloride	Decanoic acid	1:2	298.15	0.9–19.9	0.0023–0.0574	[85] [2]
222	Tetraoctylammonium chloride	Decanoic acid	1:1.5	298.15	0.9–19.9	0.0027–0.0667	[85] [2]

Table 2. *Cont.*

Ln.	HBA	HBD	Molar Ratio	T/K	P/bar	α_{CO_2}/[mol·mol^{-1}]	Ref.
223	Tetrapropylammonium chloride	Acetic acid	1:6	298.15	3.5–20.3	0.0110–0.0757	[36] [1]
224	Tetrapropylammonium chloride	Ethanolamine	1:4	298.15	4.8–20.1	0.0149–0.0628	[36] [1]
225	Tetrapropylammonium chloride	Ethanolamine	1:7	298.15	3.6–20.2	0.0754–0.1351	[36] [1]
226	Thioacetamide hydrochloride	Ethylenediamine	1:3	r.t.	1 atm	0.101	[105] [4]
227	Triethanolamine hydrochloride	Ethylenediamine	1:3	r.t.	1 atm	0.175	[105] [4]
228	Triethylmethylammonium chloride	Acetic acid	1:2	298.15	2.0–18.4	0.0036–0.0518	[36] [1]
229	Triethylmethylammonium chloride	Ethylene glycol	1:2	298.15	1.4–1.3	0.0027–0.0276	[36] [1]
230	Triethylmethylammonium chloride	Glycerol	1:2	298.15	1.5–16.5	0.0007–0.0191	[36] [1]
231	Triethylmethylammonium chloride	Glycerol–H_2O	1:2:0.05	298.15	2.3–19.8	0.0004–0.0289	[36] [1]
232	Triethylmethylammonium chloride	Glycerol–H_2O	1:2:0.11	298.15	1.4–17.4	0.0011–0.0292	[36] [1]
233	Triethylmethylammonium chloride	Lactic acid	1:2	298.15	1.4–18.6	0.0021–0.0234	[36] [1]
234	Triethylmethylammonium chloride	Levulinic acid	1:2	298.15	1.4–16.2	0.0025–0.0270	[36] [1]
235	Trimethylglycine	Glycolic	1:2	298.15	10.0	0.00764	[106] [4]
236	Trimethylglycine	Oxalic acid dihydrate	1:2	298.15	10.0	0.00348	[106] [4]
237	Trimethylglycine	Phenylacetic acid	1:2	298.15	10.0	0.00992	[106] [4]
238	Urea hydrochloride	Ethylenediamine	1:3	r.t.	1 atm	0.117	[105] [4]

[1] buchoric saturation method; [2] magnetic suspension balance; [3] pressure drop method; [4] gravimetric method.

3.1.2. Effect of Hydrogen Bond Donor

The hydrogen bond donor determines the nature of interactions between the DES and carbon dioxide, either chemical or physical. The use of amines and alkanolamines as HBDs results in a chemical reaction between the DES and CO_2, i.e., chemical absorption occurs (as presented in Figure 3), while other HBDs such as amides, glycols, sugars, and acids are responsible for physical absorption.

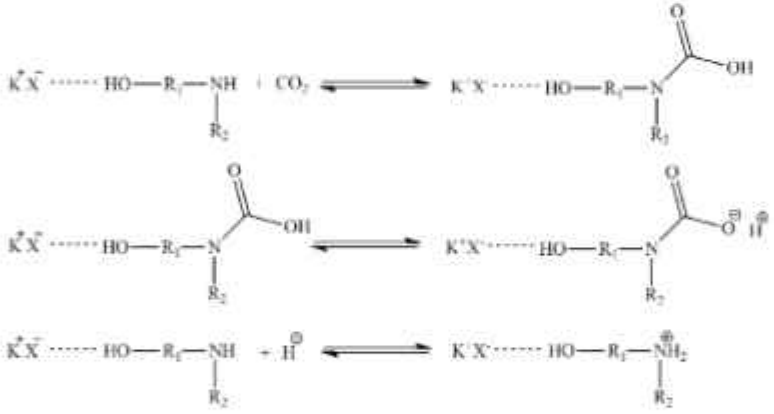

Figure 3. Mechanism of CO_2 absorption in DESs based on primary and secondary amines.

The early work of Chen et al. [68] helped to elucidate the effect of the position of hydroxyl groups on the physical absorption in choline chloride-based DESs. The results showed that higher absorption is observed for dihydric alcohols with hydroxyl groups located closer to each other in carbon scutter (2,3-butanediol) than for dihydric alcohols with hydroxyl groups placed further apart (1,4-butanediol). Ghaedi et al. [94] examined the impact of the ether groups and alkyl chain length of the HBD on DESs based on allyltriphenylphosphonium bromide (ATPPB) and diethylene glycol or triethylene glycol (TEG). At 303.15 K and 1.95 MPa, the solubility of CO_2 was higher for ATPPB:TEG DESs (1:4) (x_{CO2} = 0.5583) than for ATPPB:DEG DESs (1:4) (x_{CO2} = 0.5407). The additional ethylene group and higher free volume contributes to higher CO_2 solubility for TEG DESs [107]; hence, the additional ether group in TEG also improves the absorption capacity [108]. Similar behavior was observed for deep eutectic solvents based on TBAB and glycol or ethylene glycol [86]. The mole fraction of CO_2 for TBAB:EG (1:2) at 303.15 K and 1 MPa was 0.0429, while for TBAB:DEG (1:2) in the same conditions it was 0.0593. Lu et al. [27] conducted a study on the solubility of carbon dioxide in the eutectic mixture of levulinic acid or furfuryl alcohol and choline chloride. They concluded that solubility is higher for the levulinic acid-based DESs than for the furfuryl alcohol-based DESs, which they attributed to the higher affinity of the –COOH group towards CO_2 than that of the -OH group. These authors reported that the strength of the interactions between functional groups in the HBDs and carbon dioxide rises in the following order: amide > carbonyl group > ether bond > hydroxyl group. The only exceptions are glycerol-based DESs, for which CO_2 solubility is higher than for DESs based on HBD with a carbonyl group. Additionally, intramolecular interactions may play a key role in carbon dioxide absorption capacity. For triethylmethylammonium chloride-based DESs, the solubility follows the sequence TEMA:LA < TEMA:LV < TEMA:AC [38]. The poorest solubility, in lactic acid-based DESs, may result from the proximity of the carboxyl group and the hydroxyl group, which gives stronger intermolecular bonding than in levulinic acid or acetic acid. Consequently, the bonding is more difficult to break.

Alkanolamines and amines may be suitable components of DESs for carbon dioxide absorption. They absorb the gas chemically, which leads to higher carbon dioxide solubility than for other DESs. The solubility can be even higher than in the commonly used 30% wt. solution of monoethanolamine [97]. In general, the structural properties of alkanolamines and amines show a similar impact on their carbon dioxide absorption capacity as in other HBDs. For example, Pishro et al. [103] examined the solubility of CO_2 in triethylenetetramine (TETA), diethylenetriamine (DETA), and tetraethylenepentamine (TEPA). Taking into account the same components' molar ratios, the solubility was found to be the highest for EAHC:TETA (1:6), and slightly lower for EAHC:DETA (1:6), whereas the lowest solubility was observed for EAHC:TEPA (1:6). This led to the conclusion that carbon dioxide solubility is higher for DESs based on HBDs with a longer alkyl chain and with more amine groups in their structure. The influence of the alkyl chain length on carbon dioxide capacity might be different for DESs based on alkanolamines with only secondary amine groups. Haider et al. [96] conducted research on CO_2 solubility for 2-methylaminoethanol- and 2-ethylaminoethanol-based DESs. The absorption capacity of CO_2 for TBAB-MAE (1:4) was 0.30 mol_{CO2}/mol_{DES}, while for TBAB-EAE (1:4) it was 0.22 mol_{CO2}/mol_{DES} in the same conditions. This phenomenon was attributed to a lower steric hindrance caused by a shorter alkyl chain in the MAE-based DESs. The other important factor is the substitution of amines. Trisubstituted amines do not form carbamic acid with CO_2, and hence the absorption is simply physical, and the solubility of carbon dioxide is lower [86,109].

3.1.3. Effect of HBA/HBD Molar Ratio

The molar ratio of the hydrogen bond acceptor to the hydrogen bond donor has various effects on carbon dioxide solubility in deep eutectic solvents. For DESs based on dihydric alcohols, the effect of the HBA/HBD molar ratio depends on the structure of HBD. For ChCl:2,3-butanediol, the solubility increases from 0.0308 $mol \cdot kg^{-1}$ for

1:3 molar ratio to 0.0382 mol·kg^{-1} for 1:4 molar ratio at 110 kPa and 293.15 K, respectively, while for ChCl:1,4-butanediol and ChCl:1,2-propanediol it decreases from 0.0330 mol·kg^{-1} to 0.0306 mol·kg^{-1} and from 0.0365 mol·kg^{-1} to 0.0355 mol·kg^{-1}, respectively [68]. For ATPPB:DEG and ATPPB:TEG DESs, the solubility decreases with an increase in the amount of the HBDs from 1:4 to 1:16 in the DES, due to the decrease in the molar volume and the free volume [94]. Surprisingly, for ChCl:DEG and TBAB:DEG DESs, the increase in the HBA/HBD molar ratio from 1:3 to 1:4 enhances the solubility of carbon dioxide, which may be attributed to the weaker hydrogen bonds at higher molar ratios [66,86].

Considering phenol and its derivatives, the effect of the HBA/HBD molar ratio is also complex. For ChCl:phenol DESs, the solubility increases when the ratio changes from 1:2 to 1:4 [66]. The same behavior can be observed for ChCl:GC, DH:GC, and ACC:GC DESs [87]. Additionally, Pishro et al. [103] attributed the increase in carbon dioxide absorption capacity with an increasing HBA/HBD molar ratio for DESs based on a variety of different amines and alkanolamines acting as HBD to a drop in the DESs' viscosity. Lower viscosity results in lower diffusion resistance and thus in increasing the solvent fluidity and, consequently, in improving the mass transfer. For ChCl:MEA DESs, the absorption of CO_2 increases gradually when the molar ratio changes from 1:2 to 1:4, but a further increase in the molar ratio to 1:6 has no effect on carbon dioxide uptake [109]. Once more, this phenomenon might be explained with the hydrogen bonds' net. At higher molar ratios, the absorption of CO_2 changes and, as a result, ChCl and MEA cannot be sufficiently mixed to form hydrogen bonds. In their work, Ali et al. [97] revealed that changing the molar ratio of HBA/HBD in MTPB:MAF from 1:6 to 1:8 results in a decrease in solubility, which made these authors conclude that the formed DES possesses various properties that cannot be predicted by simply considering the contribution effect of its components.

3.1.4. Synergistic Effect

Shukla and Mikkola [92] tried to combine solvatochromic polarity parameters, which probe intermolecular interactions, with carbon dioxide absorption capacity. These parameters include:

- Electronic transition energy ($E_T(30)$) which stands for the hydrogen bond donor–acceptor forces, π–π interactions, and dipole–dipole interactions present in a solvent;
- Dipolarity/polarizability (π*) which is a measure of the electrolytic strength of the medium;
- Hydrogen bond donor acidity (α) which denotes the donating ability of the hydrogen bond donor;
- Hydrogen bond acceptor basicity (β) which denotes the strength of the solvent's hydrogen bond acceptor.

Solvatochromic polarity parameters are determined via the UV-VIS spectra of solvents by using the appropriate dyes: Reichardt's dye 30 is used for $E_T(30)$, and *N*,*N*-diethyl-4-nitroaniline for π*. The hydrogen bond acceptor basicity is defined by the spectroscopic shift of 4-nitroaniline with respect to *N*,*N*-diethyl-4-nitroaniline, while the hydrogen bond donor acidity can be calculated based on $E_T(30)$ and π*.

Shukla and Mikkola [92] investigated the influence of the HBA/HBD molar ratio on solvatochromic polarity parameters and CO_2 absorption capacity. They did not find a clear relationship between $E_T(30)$ and π* for the various DESs. For deep eutectic solvents based on protic HBAs, the reverse relationship between the value of $E_T(30)$ and carbon dioxide absorption capacity was observed, which suggests the involvement of non-polar interactions in CO_2 capture. Additionally, these researchers stated that the high carbon dioxide solubility can be attributed not to basicity but rather to the equilibrium between α and β. This so-called synergistic effect occurs when the $|\alpha - \beta|$ is equal or close to 0. Additionally, the standard enthalpy change and the standard entropy change should be positive and $E_T(30)$ should be low. In this case, there is no energy difference between the HBAs and HBDs in a DES, which means that both components make stable sites that interact with CO_2 [110].

In their other work, Shukla and Mikkola [99] observed much lower solubilities of carbon dioxide in TBAB-based DESs than in ChCl-based DESs despite the similar HBD components. On comparison of α and β, it was noticed that the synergistic effect was higher for ChCl-based DESs, which was the reason for the higher solubility of this class of DESs. The experiment on TBAB:3-amino-1-propanol showed that the reverse relationship between the molar ratio of HBA/HBD and carbon dioxide capacity can be explained via the synergistic effect. Unfortunately, there was no clear relationship between the synergistic effect and the carbon dioxide absorption capacity in AP-based DESs with different HBAs. It was suggested that other factors, such as the free volume or the strength of hydrogen interactions between the components, should be taken into consideration [111].

4. Practical Issues of Carbon Dioxide Separation

Taking into account the valuable properties of DESs, their safety and environmental friendliness in comparison to other solvents, and the ease of their synthesis, these solvents could replace other media used for gas separation. Their carbon dioxide capture capacity has ensured that a number of very promising approaches are being considered. However, considerable and constant effort needs to be made in order to use these innovative solvents on a large scale.

From the technological point of view, DESs' most valuable property is their low volatility, ensuring low solvent loss. In addition, the possibility of tuning DESs' physicochemical properties by changing the mixtures' composition and the structure of their components is a key issue in efficient process design. An important aspect of controlling the physicochemical properties of deep eutectic liquids is the addition of classical solvents. From the point of view of CO_2 separation, water is of particular importance and can be used to modulate the physicochemical properties of the solvent, especially its mass transfer properties such as viscosity. The formation of a DES aqueous mixture not only changes the physical properties of the deep eutectic solvent but also has a very large influence on its interactions with carbon dioxide, mostly due to the formation of new bonds between H_2O and the DES.

Research on DESs and water mixtures is primarily focused on the thermodynamic properties of the mixtures, and it mainly concerns DESs based on choline chloride as HBA. The effect of water content on the solubility of carbon dioxide in a DES has been investigated only in a few studies. The results for DESs based on ChCl showed that an increase in the water content results in a decrease in CO_2 solubility [112,113]. However, the results obtained for amine-based DESs show the opposite behavior. Trivedi et al. reported that a small addition of water (up to 10%) to MEACl:EDA with a 1:3 molar ratio can improve carbon dioxide solubility, but further H_2O addition leads to a reduction in CO_2 solubility [105]. Li et al. reported similar results for TMAC:MEA and TEAC:MEA deep eutectic solvents, and they observed only a slight effect of water content on a ChCl:MEA DES [109].

Some possible mechanisms of water influence on carbon dioxide capacity can be found in the literature. Su et al. reported that a decrease in the solubility of carbon dioxide with increasing water content might occur due to a decrease in the concentration of effective reactants [112]. Shukla et al. hypothesized that water competes with CO_2 for the active sites of DESs, which affects CO_2 uptake [92]. The increased solubility of carbon dioxide might be a result of weakening intermolecular hydrogen bond interactions within the DES structure by the forming of new interactions between water and the DES that increase the free volume and, in consequence, decrease the solvent viscosity [105,109].

Nevertheless, the addition of water to DESs alters many physical properties of the solvents, but the most important from the point of view of gas separation technologies is a drop in DES viscosity. In the study performed by Ma et al. [114], the viscosity of BTMA-:GLY (1:2) DES dropped from 716 to 20 mPa·s at 0.11 mole fraction of water, while the solubility increased by 25%.

For a better understanding of how H_2O interacts with DESs, a few theoretical studies based on molecular dynamics (MD) were conducted. MD simulations performed by Shah

et al. allowed for exploration of interactions in ChCl:Urea (1:2) aqueous solutions [115]. It was shown that Cl^- becomes preferentially hydrated by water compared with urea or choline chloride. Additionally, the effect of water was divided into three ranges based on the mass fraction of H_2O. In the first range (w_{H2O} < 5% wt.), the number of hydrogen bonds increases, reaching the maximum at $w_{H2O} \approx 2\%$. In the next range (from 5% to 25% wt.), choline chloride and urea molecules are hydrated by H_2O, resulting in low diffusivity. In the last range (water mass fraction above 25%), the anions and urea show high diffusivity. Additionally, this simulation indicated that chloride anions interact more strongly with water molecules than with urea molecules.

ChCl:urea (1:2), ChCl:Gly (1:2), and ChCl:EG (1:2) water systems were also studied by Zhekenov et al. [116]. Molecular dynamics simulations they carried out showed similar behavior for different DESs. Below 5% wt., H_2O molecules form H-bonds with ions and hydrogen bond donors, which leads to the absorption of water into the DES structure. Water content above 5% leads to drastic changes of DES properties by dampening the intramolecular interactions in the DES. First-principal MD simulations performed for a ChCl:urea (1:2) equimolar mixture with water showed that the addition of H_2O breaks the strong H-bonds between the H atoms of urea and the chloride anion. This is due to preferentially hydrating Cl^- by water and forming urea–water H-bonds [117]. Studies of pure ChCl:urea (1:2) at high dilution showed that, even for high molar fractions of water (x_{H2O} = 0.9), the ions are only partially hydrated. Additionally, as the water content decreases, the ion-pairing of cation and anion becomes dominant over the hydration of ions, which leads to the conclusion that the non-ideal behavior is the result of competition between these two interactions [118].

Molecular dynamics is also a powerful tool to assess the technological feasibility of DES use in separation processes. It can reveal structural information that may be hard or impossible to obtain with other techniques. The first works in this field focused on explaining the mechanism behind the formation of DESs and the freezing point depression. It was proven that, in the case of choline chloride-based DESs, a strong hydrogen bond formed between the chloride anion and the hydroxyl group of the HBD is responsible for the unique behavior of DESs [119,120]. Similar behavior was reported for HBAs with a bromide anion [121]. Migliorati et al. proved that other groups in HBAs which are capable of forming hydrogen bonds have a very large impact on the hydrogen bond network in DESs [122]. They compared the structures of choline chloride- and benzyltrimethylammonium chloride-based DESs and revealed that the -OH group in ChCl forms additional hydrogen bonds with HBD molecules, which leads to the formation of a three-dimensional arrangement of all the species. This structure is very different from those formed in a benzyltrimethylammonium chloride-based DES. The researchers additionally found that the introduction of even a small functional group leads to a change in the balance among all the different forces. Ferreira et al. examined the structure of a ChCl:propylene glycol (PG) 1:2 DES [123]. From the radial distribution function (RDF), they found that the HBD molecule is placed between CH^+ and Cl^-. Additionally, PG is surrounded with anion molecules rather than with other PG or cation molecules. Furthermore, they observed that CL^-–HBD interactions are the most common in this system, while HBD–HBD are the least common, which is the opposite of the case in the ChCl:EG (1:2) system [124]. In their study on 1,8-cinole (CN)-based DESs, Rozas et al. proved that not all HBDs interact with HBAs in the same way [125]. In the case of the CN:malic acid (MA) system, there is a negligible difference between the hydrogen bonds developed through the central and the terminal hydroxyl groups of the HBD. However, in the case of lactic acid (LA)-based DESs, the interactions of the COOH group were stronger than those of the OH group. The study on DESs containing methyltriphenylphosphonium bromide and monoethanolamine showed almost five times stronger interactions between Br^- and the hydroxyl group than with the amine group [126]. Pour et al. examined the influence of the HBA/HBD molar ratio on the strength of hydrogen bonds in ChCl:glucose deep eutectic solvents [127]. They observed a gradual decrease in the hydrogen bonds between the two species with an increase in glucose concentration.

Alizadeh et al. conducted a study in which they estimated microheterogenity in choline chloride and some of its derivatives coupled with ethylene glycol in 1:2 molar ratio [128]. They investigated the influence of the alcohol-substituted side chain, the symmetry and length of the alkyl chains, and the number of hydroxyl groups. The researchers proved microheterogenity, in some cases even strong microheterogenity, in all the systems studied. They also observed that the polar groups always tended to form one domain, while the non-polar chains were highly dislocated for the compounds, with the side chain length lower than eight carbon units. However, when carbon units were eight or more, the non-polar groups also formed connected domains, indicating strong microheterogenity.

MD can be successfully used for predicting the dynamic, physicochemical, and structural properties of deep eutectic solvents [129–131]. With the use of MD, Kumar et al. examined the solubility of CO_2, H_2S, CH_4, and N_2 in DESs based on ethaline, reline, glycine, and oxaline, and they observed the highest solubility for H_2S and the lowest for N_2 [132]. Methyl diethanoloamine and choline chloride were investigated in the separation of H_2S, CO_2, and CH_4. This study confirmed that H_2S solubility was higher than that of CH_1 [133]. However, MD needs further improvement, due to the poor estimation of transport properties, mostly via improvement of force fields, indicating that further work should be conducted [33].

To enhance CO_2 absorption capacity, a co-solvent that absorbs this gas chemically can be used. Muthu et al. [134] conducted a study in which they determined carbon dioxide absorption capacity in a ChCl:U (1:2) DES mixed with various alkanolamines. It was concluded that CO_2 uptake was higher in alkanolamine-DES systems than that observed for pure DES or aqueous solutions of alkanolamines. This conclusion is compatible with the results obtained by Sarmad et al. [100] for amine-functionalized ChCl:MAE (1:7) DES.

Additionally, in the study conducted by Li et al. [109], it was proven that the addition of inorganic salts to a DES can change its ability to absorb CO_2. DESs containing $NiCl_2$, $FeCl_3$, $CoCl_2$, or $CuCl_2$ possess the same carbon dioxide absorption capacity as pure DESs, while the addition of $ZnCl_2$, LiCl, or NH_1Cl to DESs results in higher CO_2 absorption. Ni^{2+}, Fe^{3+}, Co^{2+}, and Cu^{2+} possess unpaired electrons on their electron shells, which facilitates their easy bonding with carbonyl oxygen.

For separation purposes, DESs have been used in several configurations. One of the approaches proposed by Lian et al. incorporated an amino acid-based DES (L-arginine:ethylene glycol in 1:5 molar ratio) into the PEBAX membrane at 5–20% g/g. With an increase in DES loading, CO_2 permeability decreased, but the CO_2/N_2 selectivity increased up to 15% loading. For 15% DES loading, the selectivity increase reached 21% and the permeability loss was only 5% [136]. N_2 permeability remained almost constant, however. Considering the temperature effect, it was found that CO_2 and N_2 permeability both increase with increasing temperature, while the selectivity decreases.

Saeed et al. examined a supported liquid membrane based on PVDF and a DES composed of betaine and urea, glycerol, or ethylene glycol in 1:3 molar ratio. They obtained a permeability of 31.23 for the glycerol-based DES and 35.67 barrers for the DES based on urea, having the separation factor CO_2/CH_1 of 43.32 and 57.53, respectively [136]. Potassium carbonate with glycerol or ethylene glycol was also investigated in a supported liquid membrane system, resulting in CO_2 permeability of 34 and 20 barrers and CO_2 selectivity over CH_4 of 59 and 34, respectively [137].

Wu et al. calculated ideal selectivity for the H_2S/CO_2 system using a 1-ethyl-3-methylimidazolium chloride plus imidazole DES and obtaining the values of 30.9, 23.7, and 17.2, respectively, for 2:1; 1:1, and 1:2 ratios at 298.2 K [138]. An important technological parameter that is crucial for the economics of the process is the regenerability of the sorption media. The efficiency of the process and the operational parameters needed for the regeneration result from the strength of interactions between the DES and the gas, so the DES structure plays a crucial role, and it has been confirmed that the ratio of DES components affects the desorption process [139,140]. When physical interactions are observed, the regeneration is energy and time efficient.

In ten cycles of absorption and desorption, the capacity remained unchanged, thus showing the potential for a long-term use [138]. Cui et al. studied the reusability of [P2222][Triz]:EG (1:2) DESs. These authors claim that no discernible decrease in capacity was obtained, but from analyzing the data one can see the capacity decrease in five cycles of absorption and desorption [91].

5. Conclusions and Perspectives

Large amounts of air pollution with acid gases have driven the search for new sorption media and, to be in line with sustainable development goals, media that are environmentally friendly. This article summarizes the properties of DESs and their suitability for carbon dioxide separation. Deep eutectic solvents have attracted much attention due to their unique properties and low production cost. Their nature, especially their negligible vapor pressure and non-flammability, makes them useful and safe in gas separation processes. The impact of the hydrogen bond donor, hydrogen bond acceptor, and molar ratio need to be thoroughly analyzed to ensure high CO_2 absorption capacity and, at the same time, high selectivity in regard to other components of the purified streams. Therefore, careful selection should be performed, and the development of molecular dynamics methods would make that easier, less time consuming, and economically advantageous. Considering their tunability, DESs have high potential in separation processes, as they can be designed to obtain desirable properties and capacity for a specific application. Still, the major challenge is their relatively high viscosity. It results from the presence of hydrogen bonds and electrostatic and van der Waals interactions between the individual components of the DESs. However, even a small addition of water can significantly decrease viscosity and thus improve diffusion. The effect of water content on the solubility of carbon dioxide in a DES has been investigated only in a few studies. Computational methods for the investigation of the phase dynamics and mechanisms occurring in the systems are highly needed, as well as research on their behavior and properties in real applications. DESs are known to be solvents with satisfying CO_2 capacity and the potential for implementation in industrial processes in the near future. It is highly desirable to focus on DESs for greener applications and to conduct further analyses on the technical and economic aspects of DES utilization. Although several DESs have been broadly studied, many more studies are still needed, especially regarding functional DESs. Future research should focus on (1) designing new, cheap, and environmentally friendly DESs with high CO_2 capacity and low viscosity to make them attractive in gas separation; (2) technoeconomic research on the use of DESs in CO_2 separation; (3) the regeneration of DESs used for CO_2 capture; (4) the prediction of their properties and CO_2 absorption capacity; and (5) the impact of water content on the DES properties, CO_2 absorption capacity, and separation parameters.

Author Contributions: Conceptualization, I.C.-K.; writing—original draft preparation, B.N. and D.W.; writing—review and editing, I.C.-K. and D.W.; supervision, I.C.-K. All authors have read and agreed to the published version of the manuscript.

Funding: This research received no external funding.

Data Availability Statement: Data sharing is not applicable to this article.

Conflicts of Interest: The authors declare no conflict of interest.

References

1. Martins, M.A.R.; Pinho, S.P.; Coutinho, J.A.P. Insights into the Nature of Eutectic and Deep Eutectic Mixtures. *J. Solution Chem.* **2019**, *48*, 962–982. [CrossRef]
2. Vieira Sanches, M.; Freitas, M.R.; Oliva, M.; Mero, A.; De Marchi, L.; Cuccaro, A.; Fumagalli, G.; Mezzetta, A.; Colombo Dugoni, G.; Ferro, M.; et al. Are natural deep eutectic solvents always a sustainable option? A bioassay-based study. *Environ. Sci. Pollut. Res.* **2023**, *30*, 17268–17279. [CrossRef]

5. Shahbaz, K.; Mjalli, F.S.; Vakili-Nezhaad, G.; AlNashef, I.M.; Asadov, A.; Farid, M.M. Thermogravimetric Measurement of Deep Eutectic Solvents Vapor Pressure. *J. Mol. Liq.* **2016**, *222*, 61–66. [CrossRef]
4. Hou, Y.C.; Yao, C.F.; Wu, W.Z. Deep Eutectic Solvents: Green Solvents for Separation Applications. *Wuli Huaxue Xuebao/ Acta Phys.—Chim. Sin.* **2018**, *34*, 873–885. [CrossRef]
5. Maniam, K.K.; Paul, S. Ionic Liquids and Deep Eutectic Solvents for CO_2 Conversion Technologies—A Review. *Materials* **2021**, *14*, 4519. [CrossRef]
6. Cotroneo-Figueroa, V.P.; Gajardo-Parra, N.F.; López-Porfiri, P.; Leiva, Á.; Gonzalez-Miquel, M.; Garrido, J.M.; Canales, R.I. Hydrogen Bond Donor and Alcohol Chain Length Effect on the Physicochemical Properties of Choline Chloride Based Deep Eutectic Solvents Mixed with Alcohols. *J. Mol. Liq.* **2022**, *345*, 116986. [CrossRef]
7. López-Porfiri, P.; Brennecke, J.F.; Gonzalez-Miquel, M. Excess Molar Enthalpies of Deep Eutectic Solvents (DESs) Composed of Quaternary Ammonium Salts and Glycerol or Ethylene Glycol. *J. Chem. Eng. Data* **2016**, *61*, 4245–4251. [CrossRef]
8. Shahbaz, K.; Mjalli, F.S.; Hashim, M.A.; Alnashef, I.M. Eutectic Solvents for the Removal of Residual Palm Oil-Based Biodiesel Catalyst. *Sep. Purif. Technol.* **2011**, *81*, 216–222. [CrossRef]
9. Abbott, A.P.; Capper, G.; Davies, D.L.; Rasheed, R.K.; Tambyrajah, V. Novel Solvent Properties of Choline Chloride/Urea Mixtures. *Chem. Commun.* **2003**, *9*, 70–71. [CrossRef]
10. Shahbaz, K.; Mjalli, F.S.; Hashim, M.A.; AlNashef, I.M. Using Deep Eutectic Solvents Based on Methyl Triphenyl Phosphunium Bromide for the Removal of Glycerol from Palm-Oil-Based Biodiesel. *Energy Fuels* **2011**, *25*, 2671–2678. [CrossRef]
11. Abbott, A.P.; Boothby, D.; Capper, G.; Davies, D.L.; Rasheed, R.K. Deep Eutectic Solvents Formed between Choline Chloride and Carboxylic Acids: Versatile Alternatives to Ionic Liquids. *J. Am. Chem. Soc.* **2004**, *126*, 9142–9147. [CrossRef] [PubMed]
12. Abbott, A.P.; Ahmed, E.I.; Prasad, K.; Qader, I.B.; Ryder, K.S. Liquid Pharmaceuticals Formulation by Eutectic Formation. *Fluid Phase Equilib.* **2017**, *448*, 2–8. [CrossRef]
13. Marcus, Y. The Entropy of Deep Eutectic Solvent Formation. *Entropy* **2018**, *20*, 524. [CrossRef] [PubMed]
14. Pontes, P.V.A.; Crespo, E.A.; Martins, M.A.R.; Silva, L.P.; Neves, C.M.S.S.; Maximo, G.J.; Hubinger, M.D.; Batista, E.A.C.; Pinho, S.P.; Coutinho, J.A.P.; et al. Measurement and PC-SAFT Modeling of Solid-Liquid Equilibrium of Deep Eutectic Solvents of Quaternary Ammonium Chlorides and Carboxylic Acids. *Fluid Phase Equilib.* **2017**, *448*, 69–80. [CrossRef]
15. García, G.; Aparicio, S.; Ullah, R.; Atilhan, M. Deep Eutectic Solvents: Physicochemical Properties and Gas Separation Applications. *Energy Fuels* **2015**, *29*, 2616–2644. [CrossRef]
16. Song, Z.; Hu, X.; Wu, H.; Mei, M.; Linke, S.; Zhou, T.; Qi, Z.; Sundmacher, K. Systematic Screening of Deep Eutectic Solvents as Sustainable Separation Media Exemplified by the CO_2 Capture Process. *ACS Sustain. Chem. Eng.* **2020**, *8*, 8741–8751. [CrossRef]
17. Ravula, S.; Larm, N.E.; Mottaleb, M.A.; Heitz, M.P.; Baker, G.A. Vapor Pressure Mapping of Ionic Liquids and Low-Volatility Fluids Using Graded Isothermal Thermogravimetric Analysis. *ChemEngineering* **2019**, *3*, 42. [CrossRef]
18. Boisset, A.; Jacquemin, J.; Anouti, M. Physical Properties of a New Deep Eutectic Solvent Based on Lithium Bis[(Trifluoromethyl)Sulfonyl]Im and N-Methylacetamide as Superionic Suitable Electrolyte for Lithium Ion Batteries and Electric Double Layer Capacitors. *Electrochim. Acta* **2013**, *102*, 120–126. [CrossRef]
19. Dietz, C.H.J.T.; Creemers, J.T.; Meuleman, M.A.; Held, C.; Sadowski, G.; Van Sint Annaland, M.; Gallucci, F.; Kroon, M.C. Determination of the Total Vapor Pressure of Hydrophobic Deep Eutectic Solvents: Experiments and Perturbed-Chain Statistical Associating Fluid Theory Modeling. *ACS Sustain. Chem. Eng.* **2019**, *7*, 4047–4057. [CrossRef]
20. Marcus, Y. *Deep Eutectic Solvents*; Springer: Berlin/Heidelberg, Germany, 2019.
21. Zhang, Q.; De Oliveira Vigier, K.; Royer, S.; Jérôme, F. Deep Eutectic Solvents: Syntheses, Properties and Applications. *Chem. Soc. Rev.* **2012**, *41*, 7108–7146. [CrossRef]
22. Omar, K.A.; Sadeghi, R. Novel Nonanol-Based Deep Eutectic Solvents: Thermophysical Properties and Their Applications in Liquid-Liquid Extraction and Amino Acid Detection. *J. Mol. Liq.* **2021**, *336*, 116359. [CrossRef]
23. Nowosielski, B.; Jamnigiewicz, M.; Łuczak, J.; Śmiechowski, M.; Warmińska, D. Experimental and Predicted Physicochemical Properties of Monopropanolamine-Based Deep Eutectic Solvents. *J. Mol. Liq.* **2020**, *309*, 113110. [CrossRef]
24. Shahbaz, K.; Bonnotian, S.; Mjalli, F.S.; Hashim, M.A.; Alnashef, I.M. Densities of Ammonium and Phosphonium Based Deep Eutectic Solvents: Prediction Using Artificial Intelligence and Group Contribution Techniques. *Thermochim. Acta* **2012**, *527*, 59–66. [CrossRef]
25. Mjalli, F.S.; Murshid, G.; Al-Zakwani, S.; Hayyan, A. Monoethanolamine-Based Deep Eutectic Solvents, Their Synthesis and Characterization. *Fluid Phase Equilib.* **2017**, *448*, 30–40. [CrossRef]
26. Ghaedi, H.; Ayoub, M.; Sufian, S.; Lal, B.; Shariff, A.M. Measurement and Correlation of Physicochemical Properties of Phosphonium-Based Deep Eutectic Solvents at Several Temperatures (293.15 K–343.15 K) for CO_2 Capture. *J. Chem. Thermodyn.* **2017**, *113*, 41–51. [CrossRef]
27. Lu, M.; Han, G.; Jiang, Y.; Zhang, X.; Deng, D.; Ai, N. Solubilities of Carbon Dioxide in the Eutectic Mixture of Levulinic Acid (or Furfuryl Alcohol) and Choline Chloride. *J. Chem. Thermodyn.* **2015**, *88*, 72–77. [CrossRef]
28. Abbott, A.P.; Harris, R.C.; Ryder, K.S.; D'Agostino, C.; Gladden, L.F.; Mantle, M.D. Glycerol Eutectics as Sustainable Solvent Systems. *Green Chem.* **2011**, *13*, 82–90. [CrossRef]

29. Basiahgari, A.; Panda, S.; Gardas, R.L. Effect of Ethylene, Diethylene, and Triethylene Glycols and Glycerol on the Physicochemical Properties and Phase Behavior of Benzyltrimethyl and Benzyltributylammonium Chloride Based Deep Eutectic Solvents at 283.15-343.15 K. *J. Chem. Eng. Data* **2018**, *63*, 2613–2627. [CrossRef]
30. Mjalli, F.S.; Vakili-Nezhaad, G.; Shahbaz, K.; Alnashef, I.M. Application of the Eötvos and Guggenheim Empirical Rules for Predicting the Density and Surface Tension of Ionic Liquids Analogues. *Thermochim. Acta* **2014**, *575*, 40–44. [CrossRef]
31. Florindo, C.; Oliveira, F.S.; Rebelo, L.P.N.N.; Fernandes, A.M.; Marrucho, I.M. Insights into the Synthesis and Properties of Deep Eutectic Solvents Based on Cholinium Chloride and Carboxylic Acids. *ACS Sustain. Chem. Eng.* **2014**, *2*, 2416–2425. [CrossRef]
32. Wang, Y.; Hou, Y.; Wu, W.; Liu, D.; Ji, Y.; Ren, S. Roles of a Hydrogen Bond Donor and a Hydrogen Bond Acceptor in the Extraction of Toluene from: N -Heptane Using Deep Eutectic Solvents. *Green Chem.* **2016**, *18*, 3089–3097. [CrossRef]
33. Hansen, B.B.; Spittle, S.; Chen, B.; Poe, D.; Zhang, Y.; Klein, J.M.; Horton, A.; Adhikari, L.; Zelovich, T.; Doherty, B.W.; et al. Deep Eutectic Solvents: A Review of Fundamentals and Applications. *Chem. Rev.* **2021**, *121*, 1232–1285. [CrossRef] [PubMed]
34. Yadav, A.; Trivedi, S.; Rai, R.; Pandey, S. Densities and Dynamic Viscosities of (Choline Chloride + glycerol) Deep Eutectic Solvent and Its Aqueous Mixtures in the Temperature Range (283.15-363.15)K. *Fluid Phase Equilib.* **2014**, *367*, 135–142. [CrossRef]
35. Mjalli, F.S. Mass Connectivity Index-Based Density Prediction of Deep Eutectic Solvents. *Fluid Phase Equilib.* **2016**, *409*, 312–317. [CrossRef]
36. Haghbakhsh, R.; Raeissi, S.; Duarte, A.R.C. Group Contribution and Atomic Contribution Models for the Prediction of Various Physical Properties of Deep Eutectic Solvents. *Sci. Rep.* **2021**, *11*, 6684. [CrossRef] [PubMed]
37. Abbott, A.P.; Harris, R.C.; Ryder, K.S. Application of Hole Theory to Define Ionic Liquids by Their Transport Properties. *J. Phys. Chem. B* **2007**, *111*, 4910–4913. [CrossRef] [PubMed]
38. Sarmad, S.; Xie, Y.; Mikkola, J.P.; Ji, X. Screening of Deep Eutectic Solvents (DESs) as Green CO_2 Sorbents: From Solubility to Viscosity. *New. J. Chem.* **2016**, *41*, 290–301. [CrossRef]
39. Mjalli, F.S.; Naser, J. Viscosity Model for Choline Chloride-Based Deep Eutectic Solvents. *Asia-Pac. J. Chem. Eng.* **2015**, *10*, 273–281. [CrossRef]
40. Mjalli, F.S.; Al-Hajri, R.; Al-Muhtaseb, A.; Ahmed, O.; Nagaraju, M. Novel Amino Acid-Based Ionic Liquid Analogues: Neutral Hydroxylic and Sulfur-Containing Amino Acids. *Asia-Pac. J. Chem. Eng.* **2016**, *11*, 683–694. [CrossRef]
41. Florindo, C.; Oliveira, M.M.; Branco, L.C.; Marrucho, I.M. Carbohydrates-Based Deep Eutectic Solvents: Thermophysical Properties and Rice Straw Dissolution. *J. Mol. Liq.* **2017**, *247*, 441–447. [CrossRef]
42. Maugeri, Z.; Domínguez De María, P. Novel Choline-Chloride-Based Deep-Eutectic-Solvents with Renewable Hydrogen Bond Donors: Levulinic Acid and Sugar-Based Polyols. *RSC Adv.* **2012**, *2*, 421–425. [CrossRef]
43. D'Agostino, C.; Harris, R.C.; Abbott, A.P.; Gladden, L.F.; Mantle, M.D. Molecular Motion and Ion Diffusion in Choline Chloride Based Deep Eutectic Solvents Studied by 1H Pulsed Field Gradient NMR Spectroscopy. *Phys. Chem. Chem. Phys.* **2011**, *13*, 21383–21391. [CrossRef] [PubMed]
44. Haghbakhsh, R.; Parvaneh, K.; Raeissi, S.; Shariati, A. A General Viscosity Model for Deep Eutectic Solvents: The Free Volume Theory Coupled with Association Equations of State. *Fluid Phase Equilib.* **2018**, *470*, 193–202. [CrossRef]
45. Benguerba, Y.; Alnashef, I.M.; Erto, A.; Balsamo, M.; Ernst, B. A Quantitative Prediction of the Viscosity of Amine Based DESs Using Sσ-Profile Molecular Descriptors. *J. Mol. Struct.* **2019**, *1184*, 357–363. [CrossRef]
46. Hayyan, A.; Mjalli, F.S.; Alnashef, I.M.; Al-Wahaibi, Y.M.; Al-Wahaibi, T.; Hashim, M.A. Glucose-Based Deep Eutectic Solvents: Physical Properties. *J. Mol. Liq.* **2013**, *178*, 137–141. [CrossRef]
47. Omar, K.A.; Sadeghi, R. Novel Deep Eutectic Solvents Based on Pyrogallol: Synthesis and Characterizations. *J. Chem. Eng. Data* **2021**, *66*, 2088–2095. [CrossRef]
48. Chen, Y.; Chen, W.; Fu, L.; Yang, Y.; Wang, Y.; Hu, X.; Wang, F.; Mu, T. Surface Tension of 50 Deep Eutectic Solvents: Effect of Hydrogen-Bonding Donors, Hydrogen-Bonding Acceptors, Other Solvents, and Temperature. *Ind. Eng. Chem. Res.* **2019**, *58*, 12743–12750. [CrossRef]
49. Mjalli, F.S.; Al-Azzawi, M. Aliphatic Amino Acids as Possible Hydrogen Bond Donors for Preparing Eutectic Solvents. *J. Mol. Liq.* **2021**, *330*, 115637. [CrossRef]
50. Bagh, F.S.G.; Shahbaz, K.; Mjalli, F.S.; AlNashef, I.M.; Hashim, M.A. Electrical Conductivity of Ammonium and Phosphonium Based Deep Eutectic Solvents: Measurements and Artificial Intelligence-Based Prediction. *Fluid Phase Equilib.* **2013**, *356*, 30–37. [CrossRef]
51. Pandey, A.; Pandey, S. Solvatochromic Probe Behavior within Choline Chloride-Based Deep Eutectic Solvents: Effect of Temperature and Water. *J. Phys. Chem. B* **2014**, *118*, 14652–14661. [CrossRef]
52. Teles, A.R.R.; Capela, E.V.; Carmo, R.S.; Coutinho, J.A.P.; Silvestre, A.J.D.; Freire, M.G. Solvatochromic Parameters of Deep Eutectic Solvents Formed by Ammonium-Based Salts and Carboxylic Acids. *Fluid Phase Equilib.* **2017**, *448*, 15–21. [CrossRef] [PubMed]
53. Florindo, C.; McIntosh, A.J.S.; Welton, T.; Branco, L.C.; Marrucho, I.M. A Closer Look into Deep Eutectic Solvents: Exploring Intermolecular Interactions Using Solvatochromic Probes. *Phys. Chem. Chem. Phys.* **2017**, *20*, 206–213. [CrossRef] [PubMed]
54. Ghaedi, H.; Ayoub, M.; Sufian, S.; Lal, B.; Uemura, Y. Thermal Stability and FT-IR Analysis of Phosphonium-Based Deep Eutectic Solvents with Different Hydrogen Bond Donors. *J. Mol. Liq.* **2017**, *242*, 395–403. [CrossRef]

55. Zhao, H.; Baker, G.A.; Holmes, S. Protease Activation in Glycerol-Based Deep Eutectic Solvents. *J. Mol. Catal. B Enzym.* **2011**, *72*, 163–167. [CrossRef] [PubMed]
56. Delgado-Mellado, N.; Larriba, M.; Navarro, P.; Rigual, V.; Ayuso, M.; García, J.; Rodríguez, F. Thermal Stability of Choline Chloride Deep Eutectic Solvents by TGA/FTIR-ATR Analysis. *J. Mol. Liq.* **2018**, *260*, 37–43. [CrossRef]
57. Naser, J.; Mjalli, F.S.; Gano, Z.S. Molar Heat Capacity of Selected Type III Deep Eutectic Solvents. *J. Chem. Eng. Data* **2016**, *61*, 1608–1615. [CrossRef]
58. Siongco, K.R.; Leron, R.B.; Caparanga, A.R.; Li, M.H. Molar Heat Capacities and Electrical Conductivities of Two Ammonium-Based Deep Eutectic Solvents and Their Aqueous Solutions. *Thermochim. Acta* **2013**, *566*, 50–56. [CrossRef]
59. Zhang, K.; Li, H.; Ren, S.; Wu, W.; Bao, Y. Specific Heat Capacities of Two Functional Ionic Liquids and Two Functional Deep Eutectic Solvents for the Absorption of SO_2. *J. Chem. Eng. Data* **2017**, *62*, 2708–2712. [CrossRef]
60. Taherzadeh, M.; Haghbakhsh, R.; Duarte, A.R.C.; Raeissi, S. Estimation of the Heat Capacities of Deep Eutectic Solvents. *J. Mol. Liq.* **2020**, *307*, 112940. [CrossRef]
61. Bunquin, R.M.A.; Caparanga, A.R. Predicting the Heat Capacities of Ammonium- And Phosphonium-Based Deep Eutectic Solvents Using Artificial Neural Network. *J. Phys. Conf. Ser.* **2021**, *1893*, 012001. [CrossRef]
62. Su, H.Z.; Yin, J.M.; Liu, Q.S.; Li, C.P. Properties of Four Deep Eutectic Solvents: Density, Electrical Conductivity, Dynamic Viscosity and Refractive Index. *Wuli Huaxue Xuebao Acta Phys.—Chim. Sin.* **2015**, *31*, 1468–1473. [CrossRef]
63. Seki, S.; Tsuzuki, S.; Hayamizu, K.; Umebayashi, Y.; Serizawa, N.; Takei, K.; Miyashiro, H. Comprehensive Refractive Index Property for Room-Temperature Ionic Liquids. *J. Chem. Eng. Data* **2012**, *57*, 2211–2216. [CrossRef]
64. Murshid, G.; Mjalli, F.S.; Naser, J.; Al-Zakwani, S.; Hayyan, A. Novel Diethanolamine Based Deep Eutectic Mixtures for Carbon Dioxide (CO_2) Capture: Synthesis and Characterisation. *Phys. Chem. Liq.* **2019**, *57*, 473–490. [CrossRef]
65. Sánchez, P.B.; González, B.; Salgado, J.; José Parajó, J.; Domínguez, Á. Physical Properties of Seven Deep Eutectic Solvents Based on L-Proline or Betaine. *J. Chem. Thermodyn.* **2019**, *131*, 517–523. [CrossRef]
66. Li, G.; Deng, D.; Chen, Y.; Shan, H.; Ai, N. Solubilities and Thermodynamic Properties of CO_2 in Choline-Chloride Based Deep Eutectic Solvents. *J. Chem. Thermodyn.* **2014**, *75*, 58–62. [CrossRef]
67. Husson-Borg, P.; Majer, V.; Costa Gomes, M.F. Solubilities of Oxygen and Carbon Dioxide in Butyl Methyl Imidazolium Tetrafluoroborate as a Function of Temperature and at Pressures Close to Atmospheric Pressure. *J. Chem. Eng. Data* **2003**, *48*, 480–485. [CrossRef]
68. Chen, Y.; Ai, N.; Li, G.; Shan, H.; Cui, Y.; Deng, D. Solubilities of Carbon Dioxide in Eutectic Mixtures of Choline Chloride and Dihydric Alcohols. *J. Chem. Eng. Data* **2014**, *59*, 1247–1253. [CrossRef]
69. Deng, D.; Jiang, Y.; Liu, X.; Zhang, Z.; Ai, N. Investigation of Solubilities of Carbon Dioxide in Five Levulinic Acid-Based Deep Eutectic Solvents and Their Thermodynamic Properties. *J. Chem. Thermodyn.* **2016**, *103*, 212–217. [CrossRef]
70. Liu, F.; Chen, W.; Mi, J.; Zhang, J.Y.; Kan, X.; Zhong, F.Y.; Huang, K.; Zheng, A.M.; Jiang, L. Thermodynamic and Molecular Insights into the Absorption of H_2S, CO_2, and CH_4 in Choline Chloride plus Urea Mixtures. *AIChE J.* **2019**, *65*, e16574. [CrossRef]
71. Wu, H.; Shen, M.; Chen, X.; Yu, G.; Abdeltawab, A.A.; Yakout, S.M. New Absorbents for Hydrogen Sulfide: Deep Eutectic Solvents of Tetrabutylammonium Bromide/Carboxylic Acids and Choline Chloride/Carboxylic Acids. *Sep. Purif. Technol.* **2019**, *224*, 281–289. [CrossRef]
72. Jiang, W.J.; Zhong, F.Y.; Liu, Y.; Huang, K. Effective and Reversible Capture of NH3 by Ethylamine Hydrochloride Plus Glycerol Deep Eutectic Solvents. *ACS Sustain. Chem. Eng.* **2019**, *7*, 10552–10560. [CrossRef]
73. Jiang, W.J.; Zhang, J.B.; Zou, Y.T.; Peng, H.J.; Huang, K. Manufacturing Acidities of Hydrogen-Bond Donors in Deep Eutectic Solvents for Effective and Reversible NH3Capture. *ACS Sustain. Chem. Eng.* **2020**, *8*, 13408–13417. [CrossRef]
74. Kim, J.E.; Lim, J.S.; Kang, J.W. Measurement and Correlation of Solubility of Carbon Dioxide in 1-Alkyl-3-Methylimidazolium Hexafluorophosphate Ionic Liquids. *Fluid Phase Equilib.* **2011**, *306*, 251–255. [CrossRef]
75. Blanchard, L.A.; Gu, Z.; Brennecke, J.F. High-Pressure Phase Behavior of Ionic Liquid/CO_2 Systems. *J. Phys. Chem. B* **2001**, *105*, 2437–2444. [CrossRef]
76. Bi, Y.; Hu, Z.; Lin, X.; Ahmad, N.; Xu, J.; Xu, X. Efficient CO_2 Capture by a Novel Deep Eutectic Solvent through Facile, One-Pot Synthesis with Low Energy Consumption and Feasible Regeneration. *Sci. Total Environ.* **2020**, *705*, 135798. [CrossRef] [PubMed]
77. Jiang, B.; Zhang, H.; Zhang, L.; Zhang, N.; Huang, Z.; Chen, Y.; Sun, Y.; Tantai, X. Novel Deep Eutectic Solvents for Highly Efficient and Reversible Absorption of SO_2 by Preorganization Strategy. *ACS Sustain. Chem. Eng.* **2019**, *7*, 8347–8357. [CrossRef]
78. Wang, C.; Guo, Y.; Zhu, X.; Cui, G.; Li, H.; Dai, S. Highly Efficient CO_2 Capture by Tunable Alkanolamine-Based Ionic Liquids with Multidentate Cation Coordination. *Chem. Commun.* **2012**, *48*, 6526. [CrossRef]
79. Cui, G.; Liu, J.; Lyu, S.; Wang, H.; Li, Z.; Wang, J. Efficient and Reversible SO_2 Absorption by Environmentally Friendly Task-Specific Deep Eutectic Solvents of PPZBr + Gly. *ACS Sustain. Chem. Eng.* **2019**, *7*, 14236–14246. [CrossRef]
80. Sheng, K.; Kang, Y.; Li, J.; Xu, H.; Li, D. High-Efficiency Absorption of SO_2 by a New Type of Deep Eutectic Solvents. *Energy Fuels* **2020**, *34*, 3440–3448.
81. Zubeir, L.F.; Romanos, G.E.; Weggemans, W.M.A.; Iliev, B.; Schubert, T.J.S.; Kroon, M.C. Solubility and Diffusivity of CO_2 in the Ionic Liquid 1-Butyl-3-Methylimidazolium Tricyanomethanide within a Large Pressure Range (0.01 MPa to 10 MPa). *J. Chem. Eng. Data* **2015**, *60*, 1544–1562. [CrossRef]

82. Zubeir, L.F.; Lacroix, M.H.M.; Kroon, M.C. Low Transition Temperature Mixtures as Innovative and Sustainable CO_2 Capture Solvents. *J. Phys. Chem. B* **2014**, *118*, 14429–14441. [CrossRef]
83. Lei, Z.; Dai, C.; Chen, B. Gas Solubility in Ionic Liquids. *Chem. Rev.* **2014**, *114*, 1289–1326. [CrossRef] [PubMed]
84. Aki, S.N.V.K.; Mellein, B.R.; Saurer, E.M.; Brennecke, J.F. High-Pressure Phase Behavior of Carbon Dioxide with Imidazolium-Based Ionic Liquids. *J. Phys. Chem. B* **2004**, *108*, 20355–20365. [CrossRef]
85. Zubeir, L.F.; Van Osch, D.J.G.P.; Rocha, M.A.A.; Banat, F.; Kroon, M.C. Carbon Dioxide Solubilities in Decanoic Acid-Based Hydrophobic Deep Eutectic Solvents. *J. Chem. Eng. Data* **2018**, *63*, 913–919. [CrossRef] [PubMed]
86. Haider, M.B.; Jha, D.; Marriyappan Sivaguanam, B.; Kumar, R. Thermodynamic and Kinetic Studies of CO_2 Capture by Glycol and Amine-Based Deep Eutectic Solvents. *J. Chem. Eng. Data* **2018**, *63*, 2671–2680. [CrossRef]
87. Liu, X.; Gao, B.; Jiang, Y.; Ai, N.; Deng, D. Solubilities and Thermodynamic Properties of Carbon Dioxide in Guaiacol-Based Deep Eutectic Solvents. *J. Chem. Eng. Data* **2017**, *62*, 1448–1455. [CrossRef]
88. Altamash, T.; Nasser, M.S.; Elhamarnah, Y.; Magzoub, M.; Ullah, R.; Qiblawey, H.; Aparicio, S.; Atilhan, M. Gas Solubility and Rheological Behavior Study of Betaine and Alanine Based Natural Deep Eutectic Solvents (NADES). *J. Mol. Liq.* **2018**, *256*, 286–295. [CrossRef]
89. Akhmetshina, A.I.; Petukhov, A.N.; Mechergui, A.; Vorotyntsev, A.V.; Nyuchev, A.V.; Moskvichev, A.A.; Vorotyntsev, I.V. Evaluation of Methanesulfonate-Based Deep Eutectic Solvent for Ammonia Sorption. *J. Chem. Eng. Data* **2018**, *63*, 1896–1904. [CrossRef]
90. Yan, H.; Zhao, L.; Bai, Y.; Li, F.; Dong, H.; Wang, H.; Zhang, X.; Zeng, S. Superbase Ionic Liquid-Based Deep Eutectic Solvents for Improving CO_2 Absorption. *ACS Sustain. Chem. Eng.* **2020**, *8*, 2523–2530. [CrossRef]
91. Cui, G.; Lv, M.; Yang, D. Efficient CO_2 Absorption by Azolide-Based Deep Eutectic Solvents. *Chem. Commun.* **2019**, *55*, 1426–1429. [CrossRef]
92. Shukla, S.K.; Mikkola, J.P. Intermolecular Interactions upon Carbon Dioxide Capture in Deep-Eutectic Solvents. *Phys. Chem. Chem. Phys.* **2018**, *20*, 24591–24601. [CrossRef] [PubMed]
93. Li, X.; Liu, X.; Deng, D. Solubilities and Thermodynamic Properties of CO_2 in Four Azole-Based Deep Eutectic Solvents. *J. Chem. Eng. Data* **2018**, *63*, 2091–2096. [CrossRef]
94. Ghaedi, H.; Ayoub, M.; Sufian, S.; Shariff, A.M.; Hailegiorgis, S.M.; Khan, S.N. CO_2 Capture with the Help of Phosphonium-Based Deep Eutectic Solvents. *J. Mol. Liq.* **2017**, *243*, 564–571. [CrossRef]
95. Wang, J.; Cheng, H.; Song, Z.; Chen, L.; Deng, L.; Qi, Z. Carbon Dioxide Solubility in Phosphonium-Based Deep Eutectic Solvents: An Experimental and Molecular Dynamics Study. *Ind. Eng. Chem. Res.* **2019**, *58*, 17514–17523. [CrossRef]
96. Haider, M.B.; Kumar, R. Solubility of CO_2 and CH_4 in Sterically Hindered Amine-Based Deep Eutectic Solvents. *Sep. Purif. Technol.* **2020**, *248*, 117055. [CrossRef]
97. Ali, E.; Hadj-Kali, M.K.; Mulyono, S.; Alnashef, I.; Fakeeha, A.; Mjalli, F.; Hayyan, A. Solubility of CO_2 in Deep Eutectic Solvents: Experiments and Modelling Using the Peng-Robinson Equation of State. *Chem. Eng. Res. Des.* **2014**, *92*, 1898–1906. [CrossRef]
98. Liu, X.; Gao, B.; Deng, D. SO_2 Absorption/Desorption Performance of Renewable Phenol-Based Deep Eutectic Solvents. *Sep. Sci. Technol.* **2018**, *53*, 2150–2158. [CrossRef]
99. Shukla, S.K.; Nikjoo, D.; Mikkola, J.P. Is Basicity the Sole Criterion for Attaining High Carbon Dioxide Capture in Deep-Eutectic Solvents? *Phys. Chem. Chem. Phys.* **2020**, *22*, 966–970. [CrossRef]
100. Sarmad, S.; Nikjoo, D.; Mikkola, J.P. Amine Functionalized Deep Eutectic Solvent for CO_2 Capture: Measurements and Modeling. *J. Mol. Liq.* **2020**, *309*, 113159. [CrossRef]
101. Sze, L.L.; Pandey, S.; Ravula, S.; Pandey, S.; Zhao, H.; Baker, G.A.; Baker, S.N. Ternary Deep Eutectic Solvents Tasked for Carbon Dioxide Capture. *ACS Sustain. Chem. Eng.* **2014**, *2*, 2117–2123. [CrossRef]
102. Jiang, B.; Ma, J.; Yang, N.; Huang, Z.; Zhang, N.; Tantai, X.; Sun, Y.; Zhang, L. Superbase/Acylamido-Based Deep Eutectic Solvents for Multiple-Site Efficient CO_2 Absorption. *Energy and Fuels* **2019**, *33*, 7569–7577. [CrossRef]
103. Pishro, K.A.; Murshid, G.; Mjalli, F.S.; Naser, J. Investigation of CO_2 Solubility in Monoethanolamine Hydrochloride Based Deep Eutectic Solvents and Physical Properties Measurements. *Chin. J. Chem. Eng.* **2020**, *28*, 2848–2856. [CrossRef]
104. Ren, H.; Lian, S.; Wang, X.; Zhang, Y.; Duan, E. Exploiting the Hydrophilic Role of Natural Deep Eutectic Solvents for Greening CO_2 Capture. *J. Clean. Prod.* **2018**, *193*, 802–810. [CrossRef]
105. Trivedi, T.J.; Lee, J.H.; Lee, H.J.; Jeong, Y.K.; Choi, J.W. Deep Eutectic Solvents as Attractive Media for CO_2 Capture. *Green Chem.* **2016**, *18*, 2834–2842. [CrossRef]
106. Siani, G.; Tiecco, M.; Di Profio, P.; Guernelli, S.; Fontana, A.; Ciulla, M.; Canale, V. Physical Absorption of CO_2 in Betaine/Carboxylic Acid-Based Natural Deep Eutectic Solvents. *J. Mol. Liq.* **2020**, *315*, 113708. [CrossRef]
107. Ramdin, M.; de Loos, T.W.; Vlugt, T.J.H. State-of-the-Art of CO_2 Capture with Ionic Liquids. *Ind. Eng. Chem. Res.* **2012**, *51*, 8149–8177. [CrossRef]
108. Kanakubo, M.; Makino, T.; Taniguchi, T.; Nokami, T.; Itoh, T. CO_2 Solubility in Ether Functionalized Ionic Liquids on Mole Fraction and Molarity Scales. *ACS Sustain. Chem. Eng.* **2016**, *4*, 525–535. [CrossRef]
109. Li, Z.; Wang, L.; Li, C.; Cui, Y.; Li, S.; Yang, G.; Shen, Y. Absorption of Carbon Dioxide Using Ethanolamine-Based Deep Eutectic Solvents. *ACS Sustain. Chem. Eng.* **2019**, *7*, 10403–10414. [CrossRef]
110. Shukla, S.K.; Mikkola, J.P. Unusual Temperature-Promoted Carbon Dioxide Capture in Deep-Eutectic Solvents: The Synergistic Interactions. *Chem. Commun.* **2019**, *55*, 3939–3942. [CrossRef]

111. Cichowska-Kopczyńska, I.; Warmińska, D.; Nowosielski, B. Solubility of Carbon Dioxide in Deep Eutectic Solvents Based on 3-Amino-1-Propanol and Tetraalkylammonium Salts at Low Pressure. *Materials* **2021**, *14*, 594. [CrossRef]
112. Su, W.C.; Wong, D.S.H.; Li, M.H. Effect of Water on Solubility of Carbon Dioxide in (Aminomethanamide + 2-Hydroxy-N,N,N-Trimethylethanaminium Chloride). *J. Chem. Eng. Data* **2009**, *54*, 1951–1955. [CrossRef]
113. Xie, Y.; Dong, H.; Zhang, S.; Lu, X.; Ji, X. Effect of Water on the Density, Viscosity, and CO_2 Solubility in Choline Chloride/Urea. *J. Chem. Eng. Data* **2014**, *59*, 3344–3352. [CrossRef]
114. Ma, C.; Sarmad, S.; Mikkola, J.P.; Ji, X. Development of Low-Cost Deep Eutectic Solvents for CO_2 Capture. *Energy Procedia* **2017**, *142*, 3320–3325. [CrossRef]
115. Shah, D.; Mjalli, F.S. Effect of Water on the Thermo-Physical Properties of Reline: An Experimental and Molecular Simulation Based Approach. *Phys. Chem. Chem. Phys.* **2014**, *16*, 23900–23907. [CrossRef] [PubMed]
116. Zhekenov, T.; Toksanbayev, N.; Kazakbayeva, Z.; Shah, D.; Mjalli, F.S. Formation of Type III Deep Eutectic Solvents and Effect of Water on Their Intermolecular Interactions. *Fluid Phase Equilib.* **2017**, *441*, 43–48. [CrossRef]
117. Fetisov, E.O.; Harwood, D.B.; Kuo, I.F.W.; Warrag, S.E.E.; Kroon, M.C.; Peters, C.J.; Siepmann, J.I. First-Principles Molecular Dynamics Study of a Deep Eutectic Solvent: Choline Chloride/Urea and Its Mixture with Water. *J. Phys. Chem. B* **2018**, *122*, 1245–1254. [CrossRef]
118. Gao, Q.; Zhu, Y.; Ji, X.; Zhu, W.; Lu, L.; Lu, X. Effect of Water Concentration on the Microstructures of Choline Chloride/Urea (1:2)/Water Mixture. *Fluid Phase Equilib.* **2018**, *470*, 134–139. [CrossRef]
119. Sun, H.; Li, Y.; Wu, X.; Li, G. Theoretical Study on the Structures and Properties of Mixtures of Urea and Choline Chloride. *J. Mol. Model.* **2013**, *19*, 2433–2441. [CrossRef]
120. Perkins, S.L.; Painter, P.; Colina, C.M. Experimental and Computational Studies of Choline Chloride-Based Deep Eutectic Solvents. *J. Chem. Eng. Data* **2014**, *59*, 3652–3662. [CrossRef]
121. Naik, P.K.; Paul, S.; Banerjee, T. Physicochemical Properties and Molecular Dynamics Simulations of Phosphonium and Ammonium Based Deep Eutectic Solvents. *J. Solution Chem.* **2019**, *48*, 1046–1065. [CrossRef]
122. Migliorati, V.; Sessa, F.; D'Angelo, P. Deep Eutectic Solvents: A Structural Point of View on the Role of the Cation. *Chem. Phys. Lett. X* **2019**, *737*, 100001. [CrossRef]
123. Ferreira, E.S.C.; Voroshylova, I.V.; Figueiredo, N.M.; Pereira, C.M.; Cordeiro, M.N.D.S. Computational and Experimental Study of Propeline: A Choline Chloride Based Deep Eutectic Solvent. *J. Mol. Liq.* **2020**, *298*, 111978. [CrossRef]
124. Ferreira, E.S.C.; Voroshylova, I.V.; Pereira, C.M.; Cordeiro, M.N.D.S. Improved Force Field Model for the Deep Eutectic Solvent Ethaline: Reliable Physicochemical Properties. *J. Phys. Chem. B* **2016**, *120*, 10124–10137. [CrossRef] [PubMed]
125. Rozas, S.; Alomari, N.; Atilhan, M.; Aparicio, S. Theoretical Insights into the Cineole-Based Deep Eutectic Solvents. *J. Chem. Phys.* **2021**, *154*, 184504. [CrossRef] [PubMed]
126. Kussainova, D.; Shah, D. Structure of Monoethanolamine Based Type III DESs: Insights from Molecular Dynamics Simulations. *Fluid Phase Equilib.* **2019**, *482*, 112–117. [CrossRef]
127. Barani Pour, S.; Jahanbin Sardroodi, J.; Rastkar Ebrahimzadeh, A. The Study of Structure and Interactions of Glucose-Based Natural Deep Eutectic Solvents by Molecular Dynamics Simulation. *J. Mol. Liq.* **2021**, *334*, 115956. [CrossRef]
128. Alizadeh, V.; Celler, D.; Malberg, F.; Sánchez, P.B.; Padua, A.; Kirchner, B. Strong Microheterogeneity in Novel Deep Eutectic Solvents. *ChemPhysChem* **2019**, *20*, 1786–1792. [CrossRef]
129. Doherty, B.; Acevedo, O. OPLS Force Field for Choline Chloride-Based Deep Eutectic Solvents. *J. Phys. Chem. B* **2018**, *122*, 9982–9993. [CrossRef]
130. Altamash, T.; Atilhan, M.; Aliyan, A.; Ullah, R.; Garcia, G.; Aparicio, S. Insights into Choline Chloride-Phenylacetic Acid Deep Eutectic Solvent for CO_2 Absorption. *RSC Adv.* **2016**, *6*, 109201–109210. [CrossRef]
131. Ullah, R.; Atilhan, M.; Anaya, B.; Khraisheh, M.; Garcia, G.; Elkhattat, A.; Tariq, M.; Aparicio, S. A Detailed Study of Cholinium Chloride and Levulinic Acid Deep Eutectic Solvent System for CO_2 capture via Experimental and Molecular Simulation Approaches. *Phys. Chem. Chem. Phys.* **2015**, *17*, 20941–20960. [CrossRef]
132. Kumar, K.; Keshri, S.; Bharti, A.; Kumar, S.; Mogurampelly, S. Solubility of Gases in Choline Chloride-Based Deep Eutectic Solvents from Molecular Dynamics Simulation. *Ind. Eng. Chem. Res.* **2022**, *61*, 4659–4671. [CrossRef]
133. Jahanbakhsh-Bonab, P.; Jahanbin Sardroodi, J.; Sadegh Avestan, M. The Pressure Effects on the Amine-Based DES Performance in NG Sweetening: Insights from Molecular Dynamics Simulation. *Fuel* **2022**, *323*, 124249. [CrossRef]
134. Muthu, A.; Maheswari, U.; Palanivelu, K. Absorption of Carbon Dioxide in Alkanolamines in Deep Eutectic Solvent Medium for CO_2 Gas Separation. *J. Chem. Pharm. Sci.* **2014**, *974*, 2115.
135. Lian, S.; Li, R.; Zhang, Z.; Liu, Q.; Song, C.; Lu, S. Improved CO_2 Separation Performance and Interfacial Affinity of Composite Membranes by Incorporating Amino Acid-Based Deep Eutectic Solvents. *Sep. Purif. Technol.* **2021**, *272*, 118953. [CrossRef]
136. Saeed, U.; Khan, A.L.; Gilani, M.A.; Bilad, M.R.; Khan, A.U. Supported Deep Eutectic Liquid Membranes with Highly Selective Interaction Sites for Efficient CO_2 Separation. *J. Mol. Liq.* **2021**, *342*, 117509. [CrossRef]
137. Saeed, U.; Khan, A.U.; Khan, A.L.; Gilani, M.A.; Bilad, M.R. Separation of Carbon Dioxide by Potassium Carbonate Based Supported Deep Eutectic Liquid Membranes: Influence of Hydrogen Bond Donor. *J. Membr. Sci. Res.* **2022**, *8*. [CrossRef]
138. Wu, X.; Cheng, N.N.; Jiang, H.; Zheng, W.T.; Chen, Y.; Huang, K.; Liu, F. 1-Ethyl-3-Methylimidazolium Chloride plus Imidazole Deep Eutectic Solvents as Physical Solvents for Remarkable Separation of H2S from CO_2. *Sep. Purif. Technol.* **2021**, *276*, 119313. [CrossRef]

139. Wang, Y.; Ren, S.; Hou, Y.; Wu, W. Capture of Acidic Gases from Flue Gas by Deep Eutectic Solvents. *Processes* **2021**, *9*, 1268. [CrossRef]
140. Yang, D.; Zhang, S.; De-en, J.; Dai, S. SO_2 Absorption in EmimCl–TEG Deep Eutectic Solvents. *Phys. Chem. Chem. Phys.* **2018**, *20*, 15168–15173.

Załącznik A2

B. Nowosielski, M. Jamrógiewicz, J. Łuczak, M. Śmiechowski, D. Warmińska, Experimental and predicted physicochemical properties of monopropanolamine-based deep eutectic solvents, J. Mol. Liq. 309 (2020) 113110. https://doi.org/10.1016/j.molliq.2020.113110. **IF_{2020}: 6,16, $MNSW_{2020}$: 100**

Journal of Molecular Liquids 309 (2020) 113110

Contents lists available at ScienceDirect

Journal of Molecular Liquids

journal homepage: www.elsevier.com/locate/molliq

Experimental and predicted physicochemical properties of monopropanolamine-based deep eutectic solvents

Bartosz Nowosielski [a], Marzena Jamróg iewicz [c], Justyna Łuczak [b], Maciej Śmiechowski [a], Dorota Warmińska [a,*]

[a] Department of Physical Chemistry, Faculty of Chemistry, Gdańsk University of Technology, ul. Narutowicza 11/12, 80-233 Gdańsk, Poland
[b] Department of Process Engineering and Chemical Technology, Faculty of Chemistry, Gdańsk University of Technology, ul. Narutowicza 11/12, 80-233 Gdańsk, Poland
[c] Department of Physical Chemistry, Faculty of Pharmacy, Medical University of Gdańsk, Al. Gen. Hallera 107, 80-416 Gdańsk, Poland

ARTICLE INFO

Article history:
Received 19 February 2020
Received in revised form 2 April 2020
Accepted 7 April 2020
Available online 11 April 2020

Keywords:
DES
3-amino-1-propanol
Tetraalkylammonium salts
Physicochemical properties

ABSTRACT

In this work, the novel deep eutectic solvents (DESs) based on 3-amino-1-propanol (AP) as hydrogen bond donor (HBD) and tetrabutylammonium bromide (TBAB) or tetrabutylammonium chloride (TBAC) or tetraethylammonium chloride (TEAC) as hydrogen bond acceptors (HBAs) were synthesized with different molar ratios of 1: 4, 1: 6 and 1: 8 salt to AP. Fourier Transform Infrared Spectroscopy measurements were performed to provide an evidence of any chemical structure changes. Physical properties of the prepared DESs including densities, viscosities, refractive indices and sound velocities were measured within the temperature range of 293.15–333.15 K at the pressure of 0.1 MPa. They were analyzed in terms of estimating the effect of HBA to HBD molar ratio, anion and length of alkyl chain in a salt, and their temperature dependences were fitted by empirical equations. Thermal expansion coefficients and activation energies for viscous flow were obtained accordingly. Moreover, experimental values of density and refractive index were compared with predicted ones. For prediction of density, Rackett equation modified by Spencer and Danner and the mass connectivity index-based method were used, while refractive index was estimated by the atomic contribution method.

1. Introduction

One of the main directions of global research nowadays is the search for technologies aimed at reducing carbon dioxide emissions. This gas, mainly responsible for the occurrence of the greenhouse effect, is emitted to the atmosphere in the processes of electricity and heat production based on fossil combustion [1]. In power plants, due to the low pressure of flue gases, one of the most common technologies used for CO_2 removal is absorption using aqueous amine solutions. The highest efficiency of the CO_2 removal process is achieved by chemical absorption using a 30% aqueous solution of monoethanolamine (MEA) [2]. However, the corrosive nature of the reaction environment and its loss due to volatility make it desirable to search for alternative solvents that could replace aqueous solutions of MEA or other alkanolamines.

Since 2008, attempts have been noted in the literature to use deep eutectic mixtures for the removal of CO_2 from industrial process streams [3]. These solvents have similar physical properties as ionic liquids, are practically non-volatile and non-flammable, and exhibit high thermal and electrochemical stability, but are definitely cheaper, less toxic and often biodegradable [4–9]. As with ionic liquids, their physical properties can be controlled by changing the composition and proportions of the components making up a given eutectic mixture, so as to obtain advantageous properties for a specific application.

The research performed so far clearly shows that the solubility of carbon dioxide depends on the structure of a deep eutectic mixture, which determines not only the chemical properties of the solvent (the possibility of chemisorption or the lack thereof), but also its physical properties, including viscosity—a key parameter in the technological process [10]. It has been established, that DESs based on alkanolamines have much higher CO_2 absorption capacity than other deep eutectic solvents, for which no chemical reactions with carbon dioxide are observed [7,10]. So far, deep eutectic solvents with monoethanolamine [10–12], diethanolamine [10,12,13], triethanolamine [14] and methyldiethanolamine [10,12,13] as hydrogen bond donor and DESs based on monoethanolamine chloride [7] or *N,N*-diethylenethanolammonium chloride [14] as hydrogen bond acceptor have been studied. For these systems the physical properties such as density, viscosity, surface tension and refractive index have been determined.

In this study, novel deep eutectic solvents were prepared by introducing 3-amino-1-propanol (AP), which is a good CO_2 absorbent, as a hydrogen bond donor (HBD) coupled with tetrabutylammonium bromide (TBAB) or tetrabutylammonium chloride (TBAC) or tetraethylammonium chloride (TEAC) as hydrogen bond acceptors (HBAs). The DESs were obtained for three different salts to amine

* Corresponding author.
E-mail address: dorwarm@pg.edu.pl (D. Warmińska).

https://doi.org/10.1016/j.molliq.2020.113110
0167-7322/

molar ratios of 1:4, 1:6 and 1:8 and characterized by measuring their main physical properties such as density, viscosity, refractive index and sound velocity at temperatures from 293.15 to 333.15 K. Temperature dependences of physical properties were fitted by empirical equations, and both thermal expansion coefficients or activation energies for viscous flow were obtained accordingly. Moreover, Rackett equation modified by Spencer and Danner and the mass connectivity index-based method were used for density prediction, while the refractive index was estimated by the atomic contribution method. The influence of the size of tetraalkylammonium cation as well as the type of anion of salt on physical properties of DESs and the strength of hydrogen bond interactions between HBA and HBD were discussed.

2. Experimental

2.1. Chemicals and synthesis

The chemicals in this study, 3-amino-1-propanol, tetrabutylammonium bromide, tetrabutylammonium chloride and tetraethylammonium chloride were purchased from Sigma-Aldrich and apart from TBAC they were used as received from the supplier. Tetrabutylammonium chloride was purified by double crystallization from acetone by adding diethyl ether. All salts were dried under reduced pressure before use. TBAB at 323 K for 48 h, TBAC and TEAC at 298.15 K for several days. The corresponding information and the chemical structures of the DESs ingredients are presented in Table 1 and Fig. 1, respectively.

In this work, DESs were prepared by mass with the same molar ratio of 1:4, 1:6 and 1:8 salt to 3-amino-1-propanol. The weighing was done using an analytical balance (Mettler Toledo) with the precision of 0.1 mg. The standard uncertainty in the mass fraction was estimated to be less than $\pm 1 \cdot 10^{-4}$. The combinations of the quaternary salts and AP were mixed at 353.15 K for 1 h using a magnetic stirrer in a fume hood until a homogeneous and uniform liquid without any precipitate was formed. This is commonly described as the heating method of DES formation [15]. The final DESs, stable colourless liquids at room temperature, were kept in tight bottles to prevent any contamination from outside atmosphere that may affect the physical properties of DES. Since deep eutectic solvents are known as hygroscopic solvents, the water content of DESs was measured using a Mettler Toledo Coulometric Karl - Fischer titrator (899 Coulometer apparatus from Metrohm), as presented in Table 2.

2.2. Physical properties measurements

2.2.1. Melting point

Mettler Toledo Star One Differential Scanning Calorimeter (DSC) was used to measure the melting points of the eutectic mixtures. The measurements were made under purified nitrogen atmosphere with a flow rate of 60 mL·min^{-1}, with samples of 10–18 mg packed in standard aluminium pan. The DSC equipment was connected to the STAR® data acquisition software a dedicated computer. The heating and cooling sequence was programmed on the STAR® console which controls the DSC equipment. For the melting point determination, a temperature range from 193.15 to 298.15 K was selected with a heating rate of 1 K·min^{-1}. The uncertainty of the measurement was ±0.01 K. This procedure was performed in at least three repetitions to ensure reproducibility of the results.

2.2.2. Density

The densities of the DES samples were measured at different temperatures with a digital vibration-tube analyser (Anton Paar DMA 5000, Austria) with proportional temperature control that kept the samples at working temperature with an accuracy of ±0.01 K. The apparatus was calibrated with double distilled, deionized and degassed water, and with dry air at atmospheric pressure (0.1 MPa) according to the apparatus catalogue. The standard uncertainty of density measurement was better than 0.35 kg·m^{-3}.

2.2.3. Sound velocity

The sound velocities were determined using the sound analyser OPTIME 1.0 from OPTEL (Poland) with the standard uncertainty of 0.5 m·s^{-1} by measuring the time it takes for a pulse of ultrasound to travel from one transducer to another (*pitch-catch*) or to return to the same transducer (*pulse-echo*). The cell was thermostated at 298.15 ± 0.01 K and calibrated with double distilled water, with the value 1496.69 $m \cdot s^{-1}$ used as the sound velocity in pure water at 298.15 K.

2.2.4. Viscosity

Viscosities of the solvents were determined using LVDV-III Programmable Rheometer (cone-plate viscometer; Brookfield Engineering Laboratory, USA), controlled by a computer. The temperature of the samples was controlled within ±0.01 K using a thermostatic water bath (PolyScience 9106, USA). The display of the viscosimeter was verified with certified viscosity standard N100 and S3 provided by Cannon at 298.15 ± 0.01 K. The standard uncertainty of viscosity measurement was better than 1%.

2.2.5. Refractive index

The refractive indices were measured using an Abbe refractometer (RL-3, Poland) equipped with a thermostat for controlling the cell temperature with an accuracy of ±0.1 K. The standard uncertainty of refractive index measurement on the n_D scale was 0.0002. At least three independent measurements were taken for each sample at each temperature to assure reproducibility of the measurement.

2.2.6. Infrared spectroscopy measurements

FTIR spectra of DESs were recorded on Nicolet 8700 spectrometer (Thermo Electron Co.). An attenuated total reflection (ATR) technique was employed because of extremely strong absorption of AP for ν(OH)/ν(NH_2) stretching vibrations. For this purpose, the Specac Golden Gate single reflection accessory equipped with a diamond crystal (45° incidence angle) mounted in a heated tungsten carbide disc was used. The temperature of the 50 mL liquid sample cell atop the crystal was kept at 298.15 ± 0.1 K by the Specac West 6100+ controller maintaining the tungsten carbide disc temperature and additionally stabilized by circulating thermostated water from a Julabo F12 thermostat. The sample temperature was monitored by a thermocouple inside the cell. The spectrometer measurement chamber and the ATR accessory were purged with dry nitrogen. The sample spectra were ratioed against a background spectrum collected for an empty, dry cell obtained

Table 1
Provenance and mass fraction purity of the compounds studied.

Chemical name	Source	CAS number	Initial purity/mass fraction[a]	Purification method	Final purity/mass fraction[b]
3-amino-1-propanol (AP)	Sigma Aldrich	156-87-6	0.99	None	–
Tetrabutylammonium bromide (TBAB)	Sigma Aldrich	1643-19-2	≥0.99	None	–
Tetraethylammonium chloride (TEAC)	Sigma Aldrich	56-34-8	≥0.98	None	–
Tetrabutylammonium chloride (TBAC)	Sigma Aldrich	1112-67-0	≥0.97	Crystallization	≥0.98[c]

[a] As stated by the supplier.
[b] Determined by potentiometric titration.

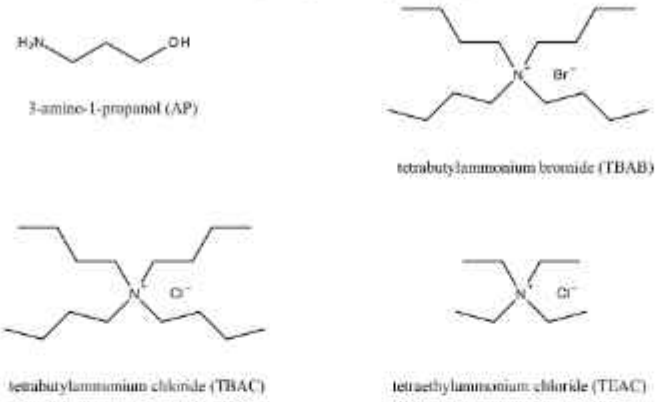

Fig. 1. Chemical structures of the DES's ingredients used in this study.

directly before each measurement. For each sample spectrum 256 scans were performed with a selected resolution of 2.0 cm^{-1}.

Spectra acquisition was controlled by OMNIC 7.3 software package (Thermo Scientific). Advanced ATR correction algorithm of the software was used to correct for normal and anomalous dispersion effects. It requires the knowledge of the crystal material, the incidence angle, the number of internal reflections and the refractive index of the sample. The spectra were further analyzed using GRAMS/32 software (Galactic Industries Corp.).

3. Results and discussion

3.1. Melting point

Differential scanning calorimetry (DSC) was used to determine the melting point and any solid state phase transitions in the present of quaternary DESs. The heating rate of 1 $K \cdot min^{-1}$ was used to increase the sensitivity of the instrument. Table 2 shows the melting points of DES. Fig. 2 (a,b,c) illustrates DSC curves for the DES systems with three HDA:HBD ratios. DSC plots for the eutectic mixtures were collected for at least three runs to ensure the reproducibility. Generally, only one endothermic peak was identified which was considered as the melting peak, but in the case of TBAB - AP 1:8 we observed a doublet form of melting peak. No phase transition peak was observed. The melting temperature in the present work is taken as the peak temperature in the heating profile. For all the studied DESs the melting points were lower than for the pure components. Moreover, the order of melting temperatures for DES at the same molar ratio of the salt to 3-amine-1-propanol is as follows: TBAB:AP > TBAC:AP > TEAC:AP, which seems to suggest that the melting temperature of salt may influence the melting temperature of deep eutectic solvents. Besides, the highest values of T_m are observed for tetrabutylammonium bromide based DESs, which T_m is greater than that of TBAC. Moreover, the comparison of the melting temperatures for DES containing tetrabutylammonium and tetraethylammonium chlorides leads to the conclusion, that the melting temperature of deep eutectic solvents increases with increasing cation alkyl chain length in the salt and T_m of salt itself.

3.2. Density

3.2.1. Experimental values

The density, viscosity, refractive index and sound velocity of the deep eutectic solvents studied were measured as a function of temperature with the range of 293.15–333.15 K and at ambient pressure. The density data are presented in Table S1 and in Fig. 3 (a,b,c).

As it can been observed, density decreases linearly with the temperature increase for all molar compositions of all nine DESs. Obviously, this is due to of the formation of larger intermolecular voids at higher temperatures, which increase the volume and decrease the density. The fitting parameters of linear equations ($d = a \cdot T + b$) correlating the effect of temperature on the density, obtained by least square analysis are listed in Table 3.

The order of density for DES at the same temperature and molar ratio of the salt to 3-amine-1-propanol is as follows: TBAB:AP (DES

Table 2
The abbreviation, molar mass, molar ratio, mass fraction, water content and melting point for chemicals used in this work.

DES		Salt		HBD		Molar ratio	Mass fraction[a]		Water content[b]	
Symbol	M_{DES}/(g·mol^{-1})		M_{salt}/(g·mol^{-1})		M_{HBD}/(g·mol^{-1})	Salt: HBD	Salt	HBD		T_m/K
DES1	124.229	TBAB	322.37	AP	75.11	1:4	0.5155	0.4845	0.00098	277.34
DES2	110.405	TBAB	322.37	AP	75.11	1:6	0.4168	0.5832	0.00033	274.41
DES3	102.580	TBAB	322.37	AP	75.11	1:8	0.3488	0.6512	0.00054	276.02; 278.6
DES4	93.265	TEAC	165.71	AP	75.11	1:4	0.3650	0.6440	0.00156	272.37
DES5	88.072	TEAC	165.71	AP	75.11	1:6	0.2692	0.7308	0.00127	272.19
DES6	85.189	TEAC	165.71	AP	75.11	1:8	0.2164	0.7836	0.00125	271.81
DES7	115.834	TBAC	277.92	AP	75.11	1:4	0.4818	0.5182	0.00178	276.29
DES8	103.891	TBAC	277.92	AP	75.11	1:6	0.3792	0.6208	0.00121	273.91
DES9	97.096	TBAC	277.92	AP	75.11	1:8	0.3168	0.6832	0.00202	277.33

[a] The standard uncertainty of DES mass fraction composition is 0.0001.
[b] Water content of DESs in mass fraction determined by Karl Fisher titration with the standard uncertainty ± 0.0001.

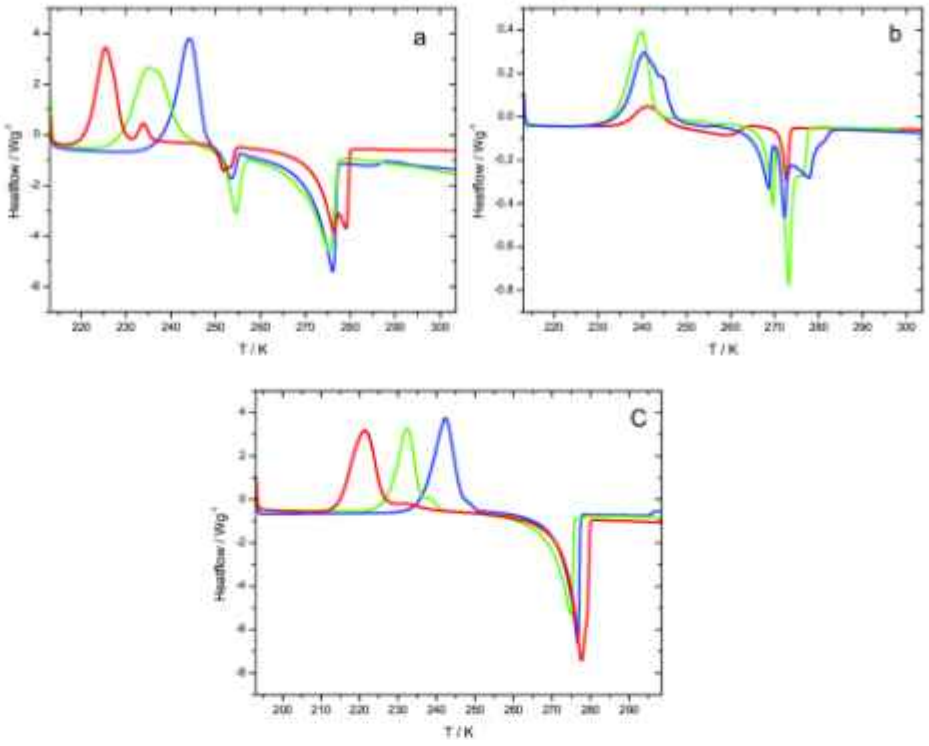

Fig. 2. DSC curves for deep eutectic solvents studied: a) TBAB:AP (DES 1–3), b) TEAC:AP (DES 4–6) and c) TBAC:AP (DES 7–9); (blue – 1:4, red – 1:5, green 1:6). (For interpretation of the references to colour in this figure legend, the reader is referred to the web version of this article.)

1–3) > TEAC:AP (DES 4–6) > TBAC:AP (DES 7–9), which seems to suggest that structure of HBA as well as HBD may have a significant effect on the density values of deep eutectic solvents. The highest values of densities are observed for TBAB-based DESs, which is attributed to the mass of bromide being greater than chloride [16,17]. Moreover, comparing the density values for DES containing tetrabutylammonium and tetraethylammonium chlorides leads to conclusion, that the density of deep eutectic solvents decreases with the increasing cation alkyl chain length in the salt. That conclusion is consistent with the density results obtained for ILs [18,19]. Apparently, packing effects taking place in case of TBAB cause the increase of relative volume of salt and as a result the decrease of the density of DES. Moreover, the higher density values obtained for TBAB:AP (DES 1–3) than those for TEAC:AP (DES 4–6) suggest that the packaging effects have smaller influence on density than the effect connected with the mass of the anion.

As is seen from Table S1 and Fig. 3, the density of DESs also depends on the HBA:HBD molar ratio. For TBAB- and TEAC-based deep eutectic solvents, the density decreases with the increasing of molar ration of 3-amine-1-propanol, while for TBAC-based DESs the opposite trend is observed. Obviously, it is the result of different relation of density of deep eutectic solvents to the density of AP. The densities of TBAB:AP (DES 1–3) and TEAC:AP (DES 4–6) are higher than the density of pure 3-amine-1-propanol, while the density of TBAC:AP (DES 7–9) is lower. Thus, when the amount of 3-amine-1-propanol in TBAC:AP (DES 7–9) increases, the density tends to the smaller density of pure AP, i.e., it decreases.

3.2.2. Prediction of density values

Generally, three methods have been reported in the literature for estimating deep eutectic solvents densities so far. Shahbaz et al. used artificial intelligence and group contribution methods for density predictions in glycerol and ethylene glycol HBD components mixed with choline chloride, diethylethanolammonium chloride, and methyltriphenylphosphonium bromide as HBA components [20,21]. Mjalli introduced the mass connectivity index-based density prediction for a set of 20 deep eutectic solvents systems comprising different salts and hydrogen bond donors [22].

In the present study, the Rackett equation [23] modified by Spencer and Danner [24] and MCI-based (mass connectivity index-) density model [28] were used and their effectiveness for density prediction of DESs based on 3-amino-1-propanol were compared.

The first approach, i.e. the modified Racket equation, requires knowledge of critical temperature, critical volume and critical pressure of DESs. Because these parameters cannot be found experimentally, they are estimated using the Lee-Kesler mixing equations suggested by Knapp et al. [25]. Moreover, the Modified Lydersen-Joback-Reid method [26] is used to found the critical properties of components of deep eutectic solvents. The calculated critical properties of DESs obtained by using above methods are presented in Table 4.

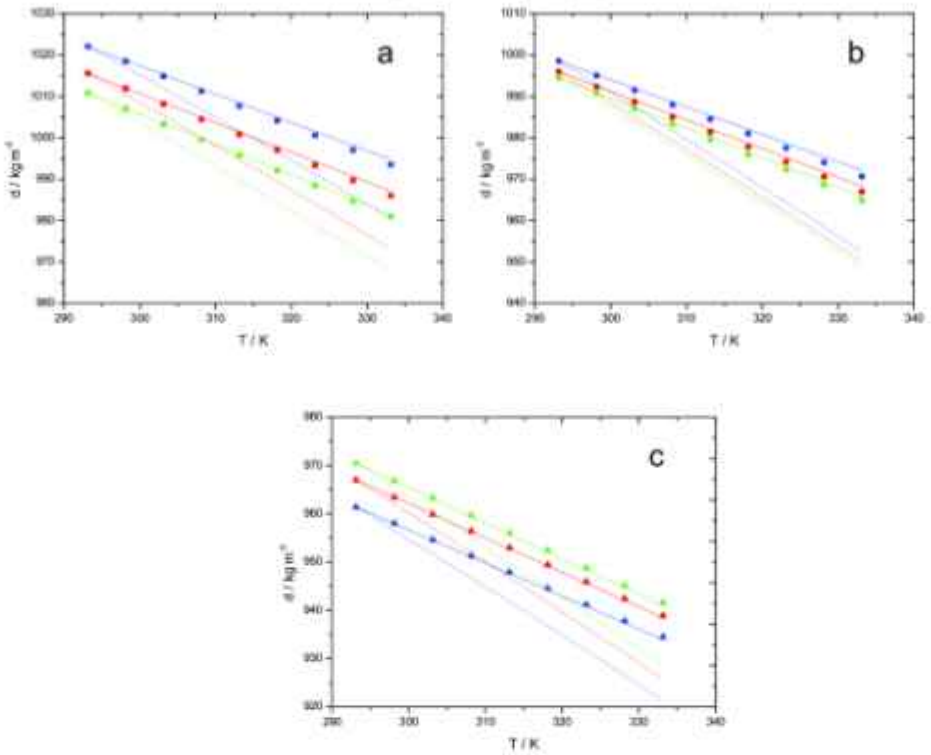

Fig. 3. Densities of deep eutectic solvents studied as a function of temperature in the range of 293.15–333.15 K and at atmospheric pressure a) TBAB:AP (DES 1–3), b) TBAC:AP (DES 4–6) and c) TBAC:AP (DES 7–9). (blue – 1:4, red – 1:5, green 1:6); solid line – modified Rackett equation, dashed line – mass connectivity index based method. (For interpretation of the references to colour in this figure legend, the reader is referred to the web version of this article.)

To predict the DES density the modified Rackett equation is employed as:

$$d = \frac{d_R}{Z_{RA}^{\varphi}} \tag{1}$$

where parameter φ is defined as

$$\varphi = \left(1-\frac{T}{T_{cm}}\right)^{2/7} - \left(1-\frac{T_R}{T_{cm}}\right)^{2/7} \tag{2}$$

and T_{cm}, d_R and T_R are critical temperature of DES, reference density and temperature, respectively. In the present study, the density at 293.15 K was chosen as the reference density. Z_{RA} is the specific compressibility factor introduced by Spencer and Danner to account for irregularities that cannot be handled by the original Racket model. It is defined as:

$$Z_{RA} = \left(\frac{V_{mc} \cdot P_{cm}}{R \cdot T_{cm}}\right)^{1/\left[1+\left(1-\frac{T}{T_{cm}}\right)^{2/7}\right]} \tag{3}$$

Table 3
Density model parameters along with root-mean-square deviations.

DES	a	b	RMSD	R^2
DES1	−0.715	1231.34	0.041	0.9999
DES2	−0.741	1232.71	0.050	0.9999
DES3	−0.745	1229.24	0.053	0.9999
DES4	−0.699	1203.31	0.051	0.9999
DES5	−0.725	1208.56	0.033	0.9999
DES6	−0.741	1211.72	0.028	0.9999
DES7	−0.673	1158.34	0.013	0.9999
DES8	−0.702	1172.88	0.030	0.9999
DES9	−0.722	1182.14	0.030	0.9999

Table 4
The calculated critical properties and mass connectivity indices of DESs used in this study and average relative deviation, where the superscript RA: Racket model, MCI: mass connectivity index- based model.

DES	T_{cm}/K	$10^3 V_{mc}$/(m³·mol⁻¹)	P_{cm}/bar	MCI	$ARD^{[RK]}$/%	$ARD^{[RA]}$/%
DES1	646.47	388.30	31.20	4.5320	0.07	0.62
DES2	636.61	390.02	34.18	5.6136	0.06	0.61
DES3	631.31	528.84	36.13	6.7102	0.03	0.64
DES4	607.30	317.13	36.81	3.7483	0.09	0.90
DES5	609.12	299.72	38.89	4.8440	0.07	0.83
DES6	620.25	290.19	40.14	5.9393	0.05	0.79
DES7	639.05	387.89	30.91	4.5323	0.03	0.68
DES8	630.91	347.90	34.10	5.6703	0.02	0.67
DES9	627.01	327.95	36.00	6.7241	0.03	0.66

where V_{298} and P_{298} are the saturated molar volume at the reference temperature and critical pressure of DES.

The second method applied in this study for the DESs density prediction, based on mass connectivity index, was introduced by Mjalli [22]. Using the training set of the experimental data consisting of 86 density values of DESs he found the semi-empirical equation for prediction of density as:

$$d(T) = d_0 - 5.197\cdot10^{-4}\lambda_{DES}^{\,0.8202}(T - T_R) \quad (4)$$

in which λ_{DES} denotes to the mass connectivity index of DES, calculated on the basis of the pure components mass connectivity indices λ. Furthermore, the values of λ are estimated from equation [27]:

$$\lambda = \sum_{i-j}^{N_b}\left(1/\sqrt{M_i M_j}\right) \quad (5)$$

where M_i and M_j are the masses of connected groups numbers (i) and (j) reported by Vaderrama et al. [28].

For 3-amine-1-propanol, tetrabutylammonium bromide, tetraethylammonium chloride and tetrabutylammonium chloride the mass connectivity indices were obtained as 0.5480, 2.3215, 1.5617 and 2.2515, respectively. Multiplying the salt and 3-amine-1-propanol mass connectivity indices by their molar quantities in the DES allowed us to calculate the mass connectivity indices of DESs, which are collected in Table 4.

Fig. 3 shows experimental and predicted densities of DESs based on 3-amino-1-propanol by the Rackett equation modified by Spencer and Danner and the model proposed by Mjalli. Moreover, the average relative deviations (ARD) between the experimental and models predicted densities are presented in Table 4. The negative variation of DES densities with temperature was captured by the Rackett equation, as well as by the MCI-based model. Moreover, the mass connectivity index model was successful in explaining this relationship with higher degree of credibility than the modified Rackett model. In all cases the Rackett predictions were underestimated with a much higher inclination with respect to temperature. The ARD values are the highest for deep eutectic solvents TEAC:AP (DES 4–6) and at the highest recorded temperature of 333.15 K are 1.87, 1.73, and 1.66% respectively. On the other hand, the MCI-based models gave ARD values of 0.15, 0.13 and 0.09% for the same systems. Thus, the obtained results indicate that the most proper method for density prediction for DESs is the method introduced by Mjalli [22].

3.2.2. Estimated thermodynamic properties of DESs

The isobaric thermal expansion coefficient α_p is defined as temperature dependence of ln(d) as expressed by the following equation:

$$\alpha_p = \frac{1}{V_m}\left(\frac{\partial V_m}{\partial T}\right)_p = -\left(\frac{\partial \ln(d)}{\partial T}\right)_p \quad (6)$$

where V_m and d are the molar volume and the density of DESs, respectively. It can be obtained by fitting the temperature dependence of ln (d) to the following straight line

$$\ln(d) = b - \alpha_p T \quad (7)$$

where b is an empirical constant. From Table 5 one can see, that α_p of DESs studied depend mainly on the molar ratio of the salt to 3-amine-1-propanol, while the dependence on the type of HBA is negligible. The smallest values of the thermal expansion coefficient were obtained for deep eutectic solvents containing the smallest amount of AP, suggesting the smallest free volumes or interstices in these solvents.

Table 5 presents also the molecular volume, standard molar entropy and lattice potential energy calculated from density at 298.15 K.

Table 5
Estimated physicochemical properties of DESs at 298.15 K at atmospheric pressure.

DES	$10^4\alpha_p/K^{-1}$	$V_{m,i}$/(nm^3)	S^o/(J K^{-1} mol^{-1})	U_{pot}/(kJ mol^{-1})
DES1	7.09	0.203	281.8	503
DES2	7.40	0.181	255.1	518
DES3	7.48	0.169	240.1	528
DES4	7.10	0.156	223.3	540
DES5	7.39	0.147	213.0	548
DES6	7.56	0.143	207.3	553
DES7	7.10	0.201	278.6	504
DES8	7.37	0.178	252.4	526
DES9	7.42	0.168	238.6	529

Standard molar entropy and lattice potential energy of the studied DESs were estimated by using the empirical equations [29]:

$$S^o = 1246.5 V_{m,i} + 29.5 \quad (8)$$

$$U_{pot} = 1981.2 (d/M)^{1/3} + 103.8 \quad (9)$$

As is seen from Table 5, the DESs exhibit low lattice energy which is an underlying reason for their liquid state at room temperature (U_{pot}, CsI = 613 kJ mol^{-1}) [30].

3.3. Viscosity

The experimental dynamic viscosity data of the binary mixtures corresponding to the applied temperature range of 293.15–333.15 K are listed in Table S2 and presented in Fig. 4 (a,b,c). As expected, temperature plays an important role in viscosity, namely decrease of this parameter was observed at higher temperatures. Higher temperatures increase kinetic energy of the ions and molecules, and weaken the attractive forces between them, promoting their movement and contributing to decreasing viscosity [31].

At lower temperatures the viscosity of DESs decreases rapidly and asymptotically approaches a lower value at higher temperatures [32]. The following tendency was noticed TBAB:AP (DES 1–3) > TBAC:AP (DES 7–9) > TEAC (DES 4–6) for a corresponding molar ratio of the compounds. In this regard, liquids composed of salts with smaller cation (shorter hydrocarbon substituent) and anion manifest lower viscosity (weaker interactions and flow resistance). All binary mixtures showed higher values of viscosity in comparison to 1-amino-1-propanol. Moreover, a decrease of the mole fraction of the salt in the system (increase of the molar ratio salt:AP) resulted in the lower values of the dynamic viscosity. For example, the viscosity of TBAB–AP at 298.15 K decreased from 84.7 to 50.2 mPa·s when the molar ratio raised from 1:4 to 1:8. Analogous relations were observed in the literature [31].

The dynamic viscosity results were further fitted with the Arrhenius and Vogel-Fulcher-Tamman (VFT) equations:

$$\eta = \eta_\infty \exp\frac{E_a}{R\cdot T} \quad (10)$$

$$\eta = \eta_0 \exp\frac{b}{T - T_0} \quad (11)$$

where η_∞, E_a/R, η_0, b, and T_0 are fitting parameters, η_∞ is the viscosity at infinite temperature, E_a is the activation energy, R is the gas constant, and T is the temperature in Kelvin. The fitting parameters determined from the experimental data along with root-mean-square deviations (RMSD) are presented in Tables 6 and 7. The E_a values calculated for the binary mixtures were found to vary from 33.4 kJ·mol^{-1} (DES 6) up to 38.5 kJ·mol^{-1} (DES 1), and reflect the abovementioned viscosity relations. The higher E_a value, the harder ions move past each other due to the interactions occurring in the fluid. DESs with the lowest salt: AP molar ratio (1:4) have higher activation energies. Based on the

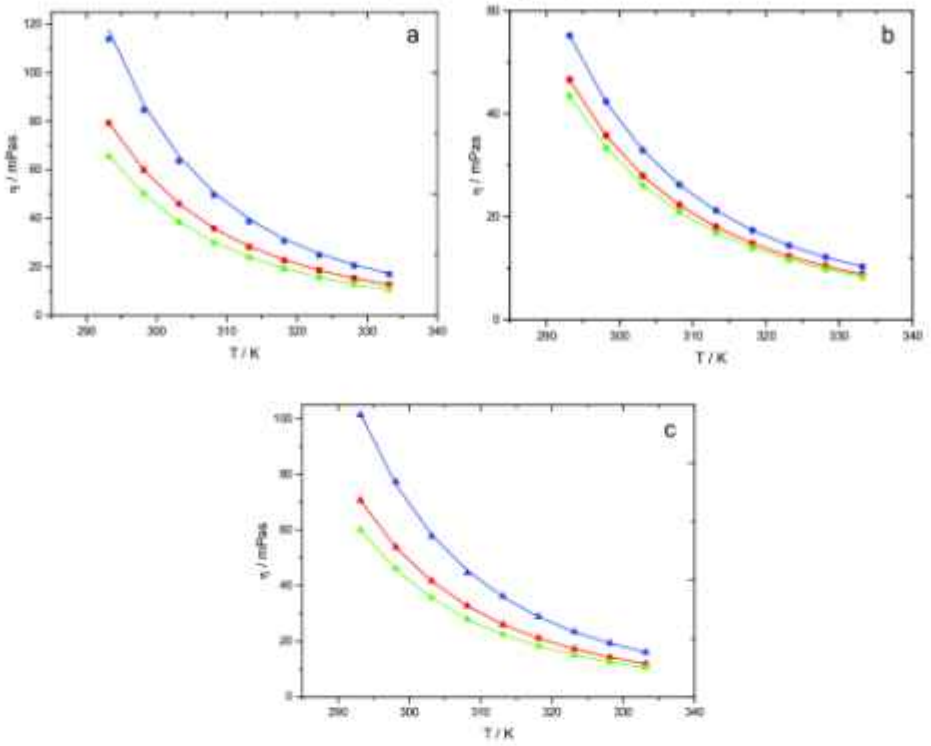

Fig. 4. Viscosities of deep eutectic solvents studied as a function of temperature in the range 293.15–333.15 K and at atmospheric pressure: a) TBAB:AP (DES 1–3), b) TEAC:AP (DES 4–6) and c) TBAC:AP (DES 7–9), (blue - 1:4, red - 1:6, green 1:8); solid line - Vogel-Fulcher-Tammann equation. (For interpretation of the references to colour in this figure legend, the reader is referred to the web version of this article.)

comparison of the correlation coefficients, R^2, and RMSD it was concluded that the VFT equation represents better fitting for the dynamic viscosity results.

3.4. Refractive index

3.4.1. Experimental values

The refractive index values of deep eutectic solvents studied at the temperature range from 293.13 to 333.15 K are presented in Table S3 and the trends are shown in Fig. 5 (a,b,c). There are several factors that have an effect on the refractive index of DESs such as type of salt, molar ratio of HBD to HBA, temperature and molecular weight of DES. The obtained results reveal that for all mixtures the values of refractive index decrease linearly with increasing the temperature. Adequate regression parameters ($n_D = a \cdot T + b$) are collected in Table 8.

Moreover, for a given temperature and molar ratio of salt to 3-amine-1-propanol, n_D value of the DESs is in the following order: TBAB:AP (DES 1–3) > TEAC:AP (DES 4–6) > TBAC:AP (DES 7–9), which is consistent with the order of density. Also, as the molecular weight of DESs decreases (see values of n_D for TBAB- and TBAC-based DESs),

Table 6
Fitting parameters for the Arrhenius equation for dynamic viscosity results determined within temperature range T = (293.15 to 333.15) K and P = 0.1 MPa.

DES	$10^3\eta_\infty$/mPa·s	$10^{-3}E_a$/J·mol^{-1}	RMSD	R^2
DES1	1.47	3.85	0.025	0.9984
DES2	1.06	3.70	0.023	0.9986
DES3	1.97	3.65	0.020	0.9988
DES4	4.62	3.40	0.024	0.9980
DES5	4.42	3.37	0.024	0.9981
DES6	4.58	3.34	0.024	0.9981
DES7	2.20	3.73	0.026	0.9982
DES8	2.60	3.60	0.020	0.9989
DES9	3.14	3.51	0.025	0.9980

Table 7
Fitting parameters for the Vogel-Fulcher-Tammann (VFT) equation, for dynamic viscosity results determined within temperature range T = (293.15 to 333.15) K and P = 0.1 MPa.

DES	η_0/mPa·s	b/K	T_0/K	RMSD	R^2
DES1	0.0316	1080.7	101.7	0.025	0.9999
DES2	0.0175	1234.0	149.0	0.011	0.9999
DES3	0.0086	1411.3	135.4	0.019	0.9999
DES4	0.0600	835.0	170.7	0.0025	0.9998
DES5	0.0539	827.8	170.7	0.0010	0.9998
DES6	0.0550	811.3	171.6	0.0023	0.9999
DES7	0.0311	1094.0	157.9	0.025	0.9997
DES8	0.0153	1261.0	143.6	0.0031	0.9999
DES9	0.0280	1034.7	157.7	0.013	0.9999

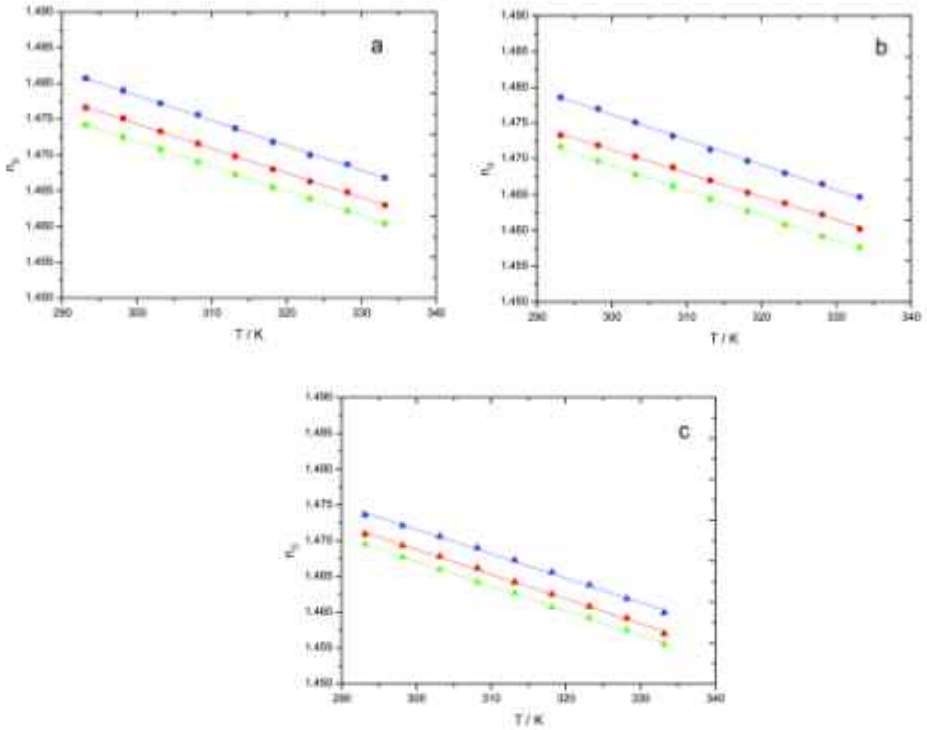

Fig. 5. Refractive indices of deep eutectic solvents studied as a function of temperature in the range 293.15–333.15 K a) TBAB:AP (DES 1–3), b) TEAC:AP (DES 4–6) and c) TBAC:AP (DES 7–9), (blue – 1:4, red – 1:6, green 1:8), solid line – linear fit. (For interpretation of the references to colour in this figure legend, the reader is referred to the web version of this article.)

the value of refractive index of deep eutectic solvents decreases at all temperatures. As it was observed for viscosities, the refractive indices decrease with an increasing of mole fraction of AP in the mixture for all DESs investigated. Obviously, it is the result of the smaller value of the refractive index of 3-amine-1-propanol comparing to that of deep eutectic solvents. Thus, when the content of AP increases in DES, the refractive index decreases.

3.4.2. Prediction of refractive index values

It is generally accepted that the atomic contribution method is more accurate than others in predicting the refractive indices of organic liquids [33]. In this method molar refraction of compound is calculated by summing its atomic and structural contribution parameters, which were determined by Wildman and Crippen using 3412 molecules data set [34]. Then, Lorentz–Lorenz equation and experimental density value of compound is employed to calculate the refractive index:

$$R_M = \frac{M}{d}\left(\frac{n^2-1}{n^2+2}\right) \tag{12}$$

In this equation R_M, M (g·mol^{-1}) and d (g·cm^{-3}) are molar refraction, molar mass and density, respectively.

In the present study, the molar refractions of pure components of DESs, i.e., the salts and 3-amine-1-propanol were initially calculated and they were found to be equal to 0.757, 87.564, 47.557 and 84.493 for AP, TBAB, TEAC and TBAC, respectively. Then, molar refraction of DESs were obtained through equation:

$$R_M = \sum_{i=1} x_i R_{Mi} \tag{13}$$

where x_i and R_{Mi} are mole fraction and molar refraction of the individual constituting salt and AP. Finally, the refractive indices were calculated by Lorentz–Lorenz equation using the experimental values of density.

Table 9 presents the calculated molar refractions and the refractive indices for all DESs together with the experimental values and relative deviations at 293.15 K. As it can be seen, the predicted data of DESs molar refractions and refractive indices are in good agreement with the experimental data. Specially, the value of ARD% obtained for refractive indices equal to 0.41% confirms that the atomic contributions

Table 8
Refractive index model parameters and regression coefficients.

DES	a	b	RMSD	R^2
DES1	−0.00035	1.5810	0.00015	0.9992
DES2	−0.00034	1.5772	0.000098	0.9998
DES3	−0.00034	1.5752	0.000063	0.9999
DES4	−0.00035	1.5810	0.00017	0.9990
DES5	−0.00033	1.5693	0.00016	0.9989
DES6	−0.00035	1.5745	0.00014	0.9993
DES7	−0.00034	1.5740	0.00025	0.9977
DES8	−0.00035	1.5723	0.00020	0.9985
DES9	−0.00035	1.5708	0.00012	0.9995

Table 9
Calculated molar refractions and predicted refractive indices of DESs at 293.15 K.

DES	$R_{M\ exp}$	$R_{M\ cal}$	%RD	n_{exp}	n_{cal}	%RD
DES1	34.570	34.029	1.57	1.4807	1.4719	0.59
DES2	30.691	30.293	1.30	1.4766	1.4694	0.49
DES3	28.522	28.170	1.24	1.4742	1.4674	0.47
DES4	26.485	26.128	1.28	1.4786	1.4715	0.49
DES5	24.819	24.591	1.47	1.4733	1.4682	0.35
DES6	23.972	23.739	0.98	1.4717	1.4664	0.37
DES7	33.838	33.556	0.84	1.4736	1.4690	0.32
DES8	30.032	29.790	0.75	1.4709	1.4668	0.28
DES9	28.061	27.855	0.74	1.4691	1.4655	0.25
ARD%			1.13			0.41

method can be considered as the suitable method for the prediction of n_D values of DESs, though the atomic contributions proposed by Wildman and Crippen were considered for neutral compounds [34].

3.5. Sound velocity

The experimental sound velocity data for all DESs as a function of temperature are summarized in Table S4 and presented in Fig. 6 (a,b, c). As it can be seen, the sound velocity, similarly to other properties, decreases with increasing tempecature. This behaviour was also reported in case of other DESs. At elevated temperature the molecules move further apart from each other, generating more free space and in the result density, viscosity, refractive index and sound velocity decrease [35–37]. Moreover, similar to most other DESs, the sound velocity of DESs investigated in the present study shows linear relationship with the temperature. Table 10 shows regression parameters ($u = a \cdot T + b$). Previously, the temperature dependence of the speed of sound was found to be nonlinear only for deep eutectic solvents based on benzyltrimethylammonium chloride and benzyltributylammonium chloride as HBAs and glycerol HBD, as well as deep eutectic solvents based on L-proline [38].

As is seen from Table 10, for a given temperature and molar ratio of salt to 3-amine-1-propanol, sound velocity of the DESs is in the following order: TEAC:AP ≫ TBAC:AP > TBAB:AP, which is opposite with the order of viscosity. Moreover, values of sound velocity obtained for TEAC-based DESs are significantly higher than those for TBAC- or TBAB-based DESs, which are similar in their magnitude. This result indicates that sound velocity is mainly determined by alkyl chain length of the HBD, while the type of anion has much smaller influence on it. Obviously, the less compact structure of TBAC:AP (DES 7–9) compared to that of TEAC:AP (DES 4–6) results in significantly smaller sound velocity value.

The sound velocity of the DESs similarly to other physical properties also depends on the molar ratio of HBA to HBD. For TBAB- and TBAC-based deep eutectic solvents sound velocity increases with increasing of molar ratio of 3-amine-1-propanol, while for TEAC-based DES the opposite trend is observed. Obviously, it is the result of different relation of the physical property of deep eutectic solvents to that of AP.

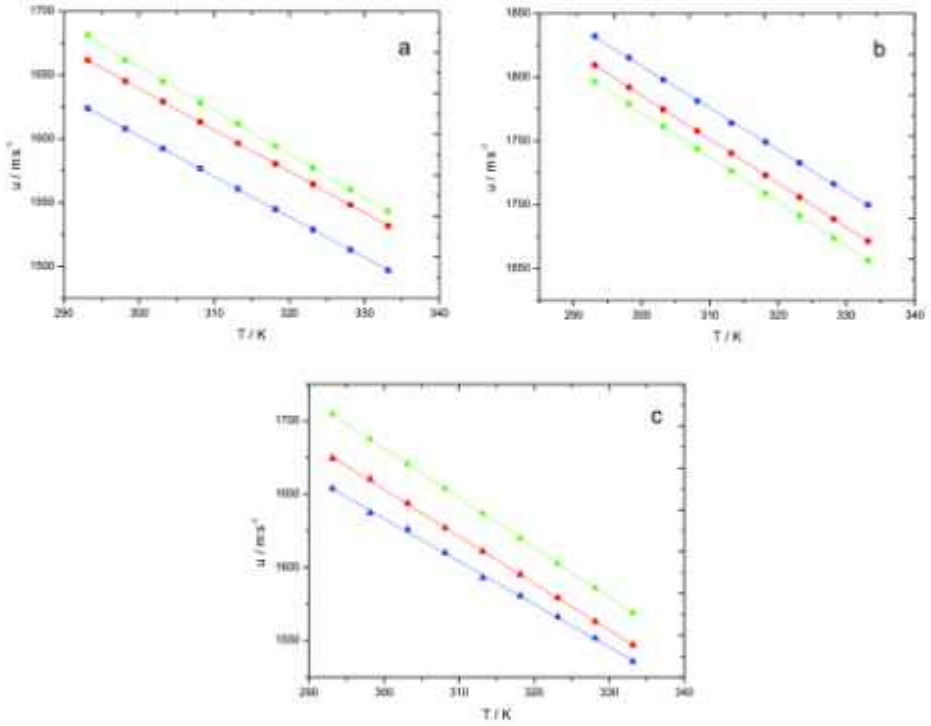

Fig. 6. Sound velocities of deep eutectic solvents studied as a function of temperature in the range 293.15–333.15 K: a) TBAB:AP (DES 1–3), b) TEAC:AP (DES 4–6) and c) TBAC:AP (DES 7–9) (blue – 1:4, red – 1:5, green 1:6), solid line – linear fit. (For interpretation of the references to colour in this figure legend, the reader is referred to the web version of this article.)

Table 10
Sound velocity model parameters and regression coefficients.

DES	a	b	RMSD	R^2
DES1	−3.17	2554.3	0.20	0.9999
DES2	−3.25	2613.5	0.20	0.9999
DES3	−3.42	2682.7	0.90	0.9997
DES4	−3.29	2706.8	0.80	0.9998
DES5	−3.45	2820.0	0.20	0.9999
DES6	−3.59	2823.3	0.10	0.9999
DES7	−2.93	2511.5	1.3	0.9992
DES8	−3.21	2616.3	0.60	0.9999
DES9	−3.39	2688.9	0.10	0.9999

3.5.1. Isentropic compressibility

Based on the experimental values of sound velocity and density, the techeologically important parameter of isentropic compressibility was estimated. It was calculated by applying the Newton-Laplace equation:

$$k_S = \frac{1}{\rho u^2} \tag{14}$$

The isentropic compressibility also gives a measure of the available free space in the liquid. From the calculated values reported in Table S5, it is observed that the κ_S changes with the increase of the temperature or increase of the amount of AP in DES in opposite trend than for that noticed for sound velocity. The smallest values of isentropic compressibility were observed for TEAC:AP (DES 4–6) for which the most compact structure is expected.

3.6. FTIR analysis of the DESs

Infrared spectroscopy is an invaluable tool for studying intermolecular interactions of aminoalcohol-based DESs [11]. The FTIR spectra of the studied DESs are shown in Fig. 7 together with the reference of pure AP spectrum.

The bands in the AP spectrum were previously ascribed in great detail [39]. The region of particular interest here is the ν(OH)/ν(NH_2) stretching vibrations range (3000–3600 cm^{-1}), distinctly sensitive to the hydrogen bonding. Pure AP is an associated liquid with as many as four hydrogen bonds formed per molecule [40] as found in molecular dynamics simulations. In DES, some of the internal hydrogen bonds are replaced by aminoalcohol to halide bonding. In water, such bonds are slightly weaker than water–water hydrogen bonds [41]. In the studied DESs, the dominant effect in the IR spectrum is the lowering of the intensity of all the AP bands due to the lower concentration of aminoalcohol. At the same time, positions of the ν(OH)/ν(NH_2) bands become slightly blue-shifted due to the emergence of OH–halide and NH–halide hydrogen bonds. Interestingly, the ν(OH) band at 3171 cm^{-1} is apparently much more perturbed by the formation of DES than the doublet of symmetric/asymmetric ν(NH_2) bands at 3288/3347 cm^{-1}, indicating it is a much more sensitive probe of the intermolecular interactions in the synthesized DESs.

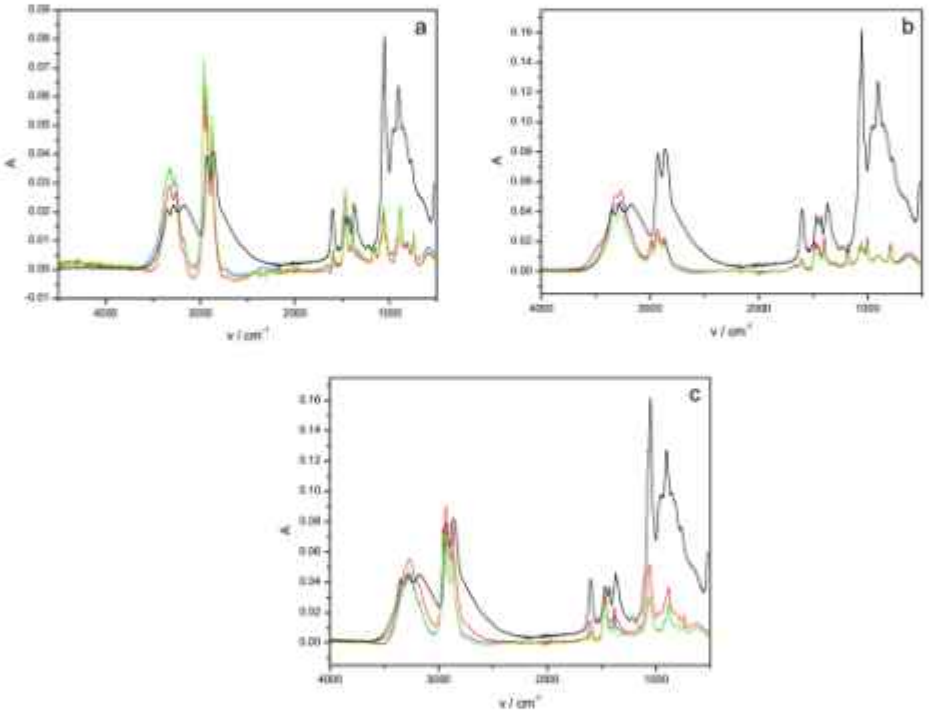

Fig. 7. The FTIR spectra of the studied DESs together with the pure AP spectrum; a) TBAB:AP (DES 1–3), b) TEAC:AP (DES 4–6) and c) TBAC:AP (DES 7–9) (blue–1:4, red – 1:6, green 1:8). (For interpretation of the references to colour in this figure legend, the reader is referred to the web version of this article.)

Below 1500 cm^{-1}, the intramolecular bands of the tetraalkylammonium cations are superimposed on the solvent background. Comparison with the pure salts (see Fig. S1), but note that spectra of some of the salts were difficult to record in an anhydrous state, reveals neither changes in band positions, nor formation of any new bands, thus confirming the lack of specific chemical interactions between the DESs components.

4. Conclusions

Experimental density, viscosity, refractive index and sound velocity for 3-amino-1-propanol plus tetrabutylammonium bromide, 3-amino-1-propanol plus tetraethylammonium chloride and 3-amino-1-propanol plus tetrabutylammonium chloride deep eutectic solvents with different molar ratios of 1:4, 1:6 and 1:8 salt to AP have been reported as a function of temperature at atmospheric pressure. From the experimental data, the thermal expansion coefficients, the activation energies for viscous flow and the isentropic compressibility of DESs were calculated.

It was found that density, refractive index and sound velocity of the studied deep eutectic solvents decrease linearly with temperature, while viscosity changes exponentially with temperature. The Vogel-Tamman-Fulcher equation better describes the dependence of viscosity on temperature than the Arrhenius equation.

Furthermore, the results revealed that the order of density and refractive index for DESs at the same temperature and molar ratio of the salt to 3-amine-1-propanol is as follows: TBAB:AP (DES 1–3) > TEAC:AP (DES 4–6) > TBAC:AP (DES 7–9), while the smallest values of viscosity and isentropic compressibility for TEAC:AP (DES 4–6) are observed.

Rackett equation modified by Spencer and Danner and the mass connectivity index-based method used for density prediction indicate that the most proper method for density prediction for the selected deep eutectic solvents is the method introduced by Mjalli. Moreover, the value of ARD% obtained for refractive indices equal to 0.41% confirms that the atomic contributions method can be considered as the suitable method to prediction of n_D of DESs.

To sum up the study, taking into account physical properties, especially viscosity, deep eutectic solvent composed of tetraethylammonium chloride and 3-amino-1-propanol appears to be the best solvent among those considered for use as an absorbent of carbon dioxide.

CRediT authorship contribution statement

Bartosz Nowosielski: Investigation, Formal analysis, Data curation, Writing - review & editing. **Marzena Jamróg iewicz:** Investigation, Formal analysis, Data curation, Writing - original draft, Writing - review & editing. **Justyna Łuczak:** Investigation, Formal analysis, Data curation, Writing - original draft, Writing - review & editing. **Maciej Śmiechowski:** Investigation, Formal analysis, Data curation, Writing - original draft, Writing - review & editing. **Dorota Warmińska:** Conceptualization, Investigation, Formal analysis, Data curation, Writing - original draft, Writing - review & editing.

Declaration of competing interest

The authors declare that they have no known competing financial interests or personal relationships that could have appeared to influence the work reported in this paper.

Appendix A. Supplementary data

Supplementary data to this article can be found online at https://doi.org/10.1016/j.molliq.2020.113110.

References

[1] N. Du, et al., Polymer nanosieve membranes for CO2-capture applications, Nat. Mater. 10 (5) (2011) 372–375.
[2] G.T. Rochelle, Amine scrubbing for CO2 capture, Science (80-.) 325 (5948) (2009) 1652–1654.
[3] X. Li, M. Hou, B. Han, X. Wang, L. Zou, Solubility of CO2 in a choline chloride + urea eutectic mixture, J. Chem. Eng. Data 53 (2) (2008) 548–550.
[4] Y. Marcus, Deep Eutectic Solvents, Springer International Publishing, 2019.
[5] S. Sarmad, J.P. Mikkola, X. Ji, Carbon dioxide capture with ionic liquids and deep eutectic solvents: a new generation of sorbents, ChemSusChem 10 (2) (2017) 324–352.
[6] I. Adeyemi, M.R.M. Abu-Zahra, I. Alnashef, Experimental study of the solubility of CO2 in novel amine based deep eutectic solvents, Energy Procedia 105 (2017) 1394–1400.
[7] T.J. Trivedi, J.H. Lee, H.J. Lee, Y.K. Jeong, J.W. Choi, Deep eutectic solvents as attractive media for CO2 capture, Green Chem. 18 (9) (2016) 2834–2842.
[8] S.K. Shukla, J.P. Mikkola, Intermolecular interactions upon carbon dioxide capture in deep-eutectic solvents, Phys. Chem. Chem. Phys. 20 (38) (2018) 24699–24707.
[9] H. Ghaedi, et al., Density, excess and limiting properties of (water and deep eutectic solvent) systems at temperatures from 293.15 K to 343.15 K, J. Mol. Liq. 248 (2017) 378–390.
[10] I. Adeyemi, M.R.M. Abu-Zahra, I. Alnashef, Novel green solvents for CO2 capture, Energy Procedia 114 (2017) 2552–2560.
[11] F.S. Mjalli, G. Murshid, S. Al-Zakwani, A. Hayyan, Monoethanolamine-based deep eutectic solvents, their synthesis and characterization, Fluid Phase Equilib. 448 (2017) 30–40.
[12] I. Adeyemi, M.R.M. Abu-Zahra, I.M. AlNashef, Physicochemical properties of alkanolamine-choline chloride deep eutectic solvents: measurements, group contribution and artificial intelligence prediction techniques, J. Mol. Liq. 256 (2018) 581–600.
[13] M.B. Haider, D. Jha, B. Marappan Sivagnanam, R. Kumar, Thermodynamic and kinetic studies of CO2 capture by glycol and amine-based deep eutectic solvents, J. Chem. Eng. Data 63 (8) (2018) 2671–2680.
[14] E. Ali, et al., Solubility of CO2 in deep eutectic solvents: experiments and modelling using the Peng-Robinson equation of state, Chem. Eng. Res. Des. 92 (10) (2014) 1898–1906.
[15] A.P. Abbott, G. Capper, D.L. Davies, R.K. Rasheed, V. Tambyrajah, Novel solvent properties of choline chloride/urea mixtures, Chem. Commun. 9 (1) (2003) 70–71.
[16] E.L. Smith, A.P. Abbott, K.S. Ryder, Deep eutectic solvents (DESs) and their applications, Chem. Rev. 114 (21) (2014) 11060–11082.
[17] Q. Zhang, K. De Oliveira Vigier, S. Royer, F. Jérôme, Deep eutectic solvents: syntheses, properties and applications, Chem. Soc. Rev. 41 (21) (2012) 7108–7146.
[18] T.L. Greaves, A. Weerawardena, C. Fong, I. Krodkiewska, C.J. Drummond, Protic ionic liquids: solvents with tunable phase behavior and physicochemical properties, J. Phys. Chem. B 110 (45) (2006) 22479–22487.
[19] S.B. Capello, et al., Effect of temperature and cationic chain length on the physical properties of ammonium nitrate-based protic ionic liquids, J. Phys. Chem. B 116 (36) (2012) 11302–11312.
[20] K. Shahbaz, S. Baroutian, F.S. Mjalli, M.A. Hashim, I.M. Alnashef, Densities of ammonium and phosphonium based deep eutectic solvents: prediction using artificial intelligence and group contribution techniques, Thermochim. Acta 527 (2012) 59–66.
[21] K. Shahbaz, F.S. Mjalli, M.A. Hashim, I.M. Alnashef, Prediction of deep eutectic solvents densities at different temperatures, Thermochim. Acta 515 (1–2) (2011) 67–72.
[22] F.S. Mjalli, Mass connectivity index-based density prediction of deep eutectic solvents, Fluid Phase Equilib. 409 (2016) 372–377.
[23] H.G. Rackett, Equation of state for saturated liquids, J. Chem. Eng. Data 15 (4) (1970) 514–517.
[24] C.F. Spencer, R.P. Danner, Improved equation for prediction of saturated liquid density, J. Chem. Eng. Data 17 (2) (1972) 236–241.
[25] H. Knapp, R. Doring, L. Oellrich, U. Plocker, J.M. Prausnitz, Vapor-liquid Equilibria for Mixtures of Low Boiling Substances, Chemistry Data Series, VI, , DECHEMA, Frankfurt, Ger. 1982, 1982.
[26] V.H. Alvarez, J.O. Valderrama, A modified Lydersen-Joback-Reid method to estimate the critical properties of biomolecules, Alimentaria 254 (2004) 55–66.
[27] M. Randić, On characterization of molecular branching, J. Am. Chem. Soc. 97 (23) (1975) 6609–6615.
[28] J.O. Valderrama, R.E. Rojas, Mass connectivity index, a new molecular parameter for the estimation of ionic liquid properties, Fluid Phase Equilib. 290 (1) (2010) 107–112.
[29] L. Glasser, Lattice and phase transition thermodynamics of ionic liquids, Thermochim. Acta 421 (1–2) (2004) 87–93.
[30] D.R. Lide, CRC Handbook of Chemistry and Physics, 85, CRC press, 2004.
[31] S. Sarmad, Y. Xie, J.P. Mikkola, X. Ji, Screening of deep eutectic solvents (DESs) as green CO2 sorbents: from solubility to viscosity, New J. Chem. 41 (1) (2017) 290–301.
[32] M.H. Ghatee, M. Zare, F. Moosavi, A.R. Zolghadr, Temperature-dependent density and viscosity of the ionic liquids 1-alkyl-3-methylimidazolium iodides: experiment and molecular dynamics simulation, J. Chem. Eng. Data 55 (9) (2010) 3084–3088.
[33] X. Cao, B.C. Hancock, N. Leyva, J. Becker, W. Yu, V.M. Masterson, Estimating the refractive index of pharmaceutical solids using predictive methods, Int. J. Pharm. 368 (1–2) (2009) 16–23.
[34] S.A. Wildman, G.M. Crippen, Prediction of physicochemical parameters by atomic contributions, J. Chem. Inf. Comput. Sci. 39 (5) (1999) 868–873.

[35] D. Lapeña, L. Lomba, M. Artal, C. Lafuente, B. Giner, Thermophysical characterization of the deep eutectic solvent choline chloride:ethylene glycol and one of its mixtures with water, Fluid Phase Equilib. 492 (2019) 1–9.
[36] P.B. Sánchez, B. González, J. Salgado, J. José Parajó, Á. Domínguez, Physical properties of seven deep eutectic solvents based on L-proline or betaine, J. Chem. Thermodyn. 131 (2019) 517–521.
[37] A. Basiszbgat, S. Panda, R.L. Gardas, Acoustic, volumetric, transport, optical and thermodynamic properties of Benzyltripropylammonium based deep eutectic solvents, Fluid Phase Equilib. 448 (2017) 41–49.
[38] A. Basiszbgat, S. Panda, R.L. Gardas, Effect of ethylene, diethylene, and triethylene glycols and glycerol on the physicochemical properties and phase behavior of benzyltrimethyl and benzyltributylammonium chloride based deep eutectic solvents at 293.15–343.15 K, J. Chem. Eng. Data 63 (7) (2018) 2613–2622.
[39] C. Cacela, M.L. Duarte, R. Fausto, Structural and vibrational characterization of 3-amino-1-propanol a concerted SCF-MO ab initio, Raman and infrared (matrix isolation and liquid phase) spectroscopy study, Spectrochim. Acta - Part A Mol. Biomol. Spectrosc. 56 (6) (2000) 1051–1064.
[40] S.M. Melnikov, M. Stern, Molecular dynamics study of the solution structure, clustering, and diffusion of four aqueous alkanolamines, J. Phys. Chem. B 122 (10) (2018) 2709–2778.
[41] J. Stangret, T. Gampe, Ionic hydration behavior derived from infrared spectra in HDO, J. Phys. Chem. A 106 (21) (2002) 5393–5402.

Supporting Information

Experimental and predicted physicochemical properties of monopropanolamine-based deep eutectic solvents

Bartosz Nowosielski[a], Marzena Jamróg iewicz[c], Justyna Łuczak[b], Maciej Śmiechowski[a], Dorota Warmińska[a,*]

[a] Department of Physical Chemistry, Faculty of Chemistry, Gdańsk University of Technology, ul. Narutowicza 11/12, 80-233 Gdańsk, POLAND

[b] Department of Process Engineering and Chemical Technology, Faculty of Chemistry, Gdańsk University of Technology, ul. Narutowicza 11/12, 80-233 Gdańsk, POLAND

[c] Department of Physical Chemistry, Faculty of Pharmacy, Medical University of Gdańsk, Al. Gen. Hallera 107, 80-416 Gdańsk, POLAND

*Corresponding author: tel.: +48583471410, fax: +48583472694, e-mail address: dorwarmi@pg.edu.pl

Table S1. Experimental densities (d / kg·m^{-3}) of deep eutectic solvents (DESs) within temperature range T = (293.15 to 333.15) K and P = 0.1 MPa[a].

T / K	DES1	DES2	DES3	DES4	DES5	DES6	DES7	DES8	DES9
293.15	1022.122	1015.628	1010.866	998.600	996.012	994.554	961.373	967.025	970.474
298.15	1018.486	1011.922	1007.055	995.054	992.363	990.818	958.034	963.433	966.855
303.15	1014.882	1008.214	1003.286	991.521	988.707	987.098	954.638	959.903	963.241
308.15	1011.298	1004.506	999.532	988.005	985.063	983.384	951.278	956.411	959.629
313.15	1007.721	1000.806	995.834	984.506	981.432	979.675	947.906	952.916	956.019
318.15	1004.165	997.106	992.136	981.023	977.812	975.953	944.555	949.410	952.410
323.15	1000.612	993.406	988.466	977.553	974.202	972.285	941.202	945.903	948.805
328.15	997.059	989.707	984.733	974.096	970.600	968.596	937.838	942.387	945.197
333.15	993.515	986.004	980.975	970.656	967.01	964.916	934.475	938.879	941.586

[a] Standard uncertainties u are $u(T)$ = 0.01 K, $u(P)$ = 0.001 MPa, $u(d)$ = 0.35 kg·m^{-3}

Table S2. Experimental viscosities (η / mPa·s) of DESs within temperature range T = (293.15 to 333.15) K and P = 0.1 MPa[a]

T / K	DES1	DES2	DES3	DES4	DES5	DES6	DES7	DES8	DES9
293.15	113.95	79.29	65.55	55.20	46.64	43.43	101.38	70.66	60.21
298.15	84.69	60.03	50.16	42.37	35.79	33.36	77.36	53.86	46.14
303.15	63.71	46.01	38.60	32.90	27.95	26.08	57.75	41.70	35.71
308.15	49.65	35.84	29.98	26.20	22.33	20.97	44.64	32.75	27.99
313.15	38.79	28.31	23.97	21.20	18.04	16.86	36.19	26.01	22.48
318.15	30.76	22.73	19.27	17.36	14.80	13.95	28.87	21.12	18.33
323.15	24.94	18.62	15.76	14.41	12.32	11.60	23.45	17.25	15.02
328.15	20.54	15.40	12.93	12.13	10.37	9.77	19.38	14.24	12.51
333.15	16.99	12.83	10.91	10.28	8.82	8.30	16.08	11.99	10.73

[a]Standard uncertainties u are $u(T)$ = 0.01 K, $u(P)$ = 0.001 MPa, $u(\eta)$ = 1%

Table S3. Experimental refractive indices (n_D) of DESs within temperature range T = (293.15 to 333.15) K and P 0.1 MPa[a]

T / K	DES1	DES2	DES3	DES4	DES5	DES6	DES7	DES8	DES9
293.15	1.4807	1.4766	1.4742	1.4786	1.4733	1.4717	1.4736	1.4709	1.4695
298.15	1.4790	1.4751	1.4725	1.4770	1.4719	1.4697	1.4721	1.4693	1.4677
303.15	1.4772	1.4733	1.4708	1.4751	1.4703	1.4678	1.4706	1.4678	1.466
308.15	1.4756	1.4716	1.4690	1.4732	1.4688	1.4662	1.469	1.4662	1.4642
313.15	1.4737	1.4698	1.4672	1.4713	1.4670	1.4644	1.4673	1.4642	1.4627
318.15	1.4718	1.4680	1.4655	1.4697	1.4653	1.4627	1.4656	1.4625	1.4607
323.15	1.4700	1.4663	1.4639	1.4680	1.4638	1.4608	1.4638	1.4608	1.4592
328.15	1.4687	1.4648	1.4622	1.4665	1.4622	1.4592	1.4619	1.4592	1.4575
333.15	1.4668	1.4630	1.4604	1.4647	1.4602	1.4576	1.4599	1.4570	1.4555

[a]Standard uncertainties u are $u(T)$ = 0.1 K, $u(P)$ = 0.001 MPa, $u(n_D)$ = 0.0002

Table S4. Experimental sound velocities (u / m·s^{-1}) of DESs within temperature range T = (293.15 to 333.15) K and P = 0.1 MPa[a]

T / K	DES1	DES2	DES3	DES4	DES5	DES6	DES7	DES8	DES9
293.15	1623.86	1661.64	1681.52	1832.07	1809.34	1796.37	1653.77	1674.49	1704.74
298.15	1607.94	1645.29	1661.67	1815.07	1791.96	1778.84	1637.23	1660.28	1687.52
303.15	1592.32	1629.24	1644.97	1797.98	1774.51	1761.26	1625.95	1643.61	1670.65
308.15	1576.70	1613.19	1628.28	1781.21	1757.79	1743.65	1609.96	1626.94	1653.77
313.15	1560.77	1596.50	1611.92	1763.98	1740.25	1726.39	1593.01	1610.93	1636.86
318.15	1544.72	1580.48	1594.50	1749.12	1723.04	1708.76	1580.46	1595.09	1619.81
323.15	1528.78	1564.24	1577.41	1732.68	1705.80	1691.24	1566.10	1579.05	1602.86
328.15	1512.84	1548.01	1560.31	1716.24	1688.57	1673.72	1551.57	1563.00	1585.91
333.15	1496.90	1531.76	1543.22	1699.80	1671.33	1656.21	1535.78	1546.95	1568.95

[a]Standard uncertainties u are $u(T)$ = 0.01 K, $u(P)$ = 0.001 MPa, $u(u)$ = 0.5 m·s^{-1}

Table S5. Isentropic compressibilities (10^{10} κ_S / Pa^{-1}) of DESs within temperature range T = (293.15 to 333.15) K and P = 0.1 MPa[a]

T / K	DES1	DES2	DES3	DES4	DES5	DES6	DES7	DES8	DES9
293.15	3.710	3.566	3.499	2.983	3.067	3.116	3.803	3.688	3.546
298.15	3.798	3.651	3.596	3.050	3.138	3.190	3.894	3.765	3.632
303.15	3.886	3.737	3.683	3.120	3.212	3.266	3.962	3.856	3.720
308.15	3.978	3.825	3.774	3.190	3.286	3.345	4.056	3.950	3.810
313.15	4.074	3.920	3.865	3.264	3.364	3.425	4.157	4.044	3.904
318.15	4.173	4.015	3.964	3.332	3.445	3.509	4.238	4.140	4.002
323.15	4.276	4.114	4.066	3.407	3.528	3.596	4.332	4.240	4.102
328.15	4.382	4.216	4.171	3.485	3.613	3.685	4.429	4.344	4.207
333.15	4.492	4.323	4.280	3.566	3.702	3.778	4.537	4.451	4.314

[a]Standard uncertainties u are $u(T)$ = 0.01 K, $u(p)$ = 0.001 MPa

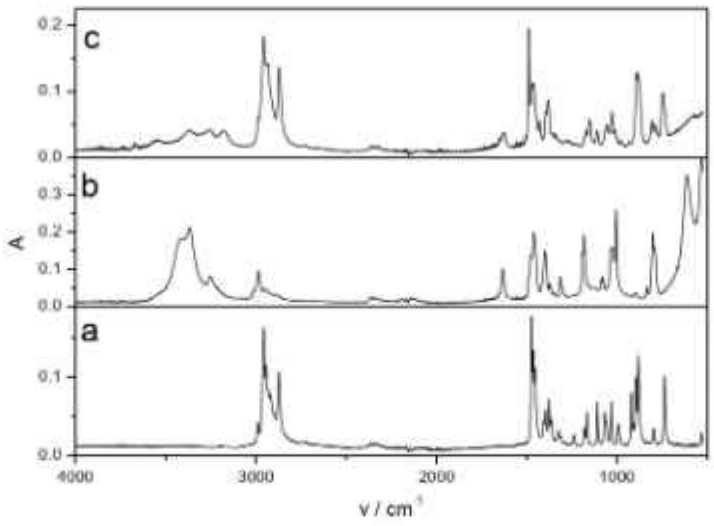

Figure S1. FTIR spectra of pure salts: a) TBAB, b) TEAC and c) TBAC.

Załącznik A3

B. Nowosielski, M. Jamrógiewicz, J. Łuczak, A. Tercjak, D. Warmińska, Effect of temperature and composition on physical properties of deep eutectic solvents based on 2-(methylamino)ethanol – measurement and prediction, J. Mol. Liq. 371 (2023) 121069. https://doi.org/10.1016/j.molliq.2022.121069. **IF_{2023}: 5,3, $MNSW_{2023}$: 100**

Journal of Molecular Liquids 371 (2023) 121069

Contents lists available at ScienceDirect

Journal of Molecular Liquids

journal homepage: www.elsevier.com/locate/molliq

Effect of temperature and composition on physical properties of deep eutectic solvents based on 2-(methylamino)ethanol – measurement and prediction

Bartosz Nowosielski [a], Marzena Jamrógiewicz [b], Justyna Łuczak [c,d], Agnieszka Tercjak [e], Dorota Warmińska [a,*]

[a] Department of Physical Chemistry, Faculty of Chemistry, Gdańsk University of Technology, ul. Narutowicza 11/12, 80-233 Gdańsk, Poland
[b] Department of Physical Chemistry, Faculty of Pharmacy, Medical University of Gdańsk, Al. Gen. Hallera 107, 80-416 Gdańsk, Poland
[c] Department of Process Engineering and Chemical Technology, Faculty of Chemistry, Gdańsk University of Technology, ul. Narutowicza 11/12, 80-233 Gdańsk, Poland
[d] Advanced Materials Center, Gdańsk University of Technology, ul. Narutowicza 11/12, 80–233 Gdańsk, Poland
[e] Group "Materials + Technologies" (GMT), Department of Chemical and Environmental Engineering, Faculty of Engineering, University of the Basque Country (UPV/EHU), Pza Europa 1, 20018 Donostia-San Sebastián, Spain

ARTICLE INFO

Article history:
Received 12 September 2022
Revised 1 December 2022
Accepted 12 December 2022
Available online 15 December 2022

Keywords:
DES
2-(methylamino)ethanol
Tetraalkylammonium salts
Thermal stability
Physical properties
Prediction models

ABSTRACT

Novel deep eutectic solvents were synthesized using 2-(methylamino)ethanol as hydrogen bond donor with tetrabutylammonium bromide or tetrabutylammonium chloride or tetraethylammonium chloride as hydrogen bond acceptors. Mixtures were prepared at different molar ratios of 1:6, 1:8 and 1:10 salt to alkanolamine and then Fourier Transform Infrared Spectroscopy measurements were performed to confirm hydrogen bonds interactions between components. Moreover, thermal properties such as melting points and thermal stability of deep eutectic solvents were determined and described. Each of important physical properties, including densities, viscosities, refractive indices and sound velocities at the temperature range of 293.15–333.15 K and the pressure of 0.1 MPa, were measured and discussed. The effect of hydrogen bond acceptor to hydrogen bond donor molar ratio, anion and length of alkyl chain for each synthesized salt according to their properties was evaluated. Additionally, the experimental values of each physicochemical parameter were compared with the predicted ones calculated using models recommended in literature. The main aim of this work was to assess the suitability of existing mathematical models for predicting the physicochemical properties of novel alkanolamine-based DESs. Empirical correlations for approximating phase behaviour or flow properties for DES systems are used in many procedures for design materials used of carbon dioxide capture purposes. The obtained results indicate that in the case of deep eutectic solvents based on 2-(methylamino)ethanol, in the absence of any experimental data, the best models for density prediction are the bonding group interaction contribution method and the group contribution model. For modelling of the refractive index it has been confirmed that a method based on the critical properties is the most satisfying. However, for the viscosity and speed of sound, the absolute average relative deviations for the methods based on critical properties exceed the measurement uncertainties found in practice. Therefore, they do not seem suitable for an accurate estimation of these properties for deep eutectic solvents based on 2-(methylamino)ethanol.

1. Introduction

In recent years, deep eutectic solvents (DESs) have been proposed as promising green media that could replace conventional industrial solvents to reduce environmental pollution and improve process efficiency [1,2]. The reason for such great interest in these media is their excellent properties similar to ionic liquids (ILs), such as negligible vapor pressure, non-flammability and good dissolving capacity of many compounds [3]. Moreover, they have several advantages over conventional ILs in that they are biodegradable, non-toxic and relatively easy and economical to prepare [4]. DESs are easy to prepare in high purity, and consist of two or three components that can interact through hydrogen bonds and/or electrostatic interaction, thus forming an eutectic mixture [2]. DESs have been reported in many applications so

* Corresponding author.
E-mail address: dorota.warmi@pg.edu.pl (D. Warmińska).

https://doi.org/10.1016/j.molliq.2022.121069
0167-7322/

far, such as metallurgy, catalysis, organic synthesis, liquid–liquid extraction and other separation processes [5678]. These neoteric solvents have also been used for gas absorption, polymer synthesis, biomass processing and drug solubilisation [9210].

The evaluation of DESs as new generation of solvents for various practical applications requires sufficient knowledge of their thermal and physical properties. Thermal properties such as melting point and decomposition temperature help to establish the operating conditions of the process. Physical properties such as density, viscosity, speed of sound and refractive index provide information on molecular interactions in the liquid that are essential for industrial device design as well as process modelling. Therefore, at present, many studies focus not only on the application, but also on the structure and physicochemical properties of deep eutectic solvents. So far, there have been a few reviews on this topic [16211]. At the same time, the interest of prediction of the physicochemical properties of deep eutectic solvents has been increased, as determining the DES characteristics by experiments at all temperatures is time consuming and costly. Some models are able to predict the physical properties of DESs only from their structural properties, allowing the rejection of deep eutectic solvents with adequate properties even before the synthesis step. The most common predictive techniques that have been the subject of recent research regarding the physical properties of DES are group/atomic contribution methods [12]. Until now, group contribution methods have been used mainly to predict the critical properties and the acentric coefficient of pure DESs [13,14,15]. In the literature, attempts to model also density, refractive index, heat capacities, speeds of sound and surface tensions of deep eutectic solvents using GC methods can be found [16121718].

In the last five years, the primary efforts have been devoted to the physicochemical characterization of DESs based on alkanolamines that have a much higher CO_2 absorption capacity than other deep eutectic solvents [19]. So far, only deep eutectic solvents with monoethanolamine (MEA) diethanolamine (DEA), methyldiethanolamine (MDEA) and monopropanolamine (AP) have been studied [20212223]. Mjalli *et al.* reported the experimental values of density, viscosity, surface tension and refractive index for the MAE combined with choline chloride, tetrabutylammonium bromide and methyltriphenylphosphium bromide [20]. Murshid *et al* presented the density, viscosity and refractive index for DESs based on DEA [21] and Adeyemi *et al.* determined the thermal stability and the physical properties such as density, viscosity, conductivity, surface tension and refractive index for MDEA based DESs containing choline chloride [22]. Our group published the values of density, viscosity, speed of sound and refractive index for AP based DESs [23] and this study is an extension of this work. Herein, a new series of DESs containing 2-(methylamino)ethanol (MAE) as hydrogen bond donor (HBD) and tetrabutylammonium bromide (TBAB) or tetrabutylammonium chloride (TBAC) or tetraethylammonium chloride (TEAC) as HBA were prepared and characterized by Fourier Transform Infrared spectroscopy (FTIR). Thermal properties of the synthesized DESs were determined using differential scanning calorimetry (DSC) and thermogravimetric analysis (TGA) techniques. Basic physical properties such as density, speed of sound, viscosity and refractive index were measured in a wide range of temperature (293.15–333.15 K). The influence of temperature, salt chain length and molar ratio of HBA to HBD has been analysed. The experimental values of physical properties have been compared with the predicted ones. Depending on the property, various methods described in the literature, including group contribution methods, were used to model it. The predictive ability of the applied methods for density, viscosity, sound velocity and the refractive index of MAE-based DESs has been discussed.

2. Materials and methods

2.1. Chemicals and DESs preparation

Table 1 presents the information about the chemicals used in this study, and Fig. 1 shows their chemical structures. 2-(methylamino)ethanol, tetrabutylammonium bromide, tetrabutylammonium chloride and tetraethylammonium chloride were purchased from Sigma-Aldrich. Tetrabutylammonium chloride was purified by double crystallization from acetone by adding diethyl ether and the others chemicals were used as received from the producer. All salts were dried under reduced pressure before use, TBAB at 323 K for 48 h, TBAC and TEAC at 298.15 K for several days.

The nine DESs were prepared by combining three different tetraalkylammonium salts and 2-(methylamino)ethanol in the molar ratio of 1:6, 1:8 and 1:10 HBA to HBD. The molar ratio of 1:6 was the lowest at which a stable DES could be obtained. Additionally, depending on DES, the eutectic composition was in the range of 1:6–1:10 M ratios, thus in order to include the effect of molar ratio on the physical properties of analysed DESs, all liquids were tested at the given ratios. This also allowed comparison of the effect of hydrogen bond acceptors on the properties of DES with the same molar ratios. The preparation was carried out by mass, using appropriate amounts of each DES component (Mettler Toledo with the precision of 0.00001 g), mixed at 353.15 K for 1 h until a homogeneous liquid without any precipitate was formed. The obtained DESs, stable colourless liquids at room temperature, were kept in tight bottles to prevent any contamination from outside atmosphere that may affect the physical properties of DES. Before experiments, the water content in DESs was measured by the Karl - Fischer Method using a Mettler Toledo Volumetric Karl – Fischer titrator (V10S). Table 2 presents its values along with the molar mass of DESs, their abbreviations, and the molar ratio and mass fraction of DES components.

2.2. DES characterization

2.2.1. Infrared spectroscopy measurements

FTIR experiments for liquid samples were performed using Jasco-4700 instrument (4000–400 cm^{-1} with 32 scans, 4 cm^{-1} resolution; Jasco Company, Tokyo, Japan). Thin film method using salt (KBr) plates was applied by placing 1 drop of the solution on one salt plate. The spectrum from a clean plate was recorded as a back-

Table 1
Provenance and mass fraction purity of the compounds studied.

Chemical name	Source	CAS number	Initial purity/ mass fraction[a]	Purification method	Final purity/ mass fraction[a]
2-(methylamino)ethanol (MAE)	Sigma Aldrich	109–83–1	≥0.98	none	–
Tetrabutylammonium bromide (TBAB)	Sigma Aldrich	1643–19–2	≥0.99	none	–
Tetraethylammonium chloride (TEAC)	Sigma Aldrich	56–34–8	≥0.98	none	–
Tetrabutylammonium chloride (TBAC)	Sigma Aldrich	1112–67–0	≥0.97	crystallization	≥0.98[b]

[a] As stated by the supplier.
[b] Determined by potentiometric titration.

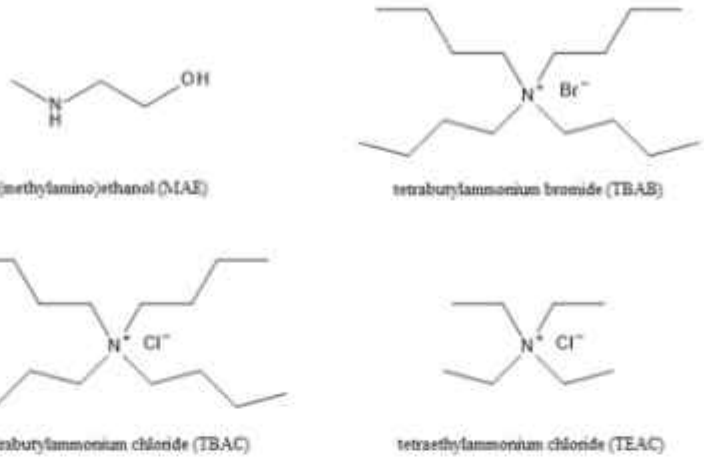

Fig. 1. Chemical structures of the DESs components used in this study.

Table 2
The abbreviation, molar mass, molar ratio, mass fraction and water content for chemicals used in this work.

DES		Salt		HBD		Molar ratio		Mass fraction[a]		Water content[b]
Symbol	M_{mix} / (g·mol^{-1})	Abbreviation	M_{salt} / (g·mol^{-1})	Abbreviation	M_{HBD} / (g·mol^{-1})	Salt	HBD	Salt	HBD	
DES1	116.601	TBAB	322.37	MAE	75.11	1	6	0.4183	0.5817	0.0015
DES2	102.072	TBAB	322.37	MAE	75.11	1	8	0.3444	0.6556	0.0018
DES3	97.675	TBAB	322.37	MAE	75.11	1	10	0.3012	0.6988	0.0020
DES4	87.915	TEAC	210.16	MAE	75.11	1	6	0.2664	0.7336	0.0017
DES5	85.200	TEAC	210.16	MAE	75.11	1	8	0.2167	0.7833	0.0018
DES6	83.390	TEAC	210.16	MAE	75.11	1	10	0.1816	0.8184	0.0021
DES7	104.336	TBAC	277.92	MAE	75.11	1	6	0.3838	0.6162	0.0020
DES8	97.829	TBAC	277.92	MAE	75.11	1	8	0.3161	0.6839	0.0025
DES9	93.574	TBAC	277.92	MAE	75.11	1	10	0.2704	0.7296	0.0028

[a] The standard uncertainty of DES mass fraction composition is 0.001.
[b] Water content of DESs in mass fraction determined by Karl Fischer titration with the standard uncertainty ± 0.0001.

ground and analysis of spectra was performed using Spectra Analysis software (Jasco Company, Tokyo, Japan). Spectra of solid samples (substrates) were recorded using dry salt KBr. The materials (1 mg) were compressed with potassium bromide (99 mg) to form a disc. Analysis were performed at 298.15 ± 0.1 K.

2.2.2. Melting point

Mettler Toledo Star One Differential Scanning Calorimeter (DSC) was used to measure the melting points of the synthesized DESs. The measurements were made under purified nitrogen atmosphere with a flow rate of 60 mL·min^{-1}, with samples of 10 – 18 mg packed in standard aluminium pan. The DSC equipment was connected to the STAR^{e} data acquisition software a dedicated computer. The heating and cooling sequence was programmed on the STAR^{e} console which controls the DSC equipment. For the melting point determination, a temperature range from 193.15 to 298.15 K was selected with a heating rate of 2 K·min^{-1}. The uncertainty of the measurement was ± 0.01 K.

2.2.3. Thermogravimetric analysis

The thermogravimetric analysis were performed using the TG 209F3 apparatus from Netzsch Group (Selb, Germany). Weighted samples (approx. 10 mg) were placed in a corundum dish. The measurement was carried out in an inert gas atmosphere-nitrogen with a flow rate of 50 mL·min^{-1} at the temperature range from 298 to 1023 K at a heating rate of 10 K·min^{-1}.

2.2.4. Density and sound velocity

The densities and the sound velocities of the DES samples were obtained at different temperatures using a digital vibration-tube analyser (Anton Paar DSA 5000, Austria) with proportional temperature control that kept the samples at working temperature with an accuracy of ± 0.01 K. Experimental frequency for the measurements of the ultrasonic velocity was equal to 3 MHz. The calibration was carried out using double distilled, deionized and degassed water, and dry air at atmospheric pressure (0.1 MPa). The standard uncertainty of density measurement was better than 0.1 kg·m^{-3} and 0.5 m·s^{-1}, respectively.

2.2.5. Viscosity

The viscosities of the DESs were measured with a LVDV-III Programmable Rheometer (cone-plate viscometer; Brookfield Engineering Laboratory, USA), controlled by a computer. The temperature of the samples was controlled within ± 0.01 K using a thermostatic water bath (PolyScience 9106, USA). The display of the viscosimeter was verified with certified viscosity standard

N100 and S3 provided by Cannon at 298.15 ± 0.01 K. The standard uncertainty of viscosity measurement was better than 2 %. At least three independent measurements were taken for each sample at each temperature to assure reproducibility of the measurement.

2.2.6. Refractive index

The refractive indices were obtained with an Abbe refractometer (RL-3, Poland) equipped with a thermostat for controlling the cell temperature with an accuracy of ± 0.1 K. The standard uncertainty of refractive index measurement on the n_D scale was 0.0002. At least three independent measurements were taken for each sample at each temperature to assure reproducibility of the measurement.

2.3. Prediction methods of DESs physical properties

2.3.1. Density modelling

Prediction of the MAE-based DESs density was performed by seven different methods described below. The two firstly applied models, Spencer – Danner procedure [25] and Mjalli *et al.* method [26], are based on the Rackett equation [24]. Generally, both models require the knowledge of the critical parameters such as the temperature, the volume and the pressure of DESs. Since these properties of DES components cannot be conveniently found experimentally, the Modified Lydersen-Joback-Reid method [27] proposed by Alvarez and Valderrama seems to be an important facilitation. The authors used Joback – Reid equations for the normal boiling temperature and the critical temperature. Additionally, Lynders equations for the critical pressure and critical volume were improved by their own modifications in parameters involved in equations. It resulted in new method which gives good results for different molecules with high molecular mass. Apart of that the critical properties of novel DES are found using the Lee-Kesler mixing equations suggested by Knapp *et al.* [28].

Prediction of DES density based on the modified Rackett equation was employed as follows:

$$d = d_R / Z_{RA}^{\varphi} \tag{1}$$

where parameter φ is defined as:

$$\varphi = (1 - T/T_{cm})^a - (1 - T_R/T_{cm})^a \tag{2}$$

and Z_{RA} is the specific compressibility factor can be calculated using:

$$Z_{RA} = \left(\frac{V_{RS} P_{cm}}{RT_{cm}}\right)^b \tag{3}$$

In equations (1)–(3), the symbols: d_R, T_R, and V_{RS} represent the reference density, reference temperature and saturated molar volume at reference temperature, respectively. The constants *a* and *b* are equal to 2/7 and $\left(1/[1 + (1 - T/T_{cm})^{2/7}]\right)$ for the modification of Spencer and Danner, while for the model proposed by Mjalli *et al.* are equal to 16/7 and $\left(25/24 + T_R/T_{cm}\right)^{16/7}$.

Going further, the density of the MAE-based DESs was predicted by the investigation performed by model introduced by Haghbakhsh *et al.* [29]. The authors used density as a databank for 149 DESs at several temperatures and a genetic programming algorithm to derive a DES density prediction model that uses the critical temperature, critical volume and acentric factor. Finally, they obtained the equation:

$$d = A_1 T_{cm}^2 + A_2 T_{cm} + A_3 \omega^{0.2251} + A_4 V_{cm} + BT \tag{4}$$

where A_{1-4} and *B* are the model's parameters presented in Table S1.

Another method of predicting the DESs densities was the bonding-group interaction contribution method introduced by Hou *et al.* [10]. Here, each group and bounding group interaction (BGI) make its own contribution to the density of the DES components.

Thus, the density can be predicted by following equation:

$$1/d = \frac{w_1}{(A_1 + B_1 T)\sum_j n_{1j}\Delta d_{1j} + A_2 + B_2 T} + \frac{w_2}{(A_1 + B_1 T)\sum_j n_{2j}\Delta d_{2j} + A_2 + B_2 T} + ww_1 w_2 T G_{ij} \tag{5}$$

where w_1 and w_2 are the mass fractions of DES components, Δd_{1j} and Δd_{2j} are the contribution values of the corresponding group *j* for density of DES components, A_1, A_2, B_1, and B_2 are the model's constants and G_{ij} is the constant that represents interactions in type III deep eutectic solvents.

Each parameters involved in presented models are presented in Table S2. For MAE-based DESs investigated in this work, only one bounding group interaction, i.e. (OH-NH) in 2-(methylamino) ethanol molecule should be considered and the values of $\sum_j n_{ij} d_j$ for TBAB, TEAC, TBAC and MAE are 0.0497; 0.0407; 0.0186 and 0.0252, respectively.

Lastly, the method by Mjalli [31] was applied for prediction of the DESs densities. It is a model based on the mass connectivity index with the semi-empirical equation as follows:

$$d = d_R - 0.0005197\,\lambda_{DES}^{0.18293}(T - T_R) \tag{6}$$

where λ_{DES} is the mass connectivity index of DES, calculated on the basis of the pure components mass connectivity indices λ, which are obtained from equation:

$$\lambda = \sum_{i=1}^{n} \left(1/\sqrt{M_i M_j}\right) \tag{7}$$

where M_i and M_j are the masses of connected groups numbers (i) and (j) reported by Vaderrama *et al.* [32].

In this work, the mass connectivity indices for 2-(methylamino) ethanol, tetrabutylammonium bromide, tetraethylammonium chloride and tetrabutylammonium chloride are obtained as 0.5428, 2.3215, 1.5617 and 2.3515, respectively. Correlation with ones calculated by multiplying the salt and MAE mass connectivity indices by their molar quantities in the DES is presented in Table 6.

Other known and applied models for predicting densities, refractive indices, heat capacities, speeds of sound, and surface tensions of novel DESs presented in this work are methods described by Haghbakhsh *et al.* in 2021 [12]. This is a group contribution (GC) and atomic contribution (AC) density models which use a 1239 point dataset.

The GC based method is expressed as:

$$d_1^G = m_{MM}\sum k_i\left(\Delta d_{1,i}^G\right)_{MM} + m_{MD}\sum l_i\left(\Delta d_{1,i}^G\right)_{MD} \tag{8}$$

$$d_2^G = m_{MM}\sum k_i\left(\Delta d_{2,i}^G\right)_{MM} + m_{MD}\sum l_i\left(\Delta d_{2,i}^G\right)_{MD} \tag{9}$$

$$d^G = \left(\frac{d_1^G}{M_w}\right)^{-0.2645} + \left(\frac{d_2^G}{M_w}\right)T^{-0.6393} + 1.3695 \tag{10}$$

while AC model is as follows:

$$d_1^A = m_{MM}\sum k_i\left(\Delta d_{1,i}^A\right)_{MM} + m_{MD}\sum l_i\left(\Delta d_{1,i}^A\right)_{MD} \tag{11}$$

$$d_2^A = m_{MM}\sum k_i\left(\Delta d_{2,i}^A\right)_{MM} + m_{MD}\sum l_i\left(\Delta d_{2,i}^A\right)_{MD} \tag{12}$$

$$d^A = \left(\frac{d_1^A}{M_w}\right)^{-0.4093} + \left(\frac{d_2^A}{M_w}\right)T^{-0.7434} + 0.5139 \tag{13}$$

where M_w is the molar mass of DES and $Ad_{i,A}$...$Ad_{i,A}$ are the contributions of each group/atom of type i for the GC and AC models. k_i and l_i indicate the number of occurrence of the functional group/atom of type i in the HBA and HBD molecules, respectively. The symbols m_{HBA} and m_{HBD} denote the normalized numbers of moles HBA or HBD. In this study, there was no need for data normalization as the number of mols of the hydrogen bond donor expressed per one mole of hydrogen bond acceptor. The G and A superscripts show the GC and AC model type, respectively.

2.3.2. Prediction of viscosity

The viscosity of deep eutectic solvents prediction was estimated by model proposed and described by Bakhtyari *et al.* [33]. Basing on a databank of 156 DESs and 1308 data points and the knowledge of the critical pressure, critical temperature, and one reference viscosity data, they developed an useful model expressed as:

$$\eta = \left[\eta_R^A + B\left(\frac{T_R - T}{T - T_R}\right)\right]^{1/A} \tag{14}$$

where the constant A is related to the critical pressure, P_{cm}:

$$A = \frac{-0.817}{P_{cm}} - 0.123 \tag{15}$$

and the constant B depend on the critical temperature, T_{cm}, as:

$$B = -1.595T_{cm} \tag{16}$$

In equation (14), the symbol η_R denotes to the viscosity at the reference temperature T_R.

For the DESs investigated in this study, the reference temperature is 293.15 K.

2.3.3. Prediction of refractive index

Four different methods were used to predict the MAE-based DESs refractive index in this work. Firstly, we applied model developed by Shahbaz *et al.* [13] and the authors applied here the molar refractions (R_M) of DESs components calculated by summing their atomic and structural contribution parameters that were determined by Wildman and Crippen [34]. The molar refraction of DESs was obtained from the equation:

$$R_M = \sum x_i R_{Mi} \tag{17}$$

where x_i and R_{Mi} are the mole fraction and molar refraction of the DES components, and its value together with the experimental value of DES density was used to calculate the refractive index by Lorentz–Lorenz equation:

$$R_M = \frac{M_w}{d}\left(\frac{n^2 - 1}{n^2 + 2}\right) \tag{18}$$

where M_w and d are the molecular weight and density of DES, respectively.

While prediction of refractive index for the components of novel DESs used in this study, the molar refractions (R_M) were found to be equal to 21.012, 87.567, 47.557 and 84.493 for MAE, TBAB, TEAC and TBAC, respectively.

The second method that we tested on the ability to predict the DESs refractive index was based on the critical properties and acentric factors developed by Taherzadeh *et al.* [35]. In the model the following equation was proposed:

$$n = A_1\omega^2 + A_2\frac{\omega^2}{M_w} + A_3P_{cm} + A_4 + B\omega/T \tag{19}$$

where A_1–A_4 and B are parameters of model presented in Table S3.

Going further, prediction of the refractive index for novel chloride and bromide-based deep eutectic solvents was performed by the group contribution model introduced by Khajeh *et al.* [18]. Unfortunately, this method does not include bromide-based deep eutectic solvents that have an amine group contained in hydrogen bond donor, therefore, in this work, the model by Khajeh *et al.* could be used to predict only the refractive indices of TEAC:MAE and TBAC:MAE. The model proposed by authors was as follows:

$$n = \sum N_i GC_i + 0.22766HBA/HBD - 0.00037T + 1.37466 \tag{20}$$

where N_i and GC_i are the number of occurrences of ith chemical substructure (functional group) and the contribution of the ith chemical substructure, respectively, T is temperature in K and HBA/HBD is molar ratio of HBA to HBD.

Lastly, we used the method described by Haghbakhsh *et al.* [12]. It is modeled on group contribution and atomic contribution and uses a large dataset of 1117 data points from 142 DESs. The GC model was expressed as:

$$n^G = (n_1^G)^{-0.2107} + (n_2^G)T^{-1.8254} + 1.3695 \tag{21}$$

while AC model was as follows:

$$n^A = (n_1^A M_w)^{-0.2975} + (n_2^A M_w)T^{-2.1023} + 1.4335 \tag{22}$$

In this work, the refractive indices of the pure components were calculated using the equations analogous to Equations (8) and (9) using the contribution of each group/atom.

2.3.4. Prediction of speed of sound

Generally, three methods were described to estimate the speed of sound of DESs, while two of them were applied in this study. The first model was proposed by Peyrovedin *et al.* [16] and required knowledge of the critical parameters of solvent. It was expressed as:

$$u = \omega(7.378M_w - 2.012T) - 2.911V_{cm} + 2514.2 \tag{23}$$

The next two were based on atomic and group contribution and were introduced on the basis 398 data points by Haghbakhsh *et al.* [12]. Unfortunately, due to the lack of NH group contribution data, the GC based model could not be used to predict the speed of sound of MAE-based DESs studied in this work. Moreover, as there is no data on the atomic contribution of the bromide ion, it was also impossible to model of the speed of sound for TBAB based DESs (DES1–DES3).

The AC based model was expressed as:

$$u^A = u_1^A + u_2^A T^{0.3278} + 1607.4690 \tag{24}$$

where the speed of sound for the pure components were calculated using the equations analogous to Equations (11) and (12) using the atomic contribution of each atom.

3. Results and discussion

3.1. FTIR characterization of DESs

Infrared spectroscopy may be used not only as standard method for identification of molecular vibrations and deformations of chemical bonds in DES, but also as a means of individual characteristic interactions of a similar chemical structures [2036]. The FTIR spectra of the studied DESs are shown in Fig. 2 together with the reference of neat 2-(methylamino)ethanol spectrum (black line at Fig. 2).

The bands in the MAE spectrum present typical region of the ν(OH)/ν(NH_2) stretching vibrations range (3900–3000 cm^{-1}), particularly sensitive to the hydrogen bonding located at 3309 cm^{-1}. The DES spectra presented maximum absorption of these interactions at 3392 cm^{-1} with TBAB salts (DES 1–3), 3378 cm^{-1} with TEAC (DES 4–6) and 3404 cm^{-1} with TBAC (DES 7–9) so there are

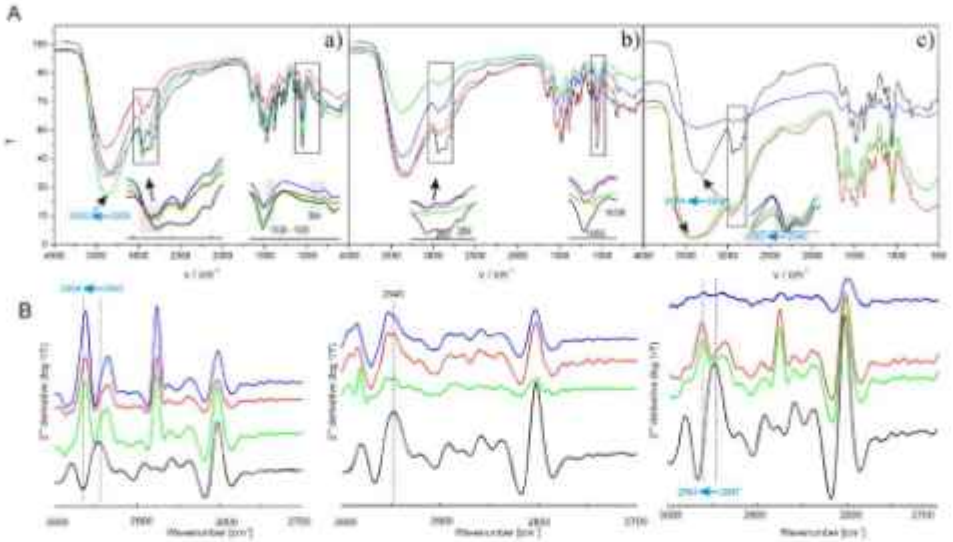

Fig. 2. A) FTIR spectra and B) their second derivatives for DES studied: a) TBAB:MAE (DES 1–3), b) TEAC:MAE (DES 4–6) and c) TBAC:MAE (DES 7–9). (blue – 1:8, red – 1:6, green – 1:10, black – neat MAE). (For interpretation of the references to colour in this figure legend, the reader is referred to the web version of this article.)

blue-shifted effects observed which mean the increase of energy. The observed frequency and intensity variations follow naturally. Interestingly, in the spectrum of TBAB:MAE the C — H stretching vibrations of the CH_2 – CH_2backbone in MEA were blue-shifted from 2943 to 2964 and from 2857 to 2873 cm^{-1}, respectively for DES 1–3. On the second derivatives of TBAC:MAE spectra blue-shifts of band 2964 — 2947 cm^{-1} are observed. In the studied DESs, the other spectroscopic effect on the spectra are observed at the range 1100-1000 cm^{-1}. The stoichiometry and amount of salt influence is visible as the change of band shape. In TBAB:MAE spectrum flattening at 1038–1020 cm^{-1} for C—N stretching amine of the 1:10 stoichiometry sample (green) is more noticeable than for the 1:6 and 1:8 samples because it corresponds to the shape of the MAE band (Fig. 2 a). In the sample containing 1:10 stoichiometry of TEAC:MAE spectrum at 1055 cm^{-1} is influenced and become deformed to more intensive one at 1035 cm^{-1} (Fig. 2 b). DES with TBAC seems as the same at this region. Substituted C—H bending at 864 cm^{-1} of each DESs spectrum is not interrupted.

3.2. Thermal properties of DESs

The obtained thermal properties of the studied DESs based on 2-(methylamino)-ethanol are shown in Table 3, as the values of melting temperature, T_m, decomposition temperatures at 10 % and 90 % weight loss, $T_{10\%}$ and $T_{90\%}$, and maximum temperatures, T_{max}. Fig. 3 presents the DSC plots and Fig. 4 shows the curves TGA with DTGA.

3.2.1. Melting point

Differential scanning calorimetry is crucial for observing the phase transition temperature of materials. DSC has been used to determine the melting point and any solid state phase transitions in the present of MAE-based DESs. Table 3 shows the melting points of DESs. Fig. 3 (a,b,c) illustrates DSC curves for the DES systems with three HDA:HBD ratios as 1:6; 1:8 and 1:10. Generally, in most curves there are doublet form endothermic peaks which are considered as melting peaks, but in the case of TBAB:MAE 1:6 we observed a single peak of melting process. For the studied DESs all the melting points were lower than for the pure components and below 298.15 K which gives them wide liquid range. Clear crystallization and melting peaks were observed for all tested DESs. Moreover, the order of melting temperatures for DES at the same molar ratio of the salt to 2-methylaminethanol is as follows: TBAB:MAE > TEAC:MAE > TBAC:MAE, which seems to suggest that the melting temperature of salt may influence the melting temperature of deep eutectic solvents. Besides, the highest values of T_m are observed for tetrabutylammonium bromide based DESs, which T_m is greater than that of TBAC. Moreover, the comparison of the melting temperatures for DES containing tetrabutylammonium and tetraethylammonium chlorides leads to the conclusion, that the melting temperature of deep eutectic solvents increases with increasing cation alkyl chain length in the salt and T_m of salt itself. The same results were obtained for DESs with 3-amino-1-propanol [23]. DSC curves are shown in Fig. 3. Additionally, it has been observed that the phase transition temperatures only for TBAB 1:8 and 1:10 are present at temperature near 250.15 K. All determined results are given in Table 3.

3.2.2. Thermogravimetric measurements

Fig. 4 presents TGA curves, i.e. the weight loss measured in % against temperature, for the studied DESs along with their pure components. In general, the curves consist of two steps– the first shows the MAE decomposition and the second corresponds to the degradation of the salt. Only for TEAC: MAE with the molar ratio of HBA to HBD of 1:10 at the lower temperature (approx. 373 K) an additional step is observed. The reason of this observation may be explained by evaporation of water. As the water content of all primary samples (see Table2) was very similar, hence the higher amount of water in TEAC: MAE (1:10) shown in the TGA

Table 3
Thermal characteristics of tested DES and MAE obtained from TGA, DTGA and DSC curves: decomposition temperatures at 10% and 90% weight loss, $T_{10\%}$ and $T_{90\%}$, maximum temperatures, T_{max}, melting temperature, T_m, heat of crystallization, ΔH_{cryst}, heat of melting, ΔH_m, and heat of other solid transitions for DESs in this work.

DES	$T_{10\%}$ / K	$T_{90\%}$ / K	T_{max1} / K	T_{max2} / K	T_m / K	ΔH_{cryst} / (kJ·K^{-1})	ΔH_m / (kJ·K^{-1})	ΔH_{other} / (kJ·K^{-1})
DES1	333.9	494.0	361.7	489.6	261.28	–	262	–
DES2	356.8	494.4	383.0	489.7	260.75	235	262, 264	250
DES3	332.2	489.9	360.6	489.5	283.83	232	259, 264	250
DES4	343.1	546.6	367.0	547.6	258.99	234	259, 262	–
DES5	340.6	543.0	368.1	548.2	258.62	235	259, 262	–
DES6	339.5	547.7	389.0	554.2	258.03	231	258, 264	–
DES7	276.8	506.1	409.8	497.9	259.02	–	255, 258	–
DES8	373.4	503.7	407.4	498.2	261.37	241	262, 255	–
DES9	367.0	490.5	404.0	486.9	263.43	233	254, 264	–
MAE	329.1	379.1	368.5	–	268.25	–	–	–

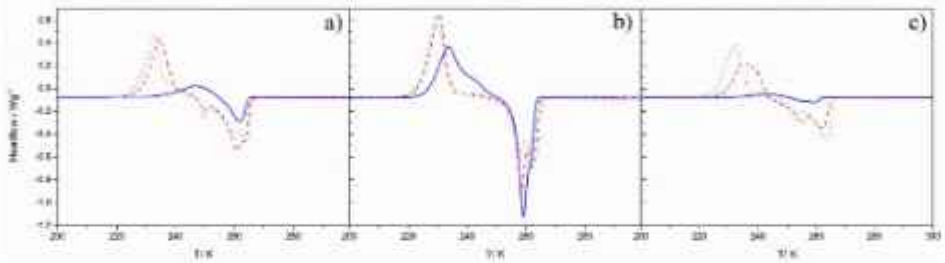

Fig. 3. DSC curves for DES studied: a) TBAB:MAE (DES 1–3), b) TEAC:MAE (DES 4–6) and c) TBAC:MAE (DES 7–9); (blue solid line – 1:9, red dashed line – 1:8, wine dotted line– 1:10). (For interpretation of the references to colour in this figure legend, the reader is referred to the web version of this article.)

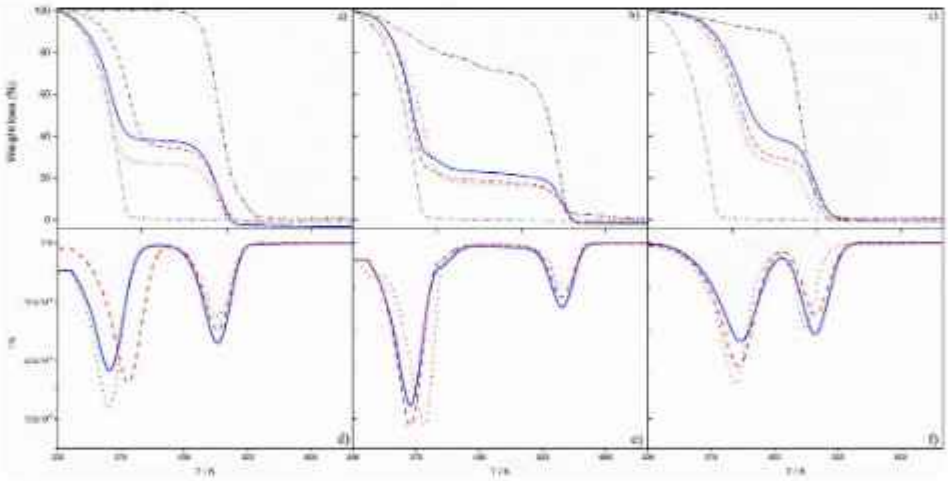

Fig. 4. TGA curves: (a, b, c) and DTGA curves: (d, e, f) obtained by thermogravimetry of DESs: a) and d) TBAB:MAE (DES 1–3), b) and e) TEAC:MAE (DES 4–6); c) and f) TBAC:MAE (DES 7–9); (blue solid line – 1:9, red dashed line – 1:8, wine dotted line – 1:10, black dash-dotted-dotted line – salt, grey dashed-dotted line – MAE). (For interpretation of the references to colour in this figure legend, the reader is referred to the web version of this article.)

curve could to be the result of moisture absorption from the atmosphere when this DES was transferred to the TGA pan.

As can be seen from the TGA plots, the stability of all DESs is in between that of their components and the order of stability is: MAE < DES < salt.

For DESs with a molar ratio of HBA to HBD equal to 1:6 and 1:10, the initial decomposition temperature measured as 10 % weight loss ($T_{10\%}$) and the first significant peak of derivative weight loss curve (T_{max1}) change according to the sequence: TBAB:MAE < TEAC:MAE < TBAC:MAE, while for DESs with the molar ratio 1:8, the order of $T_{10\%}$ is different, as is TEAC:MAE < TBAB:MAE < TBAC:MAE (Table 3). Indication of the end of the decomposition is measuring 90 % mass loss ($T_{90\%}$) and the second significant peak of derivative weight loss curve (T_{max2}). Results approved that they change regardless of the molar ratio of HBA to HBD according to: TBAB:MAE < TBAC:MAE < TEAC:MAE (Table 3). Thus, it can be concluded, that when DESs with the same molar ratio are considered, the highest thermal stability, measured by $T_{10\%}$ and T_{max1}, is found for TBAC:MAE, which is more stable than TEAC:MAE. Moreover, since the decomposition temperature observed for TBAB:MAE is lower than for TBAC:MAE, it can be claimed that DESs based on salts containing a chloride anion are more stable than those containing a bromide anion. Obviously, this correlates with the strength of the hydrogen bonds, which is stronger for the Cl^- than for Br^- and this effect seems to be stronger than the effect of the alkyl chain length in the salt because the decomposition temperature of TBAB:MAE is lower than that of TEAC:MAE. The exceptions to this rule are DESs with a molar ratio 1:8, for which an inverse $T_{10\%}$ correlation for TEAC:MAE and TBAB:MAE is observed. As the molar ratio 1:8 is the eutectic composition for TBAB:MAE (Table 3), the stronger hydrogen bonds are expected in this solvent and make it more stable. The positive effect of the eutectic composition on the thermal stability of DESs is also seen in DESs based on the same salt but differing in the molar ratio of HBA to HBD (see Fig. 4). Summing up, it can be said that our conclusions are consistent with the results obtained for phosphonium-based DES, showing that the thermal stability of DES increases with increasing length of the alkyl chain length of its components and is higher for systems with stronger hydrogen bonds interactions [37].

3.3. Experimental values of physical properties of DESs

3.3.1. Density

In this study, the density and other physical properties of the deep eutectic solvents studied were measured as a function of temperature with the range of 293.15–333.15 K and at ambient pressure. All density data are presented in Table S4. Fig. 5 depicts, as example, the obtained densities for TBAB:MAE, TEAC:MAE and TBAB:MAE at a molar ratio of 1:8.

As can be seen from Table S4, the experimental density values decrease with increasing temperature and the decrease is linear, as shown in Fig. 5. This is obviously due to the fact that at higher temperatures, more intermolecular voids are created, which increase in volume and lead to a decrease in density.

Moreover, the values of the DESs density at the same temperature and molar ratio of the salt to 2-(methylamino)ethanol are highest for TBAB based DESs and lowest when TBAC plays the role of HBA. The same order of density was found by our group for 3-amine-1-propanol based DESs consisting of the same salts, i.e. TBAB:AP > TEAC:AP > TBAC:AP [23]. The Smith and Zhang groups also postulated that bromide salts lead to denser DESs than chlorides [382].

The results obtained for TBAC:MAE and TEAC:MAE are also consistent with reports in the literature showing that the density of DESs decreases with increasing of chain length of HBD or HBA. Florindo *et al.* showed that the DESs composed of glutaric acid and levulinic acid have lower density values compared to those observed for DES based on oxalic or glycolic acids [39]. Wang *et al.* reported that the density of ethylene glycol based DESs consisting of tetraethylammonium bromide, tetrapropylammonium bromide and tetrabutylammonium bromide were 1.1596, 1.1121 and 1.0762 at 298 K, respectively [40].

As the density values for TBAB:MAE (DES 1–3) are higher than those for TEAC:MAE (DES 4–6), therefore it can concluded that the packaging effects have a smaller influence on the density than the anion weight effect (anion charge density resulting from its size).

Further inspection of results presented in Table S4 and Fig. 5 allow to claim that the DESs density depends on the HBA:HBD molar ratio. For deep eutectic solvents based on TBAB and TEAC, the density decreases as the content of MAE increases, while for TBAC-based DESs the effect of the molar ratio of HBD is negligible. It is well known that the influence of the amount of hydrogen bond donor on the density of DES depends on the molecular characteristics of HBD [2041]. For most DESs, their density decreases as the amount of HBD increases. However, in the case of DES, where there is a strong association between HBD molecules, an increase in density with the increase in the content of hydrogen bond donor was observed. Abbott *et al.* reported densities of DESs with different molar ratios of choline chloride to glycerol and found that the as the amount of HBD increased relative to the salt, the density increased [42]. In the case of the DES analyzed in this study, a dif-

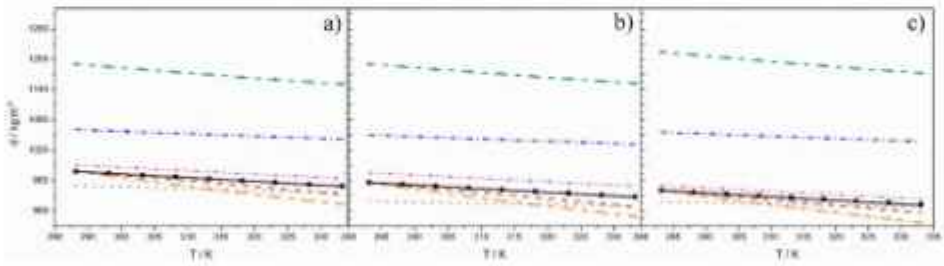

Fig. 5. Experimental values of densities (black squares) for DESs in the molar ratio 1:8 along with the predicted ones a) TBAB:MAE, b) TEAC:MAE, c) TBAC:MAE: red dashed line – method based on Rackett equation by Spencer and Danner; orange dashed line with stars – method based on Rackett equation by Mjalli; blue dashed-dotted line – method based on critical properties by Naghibzadeh *et al.*; magenta dash-dotted-dotted line – IGI based method by Hou *et al.*; black solid line – MCI based method by Mjalli; wine dotted line – GC based method by Naghibzadeh *et al.*; dark cyan dashed line with triangles – AC based method by Naghibzadeh *et al.* (For interpretation of the references to colour in this figure legend, the reader is referred to the web version of this article.)

ferent relationship between the density of deep eutectic solvents and the molar ratio of HBA to HBD seems to be related to the density of neat MAE. The densities of TBAB:MAE (DES 1–3) and TEAC:MAE (DES 4–6) are higher than those of 2-(methylamino)ethanol, while the densities of TBAC:MAE (DES 7–9) are almost the same, especially at lower temperatures. Thus, when the amount of 2-(methylamino)ethanol in TBAB:MAE (DES 1–3) and TEAC:MAE (DES 4–6) increases, the density tends to that of MAE and decreases. In the case of TBAC:MAE (DES 7–9), due to similar density of DES and neat MAE, no significant changes in density are observed as a result of changing the DES composition.

3.3.2. Viscosity

The viscosity values of MAE-based DESs are in the range of 17.43 ÷ 34.27 mPa·s at 298.15 K (see Table S5) and therefore are among the lowest of recorded so far for DESs containing ethylene glycol, ethanolamine or acetic acid [43]. Moreover, as in the case of other deep eutectic solvents, the viscosity of TBAB:MAE, TEAC:MAE and TBAC:MAE decreases greatly with increasing temperature [44,45]. According to the hole theory, as the viscosity is related to the free volume and the probability of finding holes of suitable dimensions into which solvent molecules or ions can move, this property depends on the size of the DES constituents [46]. The value of viscosity of DESs is also a result of the presence of hydrogen bonds, electrostatic and van der Waals interactions between the individual components of DESs. Thus, the viscosity depends on the chemical nature of the components, their molar ratio, water content and temperature [47]. As shown in Table S5 and Fig. 6, the lowest viscosity values for the studied systems were observed for TEAC-based DESs (DES4-6), which are smaller in size and where weaker hydrogen bonding is expected, thus this is consistent with the hole theory [46,48]. Additionally, the shorter alkyl chains in TEAC might result in weaker van der Walls interaction.

It is also observed that the values of viscosities obtained both for TBAB:MAE (DES 1-3) and TBAC:MAE (DES 7-9) are similar. Therefore, it can be claimed that for deep eutectic solvents consisting of MAE and tetraalkylammonium salts, the alkyl chain length of the salt has a greater influence on the viscosity than the anion effect.

Regardless of the salt, the viscosity of MAE-based DESs decreases as the molar ratio of HBA to HBD increases. This is due to the low molecular movement caused by the decrease in the free volume of the solvent with the compact structure of DES [49]. Similar observations that increasing the amount of HBD reduces the viscosity of DES were made by most of the authors [39,50,41]. However, it should be noted, that in the case of DESs based on hydrogen bond donors with a strong cohesive energy due to presence of intermolecular hydrogen bond network, the opposite effect was also observed. At the temperature of 298 K, the viscosities of the mixtures of choline chloride and glycerol in a molar ratio of 1:4, 1:3, 1:2 are 350, 320, and 259 mPa·s, were found, respectively [42].

Analyzing results presented in Fig. 6, it is noticed that viscosities for TBAB:MAE, TEAC:MAE and TBAC:MAE at a molar ratio of 1:8 of DESs evaluated in this work decreases nonlinearly with increasing temperature. Obviously, this is due to a significant decrease in hydrogen interactions with the temperature rising and increasing of the DES component mobility. There are two commonly used models to study the effect of temperature on DESs viscosity, namely the Arrhenius and Vogel-Fulcher-Tamman (VFT) equations [51]. The Arrhenius (1) and VFT equations (2) are expressed as:

$$\eta = \eta_\infty \exp(E_a/RT) \tag{25}$$

$$\eta = \eta_0 \exp(b/(T - T_0)) \tag{26}$$

where η_∞, E_a, η_0, b, and T_0 are fitting parameters, η_∞ is the viscosity at infinite temperature, E_a is the activation energy, R is the gas constant, and T is the temperature at Kelvin.

Tables 4 and 5 present the fitting parameters determined from the experimental data along with R^2 and root-mean-square deviations (*RMSD*). The obtained E_a values, which are the lowest for TEAC:MAE and similar for TBAB:MAE and TBAC:MAE, confirm the conclusions presented above, i.e. the higher size of the DES components and the stronger interactions between them, the higher viscosity is observed.

Comparing R^2 and *RMSD* values from Table 4 and 5 suggests the VFT equation is more suitable for fitting the dynamic viscosity results. Similar conclusions were made by for other

Table 4
Fitting parameters for the Arrhenius equation for dynamic viscosity results determined within temperature range T = (293.15 to 333.15) K and P = 0.100 MPa.

DES	$10^3 \cdot \eta_\infty$ / mPa·s	$10^{-4} \cdot E_a$ / J·mol^{-1}	R^2	RMSD
DES1	1.70	3.60	0.9977	0.60
DES2	2.70	3.43	0.9989	0.33
DES3	2.54	3.42	0.9996	0.19
DES4	8.14	3.06	0.9984	0.25
DES5	9.67	3.00	0.9986	0.21
DES6	9.52	2.99	0.9994	0.13
DES7	1.48	3.64	0.9898	1.3
DES8	3.88	3.39	0.9977	0.44
DES9	8.42	3.11	0.9939	0.89

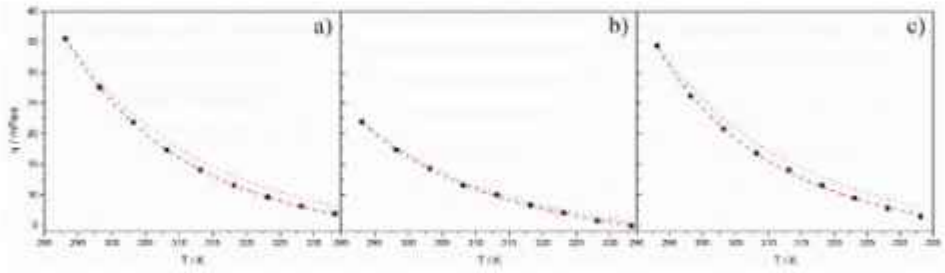

Fig. 6. Experimental values of viscosities (black squares) for DES in the molar ratio 1:8 along with the predicted ones a) TBAB:MAE, b) TEAC:MAE, c) TBAC:MAE: red dashed line – VFT equation; blue dotted line – critical properties based method by Bakhtyari *et al.* (For interpretation of the references to colour in this figure legend, the reader is referred to the web version of this article.)

Table 5
Fitting parameters for the Vogel-Fulcher-Tammar (VFT) equation for dynamic viscosity results determined within temperature range T = (293.15 to 333.15) K and P = 0.100 MPa.

DES	η_0 / mPa·s	b / K	T_0 / K	R^2	RMSD
DES1	0.0706	727.5	180.6	0.9998	0.13
DES2	0.0213	1047.8	152.0	0.9998	0.05
DES3	0.0033	1672.1	111.2	0.9998	0.08
DES4	0.0430	836.1	160.7	0.9997	0.11
DES5	0.0065	1486.5	110.1	0.9988	0.20
DES6	0.0012	2106.6	67.2	0.9990	0.17
DES7	0.0784	289.7	229.8	0.9992	0.35
DES8	0.0544	904.3	162.1	0.9989	0.30
DES9	0.0686	750.3	169.3	0.9971	0.41

Table 6
Calculated mass connectivity indices, MCI, and critical properties of DESs used in this study: critical temperature, T_{cm}, critical volume, V_{cm}, critical pressure, P_{cm}, and acentric factor, ω.

DES	T_{cm} / K	V_{cm} / cm^3·mol^{-1}	P_{cm} / bar	ω	MCI
DES1	618.12	387.61	30.37	0.723	5.3607
DES2	611.23	385.27	31.94	0.717	6.7571
DES3	607.82	354.12	32.80	0.714	7.7272
DES4	589.93	334.05	34.18	0.674	4.8599
DES5	590.04	326.60	34.96	0.679	5.8900
DES6	590.14	321.24	35.51	0.683	6.9586
DES7	612.74	386.45	30.21	0.721	5.5756
DES8	607.39	385.39	31.74	0.716	6.6978
DES9	604.24	353.82	32.74	0.713	7.7715

alcoholamine-based DES, i.e. monopropanolamine-based deep eutectic solvents [23].

3.2.3. *Refractive index*

The refractive indices obtained for the DESs studied in this work are presented in Table S6. As can be seen, their values vary from 1.4541 to 1.4602 at the temperature of 298.15 K, which is consistent with the research conducted so far showing that the refractive indices of DESs are higher than molecular solvents such as ethanol or acetone, but similar to common ILs [52].

Regardless of the molar ratio of HBA to HBD, the refractive indices at a given temperature change in the order: TBAB: MAE < TBAC: MAE < TEAC: MAE. Therefore, it can be concluded that in the case of MAE-based DESs the main factor determining the refractive index values is molecular weight of solvent. Moreover, this observation is in agreement with the order of refractive indices obtained for DESs differing in the HBA:HBD molar ratio, because the n_D decrease with increasing MAE content for all investigated DESs.

Considering the decrease in refractive index with increasing temperature, it can be said that for MAE-based DESs, as with other published DESs based on alkanolamines such as monoethanolamine, diethanolamine and 3-amino-1-propanol a linear decrease in refractive index with increasing temperature was observed [20,21,23]. This is presented in Fig. 7, which shows the obtained refractive indices for TBAB: MAE, TEAC: MAE and TBAB: MAE in the molar ratio 1:8 within the temperature range T = (293.15 to 333.15) K.

3.2.4. *Speed of sound*

The speed of sound data for the prepared MAE-based DESs measured at different temperatures are listed in Table S7 and presented in Fig. 8.

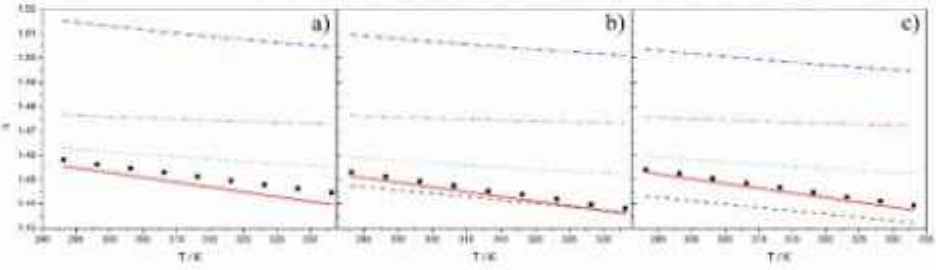

Fig. 7. Experimental values of refractive indices (black squares) for DES in the molar ratio 1:8 a) TBAB:MAE, b) TEAC:MAE, c) TBAC:MAE along with predicted ones: red solid line – method based on molar refraction by Shahsi et al.; olive dotted line – method based on critical properties by Taherzadeh et al.; blue dashed-dotted line – GC based method by Haghbakhsh et al.; magenta dashed-dotted-dotted line – AC based method by Haghbakhsh e. al.; wine dashed line – GC based method by Khajeh et al. (For interpretation of the references to colour in this figure legend, the reader is referred to the web version of this article.)

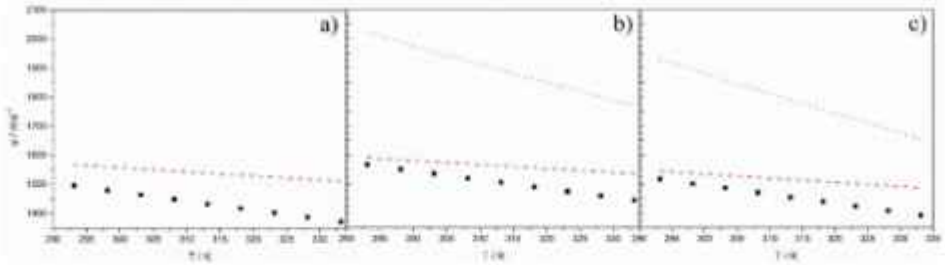

Fig. 8. Experimental values of speed of sound (black squares) for DES in the molar ratio 1:8 a) TBAB:MAE, b) TEAC:MAE, c) TBAC:MAE along with predicted ones: red dashed line – critical properties based method by Pepniendia et al.; blue dotted line – AC based method by Haghbakhsh et al.. (For interpretation of the references to colour in this figure legend, the reader is referred to the web version of this article.)

As can be seen, the speed of sound decreases with increasing temperature. This is because sound waves travel slower in less-dense materials. Moreover, as with the density and refractive index, a linear relationship between the speed of sound and temperature is observed. Similar results were obtained by Omar and Sadeghi for deep eutectic solvents based on choline chloride [53].

At a given temperature and molar ratio of salt to 2-(methylamino)ethanol, the speed of sound changes in the order: TEAC:MAE > TBAC:MAE > TBAB:MAE, which is opposite with the order of refractive index. Thus, it can be concluded that the speed of sound of MAE-based DESs also depends mainly on the molecular weight of solvent, but unlike the refractive index it increases with its value.

Besides, the speed of sound of the DESs studied, similarly to other physical properties, also is related to the molar ratio of HBA to HBD. From Table S7 and Fig. 8 clearly is seen that for all deep eutectic solvents speed of sound decreases with increasing of molar ratio of MAE.

3.4. Predicted values of physical properties of DESs

3.4.1. Density

For the DESs investigated in this study, the critical properties obtained with the Modified Lydersen-Joback-Reid [27] method connected with the Lee-Kesler-mixing equations by Knapp *et al.* [28] are presented in Table 6.

Table 7 shows the obtained values of absolute average relative deviations (%AARD) between the experimental and predicted densities of the studied novel DESs based on 2-(methylamino)ethanol. The results for all seven methods, described in the paragraph 2, are also presented in Fig. 5, which shows the experimental and modeled densities for DESs with the molar ratio 1:8. For solvents with the molar ratio of HBA to HBD equal to 1:6 and 1:10 similar relationships between the experimental and predicted values were obtained.

Results presented in Fig. 5 reveal that the density values obtained by the models proposed by Haghbakhsh *et al.* [12,29] (from both based on AC and critical properties) and Hou *et al.* [30] are overestimated, while for the remaining models are underestimated. Moreover, our calculations indicate that all models, except those proposed by Haghbakhsh *et al.*, were able to capture the density variation correctly with increasing HBA:HBD molar ratio.

The methods based on the Rackett equation by Spencer and Danner [25] or by Mjalli [26] and MCI based model have low % AARD values between 0.87 % – 1.2 %, 1.1 % – 2.5 % and 0.004 % – 0.10 %, respectively. Thus, these methods are characterized by a good prediction ability of the DESs studied so might be accepted and recommended for such purpose. However, it should be remembered that all of them require knowledge of the experimental reference density data and the critical properties of DESs, which is a huge disadvantage. The BGI [30] based model and the method based on GC proposed by Haghbakhsh *et al.* [12] allow to obtain values of %AARD equal to 1.2 % – 2.0 % and 0.68 % – 3.2 %, respectively. Therefore, both models have good predicting ability, similar to the methods discussed above, but do not require any experimental data. The highest AARD% values are for the method based on critical properties and AC based model proposed by Haghbakhsh *et al.* (8.0 % – 13 % and 11 % – 46 %, respectively).

Summarizing the obtained AARD% results for all density prediction methods, it can be concluded that in the case of novel DESs based on MAE, if we do not have any experimental data, the best methods are the BGI model and the GC model proposed by Haghbakhsh *et al.* However, if we know the density value at one temperature at least, the best density values at other temperatures might be estimated using the MCI-based method.

Table 7
Absolute average relative deviations (%AARD) for each model used for prediction of density values for DESs studied in this work.

DES	%AARD[1]	%AARD[2]	%AARD[3]	%AARD[4]	%AARD[5]	%AARD[6]	%AARD[7]
DES1	0.87	2.2	8.0	1.3	0.013	3.1	11
DES2	0.90	2.2	9.1	1.5	0.004	2.1	22
DES3	0.91	1.9	9.8	1.6	0.014	0.94	31
DES4	1.2	2.5	9.7	1.8	0.005	3.2	24
DES5	1.1	2.5	10	1.9	0.024	2.9	35
DES6	0.94	1.1	11	2.0	0.059	1.8	46
DES7	0.93	2.3	13	1.2	0.050	1.4	19
DES8	0.95	2.3	13	1.2	0.088	1.5	29
DES9	0.95	2.3	13	1.4	0.10	0.68	40

1- method based on Rackett equation by Spencer and Danner, 2- method based on Rackett equation by Mjalli, 3- method based on critical properties by Haghbakhsh *et al.*, 4-BGI based method, 5- MCI based method, 6-GC based method by Haghbakhsh *et al.*, 7- AC based method by Haghbakhsh *et al.*

3.4.2. Viscosity

Parameters *A* and *B* of the model for prediction of the viscosity proposed by Bakhtyari *et al.* [33] were calculated using the critical properties given in Table 6, and their values are presented in Table 8.

Table 9 shows the obtained values of relative deviations (%RD) and absolute average relative deviations (%AARD) in temperature range 298.15–333.15 K. As it is presented, depending on DES, % AARD varies from 5.4 % to 16 %, which is close to the global % AARD value (10.1 %) provided by the authors of this method [33]. Regardless of the temperature and composition of solvent, the predicted values were overestimated compared to the experimental ones, and the %RD increased with increasing temperature (see Fig. 6). This observation suggests that this method has better viscosity predictive ability at temperatures close to the reference temperature. The relationship between the molar ratio of HBA to HBD and the viscosity of DESs was correctly modeled by the method. However, since the calculated values of % AARD exceed the viscosity measurement uncertainties found in practice, the model developed by Bakhtyari *et al.* does not appear to be suitable for an accurate estimation of MAE-based DESs viscosity. On the other side, as the predicted values maintain the viscosity order for TBAB:MAE, TEAC:MAE and TBAC:MAE, they can be used to select an appropriate DES from among the studied solvents for a specific application.

Table 8
Calculated values of *A* and *B* parameters of DESs studied in this work.

DES	A	B
DES1	−0.14990	−980.91
DES2	−0.14858	−974.92
DES3	−0.14858	−974.92
DES4	−0.14890	−940.94
DES5	−0.14637	−941.12
DES6	−0.14601	−941.27
DES7	−0.15004	−977.33
DES8	−0.14874	−968.79
DES9	−0.14796	−961.76

3.4.3. Refractive index

Table 10 shows the absolute average relative deviations (% AARD) for the calculated refractive indices in the temperature range 298.15–333.15 K. The results are also presented in Fig. 5 including both the experimental and the predicted refractive indices for MAE-based DESs with the molar ratio 1:8. As can be seen, the predicted values calculated using the models proposed by Taherzadeh *et al.* [35] and Haghbakhsh *et al.* [12] are higher than the experimental values, while for other models they are lower. Moreover, our calculations showed that the models proposed by Shahbaz *et al.* [13] and Taherzadeh *et al.* [35] were able to predict a decrease of refractive index with an increase in the molar ratio of HBA to HBD, while others have not captured this relationship.

The best %AARD values (0.10 % – 0.29 %) were obtained using the model introduced by Shahbaz *et al.*. The major drawback of this method is that experimental density data is required to predict the refractive index.

The methods proposed by Taherzadeh *et al.* [35] and Khajeh *et al.* [18] are characterized by similar %AARD values (0.32 % – 0.81 % and 0.11 % – 0.87 % respectively), and the advantage of these models is that they do not require the use any of any experimental data, because they are based solely on critical properties or group contribution. However, as written above, the method proposed by Khajeh *et al.* could not be used for alkanolamine-based DESs that contain TBAB.

The GC and AC models proposed by Haghbakhsh *et al.* [12] have the highest %AARD values (2.8 % – 4.7 % and 1.3 % – 2.2 %, respectively), and therefore they are characterized by the worst refractive index prediction ability.

In summary, the most preferred model for prediction of refractive indices for novel MAE-based DESs is that introduced by Shahbaz *et al.*, but in the absence of experimental data on density, the method proposed by Taherzadeh *et al.* should be recommended.

Table 9
Relative deviations (%RD) and absolute average relative deviation (%AARD) for model by Bakhtyari *et al.* for prediction of viscosity values for DESs studied in this work.

T / K	DES1	DES2	DES3	DES4	DES5	DES6	DES7	DES8	DES9
	%RD								
298.15	5.2	5.2	2.9	2.9	2.5	2.1	0.33	9.6	5.3
303.15	8.1	8.1	5.3	4.7	4.1	2.2	1.6	12	7.8
308.15	11	11	8.5	7.4	5.8	5.6	0.89	17	9.2
313.15	13	13	11	11	7.7	2.2	0.86	19	8.3
318.15	15	15	13	14	7.1	4.4	3.0	21	11
323.15	18	18	15	17	6.4	5.3	8.2	22	15
328.15	20	20	17	19	11	12	12	18	19
333.15	22	22	18	23	12	13	16	10	24
%AARD	14	11	12	11	5.9	5.4	16	12	6.0

Table 10
The %AARD of each model used for prediction of refractive index values for DESs studied in this work.

DES	%AARD[1]	%AARD[2]	%AARD[3]	%AARD[4]	%AARD[5]
DES1	0.29	0.32	–	3.2	1.3
DES2	0.25	0.33	–	4.0	1.6
DES3	0.22	0.67	–	4.7	1.8
DES4	0.18	0.48	0.49	3.4	1.8
DES5	0.12	0.69	0.24	4.1	2.0
DES6	0.13	0.81	0.11	4.7	2.2
DES7	0.16	0.42	0.87	2.8	1.6
DES8	0.10	0.64	0.61	3.6	1.9
DES9	0.13	0.75	0.48	4.2	2.0

1–method based on molar refraction by Shahbaz et al., 2– method based on critical properties by Taherzadeh et al., 3– GC based method by Khajeh et al., 4– AC based method by Haghbakhsh et al., 5– GC based method by Haghbakhsh et al.

Table 11
The %AARD of each model used for prediction of speed of sound values for novel DESs studied in this work.

DES	%AARD[1]	%AARD[2a]
DES1	6.8	–
DES2	7.4	–
DES3	8.2	–
DES4	2.2	23
DES5	3.9	26
DES6	5.2	29
DES7	2.2	20
DES8	4.2	23
DES9	5.4	25

1-method based on critical properties by Peyrovedin et al.,
2-AC based method by Haghbakhsh et al.

3.4.4. Speed of sound

Fig. 8 presents the correlation between the obtained experimental data and predicted speed of sound values for novel MAE-based DESs at a molar ratio 1:8. Similar relationships between the experimental and predicted values were obtained for these DESs with a molar ratio of HBA to HBD of 1:6 and 1:10. In Table 11, the absolute average relative deviations (%AARD) for calculated speed of sound of all mixtures in the temperature range 298.15–333.15 K are collected. Our calculations show that both models tends to overestimate the speed of sound for all DESs studied. Moreover, the method based on the critical properties and the method based on atomic contribution captured the negative variation of the speed of sound values with temperature, but both failed to predict negative variability of u and MAE content. The %AARD of the first model ranges from 2.2 % to 8.2 %, while for the second model it is in the range of 20 % – 29 %. Thus, both models have a high %AARD, although the model introduced by Peyrovedin *et al.* [16] is much better than the model proposed by Haghbakhsh *et al.* [12].

4. Conclusions

In this work, experimental density, viscosity, refractive index and sound velocity for deep eutectic solvents based on 2-(methylamino)ethanol have been reported as a function of temperature at atmospheric pressure. Hydrogens bond acceptors in the studied DESs were tetrabutylammonium bromide, tetraethylammonium chloride and tetrabutylammonium chloride mixed with MAE in different molar ratios of 1:6, 1:8 and 1:10.

Spectroscopy measurements confirmed the hydrogen bonds interactions between components while thermal properties such as melting points and thermal stability of deep eutectic solvents are directly influenced by cation alkyl chain length in the salt. The results showed that for density, refractive index and speed of sound a linear negative correlation with temperature was obtained, while for viscosity the decrease with temperature was exponential.

The density of MAE-based DESs decreased with increasing chain length of HBD or HBA, but this effect was less than the effect of the anion weight. When the amount of alkanolamine in TBAB:MAE (DES 1–3) and TEAC:MAE (DES 4–6) increased, the density decreased. For TBAC:MAE (DES 7–9), due to the similar density of DES and neat MAE, no significant changes in density were observed as a result of changing the solvent composition.

The lowest viscosity values for the studied systems were observed for TEAC-based DESs (DES 4-6), which are smaller in size and where weaker hydrogen bonding is expected. Thus, in contrast to density, the alkyl chain length of the MAE-based DESs salts has a greater influence on the viscosity than the anion effect. Moreover, regardless of the salt, the viscosity decreased as the molar ratio of HBA to HBD increased.

The refractive indices of the studied DESs varied according to: TBAB:MAE < TBAC:MAE < TEAC: MAE and decreased with the decrease in salt content in the mixture. Thus, the main factor determining the refractive index of MAE-based DESs is their molecular weight. The speed of sound of TBAB:MAE, TEAC:MAE and TBAC: MAE also depends mainly on the molecular weight of the mixture, but unlike the refractive index it increases with its value. This is clearly seen both in the order of the speed of sound for DESs with different salts and for DESs with the same salts but a different molar ratio of HBA to HBD.

Moreover, models available in the literature were used and evaluated for prediction of the physicochemical properties of studied DESs. The results obtained in this work indicate that for deep eutectic solvents based on 2-(methylamino)ethanol, in the absence of any experimental data, the best models for density prediction are the bonding group interaction contribution method and the group contribution model. For modelling of refractive index, a method based on critical properties should be used. However, for viscosity or speed of sound, the methods using critical properties do not seem suitable for an accurate estimation of these properties for MAE-based DESs. The same effect, i.e. a higher % AARD value than the measurement uncertainties found in practice, was obtained for the atomic contribution method predicting the speed of sound of the DESs studied. Thus, the results indicate that new models that will be able to predict viscosity and speed of sound of alkanolamine-based DESs with lower %AARD are worth for searching.

Funding

This research did not receive any specific grant from funding agencies in the public, commercial, or not-for-profit sectors.

CRediT authorship contribution statement

Bartosz Nowosielski: Conceptualization, Methodology, Formal analysis, Investigation, Writing – original draft, Visualization, Writing – review & editing. **Marzena Jamróg-iewicz:** Investigation, Writing - review & editing. **Justyna Łuczak:** Writing – review & editing. **Agnieszka Tercjak:** Investigation. **Dorota Warmińska:** Conceptualization, Supervision, Writing – original draft, Writing - review & editing.

Data availability

Data will be made available on request.

Declaration of Competing Interest

The authors declare that they have no known competing financial interests or personal relationships that could have appeared to influence the work reported in this paper.

Appendix A. Supplementary material

Supplementary data to this article can be found online at https://doi.org/10.1016/j.molliq.2022.121089.

References

[1] K. Jafari, M.H. Fatemi, P. Estellé, Deep eutectic solvents (DESs): A short overview of the thermophysical properties and current use as base fluid for heat transfer nanofluids, J. Mol. Liq. 321 (2021) 114752.

[2] B.B. Hansen, S. Spittle, B. Chen, D. Poe, Y. Zhang, J.M. Klein, A. Horton, L. Adhikari, T. Zelovich, B.W. Doherty, B. Gurkan, E.J. Maginn, A. Ragauskas, M. Dadmun, T.A. Zawodzinski, G.A. Baker, M.E. Tuckerman, R.F. Savinell, J.R. Sangoro, Deep Eutectic Solvents: A Review of Fundamentals and Applications, Chem. Rev. 121 (3) (2021) 1232–1285.

[3] I. Wazeer, M. Hayyan, M.K. Hadj-Kali, Deep eutectic solvents: designer fluids for chemical processes, J. Chem. Technol. Biotechnol. 93 (4) (2018) 945–958, https://doi.org/10.1002/jctb.5491.

[4] Y. Marcus (Ed.), Deep Eutectic Solvents, Springer International Publishing, Cham, 2019.

[5] E. Gómez, P. Cojocaru, L. Magagnin, E. Valles, Electrodeposition of Co, Sm and SmCo from a Deep Eutectic Solvent, J. Electroanal. Chem. 658 (1–2) (2011) 18–24, https://doi.org/10.1016/j.jelechem.2011.04.015.

[6] Q. Zhang, K. De Oliveira Vigier, S. Royer, F. Jérôme, Deep eutectic solvents: Syntheses, properties and applications, Chem. Soc. Rev. 41 (21) (2012) 7108–7146, https://doi.org/10.1039/c2cs35178a.

[7] M. Pätzold, S. Siebenhaller, S. Kara, A. Liese, C. Syldatk, D. Holtmann, Deep Eutectic Solvents as Efficient Solvents in Biocatalysis, Trends Biotechnol. 37 (9) (2019) 943–959, https://doi.org/10.1016/j.tibtech.2019.03.007.

[8] F.S. Oliveira, A.B. Pereiro, L.P.N. Rebelo, I.M. Marrucho, Deep eutectic solvents as extraction media for azeotropic mixtures, Green Chem. 15 (5) (2013) 1326–1330, https://doi.org/10.1039/c3gc37030a.

[9] S. Sarmad, J.P. Mikkola, X. Ji, Carbon Dioxide Capture with Ionic Liquids and Deep Eutectic Solvents: A New Generation of Sorbents, ChemSusChem 10 (2) (2017) 324–352, https://doi.org/10.1002/cssc.201600987.

[10] M. Mokhtarpour, H. Shekaari, M.T. Zafarani-Moattar, S. Golgoun, Solubility and solvation behavior of some drugs in choline based deep eutectic solvents at different temperatures, J. Mol. Liq. 297 (2020) 111799.

[11] M. Zhang, X. Zhang, Y. Liu, K. Wu, Y. Zhu, H. Lu, B. Liang, Insights into the relationships between physicochemical properties, solvent performance, and applications of deep eutectic solvents, Environ. Sci. Pollut. Res. 28 (27) (2021) 35537–35563.

[12] R. Haghbakhsh, S. Raeissi, A.R.C. Duarte, Group contribution and atomic contribution models for the prediction of various physical properties of deep eutectic solvents, Sci. Rep. 11 (1) (2021) pp, https://doi.org/10.1038/s41598-021-85824-z.

[13] K. Shahbaz, F.S.G. Bagh, F.S. Mjalli, I.M. AlNashef, M.A. Hashim, Prediction of refractive index and density of deep eutectic solvents using atomic contributions, Fluid Phase Equilib. 354 (Sep. 2013) 304–311, https://doi.org/10.1016/j.fluid.2013.06.050.

[14] K. Shahbaz, F.S. Mjalli, M.A. Hashim, I.M. Alnashef, Prediction of deep eutectic solvents densities at different temperatures, Thermochim. Acta 515 (1–2) (2011) 67–72, https://doi.org/10.1016/j.tca.2010.12.022.

[15] N.R. Mirza, N.J. Nicholas, Y. Wu, S. Kentish, G.W. Stevens, Estimation of Normal Boiling Temperatures, Critical Properties, and Acentric Factors of Deep Eutectic Solvents, J. Chem. Eng. Data 60 (6) (2015) 1844–1854, https://doi.org/10.1021/acs.jced.5b00046.

[16] H. Peyrovedin, R. Haghbakhsh, A.R.C. Duarte, S. Raeissi, A Global Model for the Estimation of Speeds of Sound in Deep Eutectic Solvents, Molecules 25 (7) (Apr. 2020) 1626, https://doi.org/10.3390/molecules25071626.

[17] K. Shahbaz, S. Baroutian, F.S. Mjalli, M.A. Hashim, I.M. Alnashef, Densities of ammonium and phosphonium based deep eutectic solvents: Prediction using artificial intelligence and group contribution techniques, Thermochim. Acta 527 (2012) 59–66, https://doi.org/10.1016/j.tca.2011.10.010.

[18] A. Khajeh, K. Parvaneh, M. Shakourian-Fard, Refractive index prediction of deep eutectic solvents by molecular approaches, J. Mol. Liq. 332 (Jun. 2021), https://doi.org/10.1016/j.molliq.2021.115843.

[19] Z. Li, L. Wang, C. Li, Y. Cui, S. Li, G. Yang, Y. Shen, Absorption of Carbon Dioxide Using Ethanolamine-Based Deep Eutectic Solvents, ACS Sustain. Chem. Eng. 7 (12) (2019) 10403–10414.

[20] F.S. Mjalli, G. Murshid, S. Al-Zakwani, A. Hayyan, Monoethanolamine-based deep eutectic solvents, their synthesis and characterization, Fluid Phase Equilib. 448 (2017) 30–40, https://doi.org/10.1016/j.fluid.2017.03.008.

[21] G. Murshid, F.S. Mjalli, J. Naser, S. Al-Zakwani, A. Hayyan, Novel diethanolamine based deep eutectic mixtures for carbon dioxide (CO 2) capture: synthesis and characterisation, Phys. Chem. Liq. 57 (4) (2019) 473–490, https://doi.org/10.1080/00319104.2018.1491043.

[22] I. Adeyemi, M.R.M. Abu-Zahra, I.M. AlNashef, Physicochemical properties of alkanolamine-choline chloride deep eutectic solvents: Measurements, group contribution and artificial intelligence prediction techniques, J. Mol. Liq. 256 (2018) 581–590, https://doi.org/10.1016/j.molliq.2018.02.085.

[23] B. Nowosielski, M. Jamrógiewicz, J. Łuczak, M. Śmiechowski, D. Warmińska, Experimental and predicted physicochemical properties of monopropanolamine-based deep eutectic solvents, J. Mol. Liq. 309 (2020) 113110.

[24] H.G. Rackett, Equation of State for Saturated Liquids, J. Chem. Eng. Data 15 (4) (1970) 514–517, https://doi.org/10.1021/je60047a012.

[25] C.F. Spencer, R.P. Danner, Improved Equation for Prediction of Saturated Liquid Density, J. Chem. Eng. Data 17 (2) (1972) 236–241, https://doi.org/10.1021/je60053a012.

[26] F.S. Mjalli, K. Shahbaz, I.M. AlNashef, Modified Rackett equation for modelling the molar volume of deep eutectic solvents, Thermochim. Acta 614 (Aug. 2015) 185–190, https://doi.org/10.1016/j.tca.2015.06.020.

[27] V.H. Alvarez, J.O. Valderrama, A modified Lydersen-Joback-Reid method to estimate the critical properties of biomolecules, Alimentaria 254 (2004) 55–60.

[28] H. Knapp, R. Doring, L. Oellrich, U. Plocker, and J.M. Prausnitz, "Vapor-Liquid Equilibria for Mixtures of Low Boiling Substances, Chemistry Data Series, vol. VI," VI (DECHEMA, Frankfurt, Ger. 1982), 1982.

[29] R. Haghbakhsh, K. Bardool, A. Bakhtyari, A.R.C. Duarte, S. Raeissi, Simple and global correlation for the densities of deep eutectic solvents, J. Mol. Liq. 296 (Dec. 2019), https://doi.org/10.1016/j.molliq.2019.111830.

[30] X.-J. Hou, L.-Y. Yu, Y.-X. Wang, K.-J. Wu, C.-H. He, Comprehensive Prediction of Densities for Deep Eutectic Solvents: A New Bonding-Group Interaction Contribution Scheme, Ind. Eng. Chem. Res. 60 (35) (Sep. 2021) 13127–13139, https://doi.org/10.1021/acs.iecr.1c02260.

[31] F.S. Mjalli, Mass connectivity index-based density prediction of deep eutectic solvents, Fluid Phase Equilib. 409 (2016) 312–317, https://doi.org/10.1016/j.fluid.2015.09.053.

[32] J.O. Valderrama, R.E. Rojas, Mass connectivity index, a new molecular parameter for the estimation of ionic liquid properties, Fluid Phase Equilib. 297 (1) (2010) 107–112, https://doi.org/10.1016/j.fluid.2010.06.015.

[33] A. Bakhtyari, R. Haghbakhsh, A.R.C. Duarte, S. Raeissi, A simple model for the viscosities of deep eutectic solvents, Fluid Phase Equilib. 521 (Oct. 2020), https://doi.org/10.1016/j.fluid.2020.112662.

[34] S.A. Wildman, G.M. Crippen, Prediction of Physicochemical Parameters by Atomic Contributions, J. Chem. Inf. Comput. Sci. 39 (5) (Sep. 1999) 868–873, https://doi.org/10.1021/ci990307l.

[35] M. Taherzadeh, R. Haghbakhsh, A.R.C. Duarte, S. Raeissi, Generalized Model to Estimate the Refractive Indices of Deep Eutectic Solvents, J. Chem. Eng. Data 65 (8) (2020) 3965–3976, https://doi.org/10.1021/acs.jced.0c00308.

[36] I. Zahrina, K. Mulia, A. Yanuar, M. Nasikin, Molecular interactions in the betaine monohydrate-polyol deep eutectic solvents: Experimental and computational studies, J. Mol. Struct. 1158 (2018) 133–138, https://doi.org/10.1016/j.molstruc.2017.11.094.

[37] H. Ghaedi, M. Ayoub, S. Sufian, B. Lal, Y. Uemura, Thermal stability and FT-IR analysis of Phosphonium-based deep eutectic solvents with different hydrogen bond donors, J. Mol. Liq. 242 (2017) 395–403, https://doi.org/10.1016/j.molliq.2017.07.016.

[38] E.L. Smith, A.P. Abbott, K.S. Ryder, Deep Eutectic Solvents (DESs) and Their Applications, Chem. Rev. 114 (21) (2014) 11060–11082, https://doi.org/10.1021/cr300162p.

[39] C. Florindo, F.S. Oliveira, L.P.N. Rebelo, A.M. Fernandes, I.M. Marrucho, Insights into the synthesis and properties of deep eutectic solvents based on cholinium chloride and carboxylic acids, ACS Sustain. Chem. Eng. 2 (10) (2014) 2416–2425, https://doi.org/10.1021/sc500439w.

[40] Y. Wang, Y. Hou, W. Wu, D. Liu, Y. Ji, S. Ren, Roles of a hydrogen bond donor and a hydrogen bond acceptor in the extraction of toluene from N -heptane using deep eutectic solvents, Green Chem. 18 (10) (2016) 3089–3097, https://doi.org/10.1039/c5gc02909j.

[41] H. Ghaedi, M. Ayoub, S. Sufian, B. Lal, A.M. Shariff, Measurement and correlation of physicochemical properties of phosphonium-based deep eutectic solvents at several temperatures (293.15 K–343.15 K) for CO2 capture, J. Chem. Thermodyn. 113 (2017) 41–51, https://doi.org/10.1016/j.jct.2017.05.020.

[42] A.P. Abbott, R.C. Harris, K.S. Ryder, C. D'Agostino, L.F. Gladden, M.D. Mantle, Glycerol eutectics as sustainable solvent systems, Green Chem. 13 (1) (2011) 82–90, https://doi.org/10.1039/c0gc00395f.

[43] S. Sarmad, Y. Xie, J.P. Mikkola, X. Ji, Screening of deep eutectic solvents (DESs) as green CO2 sorbents: from solubility to viscosity, New J. Chem. 41 (1) (2016) 290–301, https://doi.org/10.1039/c6nj03140d.

[44] R. Saputra, R. Walvekar, M. Khalid, N.M. Mubarak, Synthesis and thermophysical properties of ethylammonium chloride-glycerol-ZnCl2 ternary deep eutectic solvent, J. Mol. Liq. 310 (Jul. 2020), https://doi.org/10.1016/j.molliq.2020.113232.

[45] N. Rodriguez Rodriguez, L. Machiels, K. Binnemans, p-Toluenesulfonic Acid-Based Deep-Eutectic Solvents for Solubilizing Metal Oxides, ACS Sustainable Chem. Eng. 7 (4) (2019) 3940–3948.

[46] A.P. Abbott, G. Capper, S. Gray, Design of Improved Deep Eutectic Solvents Using Hole Theory, ChemPhysChem 7 (4) (Apr. 2006) 803–806, https://doi.org/10.1002/cphc.200500489.

[47] T. El Achkar, H. Greige-Gerges, S. Fourmentin, Basics and properties of deep eutectic solvents: a review, Environ. Chem. Lett. 19 (4) (2021) 3397–3408, https://doi.org/10.1007/s10311-021-01225-8.

[48] A.P. Abbott, R.C. Harris, K.S. Ryder, Application of hole theory to define ionic liquids by their transport properties, J. Phys. Chem. B 111 (18) (2007) 4910–4913, https://doi.org/10.1021/jp0671998.

[49] M. Francisco, A. van den Bruinhorst, M.C. Kroon, Low-Transition-Temperature Mixtures (LTTMs): A New Generation of Designer Solvents, Angew. Chemie Int. Ed. 52 (11) (Mar. 2013) 3074–3085, https://doi.org/10.1002/anie.201207548.

[50] A. Hayyan, F.S. Mjalli, I.M. Alnashef, Y.M. Al-Wahaibi, T. Al-Wahaibi, M.A. Hashim, Glucose-based deep eutectic solvents: Physical properties, J. Mol. Liq. 178 (2013) 137–141, https://doi.org/10.1016/j.molliq.2012.11.025.

[51] S.P. Ijardar, V. Singh, R.L. Gardas, Revisiting the Physicochemical Properties and Applications of Deep Eutectic Solvents, Molecules 27 (4) (Feb. 2022) 1368, https://doi.org/10.3390/molecules27041368.

[52] S. Seki, S. Tsuzuki, K. Hayamizu, Y. Umebayashi, N. Serizawa, K. Takei, H. Miyashiro, Comprehensive refractive index property for room-temperature ionic liquids, J. Chem. Eng. Data 57 (8) (2012) 2211–2216.

[53] K.A. Omar, R. Sadeghi, Novel Thymol-based deep eutectic solvents: Thermophysical properties and their applications in Liquid-Liquid extraction and amino acid detection, J. Mol. Liq. 336 (2021) 116359.

Effect of temperature and composition on physical properties of deep eutectic solvents based on 2-(methylamino)ethanol – measurement and prediction

Bartosz Nowosielski[a], Marzena Jamróglewicz[b], Justyna Łuczak[c, d], Agnieszka Tercjak[e], Dorota Warmińska[a, *]

[a] Department of Physical Chemistry, Faculty of Chemistry, Gdańsk University of Technology, ul. Narutowicza 11/12, 80-233 Gdańsk, POLAND

[b] Department of Physical Chemistry, Faculty of Pharmacy, Medical University of Gdańsk, Al. Gen. Hallera 107, 80-416 Gdańsk, POLAND

[c] Department of Process Engineering and Chemical Technology, Faculty of Chemistry, Gdańsk University of Technology, ul. Narutowicza 11/12, 80-233 Gdańsk, POLAND

[d] Advanced Materials Center, Gdańsk University of Technology, ul. Narutowicza 11/12, 80–233 Gdańsk, POLAND[c] Department of Physical Chemistry, Faculty of Pharmacy, Medical University of Gdańsk, Al. Gen. Hallera 107, 80-416 Gdańsk, POLAND

[e] Group 'Materials + Technologies' (GMT), Department of Chemical and Environmental Engineering, Faculty of Engineering, University of the Basque Country (UPV/EHU), Pza Europa 1, 20018 Donostia-San Sebastian, Spain

*Corresponding author: Tel.:+48583471410; fax:+48583472694,
e-mail address: dorwarmi@ pg.edu.pl

Table S1 Parameters of model proposed by Haghbakhsh *et. al.* [1].

parameter	values
A_1	-0.00000113
A_2	0.002566
A_3	0.2376
A_4	-0.000467
B	-0.000464

Table S2 Parameters of model proposed by Hou *et.al.* [2].

parameter	values
A1	3.8043
A2	1.0601
B1	0.000382
B2	-0.000672
G_{SI}	0.0000342

Table S3 Parameters of model proposed by Taherzadeh *et al.* [3].

parameters	values
A_2	0.0517
A_2	-11.625
A_3	0.00227
A_4	1.3668
B	25.89

Table S4 Experimental density, d, of deep eutectic solvents within temperature range T = (293.15 to 333.15) K and P = 0.100 MPa[a].

T / K	DES1	DES2	DES3	DES4	DES5	DES6	DES7	DES8	DES9
				d / (kg·m^{-3})					
293.15	986.1	978.0	973.3	958.9	956.0	953.8	939.6	940.3	940.0
298.15	982.4	974.4	969.6	955.5	952.4	950.2	936.2	936.8	936.4
303.15	978.8	970.7	965.9	952.0	948.9	946.7	932.8	933.3	932.9
308.15	975.2	967.0	962.2	948.5	945.3	943.1	929.3	929.9	929.3
313.15	971.5	963.3	958.5	945.0	941.8	939.5	925.9	926.4	925.7
318.15	967.8	959.6	954.8	941.5	938.2	935.9	922.5	922.9	922.2
323.15	964.3	955.9	951.1	938.1	934.7	932.3	919.1	919.4	918.6
328.15	960.7	952.2	947.5	934.6	931.1	928.7	915.6	915.9	915.0
333.15	957.1	948.5	943.6	931.1	927.6	923.0	912.2	912.4	911.4

[a] Standard uncertainties u are $u(T)$ = 0.01 K, $u(p)$ = 0.001 MPa, $u(d)$ = 0.1 kg·m^{-3}

Table S5 Experimental viscosities, η, of deep eutectic solvents within temperature range T = (293.15 to 333.15) K and P = 0.100 MPa[a].

T / K	DES1	DES2	DES3	DES4	DES5	DES6	DES7	DES8	DES9
				η / (mPa·s)					
293.15	45.27	35.51	32.55	23.70	21.89	20.50	47.35	34.37	29.49
298.15	34.12	27.57	25.32	18.78	17.43	16.74	34.27	26.15	22.94
303.15	26.71	21.82	20.21	15.20	14.33	13.53	27.02	20.75	18.46
308.15	21.15	17.38	16.21	12.45	11.55	11.36	21.09	16.84	15.12
313.15	17.14	14.13	13.09	10.28	10.05	9.57	17.15	14.13	12.73
318.15	14.07	11.59	10.63	8.78	8.35	7.92	14.07	11.56	11.44
323.15	11.64	9.64	8.82	7.56	7.10	6.50	11.78	9.50	8.93
328.15	9.73	8.16	7.42	6.23	5.78	5.45	10.35	7.84	7.38
333.15	8.17	6.95	6.21	5.41	4.95	4.57	9.58	6.50	6.48

[a] Standard uncertainties u are $u(T)$ = 0.01 K, $u(p)$ = 0.001 MPa, $u(\eta)$ = 2%

Table S6 Experimental refractive indices, n_D of deep eutectic solvents within temperature range T = (293.15 to 333.15) K and P = 0.100 MPa[a].

T / K	DES1	DES2	DES3	DES4	DES5	DES6	DES7	DES8	DES9
				n_D					
293.15	1.4618	1.4583	1.4560	1.4560	1.4531	1.4510	1.4571	1.4541	1.4520
298.15	1.4602	1.4563	1.4541	1.4542	1.4511	1.4489	1.4551	1.4525	1.4504
303.15	1.4587	1.4547	1.4524	1.4526	1.4492	1.4472	1.4536	1.4505	1.4482
308.15	1.4570	1.4529	1.4504	1.4509	1.4475	1.4454	1.4519	1.4486	1.4466
313.15	1.4552	1.4511	1.4487	1.4490	1.4453	1.4437	1.4502	1.4467	1.4449
318.15	1.4537	1.4495	1.4469	1.4474	1.4438	1.4418	1.4486	1.4446	1.443
323.15	1.4519	1.4479	1.4450	1.4455	1.442	1.4399	1.4469	1.4427	1.4411
328.15	1.4505	1.4463	1.4434	1.4439	1.4397	1.4382	1.4452	1.4411	1.4392
333.15	1.4491	1.4447	1.4417	1.4424	1.4381	1.4366	1.4439	1.4393	1.4377

[a] Standard uncertainties u are $u(T)$ 0.1 K, $u(p)$ 0.001 MPa, $u(n_D)$ 0.0002

Table S7 Experimental speed of sound values, u, for DESs within temperature range T (293.15 to 333.15) K and P = 0.100 MPa[a].

T / K	DES1	DES2	DES3	DES4	DES5	DES6	DES7	DES8	DES9
				u / m·s^{-1}					
293.15	1497.5	1495.2	1494.1	1581.2	1565.5	1553.4	1521.4	1516.6	1513.3
298.15	1482.0	1479.7	1478.5	1565.6	1550.1	1538.0	1505.8	1501.0	1497.6
303.15	1466.6	1464.1	1462.9	1550.1	1534.8	1522.5	1490.2	1485.3	1482.0
308.15	1451.3	1448.7	1447.5	1534.7	1519.5	1507.1	1474.7	1469.8	1466.3
313.15	1435.8	1433.1	1431.9	1519.3	1504.6	1491.9	1459.1	1454.2	1450.5
318.15	1420.7	1417.8	1416.5	1504.3	1489.4	1476.9	1443.8	1438.9	1435.0
323.15	1405.5	1402.6	1401.2	1489.1	1474.1	1461.5	1428.6	1423.6	1419.5
328.15	1390.5	1387.3	1385.9	1473.8	1458.8	1446.3	1413.5	1408.3	1404.1
333.15	1375.4	1372.2	1370.6	1458.7	1444.6	1431.0	1398.5	1393.1	1388.5

[a] Standard uncertainties u are $u(T)$ =0.01 K, $u(p)$= 0.001 MPa, $u(u)$ = 0.5 m·s^{-1}

[1] R. Haghbakhsh, R. Bardool, A. Bakhtyari, A. R. C. Duarte, and S. Raeissi, "Simple and global correlation for the densities of deep eutectic solvents," *J. Mol. Liq.*, vol. 296, p. 111830, Dec. 2019, doi: 10.1016/j.molliq.2019.111830.

[2] X.-J. Hou, L.-Y. Yu, Y.-X. Wang, K.-J. Wu, and C.-H. He, "Comprehensive Prediction of Densities for Deep Eutectic Solvents: A New Bonding-Group Interaction Contribution Scheme," *Ind. Eng. Chem. Res.*, vol. 60, no. 35, pp. 13127–13139, Sep. 2021, doi: 10.1021/acs.iecr.1c02260.

[3] M. Taherzadeh, R. Haghbakhsh, A. R. C. Duarte, and S. Raeissi, "Generalized Model to Estimate the Refractive Indices of Deep Eutectic Solvents," *J. Chem. Eng. Data*, vol. 65, no. 8, pp. 3965–3976, Aug. 2020, doi: 10.1021/acs.jced.0c00308.

Załącznik A4

B. Nowosielski, M. Jamrógiewicz, I. Cichowska-Kopczyńska, D. Warmińska, Comprehensive evaluation of physical properties and carbon dioxide capacities of new 2-(butylamino)ethanol-based deep eutectic solvents, Pure Appl. Chem. 96 (2024) 1733–1749. https://doi.org/10.1515/pac-2024-0228. **IF_{2023}: 1,8, $MNSW_{2023}$: 140**

Research Article

Bartosz Nowosielski*, Marzena Jamrógiewicz, Iwona Cichowska-Kopczyńska and Dorota Warmińska

Comprehensive evaluation of physical properties and carbon dioxide capacities of new 2-(butylamino)ethanol-based deep eutectic solvents

https://doi.org/10.1515/pac-2024-0228

Abstract: The aim of this research was to assess the impact of the components of alkanolamine deep eutectic solvents (DESs) on the physical properties of those DESs and their carbon dioxide capacity. To achieve this goal, novel deep eutectic solvents were synthesized by using 2-(butylamino)ethanol (BAE) as the hydrogen bond donor (HBD), along with tetrabutylammonium bromide TBAB), tetrabutylammonium chloride (TBAC), or tetraethylammonium chloride (TEAC) as the hydrogen bond acceptors (HBA) at various molar ratios (1:6, 1:8, and 1:10). To confirm the presence of hydrogen bond interactions between the components Fourier Transform Infrared Spectroscopy measurements were conducted. Furthermore, thermal properties, including melting points and thermal stability, of these deep eutectic solvents as well as key physical properties, such as density, viscosity, refractive index, and sound velocity, within the temperature range of 293.15–333.15 K and at a pressure of 0.1 MPa were examined. The effect of the molar ratio of HBA to HBD, the type of anion, and the length of the alkyl chain were studied and analysed in regard to physicochemical properties. In this work, the solubility of carbon dioxide in DESs derived from 2-(butylamino)ethanol, 3-aminopropan-1-ol (AP), and 2-(methylamino)ethanol (MAE) was measured. The highest CO_2 capacity was found for TEAC:MAE 1:10 DES characterized by the shortest alkyl chain length in both HBA and HBD molecules, the highest amine content, and the lowest viscosity. Additionally, the effect of water addition on carbon dioxide solubility was explored. The results showed that the influence of water on CO_2 solubility varies with the type of DES. In general, this work highlighted that DESs can serve as effective media for carbon dioxide capture, and their performance can be tailored by changing the type of hydrogen bond acceptor or donor, their molar ratio and by the addition of water.

Keywords: 2-(butylamino)ethanol; alkanolamine-based DES; carbon dioxide capacity; physical properties; tetraalkylammonium salts; thermal stability.

***Corresponding author: Bartosz Nowosielski**, Department of Physical Chemistry, Faculty of Chemistry, Gdańsk University of Technology, ul. Narutowicza 11/12, 80-233 Gdańsk, Poland; and Maritime Advanced Research Centre, Szczecińska 65, 80-392 Gdańsk, Poland, Tel.: +48583471410; fax: +48583472694, e-mail: bartosz.nowosielski@pg.edu.pl, https://orcid.org/0000-0003-0941-5707

Marzena Jamrógiewicz, Department of Physical Chemistry, Faculty of Pharmacy, Medical University of Gdańsk, Al. Gen. Hallera 107, 80-416 Gdańsk, Poland

Iwona Cichowska-Kopczyńska, Department of Process Engineering and Chemical Technology, Faculty of Chemistry, Gdańsk University of Technology, ul. Narutowicza 11/12, 80-233 Gdańsk, Poland

Dorota Warmińska, Department of Physical Chemistry, Faculty of Chemistry, Gdańsk University of Technology, ul. Narutowicza 11/12, 80-233 Gdańsk, Poland

Introduction

In recent years, deep eutectic solvents (DESs) have garnered significant attention as promising environmentally friendly alternatives to traditional industrial solvents. This shift is driven by their potential to reduce environmental pollution and enhance process efficiency. These solvents exhibit excellent properties, similar to those presented by to ionic liquids (ILs), such as very low vapor pressure, non-flammability and effective solvation capabilities for various compounds[1]. Furthermore, DESs offer several advantages over conventional ILs. They are biodegradable, less-toxic, and comparatively cost-effective and easy to prepare[2]. DESs can be readily synthesized with high purity and typically consist of two or three components that can interact through hydrogen bonds and/or electrostatic forces, resulting in the formation of an eutectic mixture[3]. DESs have found applications across various fields, including metallurgy, catalysis, organic synthesis, liquid-liquid extraction, and other separation processes.[4–7] These innovative solvents have also been employed in gas absorption, polymer synthesis, biomass processing, and drug solubilization.[3,8,9]

Recently, there has been a notable emphasis on the physicochemical examination of DESs and their CO_2 capacity, particularly those incorporating amines or alkanolamines are put into extensive examination. These DESs exhibit a considerably greater CO_2 absorption capacity than other solvents.[10] Besides temperature, many factors can influence the carbon dioxide solubility in DESs. One of the most important issues to consider is the type of hydrogen bond donor (HBD) and acceptor (HBA) and their molar ratios.[11] Sarmad et al. performed studies on carbon dioxide solubility in DESs composed of TBAB and ethanolamine.[12] They showed that changing the molar ratio from 1:6 to 1:7 increased the solubility. Pishro et al. studied the effect of the alkyl chain length of amine-based DESs conjugated with monoethanolamine hydrochloride (MEACl) on CO_2 absorption ability.[13] They observed increase in carbon dioxide solubility with an increase in alkyl chain length in HBD molecule. Jo et al. evaluated the effect of amine type on carbon dioxide solubility using DESs composed of potassium prolinate or glycinate as HBA and monoethanolamine (MEA), diethanolamine (DEA), or methyldiethanolamine (MDEA) as HBA.[14] They showed that regardless of HBA used, the solubilities followed the order of amine: primary > secondary > tertiary. Different results were obtained by Park et al.[15] They combined triethylenetetramine hydrochloride (TETACl) with MEA, DEA, or MDEA to form DESs with high CO_2 absorption capacities. The highest carbon dioxide solubilities were observed in tertiary amines while the lowest in primary amines. The best results for MDEA-based DES were explained by the increase in the rate of carbon dioxide solubility constant when tertiary amines are blended with lower-order amine molecules, in this case TETACl, which played role of HBA.

The effect of water content on the solubility of carbon dioxide in DES was investigated only in a few studies and it was established that it depends strongly on compounds of which deep eutectic solvent is formed of. The results for DESs based on choline chloride (ChCl) showed that increasing water content results in decreasing CO_2 solubility.[16,17] However, results obtained for amine-based DESs show other behavior. Trivedi et al. reported that a small addition of water (up to 10 %) in [MEACl]:[EDA] with a 1:3 molar ratio system can improve carbon dioxide solubility, but further increase in the water content results in a reduction of solubility.[18] Anwer et al. studied the effect of water addition on the solubility of CO_2 in ChCl-based DESs combined with amines including MEA, DEA, or MDEA.[19] The results showed that in case of primary and secondary amines, namely MEA- and DEA-based DESs, the addition of 5 wt% water results in drop in carbon dioxide capacity. However, in the case of MDEA-based DESs, an increase in CO_2 solubility was observed. It was associated with the tertiary amine MDEA forming bicarbonate during CO_2 capture. Interestingly, further addition of water to 10 wt% and 15 wt% resulted in higher absorption values in case of MEA and DEA-based DESs compared to pure DESs. In the literature, various potential mechanisms for the impact of water on carbon dioxide solubility have been proposed. Su et al. suggested that the reduction in carbon dioxide solubility with increasing water content could be attributed to a decrease in the concentration of active reactants.[16] Meanwhile, Shukla et al. theorized that water competes with CO_2 for the active sites within deep eutectic solvents, thereby reducing CO_2 absorption.[20] However, in our opinion, the increased solubility of carbon dioxide may result from a weakening of the intermolecular interactions by creating new interactions with DES and hence CO_2 can react with DES more efficiently.

In this study, we have developed a novel series of deep eutectic solvents by incorporating 2-(butylamino) ethanol (BAE) as the hydrogen bond donor and using tetrabutylammonium bromide (TBAB), tetrabutylammonium chloride (TBAC), or tetraethylammonium chloride (TEAC) as the hydrogen bond acceptor. These DESs were characterized through Fourier Transform Infrared spectroscopy (FTIR). The thermal properties of the synthesized DESs were assessed by differential scanning calorimetry (DSC) and thermogravimetric analysis (TGA) techniques. Additionally, various fundamental physicochemical properties, such as density, speed of sound, viscosity, and refractive index, were measured over a wide temperature range (293.15–333.15 K). We conducted a comprehensive analysis to investigate the impact of temperature, the length of the salt chain, and the molar ratio of HBA to HBD. This analysis was then compared with DESs previously studied by our research group, which were based on 3-aminopropan-1-ol (AP) and 2-(methylamino)ethanol (MAE).[21,22] Furthermore, we examined the solubility of carbon dioxide in these DESs using gravimetric method and explored the effects of alkyl chain length, the type of anion, the order of the amine, and the influence of water addition on carbon dioxide solubility.

Materials and methods

Chemicals and DESs preparation

Table 1 presents the information about the chemicals used in this study, and Fig. 1 shows their chemical structures. 2-(butylamino)ethanol, 3-aminopropan-1-ol, 2-(methylamino)ethanol tetrabutylammonium bromide, tetrabutylammonium chloride and tetraethylammonium chloride were purchased from Sigma-Aldrich. Tetrabutylammonium chloride was purified by double crystallization from acetone by adding diethyl ether while the other chemicals were used as received from the producer. All salts were dried under reduced pressure before use, TBAB at 323 K for 48 h, TBAC and TEAC at 298.15 K for several days.

The nine deep eutectic solvents were synthesized through the combination of three distinct tetraalkylammonium salts and 2-(butylamino)ethanol in the molar ratios of 1:6, 1:8 and 1:10 HBA to HBD. The molar ratio of 1:6 was the lowest at which a stable DES could be obtained. Furthermore, for TBAC/BAE, the eutectic composition was in the range of molar ratios 1:6–1:10. Thus in order to investigate the influence of molar ratio on the physical properties of the DESs, all liquids were tested at the specified ratios. This approach also facilitated the comparison of the impact of hydrogen bond acceptors on the properties of DESs with the same molar ratios. The preparation of solvents was carried out by mass, using appropriate amounts of each DES component (Mettler Toledo balance with the precision of 0.00001 g). The components were thoroughly mixed at a temperature of 353.15 K for 1 hour until a homogeneous liquid, devoid of any precipitate, was obtained. The resulting DESs were colorless and exhibited stability at room temperature. To maintain their integrity, the DESs were stored in tightly sealed containers to prevent contamination from the external atmosphere, which could potentially influence their physical properties. Prior to conducting experiments, the water content in DESs was determined by the Karl – Fischer Method using a Mettler Toledo Volumetric Karl – Fischer titrator (V105). Table 2 presents its values along with the molar mass of DESs, their abbreviations, and the molar ratio and mass fraction of DES components.

Table 1: Provenance and mass fraction purity of the compounds studied.

Chemical name	Source	CAS number	Initial purity/mass fraction[a]	Purification method	Final purity/mass fraction[a]
2-(butylamino)ethanol (BAE)	Sigma Aldrich	111-75-1	≥0.98	None	–
3-Aminopropan-1-ol (AP)	Sigma Aldrich	156-87-6	0.99	None	–
2-(methylamino)ethanol (MAE)	Sigma Aldrich	109-83-1	≥0.98	None	–
Tetrabutylammonium bromide (TBAB)	Sigma Aldrich	1643-19-2	≥0.99	None	–
Tetraethylammonium chloride (TEAC)	Sigma Aldrich	56-34-8	≥0.98	None	–
Tetrabutylammonium chloride (TBAC)	Sigma Aldrich	1112-67-0	≥0.97	Crystallization	≥0.98[b]

[a]As stated by the supplier. [b]Determined by potentiometric titration.

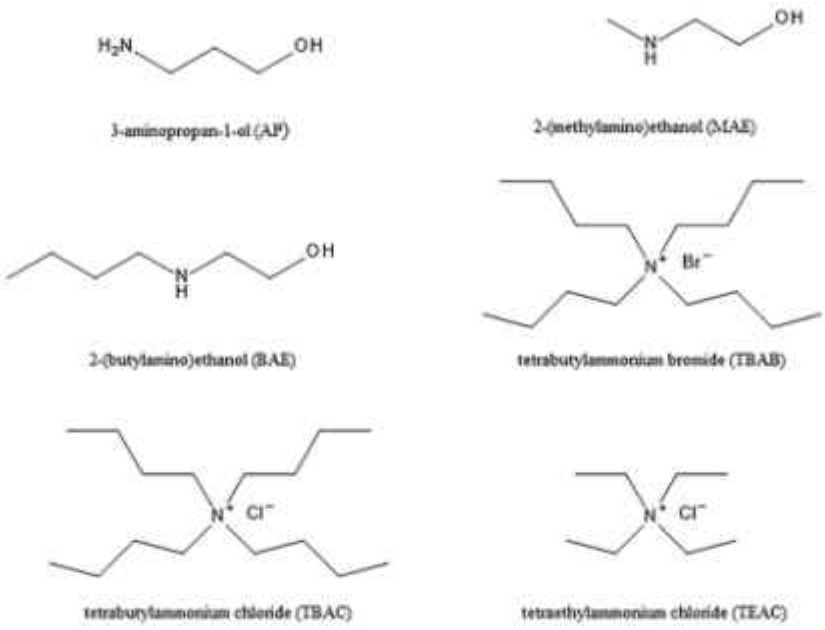

Fig. 1: Chemical structures of the DESs components used in this study.

The preparation procedure of DESs containing 3-aminopropan-1-ol[35] and 2-(methylamino)ethanol[37] was described in our earlier works. Molar mass, molar ratio, mass fraction and water content for those DESs are presented in Table S1 and Table S2.

Table 2: The abbreviation, molar mass, molar ratio, mass fraction and water content for chemicals used in synthesis of 2-(butylamino) ethanol-based DESs.

DES		Salt		HBD		Molar ratio		Mass fraction[a]		Water content[b]
Symbol	$M_{DES}/10^3$ kg mol^{-1}	Abbreviation	M_{salt}/g mol^{-1}	Abbreviation	M_{HBD}/g mol^{-1}	Salt	HBD	Salt	HBD	-
DES1	146.503	TBAB	322.37	BAE	117.19	1	6	0.3144	0.6856	0.00059
DES2	140.100	TBAB	322.37	BAE	117.19	1	8	0.2568	0.7431	0.00064
DES3	135.553	TBAB	322.37	BAE	117.19	1	10	0.2128	0.7872	0.00066
DES4	124.141	TEAC	210.16	BAE	117.19	1	6	0.1912	0.8088	0.00123
DES5	122.584	TEAC	210.16	BAE	117.19	1	8	0.1503	0.8497	0.00139
DES6	121.606	TEAC	210.16	BAE	117.19	1	10	0.1240	0.8760	0.00151
DES7	140.185	TBAC	277.92	BAE	117.19	1	6	0.2836	0.7164	0.00210
DES8	134.994	TBAC	277.92	BAE	117.19	1	8	0.2280	0.7720	0.00249
DES9	131.836	TBAC	277.92	BAE	117.19	1	10	0.1921	0.8079	0.00266

[a]The standard uncertainty of DES mass fraction composition is 0.001. [b]Water content of DESs in mass fraction determined by Karl Fisher titration with the standard uncertainty ±0.0001.

DES characterization

Infrared spectroscopy measurements

The Jasco-4700 instrument (Jasco Company, Tokyo, Japan), was utilized to perform FTIR experiments on liquid samples. The experiments covered a spectral range of 4000–400 cm^{-1} with 32 scans and a resolution of 4 cm^{-1}. To perform the experiments, the thin film method utilizing salt (KBr) plates was implemented. A single drop of the liquid solution was placed on one of the salt plates. Before recording the spectrum, a background spectrum was obtained from a clean plate. The analysis of the spectra was carried out using the Spectra Analysis software (Jasco Company in Tokyo, Japan). For solid samples (substrates), the spectra were recorded using dry salt KBr. In this case, the materials (1 mg) were compressed with potassium bromide (99 mg) to form a disc. The analysis was conducted at a temperature of 298.15 ± 0.1 K.

Melting point

The melting points of the synthesized DESs were determined using the Mettler Toledo Star One Differential Scanning Calorimeter (DSC). The measurements were conducted in a purified nitrogen atmosphere with a flow rate of 60 mL min^{-1}. The samples, weighing between 10 and 18 mg, were placed in standard aluminium pans. The DSC equipment was connected to a dedicated computer running the STAR® data acquisition software. The heating and cooling sequence was programmed on the STAR® console, which controlled the DSC equipment. A temperature range of 193.15–298.15 K, with a heating rate of 2 K min^{-1}, was selected for the determination of the melting point. The measurement uncertainty was ±0.01 K.

Thermogravimetric analysis

The TG 209F3 apparatus from Netzsch Group (Selb, Germany) was employed for the thermogravimetric analyses. Approximately 10 mg of samples were carefully positioned in a corundum dish for testing. The measurements were conducted in a nitrogen atmosphere with a flow rate of 50 ml min^{-1}, spanning temperatures from 298 to 1023 K, and a heating rate of 10 K min^{-1}.

Density and sound velocity

The densities and the sound velocities of the DES samples were obtained at different temperatures using a digital vibration-tube analyser (Anton Paar DSA 5000, Austria) with proportional temperature control that kept the samples at working temperature with an accuracy of ±0.01 K. Experimental frequency for the measurements of the ultrasonic velocity was equal to 3 MHz. The calibration was carried out using double distilled, deionized and degassed water, and dry air at atmospheric pressure (0.1 MPa). The standard uncertainty of density measurement was better than 0.1 kg m^{-3} and 0.5 m s^{-1}, respectively.

Viscosity

The DESs' viscosities were determined using a computer controlled LVDV-III Programmable Rheometer (cone-plate viscometer; Brookfield Engineering Laboratory, USA). The sample temperature was regulated within ±0.01 K using a thermostatic water bath (PolyScience 9106, USA). The viscometer's accuracy was confirmed using a certified viscosity standard N100 and S3 provided by Cannon at 298.15 ± 0.01 K. The uncertainty in viscosity measurement was less than 2 %, and each sample was measured independently at least three times at each temperature to ensure reproducibility.

Refractive index

The Abbe refractometer (RL-3, Poland) was employed to measure the refractive indices, with a thermostat ensuring the cell temperature was controlled with an accuracy of ± 0.1 K. The standard uncertainty of the refractive index measurements on the n_D scale was 0.0002. To validate the reproducibility of the measurements, a minimum of three independent measurements were taken for each sample at every temperature.

CO_2 solubility measurement by gravimetric

The CO_2 absorption capacity was measured by gravimetric method using the experimental setup shown in Fig. 2. The setup consists of a gas tight measuring cell (3) placed in a thermostat bath (PolyScience 9106, Warrington, PA, USA) (2) and connected to a gas supply container (1) and vacuum oil pump.

For each experiment, 1 ml of DES was injected into the measuring cell (1). The cell was properly sealed and placed in the thermostat water bath. The temperature was kept constant with an accuracy of ±0.1 K. The system was then evacuated using a vacuum oil pump and the vacuum was applied until the pressure in the system did not change in order to ensure complete gas desorption from the DES sample Then carbon dioxide was introduced into the cell at 7.5 ml/min flow rate. The gas flow was increased to 15 ml/min when the DES viscosity increased during the absorption process and no bubbles were observed. The mass of the cell was determined using an analytical balance (RADWAG) with an accuracy of ±0.1 mg in regular time intervals. The measurement was finished when the weight of the sample remained constant. The final solubility values were calculated at 0.1 MPa pressure.

Results and discussion

FTIR characterization of DESs

Infrared spectroscopy serves as a valuable tool for examining the intermolecular interactions among molecules within DESs.[22] The FTIR spectra of the investigated DESs are displayed in Figure S1, alongside the spectra of pure BAE, TBAB, TBAC, TEAC.

The ν(OH)/ν(NH) stretching vibration bands, located at range a 3900–3000 cm^{-1}, are a great probe of hydrogen bond interactions. For neat BAE, the maximum of this band is located at 3301.5 cm^{-1}. The peak positions of

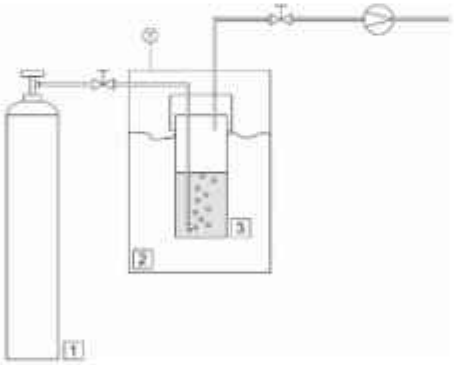

Fig. 2: Schematic diagram of the gas solubility setup (1 – gas supply; 2 – thermostatic water bath; 3 – measuring cell).

ν(OH)/ν(NH) stretching vibration bands for all DESs studied are shown in Figure S1. Interestingly, regardless of DES components and molar HBA/HBD ratio, these maxima exhibit a blue-shift compared to pure BAE. This blue-shift corresponds to an increase in energy resulting from the formation of new hydrogen bonds between BAE and tetraalkylammonium halides. Furthermore, the other bands observed in the DES spectra remain unaltered compared to those of the pure components, indicating the absence of any chemical reactions between the molecules within the DESs.

The most significant shift is evident in TEAC:BAE (1:6), indicating the strongest hydrogen bond interactions within this DES, while the smallest shift is observed in TBAC:BAE (1:6). When BAE is added, thereby increasing the HBA/HBD molar ratio from 1:6 to 1:8, the blue-shift effect diminishes in case of TBAB and TEAC-based DESs. Further additions of BAE have minimal impact on the positions of the ν(OH)/ν(NH) stretching vibration bands. Interestingly, the maxima for TBAC:BAE DESs remain unchanged regardless of the HBA/HBD molar ratio.

Thermal properties of DESs

The obtained thermal properties of the studied DESs based on 2-(butylamino)-ethanol are shown in Table 3, as the values of melting temperature, T_m, decomposition temperatures at 10 % and 90 % weight loss, $T_{10\,\%}$ and $T_{90\,\%}$, and maximum temperatures, T_{max}. Figure S2 presents the DSC plots and Figure S3 shows the TGA and DTGA curves.

Melting point

Differential scanning calorimetry was used to determination of melting points and any solid-state phase transitions of BAE-based DESs. Table 3 provides an overview of the melting points of these DESs. Meanwhile, Figure S2(a, b, c) illustrates the DSC curves for DES systems with three different HDA:HBD ratios – namely, 1:6, 1:8, and 1:10.

In most of the DSC curves, a distinctive pattern appears, characterized by singlet-shaped endothermic peaks, indicative of melting points. However, notable exceptions were observed in the case of TEAC:BAE 1:6 and TBAB:BAE 1:10, where a double peak signifies the melting process. Importantly, for all the studied DESs, their melting points are consistently lower than those of the individual components and remain below 269.86 K, affording them a wide liquid range.

Table 3: Thermal characteristics obtained from TGA, DTGA and DSC curves: decomposition temperatures at 10 % and 90 % weight loss, $T_{10\,\%}$ and $T_{90\,\%}$, maximum temperatures, T_{max}, melting temperature, T_m, for BAE-based DESs.

DES	$T_{10\,\%}$/K	$T_{90\,\%}$/K	T_{max1}/K	T_{max2}/K	T_m/K
DES1	372.0	502.3	412.1	492.5	267.33
DES2	371.2	499.2	409.6	492.3	267.63
DES3	371.6	497.3	410.4	492.8	269.82
DES4	347.3	550.2	396.0	549.1	269.17
DES5	358.6	544.5	411.1	552.1	269.70
DES6	379.3	529.5	427.5	554.2	269.86
DES7	363.3	492.8	418.6	483.5	268.16
DES8	365.7	487.8	414.9	483.3	266.55
DES9	352.6	487.9	397.0	484.3	267.20
BAE	364.8	422.1	412.1	–	271.00

Clear crystallization and melting peaks are observed for all the studied DESs. Furthermore, when considering DESs with the same molar ratio of salt to 2-(butylamino)ethanol, the order of melting temperatures is as follows: TEAC:BAE > TBAB:BAE > TBAC:BAE. This sequence implies that the melting temperature of the salt may indeed influence the melting temperature of deep eutectic solvents.

Additionally, the higher melting temperature values found for TBAB-based DESs, in comparison to those of TBAC-based, suggest that the type of anion have an effect on melting point of DES. Surprisingly, a comparison of the melting temperatures of DESs containing tetrabutylammonium and tetraethylammonium chlorides showed increase of melting temperature with a decrease in alkyl chain length. The opposite observations were made for DESs featuring 3-aminopropan-1-ol[23] and 2-(methylamino)ethanol.[22] This difference might be due to high steric hindrances between TBAC and BAE molecules, which can weaken the hydrogen bond network in TBAC-based DESs, and result in lower melting temperature.

Thermogravimetric measurements

Figure S3 presents TGA curves, *i.e.* the weight loss measured in % against temperature, for the studied DESs along with their pure components. In general, the curves consist of two steps– the first shows the BAE decomposition and the second corresponds to the degradation of the salt.

As can be seen from the TGA plots, the stability of TBAB and TBAC-based DESs is in between that of their components and the order of stability is: BAE < DES < salt. The initial decomposition temperature measured as 10 % weight loss ($T_{10\,\%}$) for those DESs oscillate around the temperature of pure BAE, while the end of the decomposition measured as 90 % mass loss ($T_{90\,\%}$) is higher. In general, the increase of BAE content in the mentioned DESs results in lower thermal stability. For TEAC-based DESs however, thermal stability increases distinctly with an increase of BAE content. As can be observed in Figure S3, decomposition of TEAC starts earlier than BAE which results in lower thermal stability in the case of TEAC rich DESs. Liu et al. performed TGA studies on the effect of HBA/HBD molar ratio on the thermal stability of ChCl:urea DESs.[24] They found that at higher ChCl contents, there is no sufficient amount of choline chloride to form hydrogen bonds with urea, so "excess" ChCl acts as an impurity towards formed DES, which results in a different thermogram curve than for DESs with other HBA/HBD molar ratios. The similar situation can be observed in our case for TEAC:BAE (DES4 and DES5).

For DESs with a molar ratio of HBA to HBD equal to 1:6 and 1:8, the $T_{10\,\%}$ values change according to the sequence: TEAC:BAE < TBAC:BAE < TBAB:BAE, while for DESs with the molar ratio 1:10, the order of $T_{10\,\%}$ is different, as is TBAC:BAE < TBAB:BAE < TEAC:BAE (Table 3). As the temperature of decomposition of TBAB-based DESs is always higher than TBAC-based ones it can be concluded that the anion has impact on DESs thermal stability. In the case of MAE-based DESs, the more stable DESs were those based on TBAC due to stronger hydrogen bonds formed by Cl^- than for Br^-.[21,22] However, BAE molecule has a long alkyl chain that provides steric hindrance which possibly can influence the hydrogen bond strength between amine group and the halide anion. Bromide anion has higher ionic radii than Cl^- i.e. is placed further from tetrabutylammonium cation and possibly can interact more effectively with BAE molecule resulting in higher thermal stability.

Comparison of TBAC and TEAC-based at a molar ratio 1:6 and 1:8 shows that thermal stability increases with an increase of alkyl chain length in HBA. Similar results were obtained for phosphonium-based DESs.[25] However, at a molar composition of 1:10 the thermal stability is reversed. It could be due to smaller steric hindrances between TEAC and BAE molecules than between TBAC and BAE, which allows to form more complicated hydrogen bond neat in TEAC-based DESs, resulting in higher thermal stability at a molar ratio 1:10.

Physical properties of DESs

Density

The density data measured as a function of temperature in the range of 293.15–333.15 K are shown in Fig. 3 and Table S3.

Similarly to other deep eutectic solvents, the density of studied systems decreases linearly with temperature.[3] At elevated temperatures, the volume of the solvent increases due to the formation of more intermolecular voids, leading to a decrease in density.

Comparing DESs at the same HBA/HBD molar ratio and temperature, the density values follow the order TBAB:BAE > TEAC:BAE > TBAC:BAE. The same order of densities was found by our group for DESs based on other alkanolamines i.e. 2-(methylamino)ethanol (MAE) and 3-aminopropan-1-ol (AP).[21,22] The highest densities for TBAB-based DESs are obviously due to the higher molar mass of bromide anion compared to chloride anion.[5,26]

Analysis of the density results obtained for TBAC:BAE and TEAC:BAE shows the influence of HBA alkyl chain length on the density of DES. The higher density for TEAC-based DESs indicates that shorter alkyl chains lead to higher density. This is due to the smaller free volume resulting from the packing effect occurring in such solvents. The same behavior was observed for other tetraalkylammonium-based DESs combined with alkanolamines, lactic acid or glycols.[21,22,27]

Another factor that could be discussed is the effect of HBA/HBD molar ratio on density. Regardless of the HBA used, the density of DES decreases with increasing BAE content. This behavior is consistent with other literature reports.[25,28] It is worth mentioning that in the case of TBAC-based DESs, different relations were observed in DESs composed of 3-aminopropan-1-ol or 2-(methylamino)ethanol as hydrogen bond donor. As shown in our previous studies, for TBAC:AP DES, the density increases with increasing AP content, while in the case of TBAC:MAE DES, the HBA/HBD molar ratio seems to have a negligible effect on the density values.[21,22] It could be attributed to the different association effect between DES molecules and the relationship between DES density and HBA/HBD molar ratio may be also dependent on density of neat alkanolamine.[29] The densities of TBAC:AP are lower than pure AP, TBAC:MAE are similar to neat MAE while for TBAC:BAE are higher than pure BAE.

Connection of density values for DESs presented in this study, as well as in our previous studies for AP and MAE-based deep eutectic solvents, with the same HBA/HBD molar ratio, shows the effect of HBD on this property. The relationship between various DES at a molar ratio 1:6 is presented in Figure S4. Regardless of hydrogen bond acceptor used, DESs based on AP have the highest density, while those composed of BAE have the lowest.[21,22] For example, the density of TBAB:AP 1:6 is 1015.6 kg m^{-3}; TBAB:MAE is 986.1 kg m^{-3} while for TBAB:BAE 1:6 is 937.6 kg m^{-3} in 293.15 K. This behavior of density values for 2-(butylamino)ethanol can be correlated with longest alkyl chains for this HBD. The decrease of density with an increase in alkyl chain length was also shown by

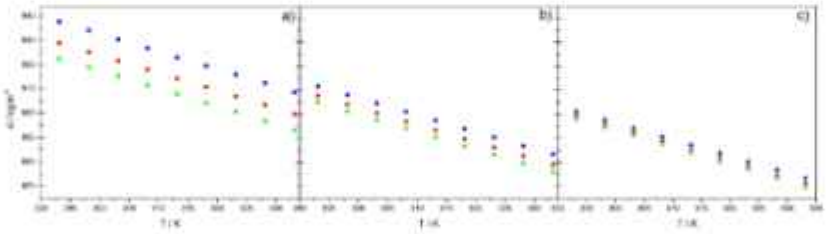

Fig. 3: Densities of deep eutectic solvents containing BAE studied as a function of temperature in the range of 293.15–333.15 K and at atmospheric pressure (a) TBAB:BAE (DES 1–3), (b) TEAC:BAE (DES 4–6) and (c) TBAC:BAE (DES 7–9), (blue – 1:6, red – 1:8, green – 1:10).

Florindo et al. for carboxyl acid-based DESs.[39] The only difference between AP and MAE is that AP is a primary amine while MAE is a secondary one. Therefore, AP may form more hydrogen bonds with HBA, leading to higher density values.

Viscosity

The experimental dynamic viscosity data of the studied DESs, obtained at the temperature range of 293.15–333.15 K., are presented in Table S4 and Fig. 4. As can be seen, Fig. 4 shows the non-linear decrease in viscosity with temperature. It is well known phenomenon occurring both for DESs and ILs.[31–33] On the one hand, it is the effect of weakening of molecular interactions between components of DES, which affects the mobility of species in DES having a major impact on this parameter.[34] On the other hand, it can be explained using a hole theory.[35] The underlying concept of this theory suggests that the viscosity of a liquid is influenced by the presence of appropriately sized gaps that enable the movement of ions. In this context, factors like steric hindrances play a more significant role in influencing viscosity compared to the interactions between HBA and HBD. As the temperature rises, the liquid contains a greater number of larger gaps. As a result, deep eutectic solvents exhibit lower viscosity.

The inspection of both Table S4 and Fig. 4 shows that the lowest viscosities are observed for TEAC (DES4-6) based DESs, while the highest for TBAB (DES1-3) based. A relatively low difference between viscosities of TBAB and TBAC-based DESs, and a higher difference between TBAC and TEAC-based DESs suggests that alkyl chain length has a greater impact on viscosity than anion of salt.[36] Additionally, higher molecular mass of DESs components also results in higher viscosity of deep eutectic solvent.[37]

The addition of HBD i.e. changing the HBA/HBD molar ratio in DES composition results in drop in viscosity. This is directly linked to the increase of the solvent's free volume and molecular motion of species.[38] Similar results were observed for other DESs in the literature.[12]

For TBAB-based DESs (at molar ratio 1:6) at 293.15 K, the viscosities follow the order AP[25]>BAE > MAE[23] with values 79.3 mPas, 60.6 mPas and 45.3 mPas respectively. This relationships are unchanged in the case of other HBAs which is shown in Figure S5. The highest viscosity of AP-based DESs might be attributed to the 3-aminopropan-1-ol's capability to create a greater number of hydrogen bonds than both 2-(methylamino)ethanol and 2-(butylamino)ethanol. Furthermore, long alkyl chains of BAE could potentially be arrange in layers, which can reduce species mobility, thereby resulting in a higher viscosity of BAE-based DESs compared to MAE-based.

Arrhenius and Vogel-Fulcher-Tamman (VFT) equations are the most commonly used for fitting experimental viscosity to temperature data in the case of deep eutectic solvents.[33] The Arrhenius (1) and VFT equations (2) are expressed as:

$$\eta = \eta_\infty e^{\frac{E_a}{RT}} \tag{1}$$

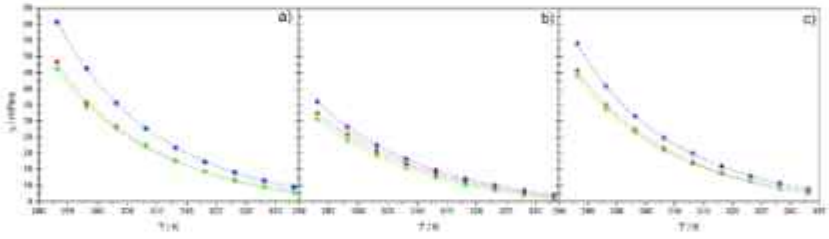

Fig. 4: Viscosities of deep eutectic solvents containing BAE studied as a function of temperature in the range 293.15–333.15 K and at atmospheric pressure (a) TBAB:BAE (DES 1–3), (b) TEAC:BAE (DES 4–6) and (c) TBAC:BAE (DES 7–9) (blue – 1:6, red – 1:8, green – 1:10); dashed line – Vogel-Fulcher-Tamman equation.

$$\eta = \eta_\infty e^{\frac{E_a}{RT}} \quad (2)$$

where η_∞, E_a, η_0, b and T_o are fitting parameters, η_∞ is the viscosity at infinite temperature, E_a is the activation energy, R is the gas constant, and T is the temperature in Kelvin. Table S5 and Table S6 contain the fitting parameters determined from the experimental data along with R^2 and root-mean-square deviations (*RMSD*). The activation energies (E_a) can be useful for assessing the interactions occurring in liquid solvents. High E_a values indicate stronger intermolecular interactions, which lead to a drop in ions mobility. This is reflected in increased viscosity. Thus, the calculated E_a values align with the previously outlined viscosity relationships. The statistics metrics i.e. R^2 and *RMSD* values suggest that the VFT equation is better suited for fitting the viscosity data of DESs.

Refractive index

Figure 5 and Table S7 provide a summary of the refractive indices for the DESs examined in this study. The refractive indices at a specific temperature, regardless of the molar ratio of the HBA to the HBD, are in the following sequence: TBAB:BAE > TBAC:BAE > TEAC:BAE. Such observation can lead to a conclusion that n_D is primarily dependent of the molecular mass of DESs. The effect of alkyl chain length is not as pronounced as molecular mass when it comes to n_D values; TBAC and TEAC have similar n_D values, although TBAC-based DESs tend to show slightly higher values. This observation aligns with the refractive index trend observed among DESs with varying HBA:HBD molar ratios, as the refractive index decreases with an increasing BAE content across all examined DESs. It is noteworthy that BAE-based DESs exhibit a linear decrease in refractive index with rising temperature, similar to previously reported findings for DESs based on sulfosalicylic acid[40], benzylic acid[41], 2-(methylamino)ethanol[22], and 3-aminopropan-1-ol.[21]

Moreover, the effect of HBD on refractive indices values is shown in Figure S6. DESs based on BAE exhibit the lowest refractive indices when compared to those based on AP[21] and MAE.[22] In the case of TBAB-based DESs, at a molar ratio 1:6, combined with AP, MAE, BAE the values of refractive indices in 293.15 K are 1.4766; 1.4618 and 1.4595 respectively. This shows that molar mass does not play a significant role in the case of various hydrogen bond donors, unlike its role in different hydrogen bond acceptors. It is clear that the length of the alkyl chains in HBD determines the DESs n_D values. Another important factor could be the type of amine used as the HBD. The greatest n_D values are seen in the primary amine AP, whereas secondary amines like MAE and BAE have comparable but unmistakably lower refractive indices than AP.

Speed of sound

Table S8 and Fig. 6 illustrate the relationship between temperature and sound velocity across the various studied DESs. When DESs based on TBAB and TBAC are compared, regardless of the molar ratio of HBA/HBD, an inverse correlation appears between molecular mass and sound velocity values. Specifically, DESs based on TBAC exhibit

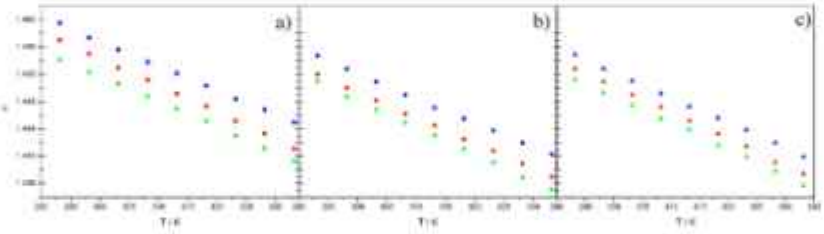

Fig. 5: Refractive indices of deep eutectic solvents containing BAE studied as a function of temperature in the range of 293.15–333.15 K and at atmospheric pressure (a) TBAB:BAE (DES 1–3), (b) TEAC:BAE (DES 4–6) and (c) TBAC:BAE (DES 7–9), (blue – 1:4, red – 1:5, green – 1:8).

higher sound velocity values. The highest values found for DESs based on TEAC further highlight the significant influence of alkyl chain length on sound velocity. As for the other properties, an increase of the HBD content leads to a decrease in sound velocity in the case of all deep eutectic solvents studied. Kianpour et al. reported a similar finding for ninhydrin based DESs.[42] Moreover, a linear decrease in sound velocity with increased temperature was observed.

Figure S7 shows the influence of HBD on the speed of sound values. The highest values of sound velocity for alkanolamines based DESs studied by our group were found to be for the ones containing 3-aminopropan-1-ol.[21] It could be attributed to the fact, that AP is first order amine, which can form a more complex hydrogen bonds network. It makes AP-based DESs denser and more suitable for traveling sound waves in the proper time without facing the retardants. The higher values of sound velocities of MAE-based[22] DESs compared to BAE-based ones are due to shorter alkyl chains in MAE molecules.

Solubility of CO_2 in alkanolamine-based DESs

The carbon dioxide capacities of pure DESs used in this study are presented in Table 4, and the bold values indicate DESs with highest CO_2 absorption capacities. The solubility values of CO_2 in TBAB:AP 1:4 (0.49 mol_{CO2} mol_{DES}^{-1}) were close to those reported by Shulka and Mikkola (0.51 mol_{CO2} mol_{DES}^{-1}).[20] The dissolution of CO_2 occurs due to physical, chemical or mixed sorption mechanism. Within the range of DESs selected for this study, the presence of alkanolamines as HBD induced a mixed mechanism of CO_2 absorption.[20] To confirm this, for DESs composed of TBAB with AP, MAE and BAE at a molar ratio 1:6, FTIR spectra were recorded before and after the reaction of DES and carbon dioxide. The diagrams are presented in Figure S8. The presence of a new band around 2360 cm^{-1} for all spectra studied can be attributed to asymmetric O=C=O stretching vibration and it is represents physically absorbed CO_2.[43] In addition, new bands at 1306 cm^{-1}, 1376 cm^{-1} and 1405 cm^{-1} were observed for AP, MAE and BAE, respectively. They result from the C=O vibration of the carbamate species, which confirms the chemical reaction between DES and CO_2 molecules.[44]

In Figure S9, the examples of the carbon dioxide absorption kinetics for DESs composed of various HBA and HBD and molar ratios are presented. Figure S9a shows the effect of hydrogen bond acceptor on CO_2 uptake kinetics in AP-based DESs. At the initial step, absorption is rapid and the rate is similar for all presented DESs. Further, the process slows down and the lowest capacity is observed for TBAB-based DES, which also has the highest viscosity. The exceptions are DESs with BAE as HBD and AP with 1:6 ratio. Figure S9b presents the effect of hydrogen bond donor on CO_2 absorption isotherms for TBAC-based DESs. The kinetics and CO_2 absorption capacities follow the order of BAE < AP < MAE. The increasing content of HBD results in higher carbon dioxide capacity (Figure S9c) and thus more rapid kinetics.

Absorption capacities of DESs based on the same molar ratio (1:6) composed of various hydrogen bond acceptors and donors are presented in Fig. 7. Taking into account the CO_2 capacity of TBAB and TBAC-based DESs the influence of the anion type on the absorption capacity is clearly visible. Higher solubilities are observed for

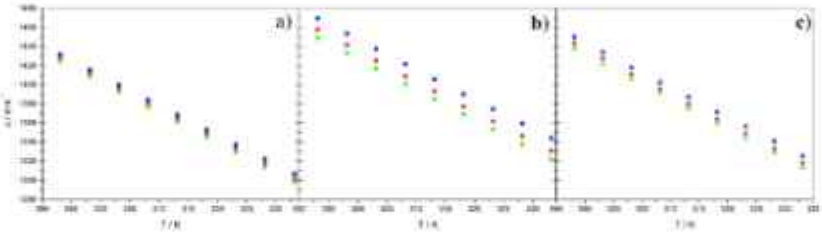

Fig. 6: Sound velocities of deep eutectic solvents containing BAE studied as a function of temperature in the range of 293.15–333.15 K and at atmospheric pressure (a) TBAB:BAE (DES 1–3), (b) TEAC:BAE (DES 4–6) and (c) TBAC:BAE (DES 7–9), (blue – 1:4, red – 1:6, green – 1:8).

Table 4: Carbon dioxide capacity of studied of BAE-based DESs under the pressure 1 bar.

DES	$c/g_{CO2}\,g_{DES}^{-1}$
TBAB:AP 1:4	0.175
TBAB:AP 1:6	0.177
TBAB:AP 1:8	0.184
TBAC:AP 1:4	0.153
TBAC:AP 1:6	0.185
TBAC:AP 1:8	0.186
TEAC:AP 1:4	0.157
TEAC:AP 1:6	0.192
TEAC:AP 1:8	0.201
TBAB:MAE 1:6	0.161
TBAB:MAE 1:8	0.185
TBAB:MAE 1:10	0.193
TBAC:MAE 1:6	0.186
TBAC:MAE 1:8	0.194
TBAC:MAE 1:10	0.202
TEAC:MAE 1:6	**0.209**
TEAC:MAE 1:8	**0.219**
TEAC:MAE 1:10	**0.223**
TBAB:BAE 1:6	0.142
TBAB:BAE 1:8	0.148
TBAB:BAE 1:10	0.153
TBAC:BAE 1:6	0.128
TBAC:BAE 1:8	0.138
TBAC:BAE 1:10	0.140
TEAC:BAE 1:6	0.153
TEAC:BAE 1:8	0.164
TEAC:BAE 1:10	0.178

DESs based on HBA containing Cl^-. Moreover, the longer the alkyl chain in the HBA structure, the higher absorption capacity is observed. Literature data report similar observations regarding anion and alkyl chain length for DESs based on ethanolamine.[10] Interestingly, reverse trend was reported for DESs that absorb CO_2 physically.[32,41] Thus lower CO_2 absorption in DESs composed BAE than AP or MAE might suggest a greater proportion of physical absorption in those DESs. This can be further confirmed by the molecular volume (V_m) of those DESs. The values of this property are reported in Table S10. The lowest value of V_m in the case of TEAC-based DESs shows the origin of the poorest solubility values and yet again confirms the greater influence of physical phenomena in this type of DESs.

In general, the carbon dioxide capacity follows the HBD order: BAE < AP < MAE. The only exception is TBAB:AP 1:6 DES. Molecular dynamics studies revealed different factors that influence CO_2 solubility in DESs with physical and chemical mechanism. Altamash et al. showed that the strength of interactions between phenylacetic acid-based DES and CO_2 is almost half lower than for levulinic acid-based ones.[40] They suggested that there are other factors, such as the volume rearrangement of DES (i.e. its free volume), that play a key role in the physical absorption of carbon dioxide in DESs. On the other hand, the studies conducted by Shukla and Mikkola[20] showed lower carbon dioxide absorption for DES composed of 1-methylimidazolium chloride and ethylenediamine (HMIMCl:EDA) than for monoethaloammonium chloride and ethylenediamine (MEACl:EDA) at various molar ratios. They concluded that the strength of hydrogen bond interactions between DESs components plays a key role in their CO_2 sorption abilities. Due to more acidic protons in HMIMCl molecule than in MEACl, EDA is more strongly coordinated by HMIMCl. It results in weaker interactions between HMIMCl:EDA DES and carbon dioxide, thus causes lower absorption capacities in comparison to MEACl:EDA. These observations are crucial in understanding influence of HBD on carbon dioxide capacities in studied DESs. The lower carbon dioxide capacity of AP-based DESs than that of MAE-based might be attributed to the fact, that as AP is a primary amine, it can form

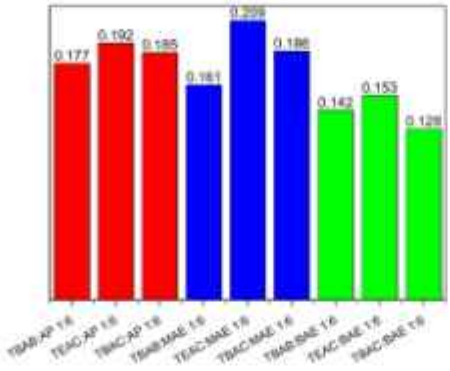

Fig. 7: Absorption capacities ($g_{CO2}\ g_{DES}^{-1}$) at molar ratio 1:6 for TBAB, TEAC or TBAC coupled with: blue – AP; red – MAE; green – BAE.

more complex hydrogen bond structures with HBA than MAE thus AP-based DESs cannot interact with CO_2 as efficiently as MAE- based ones. It is in line with results obtained for pure alkanolamines.[47] For BAE based DESs the limiting factor for absorption appears to be the low free volume of solvent caused by longer alkyl chains.

The last important factor that influences carbon dioxide solubility in pure DESs is HBA/HBD molar ratio. Regardless of HBA and HBD used, the carbon dioxide solubility increases with an increase of alkanolamine content. This trend was also observed by Li et al.[22] for DESs composed of choline chloride and ethanolamine. Once again this phenomenon was correlated with weakening of hydrogen bonds between HBA and HBD upon HBD addition.

Solubility of CO_2 in DESs mixtures with water

Figure 8 illustrates the impact of water addition on the carbon dioxide capacity of DESs at a molar ratio of HBD to HBA of 1:6. The presence of water can either enhance or diminish the CO_2 absorption capacity of DESs. For MAE-based DESs, the addition of 0.5 % wt water results in approximately 11 % increase in CO_2 solubility (from 0.161 to 0.179 $g_{CO2}\ g_{DES}^{-1}$) (from 0.161 to 0.179 $g_{CO2}\ g_{DES}^{-1}$). The 1 % wt water mixtures also present higher absorption capacities, equal to 0.171 $g_{CO2}\ g_{DES}^{-1}$. Further water content increase results in the decrease of CO_2 capacity in comparison to pure DES, namely drop from 0.161 to 0.123 $g_{CO2}\ g_{DES}^{-1}$. For AP and BAE based DESs, even a small amount of water added reduces the absorption capacities.

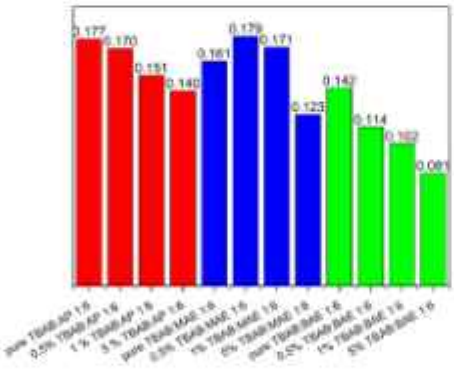

Fig. 8: Absorption capacities ($g_{CO2}\ g_{DES}^{-1}$) for studied DESs at molar ratio 1:6 and their water mixtures composed of TBAB, TEAC or TBAC coupled with: red – AP; blue – MAE; green – BAE.

Taking into account the capacity of pure DES and pure water as well as the mass fraction of the solution components, calculations of the CO_2 capacity of the solutions were carried out assuming additivity of solubility. The theoretical capacity presented in Table S9 represents the sum of solubility shares in pure components.

There are several hypotheses on molecular mechanisms related to the influence of water addition on carbon dioxide absorption capacities. According to Su et al., an increase in water content may lead to a reduction in the solubility of carbon dioxide, potentially caused by a decline in the concentration of active reactants i.e. molecules that can interact with CO_2 effectively.[16]

In TBAB:AP and TBAB: BAE systems all of the solutions studied presented lower CO_2 capacity than the theoretical value simply summing up the solubility in pure components. A very strong effect was observed for TBAB:BAE. The addition of 5 % of water resulted in a 40 % decrease in solubility (from 0.134 to 0.081 $g_{CO2}g_{DES}^{-1}$) (from 0.134 to 0.081 $g_{CO2}g_{DES}^{-1}$) compared to the summed solubility in pure components (water and DES). In TBAB:MAE 0.5 and 1 % solutions the capacity was equal to respectively 0.179 and 0.171 and was higher than the theoretical one (0.160 and 0.159 $g_{CO2}g_{DES}^{-1}$). Trivedi et al. suggested that the addition of water results in the formation of new hydrogen bonds between DES and water molecules, this leads to the weakening of interactions between DES molecules[19] and thus in a higher free volume of solvent and allows DESs molecules to interact more efficiently with carbon dioxide. Our research group's investigations into binary mixtures of water with alkanolamine-based DESs revealed the strongest interactions between water and those based on MAE.[40] In line with the absorption capacities of water-DES mixtures, it can be deduced that the strength of hydrogen bonds formed between water and DESs plays a pivotal role in determining whether the addition of water to a DES will enhance or diminish its carbon dioxide solubility capabilities.

Conclusions

The presented results and discussion are a comprehensive evaluation of our newly synthesized and recently studied deep eutectic solvents. This study presents experimental data of the FTIR spectra, thermal properties, density, viscosity, refractive index, and sound velocity of deep eutectic solvents derived from 2-(butylamino) ethanol, with a focus on their temperature-dependent behaviour at the atmospheric pressure. The DESs taken under investigation in this work featured tetrabutylammonium bromide, tetraethylammonium chloride, and tetrabutylammonium chloride as hydrogen bond acceptors, combined with 2-(butylamino)ethanol (BAE) in varying molar ratios of 1:6, 1:8, and 1:10. The mentioned properties were also compared with those previously obtained for 3-aminopropan-1-ol (AP) and 2-(methylamino)ethanol (MAE) based DESs. The measurements showed a crucial effect of alkyl chain length, HBA/HBD molar ratio, anion's molecular weight and type of amine on physiochemical properties of studied DESs.

Furthermore, the carbon dioxide capacity of present BAE and earlier obtained AP and MAE-based DESs was studied. The impact of HBA, HBD and their molar ratio on carbon dioxide solubility in deep eutectic solvents was explored and compared to sum up this project. The findings demonstrated that both the length of the alkyl chain and the type of anion exert influence on carbon dioxide solubility. In the case of AP and MAE-based DESs, an increase in alkyl chain length resulted in decreased solubility, whereas for BAE-based DESs, this relationship was inverted. Additionally, both alkyl chain length and the type of amine influenced the carbon dioxide capacities in DESs. The long alkyl chains in BAE molecules acted as steric hindrance, leading to the lowest carbon dioxide solubilities. More intricate interactions between AP molecules and HBA salts resulted in lower carbon dioxide solubility compared to MAE-based DESs. In the case of all studied DESs, higher content of HBD increased in CO_2 capacity This underscored the crucial role of the interaction strength between DES components and carbon dioxide solubility.

Finally, the effect of water content in DES on carbon dioxide capacity was studied. Results showed that the addition of water could either decrease or increase carbon dioxide solubility in DESs. In the case of AP and BAE-based DESs, even a small amount of added water led to a reduction in carbon dioxide solubility. However, in MAE-based DESs, the addition of 0.5 % or 1 % water resulted in an increase in CO_2 absorption capacity. This indicates that the strength of interactions between DESs and water molecules plays a pivotal role in the effects of water addition on carbon dioxide solubility.

Research funding: This research did not receive any specific grant from funding agencies in the public, commercial, or not-for-profit sectors.

References

1. Wazeer, I.; Hayyan, M.; Hadj-Kali, M. K. Deep Eutectic Solvents: Designer Fluids for Chemical Processes. *J. Chem. Technol. Biotechnol.* **2018**, *93* (4), 945–958. https://doi.org/10.1002/jctb.5491.
2. Marcus, Y. *Deep Eutectic Solvents*, Springer: Switzerland, 2019.
3. Hansen, B. B.; Spittle, S.; Chen, B.; Poe, D.; Zhang, Y.; Klein, J. M.; Horton, A.; Adhikari, L.; Zelovich, T.; Doherty, B. W.; Gurkan, B.; Maginn, E. J.; Ragauskas, A.; Dadmun, M.; Zawodzinski, T. A.; Baker, G. A.; Tuckerman, M. E.; Savinell, R. F.; Sangoro, J. R. Deep Eutectic Solvents: A Review of Fundamentals and Applications. *Chem. Rev.* **2021**, *121* (3), 1232–1285. https://doi.org/10.1021/acs.chemrev.0c00385.
4. Gómez, E.; Cojocaru, P.; Magagnin, L.; Valles, E. Electrodeposition of Co, Sm and SmCo from a Deep Eutectic Solvent. *J. Electroanal. Chem.* **2011**, *658* (1–2), 18–24. https://doi.org/10.1016/j.jelechem.2011.04.015.
5. Zhang, Q.; De Oliveira Vigier, K.; Royer, S.; Jérôme, F. Deep Eutectic Solvents: Syntheses, Properties and Applications. *Chem. Soc. Rev.* **2012**, *41* (21), 7108–7146. https://doi.org/10.1039/c2cs35178a.
6. Pätzold, M.; Siebenhaller, S.; Kara, S.; Liese, A.; Syldatk, C.; Holtmann, D. Deep Eutectic Solvents as Efficient Solvents in Biocatalysis. *Trends Biotechnol.* **2019**, *37* (9), 943–959. https://doi.org/10.1016/j.tibtech.2019.03.007.
7. Oliveira, F. S.; Pereiro, A. B.; Rebelo, L. P. N.; Marrucho, I. M. Deep Eutectic Solvents as Extraction Media for Azeotropic Mixtures. *Green Chem.* **2013**, *15* (5), 1326–1330. https://doi.org/10.1039/c3gc37030e.
8. Sarmad, S.; Mikkola, J. P.; Ji, X. Carbon Dioxide Capture with Ionic Liquids and Deep Eutectic Solvents: A New Generation of Sorbents. *ChemSusChem* **2017**, *10* (2), 324–352. https://doi.org/10.1002/cssc.201600987.
9. Mokhtarpour, M.; Shekaari, H.; Zafarani-Moattar, M. T.; Golgoun, S. Solubility and Solvation Behavior of Some Drugs in Choline based Deep Eutectic Solvents at Different Temperatures. *J. Mol. Liq.* **2020**, *297*, 111799. https://doi.org/10.1016/j.molliq.2019.111799.
10. Li, Z.; Wang, L.; Li, C.; Cui, Y.; Li, S.; Yang, G.; Shen, Y. Absorption of Carbon Dioxide Using Ethanolamine-Based Deep Eutectic Solvents. *ACS Sustain. Chem. Eng.* **2019**, *7* (12), 10403–10414. https://doi.org/10.1021/acssuschemeng.9b00555.
11. Cichowska-Kopczyńska, I.; Nowosielski, B.; Warminska, D. Deep Eutectic Solvents: Properties and Applications in CO2 Separation. *Molecules* **2023**, *28* (14), 5293. https://doi.org/10.3390/molecules28145293.
12. Sarmad, S.; Xie, Y.; Mikkola, J. P.; Ji, X. Screening of Deep Eutectic Solvents (DESs) as Green CO2 Sorbents: from Solubility to Viscosity. *New J. Chem.* **2016**, *41* (1), 290–301. https://doi.org/10.1039/c6nj03148d.
13. Pishro, K. A.; Murshid, G.; Mjalli, F. S.; Naser, J. Investigation of CO2 Solubility in Monoethanolamine Hydrochloride based Deep Eutectic Solvents and Physical Properties Measurements. *Chinese J. Chem. Eng.* **2020**, *28* (11), 2848–2856. https://doi.org/10.1016/j.cjche.2020.07.004.
14. Jo, J.; Park, J.; Kwon, S.; Park, M.; Jung, J.; Yoo, Y.; Kang, D. Revolutionizing CO2 Capture: Molecular Complexes of Deep Eutectic Solvents with Enhanced Hydrogen Bond Accepting Interaction for Superior Absorption Performance. *J. Environ. Chem. Eng.* **2023**, *11* (3), 110108. https://doi.org/10.1016/j.jece.2023.110108.
15. Park, M.; Kwon, S.; Park, J.; Jo, J.; Yoo, Y.; Kang, D. Tailoring the Characteristics of Deep Eutectic Solvents Comprising Quaternized Linear Polyamine based on the Order of Amines for CO2 Capture. *Chem. Eng. J.* **2023**, *468*, 143552. https://doi.org/10.1016/j.cej.2023.143552.
16. Su, W. C.; Wong, D. S. H.; Li, M. H. Effect of Water on Solubility of Carbon Dioxide in (Aminomethanamide + 2-Hydroxy-N,N,N-Trimethylethanaminium Chloride). *J. Chem. Eng. Data* **2009**, *54* (6), 1951–1955. https://doi.org/10.1021/je900078k.
17. Xie, Y.; Dong, H.; Zhang, S.; Lu, X.; Ji, X. Effect of Water on the Density, Viscosity, and CO2 Solubility in Choline Chloride/Urea. *J. Chem. Eng. Data* **2014**, *59* (11), 3344–3352. https://doi.org/10.1021/je500320t.
18. Trivedi, T. J.; Lee, J. H.; Lee, H. J.; Jeong, Y. K.; Choi, J. W. Deep Eutectic Solvents as Attractive Media for CO2 Capture. *Green Chem.* **2016**, *18* (9), 2834–2842. https://doi.org/10.1039/c5gc02319j.
19. Anwer, S.; Alkhatib, I. I. I.; Salih, H. A.; Vega, L. F.; Alnashef, I. Investigating the Role of Water on CO2 Capture by Amine-based Deep Eutectic Solvents through a Combined Experimental-Molecular Modeling Approach. *Sep. Purif. Technol.* **2024**, *330*, 125350. https://doi.org/10.1016/j.seppur.2023.125350.
20. Shukla, S. K.; Mikkola, J. P. Intermolecular Interactions upon Carbon Dioxide Capture in Deep-Eutectic Solvents. *Phys. Chem. Chem. Phys.* **2018**, *20* (38), 24591–24601. https://doi.org/10.1039/c8cp03724h.
21. Nowosielski, B.; Jamróz-Niemczyk, M.; Łuczak, J.; Śmiechowski, M.; Warminska, D. Experimental and Predicted Physicochemical Properties of Monopropanolamine-based Deep Eutectic Solvents. *J. Mol. Liq.* **2020**, *309*, 113110. https://doi.org/10.1016/j.molliq.2020.113110.
22. Nowosielski, B.; Jamróz-Niemczyk, M.; Łuczak, J.; Tercjak, A.; Warminska, D. Effect of Temperature and Composition on Physical Properties of Deep Eutectic Solvents based on 2-(Methylamino)ethanol – Measurement and Prediction. *J. Mol. Liq.* **2023**, *371*, 121069. https://doi.org/10.1016/j.molliq.2022.121069.
23. Mjalli, F. S.; Murshid, G.; Al-Zakwani, S.; Hayyan, A. Monoethanolamine-based Deep Eutectic Solvents, their Synthesis and Characterization. *Fluid Phase Equil.* **2017**, *448*, 30–40. https://doi.org/10.1016/j.fluid.2017.03.008.
24. Liu, S.; Yu, D.; Chen, Y.; Shi, R.; Zhou, F.; Mu, T. High-Resolution Thermogravimetric Analysis Is Required for Evaluating the Thermal Stability of Deep Eutectic Solvents. *Ind. Eng. Chem. Res.* **2022**, *61* (38), 14347–14354. https://doi.org/10.1021/acs.iecr.2c02240.

25. Ghaedi, H.; Ayoub, M.; Sufian, S.; Lal, B.; Uemura, Y. Thermal Stability and FT-IR Analysis of Phosphonium-based Deep Eutectic Solvents with Different Hydrogen Bond Donors. *J. Mol. Liq.* **2017**, *242*, 395–403. https://doi.org/10.1016/j.molliq.2017.07.016.
26. Smith, E. L.; Abbott, A. P.; Ryder, K. S. Deep Eutectic Solvents (DESs) and Their Applications. *Chem. Rev.* **2014**, *114* (21), 11060–11082. https://doi.org/10.1021/cr300162p.
27. Wang, Y.; Hou, Y.; Wu, W.; Liu, D.; Ji, Y.; Ren, S. Roles of a Hydrogen Bond Donor and a Hydrogen Bond Acceptor in the Extraction of Toluene from N-Heptane using Deep Eutectic Solvents. *Green Chem.* **2016**, *18* (10), 3089–3097. https://doi.org/10.1039/c5gc02989k.
28. Ghaedi, H.; Ayoub, M.; Sufian, S.; Lal, B.; Shariff, A. M. Measurement and Correlation of Physicochemical Properties of Phosphonium-based Deep Eutectic Solvents at Several Temperatures (293.15 K–343.15 K) for CO2 Capture. *J. Chem. Thermodyn.* **2017**, *113*, 41–51. https://doi.org/10.1016/j.jct.2017.05.020.
29. Abbott, A. P.; Harris, R. C.; Ryder, K. S.; D'Agostino, C.; Gladden, L. F.; Mantle, M. D. Glycerol Eutectics as Sustainable Solvent Systems. *Green Chem.* **2011**, *13* (1), 82–90. https://doi.org/10.1039/c0gc00395f.
30. Florindo, C.; Oliveira, F. S.; Rebelo, L. P. N. N.; Fernandes, A. M.; Marrucho, I. M. Insights into the Synthesis and Properties of Deep Eutectic Solvents based on Cholinium Chloride and Carboxylic Acids. *ACS Sustain. Chem. Eng.* **2014**, *2* (10), 2416–2425. https://doi.org/10.1021/sc500439w.
31. Sun, W.; Liu, Q.; Zhao, J.; Muhammad Ali, H.; Said, Z.; Liu, C. Experimental Study on Sodium Acetate Trihydrate/Glycerol Deep Eutectic Solvent Nanofluids for Thermal Energy Storage. *J. Mol. Liq.* **2023**, *372*, 121164. https://doi.org/10.1016/j.molliq.2022.121164.
32. Gajardo-Parra, N. F.; Lubben, M. J.; Winnert, J. M.; Leiva, Á.; Brennecke, J. F.; Canales, R. I. Physicochemical Properties of Choline Chloride-based Deep Eutectic Solvents and Excess Properties of their Pseudo-Binary Mixtures with 1-Butanol. *J. Chem. Thermodyn.* **2019**, *133*, 272–284. https://doi.org/10.1016/j.jct.2019.02.010.
33. Ochędzan-Siodłak, W.; Dziubek, K.; Siodlak, D. Densities and Viscosities of Imidazolium and Pyridinium Chloroaluminate Ionic Liquids. *J. Mol. Liq.* **2013**, *177*, 85–93. https://doi.org/10.1016/j.molliq.2012.10.001.
34. Qin, H.; Hu, X.; Wang, J.; Cheng, H.; Chen, L.; Qi, Z. Overview of Acidic Deep Eutectic Solvents on Synthesis, Properties and Applications. *Green Energy Environ.* **2020**, *5* (1), 8–21. https://doi.org/10.1016/j.gee.2019.03.002.
35. Abbott, A. P.; Capper, G.; Gray, S. Design of Improved Deep Eutectic Solvents Using Hole Theory. *ChemPhysChem* **2006**, *7* (4), 803–806. https://doi.org/10.1002/cphc.200500489.
36. Omar, K. A.; Sadeghi, R. New Chloroacetic Acid-based Deep Eutectic Solvents for Solubilizing Metal Oxides. *J. Mol. Liq.* **2022**, *347*, 118393. https://doi.org/10.1016/j.molliq.2021.118393.
37. Omar, K. A.; Sadeghi, R. Novel Ninhydrin-based Deep Eutectic Solvents for Amino Acid Detection. *J. Mol. Liq.* **2020**, *303*, 112644. https://doi.org/10.1016/j.molliq.2020.112644.
38. Francisco, M.; van den Bruinhorst, A.; Kroon, M. C. Low-Transition-Temperature Mixtures (LTTMs): A New Generation of Designer Solvents. *Angew. Chemie Int. Ed.* **2013**, *52* (11), 3074–3085. https://doi.org/10.1002/anie.201207548.
39. Ijardar, S. P.; Singh, V.; Gardas, R. L. Revisiting the Physicochemical Properties and Applications of Deep Eutectic Solvents. *Molecules* **2022**, *27* (4), 1368. https://doi.org/10.3390/molecules27041368.
40. Zinov'eva, I. V.; Fedorov, A. Y.; Milevskii, N. A.; Zakhodyaeva, Y. A.; Voshkin, A. A. A Deep Eutectic Solvent Based on Choline Chloride and Sulfosalicylic Acid: Properties and Applications. *Theor. Found. Chem. Eng.* **2021**, *55* (3), 371–379. https://doi.org/10.1134/S0040579521030246.
41. Omar, K. A.; Sadeghi, R. Novel Benzilic Acid-based Deep-Eutectic-Solvents: Preparation and Physicochemical Properties Determination. *Fluid Phase Equil.* **2020**, *522*, 112752. https://doi.org/10.1016/j.fluid.2020.112752.
42. Kianpour, A.; Omar, K. A.; Sadeghi, R. Novel Deep Eutectic Solvents: Physical Properties and Their Application in Amino Acid Detection. *J. Chem. Eng. Data* **2022**, *67* (6), 1421–1427. https://doi.org/10.1021/acs.jced.2c00152.
43. Haider, M. B.; Hussain, Z.; Kumar, R. CO2 Absorption and Kinetic Study in Ionic Liquid Amine Blends. *J. Mol. Liq.* **2016**, *224*, 1025–1031. https://doi.org/10.1016/j.molliq.2016.10.044.
44. Danon, A.; Stair, P. C.; Weitz, E. FTIR Study of CO2 Adsorption on Amine-Grafted SBA-15: Elucidation of Adsorbed Species. *J. Phys. Chem. C* **2011**, *115* (23), 11540–11549. https://doi.org/10.1021/jp200914v.
45. Zubeir, L. F.; Van Osch, D. J. G. P.; Rocha, M. A. A.; Banat, F.; Kroon, M. C. Carbon Dioxide Solubilities in Decanoic Acid-Based Hydrophobic Deep Eutectic Solvents. *J. Chem. Eng. Data* **2018**, *63* (4), 913–919. https://doi.org/10.1021/acs.jced.7b00534.
46. Altamash, T.; Atilhan, M.; Aliyan, A.; Ullah, R.; Garcia, G.; Aparicio, S. Insights into Choline Chloride-Phenylacetic Acid Deep Eutectic Solvent for CO2 Absorption. *RSC Adv.* **2016**, *6* (110), 109201–109210. https://doi.org/10.1039/c6ra22312e.
47. Narku-Tetteh, J.; Muchan, P.; Idem, R. Effect of Alkanol Chain Length of Primary Alkanolamines and Alkyl Chain Length of Secondary and Tertiary Alkanolamines on their CO2 Capture Activities. *Sep. Purif. Technol.* **2017**, *187*, 453–467. https://doi.org/10.1016/j.seppur.2017.07.004.
48. Nowosielski, B.; Jamróz-Niemczyk, M.; Łuczak, J.; Warmińska, D. Novel Binary Mixtures of Alkanolamine Based Deep Eutectic Solvents with Water – Thermodynamic Calculation and Correlation of Crucial Physicochemical Properties. *Molecules* **2022**, *27* (3), 788. https://doi.org/10.3390/molecules27030788.

Supplementary Material: This article contains supplementary material (https://doi.org/10.1515/pac-2024-0228).

Table S1 The abbreviation, molar mass, molar ratio, mass fraction and water content for chemicals used in synthesis of 3-aminepropan-1-ol based DESs.

DES		Salt		HBD		Molar ratio		Mass fraction[a]		Water content[b]
Symbol	M_{DES} / g mol^{-1}	Abbreviation	M_{salt} / g mol^{-1}	Abbreviation	M_{HBD} / g mol^{-1}	Salt	HBD	Salt	HBD	
DES10	124.229	TBAB	322.37	AP	75.11	1	4	0.5155	0.4845	0.00066
DES11	110.405	TBAB	322.37	AP	75.11	1	6	0.4168	0.5832	0.00053
DES12	102.580	TBAB	322.37	AP	75.11	1	8	0.3488	0.6512	0.00054
DES13	93.265	TEAC	165.71	AP	75.11	1	4	0.3650	0.6440	0.00156
DES14	88.072	TEAC	165.71	AP	75.11	1	6	0.2692	0.7308	0.00127
DES15	85.189	TEAC	165.71	AP	75.11	1	8	0.2164	0.7836	0.00125
DES16	115.834	TBAC	277.92	AP	75.11	1	4	0.4818	0.5182	0.00178
DES17	103.851	TBAC	277.92	AP	75.11	1	6	0.3792	0.6208	0.00121
DES18	97.696	TBAC	277.92	AP	75.11	1	8	0.3168	0.6832	0.00202

[a] The standard uncertainty of DES mass fraction composition is 0.001

[b] Water content of DESs in mass fraction determined by Karl Fisher titration with the standard uncertainty ±0.0001.

Table S2 The abbreviation, molar mass, molar ratio, mass fraction and water content for chemicals used in synthesis of 2-(methylamino)ethanol based DESs.

DES		Salt		HBD		Molar ratio		Mass fraction[a]		Water content[b]
Symbol	M_{DES} / g·mol^{-1}	Abbreviation	M_{salt} / g·mol^{-1}	Abbreviation	M_{HBD} / g·mol^{-1}	Salt	HBD	Salt	HBD	
DES19	110.601	TBAB	322.37	MAE	75.11	1	6	0.4183	0.5817	0.00154
DES20	102.072	TBAB	322.37	MAE	75.11	1	8	0.3444	0.6556	0.00183
DES21	97.675	TBAB	322.37	MAE	75.11	1	10	0.3012	0.6988	0.00204
DES22	87.915	TEAC	210.16	MAE	75.11	1	6	0.2664	0.7336	0.00168
DES23	85.206	TEAC	210.16	MAE	75.11	1	8	0.02167	0.7833	0.00182
DES24	83.390	TEAC	210.16	MAE	75.11	1	10	0.1816	0.8184	0.00210
DES25	104.336	TBAC	277.92	MAE	75.11	1	6	0.3838	0.6162	0.00203
DES26	97.629	TBAC	277.92	MAE	75.11	1	8	0.3161	0.6839	0.00247
DES27	93.574	TBAC	277.92	MAE	75.11	1	10	0.2704	0.7296	0.00276

[a] The standard uncertainty of DES mass fraction composition is 0.001

[b] Water content of DESs in mass fraction determined by Karl Fisher titration with the standard uncertainty ±0.0001.

Table S3. Experimental densities of deep eutectic solvents (DESs) within temperature range T = (293.15 to 333.15) K and P = 0.1 MPa[a].

T / K	DES1	DES2	DES3	DES4	DES5	DES6	DES7	DES8	DES9
				d / kg·m−3					
293.15	937.6	928.9	922.4	911.5	907.7	904.9	901.1	899.5	898.2
298.15	934.0	925.2	918.8	908.0	904.1	901.3	897.7	896.0	894.6
303.15	930.3	921.6	915.1	904.5	900.5	897.7	894.2	892.5	891.1
308.15	926.7	917.9	911.5	901.0	896.9	894.1	890.7	888.9	887.5
313.15	923.1	914.2	907.8	897.5	893.4	890.5	887.3	885.4	884.0
318.15	919.5	910.6	904.1	893.9	889.8	886.9	883.8	881.9	880.4
323.15	915.9	906.9	900.4	890.4	886.2	883.2	880.4	878.4	876.8
328.15	912.2	903.2	896.7	886.9	882.6	879.6	876.9	874.8	873.2
333.15	908.6	899.6	893.0	883.4	879.0	875.9	873.4	871.3	869.7

[a] Standard uncertainties u are $u(T)$ 0.01 K, $u(p)$ 0.001 MPa, $u(d)$ 0.1 kg·m^{-3}

Table S4 Experimental viscosities, η, of deep eutectic solvents within temperature range T (293.15 to 333.15) K and P 0.100 MPa[a].

T / K	DES1	DES2	DES3	DES4	DES5	DES6	DES7	DES8	DES9
				η / mPa·s					
293.15	60.6	48.3	46.2	36.0	32.4	30.6	54.0	45.7	44.0
298.15	46.4	35.0	34.9	28.2	25.9	24.1	40.8	34.9	33.6
303.15	35.6	28.3	27.9	22.4	20.6	19.3	31.5	27.2	26.5
308.15	27.6	22.3	22.2	18.2	16.6	15.4	24.7	21.5	20.8
313.15	21.7	17.7	17.4	14.7	13.5	12.5	19.9	17.2	16.6
318.15	17.3	14.2	14.2	12.1	11.1	10.3	15.9	13.9	13.7
323.15	14.0	11.6	11.5	10.0	9.2	8.5	12.9	11.3	11.2
328.15	11.5	9.6	9.5	8.4	7.6	7.0	10.6	9.3	9.2
333.15	9.5	7.8	7.8	7.1	6.4	5.9	8.8	7.7	7.6

[a] Standard uncertainties u are $u(T)$ =0.01 K, $u(p)$= 0.001 MPa, $u(\eta)$ = 2%

Table S5. Fitting parameters for the Arrhenius equation for dynamic viscosity results of BAE-based DESs determined within temperature range T = (293.15 to 333.15) K and P = 0.1 MPa.

DES	η_∞ / 10^5 mPa·s	E_a /·10^{-4} J mol^{-1}	R^2	RMSD
DES1	0.79	3.86	0.9997	0.31
DES2	0.86	3.76	0.9981	0.59
DES3	1.52	3.64	0.9986	0.47
DES4	3.57	3.38	0.9996	0.21
DES5	3.84	3.33	0.9999	0.09
DES6	2.92	3.38	0.9999	0.09
DES7	1.00	3.77	0.9991	0.45
DES8	1.23	3.68	0.9995	0.28
DES9	1.50	3.63	0.9993	0.33

Table S6 Fitting parameters for the Vogel-Fulcher-Tammann (VFT) equation for dynamic viscosity results of BAE-based DESs determined within temperature range T = (293.15 to 333.15) K and P = 0.1 MPa.

DES	η_0 / mPa·s	B / K	T_0 / K	R^2	RMSD
DES1	0.0011	2113.8	99.6	0.99993	0.019
DES2	0.0194	1055.8	158.0	0.99933	0.019
DES3	0.0042	1604.7	120.7	0.99913	0.013
DES4	0.0055	1548.3	117.0	0.99998	0.002
DES5	0.0003	2886.5	46.2	0.99992	0.078
DES6	0.0006	2455.3	68.2	0.99997	0.045
DES7	0.0110	1264.1	144.5	0.99996	0.009
DES8	0.0039	1608.5	121.7	0.99999	0.001
DES9	0.0066	1428.3	131.0	0.99991	0.013

Table S7 Experimental refractive indices, n_D of deep eutectic solvents within temperature range T = (293.15 to 333.15) K and P = 0.100 MPa[a].

T / K	DES1	DES2	DES3	DES4	DES5	DES6	DES7	DES8	DES9
				n_D					
293.15	1.4595	1.4570	1.4541	1.4547	1.4520	1.4510	1.4549	1.4528	1.4512
298.15	1.4573	1.4550	1.4523	1.4528	1.4500	1.4487	1.4528	1.4509	1.4493
303.15	1.4556	1.4529	1.4506	1.4509	1.4482	1.4468	1.4510	1.4490	1.4474
308.15	1.4538	1.4511	1.4488	1.4490	1.4462	1.4449	1.4492	1.4472	1.4455
313.15	1.4521	1.4491	1.4469	1.4471	1.4445	1.4431	1.4473	1.4452	1.4439
318.15	1.4503	1.4473	1.4451	1.4455	1.4425	1.4411	1.4456	1.4433	1.4417
323.15	1.4484	1.4452	1.4430	1.4438	1.4408	1.4391	1.4439	1.4415	1.4399
328.15	1.4468	1.4433	1.4412	1.4420	1.4389	1.4369	1.4420	1.4391	1.4378
333.15	1.4450	1.4411	1.4393	1.4403	1.4370	1.4351	1.4399	1.4374	1.4357

[a] Standard uncertainties u are $u(T)$ 0.1 K, $u(p)$ 0.001 MPa, $u(n_D)$ 0.0002

Table S8 Experimental speed of sound values, u, for DESs within temperature range T (293.15 to 333.15) K and P = 0.100 MPa[a].

T / K	DES1	DES2	DES3	DES4	DES5	DES6	DES7	DES8	DES9
				u / m·s^{-1}					
293.15	1431.7	1427.5	1424.8	1453.5	1441.4	1433.2	1450.2	1443.5	1438.5
298.15	1415.7	1411.5	1408.7	1437.5	1425.3	1417.1	1434.2	1427.5	1422.5
303.15	1399.8	1395.5	1392.6	1421.7	1409.4	1401.0	1418.4	1411.6	1406.7
308.15	1384.0	1379.7	1376.7	1406.0	1393.4	1385.1	1402.7	1395.9	1391.0
313.15	1368.4	1364.0	1360.9	1390.4	1377.6	1369.3	1387.2	1380.2	1375.5
318.15	1352.9	1348.3	1345.2	1374.9	1361.9	1353.5	1371.7	1364.6	1360.0
323.15	1337.4	1332.7	1329.5	1359.4	1346.3	1337.8	1356.3	1349.1	1344.5
328.15	1321.8	1317.2	1313.8	1344.0	1330.7	1322.1	1340.9	1333.6	1328.9
333.15	1306.5	1301.7	1298.2	1453.5	1441.4	1433.2	1325.5	1318.1	1313.5

[a] Standard uncertainties u are $u(T)$ =0.01 K, $u(p)$= 0.001 MPa, $u(u)$ = 0.5 m·s^{-1}

Table S9 Theoretical calculation of the CO_2 capacity of different solutions of TBAB ($g_{CO2}\ g_{DES}^{-1}$).

DES	%wt. of water in aqueous solutions of DES	c exp. /$g_{CO2}\ g_{DES}^{-1}$	c theor. /$g_{CO2}\ g_{DES}^{-1}$	increase/decrease / %
TBAB:AP	0	0.177	-	-
	0.5	0.170	0.176	-3
	1	0.151	0.175	-14
	5	0.140	0.168	-27
TBAB:MAE	0	0.161	-	-
	0.5	0.179	0.160	12
	1	0.171	0.159	7
	5	0.123	0.152	-19
TBAB:BAE	0	0.142	-	-
	0.5	0.114	0.141	-19
	1	0.102	0.140	-27
	5	0.081	0.134	-40

Table S10 Molecular volume of BAE-based DESs at 298.15 K.

DES	$V_m / 10^4\ m^3 mol^{-1}$
DES1	1.57
DES2	1.51
DES3	1.47
DES4	1.37
DES5	1.36
DES6	1.35
DES7	1.56
DES8	1.51
DES9	1.47

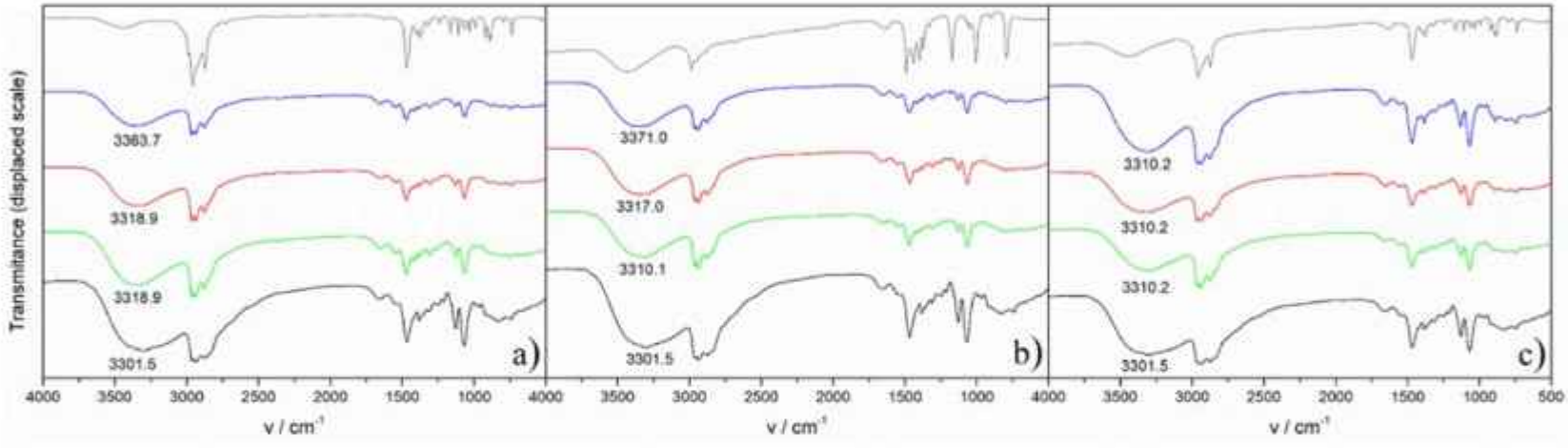

Figure S1 FTIR spectra for DESs containing BAE: a) TBAB:BAE (DES 1–3), b) TEAC:BAE (DES 4–6) and c) TBAC:BAE (DES 7–9); (blue – 1:6, red – 1:8,green – 1:10; black –neat BAE, grey - corresponding ammonium salt).

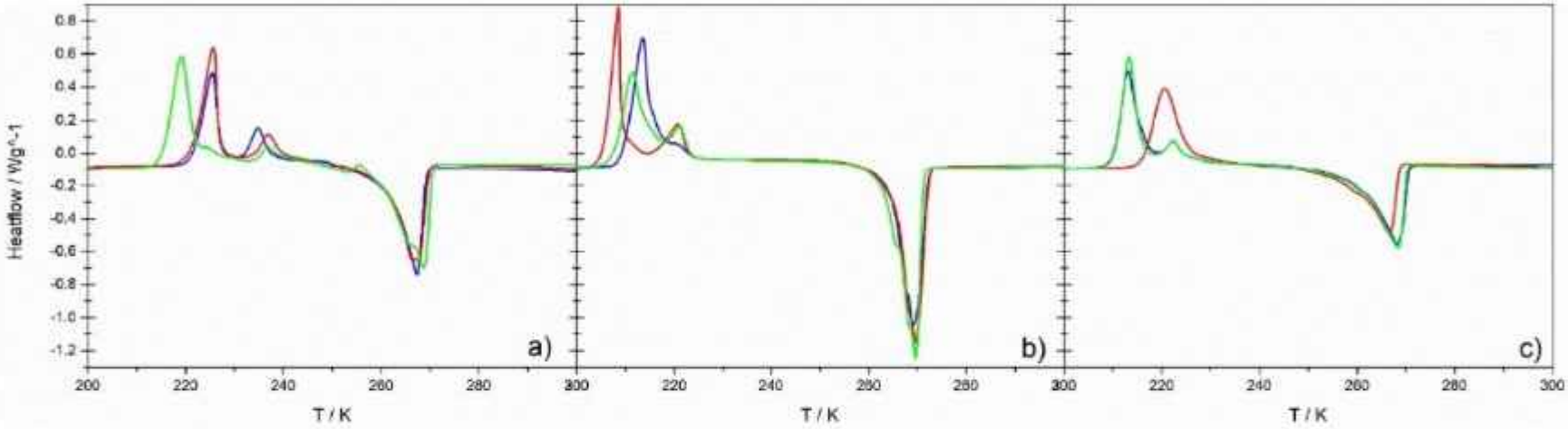

Figure S2 DSC curves for DESs containing BAE: a) TBAB:BAE (DES 1-3) , b) TEAC:BAE (DES 4-6) and c) TBAC:BAE (DES 7-9); (blue line – 1:6, red line – 1:8, green line– 1:10).

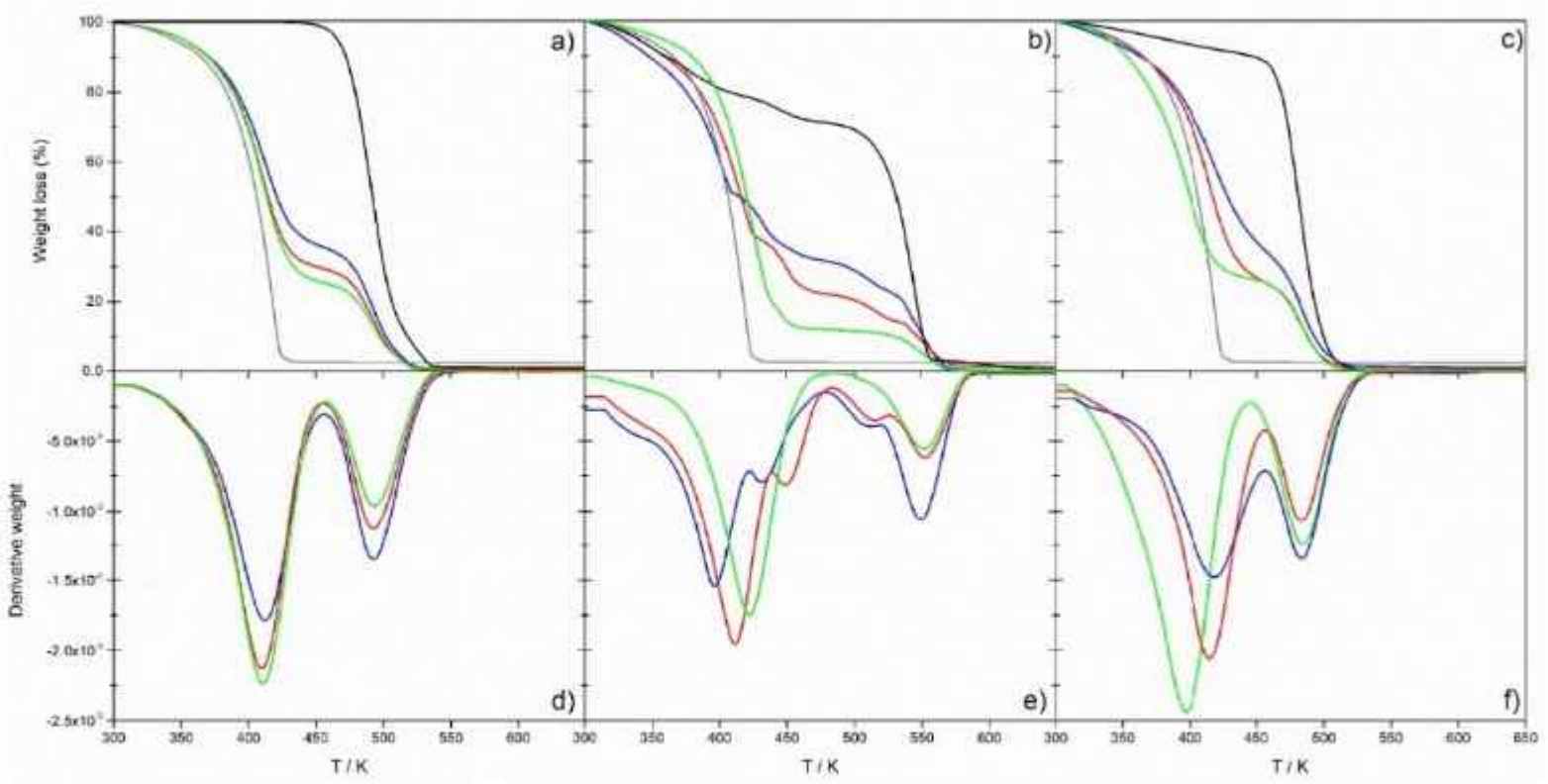

Figure S3 TGA curves: (a, b, c) and DTGA curves: (d, e, f) obtained by thermogravimetry of DESs containing BAE: a) and d) TBAB:BAE (DES 1-3) , b) and e) TEAC:BAE (DES 4-6); c) and f) TBAC:BAE (DES 7-9); (blue line – 1:6, red line – 1:8, green line – 1:10, black– salt, grey– BAE).

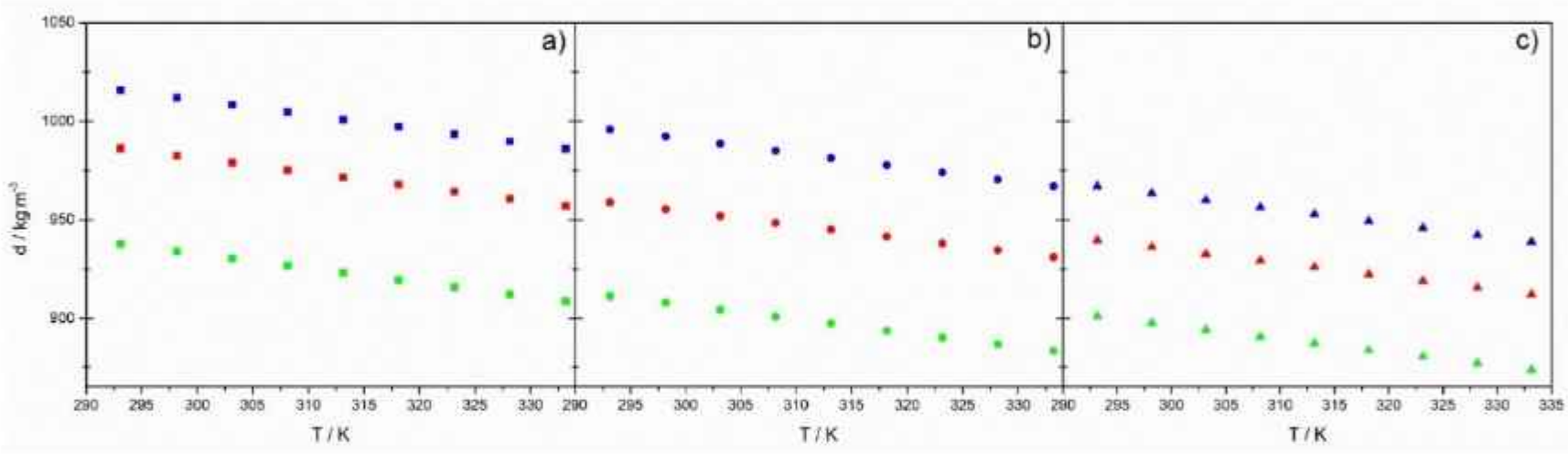

Figure S4 Densities of deep eutectic solvents studied as a function of temperature in the range of 293.15–333.15 K and at atmospheric pressure for various DESs at molar ratio 1:6 a) TBAB-based b) TEAC-based and c) TBAC-based (blue -AP, red – MAE, green BAE.

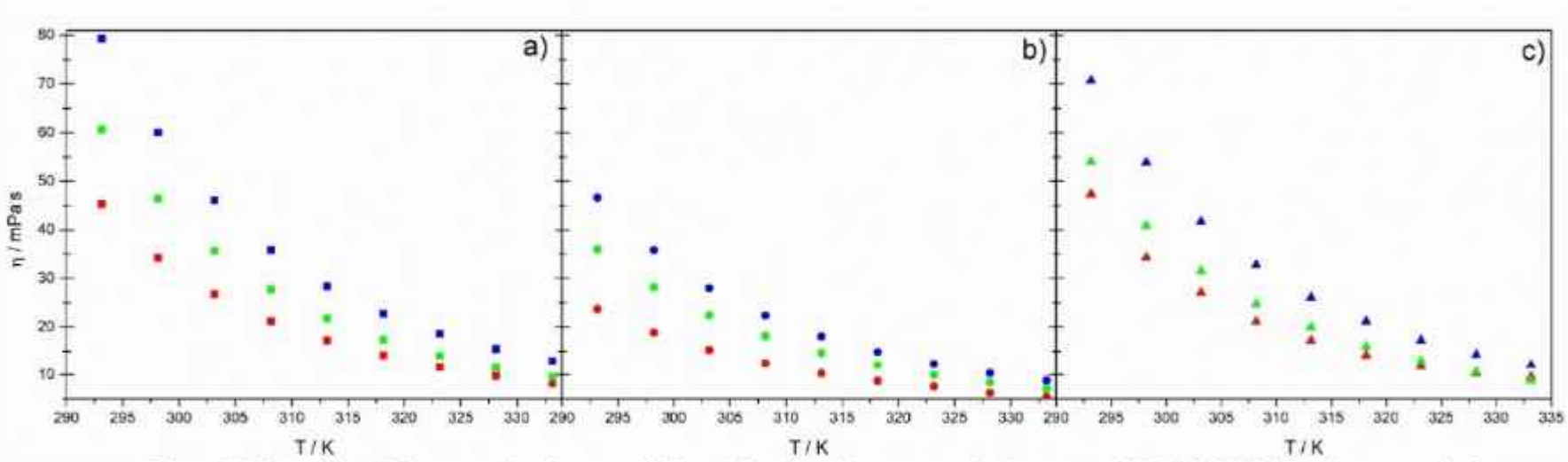

Figure S5 Viscosities of deep eutectic solvents studied as a function of temperature in the range of 293.15–333.15 K and at atmospheric pressure for various DESs at molar ratio 1:6 a) TBAB-based b) TEAC-based and c) TBAC-based (blue -AP, red – MAE, green BAE

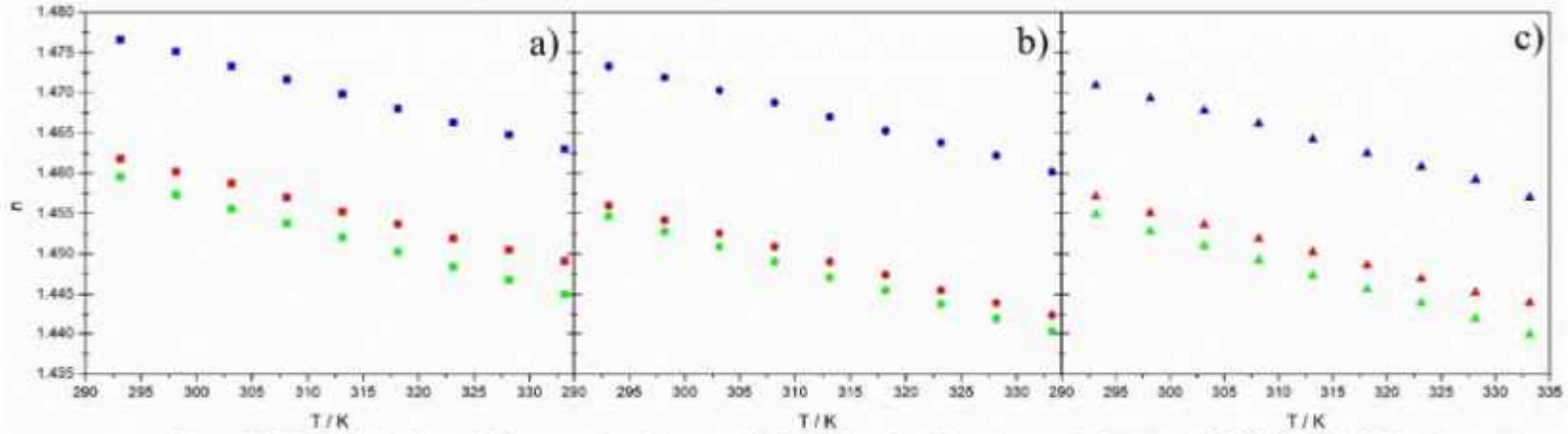

Figure S6 Refractive indices of deep eutectic solvents studied as a function of temperature in the range of 293.15–333.15 K and at atmospheric pressure for various DESs at molar ratio 1:6 a) TBAB-based b) TEAC-based and c) TBAC-based (blue -AP, red – MAE, green BAE

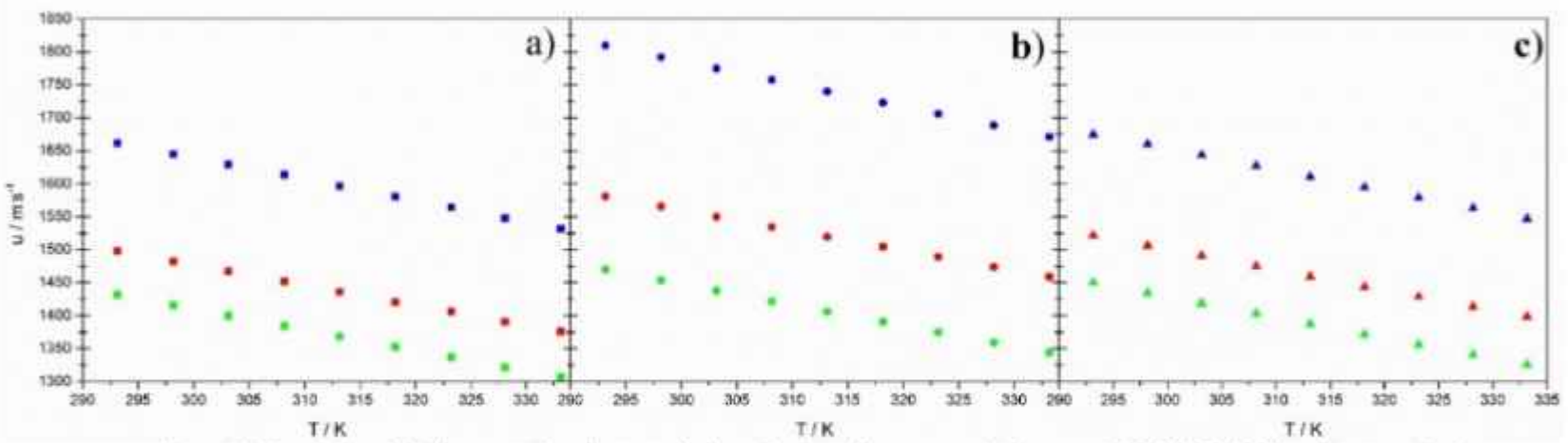

Figure S7 Speed of sound of deep eutectic solvents studied as a function of temperature in the range of 293.15–333.15 K and at atmospheric pressure for various DESs at molar ratio 1:6 a) TBAB-based b) TEAC-based and c) TBAC-based (blue -AP, red – MAE, green BAE.

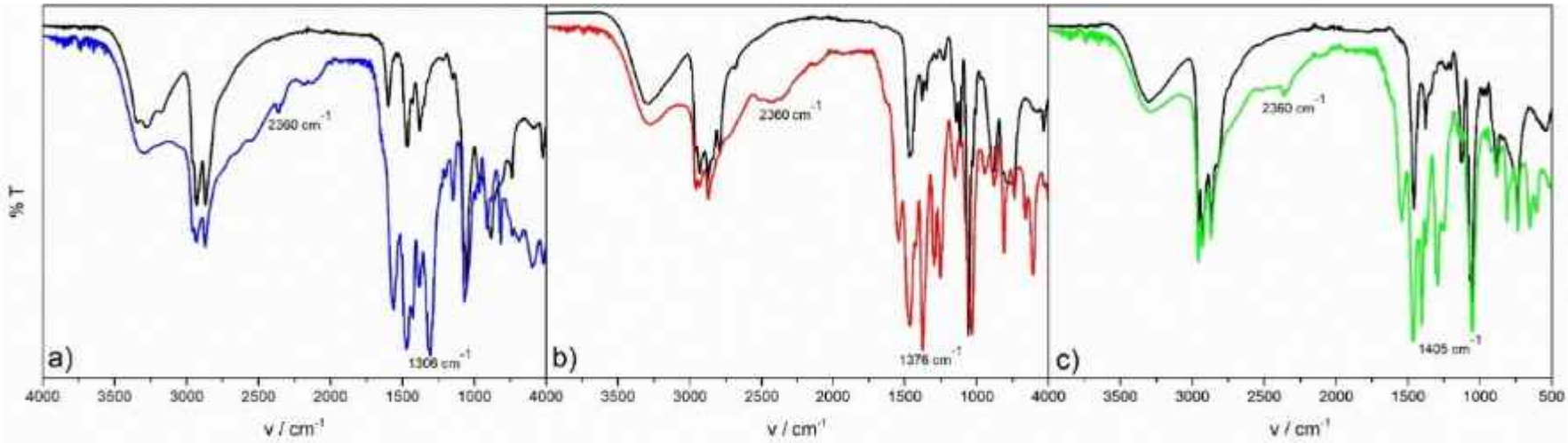

Figure S8 FTIR spectra of pure DESs (black line) and different TBAB based DESs after CO_2 absorption (colour line) a) TBAB:AP 1:6; b) TBAB:MAE 1:6; c) TBAB:BAE 1:6.

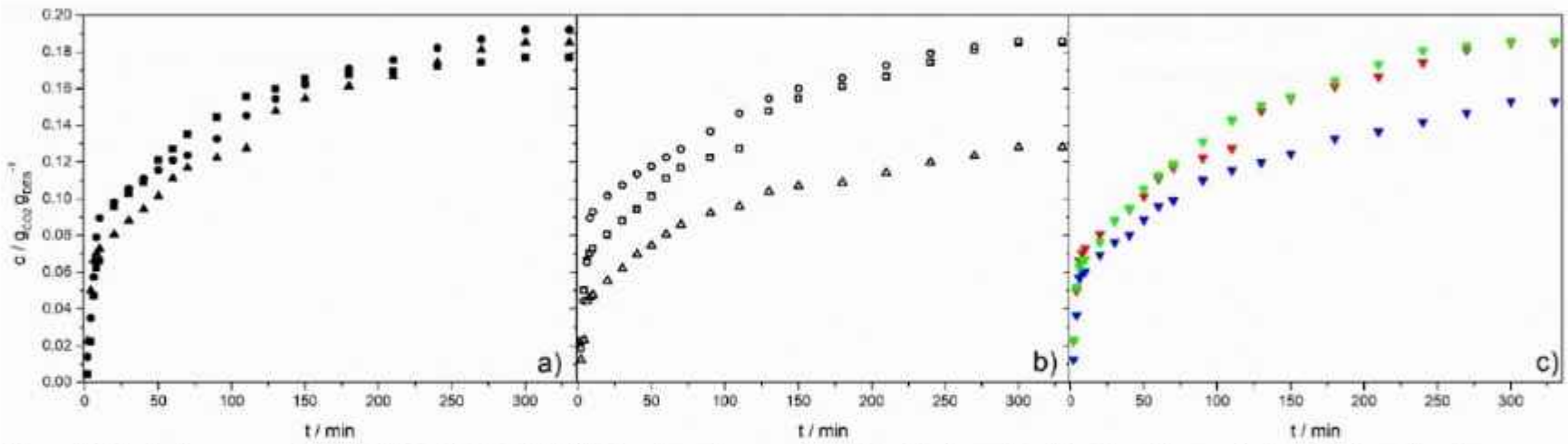

Figure S9 The influence on a) HBA; b) HBD c) HBA/HBD molar ratio on carbon dioxide absorption kinetics. The symbols and colors denotes ■ – TBAB:AP 1:6 ● - TEAC:AP 1:6 ▲ - TBAC:AP 1:6; □ – TBAC:AP 1:6 ○ - TBAC:MAE 1:6 △ - TBAC:BAE 1:6 ▼ - TBAC:AP; blue 1:4; red 1:6; green 1:

Załącznik A5

B. Nowosielski, M. Jamrógiewicz, J. Łuczak, D. Warmińska, Novel Binary Mixtures of Alkanolamine Based Deep Eutectic Solvents with Water—Thermodynamic Calculation and Correlation of Crucial Physicochemical Properties, Molecules 27 (2022) 788. https://doi.org/10.3390/molecules27030788. **IF_{2022}: 4,6, $MNSW_{2022}$: 140**

molecules

Article

Novel Binary Mixtures of Alkanolamine Based Deep Eutectic Solvents with Water—Thermodynamic Calculation and Correlation of Crucial Physicochemical Properties

Bartosz Nowosielski [1], Marzena Jamróg iewicz [2], Justyna Łuczak [3] and Dorota Warmińska [3,*]

[1] Department of Physical Chemistry, Faculty of Chemistry, Gdańsk University of Technology, ul. Narutowicza 11/12, 80-233 Gdańsk, Poland; bartosz.nowosielski@pg.edu.pl
[2] Department of Physical Chemistry, Faculty of Pharmacy, Medical University of Gdańsk, Al. Gen. Hallera 107, 80-416 Gdańsk, Poland; marzena.jamrogiewicz@gumed.edu.pl
[3] Department of Process Engineering and Chemical Technology, Faculty of Chemistry, Gdańsk University of Technology, ul. Narutowicza 11/12, 80-233 Gdańsk, Poland; justyna.luczak@pg.edu.pl
* Correspondence: dorwarm@pg.edu.pl; Tel.: +48-583471410

Abstract: This paper demonstrates the assessment of physicochemical and thermodynamic properties of aqueous solutions of novel deep eutectic solvent (DES) built of tetrabutylammonium chloride and 3-amino-1-propanol or tetrabutylammonium bromide and 3-amino-1-propanol or 2-(methylamino)ethanol or 2-(butylamino)ethanol. Densities, speeds of sound, refractive indices, and viscosities for both pure and aqueous mixtures of DES were investigated over the entire range of compositions at atmospheric pressure and T = (293.15 - 313.15) K. It was concluded that the experimental data were successfully fitted using the Jouyban–Acree model with respect to the concentration. Obtained results showed that this mathematical equation is an accurate correlation for the prediction of aqueous DES properties. Key physicochemical properties of the mixtures—such as excess molar volumes, excess isentropic compressibilities, deviations in viscosity, and deviations in refractive indices—were calculated and correlated by the Redlich–Kister equation with temperature-dependent parameters. The non-ideal behavior of the studied systems were also evaluated by using the Prigogine–Flory–Patterson theory and the results were interpreted in terms of interactions between the mixture components.

Keywords: DES; deep eutectic solvents; aqueous mixtures; excess properties; JAM; PFP

check for updates

Citation: Nowosielski, B.; Jamróg iewicz, M.; Łuczak, J.; Warmińska, D. Novel Binary Mixtures of Alkanolamine Based Deep Eutectic Solvents with Water—Thermodynamic Calculation and Correlation of Crucial Physicochemical Properties. *Molecules* **2022**, *27*, 788. https://doi.org/10.3390/molecules27030788

Academic Editor: Reza Haghbakhsh

Received: 29 December 2021
Accepted: 25 January 2022
Published: 29 January 2022

1. Introduction

Deep eutectic solvents (DES) are very important and well-known components or materials used often in chemistry but also in other industries as pharmacy, chemical technology as an inexpensive solvent/component being sustainable alternative to the conventional organic solvents which are non-ecological. Currently, the advancement of different DES had enabled the production of materials for unique purpose for reaction medium, biodiesel processes, metal electrodeposition, nanotechnology, and others [1]. Global research is still focused on the developing new innovative DES which will probably replace non-ecological classic solvents as well [2,3].

Deep eutectic solvents, based on urea and quaternary ammonium salts, were first reported by Abbott et al. [4]. Since then many derivatives have been invented and applied. Generally, DESs are built from hydrogen bond acceptor (HBA) and hydrogen bond donor (HBD) in the appropriate molar ratio forming complexes through hydrogen bonds. As a result, deep eutectic solvents have a lower melting point than their components [5].

DESs share many properties with room temperature ionic liquid (RTIL). They are practically non-volatile and non-flammable, and exhibit high thermal and electro-chemical stability, but are definitely cheaper, less toxic, and often biodegradable in comparison

with RTIL [6]. Additionally, since the physical properties of DES are dependent on the composition and proportions of the components making up a given eutectic mixture, it is possible to propose a particular composition whose properties should be applied specifically [1,7].

Deep eutectic solvents are highly hygroscopic liquids, so trace amounts of water are often unavoidable as impurity [8]. However, depending on the application, water can be deliberately added to the DES to modulate the physicochemical properties of the solvent, especially mass transfer properties such as viscosity.

Aqueous mixtures of DES have already been used in nanoparticle synthesis [9], carbon dioxide absorption [10,11], and as media in chemical reactions [12]. Some conflicting information is found in the literature regarding the impact of water in DES on processes of CO_2 absorption. Su et al. [10] discovered that even a small addition of water to DES composed of choline chloride (ChCl) and urea reduces the solubility of carbon dioxide, while Li et al. [11] concluded that the solubility of CO_2 increases in tetramethylammonium chloride and monoethanolamine DES after the addition of H_2O, and reaches a maximum at 10% water content. Therefore, since the water content has a great influence on the physicochemical properties of deep eutectic solvents, it is crucial to control it in aqueous DES solutions from a technological point of view and in further application. A significant part of the research carried out so far has been devoted to the properties of pseudo-pure DES [13–16]. Thermodynamic properties of aqueous DESs are also rarely published [17]. Kuddushi et al. measured densities of aqueous solution of DES composed of ChCl with glutaric acid and malonic acid [18]. They calculated excess molar volume (V_m^E) for those systems that found to be negative, indicating strong interactions between water and DES molecules. Additionally, volumetric properties were described for such aqueous DES systems as: allyltriphenyl phosphonium bromide (ATPPB) with diethylene glycol (DEG) [19] or triethylene glycol (TEG) [20], ChCl with ethylene glycol or glycerol [21] and ChCl with lactic acid [22].

Studies that consider other properties of aqueous DES solutions—such as acoustic properties [18], refractive indices [21,23], and viscosities [23,24]—are still rare and not popular. All of them confirm that the interactions between DES and water molecules significantly influence on thermodynamic properties of aqueous DES solutions.

In general, most of the research that has been carried out to date on deep eutectic solvents as potential CO_2 absorbers are devoted to DESs in which physical absorption of carbon dioxide occurs. The carbon dioxide absorption capacity in those DESs is lower than that in commercially used absorbers therefore their potential application in industry is significantly limited. Therefore, the aim of this work is to characterize and better understand the water solutions of deep eutectic solvents based on alkanolamines with chemical absorption capacity in terms of their suitability for the effective separation of carbon dioxide from gas streams at relatively low pressure. It is known from the literature that carbon dioxide capacity, apart from others factors, depends also on the strength of intermolecular interactions between DES components [25,26]. As the interactions between HBA and HBD increase, the CO_2 solubility decreases. Similar effects can be expected for aqueous solutions of DESs, where increasing strength of the DES-H2O interactions might result in a decrease of carbon dioxide capacity due to the weaker interactions between CO_2 and DES [27]. The final effect of the presence of water in DES on the solubility of CO_2 will also depend on which of the components (DES or water) will have the greater affinity for the gas absorbed. Herein, we prepared deep eutectic solvents built of tetrabutylammonium bromide with 3-amino-1-propanol (AP), 2-(methylamino)ethanol (MAE), or 2-(butylamino)ethanol (BAE) and tetrabutylammonium chloride (TBAC) with AP, at 1:6 molar ratios. Then, the physicochemical properties of pure and aqueous solutions of DESs as density, speed of sound, viscosity, and refractive index were measured, and Jouyban–Acree predictive model (JAM) was used to correlate the experimental data. Several mathematical models for the correlation of physical properties of binary mixtures can be found in the literature [28]. However, these models were used mainly to correlate the

density of mixtures. Thus, we decided to use the JAM equation, as so far it has also been used to predict the viscosity of two-component mixtures of classical solvents [29]. Thermodynamic excess properties—including excess molar volume, excess isobaric thermal expansion, excess isentropic compressibility, deviation in refractive indices, deviation in viscosities, and excess Gibbs energy of activation for viscous flow—were calculated and correlated by the Redlich–Kister-type polynomial equation considered as the most common and accurate mathematical model for this purpose. Prigogine–Flory–Patterson Theory (PFP) was used to correlate the experimental excess molar volume as the most accepted theory to interpret the behavior of non-ideal liquid solution, which has been applied to many mixtures of classical solvents as well as to systems containing ionic liquids and some aqueous solutions of DESs. The effect of the HBA anion type of obtained DES solutions was evaluated as well as the order and length of the alkyl chain of each alkanolamine were discussed. The influence of temperature on thermodynamic properties of DES solutions was also involved in this study.

2. Materials and Methods

2.1. Chemicals

The chemicals used in this study—3-amino-1-propanol (AP), 2-(methylamino)ethanol (MAE), 2-(butylamino)ethanol (BEA), tetrabutylammonium bromide (TBAB), and tetrabutylammonium chloride (TBAC)—were purchased from Sigma-Aldrich. TBAC was purified by double crystallization from acetone by adding diethyl ether. All salts were dried under reduced pressure before use, TBAB at 323 K for 48 h while TBAC at 298.15 K for several days. The corresponding information and the chemical structures of the DESs components are presented in Table 1.

Table 1. Provenance, mass fraction purity, and chemical structures of the compounds studied.

Chemical Name	Source	CAS Number	Molecular Weight M/(g·mol^{-1})	Mass Fraction Purity	Chemical Structure
3-amino-1-propanol (AP)	Sigma Aldrich	156-87-6	75.11	0.99 [a]	
2-(methylamino)-ethanol (MEA)	Sigma Aldrich	109-83-1	75.11	≥98 [a]	
2-(butylamino)-ethanol (BEA)	Sigma Aldrich	111-75-1	117.19	≥98 [a]	
tetrabutylammonium bromide (TBAB)	Sigma Aldrich	1643-19-2	322.37	≥0.99 [a]	
tetrabutylammonium chloride (TBAC)	Sigma Aldrich	1112-67-0	277.92	≥0.98 [b]	

[a] As stated by supplier. [b] After crystalization, determined by potentiometric titration.

2.2. Preparation of DESs and Their Aqueous Solutions

DESs were prepared by mass with the same molar ratio of 1:6 salt to amino alcohol. The weighing was done using an analytical balance (Mettler Toledo) with the precision

of 0.1 mg. The standard uncertainty in the mass fraction was estimated to be less than $\pm 1 \times 10^{-4}$. The combinations of the quaternary ammonium salts and AP/MAE/BEA were mixed at 353.15 K for 1 h using a magnetic stirrer in a fume hood until a homogeneous and uniform liquid without any precipitate was formed. Water content of DESs was measured using a Mettler Toledo Coulometric Karl–Fischer titrator (899 Coulometer apparatus from Metrohm) and it was found to be less than 0.0016 mass fraction. Table 2 displays the abbreviation of chemicals and DESs along with their molar mass, molar ratio, mass fraction, and water content.

Table 2. Abbreviations of chemicals and DESs along with their molar mass, molar ratio, mass fraction, and water content.

Symbol	HBA	HBD	Molar Ratio	M_{DES}/ (g·mol^{-1})	Mass Fraction of HBA [a]	Water Content [b]
DES1	TBAB	AP	1:6	110.449	0.4172	0.00059
DES2	TBAC	AP	1:6	104.091	0.3815	0.00121
DES3	TBAB	MAE	1:6	110.433	0.4170	0.00118
DES4	TBAB	BAE	1:6	146.519	0.3145	0.00159

[a] The standard uncertainty of DES mass fraction composition is 0.0001. [b] Water content of DESs in mass fraction determined by Karl Fisher titration with the standard uncertainty ±0.0001.

Deionized, double distilled, degassed water with a specific conductance of 1.15×10^{-6} S·cm^{-1} was used for the preparation of aqueous mixtures of DESs. The water contents in DES was accounted for upon solution preparation.

2.3. *Physical Properties Measurements*

2.3.1. Density and Speed of Sound

Measurements of density and speed of sound were performed by using a digital vibration-tube analyzer (Anton Paar DSA 5000, Graz, Austria) with proportional temperature control that kept the samples at working temperature with an accuracy of 0.01 K. Experimental frequency for the measurements of the ultrasonic speed was equal to 3 MHz. The apparatus was calibrated with double distilled deionized and degassed water and dry air at atmospheric pressure according to the apparatus catalog procedure. The experimental uncertainty of density and ultrasonic velocity measurements was better than 35×10^{-3} kg m^{-3} and 2×10^{-1} m s^{-1}, respectively.

2.3.2. Viscosity

Viscosities of the solvents were determined using LVDV-III Programmable Rheometer (cone-plate viscometer; Brookfield Engineering Laboratory, USA), controlled by a computer. The temperature of the samples was controlled within ± 0.01K using a thermostatic water bath (PolyScience 9106, Niles, IL, USA). The display of the viscosimeter was verified with certified viscosity standard N100 and S3 provided by Cannon at 298.15 ± 0.01 K. The standard uncertainty of viscosity measurement was better than 1%.

2.3.3. Refractive Index

The refractive indices were measured using an Abbe refractometer (RL-3, Warsaw, Poland) equipped with a thermostat for controlling the cell temperature with an accuracy of ±0.1 K. The standard uncertainty of refractive index measurement on the n_D scale was 0.0002. At least three independent measurements were taken for each sample at each temperature to assure reproducibility of the measurement.

2.3.4. Isobaric Heat Capacity

A Mettler Toledo Star One differential scanning calorimeter (DSC), STAR-1 System (Mettler Toledo, Greifensee, Switzerland), was used to measure specific heat capacities of novel DESs. The DSC instrument was calibrated by the indium standard prior to sample

measurements. During the measurement, an inert atmosphere was created under a nitrogen flow of 60 mL min^{-1}. The sapphire method for cp determination was used [30]. A 'baseline' or blank measurement was performed for heating rate 10 K min^{-1}. All of the results obtained were blank curve corrected and performed twice. The test material and the reference were placed into individual aluminium crucibles which were then sealed with pierced lids. The data from the DSC were recorded and then analyzed to obtain the *Cp* from the data.

3. Results and Discussion

3.1. Physical Properties of Binary Mixtures

The experimental values of density, speed of sound, viscosity, and refractive indices for aqueous solutions of DESs consisting of tetrabutylammonium bromide and 3-amino-1-propanol or 2-(methylamino)ethanol or 2-(butylamino)ethanol and for the aqueous solutions of DES built of tetrabutylammonium chloride and 3-amino-1-propanol over the entire range of compositions at temperatures ranging from 293.15 K to 313.15 K are reported in Tables S1–S4. Moreover, in Figure 1 the physical properties are plotted as a function of the DES molar fraction at 298.15 K for all systems studied. As it can be observed, depending on the properties, its dependence on the deep eutectic solvent content varies. Moreover, all trends are nonlinear, indicating deviation from the ideal course.

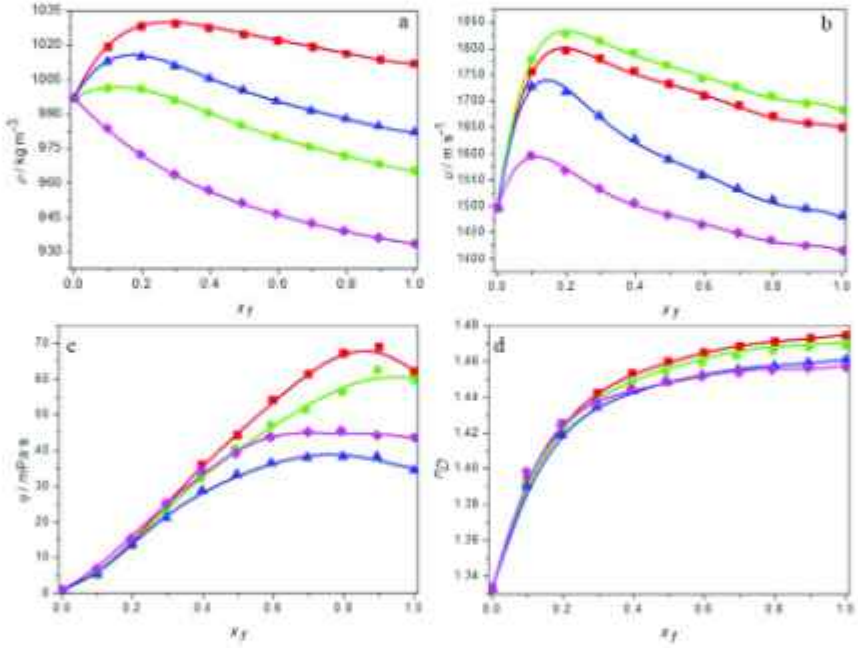

Figure 1. The dependence of the physical properties of aqueous solutions of DESs on molar fraction of deep eutectic solvent at 298.15K: (**a**) density; (**b**) speed of sound; (**c**) viscosity; (**d**) refractive index. ■ DES1; ● DES2; ▲ DES3; ♦ DES4; —, Equation (1).

Taking into account the density, its values decrease in the whole range of DES concentrations only for aqueous TBAB:BAE (DES4) solutions for which a negative deviation from ideal behavior is observed. For the other systems, the density increases with increasing DES

concentration at low deep eutectic solvent content, reaches its maximum value at certain molar fraction of DES, and afterwards begins to decrease. The composition of the solution with the highest density depends on both the amino alcohol and the salt.

The dependence of the sound velocity and viscosity of aqueous DES solutions on the molar fraction of DES also shows a maximum. However, in the case of viscosity, unlike the speed of sound and the density, it occurs at high DES content. The refractive index increases monotonically in the whole range of DES concentrations for all systems.

When the temperature dependence is considered, one can observe that all properties decrease with the increase of temperature as the result of thermal expansion.

The experimental values of of density, speed of sound, viscosity, and refractive indices of binary mixtures were correlated by using of Jouyban–Acree model [29,31–33]. This mathematical model uses the physicochemical properties of the individual solvents as input data and a number of curve-fitting parameters represent the effects of solvent–solvent interactions in the solution

$$lny = x_1 lny_1 + x_2 lny_2 + \frac{x_1 x_2}{T} \sum_{i=0}^{i=n} J_i (x_1 - x_2)^2 \quad (1)$$

The y, y_1, and y_2 are the physical properties of the mixture, deep eutectic solvent and water, at specific temperature. The x_1 and x_2 are mole fractions of DES and water, respectively. The J_i terms are coefficients of the model computed by using a zero-intercept regression analysis

$$lny - x_1 lny_1 - x_2 lny_2 = \frac{x_1 x_2}{T} \sum_{i=0}^{i=n} J_i (x_1 - x_2)^2 \quad (2)$$

Root mean square deviation of fit (RMSD) and the average deviation (ARD %) were calculated according to the following equations

$$RMSD = \left[\frac{\sum \left(Y_{exp} - Y_{pred} \right)^2}{n - k} \right]^{1/2} \quad (3)$$

$$ARD\ \% = \frac{100}{n} \sum \frac{\left| y_{exp} - y_{pred} \right|}{y_{pred}} \quad (4)$$

where n is the number of experimental data, k is the number of parameters of model and Y is equal to lny.

Parameters J_i of Equation (1), root mean square deviation of fit (RMSD) and the corresponding average relative deviation (ARD %) for the systems studied at T = (293.15 to 313.15) K are presented in Table S5 (Supplementary Materials).

Moreover, the values of density, speed of sound, viscosity, and refractive index obtained by JAM are depicted as the smoothed solid lines in Figure 1. As can be seen, the Jouyban–Acree model correlates the experimental physical properties satisfactorily, especially for density and refractive index, for which average relative deviations are the same order as the experimental uncertainty. Thus, the JAM can be considered a reliable model for predicting the densities and refractive indices as well as it can be used for estimation of the speeds of sound and viscosity of aqueous DES solutions, for which, however, higher ARD % are observed.

3.2. Volumetric Properties

3.2.1. Excess Molar Volume

The excess molar volumes (V^E) were calculated using the experimental density data according to the following equation

$$V^E = \frac{x_1M_1 + x_2M_2}{\rho} - \frac{x_1M_1}{\rho_1} - \frac{x_2M_2}{\rho_2} \quad (5)$$

where d is the density of the mixture and x_i, M_i, and ρ_i are: the mole fraction, the molar mass and density of DES ($i = 1$) and water ($i = 2$), respectively.

The obtained values of V^E are presented in Tables S1–S4 and plotted as a function of the DES mole fraction, x_1, in Figure 2. Figure 2a shows the plots of V^E against mole fraction of DES for all studied mixtures at 298.15 K and Figure 2b depicts the temperature dependence of excess molar volumes for the system (TBAB:BAE + water) as an example. It can be observed in these figures that the curves of V^E are asymmetrical and their values are negative over the whole composition and temperature range. The minimum was found between mol fraction of 0.35 and 0.4 of DES equal to −0.98 for DES1, −1.00 for DES2, −1.13 for DES3, −1.02 for DES4. The asymmetry of the curves is due to the difference between the molar volumes of the components mixture.

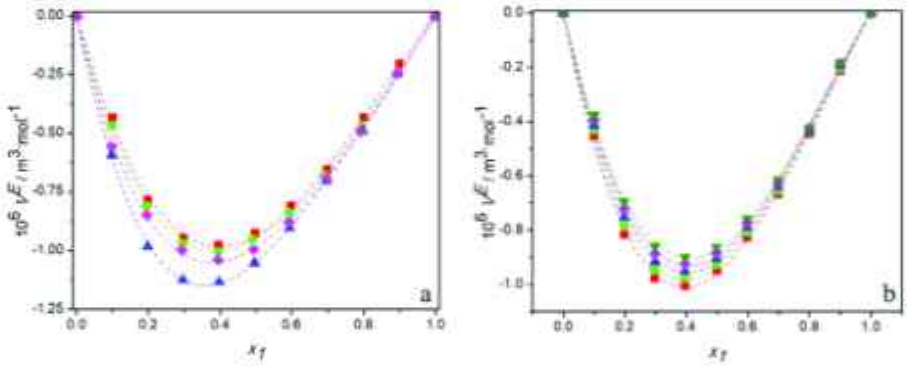

Figure 2. Dependence of the excess molar volume of aqueous solutions of DESs on molar fraction of deep eutectic solvent: (**a**) at 298.15 K for ■ DES1; ● DES2; ▲ DES3; ♦ DES4; (**b**) for DES1 at 298.15 K (■); 298.15 K (●); 303.15 K (▲); 308.15 K (♦); 313.15 K (▼); —, Equation (6).

In Figure 2, the dashed lines represent the correlated values according to the Redlich–Kister polynomial [31]

$$V^E = x_1x_2\sum_{i=0}^{2} A_i(x_1 - x_2)^i \quad (6)$$

where the A_i values are adjustable parameters.

As it can be seen, the calculated values agree very well with the experimental data. The A_i values were determined using the least squares method and they are listed in Tables S6–S9, along with their RMSD. For all systems, excess molar volumes were correlated using three-parameter Redlich–Kister polynomial equation.

The negative values of excess molar volumes can be explained based on the strength of the specific interactions, size, and shape of molecules. When DES is added to water, the intra-molecular interactions between DES or water molecules are disrupted and new hydrogen bonding interactions between water and chloride/bromide anion of HBA and between water and -OH group and $-NH_2$ group or –NH of amino alcohol are forming. Moreover, water molecules—as much smaller than the deep eutectic solvent one—may

fit into the interstices of the DES. Therefore, the filling effect of water in the interstices of DES, and the strong hydrogen bonding interactions between the unlike components of the systems, all lead to the negative values of the excess molar volumes.

The temperature dependence of the excess molar volumes can determine what kind of effect—i.e., the packing phenomenon or the strong forces between the components—is responsible for the negative values of V^E. In general, as temperature increases, the specific interactions break down and due to the increased thermal fluctuation, more holes of sufficient size for the accommodation of the unlike component are formed. These effects influence the excess molar volume in a reverse manner. A decrease of specific interactions causes an increase in V^E values, while a loosening of the DES structure leads to a decrease of excess molar volume with temperature. Thus, the observed increase of V^E with rising temperature for all systems investigated suggests that specific interactions determine the volumetric behavior of aqueous solutions of deep eutectic solvents based on alcohol amine. A similar phenomenon was observed by other researchers for aqueous solutions of DES based on choline chloride [18,21,22,24,35–38] or allyltriphenylphosphonium bromide [19,20]. What is interesting, for the (DES + alcohol) systems, due to the decrease in the excess molar volume with temperature, the dominance of the packing effect was postulated [39,40].

The dominance of specific interactions in the aqueous solutions of the DESs studied can be confirmed by the Prigogine–Flory–Patterson (PFP) theory [41–45]. This theory has been originally used in interpreting the values of the excess molar volumes of binary systems formed by polar compounds which do not form strong electrostatic or hydrogen bond interactions. Over time, however, it has emerged that the use of the Flory formalism can still provide an interesting correlation between the excess volumes of more complex mixtures. So far, the PFP theory has been successfully applied to predict and model the excess molar volumes of many mixtures containing ionic liquids [46–50] and some aqueous systems with deep eutectic solvents [18,51,52].

According to the PFP theory, the excess molar volume contains three contributions: an interactional contribution, a free volume contribution, and a pressure contribution. The expression for V^E is given as

$$\frac{V^E}{x_1V_1^* + x_2V_2^*} = \frac{\left(\tilde{V}^{1/3} - 1\right)\tilde{V}^{2/3}\psi_1\Theta_2\chi_{12}}{\left[(4/3)\tilde{V}^{-1/3} - 1\right]P_1^*} + \frac{-\left(\tilde{V}_1 - \tilde{V}_2\right)^2\left[(14/9)\tilde{V}^{-1/3} - 1\right]\psi_1\psi_2}{\left[(4/3)\tilde{V}^{-1/3} - 1\right]\tilde{V}} + \frac{\left(\tilde{V}_1 - \tilde{V}_2\right)(P_1^* - P_2^*)\psi_1\psi_2}{P_2^*\psi_1 + P_1^*\psi_2} \quad (7)$$

where V^E is excess molar volume, x mole fraction, V^* characteristic volume, P^* characteristic pressure, ψ molecular contact energy fraction, θ molecular surface fraction, $\tilde{V}$ reduced volume, and χ_{12} interactional parameter.

The reduced volume for pure substance i is defined in terms of the thermal expansion coefficients, α_i, as

$$\tilde{V}_i = \left(\frac{1 + \frac{4}{3}\alpha_i T}{1 + \alpha_i T}\right)^3 \quad (8)$$

The reduced volume of mixture, $\tilde{V}$, is calculated from

$$\tilde{V} = \psi_1\tilde{V}_1 + \psi_2\tilde{V}_2 \quad (9)$$

where the molecular contact energy fraction, ψ, is expressed by: $\psi_1 = 1 - \psi_2 = \frac{\phi_1 P_1^*}{\phi_1 P_1^* + \phi_2 P_2^*}$ with the hardcore volume fraction, ϕ, calculated from $\phi_1 = 1 - \phi_2 = \frac{x_1 V_1^*}{x_1 V_1^* + x_2 V_2^*}$.

The characteristic volume, V_i^*, is calculated from the molar volume from the expression $V_i^* = \frac{V_i^0}{\tilde{V}_i}$ and the characteristic pressure is expressed by

$$P_i^* = \frac{\alpha_i}{\kappa_{Ti}} T\tilde{V}_i^2 \quad (10)$$

where κ_{Tj} is the isothermal compressibility obtained from the isentropic compressibility from the thermodynamic relation

$$\kappa_{Tj} = \kappa_{Sj} + \frac{V_j^0 a_j^2 T}{C_{pj}} \tag{11}$$

with the isobaric heat capacity, C_{pj}.

The molecular surface fraction of component 2 is given by: $\Theta_2 = \frac{\phi_2}{\phi_1 \frac{s_1}{s_2} + \phi_2}$, in which the ratio of the surface contact sites per segment is given by

$$\frac{s_1}{s_2} = \left(\frac{v_2^*}{v_1^*}\right)^{\frac{1}{3}} \tag{12}$$

In present study, the thermal expansion coefficient, a_p, defined as: $a_p = \frac{1}{V}\left(\frac{\partial V}{\partial T}\right)_p$, was calculated by use the temperature dependence of density, which was found to be the second-order polynomial equation.

The isobaric heat capacity of DESs was determined experimentally. Table S10 shows, for all pure DESs used in this work, the thermal expansion coefficient, the isobaric heat capacity and the Flory parameters necessary for the application of the PFP theory. The results of our experiments compare the Cp of DES1–DES4. Quite noticeable differences are observed. Generally, the *Cp* values [J·mol $^{-1}$ K $^{-1}$] are arranged in order: DES 3 < DES 2 < DES 1 < DES 4 at set temperature points.

According to the PFP theory, for the separation of the values of excess molar volume into three contributions, the interactional parameter χ_{12} must be found. In the present study, it has been done by minimalization of the objective function, considering deviations in the prediction of the excess volume, defined as

$$OF = \sum_{i=1}^{n}\left(V_{exp}^E - V_{calc}^E\right)^2 \tag{13}$$

In calculations, the value of the interactional parameter χ_{12} was assumed to be independent on the composition of mixture. Figure 3 shows the composition dependence of calculated excess molar volume, together with the three contributions (V_{int}^E, V_{fo}^E, V_{p}^E), compared with the experimental V^E data for each system studied at 298.15 K.

Moreover, Table 3 reports the adjusted values of interactional parameter χ_{12} and calculated three contributions to excess molar volume for the binary mixtures of deep eutectic solvents with water at all temperatures investigated and at $x_1 = 0.4$ together with RMSD.

Study of the data presented in Table 3 as well as an analysis of Figure 3 reveals that the interactional contribution is always negative and it seems to be the most important to explain the values of the excess molar volume. It decides about the sign and magnitude of the V^E due to its greater value compared to the other two contributions for all investigated systems at all temperatures. The free volume contribution, which is a measure of geometrical accommodation, is negative but its magnitude is much smaller than for the interactional contributions. Therefore, it can be said that the PFP model confirms the conclusions resulting from the dependence of excess molar volume on the temperature, postulating little significance of the packing effect for the systems studied. The third contribution is the result of differences in internal pressure and in the reduced volumes of the components. It is positive, its magnitude is smaller than the interactional contribution and decreases distinctly with temperature.

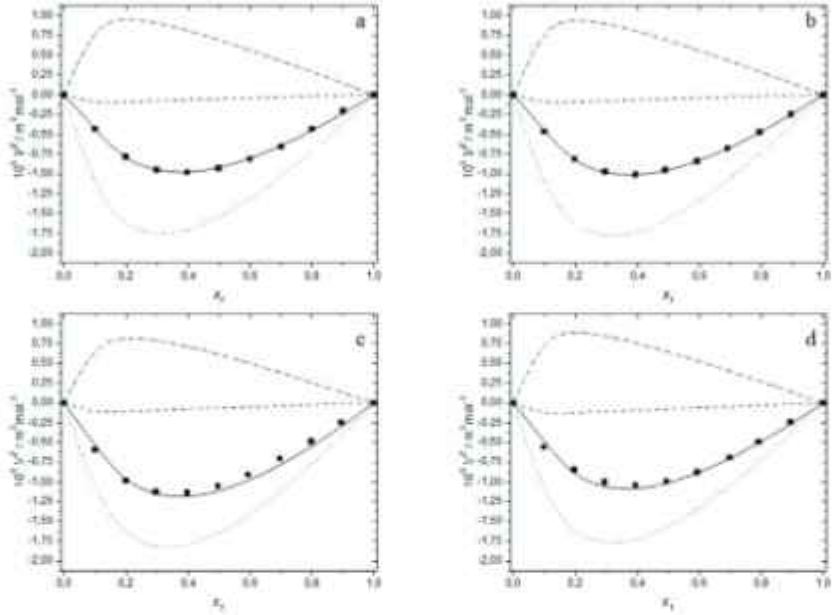

Figure 3. The dependence of the excess molar volume of aqueous solutions of DESs on molar fraction of deep eutectic solvent at 298.15 K: (**a**) for DES1; (**b**) for DES2; (**c**) for DES3; (**d**) for DES4; (■) experimental data; (—) calculated using the PFP model; (… … …) interactional contribution (V^E_{int}); (– – –), free volume contribution (V^E_{fv}); (– · –), characteristic pressure contribution (V^E_{p*}).

Table 3. Calculated values of the interactional parameter χ12, root mean square deviation of fit RMSD, and the three contributions (V^E_{int}, V^E_{fv}, V^E_{p*}) from the PFP theory to the excess molar volumes for the binary mixtures of deep eutectic solvents with water at x1 = 0.4 and T = (293.15 − 313.15) K.

T/K	293.15	298.15	303.15	308.15	313.15
			DES_1 (1) + water (2)		
10^{-6} χ12/J·m^{-3}	−393.3	−354.2	−317.6	−283.2	−252.1
10^6 V^E_{int}/m^3·mol^{-1}	−1.932	−1.726	−1.534	−1.359	−1.205
10^6 V^E_{fv}/m^3·mol^{-1}	0.979	0.814	0.661	0.522	0.398
10^6 V^E_{p*}/m^3·mol^{-1}	−0.062	−0.064	−0.066	−0.039	−0.053
RMSD	0.018	0.016	0.022	0.033	0.046
			DES_2 (1) + water (2)		
10^{-6} χ12/J·m^{-3}	−397.7	−358.5	−321.7	−287.2	−256.0
10^6 V^E_{int}/m^3·mol^{-1}	−1.960	−1.752	−1.559	−1.384	−1.230
10^6 V^E_{fv}/m^3·mol^{-1}	0.964	0.806	0.652	0.513	0.390
10^6 V^E_{p*}/m^3·mol^{-1}	−0.062	−0.065	−0.064	−0.060	−0.053
RMSD	0.020	0.006	0.008	0.020	0.033
			DES_3 (1) + water (2)		
10^{-6} χ12/J·m^{-3}	−324.1	−294.1	−266.0	−241.2	−218.9
10^6 V^E_{int}/m^3·mol^{-1}	−2.031	−1.818	−1.624	−1.454	−1.305
10^6 V^E_{fv}/m^3·mol^{-1}	0.888	0.716	0.559	0.421	0.301
10^6 V^E_{p*}/m^3·mol^{-1}	−0.078	−0.081	−0.079	−0.074	−0.067
RMSD	0.080	0.068	0.054	0.040	0.029

Table 3. *Cont.*

T/K	293.15	298.15	303.15	308.15	313.15
			DES_6 (1) + water (2)		
$10^{-6}\,\chi_{12}/J{\cdot}m^{-3}$	−245.4	−217.4	−190.9	−166.9	−145.5
$10^6\,V_E^E/m^3{\cdot}mol^{-1}$	−1.989	−1.750	−1.529	−1.332	−1.158
$10^6\,V_{int}^E/m^3{\cdot}mol^{-1}$	0.946	0.761	0.591	0.438	0.302
$10^6\,V_{fv}^E/m^3{\cdot}mol^{-1}$	−0.091	−0.096	−0.097	−0.094	−0.087
RMSD	0.062	0.045	0.031	0.027	0.033

For deeper analysis of the obtained results, the percentage of the three contributions in excess molar volume was calculated. Figure 4 presents the obtained results at 298.15 K.

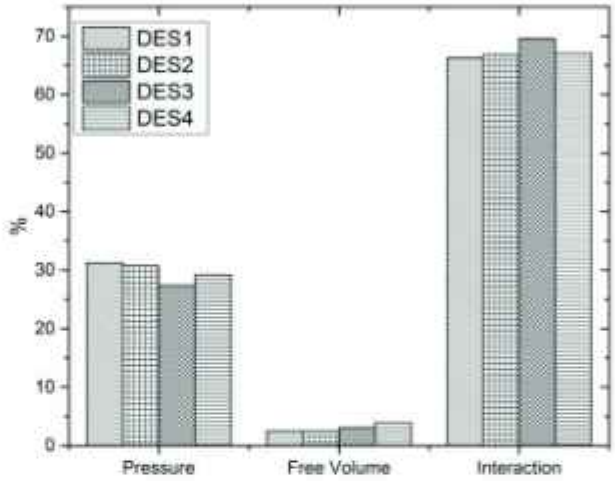

Figure 4. Percentages of the three contributions in excess molar volume of aqueous solutions of DESs for $x_L = 0.4$ at 298.15 K.

As can be seen, the interactional contribution and the characteristic pressure contribution determine the order of the excess molar volume observed for the studied systems, which is as follows: TBAB:MAE (DES 3) < TBAB:BAE (DES 4) < TBAC:AP (DES 2) ≈ TBAB:AP (DES 1). The free volume fraction has practically no effect on the excess molar volume, and its absolute value increases with the length of the alkyl chain in the amino alcohol.

Moreover, the results show that the anion of the salt in DES does not practically effect on the value of excess molar volume. As depicted in Figures 3 and 4, almost identical interactional contribution, free volume contribution and characteristic pressure contribution are observed for aqueous solutions of TBAC:AP (DES 2) and TBAB:AP (DES 1).

Further analysis of Table 3 shows that the interactional contribution is mainly responsible for the increase of excess molar volume with increasing temperature. The decrease in its absolute value is greater than the decrease of the positive characteristic pressure contribution, and consequently the excess volumes of the studied systems increase with temperature. The percentage of free volume contribution increases with increasing temperature, but due to the low absolute values V_{int}^E, it has no influence on the excess molar volume or its dependence on temperature.

Summing up, it is evident from Figure 3 that the PFP theory predicts the experimental data satisfactorily. Thus, while the PFP theory does not take into account the strong

interactions between components—such as electrostatic, hydrogen bonding, and complex formation—we can infer that the PFP model reproduces the main characteristics of the experimental data by using only one fitted parameter to describe excess molar volume.

3.2.2. Excess of Thermal Expansion

As the temperature dependence of density was found to be second order polynomial, type: $\ln(\rho) = at^2 + bt + c$, the isobaric thermal expansion coefficients at different temperatures were derived according to the equation

$$\alpha_p = \frac{1}{V}\left(\frac{\delta V}{\delta T}\right)_\mu = -\frac{1}{\rho}\left(\frac{\delta \rho}{\delta T}\right)_\rho = -\left(\frac{\delta ln\rho}{\delta T}\right)_\rho = -(2a + b) \quad (14)$$

Then, excess thermal expansion, $\Delta\alpha_p$, was calculated using the equation

$$\Delta\alpha_p = \alpha_p - \sum_{i=1}^{n} \Phi_i \alpha_{p,i} \quad (15)$$

where Φ_i is the volume fraction of pure component i, defined as $\phi_i = x_i V_i / \sum_i x_i V_i$. The values of α_p and $\Delta\alpha_p$ are given in Tables S1–S6 in Supporting Material and variation of the excess thermal expansion with DES mole fraction, x_1, is plotted in Figure 5.

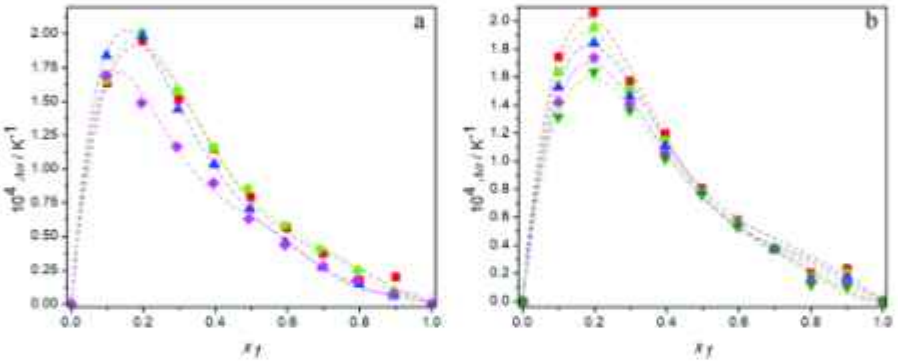

Figure 5. Dependence of the excess thermal expansion of aqueous solutions of DESs on molar fraction of deep eutectic solvent: (a) at 298.15 K for ■ DES1; • DES2; ▲ DES3; ♦ DES4; (b) for DES1 at 293.15 K (■); 298.15 K (•); 303.15 K (▲); 308.15 K (♦); 313.15 K (▼); —, Equation (6).

It can be seen that the values of excess thermal expansion are positive in the entire composition range for all systems studied, regardless of temperature. Since positive $\Delta\alpha_p$ are typical for the systems containing molecules capable to self-associate, the obtained results confirm strong hydrogen bonds between water molecules or between molecules of deep eutectic solvents, the strength of which decreases with temperature, as indicated by a reduction in excess thermal expansion with temperature [53]. Moreover, the less positive values of excess thermal expansion obtained for the (TBAB:BAE (DES 4) + water) system indicate the weakest hydrogen bond interactions between molecules of this DES compared to the others.

3.2.3. Partial Molar Volumes

The partial molar volumes of the studied DESs and water in their binary mixtures, $\overline{V}_1$ and $\overline{V}_2$, were calculated from the Equations (16) and (17), using the parameters of Redlich Kister equation (Tables S6–S9) and the molar volumes of the pure components, V_1^o and V_2^o

$$\overline{V}_1 = V_1^o + (x_1 - 1)^2 \sum_{i=0}^{j} A_i (2x_1 - 1)^i + 2x_1 (1 - x_1)^2 \sum_{i=0}^{j} A_i i (2x_1 - 1)^{i-1} \quad (16)$$

$$\overline{V}_2 = V_2^o + x_1{}^2 \sum_{i=0}^{j} A_i (2x_1 - 1)^i - 2x_1{}^2 (1 - x_1) \sum_{i=0}^{j} A_i i (2x_1 - 1)^{i-1} \quad (17)$$

The obtained values of the partial molar volumes together with the molar volumes of pure components are presented in Table S11 in Supplementary Material. As can be seen, at all studied temperatures, the molar volumes of the interacting compounds in the pure state were higher than their corresponding values in the mixture, indicating the reduction in volume upon adding a deep eutectic solvent to water. Figure 6 shows the excess partial molar volumes of the components at 298.15 K. These properties were calculated from definition as: $\overline{V}_i^E = \overline{V}_i - V_i^o$ and their values are negative over the whole composition range. In general, the negative $\overline{V}_1^E$ and $\overline{V}_2^E$ values indicate the presence of significant solute–solvent interactions between unlike molecules, whereas the positive $\overline{V}_1^E$ and $\overline{V}_2^E$ values indicate the presence of solute–solute or solvent–solvent interactions between like molecules in the mixture [54]. In the present work, the negative excess partial molar volumes of the components indicate that the DES—water interactions are stronger than the DES—DES or the water–water interactions, what is consistent with the conclusions from excess molar volumes.

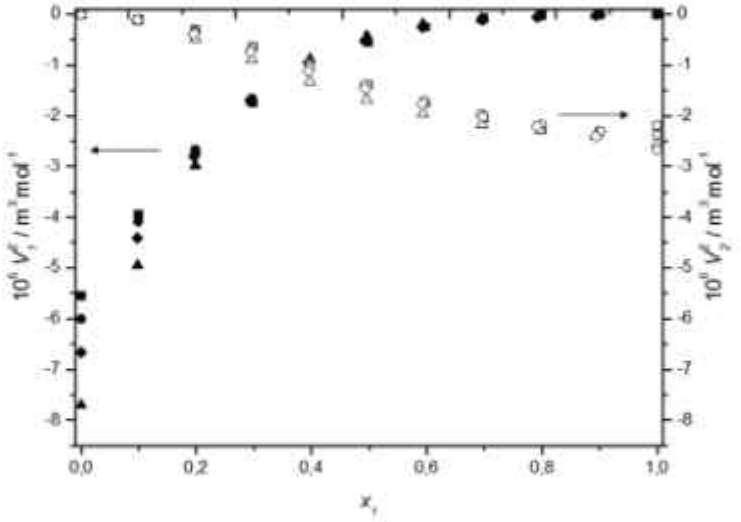

Figure 6. Dependence of the excess partial molar volume $\overline{V}_1^E$ of ■ DES1, ● DES2, ▲ DES3, ♦ DES4, and water $\overline{V}_2^E$ in □ DES1, ○ DES2, △ DES3, ◇ DES4 on molar fraction of deep eutectic solvent at 298.15 K.

Since the partial molar properties at infinite dilution provide useful information about the interactions between components of a mixture that are independent on composition, their values for DES and water were calculated.

The partial molar volumes at infinite dilution of DES were obtained by setting $x_1 = 0$ in Equation (18) as

$$\overline{V}_1^{\infty} = V_1^{\circ} + \sum_{i=0}^{i} A_i(-1)^i \tag{18}$$

Similarly, setting $x_1 = 1$ in Equation (19) allowed to estimate the partial molar volumes at infinite dilution of water

$$\overline{V}_2^{\infty} = V_2^{\circ} + \sum_{i=0}^{i} A_i \tag{19}$$

Table 4 presents the obtained values of partial molar volumes at infinite dilutions of DES and water in their binary systems.

Table 4. Partial molar volumes at infinite dilution of DES and water in their binary mixtures at T = (293.15 to 313.15) K and at atmospheric pressure (0.1 MPa).

T/K	$10^6\,\overline{V}_1^{\infty}$/ $m^3 \cdot mol^{-1}$	$10^6\,\overline{V}_1^{E,\infty}$/ $m^3 \cdot mol^{-1}$	$10^6\,\overline{V}_2^{\infty}$/ $m^3 \cdot mol^{-1}$	$10^6\,\overline{V}_2^{E,\infty}$/ $m^3 \cdot mol^{-1}$	$10^6\,\overline{V}_1^{\infty}$/ $m^3 \cdot mol^{-1}$	$10^6\,\overline{V}_1^{E,\infty}$/ $m^3 \cdot mol^{-1}$	$10^6\,\overline{V}_2^{\infty}$/ $m^3 \cdot mol^{-1}$	$10^6\,\overline{V}_2^{E,\infty}$/ $m^3 \cdot mol^{-1}$
	DES 1 + water				**DES 2 + water**			
293.15	102.91	−5.83	15.94	−2.11	101.10	−6.34	15.58	−2.47
298.15	103.60	−5.54	15.88	−2.19	101.82	−6.01	15.69	−2.38
303.15	104.32	5.22	16.13	1.96	102.51	5.71	15.79	2.30
308.15	105.00	4.95	16.24	1.88	103.18	5.44	15.89	2.24
313.15	105.65	−4.70	16.31	−1.85	103.84	−5.19	15.98	−2.17
	DES 3 + water				**DES 4 + water**			
293.15	104.00	8.04	15.45	2.6	149.34	6.98	15.29	2.75
298.15	104.75	−7.70	15.52	−2.54	150.27	−6.66	15.40	−2.67
303.15	105.47	−7.39	15.60	−2.49	151.17	−6.36	15.50	−2.60
308.15	106.18	−7.10	15.69	−2.43	152.06	−6.09	15.59	−2.53
313.15	106.88	6.83	15.77	2.39	152.94	5.83	15.68	2.47

As can be seen, both the partial molar volumes and the excess partial molar volumes at infinite dilution increase with the increasing temperature. Such results seem to indicate that the weakening of hydrogen bond interactions between DES and water molecules with increase in temperature is the most important factor controlling the properties of the systems and it dominates over the packing effect. Moreover, the excess partial molar volumes at infinite dilution of DES change in the order TBAB:MAE (DES 3) < TBAB:BAE (DES 4) < TBAC:AP (DES 2) < TBAB:AP (DES 1) confirming the conclusions obtained on the basis of excess molar volumes. The dependence of excess partial molar volumes at infinite dilution of water on the DES: TBAB:BAE (DES 4) ≤ TBAB:MAE (DES 3) < TBAC:AP (DES 2) < TBAB:AP (DES 1) is similar and only the reordering of DES4 and DES3 takes place. However, taking into an account the uncertainty of partial molar volume at infinite dilution, it can be said, that the $\overline{V}_2^{E,\infty}$ for systems (DES4+water) and (DES3+water) are practically equal.

3.3. *Excess Isentropic Compressibility*

The isentropic compressibilities of aqueous solutions of DESs were estimated using experimental values of densities and sound velocities by the Laplace equation

$$\kappa_S = -\frac{1}{V_m}\left(\frac{\partial V_m}{\partial P}\right)_S = \frac{1}{u^2 \cdot \rho} \tag{20}$$

providing the link between thermodynamics and acoustics.

Then, according to the approach developed by Benson et al. [55], the excess isentropic compressibility was calculated as

$$\kappa_S^E = \kappa_S - \sum_i \Phi_i \kappa_{S,i} - T \sum_i \Phi_i V_i a_{p,i}^2 / C_{p,i} + T \sum_i x_i V_i \left(\sum_i \Phi_i a_{p,i} \right)^2 / \sum_i x_i C_{p,i} \quad (21)$$

Tables S1–S4 in Supplementary Material present the experimental values of sound velocity and the calculated values of excess isentropic compressibility for aqueous solutions of DESs made of tetrabutylammonium bromide and 3-amino-1-propanol or 2-(methylamino)ethanol or 2-(butylamino)ethanol and for the aqueous solutions of DES built of tetrabutylammonium chloride and 3-amino-1-propanol over the entire range of compositions at temperatures ranging from 293.15 K to 313.15 K. Figure 7a shows the plots of κ_S^E against mole fraction of DES for the all studied mixtures at 298.15 K and Figure 7b depicts the temperature dependence of excess isentropic compressibility for the system (TBAB:AP +water) as an example. It is evident that the curves are remarkably asymmetric, with their minima shifted towards a rich mole fraction of water, even more than the excess molar volume curves are.

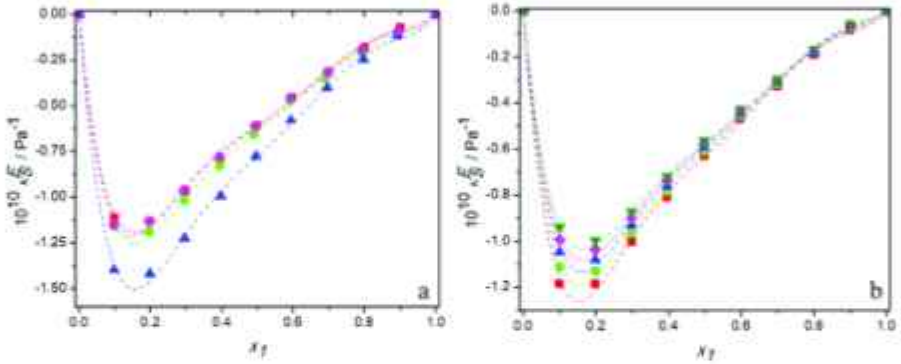

Figure 7. Dependence of the excess isentropic compressibility of aqueous solutions of DESs on molar fraction of deep eutectic solvent: (**a**) at 298.15 K for ■ DES1; • DES2; ▲ DES3; ♦ DES4; (**b**) for DES1 at 298.15 K (■); 298.15 K (•); 303.15 K (▲); 308.15 K (♦); 313.15 K (▼); —, Equation (6).

In these figures, it can be also seen that the values of κ_S^E are negative for all systems over the entire range of the mole fraction as well as the temperature range. This indicates that the mixtures might be less compressible than the corresponding ideal mixtures due to a closer approach and stronger interactions between the unlike molecules of the mixtures. The negative values of excess isentropic compressibility for the binary systems follow the order: TBAB:MAE (DES 3) < TBAB:BAE (DES 4) ≈ TBAC:AP (DES 2) ≈ TBAB:AP (DES 1). Thus, the behavior of the excess isentropic compressibility seems to be consistent with the obtained values of the excess molar volume, which suggests that the interactions and the packing effect dominate in aqueous solutions of TBAB:MAE and do not practically depend on the anion of the salt in DES.

Moreover, as can be seen in Figure 7b, the values of κ_S^E become less negative with increasing temperature for all systems at a fixed composition. It is due to the reduction of interactions between unlike molecules, what has already been suggested by volumetric properties. Indeed, the increase in temperature also increases the thermal motion of the molecules and enlargement of interstices. However, the decrease in hydrogen bonding is

greater and, in the result, the excess molar compressibility of all aqueous solutions of DES decreases with increasing temperature.

3.4. Deviations in Refractive Index

From refractive indices the deviations in refractive index, Δn_D, were calculated using the equation

$$\Delta n_D = n_D - \sum_{i=1}^{n} \Phi_i n_{Di} \quad (22)$$

where n_D and n_{Di} are the refractive index of a mixture and a pure component i, respectively and Φ_i denotes the volume fraction of a pure component i.

Tables S1–S4 in Supplementary Material present the experimental values of refractive index and calculated values of the deviations in refractive index for aqueous solutions of DESs over the entire range of compositions at temperatures ranging from 293.15 K to 313.15 K. Figure 8a shows the plots of Δn_D against mole fraction of DES for the all studied mixtures at 298.15 K and Figure 8b depicts the temperature dependence of deviations in refractive index for the system (TBAB:AP +water) as an example.

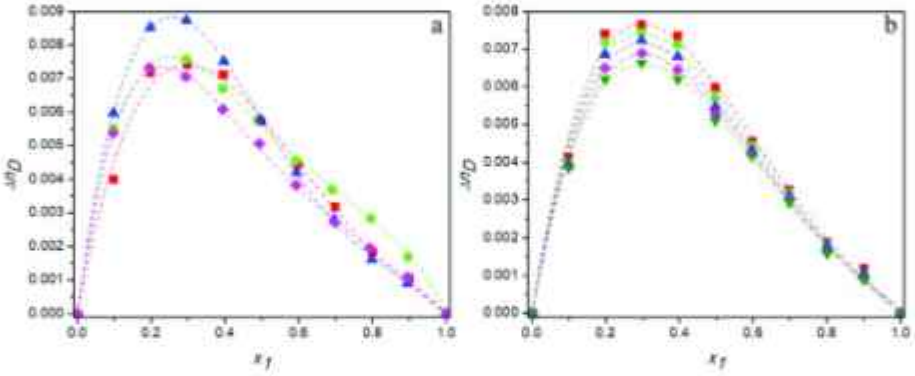

Figure 8. Dependence of the deviations in refractive of aqueous solutions of DESs on molar fraction of deep eutectic solvent: (**a**) 298. 15 K for ■ DES1; ● DES2; ▲ DES3; ♦ DES4; (**b**) for DES1 at 298.15 K (■); 298.15 K (●); 303.15 K (▲); 308.15 K (♦); 313.15 K (▼); —, Equation (6).

As can be seen from Figure 8, the values of deviations in refractive index are positive over the whole composition range of binary mixtures and their dependences on mole fraction of DES are asymmetrical.

It is known that deviations of refractive index are negatively correlated with excess molar volumes [56]. If excess molar volume is negative, then there will be less free volume available than in an ideal mixture and the photons will interact more strongly with the components of the solution. As a result, light will travel with a weaker velocity in the mixture and its refractive index will be higher than in an ideal solution. Thus, positive deviations of refractive index will be observed.

This phenomenon occurs in all systems investigated in the present study and it is the strongest for TBAB:MAE (DES 3). Therefore, the obtained deviations of refractive index confirm the conclusion regarding the strongest interactions between this deep eutectic solvent and water molecules compared to other DESs studied. Moreover, as the values Δn_D increase with decreasing temperature, they indicate an increase in the number of hydrogen bonds at lower temperatures, which corresponds with the results of densitometric and acoustic research.

3.5. Deviations in Viscosity and Excess Gibbs Energy of Activation for Viscous Flow

Based on the viscosities of the mixtures, the viscosity deviations $\Delta\eta$ were obtained according to the equation

$$\Delta\eta = \eta - \exp(x_1 ln\eta_1 + x_2 ln\eta_2) \quad (23)$$

which uses the viscosity of the ideal mixture as suggested by Arrhenius.

The excess Gibbs energy of activation for viscous flow ΔG^E, was calculated using the equation

$$\Delta G^E = RT[\ln(\eta V_m) - (x_1 \ln(\eta_1 V_1) + x_2 \ln(\eta_2 V_2)] \quad (24)$$

where R is the gas constant and T is the absolute temperature. The symbols η_1, η_2, V_1, and V_2 represent viscosity of DES, viscosity of water, molar volume of DES, and molar volume of water, respectively.

Tables S1–S4 in Supplementary Material present the experimental values of viscosity, calculated values of the viscosity deviations and the excess Gibbs energy of activation for viscous flow for aqueous solutions of DESs over the entire range of compositions at temperatures ranging from 293.15 K to 313.15 K. Figure 9a,b show the plots of $\Delta\eta$ and ΔG^E against mole fraction of DES for the all studied mixtures at 298.15 K. Figure 9c,d depict the temperature dependence of viscosity deviations and the temperature dependence of the excess Gibbs energy of activation for viscous flow for the system (TBAB:BAE +water) as an example.

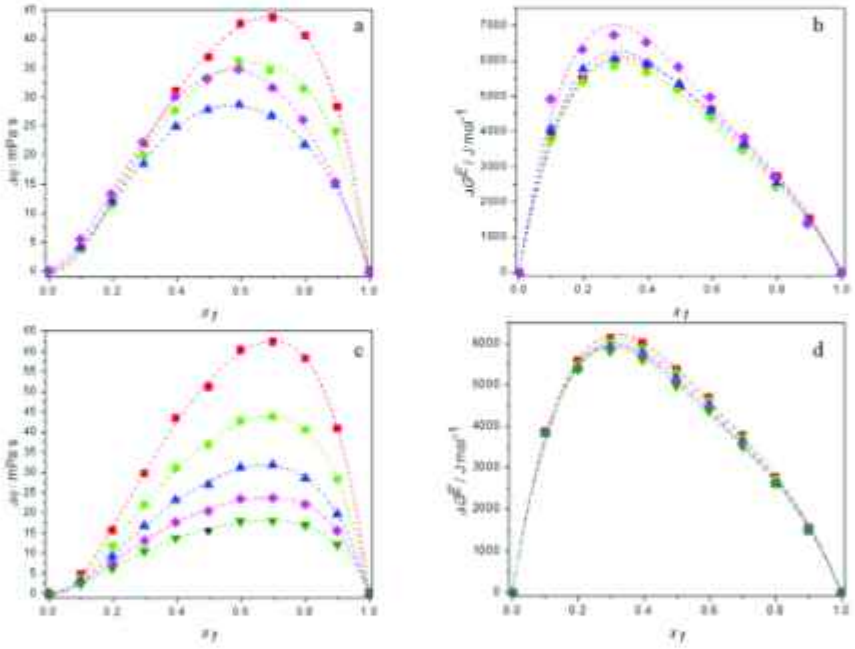

Figure 9. Dependence of the deviations in viscosity and the excess Gibbs energy of activation of aqueous solutions of DESs on molar fraction of deep eutectic solvent: (**a**,**b**) at 298.15 K for ■ DES1; • DES2; ▲ DES3; ♦ DES4; (**c**,**d**) for DES1 at 298.15 K (■); 298.15 K (•); 303.15 K (▲); 308.15 K (♦); 313.15 K (▼); —, Equation (6).

It is clearly visible that the viscosity deviations of all mixtures are positive in the whole range of composition. It is known that the viscosity of a mixture is related to the liquid structure [57]. Therefore, the viscosity deviation depends on molecular interactions as well as on the size and shape of the molecules forming the solution. The positive viscosity deviations are observed in mixtures with strong specific interactions like hydrogen bonding interactions, whereas the interstitial accommodation of one component with the other within the mixture leads to negative $\Delta\eta$ values [58]. For our DES systems, the predominant effect is the hydrogen bonding, that leads to positive $\Delta\eta$ values.

The order of viscosity deviations is the same as for the viscosity of the studied systems and is as follows: TBAB:AP (DES 1) > TBAC:AP (DES 2) > TBAB:BAE (DES 4) > TBAB:MAE (DES 3). It is different from those obtained for excess molar volume or excess compressibility. Thus, it can concluded that the values of viscosity deviations are determined not only by the interactions between unlike molecules, but also by other effects as shape of the molecules.

Estimation of the results obtained and presented in Figure 9 confirm the temperature dependence of the viscosity deviations in the studied systems because the values of $\Delta\eta$ become less positive with increasing temperature. This is due to the weakening of the interactions between the molecules present in the solution, which seem to dominate over the penetration phenomenon that obviously increases with temperature.

The positive values of excess Gibbs energy of activation presented in Figure 9a,b once again approve the dominance of specific interactions—i.e., hydrogen bonding between DES and water molecules occurring in the studied systems—which become weaker as temperature increases [58].

3.6. Correlations of Excess Properties

Similarly, as in a case of excess molar volumes, in order to correlate the calculated excess thermal expansions, excess isentropic compressibilities, deviations in refractive index, deviations in viscosity, and excess Gibbs energy of activation for viscous flow with the composition, the Redlich–Kister polynomial equation was applied [34]

$$Y^E = x_1 x_2 \sum_{i=0}^{n} A_i (x_1 - x_2)^i \tag{25}$$

where the A_i values are adjustable parameters. They were determined using the least squares method and their values are listed in Tables S6–S9 along with root mean square deviations of fit (RMSD). In order to obtain RMSD close to the experimental uncertainty, a different degree of the polynomial equation was chosen depending on the property and DES. For almost all systems, excess molar volumes, deviations in refractive index, and excess Gibbs energy of activation for viscous flow with composition were correlated using free-parameter Redlich–Kister polynomial equation. For viscosity deviations and excess isentropic compressibilities, a better fit was obtained for four-parameter and for five-parameter Redlich–Kister polynomial equation, respectively. In case of excess thermal expansions four-parameter for DES1 and DES 2 and five-parameter Redlich–Kister polynomial for DES3 and DES5 were chosen.

In Figures 2, 5 and 7–9, the dashed lines represent the correlated values according to the Redlich–Kister equation. As it can be seen, the calculated values agree very well with the experimental data. Thus, the Redlich–Kister equation perfectly represents the data over the experimental temperature range for the novel DES + water binary systems studied in this work.

4. Conclusions

The presented novel DESs built of tetrabutylammonium chloride and 3-amino-1-propanol or tetrabutylammonium bromide and 3-amino-1-propanol or 2-(methylamino)ethanol or 2-(butylamino)ethanol were found to be attractive in their properties, mostly for further evaluation and optimization during development of inexpensive eco-solvents or other

valuable material. Most important physicochemical properties have been demonstrated in details such as density, speed of sound, refractive index, and viscosity which were measured for their aqueous solutions over the entire range of compositions at atmospheric pressure and T = (293.15 − 313.15). The chosen Jouyban–Acree model was successfully used to correlate the experimental physical properties with respect to the concentration, and the results showed that this mathematical equation is an accurate correlation for the prediction of aqueous DES properties.

Excess molar volumes, excess isentropic compressibilities, deviations in viscosity, and deviations in refractive indices were calculated to study nonideal behavior of binary mixtures and they were correlated by the Redlich–Kister equation with temperature-dependent parameters. Excess molar volumes and excess compressiblities were negative and deviations in viscosity and deviations in refractive index were positive over the entire range of composition and temperature, suggesting strong intermolecular interactions among unlike molecules. Moreover, the temperature dependences of the excess molar volumes and compressibilities indicate that, in the studied systems, hydrogen bonding prevails over the packing effect (non-specific interactions).

The dominance of specific interactions in the aqueous solutions of the DESs also was confirmed by the Prigogine–Flory–Patterson (PFP) theory, which was applied to excess molar volumes.

The calculated negative values of the excess partial molar volumes of DESs and water demonstrated sufficient DES—water interactions which are stronger than the DES—DES or the water–water ones will probably facilitate the efficient utilization of DES.

In terms of the suitability of the water mixtures of the studied DES for the effective separation of carbon dioxide from gas streams at relatively low pressure, the obtained values of the excess properties allow us to assume that the best absorbent would be TBAB:AP, and the worst of TBAB:MAE.

Supplementary Materials: The following supporting information can be found online: Table S1: Densities ρ, excess molar volumes V^E, isobaric thermal expansion coefficients α_p, excess thermal expansion $\Delta\alpha_p$, speeds of sound u, excess isentropic compressibilities κ_S^E, viscosities η, viscosity deviations $\Delta\eta$, excess Gibbs free energy of activation of viscous flow ΔG^E, refractive indices n_D, refractive index deviations Δn_D as functions of mole fraction, x_1 of DES for TBAB:AP (DES1) + water mixtures at the temperatures (293.15 to 303.15) K and atmospheric pressure; Table S2: Densities ρ, excess molar volumes V^E, isobaric thermal expansion coefficients α_p, excess thermal expansion $\Delta\alpha_p$, speeds of sound u, excess isentropic compressibilities κ_S^E, viscosities η, viscosity deviations $\Delta\eta$, excess Gibbs free energy of activation of viscous flow ΔG^E, refractive indices n_D, refractive index deviations Δn_D as functions of mole fraction, x_1 of DES for TBAC:AP (DES2) + water mixtures at the temperatures (293.15 to 303.15) K and atmospheric pressure; Table S3:Densities ρ, excess molar volumes V^E, isobaric thermal expansion coefficients α_p, excess thermal expansion $\Delta\alpha_p$, speed of sounds u, excess isentropic compressibilities κ_S^E, viscosities η, viscosity deviations $\Delta\eta$, excess Gibbs free energy of activation of viscous flow ΔG^E, refractive indices n_D, refractive index deviations Δn_D as functions of mole fraction, x_1 of DES for TBAB:MAE (DES3) + water mixtures at the temperatures (293.15 to 303.15) K and atmospheric pressure; Table S4: Densities ρ, excess molar volumes V^E, isobaric thermal expansion coefficients α_p, excess thermal expansion $\Delta\alpha_p$, speed of sound u, excess isentropic compressibilities κ_S^E, viscosities η, viscosity deviations $\Delta\eta$, excess Gibbs free energy of activation of viscous flow ΔG^E, refractive indices n_D, refractive index deviations Δn_D as functions of mole fraction, x_1 of DES for TBAB:BAE (DES4) + water mixtures at the temperatures (293.15 to 303.15) K and atmospheric pressure; Table S5: Parameters of the JAM equation, together with RMSD and ARD% for density, speed of sound, viscosity and refractive index of DES (1) + water (2) systems at different temperatures; Table S6: Parameters A_i of Equation (6) and the corresponding RSMD f for TBAB:AP (DES1) + water mixtures at the temperatures (293.15 to 303.15) K and atmospheric pressure; Table S7. Parameters A_i of Equation (6) and the corresponding RSMD for TBAC:AP (DES2) + water mixtures at the temperatures (293.15 to 303.15) K and atmospheric pressure; Table S8: Parameters A_i of Equation (6) and the corresponding RSMD for TBAB:MAE (DES3) + water mixtures at the temperatures (293.15 to 303.15) K and atmospheric pressure; Table S9: Parameters A_i of Equation (6) and the corresponding RSMD for TBAB:BAE (DES4) + water mixtures at the temperatures (293.15 to

303.15) K and atmospheric pressure; Table S10: Isobaric thermal expansion coefficient (α_p), isochoric molar heat capacity (C_P), Flory theory parameters: characteristic volume (V*), reduce volume (V), characteristic pressure (P*), and ratio of molecular surface to volume ratio (S1/S2) of DES to water; Table S11: Partial molar volumes of DESs and water in their binary mixtures at T = (293.15 to 313.15) K and at atmospheric pressure (0.1 MPa).

Author Contributions: Conceptualization, D.W. and B.N.; Methodology, D.W., B.N. and J.L.; Investigation, B.N. and M.J.; Data curation, D.W. and B.N.; Writing—original draft preparation, D.W. and B.N.; Writing—review and editing, J.L. and M.J.; Supervision, D.W. All authors have read and agreed to the published version of the manuscript.

Funding: This research received no external funding.

Institutional Review Board Statement: Not applicable.

Informed Consent Statement: Not applicable.

Data Availability Statement: The data presented in this study are available on request from the corresponding author. The data are not publicly available due to the lack of requirements of Gdansk University of Technology and Medical University of Gdansk.

Conflicts of Interest: The authors declare no conflict of interest.

References

1. Marcus, Y. *Deep Eutectic Solvents*; Springer International Publishing: Cham, Switzerland, 2019.
2. Leron, R.B.; Wong, D.S.H.; Li, M.H. Densities of a deep eutectic solvent based on choline chloride and glycerol and its aqueous mixtures at elevated pressures. *Fluid Phase Equilib.* **2012**, *335*, 32–38. [CrossRef]
3. Liu, Y.; Friesen, J.B.; McAlpine, J.B.; Lankin, D.C.; Chen, S.N.; Pauli, G.F. Natural Deep Eutectic Solvents: Properties, Applications, and Perspectives. *J. Nat. Prod.* **2018**, *81*, 679–690. [CrossRef] [PubMed]
4. Abbott, A.P.; Capper, G.; Davies, D.L.; Rasheed, R.K.; Tambyrajah, V. Novel solvent properties of choline chloride/urea mixtures. *Chem. Commun.* **2003**, *9*, 70–71. [CrossRef] [PubMed]
5. Dai, Y.; van Spronsen, J.; Witkamp, G.J.; Verpoorte, R.; Choi, Y.H. Natural deep eutectic solvents as new potential media for green technology. *Anal. Chim. Acta* **2013**, *766*, 61–68. [CrossRef]
6. Sarmad, S.; Mikkola, J.P.; Ji, X. Carbon Dioxide Capture with Ionic Liquids and Deep Eutectic Solvents: A New Generation of Sorbents. *ChemSusChem* **2017**, *10*, 324–352. [CrossRef]
7. Alomar, M.K.; Hayyan, M.; Alsaadi, M.A.; Akib, S.; Hayyan, A.; Hashim, M.A. Glycerol-based deep eutectic solvents: Physical properties. *J. Mol. Liq.* **2016**, *215*, 98–103. [CrossRef]
8. Garcia, G.; Aparicio, S.; Ullah, R.; Atilhan, M. Deep eutectic solvents: Physicochemical properties and gas separation applications. *Energy Fuels* **2015**, *29*, 2616–2644. [CrossRef]
9. Liao, H.G.; Jiang, Y.X.; Zhou, Z.Y.; Chen, S.P.; Sun, S.G. Shape-controlled synthesis of gold nanoparticles in deep eutectic solvents for studies of structure-functionality relationships in electrocatalysis. *Angew. Chem.-Int. Ed.* **2008**, *47*, 9100–9103. [CrossRef]
10. Su, W.C.; Wong, D.S.H.; Li, M.H. Effect of water on solubility of carbon dioxide in (aminomethanamide + 2-hydroxy-*N*,*N*,*N*-trimethylethanaminium chloride). *J. Chem. Eng. Data* **2009**, *54*, 1951–1955. [CrossRef]
11. Li, Z.; Wang, L.; Li, C.; Cui, Y.; Li, S.; Yang, G.; Shen, Y. Absorption of Carbon Dioxide Using Ethanolamine-Based Deep Eutectic Solvents. *ACS Sustain. Chem. Eng.* **2019**, *7*, 10403–10414. [CrossRef]
12. Ahmadi, R.; Hemmateenejad, B.; Safavi, A.; Shojaeifard, Z.; Shahsavar, A.; Mohajeri, A.; Dokoohaki, M.H.; Zolghadr, A.R. Deep eutectic-water binary solvent associations investigated by vibrational spectroscopy and chemometrics. *Phys. Chem. Chem. Phys.* **2018**, *20*, 18463–18473. [CrossRef] [PubMed]
13. Nowosielski, B.; Jamróg iewicz, M.; Łuczak, J.; Śmiechowski, M.; Warmińska, D. Experimental and predicted physicochemical properties of monopropanolamine-based deep eutectic solvents. *J. Mol. Liq.* **2020**, *309*, 113110. [CrossRef]
14. Omar, K.A.; Sadeghi, R. Novel benzilic acid-based deep-eutectic-solvents: Preparation and physicochemical properties determination. *Fluid Phase Equilib.* **2020**, *522*, 112752. [CrossRef]
15. Hayyan, A.; Hadj-Kali, M.K.; Salleh, M.Z.M.; Hashim, M.A.; Rubaidi, S.R.; Hayyan, M.; Zulkifli, M.; Rashid, S.N.; Mirghani, M.E.S.; Ali, E.; et al. Characterization of tetraethylene glycol-based deep eutectic solvents and their potential application for dissolving unsaturated fatty acids. *J. Mol. Liq.* **2020**, *312*, 113284. [CrossRef]
16. van Osch, D.J.G.P.; Dietz, C.H.J.T.; Warrag, S.E.E.; Kroon, M.C. The Curious Case of Hydrophobic Deep Eutectic Solvents: A Story on the Discovery, Design, and Applications. *ACS Sustain. Chem. Eng.* **2020**, *8*, 10591–10612. [CrossRef]
17. Ma, C.; Laaksonen, A.; Liu, C.; Lu, X.; Ji, X. The peculiar effect of water on ionic liquids and deep eutectic solvents. *Chem. Soc. Rev.* **2018**, *47*, 8685–8720. [CrossRef]

18. Kaddushi, M.; Nangala, G.S.; Rajput, S.; Ijardar, S.P.; Malek, N.I. Understanding the peculiar effect of water on the physicochemical properties of choline chloride based deep eutectic solvents theoretically and experimentally. *J. Mol. Liq.* **2019**, *278*, 607–615. [CrossRef]
19. Ghaedi, H.; Ayoub, M.; Sufian, S.; Shariff, A.M.; Murshid, G.; Hailegiorgis, S.M.; Khan, S.N. Density, excess and limiting properties of (water and deep eutectic solvent) systems at temperatures from 293.15 K to 343.15 K. *J. Mol. Liq.* **2017**, *248*, 378–390. [CrossRef]
20. Ghaedi, H.; Ayoub, M.; Sufian, S.; Hailegiorgis, S.M.; Murshid, G.; Farrukh, S.; Khan, S.N. Experimental and prediction of volumetric properties of aqueous solution of (allyltriphenylPhosphonium bromide—Triethylene glycol) deep eutectic solvents. *Thermochim. Acta* **2017**, *657*, 123–133. [CrossRef]
21. Leron, R.B.; Soriano, A.N.; Li, M.H. Densities and refractive indices of the deep eutectic solvents (choline chloride+ethylene glycol or glycerol) and their aqueous mixtures at the temperature ranging from 298.15 to 333.15K. *J. Taiwan Inst. Chem. Eng.* **2012**, *43*, 551–557. [CrossRef]
22. Kumar, A.K.; Shah, E.; Patel, A.; Sharma, S.; Dixit, G. Physico-chemical characterization and evaluation of neat and aqueous mixtures of choline chloride + lactic acid for lignocellulosic biomass fractionation, enzymatic hydrolysis and fermentation. *J. Mol. Liq.* **2018**, *271*, 540–549. [CrossRef]
23. Siongco, K.R.; Leron, R.B.; Li, M.H. Densities, refractive indices, and viscosities of N,N-diethylethanol ammonium chloride-glycerol or -ethylene glycol deep eutectic solvents and their aqueous solutions. *J. Chem. Thermodyn.* **2013**, *65*, 65–72. [CrossRef]
24. Yadav, A.; Pandey, S. Densities and viscosities of (choline chloride + urea) deep eutectic solvent and its aqueous mixtures in the temperature range 293.15 K to 363.15 K. *J. Chem. Eng. Data* **2014**, *59*, 2221–2229. [CrossRef]
25. Li, G.; Deng, D.; Chen, Y.; Shan, H.; Ai, N. Solubilities and thermodynamic properties of CO_2 in choline-chloride based deep eutectic solvents. *J. Chem. Thermodyn.* **2014**, *75*, 58–62. [CrossRef]
26. Haider, M.B.; Jha, D.; Sivagnanam, B.M.; Kumar, R. Thermodynamic and Kinetic Studies of CO_2 Capture by Glycol and Amine-Based Deep Eutectic Solvents. *J. Chem. Eng. Data* **2018**, *63*, 2671–2680. [CrossRef]
27. Trivedi, T.J.; Lee, J.H.; Lee, H.J.; Jeong, Y.K.; Choi, J.W. Deep eutectic solvents as attractive media for CO_2 capture. *Green Chem.* **2016**, *18*, 2834–2842. [CrossRef]
28. Barzegar-Jalali, M.; Jalali, P.; Jouyban, A. Thermodynamic study of the aqueous pseudo-binary mixtures of betaine-based deep eutectic solvents at T = (293.15 to 313.15) K. *Phys. Chem. Liq.* **2022**, 1–16. [CrossRef]
29. Jouyban, A.; Khoubnasabjafari, M.; Vaez-Gharamaleki, Z.; Fekari, Z.; Acree, W.E. Calculation of the viscosity of binary liquids at various temperatures using Jouyban–Acree model. *Chem. Pharm. Bull.* **2005**, *53*, 519–523. [CrossRef]
30. Abu-Bakar, A.S.; Cran, M.J.; Moinuddin, K.A.M. Experimental investigation of effects of variation in heating rate, temperature and heat flux on fire properties of a non-charring polymer. *J. Therm. Anal. Calorim.* **2019**, *137*, 447–459. [CrossRef]
31. Acree, W.E. Mathematical representation of thermodynamic properties. Part 2. Derivation of the combined nearly ideal binary solvent (NIBS)/Redlich–Kister mathematical representation from a two-body and three-body interactional mixing model. *Thermochim. Acta* **1992**, *198*, 71–79. [CrossRef]
32. Jouyban, A.; Fathi-Azarbayjani, A.; Khoubnasabjafari, M.; Acree, W.E. Mathematical representation of the density of liquid mixtures at various temperatures using Jouyban–Acree model. *Indian J. Chem. Sect. A Inorg. Phys. Theor. Anal. Chem.* **2005**, *44*, 1553–1560.
33. Rodriguez, G.A.; Delgado, D.R.; Martinez, F.; Fakhree, M.A.A.; Jouyban, A. Volumetric properties of glycerol formal + propylene glycol mixtures at several temperatures and correlation with the Jouyban–Acree model. *J. Solut. Chem.* **2012**, *41*, 1477–1494. [CrossRef]
34. Redlich, O.; Kister, A.T. Algebraic Representation of Thermodynamic Properties and the Classification of Solutions. *Ind. Eng. Chem.* **1948**, *40*, 345–348. [CrossRef]
35. Shah, D.; Mjalli, F.S. Effect of water on the thermo-physical properties of Reline: An experimental and molecular simulation based approach. *Phys. Chem. Chem. Phys.* **2014**, *16*, 23900–23907. [CrossRef] [PubMed]
36. Gabriele, F.; Chiarini, M.; Germani, R.; Tiecco, M.; Spreti, N. Effect of water addition on choline chloride/glycol deep eutectic solvents: Characterization of their structural and physicochemical properties. *J. Mol. Liq.* **2019**, *291*, 111301. [CrossRef]
37. Yadav, A.; Kar, J.R.; Verma, M.; Naqvi, S.; Pandey, S. Densities of aqueous mixtures of (choline chloride + ethylene glycol) and (choline chloride + malonic acid) deep eutectic solvents in temperature range 283.15–363.15 K. *Thermochim. Acta* **2015**, *600*, 95–101. [CrossRef]
38. Harifi-Mood, A.R.; Buchner, R. Density, viscosity, and conductivity of choline chloride + ethylene glycol as a deep eutectic solvent and its binary mixtures with dimethyl sulfoxide. *J. Mol. Liq.* **2017**, *225*, 689–695. [CrossRef]
39. Sas, O.G.; Fidalgo, R.; Domínguez, I.; Macedo, E.A.; González, B. Physical properties of the pure deep eutectic solvent, [ChCl][Lev] (1:2) DES, and its binary mixtures with alcohols. *J. Chem. Eng. Data* **2016**, *61*, 4191–4202. [CrossRef]
40. Kim, K.S.; Park, B.H. Volumetric properties of solutions of choline chloride + glycerol deep eutectic solvent with water, methanol, ethanol, or iso-propanol. *J. Mol. Liq.* **2018**, *254*, 272–279. [CrossRef]
41. Flory, P.J. Statistical Thermodynamics of Liquid Mixtures. *J. Am. Chem. Soc.* **1965**, *87*, 1833–1838. [CrossRef]
42. Abe, A.; Flory, P.J. The Thermodynamic Properties of Mixtures of Small, Nonpolar Molecules. *J. Am. Chem. Soc.* **1965**, *87*, 1838–1846. [CrossRef]
43. Prigogine, I. *The Molecular Theory of Solutions*; North Holland Publishing Co.: Amsterdam, The Netherlands, 1957.
44. Patterson, D.; Delmas, G. Corresponding states theories and liquid models. *Discuss. Faraday Soc.* **1970**, *49*, 98–105. [CrossRef]

45. Costas, M.; Patterson, D. Volumes of mixing and the P* effect: Part II. Mixtures of alkanes with liquids of different internal pressures. *J. Solut. Chem.* **1982**, *11*, 807–821. [CrossRef]
46. Vaid, Z.S.; More, U.U.; Oswal, S.B.; Malek, N.I. Experimental and theoretical excess molar properties of imidazolium based ionic liquids with isomers of butanol. *Thermochim. Acta* **2016**, *634*, 38–47. [CrossRef]
47. Aangothu, S.R.; Munnangi, S.R.; Raju, K.T.S.S.; Bollikolla, H.B. An experimental investigation of molecular interactions between [Emim][triflate] ionic liquid & 2-alkoxyethanols and theoretical comparison by PFP theory. *J. Chem. Thermodyn.* **2019**, *138*, 43–50. [CrossRef]
48. Chaudhary, N.; Nain, A.K. Physicochemical studies of intermolecular interactions in 1-butyl-3-methylimidazolium tetrafluoroborate + benzonitrile binary mixtures at temperatures from 293.15 to 318.15 K. *Phys. Chem. Liq.* **2020**, *59*, 358–381. [CrossRef]
49. Fatima, U.; Riyazuddeen; Anwar, N. Effect of Solvents and Temperature on Interactions in Binary and Ternary Mixtures of 1-Butyl-3-methylimidazolium Trifluoromethanesulfonate with Acetonitrile or/and N, N-Dimethylformamide. *J. Chem. Eng. Data* **2018**, *63*, 4288–4305. [CrossRef]
50. Fatima, U.; Riyazuddeen; Anwar, N.; Montes-Campos, H.; Varela, L.M. Molecular dynamic simulation, molecular interactions and structural properties of 1-butyl-3-methylimidazolium bis(trifluoromethylsulfonyl)imide + 1-butanol/1-propanol mixtures at (298.15–323.15) K and 0.1 M Pa. *Fluid Phase Equilib.* **2018**, *472*, 9–21. [CrossRef]
51. Haghbakhsh, R.; Raeissi, S. Excess volumes of mixtures consisting of deep eutectic solvents by the Prigogine–Flory–Patterson theory. *J. Mol. Liq.* **2018**, *272*, 731–737. [CrossRef]
52. Shekaari, H.; Zafarani-Moattar, M.T.; Mokhtarpour, M.; Faraji, S. Volumetric and compressibility properties for aqueous solutions of choline chloride based deep eutectic solvents and Prigogine–Flory–Patterson theory to correlate of excess molar volumes at T = (293.15 to 308.15) K. *J. Mol. Liq.* **2019**, *289*, 111077. [CrossRef]
53. Vranes, M.; Papović, S.; Tot, A.; Zec, N.; Gadžurić, S. Density, excess properties, electrical conductivity and viscosity of 1-butyl-3-methylimidazolium bis(trifluoromethylsulfonyl)imide + γ-butyrolactone binary mixtures. *J. Chem. Thermodyn.* **2014**, *76*, 161–171. [CrossRef]
54. Hawrylak, B.; Gracie, K.; Palepu, R. Thermodynamic properties of binary mixtures of butanediols with water. *J. Solut. Chem.* **1998**, *27*, 17–31. [CrossRef]
55. Benson, G.C.; Kiyohara, O. Evaluation of excess isentropic compressibilities and isochoric heat capacities. *J. Chem. Thermodyn.* **1979**, *11*, 1061–1064. [CrossRef]
56. Brocos, P.; Piñeiro, Á.; Bravo, R.; Amigo, A. Refractive indices, molar volumes and molar refractions of binary liquid mixtures: Concepts and correlations. *Phys. Chem. Chem. Phys.* **2003**, *5*, 550–557. [CrossRef]
57. Nabi, F.; Malik, M.A.; Jesudason, C.G.; Al-Thabaiti, S.A. A review of molecular interactions in organic binary mixtures. *Korean J. Chem. Eng.* **2014**, *31*, 1505–1517. [CrossRef]
58. Garcia, B.; Alcalde, R.; Leal, J.M.; Matos, J.S. Shear viscosities of the N-methylformamide- And N,N-dimethylformamide-(C1-C10) alkan-1-ol solvent systems. *J. Chem. Soc.-Faraday Trans.* **1997**, *93*, 1115–1118. [CrossRef]

Novel binary mixtures of alkanolamine based deep eutectic solvents with water - thermodynamic calculation and correlation of crucial physicochemical properties

Bartosz Nowosielski[a], Marzena Jamrógiewicz[b], Justyna Łuczak[c], Dorota Warmińska[a*]

[a] Department of Physical Chemistry, Faculty of Chemistry, Gdańsk University of Technology, ul. Narutowicza 11/12, 80-233 Gdańsk, POLAND

[b] Department of Physical Chemistry, Faculty of Pharmacy, Medical University of Gdańsk, Al. Gen. Hallera 107, 80-416 Gdańsk, POLAND

[c] Department of Process Engineering and Chemical Technology, Faculty of Chemistry, Gdańsk University of Technology, ul. Narutowicza 11/12, 80-233 Gdańsk, POLAND

*Corresponding author: Tel.:+48583471410; fax:+48583472694,
E-mail address: dorwarmi@ pg.edu.pl

Table S1. Densities ρ, excess molar volumes V^E, isobaric thermal expansion coefficients α_p, excess thermal expansion $\Delta\alpha_p$, speeds of sound u, excess isentropic compressibilities k_S^E, viscosities η, viscosity deviations $\Delta\eta$, excess Gibbs free energy of activation of viscous flow ΔG^{*E}, refractive indices n_D, refractive index deviations Δn_D as functions of mole fraction, x_1 of DES for TBAB:AP (DES1) + water mixtures at the temperatures (293.15 to 303.15) K and atmospheric pressure. [a]

x_1	ρ / kg·m^{-3}	$10^6 V_m^E$ / m^3·mol^{-1}	$10^4 \alpha_p$ / K^{-1}	$10^4 \Delta\alpha_p$ / K^{-1}	u / m·s^{-1}	$10^{10} k_S^E$ / Pa^{-1}	η / mPa·s	$\Delta\eta$ / mPa·s	ΔG^{*E} / J·mol^{-1}	n_D	Δn_D
293.15 K											
0.0000	998.20	0.000	2.119	0.000	1482.52	0.000	1.05	0.000	0.00	1.3340	0.00000
0.0994	1022.32	-0.453	5.944	1.742	1767.38	-1.185	6.47	4.843	3874.91	1.3950	0.00413
0.1981	1032.09	-0.817	7.296	2.057	1811.29	-1.185	18.21	15.695	5585.67	1.4266	0.00742
0.2979	1033.23	-0.979	7.437	1.569	1796.62	-1.002	33.67	29.766	6123.90	1.4440	0.00764
0.3961	1031.40	-1.006	7.477	1.196	1772.86	-0.810	49.46	43.439	6022.89	1.4550	0.00736
0.4983	1028.66	-0.950	7.390	0.802	1748.67	-0.627	60.74	51.292	5373.26	1.4620	0.00599
0.5987	1025.68	-0.827	7.393	0.581	1727.08	-0.467	75.12	60.412	4709.86	1.4667	0.00456
0.6999	1022.93	-0.668	7.356	0.368	1707.97	-0.325	85.40	62.416	3790.44	1.4702	0.00326
0.8000	1020.02	-0.445	7.325	0.198	1688.58	-0.187	93.99	58.259	2775.90	1.4726	0.00187
0.9000	1017.55	-0.211	7.473	0.233	1675.64	-0.083	96.45	40.920	1565.90	1.4750	0.00118
1.0000	1015.71	0.000	7.334	0.000	1666.29	0.000	86.30	0.000	0.00	1.4764	0.00000
298.15 K											
0.0000	997.05	0.000	2.565	0.000	1496.8	0.000	0.90	0.000	0.00	1.3331	0.00000
0.0994	1019.24	-0.432	6.110	1.634	1757.08	-1.113	5.25	3.879	3852.17	1.3937	0.00400
0.1981	1028.31	-0.784	7.376	1.950	1796.54	-1.131	13.92	11.837	5487.88	1.4250	0.00717
0.2979	1029.38	-0.947	7.517	1.515	1781.00	-0.965	25.20	22.023	6025.66	1.4423	0.00742
0.3961	1027.54	-0.978	7.530	1.150	1756.80	-0.783	35.95	31.134	5892.31	1.4532	0.00712
0.4983	1024.84	-0.928	7.451	0.791	1732.43	-0.609	44.31	36.886	5284.13	1.4601	0.00572
0.5987	1021.89	-0.809	7.432	0.567	1710.67	-0.454	54.10	42.745	4620.34	1.4649	0.00443
0.6999	1019.16	-0.655	7.397	0.371	1691.51	-0.317	61.29	43.856	3719.78	1.4684	0.00318
0.8000	1016.25	-0.434	7.331	0.178	1671.67	-0.181	67.26	40.626	2723.50	1.4708	0.00182
0.9000	1013.78	-0.203	7.457	0.200	1657.12	-0.072	69.02	28.345	1535.51	1.4731	0.00106
1.0000	1011.99	0.000	7.343	0.000	1649.50	0.000	62.12	0.000	0.00	1.4746	0.00000
303.15 K											
0.0000	995.65	0.000	3.010	0.000	1509.53	0.000	0.79	0.000	0.00	1.3322	0.00000
0.0994	1016.09	-0.412	6.275	1.526	1746.66	-1.049	4.39	3.204	3835.67	1.3925	0.00394

0.1981	1024.50	-0.752	7.456	1.844	1781.64	-1.082	11.06	9.285	5408.30	1.4234	0.00687
0.2979	1025.50	-0.918	7.597	1.463	1765.20	-0.931	19.47	16.803	5921.86	1.4407	0.00723
0.3961	1023.66	-0.951	7.583	1.105	1740.68	-0.760	27.16	23.176	5766.31	1.4514	0.00680
0.4983	1021.02	-0.906	7.513	0.781	1715.83	-0.591	33.07	27.023	5155.10	1.4583	0.00546
0.5987	1018.09	-0.792	7.471	0.553	1694.24	-0.443	40.39	31.278	4518.31	1.4632	0.00433
0.6999	1015.39	-0.642	7.438	0.374	1674.98	-0.309	45.65	31.870	3634.30	1.4667	0.00310
0.8000	1012.58	-0.433	7.336	0.157	1656.35	-0.182	49.32	28.582	2618.91	1.4691	0.00178
0.9000	1009.99	-0.193	7.441	0.168	1639.39	-0.065	50.84	19.640	1459.93	1.4714	0.00104
1.0000	1008.28	0.000	7.351	0.000	1632.76	0.000	46.94	0.000	0.00	1.4729	0.00000
308.15 K											
0.0000	994.03	0.000	3.455	0.000	1520.29	0.000	0.69	0.000	0.00	1.3314	0.00000
0.0994	1012.87	-0.393	6.441	1.420	1736.11	-0.992	3.72	2.698	3859.25	1.3913	0.00388
0.1981	1020.68	-0.723	7.536	1.738	1766.28	-1.038	8.96	7.451	5377.72	1.4217	0.00650
0.2979	1021.59	-0.888	7.677	1.410	1749.37	-0.901	15.33	13.092	5860.90	1.4389	0.00689
0.3961	1019.77	-0.925	7.636	1.060	1724.41	-0.739	21.05	17.752	5695.79	1.4495	0.00646
0.4983	1017.18	-0.885	7.575	0.771	1699.51	-0.578	25.34	20.402	5080.02	1.4565	0.00528
0.5987	1014.28	-0.775	7.511	0.540	1677.87	-0.434	30.69	23.349	4445.32	1.4614	0.00420
0.6999	1011.61	-0.629	7.479	0.378	1658.56	-0.304	34.65	23.700	3578.47	1.4649	0.00302
0.8000	1008.85	-0.426	7.342	0.137	1638.97	-0.175	38.32	22.062	2640.15	1.4672	0.00163
0.9000	1006.24	-0.185	7.425	0.136	1622.30	-0.061	39.70	15.568	1509.07	1.4695	0.00091
1.0000	1004.58	0.000	7.359	0.000	1615.89	0.000	35.82	0.000	0.00	1.4711	0.00000
313.15 K											
0.0000	992.22	0.000	3.901	0.000	1529.42	0.000	0.61	0.000	0.00	1.3305	0.00000
0.0994	1009.57	-0.375	6.607	1.314	1725.05	-0.940	3.16	2.268	3853.31	1.3900	0.00386
0.1981	1016.81	-0.695	7.616	1.634	1751.15	-0.998	7.44	6.138	5370.01	1.4199	0.00620
0.2979	1017.65	-0.86	7.757	1.359	1733.12	-0.873	12.36	10.454	5816.30	1.4370	0.00663
0.3961	1015.87	-0.900	7.688	1.016	1708.21	-0.719	16.53	13.754	5611.03	1.4475	0.00619
0.4983	1013.31	-0.864	7.636	0.761	1683.20	-0.564	19.63	15.526	4982.33	1.4545	0.00510
0.5987	1010.47	-0.758	7.550	0.526	1661.22	-0.424	23.86	17.835	4378.55	1.4595	0.00417
0.6999	1007.82	-0.616	7.520	0.381	1642.16	-0.298	26.82	17.945	3518.32	1.4629	0.00293
0.8000	1005.15	-0.421	7.347	0.116	1621.35	-0.166	29.92	16.906	2619.11	1.4652	0.00157
0.9000	1002.53	-0.181	7.409	0.104	1605.15	-0.055	31.17	12.091	1516.01	1.4675	0.00089
1.0000	1000.89	0.000	7.368	0.000	1599.37	0.000	27.97	0.000	0.00	1.4691	0.00000

[a] Standard uncertainties u are: $u(T)$ =0.01 K for density, speed of sound and viscosity and $u(T)$ = 0.1 K for refractive index, $u(p)$ = 10 kPa, $u(x_i)$ = $1 \cdot 10^{-4}$, $u(\rho)$ = 0.035 kg·m^{-3}, $u(u)$ = 0.2 m·s^{-1}, $u_r(\eta)$ = 1% , $u(n_D)$ = 0.0002

Table S2. Densities ρ, excess molar volumes V^E, isobaric thermal expansion coefficients α_p , excess thermal expansion $\Delta\alpha_p$, speeds of sound u, excess isentropic compressibilities k_S^E, viscosities η, viscosity deviations $\Delta\eta$, excess Gibbs free energy of activation of viscous flow ΔG^{*E}, refractive indices n_D, refractive index deviations Δn_D as functions of mole fraction, x_1 of DES for TBAC:AP (DES2) + water mixtures at the temperatures (293.15 to 303.15) K and atmospheric pressure. [a]

x_1	ρ / kg·m^{-3}	$10^6 V_m^E$ / m^3·mol^{-1}	$10^3\alpha_p$ / K^{-1}	$10^4\Delta\alpha_p$ / K^{-1}	u / m·s^{-1}	$10^{10} k_S^E$ / Pa^{-1}	η / mPa·s	$\Delta\eta$ / mPa·s	ΔG^{*E} / J·mol^{-1}	n_D	Δn_D
293.15 K											
0.0000	998.20	0.000	2.134	0.000	1482.52	0.000	1.05	0.000	0.00	1.3340	0.00000
0.0982	1004.94	-0.488	6.083	1.915	1788.22	-1.229	6.29	4.683	3813.83	1.3935	0.00580
0.1964	1004.60	-0.843	7.265	2.062	1843.38	-1.243	17.39	14.929	5494.35	1.4225	0.00759
0.2947	999.85	-1.002	7.469	1.642	1831.12	-1.056	30.98	27.194	5968.10	1.4392	0.00784
0.3943	994.14	-1.032	7.437	1.188	1808.34	-0.856	44.48	38.604	5810.89	1.4494	0.00690
0.4899	988.81	-0.974	7.407	0.866	1785.23	-0.674	56.32	47.277	5324.20	1.4563	0.00612
0.5921	983.76	-0.855	7.360	0.586	1763.55	-0.504	65.59	51.626	4507.89	1.4613	0.00496
0.6905	979.41	-0.692	7.359	0.411	1744.52	-0.356	71.07	48.982	3522.16	1.4651	0.00416
0.7946	975.37	-0.483	7.351	0.255	1727.25	-0.220	77.89	44.519	2461.07	1.4679	0.00308
0.8959	971.90	-0.250	7.307	0.095	1713.19	-0.105	85.81	33.748	1421.25	1.4698	0.00191
1.0000	968.86	0.000	7.305	0.000	1700.32	0.000	82.77	0.000	0.00	1.4705	0.00000
298.15 K											
0.0000	997.04	0.000	2.575	0.000	1496.80	0.000	0.90	0.000	0.00	1.3331	0.00000
0.0982	1001.83	-0.464	6.192	1.750	1778.69	-1.161	5.06	3.705	3767.13	1.3921	0.00550
0.1964	1000.91	-0.809	7.344	1.953	1827.99	-1.188	13.34	11.299	5400.17	1.4210	0.00733
0.2947	996.10	-0.970	7.544	1.581	1814.97	-1.019	23.10	20.014	5853.61	1.4376	0.00757
0.3943	990.43	-1.005	7.508	1.158	1791.82	-0.829	32.34	27.631	5672.78	1.4478	0.00670
0.4899	985.13	-0.951	7.468	0.852	1768.62	-0.656	40.43	33.305	5186.02	1.4545	0.00577
0.5921	980.13	-0.838	7.410	0.580	1742.83	-0.476	47.04	36.223	4395.99	1.4594	0.00455
0.6905	975.80	-0.678	7.396	0.406	1727.69	-0.349	51.46	34.653	3457.91	1.4631	0.00369
0.7946	971.78	-0.473	7.371	0.248	1710.02	-0.215	56.44	31.454	2424.21	1.4661	0.00284
0.8959	968.35	-0.247	7.327	0.097	1695.62	-0.102	62.41	24.102	1418.02	1.4680	0.00169
1.0000	965.32	0.000	7.315	0.000	1682.88	0.000	59.81	0.000	0.00	1.4689	0.00000
303.15 K											
0.0000	995.65	0.000	3.016	0.000	1509.53	0.000	0.79	0.000	0.00	1.3322	0.00000
0.0982	998.74	-0.444	6.301	1.585	1768.06	-1.095	4.20	3.029	3732.44	1.3907	0.00528
0.1964	997.19	-0.777	7.422	1.844	1812.73	-1.138	10.64	8.903	5333.74	1.4194	0.00709

0.2947	992.34	-0.939	7.618	1.520	1798.92	-0.984	17.89	15.305	5758.47	1.4357	0.00715
0.3943	986.70	-0.978	7.578	1.129	1775.40	-0.805	24.43	20.548	5550.79	1.4460	0.00647
0.4899	981.45	-0.928	7.529	0.838	1751.99	-0.638	30.08	24.297	5055.75	1.4527	0.00560
0.5921	976.49	-0.820	7.460	0.575	1726.03	-0.463	35.17	26.529	4305.18	1.4576	0.00443
0.6905	972.20	-0.664	7.432	0.402	1710.85	-0.341	38.66	25.456	3402.54	1.4612	0.00351
0.7946	968.20	-0.463	7.392	0.241	1693.30	-0.211	42.88	23.544	2420.68	1.4640	0.00249
0.8959	964.81	-0.242	7.348	0.100	1678.51	-0.099	47.33	18.160	1433.04	1.4658	0.00127
1.0000	961.80	0.000	7.325	0.000	1665.99	0.000	44.78	0.000	0.00	1.4671	0.00000
308.15 K											
0.0000	994.03	0.000	3.457	0.000	1520.29	0.000	0.69	0.000	0.00	1.3314	0.00000
0.0982	995.58	-0.425	6.410	1.421	1757.38	-1.039	3.67	2.661	3828.70	1.3897	0.00505
0.1964	993.45	-0.747	7.500	1.735	1797.30	-1.094	8.70	7.222	5322.88	1.4184	0.00688
0.2947	988.55	-0.909	7.693	1.460	1782.62	-0.953	14.2	12.029	5713.07	1.4347	0.00696
0.3943	982.95	-0.951	7.648	1.100	1758.52	-0.782	18.92	15.703	5472.45	1.4448	0.00610
0.4899	977.75	-0.906	7.590	0.824	1735.23	-0.623	23.22	18.491	4993.20	1.4515	0.00525
0.5921	972.85	-0.802	7.510	0.570	1708.88	-0.451	27.45	20.476	4292.79	1.4563	0.00399
0.6905	968.58	-0.650	7.468	0.398	1693.99	-0.334	30.54	20.032	3439.23	1.4599	0.00308
0.7946	964.63	-0.454	7.413	0.234	1676.43	-0.207	33.23	18.034	2427.03	1.4627	0.00207
0.8959	961.26	-0.238	7.368	0.102	1661.65	-0.098	35.89	13.275	1401.48	1.4646	0.00096
1.0000	958.28	0.000	7.336	0.000	1648.89	0.000	34.23	0.000	0.00	1.4662	0.00000
313.15 K											
0.0000	992.21	0.000	3.898	0.000	1529.42	0.000	0.61	0.000	0.00	1.3305	0.00000
0.0982	992.34	-0.408	6.519	1.258	1746.33	-0.987	3.14	2.259	3841.10	1.3882	0.00483
0.1964	989.68	-0.718	7.578	1.627	1781.41	-1.052	7.43	6.156	5388.88	1.4167	0.00667
0.2947	984.73	-0.880	7.767	1.401	1766.25	-0.925	11.33	9.482	5642.12	1.4328	0.00670
0.3943	979.18	-0.926	7.718	1.071	1741.86	-0.762	15.00	12.297	5412.64	1.4428	0.00584
0.4899	974.03	-0.883	7.651	0.811	1718.48	-0.609	17.74	13.816	4860.83	1.4495	0.00506
0.5921	969.19	-0.785	7.560	0.566	1692.08	-0.441	21.26	15.547	4218.20	1.4543	0.00386
0.6905	964.96	-0.637	7.504	0.394	1676.87	-0.327	24.19	15.697	3441.56	1.4577	0.00279
0.7946	961.05	-0.445	7.434	0.227	1659.64	-0.204	26.42	14.286	2456.99	1.4604	0.00172
0.8959	957.72	-0.233	7.389	0.104	1644.80	-0.096	28.01	10.187	1399.79	1.4623	0.00064
1.0000	954.77	0.000	7.346	0.000	1631.99	0.000	26.61	0.000	0.00	1.4642	0.00000

[a] Standard uncertainties u are: $u(T)$ =0.01 K for density, speed of sound and viscosity and $u(T)$ = 0.1 K for refractive index, $u(p)$ = 10 kPa, $u(x_i)$ = $1 \cdot 10^{-4}$ $u(\rho)$ = 0.035 kg·m^{-3}, $u(u)$ = 0.2 m·s^{-1}, $u_r(\eta)$ = 1% , $u(n_D)$ = 0.0002

Table S3. Densities ρ, excess molar volumes V^E, isobaric thermal expansion coefficients α_p , excess thermal expansion $\Delta\alpha_p$, speed of sounds u, excess isentropic compressibilities k_S^E, viscosities η, viscosity deviations $\Delta\eta$, excess Gibbs free energy of activation of viscous flow ΔG^{*E}, refractive indices n_D, refractive index deviations Δn_D as functions of mole fraction, x_1 of DES for TBAB:MAE (DES3) + water mixtures at the temperatures (293.15 to 303.15) K and atmospheric pressure. [a]

x_1	ρ / kg·m^{-3}	$10^6 V_m^E$ / m^3·mol^{-1}	$10^4 \alpha_p$ / K^{-1}	$10^4 \Delta\alpha_p$ / K^{-1}	u / m·s^{-1}	$10^{10} k_S^E$ / Pa^{-1}	η / mPa·s	$\Delta\eta$ / mPa·s	ΔG^{*E} / J·mol^{-1}	n_D	Δn_D
293.15 K											
0.0000	998.20	0.000	2.119	0.000	1482.52	0.000	1.05	0.000	0.00	1.3340	0.00000
0.0978	1016.19	-0.617	6.186	1.965	1738.92	-1.463	6.76	5.235	4147.73	1.3921	0.00631
0.1982	1018.89	-1.017	7.364	2.083	1731.41	-1.462	18.26	16.039	5912.10	1.4208	0.00888
0.2957	1014.71	-1.155	7.383	1.489	1686.27	-1.251	28.68	25.463	6229.61	1.4360	0.00899
0.3970	1009.27	-1.159	7.375	1.060	1641.46	-1.009	39.11	34.394	6071.66	1.4452	0.00780
0.4958	1004.09	-1.072	7.323	0.716	1604.42	-0.786	45.73	38.886	5492.02	1.4506	0.00602
0.5935	999.33	-0.917	7.280	0.457	1574.10	-0.587	50.05	40.149	4711.38	1.4543	0.00439
0.6956	995.01	-0.713	7.264	0.266	1548.23	-0.404	51.50	36.934	3692.97	1.4572	0.00298
0.7979	991.43	-0.494	7.279	0.141	1527.38	-0.248	51.65	30.199	2575.62	1.4594	0.00175
0.8940	988.31	-0.248	7.301	0.057	1510.73	-0.117	51.65	20.805	1495.23	1.4613	0.00101
1.0000	985.67	0.000	7.342	0.000	1496.77	0.000	46.05	0.000	0.00	1.4627	0.00000
298.15 K											
0.0000	997.05	0.000	2.565	0.000	1496.80	0.000	0.90	0.000	0.00	1.3331	0.00000
0.0978	1013.00	-0.593	6.341	1.839	1727.94	-1.399	5.35	4.064	4059.50	1.3905	0.00598
0.1982	1015.12	-0.984	7.459	1.981	1717.11	-1.420	13.77	11.911	5765.79	1.4190	0.00853
0.2957	1010.94	-1.125	7.483	1.441	1671.56	-1.224	21.14	18.495	6065.45	1.4342	0.00874
0.3970	1005.53	-1.135	7.465	1.036	1626.62	-0.992	28.75	24.922	5931.15	1.4433	0.00752
0.4958	1000.40	-1.053	7.403	0.706	1589.56	-0.776	33.30	27.813	5350.14	1.4487	0.00579
0.5935	995.67	-0.903	7.355	0.459	1559.06	-0.580	36.52	28.685	4593.14	1.4524	0.00420
0.6956	991.38	-0.705	7.327	0.271	1533.11	-0.401	38.12	26.751	3626.27	1.4553	0.00282
0.7979	987.82	-0.490	7.331	0.146	1512.16	-0.246	38.33	21.820	2530.01	1.4575	0.00161
0.8940	984.70	-0.247	7.344	0.062	1495.39	-0.116	38.31	14.869	1461.16	1.4594	0.00089
1.0000	982.05	0.000	7.372	0.000	1481.33	0.000	34.50	0.000	0.00	1.4609	0.00000
303.15 K											
0.0000	994.03	0.000	3.010	0.000	1509.53	0.000	0.79	0.000	0.00	1.3322	0.00000
0.0978	1006.45	-0.571	6.496	1.713	1716.80	-1.341	4.42	3.300	4006.30	1.3889	0.00568
0.1982	1007.48	-0.952	7.555	1.880	1702.63	-1.382	10.86	9.267	5658.63	1.4172	0.00823

0.2957	1003.31	-1.097	7.582	1.394	1656.36	-1.200	16.31	14.066	5937.07	1.4323	0.00846
0.3970	997.97	-1.110	7.556	1.013	1611.59	-0.978	21.90	18.700	5799.91	1.4414	0.00732
0.4958	992.94	-1.034	7.484	0.697	1574.83	-0.769	25.07	20.533	5209.02	1.4467	0.00555
0.5935	988.31	-0.889	7.430	0.462	1543.96	-0.575	27.41	21.017	4461.74	1.4504	0.00400
0.6956	984.08	-0.696	7.391	0.276	1517.78	-0.397	28.15	18.988	3468.73	1.4533	0.00265
0.7979	980.55	-0.484	7.383	0.152	1496.98	-0.245	28.83	15.692	2431.52	1.4555	0.00147
0.8940	977.46	-0.244	7.387	0.066	1480.08	-0.115	29.47	11.036	1430.64	1.4574	0.00078
1.0000	974.81	0.000	7.403	0.000	1465.91	0.000	26.78	0.000	0.00	1.4590	0.00000
308.15 K											
0.0000	994.03	0.000	3.455	0.000	1520.29	0.000	0.69	0.000	0.00	1.3314	0.00000
0.0978	1006.45	-0.550	6.651	1.588	1705.28	-1.291	3.73	2.761	4013.42	1.3876	0.00542
0.1982	1007.48	-0.922	7.650	1.780	1688.00	-1.349	8.78	7.421	5612.26	1.4157	0.00790
0.2957	1003.31	-1.069	7.682	1.347	1641.36	-1.180	12.76	10.858	5835.10	1.4308	0.00819
0.3970	997.97	-1.087	7.646	0.990	1596.47	-0.967	17.17	14.483	5726.92	1.4399	0.00711
0.4958	992.94	-1.016	7.564	0.688	1559.75	-0.763	20.22	16.460	5225.68	1.4452	0.00536
0.5935	988.31	-0.875	7.505	0.465	1528.83	-0.571	21.73	16.479	4446.77	1.4489	0.00384
0.6956	984.08	-0.686	7.454	0.281	1502.71	-0.395	22.37	14.924	3469.99	1.4518	0.00251
0.7979	980.55	-0.478	7.435	0.157	1481.63	-0.243	22.88	12.315	2438.83	1.4540	0.00135
0.8940	977.46	-0.241	7.430	0.071	1464.88	-0.115	23.35	8.673	1442.26	1.4559	0.00066
1.0000	974.81	0.000	7.433	0.000	1450.59	0.000	21.09	0.000	0.00	1.4576	0.00000
313.15 K											
0.0000	992.22	0.000	3.901	0.000	1529.42	0.000	0.61	0.000	0.00	1.3305	0.00000
0.0978	1003.07	-0.531	6.806	1.464	1693.90	-1.247	3.18	2.331	4011.77	1.3861	0.00518
0.1982	1003.61	-0.893	7.746	1.681	1672.92	-1.319	7.25	6.072	5580.17	1.4140	0.00764
0.2957	999.43	-1.043	7.782	1.300	1626.16	-1.163	10.25	8.616	5758.91	1.4289	0.00784
0.3970	994.13	-1.063	7.736	0.968	1581.28	-0.957	13.63	11.349	5644.25	1.4381	0.00693
0.4958	989.17	-0.997	7.645	0.679	1544.61	-0.757	15.94	12.772	5140.47	1.4433	0.00514
0.5935	984.58	-0.861	7.580	0.468	1514.04	-0.570	17.07	12.688	4363.91	1.4470	0.00365
0.6956	980.41	-0.677	7.517	0.286	1487.62	-0.394	17.33	11.178	3360.36	1.4499	0.00235
0.7979	976.90	-0.473	7.487	0.163	1466.54	-0.243	17.86	9.218	2357.62	1.4521	0.00121
0.8940	973.82	-0.238	7.473	0.076	1449.56	-0.113	18.17	6.276	1360.62	1.4540	0.00055
1.0000	971.19	0.000	7.463	0.000	1435.41	0.000	16.92	0.000	0.00	1.4558	0.00000

[a] Standard uncertainties u are: $u(T)$ =0.01 K for density, speed of sound and viscosity and $u(T)$ = 0.1 K for refractive index, $u(p)$ = 10 kPa, $u(x_i)$ = $1 \cdot 10^{-4}$ $u(\rho)$ = 0.035 kg·m^{-3}, $u(u)$ = 0.2 m·s^{-1}, $u_r(\eta)$ = 1% , $u(n_D)$ = 0.0002

Table S4. Densities ρ, excess molar volumes V^E, isobaric thermal expansion coefficients α_p , excess thermal expansion $\Delta\alpha_p$, speed of sound u, excess isentropic compressibilities k_S^E, viscosities η, viscosity deviations $\Delta\eta$, excess Gibbs free energy of activation of viscous flow ΔG^{*E}, refractive indices n_D, refractive index deviations Δn_D as functions of mole fraction, x_1 of DES for TBAB:BAE (DES4) + water mixtures at the temperatures (293.15 to 303.15) K and atmospheric pressure. [a]

x_1	ρ / kg·m^{-3}	$10^6 V_m^E$ / m^3·mol^{-1}	$10^4 \alpha_p$ / K^{-1}	$10^4\Delta\alpha_p$ / K^{-1}	u / m·s^{-1}	$10^{10} k_S^E$ / Pa^{-1}	η / mPa·s	$\Delta\eta$ / mPa·s	ΔG^{*E} / J·mol^{-1}	n_D	Δn_D
293.15 K											
0.0000	998.20	0.000	2.119	0.000	1482.52	0.000	1.05	0.000	0.00	1.334	0.00000
0.0975	987.04	-0.583	6.633	1.805	1605.54	-1.196	8.64	7.086	4982.17	1.3999	0.00554
0.1951	976.01	-0.879	7.459	1.543	1580.95	-1.160	20.06	17.758	6430.49	1.4261	0.00750
0.2936	967.54	-1.030	7.684	1.177	1548.49	-0.980	33.26	29.838	6827.16	1.4391	0.00735
0.3943	960.63	-1.069	7.754	0.874	1521.14	-0.791	46.71	41.580	6664.02	1.4464	0.00631
0.4930	955.07	-1.019	7.753	0.624	1499.17	-0.620	54.37	46.739	5974.18	1.4509	0.00525
0.5925	950.31	-0.896	7.738	0.426	1480.24	-0.461	60.92	49.533	5120.29	1.4537	0.00399
0.6975	946.07	-0.708	7.726	0.269	1463.88	-0.314	62.40	45.023	3933.83	1.4558	0.00286
0.7920	942.81	-0.502	7.731	0.171	1451.18	-0.196	62.48	37.068	2782.20	1.4573	0.00208
0.8938	939.77	-0.247	7.718	0.069	1440.66	-0.091	60.29	22.015	1421.51	1.4585	0.00129
1.0000	937.31	0.000	7.725	0.000	1431.73	0.000	58.66	0.000	0.00	1.4589	0.00000
298.15 K											
0.0000	997.05	0.000	2.565	0.000	1496.80	0.000	0.90	0.000	0.00	1.3331	0.00000
0.0975	983.73	-0.557	6.769	1.693	1596.27	-1.152	6.85	5.536	4912.72	1.3984	0.00537
0.1951	972.34	-0.847	7.570	1.488	1567.74	-1.132	15.28	13.361	6321.05	1.4244	0.00731
0.2936	963.80	-0.999	7.793	1.165	1533.63	-0.961	25.00	22.181	6725.16	1.4372	0.00705
0.3943	956.88	-1.041	7.871	0.896	1505.66	-0.778	34.26	30.101	6533.68	1.4445	0.00608
0.4930	951.35	-0.996	7.837	0.633	1483.43	-0.611	39.21	33.109	5824.06	1.4490	0.00506
0.5925	946.62	-0.878	7.811	0.438	1464.64	-0.457	43.81	34.829	4982.49	1.4518	0.00382
0.6975	942.40	-0.695	7.787	0.279	1448.91	-0.318	45.11	31.617	3825.30	1.4539	0.00271
0.7920	939.16	-0.493	7.776	0.174	1435.02	-0.192	45.50	26.028	2704.65	1.4554	0.00195
0.8938	936.14	-0.243	7.757	0.073	1424.82	-0.092	44.27	15.354	1375.95	1.4565	0.00108
1.0000	933.69	0.000	7.754	0.000	1415.72	0.000	43.66	0.000	0.00	1.4571	0.00000
303.15 K											
0.0000	995.65	0.000	3.010	0.000	1509.53	0.000	0.79	0.000	0.00	1.3322	0.00000
0.0975	980.38	-0.534	6.904	1.581	1587.12	-1.117	5.65	4.507	4874.04	1.3969	0.00526
0.1951	968.65	-0.818	7.681	1.433	1553.86	-1.106	12.20	10.555	6259.26	1.4226	0.00709

0.2936	960.03	-0.969	7.903	1.153	1518.73	-0.945	19.53	17.157	6650.31	1.4353	0.00684
0.3943	953.10	-1.012	7.987	0.920	1490.41	-0.768	25.84	22.381	6400.73	1.4425	0.00583
0.4930	947.61	-0.973	7.921	0.642	1467.70	-0.604	29.54	24.534	5709.66	1.4470	0.00485
0.5925	942.91	-0.859	7.885	0.451	1449.33	-0.456	32.86	25.589	4876.35	1.4498	0.00365
0.6975	938.73	-0.682	7.847	0.290	1432.25	-0.309	33.81	23.043	3733.45	1.4519	0.00256
0.7920	935.51	-0.483	7.822	0.178	1418.25	-0.184	34.21	18.867	2633.52	1.4534	0.00182
0.8938	932.51	-0.238	7.796	0.077	1408.61	-0.088	33.47	11.005	1331.17	1.4545	0.00096
1.0000	930.07	0.000	7.783	0.000	1399.85	0.000	33.43	0.000	0.00	1.4552	0.00000
308.15 K											
0.0000	994.03	0.000	3.455	0.000	1520.29	0.000	0.69	0.000	0.00	1.3314	0.00000
0.0975	976.97	-0.511	7.040	1.471	1577.06	-1.084	4.69	3.708	4861.36	1.3954	0.00514
0.1951	964.91	-0.789	7.793	1.379	1539.85	-1.082	9.91	8.511	6243.95	1.4208	0.00690
0.2936	956.21	-0.939	8.012	1.141	1503.75	-0.930	15.55	13.552	6620.04	1.4333	0.00657
0.3943	949.28	-0.982	8.104	0.943	1474.09	-0.753	20.44	17.562	6380.94	1.4405	0.00565
0.4930	943.84	-0.948	8.005	0.652	1451.90	-0.596	22.94	18.826	5661.78	1.4449	0.00463
0.5925	939.19	-0.839	7.958	0.464	1433.59	-0.451	25.10	19.196	4803.08	1.4477	0.00346
0.6975	935.04	-0.667	7.908	0.301	1416.38	-0.305	25.76	17.131	3667.46	1.4498	0.00241
0.7920	931.85	-0.474	7.867	0.182	1402.68	-0.183	26.39	14.240	2610.80	1.4513	0.00168
0.8938	928.87	-0.234	7.835	0.081	1392.95	-0.087	25.82	8.252	1318.63	1.4524	0.00085
1.0000	926.45	0.000	7.813	0.000	1384.17	0.000	25.81	0.000	0.00	1.4532	0.00000
313.15 K											
0.0000	992.22	0.000	3.901	0.000	1529.42	0.000	0.61	0.000	0.00	1.3305	0.00000
0.0975	973.50	-0.490	7.176	1.681	1566.84	-1.057	3.92	3.062	4827.81	1.3941	0.00493
0.1951	961.13	-0.761	7.904	1.609	1526.93	-1.069	8.14	6.932	6217.66	1.4194	0.00667
0.2936	952.37	-0.909	8.122	1.366	1488.46	-0.915	12.92	11.208	6658.46	1.4319	0.00639
0.3943	945.41	-0.950	8.221	1.148	1459.07	-0.747	16.24	13.811	6330.27	1.4391	0.00549
0.4930	940.05	-0.923	8.089	0.797	1436.26	-0.591	17.98	14.546	5593.38	1.4434	0.00438
0.5925	935.44	-0.819	8.032	0.578	1417.33	-0.444	19.50	14.634	4727.97	1.4462	0.00323
0.6975	931.33	-0.652	7.968	0.384	1400.79	-0.304	20.08	13.044	3612.81	1.4483	0.00219
0.7920	928.18	-0.464	7.913	0.224	1388.11	-0.190	20.42	10.629	2548.67	1.4499	0.00157
0.8938	925.23	-0.229	7.874	0.105	1377.38	-0.087	20.29	6.295	1305.52	1.4510	0.00074
1.0000	922.83	0.000	7.842	0.000	1368.57	0.000	20.30	0.000	0.00	1.4519	0.00000

[a] Standard uncertainties u are: $u(T)$ =0.01 K for density, speed of sound and viscosity and $u(T)$ = 0.1 K for refractive index, $u(p)$ = 10 kPa, $u(x_i)$ = $1 \cdot 10^{-4}$ $u(\rho)$ = 0.035 kg·m^{-3}, $u(u)$ = 0.2 m·s^{-1}, $u_r(\eta)$ = 1% , $u(n_D)$ = 0.0002

Table S5 Parameters of the JAM equation, together with *RMSD* and *ARD%* for density, speed of sound, viscosity and refractive index of DES (1) + water (2) systems at different temperatures.

T / K	293.15	298.15	303.15	308.15	313.15	293.15	298.15	303.15	308.15	313.15
					ρ / kg·m^{-3}					
		DES1 (1) + water (2)					DES2 (1) + water (2)			
A_0	24.8275	23.7395	22.6995	21.7383	20.8103	5.7143	4.2731	2.8780	1.5468	0.2672
A_1	-27.0200	-25.8625	-24.7000	-23.6118	-22.6113	-13.9849	-12.6833	-11.3833	-10.1036	-8.8636
A_2	26.7075	24.7500	23.0350	21.3838	19.9113	16.3915	14.9069	13.3060	11.7903	10.3483
A_3	-17.9650	-16.4675	-15.1600	-13.9238	-12.6038	-9.7227	-7.6083	-5.9668	-4.4809	-3.0999
A_4	-	-	-	-	-	-0.5512	-1.9659	-2.6380	-3.2256	-3.7564
R^2	0.9999	0.9999	0.9999	0.9999	0.9999	0.9996	0.9994	0.9993	0.9992	0.9990
RMSD	0.00017	0.00016	0.00013	0.00013	0.00013	0.00014	0.00014	0.00013	0.00011	0.00010
ARD%	0.0094	0.0086	0.0068	0.0063	0.0064	0.0073	0.0074	0.0067	0.0060	0.0054
		DES3 (1) + water (2)					DES4 (1) + water (2)			
A_0	13.5545	12.3320	11.1835	10.0645	8.9810	-15.2749	-17.2111	-19.0931	-20.9427	-22.7449
A_1	-21.6575	-20.4875	-19.3300	-18.2375	-17.1650	6.3675	7.8770	9.3910	10.8915	12.4003
A_2	29.3125	27.2200	25.2725	23.4350	21.7125	-4.3187	-5.4068	-6.4975	-7.5559	-8.5685
A_3	-23.8975	-21.7775	-19.915	-18.1625	-16.5600	-4.6725	-1.7230	0.9155	3.3840	5.6678
A_4	-	-	-	-	-	7.7956	4.6164	1.7841	-0.8624	-3.3666
R^2	0.9991	0.9992	0.9993	0.9993	0.9994	0.9995	0.9998	0.9995	0.9999	0.9999
RMSD	0.00037	0.00032	0.00027	0.00024	0.00020	0.00016	0.00011	0.00008	0.00005	0.00004
ARD%	0.020	0.017	0.015	0.012	0.010	0.0087	0.0062	0.0039	0.0026	0.0018
					u / m·s^{-1}					
		DES1 (1) + water (2)					DES2 (1) + water (2)			
A_0	126.286	116.013	108.149	100.740	92.017	136.992	128.015	120.735	111.169	103.579
A_1	-127.313	-121.125	-113.488	-106.725	-101.388	-138.025	-133.000	-126.000	-121.438	-115.475
A_2	114.750	112.000	112.450	106.125	99.588	126.350	125.250	122.000	117.500	112.213
A_3	-258.188	-243.875	-228.613	-214.475	-201.663	-263.275	-242.500	-225.000	-209.063	-193.475

A_4	234.594	206.188	177.731	161.500	145.525	248.038	225.250	203.875	186.656	172.494
R^2	0.9994	0.9994	0.9994	0.9994	0.9995	0.9995	0.9992	0.9993	0.9992	0.9992
RMSD	0.0025	0.0024	0.0020	0.0022	0.0016	0.0023	0.0026	0.0034	0.0023	0.0021
%ARD	0.14	0.13	0.11	0.12	0.09	0.12	0.15	0.19	0.13	0.12
		DES3 (1) + water (2)					DES4 (1) + water (2)			
A_0	86.371	79.321	67.809	59.512	51.428	34.050	22.706	11.316	0.518	-9.699
A_1	-106.713	-98.563	-93.988	-87.900	-81.000	-41.275	-32.387	-25.325	-16.862	-9.175
A_2	96.600	93.250	87.200	82.975	77.875	28.975	25.025	14.037	9.713	9.487
A_3	-293.088	-272.938	-254.113	-236.400	-221.500	-179.525	-162.913	-146.125	-130.338	-113.775
A_4	307.944	284.219	264.731	244.288	227.063	213.100	189.619	177.631	158.275	135.331
R^2	0.9981	0.9982	0.9983	0.9983	0.9983	0.9957	0.9955	0.9951	0.9948	0.9946
RMSD	0.0044	0.0044	0.0039	0.003	0.0027	0.0032	0.0027	0.0024	0.0020	0.0017
%ARD	0.22	0.22	0.20	0.15	0.13	0.16	0.14	0.12	0.10	0.08
					η / mPas					
		DES1 (1) + water (2)					DES2 (1) + water (2)			
A_0	2197.11	2136.93	2070.94	2019.88	1968.01	2097.76	2027.09	1961.63	1929.09	1877.78
A_1	-1403.39	-1356.08	-1317.26	-1308.93	-1310.74	-1544.04	-1499.41	-1459.13	-1336.26	-1291.43
A_2	1449.19	1447.63	1428.56	1539.63	1614.44	1287.94	1331.56	1407.88	1493.06	1646.63
A_3	-450.26	-515.33	-644.89	-599.68	-583.61	-518.41	-517.04	-501.88	-831.89	-924.68
R^2	0.9998	0.9998	0.9997	0.9996	0.9996	0.9994	0.9994	0.9995	0.9995	0.9998
RMSD	0.016	0.016	0.017	0.021	0.019	0.027	0.025	0.023	0.022	0.014
%ARD	0.89	0.90	0.97	1.14	1.11	1.57	1.47	1.35	1.31	0.79
		DES3 (1) + water (2)					DES4 (1) + water (2)			
A_0	2186.81	2114.56	2034.01	2009.49	1958.05	2307.65	2227.63	2157.71	2120.71	2307.65
A_1	-1527.24	-1458.39	-1475.74	-1383.16	-1380.75	-1459.50	-1458.38	-1447.00	-1483.13	-1459.50
A_2	1537.94	1511.69	1500.44	1499.06	1478.75	707.25	756.63	814.38	822.75	707.25
A_3	-936.61	-944.76	-875.61	-1011.79	-1100.25	-1744.50	-1682.63	-1697.50	-1607.38	-1744.50
A_4	-	-	-	-	-	1861.75	1748.00	1651.56	1659.44	1861.75
R^2	0.9994	0.9994	0.9991	0.9984	0.9982	0.9994	0.9992	0.9993	0.9991	0.9992

RMSD	0.029	0.027	0.032	0.041	0.042	0.031	0.033	0.030	0.032	0.032
%ARD	1.66	1.54	1.84	2.24	2.31	1.63	1.76	1.62	1.72	1.72
					n_D					
		DES1 (1) + water (2)					DES2 (1) + water (2)			
A_0	47.4950	47.9388	48.3913	48.7650	49.0938	45.5112	45.9000	46.3138	46.7975	47.1188
A_1	-36.1950	-36.4238	-36.6013	-36.5350	-36.5387	-32.7513	-33.5775	-33.6663	-34.5525	-34.8613
A_2	34.4450	34.8513	35.4238	35.6050	35.9413	36.2188	36.4450	36.0763	36.3975	36.1013
A_3	-24.9000	-25.5913	-26.3188	-27.5150	-28.4463	-28.1588	-27.6875	-29.1488	-29.4275	-30.1938
R^2	0.9996	0.9996	0.9996	0.9995	0.9995	0.9993	0.9993	0.9993	0.9994	0.9994
RMSD	0.00055	0.00053	0.00053	0.00056	0.00059	0.00068	0.00067	0.00065	0.00063	0.00061
%ARD	0.032	0.031	0.031	0.032	0.035	0.038	0.037	0.037	0.035	0.034
		DES3 (1) + water (2)					DES4 (1) + water (2)			
A_0	43.7650	44.1175	44.4300	44.8650	45.1475	45.1613	45.4413	45.7138	45.9388	46.3888
A_1	-34.9100	-35.2425	-35.5825	-35.9075	-36.1875	-36.0987	-36.3288	-36.6013	-36.8012	-37.4362
A_2	35.4550	35.4125	35.3850	35.3950	35.4025	46.8688	47.0938	47.4063	47.6563	48.1063
A_3	-26.8750	-26.7625	-26.6325	-26.7675	-26.9275	-42.2863	-43.1663	-43.7638	-44.2138	-44.2988
R^2	0.9993	0.9994	0.9994	0.9994	0.9994	0.9981	0.9981	0.9981	0.9981	0.9982
RMSD	0.00064	0.00061	0.00059	0.00059	0.00058	0.0012	0.0011	0.0011	0.0011	0.0011
%ARD	0.036	0.034	0.033	0.032	0.033	0.064	0.064	0.064	0.063	0.063

Table S6. Parameters A_i of Eq. (6) and the corresponding *RSMD* f for TBAB:AP (DES1) + water mixtures at the temperatures (293.15 to 303.15) K and atmospheric pressure.

Function	T / K	A_0	A_1	A_2	A_3	A_4	RMSD
				DES1 (1) + water (2)			
$10^6\ V^E$ / m^3·mol^{-1}	293.15	-3.840	1.863	-0.129	-	-	0.018
	298.15	-3.749	1.754	-0.007	-	-	0.018
	303.15	-3.669	1.631	0.079	-	-	0.018
	308.15	-3.584	1.531	0.169	-	-	0.018
	313.15	-3.499	1.428	0.223	-	-	0.018
$10^4\ \Delta\alpha_p$ / K^{-1}	293.15	3.016	-6.327	11.333	-7.618	-	0.023
	298.15	2.999	-6.024	10.333	-7.210	-	0.019
	303.15	3.012	-5.738	9.335	-6.808	-	0.035
	308.15	2.930	-5.450	8.342	-6.409	-	0.015
	313.15	2.905	-5.157	7.353	-6.013	-	0.015
$10^{10}\ k_S^E$ / Pa^{-1}	293.15	-2.532	2.831	-2.489	7.174	-7.083	0.0084
	298.15	-2.451	2.745	-2.487	6.687	-6.168	0.0076
	303.15	-2.385	2.648	-2.562	6.213	-5.288	0.0074
	308.15	-2.311	2.590	-2.470	5.796	-4.740	0.0067
	313.15	-2.269	2.518	-2.384	5.430	-4.231	0.0056
$\Delta\eta$ / mPa·s	293.15	210.80	172.56	63.53	124.95	-	0.28
	298.15	150.86	115.90	41.61	86.34	-	0.15
	303.15	111.51	80.56	23.86	52.64	-	0.14
	308.15	83.62	54.50	26.76	55.38	-	0.09
	313.15	63.96	37.74	24.30	47.84	-	0.08
ΔG^E / J·mol^{-1}	293.15	21652	-14563	13324	-	-	84
	298.15	21233	-14378	13376	-	-	93
	303.15	20769	-14423	13306	-	-	112
	308.15	20408	-14287	14249	-	-	110
	313.15	20046	-14306	14901	-	-	108
Δn_D	293.15	0.02405	-0.02670	0.01050	-	-	0.000098
	298.15	0.02333	-0.02580	0.01018	-	-	0.000095
	303.15	0.02248	0.02475	0.01058	-	-	0.000081
	308.15	0.02158	0.02365	0.00953	-	-	0.000061
	313.15	0.02100	0.02250	0.00940	-	-	0.000049

Table S7. Parameters A_i of Eq. (6) and the corresponding *RSMD* for TBAC:AP (DES2) + water mixtures at the temperatures (293.15 to 303.15) K and atmospheric pressure.

Function	T / K	A_0	A_1	A_2	A_3	A_4	*RMSD*
				DES2 (1) + water (2)			
$10^6\ V^E$ / m^3·mol^{-1}	293.15	-3.892	1.937	-0.511	-	-	0.013
	298.15	-3.801	1.815	-0.390	-	-	0.013
	303.15	-3.710	1.706	-0.297	-	-	0.012
	308.15	-3.621	1.603	-0.218	-	-	0.012
	313.15	-3.533	1.507	-0.147	-	-	0.011
	293.15	3.100	-5.499	11.699	-11.308	-	0.016

$10^4\,\Delta\alpha_p$ / K^{-1}	298.15	3.101	-5.451	10.574	-9.668	-	0.011
	303.15	3.088	-5.412	9.451	-8.033	-	0.008
	308.15	3.088	-5.366	8.333	-6.402	-	0.006
	313.15	3.087	-5.325	7.218	-4.775	-	0.008
$10^{10}\,k_S^E$ / Pa^{-1}	293.15	-2.674	2.973	-2.636	7.238	-7.503	0.0089
	298.15	-2.587	2.927	-2.676	6.588	-6.704	0.0090
	303.15	-2.508	2.870	-2.648	6.054	-5.996	0.0083
	308.15	-2.426	2.822	-2.610	5.580	-5.427	0.0073
	313.15	-2.379	2.757	-2.545	5.143	-4.959	0.0068
$\Delta\eta$ / mPa·s	293.15	186.34	107.75	7.62	119.36	-	0.48
	298.15	131.40	69.93	12.51	91.90	-	0.31
	303.15	96.61	47.32	17.87	76.02	-	0.21
	308.15	74.69	40.07	14.30	42.15	-	0.10
	313.15	57.16	30.35	18.05	31.69	-	0.06
ΔG^E / J·mol^{-1}	293.15	20791	-15851	11984	-	-	105
	298.15	20268	-15531	12383	-	-	104
	303.15	19795	-15202	13049	-	-	100
	308.15	19622	-15047	13933	-	-	141
	313.15	19271	-14950	15285	-	-	147
Δn_D	293.15	0.02351	0.02009	0.02854	0.01186	-	0.000056
	298.15	0.02213	0.02198	0.02683	0.00743	-	0.000062
	303.15	0.02174	0.02009	0.02271	0.01261	-	0.000045
	308.15	0.02006	0.02169	0.02104	0.01136	-	0.000061
	313.15	0.01940	0.02135	0.01775	0.01340	-	0.000050

Table S8 Parameters A_i of Eq. (6) and the corresponding *RSMD* for TBAB:MAE (DES3) + water mixtures at the temperatures (293.15 to 303.15) K and atmospheric pressure.

Function	T / K	A_0	A_1	A_2	A_3	A_4	*RMSD*
				DES3 (1) + water (2)			
$10^6\,V^E$ / m^3·mol^{-1}	293.15	-4.274	2.720	-1.044	-	-	0.011
	298.15	-4.200	2.580	-0.924	-	-	0.011
	303.15	-4.126	2.452	-0.816	-	-	0.010
	308.15	-4.051	2.335	-0.717	-	-	0.010
	313.15	-3.977	2.221	-0.633	-	-	0.010
$10^4\,\Delta\alpha_p$ / K^{-1}	293.15	2.765	-5.444	7.854	-12.486	8.919	0.015
	298.15	2.732	-5.304	7.553	-11.321	7.769	0.014
	303.15	2.696	-5.166	7.256	-10.159	6.625	0.015
	308.15	2.672	-5.024	6.963	-9.000	5.485	0.014
	313.15	2.642	-4.891	6.668	-7.846	4.348	0.014
$10^{10}\,k_S^E$ / Pa^{-1}	293.15	-3.164	3.551	-2.920	8.644	-9.214	0.0120
	298.15	-3.106	3.531	-2.911	8.059	-8.443	0.0108
	303.15	-3.070	3.505	-2.864	7.535	-7.827	0.0097
	308.15	-3.036	3.489	-2.846	7.071	-7.230	0.0088
	313.15	-3.018	3.446	-2.814	6.704	-6.730	0.0082
$\Delta\eta$ / mPa·s	293.15	155.32	50.59	-29.09	71.03	-	0.16

	298.15	111.72	35.88	-17.09	48.62	-	0.10
	303.15	82.12	18.82	-11.04	44.44	-	0.11
	308.15	64.46	16.44	-8.22	29.55	-	0.11
	313.15	50.02	10.03	-7.77	20.57	-	0.09
	293.15	21711	-16843	14212	-	-	157
	298.15	21183	-16342	14037	-	-	157
ΔG^E / J·mol^{-1}	303.15	20579	-16359	13958	-	-	155
	308.15	20452	-15983	14035	-	-	183
	313.15	20103	-16232	13937	-	-	196
	293.15	0.02393	-0.03685	0.02643	-	-	0.000023
	298.15	0.02318	-0.03580	0.02423	-	-	0.000020
Δn_D	303.15	0.02245	-0.03500	0.02230	-	-	0.000027
	308.15	0.02163	-0.03415	0.02023	-	-	0.000024
	313.15	0.02088	-0.03335	0.01863	-	-	0.000035

Table S9 Parameters A_i of Eq. (6) and the corresponding *RSMD* for TBAB:BAE (DES4) + water mixtures at the temperatures (293.15 to 303.15) K and atmospheric pressure.

Function	T / K	A_0	A_1	A_2	A_3	A_4	*RMSD*
			DES4 (1) + water (2)				
$10^6 V^E$ / m^3·mol^{-1}	293.15	-4.045	2.112	-0.822	-	-	0.019
	298.15	-3.954	1.994	-0.710	-	-	0.017
	303.15	-3.860	1.884	-0.621	-	-	0.016
	308.15	-3.763	1.779	-0.548	-	-	0.015
	313.15	-3.662	1.680	-0.490	-	-	0.014
$10^4 \Delta\alpha_p$ / K^{-1}	293.15	2.570	-3.022	2.439	-13.078	15.448	0.026
	298.15	2.615	-3.185	2.404	-11.655	13.894	0.025
	303.15	2.632	-3.385	2.349	-10.245	12.347	0.025
	308.15	2.710	-3.521	2.324	-8.834	10.806	0.025
	313.15	3.299	-4.296	2.684	-9.634	11.835	0.030
$10^{10} k_S^E$ / Pa^{-1}	293.15	-2.469	2.659	-1.919	7.471	-8.403	0.0110
	298.15	-2.444	2.599	-1.975	7.146	-7.802	0.0100
	303.15	-2.436	2.580	-1.805	6.840	-7.601	0.0094
	308.15	-2.391	2.544	-1.838	6.581	-7.193	0.0083
	313.15	-2.366	2.535	-1.999	6.310	-6.681	0.0086
$\Delta\eta$ / mPa·s	293.15	190.38	80.90	-55.30	24.71	-	0.18
	298.15	135.50	48.85	-35.76	24.08	-	0.14
	303.15	100.35	30.76	-24.54	17.62	-	0.09
	308.15	76.61	17.27	-15.40	17.10	-	0.08
	313.15	59.55	6.93	-12.38	22.52	-	0.07
ΔG^E / J·kmol^{-1}	293.15	23563	-19656	16934	-	-	299
	298.15	23008	-19563	16883	-	-	291
	303.15	22545	-19569	17015	-	-	289
	308.15	22329	-19709	17139	-	-	281
	313.15	22100	-19957	17170	-	-	260
Δn_D	293.15	0.02000	-0.02513	0.02695	-	-	0.000029
	298.15	0.01929	-0.02399	0.02551	-	-	0.000027
	303.15	0.01854	-0.02324	0.02481	-	-	0.000024
	308.15	0.01773	-0.02273	0.02413	-	-	0.000029
	313.15	0.01686	-0.02321	0.02319	-	-	0.000020

Table S10 Isobaric thermal expansion coefficient (α_p), isochoric molar heat capacity(C_V), Flory theory parameters: characteristic volume(V^*), reduce volume ($\tilde{V}$), characteristic pressure (P^*), and ratio of molecular surface to volume ratio (S_1/S_2) of DES to water.

DES	T / K	$10^4\alpha$ / K^{-1}	C_V / $J{\cdot}mol^{-1}{\cdot}K^{-1}$	$10^6 V^*$ / $m^3{\cdot}mol^{-1}$	$\tilde{V}$	10^9P^* / Pa	S_1/S_2
DES1							
	293.15	7.334	257.4	91.563	1.188	7.199	0.571
	298.15	7.343	260.7	91.670	1.191	7.209	0.569
	303.15	7.351	264.0	91.780	1.194	7.215	0.566
	308.15	7.359	268.4	91.890	1.196	7.221	0.564
	313.15	7.368	272.8	92.003	1.199	7.226	0.562
DES2							
	293.15	7.305	249.8	90.515	1.187	7.111	0.573
	298.15	7.315	250.9	90.618	1.190	7.110	0.571
	303.15	7.325	252.9	90.721	1.193	7.115	0.568
	308.15	7.336	254.0	90.827	1.196	7.110	0.566
	313.15	7.346	256.1	90.934	1.199	7.108	0.564
DES3							
	293.15	7.342	187.7	94.326	1.188	5.550	0.565
	298.15	7.372	190.7	94.399	1.191	5.574	0.563
	303.15	7.403	194.7	94.473	1.195	5.601	0.561
	308.15	7.433	203.2	94.549	1.198	5.646	0.559
	313.15	7.463	212.4	94.627	1.202	5.690	0.557
DES4							
	293.15	7.725	284.2	130.676	1.196	5.255	0.507
	298.15	7.754	288.2	130.796	1.200	5.266	0.505
	303.15	7.783	290.6	130.918	1.203	5.270	0.503
	308.15	7.813	294.0	131.044	1.207	5.277	0.501
	313.15	7.842	297.9	131.173	1.210	5.282	0.499
Water							
	293.15	2.120	75.4	17.031	1.060	1.520	-
	298.15	2.565	75.3	16.843	1.073	1.945	-
	303.15	3.010	75.3	16.661	1.086	2.405	-
	308.15	3.455	75.2	16.485	1.099	2.898	-
	313.15	3.901	75.2	16.315	1.113	3.420	-

Table S11 Partial molar volumes of DESs and water in their binary mixtures at T = (293.15 to 313.15) K and at atmospheric pressure (0.1 MPa)[a]

x_1	$10^6\,\bar{V}_1$ / $m^3 \cdot mol^{-1}$	$10^6\,\bar{V}_2$ / $m^3 \cdot mol^{-1}$	$10^6\,\bar{V}_1$ / $m^3 \cdot mol^{-1}$	$10^6\,\bar{V}_2$ / $m^3 \cdot mol^{-1}$	$10^6\,\bar{V}_1$ / $m^3 \cdot mol^{-1}$	$10^6\,\bar{V}_2$ / $m^3 \cdot mol^{-1}$	$10^6\,\bar{V}_1$ / $m^3 \cdot mol^{-1}$	$10^6\,\bar{V}_2$ / $m^3 \cdot mol^{-1}$	$10^6\,\bar{V}_1$ / $m^3 \cdot mol^{-1}$	$10^6\,\bar{V}_2$ / $m^3 \cdot mol^{-1}$
T / K	293.15		298.15		303.15		308.15		313.15	
DES1 (1) + water (2)										
0.0000	102.91	18.05	103.60	18.07	104.32	18.09	105.00	18.12	105.65	18.16
0.0994	104.68	18.03	105.20	18.05	105.79	18.07	106.33	18.10	106.87	18.13
0.1981	106.03	17.98	106.45	17.98	106.96	18.01	107.42	18.03	107.89	18.06
0.2979	107.04	17.88	107.41	17.88	107.87	17.91	108.30	17.93	108.73	17.95
0.3961	107.75	17.75	108.10	17.73	108.54	17.77	108.95	17.79	109.36	17.82
0.4983	108.24	17.56	108.59	17.53	109.03	17.59	109.43	17.61	109.83	17.64
0.5987	108.53	17.32	108.90	17.29	109.32	17.37	109.73	17.41	110.13	17.44
0.6999	108.68	17.04	109.06	17.00	109.49	17.12	109.89	17.17	110.29	17.21
0.8000	108.74	16.71	109.13	16.67	109.55	16.83	109.95	16.90	110.36	16.95
0.9000	108.75	16.35	109.14	16.30	109.55	16.50	109.96	16.59	110.36	16.65
1.0000	108.74	15.94	109.14	15.88	109.54	16.13	109.95	16.24	110.35	16.31
V_i^*	108.74	18.05	109.14	18.07	109.54	18.09	109.95	18.12	110.35	18.16
DES2 (1) + water (2)										
0.0000	101.23	18.05	101.94	18.07	102.63	18.09	103.30	18.12	103.95	18.16
0.0986	103.22	18.04	103.78	18.06	104.32	18.08	104.87	18.11	105.40	18.14
0.1973	104.69	17.99	105.15	18.01	105.62	18.03	106.08	18.05	106.54	18.08
0.2961	105.74	17.91	106.15	17.92	106.57	17.93	106.99	17.95	107.41	17.98
0.3962	106.46	17.76	106.86	17.77	107.25	17.79	107.65	17.81	108.05	17.84
0.4925	106.91	17.57	107.30	17.58	107.69	17.60	108.08	17.63	108.48	17.66
0.5954	107.20	17.29	107.59	17.32	107.98	17.35	108.38	17.38	108.78	17.42
0.6946	107.34	16.97	107.74	17.01	108.14	17.05	108.53	17.1	108.93	17.15
0.7996	107.41	16.56	107.81	16.62	108.21	16.69	108.61	16.75	109.01	16.82
0.9019	107.43	16.12	107.83	16.20	108.23	16.28	108.62	16.37	109.02	16.45
1.0000	107.43	15.66	107.83	15.76	108.23	15.86	108.62	15.96	109.02	16.05
V_i^*	107.44	18.05	107.83	18.07	108.23	18.09	108.62	18.12	109.02	18.16
DES3 (1) + water (2)										
0.0000	104.00	18.05	104.75	18.07	105.47	18.09	106.18	18.12	106.88	18.16

0.0978	106.93	18.06	107.51	18.07	108.07	18.10	108.64	18.12	109.20	18.15
0.1982	109.00	18.05	109.48	18.06	109.95	18.08	110.42	18.10	110.90	18.13
0.2957	110.33	18.00	110.75	18.01	111.17	18.02	111.60	18.05	112.04	18.06
0.3970	111.17	17.88	111.57	17.88	111.98	17.89	112.39	17.90	112.80	17.92
0.4958	111.64	17.67	112.03	17.67	112.43	17.69	112.84	17.70	113.26	17.73
0.5935	111.87	17.38	112.27	17.39	112.68	17.41	113.09	17.43	113.51	17.46
0.6956	111.97	16.98	112.38	17.00	112.80	17.04	113.21	17.07	113.63	17.11
0.7979	112.01	16.50	112.43	16.55	112.84	16.59	113.26	16.65	113.69	16.70
0.8940	112.03	16.01	112.44	16.07	112.86	16.13	113.28	16.20	113.70	16.27
1.000	112.04	15.45	112.45	15.52	112.87	15.60	113.29	15.69	113.71	15.77
V_i^o	112.04	18.05	112.45	18.07	112.87	18.09	113.29	18.12	113.71	18.16
DES4 (1) + water (2)										
0.0000	149.34	18.05	150.27	18.07	151.17	18.09	152.06	18.12	152.94	18.16
0.0975	151.75	18.05	152.52	18.07	153.29	18.09	154.05	18.12	154.82	18.15
0.1951	153.45	18.02	154.13	18.04	154.81	18.06	155.50	18.08	156.19	18.11
0.2936	154.61	17.95	155.24	17.96	155.87	17.98	156.51	18.00	157.17	18.03
0.3943	155.37	17.81	155.97	17.82	156.58	17.83	157.21	17.85	157.84	17.88
0.4930	155.81	17.58	156.41	17.60	157.02	17.62	157.63	17.64	158.25	17.68
0.5925	156.06	17.27	156.67	17.30	157.27	17.33	157.89	17.36	158.51	17.40
0.6975	156.20	16.85	156.81	16.90	157.42	16.94	158.03	16.99	158.66	17.04
0.7920	156.26	16.41	156.87	16.47	157.49	16.53	158.10	16.59	158.72	16.66
0.8938	156.30	15.88	156.91	15.96	157.52	16.04	158.14	16.12	158.76	16.20
1.0000	156.32	15.29	156.93	15.40	157.54	15.50	158.15	15.59	158.77	15.68
V_i^o	156.32	18.05	156.93	18.07	157.54	18.09	158.15	18.12	158.77	18.16

Załącznik A6

I. Cichowska-Kopczyńska, D. Warmińska, **B. Nowosielski,** Solubility of carbon dioxide in deep eutectic solvents based on 3-amino-1-propanol and tetraalkylammonium salts at low pressure, Materials 14 (2021) 1–14. https://doi.org/10.3390/ma14030594. **IF_{2021}: 3,75, $MNSW_{2021}$: 140**

materials

MDPI

Article

Solubility of Carbon Dioxide in Deep Eutectic Solvents Based on 3-Amino-1-Propanol and Tetraalkylammonium Salts at Low Pressure

Iwona Cichowska-Kopczyńska [1,*], Dorota Warmińska [2] and Bartosz Nowosielski [2]

[1] Department of Process Engineering and Chemical Technology, Faculty of Chemistry, Gdańsk University of Technology, 80-233 Gdańsk, Poland

[2] Department of Physical Chemistry, Faculty of Chemistry, Gdańsk University of Technology, 80-233 Gdańsk, Poland; dorota.warminska@pg.edu.pl (D.W.); bartosz.nowosielski@pg.edu.pl (B.N.)

* Correspondence: iwona.kopczynska@pg.edu.pl

Abstract: Deep eutectic solvents (DESs) became an object of a great interest as an alternative to ionic liquids (ILs) and commonly used in CO_2 capture amine solutions. In the present study, five different DESs based on 3-amino-1-propanol as physical-chemical CO_2 absorbents were used. The composition was chosen in order to estimate the effects of hydrogen bond acceptor:hydrogen bond donor (HBA:HBD) molar ratio, anion type and length of alkyl chain of composing salt. The Fourier Transform Infrared (FTIR) spectroscopy was used to confirm chemical reaction. The solubility of CO_2 was measured at low pressures up to 170 kPa at the temperature range of 293–318 K. Viscosity, polarity and Kamlet–Taft parameters were determined in order to estimate the dependences of the parameters and the CO_2 capacity. CO_2 uptake was observed to improve with decreasing molar ratio of hydrogen bond donor. Comparing the CO_2 capacity of [TBAC]-based DESs, at the approximate pressure of 50 kPa, it was observed that the capacity increased in the following order of molar ratios—1:8 < 1:6 < 1:4 and a decrease in molar ratio from 1:8 to 1:4 resulted in about a 100% increase of capacity. Compared to [TBAC][AP] DESs, the [TEAC][AP] 1:4 and [TBAB][AP] 1:4 exhibited higher CO_2 uptake, though the best results were obtained for [TBAB][AP].

Keywords: carbon dioxide; capacity; solubility; equilibrium; deep eutectic solvent

Citation: Cichowska-Kopczyńska, I.; Warmińska, D.; Nowosielski, B. Solubility of Carbon Dioxide in Deep Eutectic Solvents Based on 3-Amino-1-Propanol and Tetraalkylammonium Salts at Low Pressure. *Materials* **2021**, *14*, 594. https://doi.org/10.3390/ma14030594

Academic Editor: Magdalena Maciejewska

Received: 31 December 2020
Accepted: 25 January 2021
Published: 27 January 2021

1. Introduction

Carbon dioxide is considered as a key gas in the enhancement of global warming and climate change. Increasing global CO_2 emissions forced researchers to comprehensively investigate its capture and storage technologies that should be efficient and economic. Approximately 40% of total emission of carbon dioxide comes from fossil fuel-based power plants, making them perfect targets for immediate CO_2 reductions [1]. Therefore, removal of CO_2 from exhaust streams is of particular importance in terms of atmosphere protection. Several methods of CO_2 capture were extensively studied over the last decades. The most widely used technology is chemical absorption involving aqueous amino acid salts, ammonia and alkanolamines. It has been established so far that aqueous amino acid salts from neutralization of amino acids with an organic base such as an amine showed better CO_2 absorption capacity than amino acid salts formed by neutralization of amino acids with an inorganic base such as potassium hydroxide [2,3].

The research performed by Bai and Yeh showed that the maximum CO_2 removal efficiency by an ammonia absorber can reach 99% and the CO_2 loading capacity can approach 1.20 g CO_2/g NH_3 [4].

However, because of smaller toxicity compared to ammonia and higher efficiency compared to amino acids, the most often used in industrial CO_2 separation are alkanolamines [5,6]. Commercially, a 30% aqueous solution of monoethanolamine (MEA), as

the most effective and cheapest, is used [7]. A major problem in the usage of alkanolamines for CO_2 absorption is equipment corrosion and cost of regeneration [8].

In the last decades much attention was given to the ionic liquids (ILs), considered as a "greener" replacement for amines, that present many advantages. They have negligible vapor pressure, which is of particular importance from the point of view of industrial applications, they are non-flammable, present high thermal stability, can be easily tuned for a specific application and are able to absorb a wide range of chemicals, including CO_2 [9,10]. The majority of research reports concludes that ILs absorb carbon dioxide physically. Physical absorption results in a low cost of solvent regeneration, but it strongly limits their applications in CO_2 capture at low partial pressure of post-combustion flue gas [11]. Industrial use of ionic liquids is very poor, mainly because of the high price, which excludes them from bulk applications. Moreover, there are data exhibiting their toxicity and non-biodegradability [12,13].

Therefore, to overcome the shortcomings of ILs, deep eutectic solvents (DESs) started to be considered as new absorbents for CO_2 capture. Similar to ILs, deep eutectic solvents are practically non-volatile and non-flammable, exhibit high thermal and electro-chemical stability, but are definitely cheaper, less toxic and often biodegradable, which makes them better solvents for carbon dioxide absorption [14]. They are obtained by simply mixing two substances, a hydrogen bond donor and acceptor, resulting in an eutectic mixture with melting point lower than that of each of the two components of DES. Physical properties of DESs are tunable and can be controlled by changing the composition and proportions of the components to obtain properties essential for a particular application [15].

The carbon dioxide absorption in deep eutectic solvents can be physical, chemical or mixed depending on the compounds used to obtain DES [16]. The majority of works is focused on deep eutectic solvents in which physical absorption of carbon dioxide occurs, mainly based on choline chloride (ChCl) acting as a hydrogen bond acceptor (HBA) and urea, glycols and carboxylic acids as hydrogen bond donors (HBDs) [14]. These systems are characterized by CO_2 capacity similar to that of ILs and by lower CO_2 solubility than aqueous solutions of hydroxyamines (e.g., at 298 K and 10 bar in ChCl:TEG CO_2 solubility is equal to 2.0 wt.% while in aqueous 30% MEA it is 11.95 wt.%) [17–20].

To improve carbon dioxide absorption capacity, deep eutectic solvents based on alkanolamines or amines as HBDs were introduced. Ali et al. [19] reported series of DESs which were composed of choline chloride, methyltriphenylphosphonium bromide (MTPPB) and tetrabutylammonium-bromide (TBAB) as HBAs and ethanolamine (MEA), diethanolamine (DEA) and triethanolamine (TEA) as HBDs. The obtained results show that solubility of CO_2 in alkanolamine-based DESs is higher than for glycol-based. Additionally, it was shown that for MTPPB-based DESs, increasing the fraction of MEA results in the decrease of CO_2 solubility. Adeyemi et al. [21] reported ChCl-based DESs coupled with MEA, DEA and methyldiethanolamine (MDEA) at three different molar ratios of 1:6, 1:8 and 1:10. The authors observed that the solubility of carbon dioxide in amine-based DESs is much higher (approx. 0.3 g of CO_2/g of ChCl-MEA 1:8) than for 30 wt.% MEA solution (approx. 0.1 g of CO_2/g of solvent). The highest carbon dioxide absorption was reported for ChCl-MEA and the lowest was for ChCl-MDEA. Additionally, they concluded that as a molar ratio of amine increases, the solubility of CO_2 also increases. Haider et al. [22] described the influence of HBAs (ChCl and TBAB) on carbon dioxide absorption in ethylene glycol (EG), diethylene glycol (DEG), MDEA and DEA-based DESs. The authors reported that the highest absorption was obtained in TBAB-based DESs which was explained due to increase in free volume in TBAB-based DESs in comparison to ChCl-based DESs. Trivedi et al. [13] described novel deep eutectic solvents based on various amine hydrochlorides, namely—(MEACl), (TEACl), urea hydrochloride (UCl) and thioacetamide hydrochloride (TAECl), as HBAs and ethylenediamine (EDA) as an HBD. High gravimetric uptakes of carbon dioxide were reported with the greatest value for MEACl-EDA (mole ratio 1:3) being 31.8 wt.%

Herein, a carbon dioxide absorption capacity of previously described by our group [23] 3-amino-1-propanol (AP)-based deep eutectic solvents is reported. AP was mixed with tetrabutylammonium bromide (TBAB) or tetrabutylammonium chloride (TBAC) or tetraethylammonium chloride (TEAC), which act as hydrogen bond acceptors to form DESs. The experiments were conducted at temperature range from 293.15 to 318.15 K at low pressures of CO_2. Additionally, the effect of mole ratio of TBAC and AP on CO_2 capacity was examined.

2. Materials and Methods

The chemicals used in this study, tetrabutylammonium chloride, tetrabutylammonium bromide, tetraethylammonium chloride and 3-amino-1-propanol were purchased from Sigma-Aldrich (Saint Louis, MO, USA) and were used as received, only TBAC was purified by double crystallization from acetone by adding diethyl ether. Prior to synthesis the salts were dried in a vacuum oven (Thermo Scientific, Waltham, MA, USA), at 323 K for 48 h and 298.15 K for 3 days, respectively for TBAB and both TBAC and TEAC. Corresponding data are presented in Table 1. Figure 1 shows the structures of compounds used for DES preparation. Carbon dioxide was supplied by Oxygen S.C. Gdansk (Gdansk, Poland) with purity grade 5.0.

Table 1. Sources and mass fraction purity of used chemicals.

Chemical Name	Source	CAS Number	Purity/Mass Fraction [a]
3-amino-1-propanol [AP]	Sigma Aldrich	157-87-6	0.99
Tetrabutylammonium bromide [TBAB]	Sigma Aldrich	1643-19-2	≥0.99
Tetrabutylammonium chloride [TBAC]	Sigma Aldrich	1112-67-0	≥0.99
Tetraethylammonium chloride [TEAC]	Sigma Aldrich	56-34-8	≥0.99

[a]—according to the supplier.

HBD:

3-amino-1-propanol (AP)

HBA:

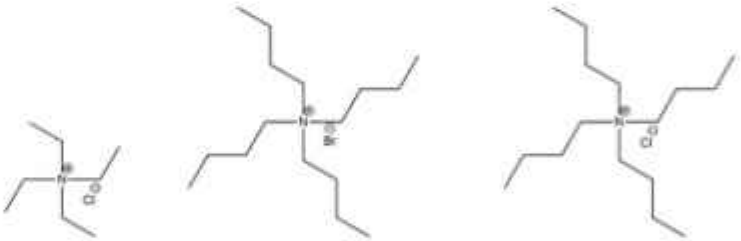

tetraethylammonium chloride (TEAC) tetrabutylammonium bromide (TBAB) tetrabutylammonium chloride (TBAC)

Figure 1. Structures of compounds used for deep eutectic solvents (DES) preparation.

2.1. Synthesis of Deep Eutectic Solvents

The absorbents were prepared by mixing TBAB, TBAC and TEAC with 3-amino-1-propanol at the molar ratios of 1:4, 1:6 and 1:8. Weighting was done with an electronic balance (Mettler Toledo, Columbus, OH, USA) with the precision of 0.1 mg. The HBD and HBA were mixed at 353.15 K for 1 h with a magnetic stirrer until homogeneous liquid was obtained. Resulting DESs were stored in gas-tight bottles at room temperature.

Before experiments DESs were dried in a vacuum dryer (Thermo Scientific, Waltham, MA, USA) at 343.15 K for 48 h. Water content was then determined using Karl Fischer titration method using 831 KF Coulometer apparatus from (Metrohm, Herisau, Switzerland). The contents of H_2O were lower than the 0.002 weight fraction.

2.2. Properties of Deep Eutectic Solvents

2.2.1. Viscosity Measurements

Viscosity was measured at temperatures ranging from 298.15 to 318.15 K and at atmospheric pressure. The LVDV-III Programmable Rheometer (Searle cone-plate viscometer; Brookfield Engineering Laboratory, Middleboro, MA, USA), controlled by a computer, was used to carry out measurements. To control the temperature of the samples within ±0.01 K accuracy, a thermostatic water bath (PolyScience 9106, Warrington, PA, USA) was used. CP-40 cone (angle 0.8°, radius 2.4 cm) and 0.5 ml deep eutectic solvent were used. The ratio of shear stress (N/m^2) and shear rate ($1/s$) at 10 points was used to obtain flow curves which were used to calculate the dynamic viscosity. The viscometer was adjusted with certified viscosity standard N100 and S3 provided by Cannon at 298.15 ± 0.01 K. The standard uncertainty of viscosity measurement was better than 1%.

2.2.2. Polarity and Kamlet-Taft Parameters

Ultraviolet visible (UV-vis) absorption spectra of three solvatochromic dyes (Reichardt's dye, N,N-diethyl-4-nitro-aniline, and 4-nitroaniline) dissolved in DESs were taken in a quartz cell with a light path length of 10 mm on a Thermo Scientific™ Evolution™ 300 spectrophotometer (Thermo Scientific, Waltham, MA, USA). Individual stock solutions of Reichardt's dye, N,N-diethyl-4-nitroaniline and 4-nitroaniline were prepared in methanol. To prepare a given dye/DES solution, the appropriate amount of the dye stock solution was micropipetted into the Eppendorf flask and methanol was evaporated under a vacuum. The DES was then added and stirred until complete dissolution of the dye was achieved. Next, the resultant solution was transferred into the quartz cuvette, and the UV-vis spectra were recorded at room temperature.

2.3. Infrared Spectroscopy Measurements

To characterize the DESs before and after saturation with CO_2 an attenuated total reflectance Fourier transforms infrared spectroscopy (ATR-FTIR) was used. For this purpose, the Nicolet 8700 spectrometer (Thermo Electron Co., Waltham, MA, USA) was applied. Employment of an attenuated total reflection (ATR) was needed because of the strong $\nu(OH)/\nu(NH_2)$ stretching vibrations of AP. The Specac Golden Gate single reflection accessory with a diamond crystal (45°) mounted in a heated tungsten carbide disc was used. The temperature of the sample was kept at 298.15 ± 0.1 K by circulating thermostated water from a Julabo F12 thermostat. The spectrometer was purged with dry nitrogen (Oxygen Gdansk, Gdansk, Poland). Prior to each experiment, the sample spectra were ratioed against a background spectrum collected for an empty, dry cell. For each spectrum, 256 scans were performed with a selected resolution of 2.0 cm^{-1}. Spectra acquisition was controlled by OMNIC 7.3 software package (version 7.3, Thermo Scientific, Waltham, MA, USA). The spectra were analyzed using GRAMS/32 software (version 4.01A, Galactic Industries Corp., Salem, NH, USA).

2.4. CO_2 Solubility

Schematic diagram of the equipment used for CO_2 solubility measurement is presented in Figure 2. The experimental setup consisted of a stainless steel equilibrium chamber (1) equipped with a water jacket connected to the water bath temperature controller (PolyScience 9106, Warrington, PA, USA) (2), to a gas container (3) and to a vacuum pump (5). The equilibrium cell had a magnetic mixer (IKA, Staufen im Breisgau, Germany), (4) in order to mix the fluids and to provide that equilibrium state was reached faster. The volume of the cell was 7.8 ± 0.01 cm^3. A volume of about 1 cm^3 of DES was injected to

the cell. The actual amount was determined gravimetrically using RADWAG analytical balance. The cell, absorbent and gas container were degassed with the vacuum pump (VALUE, Wenling, China). The gas container was then filled with CO_2 from a gas reservoir (6). Subsequently, both the equilibrium cell and the gas container were thermostated at a given temperature. The experimental uncertainty for the temperature was ±0.1 K. When the temperature of fluids was equal and stable, the gas was injected to the equilibrium cell and a starting pressure was recorded. The pressure was measured by an Aplisens PC-28 transducer. As the CO_2 was absorbed, the pressure in the cell decreased. When the equilibrium was reached, meaning the pressure in the cell did not change, the equilibrium pressure was recorded. The amount of CO_2 absorbed was calculated using Equation (1).

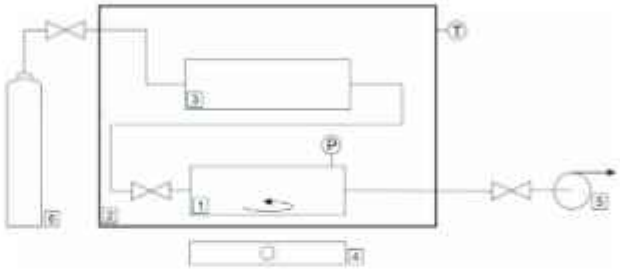

Figure 2. Schematic diagram of the equipment used for CO_2 solubility measurement (1—equilibrium cell, 2—thermostat with temperature sensor, 3—gas container, 4—magnetic stirrer, 5—vacuum pump, 6—gas reservoir).

3. Results

The initial amount of solute (n_0) was obtained from Equation (1):

$$n_0 = \frac{p_0 V}{Z_2 RT} \tag{1}$$

where V is the volume of the gas phase in the measuring chamber, p_0 is the initial gas pressure, R is the universal gas constant, T—temperature, Z_2—is the compressibility factor expressed with Equation (2):

$$Z_2 = 1 + \frac{pB_{22}}{RT} \tag{2}$$

where B_{22} is the second virial coefficient for pure CO_2. The quantity of solute present in the gas phase was calculated with Equation (3):

$$n_1 = \frac{p_1 V}{Z_2 RT} \tag{3}$$

The amount of CO_2 dissolved in the solvent is represented by the difference in CO_2 mole values and was calculated by:

$$n_l = n_0 - n_1 \tag{4}$$

At zero time the gas was put in contact with eutectic solvent and after that the decrease of pressure was observed due to the solubilization of the CO_2 in DES. At low pressures, the equilibrium was reached within 24 h, though the higher pressure the more time was needed for equilibration, reaching 14 days. The reason was increasing viscosity and resulting diffusion resistance. Higher viscosity creates several effects, like slower diffusion of CO_2 to the bulk solvent, inhibition of movement of CO_2-loaded solvent to the bulk liquid and hindrance in diffusion of free solvent to the gas–liquid interface. Moreover, the higher viscosity the slower is the heat transfer. Therefore, when viscosity decreases due

to increase of temperature, the equilibrium state is obtained faster. For that reason the more CO_2 was added to the cell, the longer the time of equilibration. Temperature increase resulted in an increase in pressure caused by temperature change and by the change in solubility. After the equilibrium was reached at 293 K and the temperature was raised, it took a maximum of 2 h to reach the equilibrium again. The increase in temperature results first of all in lower viscosity and second of all lower gas solubility, therefore during the experiment the increase in equilibrium pressure was observed when the temperature raised. The time of equilibration was very short and that indicated easy regeneration of DESs used in the study.

Viscosity plays a key role in mass and heat transfer and affects the economy of the process, operation parameters and the design of the unit itself. Among examined DESs [TEAC][AP] showed the lowest viscosity, and a higher one was observed for [TBAC][AP] and the highest for [TBAB][AP]. This affected the overall solvent transport properties, i.e., kinetics of absorption and the time of equilibration.

The observed CO_2 uptake values were relatively high for all DESs, as 3-amino-1-propanol exhibits a high reaction rate with CO_2 and therefore even at low pressures gives good results.

The shape of the absorption curve is polynomial at the pressure range studied within this research (Figure 3). This is mainly due to the chemical reaction that takes place and is in agreement with the research performed by Dong et al. who obtained similar results for the solution of 1-amino-1-propanol. The authors observed an inflection point above 100 kPa [24].

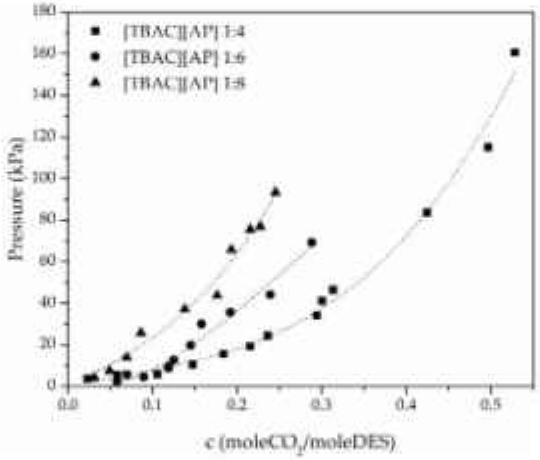

Figure 3. CO_2 uptake by DES with different molar ratio.

The values obtained for [TBAB][AP] 1:4 were close to that reported by Shukla et al. [25], around 0.51 moleCO_2/moleDES at atmospheric pressure. CO_2 capture in DESs can be tailored by varying the molar ratio of the hydrogen bond donor, changing the strength of the hydrogen bond between components or by affecting the physical absorption in a form of the size of the HBA. Due to the chemisorption occurring in DESs used in this study, the CO_2 uptake was much higher than in DESs as physical absorbents, such as for example tetrabutylammonium bromide coupled with methyldiethanol that was studied by Haider and gave a capacity of 0.29 moleCO_2/mole solvent at high pressure of 1 MPa and 303.15 K [22].

For the example of [TBAC][AP], CO_2 uptake was observed to improve with decreasing molar ratio of hydrogen bond donor (3-amino-1-propanol), as shown in Figure 3. The CO_2 absorption at the approximate pressure in TBAC-based DESs increased about 100% from 1:8 to 1:4, whereas 1:6 was between. As presented in Figure 4, compared to [TBAC][AP] DESs, the [TEAC][AP] 1:4 and [TBAB][AP] 1:4 exhibited higher CO_2 uptake, though the best results were obtained for [TBAB][AP].

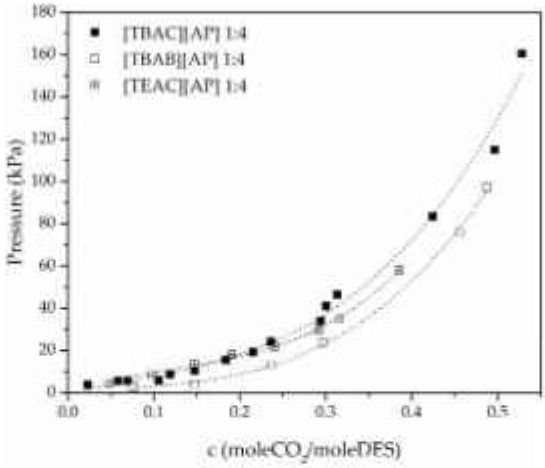

Figure 4. CO_2 uptake in different DESs of 1:4 molar ratio.

Literature describes the cases where the CO_2 absorption trend varies depending on the HBD and HBA ratio. For example, Zhang et al. conducted research on absorption in tetraethylenetetramine chloride [TETEA.Cl] and ethylene glycol [EG] or diethylene glycol [DG] and discovered that the CO_2 capacity for [TETEA.Cl][DG] increases from 1:1 to 1:2 and then decreases up to 1:7 and for [TETEA.Cl][EG] increases from 1:1 to 1:3 and further decreases [26]. However, for MEA in the role of HBD and choline chloride, tetraethylammonium chloride and tetramethylammonium chloride as HBA, Zhuo et al. reported increasing CO_2 absorption from 1:2 up to 1:6. Surprisingly, the authors reported also increase of CO_2 capacity when increasing temperature, suggesting that the reaction is endothermic [27]. Furthermore, Adeyemi et al. reported increasing CO_2 capacity of [ChCl][MEA] and [ChCl][DEA] from 1:6 to 1:10 [21].

The comparison of CO_2 solubility in the studied DESs indicates that the CO_2 solubility decreases with increasing alkyl chain length of the hydrogen bond acceptor. Moreover, exchange of the anion of the composing salt from Br^- to Cl^- results in a significant decrease in solubility.

The rate of CO_2 absorption for DESs with different molar ratio of HBA:HBD is shown in Figure 5. The graph applies to the first measuring point for each liquid, however, at different CO_2 pressures, the trend does not coincide with the total CO_2 capacity of the DESs. In the first 20 min of absorption after the CO_2 was introduced to the cell, the rate of the absorption was similar for all three molar ratios. Then, there was another approximately 20 min when the rate of absorption was in the following order—1:8 > 1:6 > 1:4, which was in agreement with the initial viscosity of the pure DESs (Table 2). After that, the rate of the process dramatically decreased in the case of 1:4 DES whereas the 1:6 and 1:8 solutions stayed close. A temperature increase during the stage of high absorption rate was not observed, however the temperature inside the cell was not directly measured, but the measuring cell was kept in the thermostated water bath of a high volume in comparison to

the volume of the cell. Taking into account the highly exothermic reaction and its effect on viscosity and energy of the system, it is likely that thermal effects play an important role in that phenomena and it is worth evaluating together with the changes of viscosity during the absorption. In comparison to different HBAs with the same HBA:HBD ratio, the absorption rate at the initial stage was the highest for DES with the highest viscosity, and the lowest for the [TEAC][AP], which has the lowest viscosity (Figure 6). Until equilibrium was reached, the rate for DESs based on the chloride salts stayed close, whereas for [TBAB][AP] the rate was much higher.

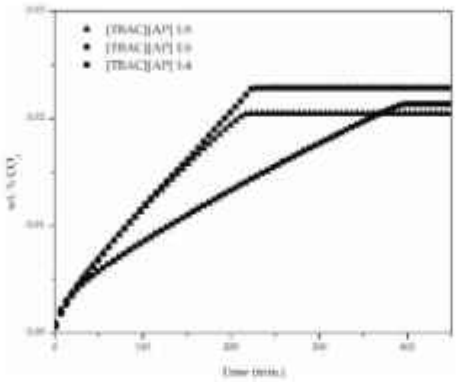

Figure 5. Time-dependent CO_2 absorption of DESs with different molar ratio of HBA and HBD.

Table 2. Thermophysical properties of the DES at p = 0.1 MPa, 298.15 K and comparison with literature data.

DES	Molar Ratio	η/(mPa.s)	$E_T(30)$/(kcal/mol)	π	α	β	|α − β|
TBAB-AP	1:4	84.69	48.7 (48.5 [a])	1.07 (1.02 [a])	0.37 (0.39 [a])	1.00 (0.90 [a])	0.63
TEAC-AP	1:4	42.37	56.7	1.10	0.87	0.92	0.05
TBAC-AP	1:4	77.36	63.0	1.13	1.18	0.90	0.28
TBAC-AP	1:6	53.86	56.8	1.02	0.90	1.25	0.34
TBAC-AP	1:8	46.14	48.8	1.04	0.40	1.05	0.65

[a] Experimental data reported by Shukla and Mikkola [73].

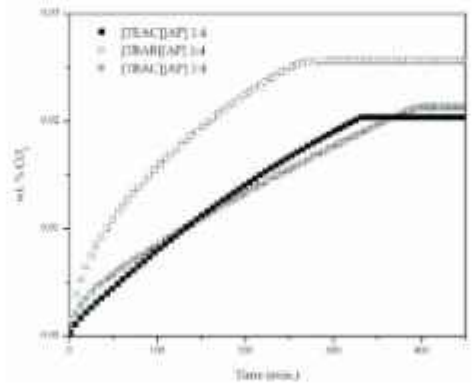

Figure 6. Time-dependent CO_2 absorption of DESs with different hydrogen bond acceptors (HBAs).

In general, the time of reaching equilibrium was short at low pressures, however increasing CO_2 pressure resulted in a very long time of equilibration. This is attributed to the increasing viscosity [28] upon CO_2 absorption that causes higher resistance of diffusion and hindrance in migration of CO_2 molecules [29,30]. The observed increase of viscosity was very high. Idris et al. performed a study on viscosity of 3-amino-1-propanol water solution unloaded and loaded with CO_2 and they reported about a 73% viscosity increase of 0.5 wt.% [AP] solution at 0.058 mole fraction of CO_2 (from 7.58 to 13.14 mPas) at 298.15 K [28]. Trivedi et al. also reported a dramatic increase in viscosity of DESs, for example for [MEACl][EDA], after 2.5 min of saturation the viscosity increased from 21.6 to 3995 cP at 30 °C [30].

Detailed results and analysis of physicochemical properties were provided elsewhere by Nowosielski et al. [23]. Within this paper, viscosity at 298.15 K and at atmospheric pressure (p = 0.1 MPa) and solvatochromic parameters at room temperature are presented. As the 3-amino-1-propanol is liquid at room temperature with viscosity of 30.43 mPa·s [28], while the HBA is not, the viscosity of all DESs is higher than that of pure [AP] and decreases with the increase of HBD to HBA ratio. As can be seen from Table 2, the experimental values of solvatochromic parameters were in good agreement with values found in the literature.

Taking into account $E_T(30)$, it was observed that the higher electronic transition energy results in higher CO_2 solubility (Figure 7). Moreover, as described by Shukla et al. [31] the relative value of α-β describes the nature of interactions between DESs and CO_2. The closer the strengths of the donor and acceptor are, the more favored the synergistic action and the higher the CO_2 capacity observed (Figure 8). This phenomenon can be considered in the prediction of the optimum HBA:HBD ratio for a specific DES, though it should not be used for comparison of DESs with different types of composing agents. This was confirmed by Shukla and Mikkola [25] who studied [TBAB][AP] and [HMIMCl][AP] and observed an increase in CO_2 capacity with increasing [AP] content, due to the favored synergistic effect. Our results confirm that the CO_2 uptake in DESs depends on the equilibrium between α and β that describes the intermolecular interactions between the HBD and HBA.

The solubility over the series of DESs used in this study varies as follows—[TBAB][AP] > [TEAC][AP] > [TBAC][AP]. With regard to the synergistic effect, [TEAC][AP] should have the best solubility, but apart from the basicity and acidity of DESs components, the solubility is influenced by the free volume and the strength of hydrogen interactions between the components. Solubility increases with increasing free volume and decreases with increasing strength of hydrogen interactions. Apparently, the superimposition of all these effects determines the ability of the DESs to dissolve carbon dioxide. The synergistic effect is most evident in the case of [TEAC], while in the case of [TBAB] the free volume favors the CO_2 absorption. Moreover, the relative special position of the functional groups in the molecule is essential. According to Shukla et al., the presence of AP with an acidic proton –OH is crucial in CO_2 capture. As the –OH group is at the α position to NH_2 it stabilizes CO_2 at the carbamic acid form [25].

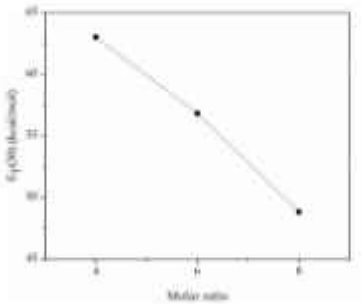

Figure 7. Effect of HBD:HBA ratio on $E_T(30)$.

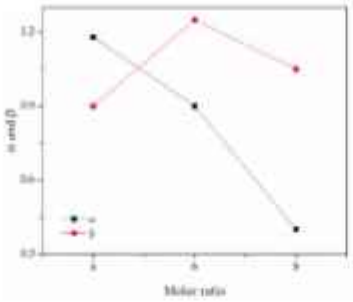

Figure 8. Effect of HBD:HBA ratio on acidity and basicity.

It has been established that in deep eutectic solvents based on alkanolamines, chemisorption of carbon dioxide occurs [22,32]. The reaction of CO_2 and DESs results from the content of primary alkanolamine AP and the reactions of its functional groups $–NH_2$ and –OH:

$$–NH_2 + CO_2 = –NHCOO^- H^+$$

$$–OH + CO_2 = –OCOO^- H^+$$

However, according to Astarita and other authors [33,34], the latter reaction is negligible due to the conditions needed and the main product of the reaction is carbamate. The molecule 3-amine-1-propanol follows the mechanism presented in Figure 9. As can be seen, due to the reaction, carbamate is formed [30].

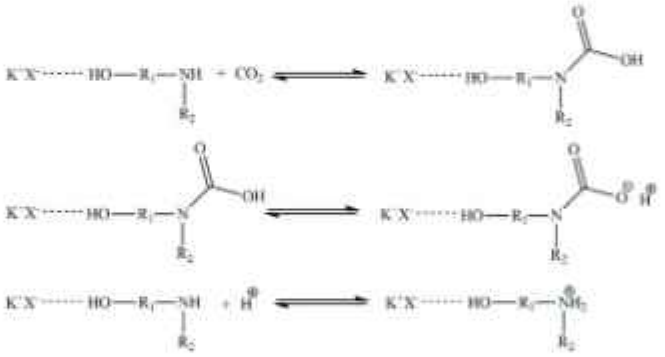

Figure 9. Scheme of alkanolamine and CO_2 reactions.

Figure 10 presents the FTIR spectra of [TBAC][AP] 1:4 before and after CO_2 absorption. As can be seen, after carbon dioxide absorption in the [TBAC][AP] 1:4, new peaks in the fingerprint region at 1311 and 1150 cm^{-1} appear. It is clear that they belong to N-C=O(O) and C-N stretching in formed carbamate due to reaction of CO_2 and alkanolamine [32]. Similar new peaks were observed in [TBAB][AP] and [TEAC][AP] spectra, however the positions of the ν(N-C=O(O)) bands become slightly red-shifted while the frequency of C-N stretching is practically constant for all DESs. The frequency of N-C=O(O) band changes is

in the order [TBAB][AP] > [TBAC][AP] > [TEAC][AP]. Thus, it depends both on an anion and a cation of the hydrogen bond donor.

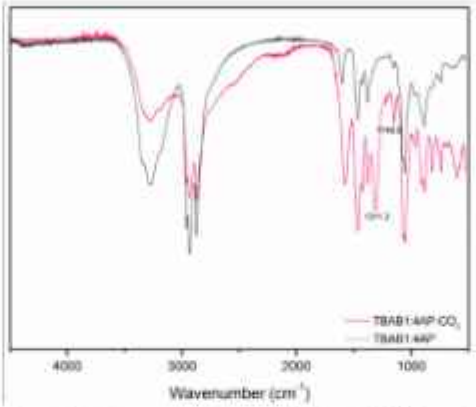

Figure 10. Spectroscopic analysis of [TBAC][AP] 1:4 before and after CO_2 absorption.

The reaction results in the temperature rise at the interfacial film. According to Camacho [34] it is dependent on the AP concentration and can be significant at certain conditions and can cause evaporation to the gas phase.

According to data provided by Benamor et al., stability of carbamates based on 3-amino-1-propanol is higher than of other amines like MEA or DEA. The authors also reported that AP carbamate is less sensitive to the temperature than other two. Still, the equilibrium constant for 3-amino-1-propanol carbamate formation was decreasing as the temperature increased, as the reaction is exothermal [35].

4. Conclusions

In the present study, the CO_2 solubility in five different DESs at several temperature points and varying pressure was investigated. Viscosity and polarity data were also reported. It was found that CO_2 uptake was improving with decreasing molar ratio of 3-amino-1-propanol. For [TBAC]-based DESs, the CO_2 capacity at the approximate pressure was in the following order—1:8 > 1:6 > 1:4. Considering the impact of the anion of tetrabutylammonium salt, it was found that DES with a bromide anion, namely [TBAB][AP] 1:4 exhibited higher CO_2 uptake than chloride-based DES. In the estimation of absorption kinetics, several stages with different characteristics were observed, and the rate of CO_2 absorption for DESs with different molar ratios of HBA:HBD was found to be similar for all three molar ratios at the initial stage, then there was another stage when the rate of absorption was in the following order—1:8>1:6>1:4, which was in agreement with the initial viscosity of the pure DESs, after that the rate of the process dramatically decreased in case of 1:4 DES whereas that of 1:6 and 1:8 stayed close. It was also observed that the rate of absorption was dependent on the anion of the composing salt. The evaluation of such behavior should be an object of interest for another study combining the changes of viscosity and thermal micro effects during the absorption.

Author Contributions: Conceptualization, I.C.-K. and D.W.; methodology, I.C.-K.; formal analysis, I.C.-K. and D.W.; investigation, B.N.; resources, I.C.-K. and D.W.; data curation, B.N.; writing—original draft preparation, I.C.-K.; writing—review and editing, I.C.-K., D.W. and B.N.; supervision, I.C.-K. All authors have read and agreed to the published version of the manuscript.

Funding: This research received no external funding.

Data Availability Statement: Data available on request due to privacy restrictions.

Conflicts of Interest: The authors declare no conflict of interest.

References

1. Spigarelli, B.P.; Kawatra, S.K. Opportunities and challenges in carbon dioxide capture. *J. CO2 Util.* **2013**, *1*, 69–87. [CrossRef]
2. Kang, D.; Park, S.; Jo, H.; Min, J.; Park, J. Solubility of CO_2 in Amino-acid-based solutions of (Potassium Sarcosinate), (Potassium Alaninate + Piperazine), and (Potassium Serinate + Piperazine). *J. Chem. Eng. Data* **2013**, *58*, 1787–1791. [CrossRef]
3. Aronu, U.E.; Svendsen, H.; Hoff, K.A. Investigation of amine amino acid salts for carbon dioxide absorption. *Int. J. Greenh. Gas Control* **2010**, *4*, 771–775. [CrossRef]
4. Bai, H.; Yeh, A.C. Removal of CO_2 greenhouse gas by ammonia scrubbing. *Ind. Eng. Chem. Res.* **1997**, *36*, 2490–2493. [CrossRef]
5. Wang, M.; Lawal, A.; Stephenson, P.; Sidders, J.A.; Ramshaw, C. Post-combustion CO_2 capture with chemical absorption: A state-of-the-art review. *Chem. Eng. Res. Des.* **2011**, *89*, 1609–1624. [CrossRef]
6. Olajire, A.A. CO_2 capture and separation technologies for end-of-pipe applications—A review. *Energy* **2010**, *35*, 2610–2628. [CrossRef]
7. Rochelle, G.T. Amine scrubbing for CO_2 capture. *Science* **2009**, *325*, 1652–1654. [CrossRef]
8. Alam Chowdhury, F.; Yamada, H.; Higashii, T.; Goto, K.; Onoda, M. CO_2 capture by tertiary amine absorbents: A performance comparison study. *Ind. Eng. Chem. Res.* **2013**, *52*, 8323–8331. [CrossRef]
9. Aghaie, M.; Rezaei, N.; Zendehboudi, S. A systematic review on CO_2 capture with ionic liquids: Current status and future prospects. *Renew. Sustain. Energy Rev.* **2018**, *96*, 502–525. [CrossRef]
10. Marsh, K.N.; Boxall, J.A.; Lichtenthaler, R. Room temperature ionic liquids and their mixtures—A review. *Fluid Phase Equilibria* **2004**, *219*, 93–98. [CrossRef]
11. Raksajati, A.; Ho, M.; Wiley, D. Solvent development for post-combustion CO_2 capture: Recent development and opportunities. *MATEC Web Conf.* **2018**, *156*, 03015. [CrossRef]
12. Oliveira, M.V.; Vidal, B.T.; De Melo, C.M.; Miranda, R.D.C.D.; Soares, C.M.F.; Coutinho, J.A.; Ventura, S.P.M.; Maltedi, S.; Lima, Á.S. (Eco)toxicity and biodegradability of protic ionic liquids. *Chemosphere* **2016**, *147*, 460–466. [CrossRef] [PubMed]
13. Krishnan, A.; Gopinath, K.P.; Vo, D.-V.N.; Malolan, R.; Nagarajan, V.M.; Arun, J. Ionic liquids, deep eutectic solvents and liquid polymers as green solvents in carbon capture technologies: A review. *Environ. Chem. Lett.* **2020**, *18*, 1–24. [CrossRef]
14. Sarmad, S.; Mikkola, J.-P.; Ji, X. Carbon dioxide capture with ionic liquids and deep eutectic solvents: A new generation of sorbents. *ChemSusChem* **2017**, *10*, 324–352. [CrossRef]
15. Marcus, Y. *Deep Eutectic Solvents*; Springer Science and Business Media LLC: Berlin/Heidelberg, Germany, 2019.
16. Zhang, Y.; Ji, X.; Lu, X. Choline-based deep eutectic solvents for CO_2 separation: Review and thermodynamic analysis. *Renew. Sustain. Energy Rev.* **2018**, *97*, 436–455. [CrossRef]
17. Leron, R.B.; Li, M.-H. Solubility of carbon dioxide in a eutectic mixture of choline chloride and glycerol at moderate pressures. *J. Chem. Thermodyn.* **2013**, *57*, 131–136. [CrossRef]
18. Li, G.; Deng, D.; Chen, Y.; Shan, H.; Ai, N. Solubilities and thermodynamic properties of CO_2 in choline-chloride based deep eutectic solvents. *J. Chem. Thermodyn.* **2014**, *75*, 58–62. [CrossRef]
19. Ali, E.; Hadj-Kali, M.K.; Mulyono, S.; Alnashef, I.M.; Fakeeha, A.; Mjalli, F.S.; Hayyan, A. Solubility of CO_2 in deep eutectic solvents: Experiments and modelling using the Peng–Robinson equation of state. *Chem. Eng. Res. Des.* **2014**, *92*, 1898–1906. [CrossRef]
20. Francisco, M.; Bruinhorst, A.; Zubeir, L.F.; Peters, C.C.; Kroon, M.C. A new low transition temperature mixture (LTTM) formed by choline chloride + lactic acid: Characterization as solvent for CO_2 capture. *Fluid Phase Equilibria* **2013**, *340*, 77–84. [CrossRef]
21. Adeyemi, I.; Abu-Zahra, M.R.; Al-Nashef, I.M. Novel green solvents for CO_2 capture. *Energy Procedia* **2017**, *114*, 2552–2560. [CrossRef]
22. Haider, M.B.; Jha, D.; Sivagnanam, B.M.; Kumar, R. Thermodynamic and kinetic studies of CO_2 capture by glycol and amine-based deep eutectic solvents. *J. Chem. Eng. Data* **2018**, *63*, 2671–2680. [CrossRef]
23. Nowosielski, B.; Jamrógiewicz, M.; Łuczak, J.; Śmiechowski, M.; Warmińska, D. Experimental and predicted physicochemical properties of monopropanolamine-based deep eutectic solvents. *J. Mol. Liq.* **2020**, *309*, 113110–113122. [CrossRef]
24. Deng, L.; Chen, J.; Gao, G. Solubility of carbon dioxide in aqueous solutions of 3-amino-1-propanol. *J. Chem. Eng. Data* **2010**, *55*, 1030–1034. [CrossRef]
25. Shukla, S.K.; Mikkola, J.-P. Intermolecular interactions upon carbon dioxide capture in deep-eutectic solvents. *Phys. Chem. Chem. Phys.* **2018**, *20*, 24591–24601. [CrossRef]
26. Zhang, K.; Hou, Y.; Wang, Y.; Wang, K.; Ren, S.; Wu, W. Efficient and reversible absorption of CO_2 by functional deep eutectic solvents. *Energy Fuels* **2018**, *32*, 7727–7733. [CrossRef]
27. Li, Z.; Wang, L.; Li, C.; Cui, Y.; Li, S.; Yang, G.; Shen, Y. Absorption of carbon dioxide using ethanolamine-based deep eutectic solvents. *ACS Sustain. Chem. Eng.* **2019**, *7*, 10403–10414. [CrossRef]
28. Idris, Z.; Kummamuru, N.B.; Eimer, D.A. Viscosity measurement and correlation of unloaded and CO_2-loaded 3-amino-1-propanol solution. *J. Chem. Eng. Data* **2018**, *63*, 1454–1459. [CrossRef]
29. Saravanamurugan, S.; Kunov-Kruse, A.J.; Fehrmann, R.; Riisager, A. Amine-functionalized amino acid-based ionic liquids as efficient and high-capacity absorbents for CO_2. *ChemSusChem* **2014**, *7*, 897–902. [CrossRef]

30. Trivedi, T.J.; Lee, J.H.; Lee, H.J.; Jeong, Y.K.; Choi, J.W. Deep eutectic solvents as attractive media for CO_2 capture. *Green Chem.* **2016**, *18*, 2834–2842. [CrossRef]
31. Shukla, S.K.; Mikkola, J.-P. Unusual temperature-promoted carbon dioxide capture in deep-eutectic solvents: The synergistic interactions. *Chem. Commun.* **2019**, *55*, 3939–3942. [CrossRef]
32. Sarmad, S.; Nikjoo, D.; Mikkola, J.-P. Amine functionalized deep eutectic solvent for CO_2 capture: Measurements and modeling. *J. Mol. Liq.* **2020**, *309*, 113159. [CrossRef]
33. Astarita, G.; Marrucci, G.; Gioia, F. The influence of carboration ratio and total amine concentration on carbon dioxide absorption in aqueous monoethanolamine solutions. *Chem. Eng. Sci.* **1964**, *19*, 95–103. [CrossRef]
34. Camacho, B.F.; Sunchez, S.; Pacheco, R. Thermal effects during the absorption of CO_2 in aqueous solutions of 3-amino-1-propanol. *Chem. Eng. Technol.* **2000**, *23*, 1073–1080. [CrossRef]
35. Benamor, A.; Al-Marri, M.J.; Hawari, A. Experimental determination of carbamate formation and amine protonation constants in 3-amino-1-propanol–CO_2–H_2O system and their temperature dependency. *Int. J. Greenh. Gas Control* **2015**, *37*, 237–242. [CrossRef]

Załącznik A7

B. Nowosielski, D. Warmińska, I. Cichowska-Kopczyńska, CO_2 Separation Using Supported Deep Eutectic Liquid Membranes Based on 1,2-propanediol, ACS Sustain. Chem. Eng. 11 (2023) 4093–4105. https://doi.org/10.1021/acssuschemeng.2c06278. **IF_{2023}: 7,1, $MNSW_{2023}$: 140**

ACS Sustainable Chemistry & Engineering

pubs.acs.org/journal/ascecg

Research Article

CO_2 Separation Using Supported Deep Eutectic Liquid Membranes Based on 1,2-propanediol

Bartosz Nowosielski, Dorota Warmińska, and Iwona Cichowska-Kopczyńska*

Cite This: ACS Sustainable Chem. Eng. 2023, 11, 4093−4105

Read Online

ACCESS | Metrics & More | Article Recommendations | Supporting Information

ABSTRACT: In this work, deep eutectic solvents (DESs) composed of choline chloride, acetylcholine chloride or tetrabutylammonium chloride, and 1,2-propanediol were used as a liquid phase for polypropylene-based supported liquid membranes (SLMs) and evaluated for the separation of carbon dioxide from CO_2/N_2 mixtures. Fourier transform infrared spectra were obtained to confirm DES formation, and the thermal stability of solvents was investigated using thermogravimetric analysis. The physicochemical properties of DESs and carbon dioxide solubility were determined in a temperature range of 293.15−313.15 K. The effects of the hydrogen bond acceptor structure and the acceptor/donor molar ratio in regard to properties and CO_2 separation potential were discussed. The permeability of CO_2 and N_2 in DES-based SLMs was determined, and the ideal CO_2/N_2 selectivity was calculated. The gas permeation results of the 1,2-propanediol-based DES based supported liquid membranes showed that the permeability of CO_2 varied from 86 to 152 barrers in 293.15 K. Similarly, the ideal CO_2/N_2 selectivity varied from 21 to 30. The performance of DES−SLMs was compared with the competing imidazolium-based supported ionic liquid membranes and proved DES−SLMs as a promising alternative considering their green potential and comparable gas separation performance.

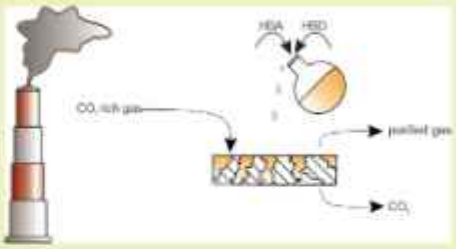

KEYWORDS: *deep eutectic solvents, supported liquid membranes, CO_2 separation, 1,2-propanediol*

INTRODUCTION

As global warming continues, new technologies are being sought to reduce emissions of carbon dioxide, which is one of the main greenhouse gases that also include water vapor, methane, volatile organic compounds, nitrous oxide, and ozone. The most important method proposed for this purpose is CO_2 capture and storage (CCS).[1] CCS technology involves capturing waste CO_2, transporting the captured CO_2 to a storage site and depositing it in a safe place. Although CO_2 deposition is currently considered the biggest problem in the process of carbon dioxide removal, its capture is not insignificant. So far, cryogenic distillation and absorption using aqueous alkanoamine solutions have been used at an industrial level for CO_2 capture.[1,2] However, both technologies used for carbon dioxide absorption have many disadvantages, such as high possibility of equipment corrosion and high energy consumption;[3] therefore, new technologies should be developed for this purpose. In recent years, membrane separation has been recognized as a cost-effective technology to reduce CO_2 emissions, and in addition to polymer-based membranes, supported liquid membranes (SLMs) have been introduced.[1] They are composed of polymeric support and liquid held in pores of support by capillary forces. The first liquids immobilized in a porous support for carbon dioxide separation were aqueous solutions of amines, and since 2002, ionic liquids (ILs) have been used and examined in gas separation.[4−6] It was found that supported ionic liquid membranes show high selectivity compared to the polymer membrane itself.[7] However, due to the high price, complex synthesis, and low biodegradability of ILs, their alternatives are still being sought. Most recently, deep eutectic solvents (DESs) have been used in SLM as a new substitute to ionic liquids[10−14] and their CO_2 capacity was proven.[15] DES-based SLMs have also become the subject of research in the field of olefin/paraffin separation, biotechnology, extraction, water purification, and energy processing and storage.[16−19]

In general, DESs consist of two components, namely, a hydrogen bond acceptor (HBA) and a hydrogen bond donor (HBD), and have similar physical properties to ionic liquids, are practically nonvolatile and nonflammable, and exhibit high

Received: October 20, 2022
Revised: February 17, 2023
Published: March 1, 2023

https://doi.org/10.1021/acssuschemeng.2c06278
ACS Sustainable Chem. Eng. 2023, 11, 4093−4105

Table 1. Provenance and Mass Fraction Purity of the Compounds Studied

chemical name	M/(g·mol^{-1})	source	CAS number	initial purity/mass fraction[a]	purification method	final purity/mass fraction[b]
choline chloride (ChCl)	139.62	Sigma-Aldrich	67−48−1	≥0.98	none	
acetylcholine chloride (AChCl)	181.66	Sigma-Aldrich	60−31−1	≥0.98	none	
tetrabutylammonium chloride (TBAC)	277.92	Sigma-Aldrich	1112−67−0	≥0.97	crystallization	≥0.98[b]
1,2-propanediol	76.09	Sigma-Aldrich	57−55−6	≥0.995	none	

[a]As stated by the supplier. [b]Determined by potentiometric titration.

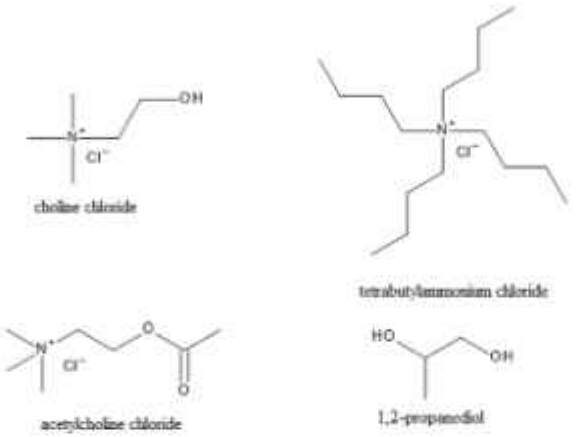

Figure 1. Chemical structures of chemicals used in this study.

thermal properties and electrochemical stability but are definitely cheaper, less toxic, and often biodegradable.[20]

To the best of our best knowledge, one the first DES-based SLMs for carbon dioxide separation has been reported by Amira et al.[21] The authors impregnated DES consisting of choline chloride (ChCl) and ethylene glycol (EG) (with a 1:3 molar ratio of HBA to HBD) into the polyvinylidenefluoride-*co*-polytetrafluoroethylene (PVDF-*co*-PTFE) polymer and used the obtained SLM for CO_2/N_2 separation. According to their results, ChCl-ethylene glycol DES/PVDF-*co*-PTFE SLM had a CO_2/N_2 ideal selectivity of 2.0. Ishaq et al. reported the permeation performance of poly(vinylidene difluoride) (PVDF) DES-based composite SLM in CO_2 separation. They found that among studied membranes, the SLMs containing DES based on monoethanolamine showed excellent selectivity of CO_2 equal to 70.47 and 78.86 for CO_2/CH_4 and CO_2/N_2, respectively.[15,22,23] Saeed et al. also examined supported liquid membrane based on PVDF, but in their research, they used DESs composed of betaine and urea/glycerol/ethylene glycol or DESs consisting of choline chloride and tartaric acid/malic acid/oxalic acid or DES based on potassium carbonate.[24−26] The authors showed that the separation factor CO_2/CH_4 for the studied SLMs was up to 60.16. Lian et al. incorporated an amino acid-based DES (L-arginine + ethylene glycol 1:5 molar ratio) to the PEBAX membrane at 5−20% g/g. The results showed that with the increase of DES loading the CO_2 permeability decreased, but the CO_2/N_2 selectivity increased up to 15% loading. For 15% DES loading, the selectivity increase reached 21% and the permeability loss was only 5%.[27] Craveiro et al. studied the poly(tetrafluoroethylene) (PTFE) membrane coated by choline chloride-based DESs with the addition of carbonic anhydrase.[14] They reported the highest CO_2 permeability for ChCl-urea (U)-based SLM and the highest CO_2/N_2 ideal selectivity for ChCl-glycerol based SLM. Castro et al. used choline chloride-levulinic acid to impregnate a PFTE membrane and investigated the effect of water on the permeation performance of this DES-based SLM in CO_2 separation.[28] They found that as the water content increased, both the permeability and the selectivity of CO_2/N_2 decreased.

In this work, it was the first time that deep eutectic solvents based on 1,2-propanediol were immobilized into a porous polypropylene support and evaluated for the separation of CO_2 from the CO_2/N_2 mixture. DESs were synthesized by mixing 1,2-propanediol with choline chloride, acetylcholine chloride, or tetrabutylammonium chloride, and Fourier transform infrared spectroscopy was studied to confirm the DES formation. The solubility of carbon dioxide in synthesized solvents and their physical properties, such as thermal stability, density, viscosity, and refractive index, were measured at a temperature range of 293.15−313.15 K. The effects of the hydrogen bond acceptor structure and the hydrogen bond acceptor/hydrogen bond donor molar ratio were discussed. Finally, the permeability of CO_2 and N_2 in DES-based SLMs was measured, and the ideal CO_2/N_2 selectivity was calculated and compared with competing high-performance imidazolium-based SILMs. The effect of operating conditions on membrane separation performance was also analyzed.

https://doi.org/10.1021/acssuschemeng.2c06278
ACS Sustainable Chem. Eng. 2023, 11, 4093−4100

Table 2. DES Specifications

symbol	HBA	HBA/HBD mole ratio	M_{DES}/(g·mol^{-1})	molar fraction[a] HBD	water content[b]
DES-A1	choline chloride	1:3.019	91.899	0.7512	0.00175
DES-A2	choline chloride	1:4.021	88.744	0.8008	0.00121
DES-B1	acetylcholine chloride	1:2.990	102.552	0.7493	0.00217
DES-C1	tetrabutylammonium chloride	1:2.987	126.713	0.7492	0.00234

[a]The standard uncertainty of the HBD molar fraction composition is 0.001. [b]Water content of DESs in mass fraction determined by the Karl−Fischer titration with the standard uncertainty ±0.0001.

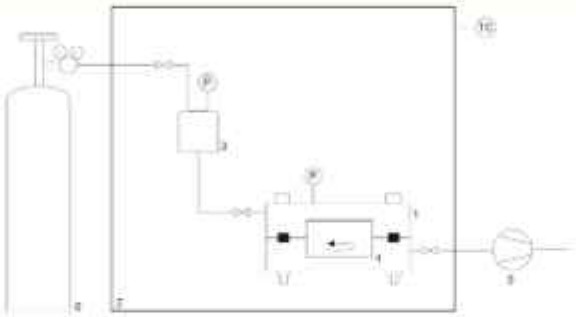

Figure 2. CO_2 experimental setup of gas solubility determination via isochoric saturation method (1, equilibrium cell; 2, thermostatic chamber; 3, intermediate gas tank; 4, magnetic stirrer; 5, vacuum pump; 6, gas tank).

EXPERIMENTAL SECTION

Materials. Table 1 presents the information about the chemicals used in this study, and in Figure 1 their chemical structures are presented. 1,2-Propanediol, choline chloride, acetylcholine chloride, and tetrabutylammonium chloride were purchased from Sigma-Aldrich (Saint Louis). Tetrabutylammonium chloride was purified by double crystallization from acetone by adding diethyl ether and the remaining chemicals were used as received from the producer. All salts were dried under reduced pressure before use for several days, choline chloride at 323.15 K and acetylcholine chloride and TBAC at 298.15 K. Polypropylene (PP) membranes with a pore size of 0.2 μm, a porosity of 80%, and a thickness of 9.3×10^{-5} m were obtained from Pall Corporation (New York). Carbon dioxide (0.9995 purity) and nitrogen (0.9998 purity) gases were supplied by Oxygen S.C. (Gdańsk, Poland).

Preparation of DESs. The DESs were prepared by mixing 1,2-propanediol with three different salts: choline chloride, acetylcholine chloride, and tetrabutylammonium chloride in a molar ratio of 1:3 HBA to HBD. For comparison, the DES containing choline chloride in a molar ratio of 1:4 was also prepared. The preparation was carried out by mass using appropriate amounts of each DES component (Mettler Toledo with a precision of 0.00001 g) and mixed at 343.15 K for 1 h until a homogeneous liquid without any precipitate was formed. The obtained DESs, stable colorless liquids at room temperature, were kept in tight bottles to prevent any contamination that may affect the physical properties. Before experiments, the water content in DESs was determined by the Karl−Fischer method using a Mettler Toledo volumetric Karl−Fischer titrator (V108). Table 2 presents its values along with the molar mass of DESs, their abbreviations, and the molar ratio and molar fraction of DES components.

Membrane Fabrication. The DES−SLMs were fabricated using the polypropylene porous support according to the well-known procedure described in the literature.[29−31] In the first step, both the DES and the polypropylene membrane were placed under vacuum at 323.15 K for 4 h to remove traces of gases and water from the pores. Thereafter, the polypropylene support was saturated with 0.1 cm^3 of DES per 1 cm^2 of the membrane. The excess liquid was removed with paper tissue, and the procedure was repeated until the weight of the membrane was stable. Then, the final mass of the liquid was compared to the theoretical calculations and if the saturation was close to 100% the membrane was used in separation experiments.

Thermogravimetric Analysis. The thermogravimetric analyses were performed using the TG 209F3 apparatus from Netzsch Group (Selb, Germany). Weighted samples (approx. 10 mg) were placed in a corundum dish. The measurement was carried out in an inert gas atmosphere-nitrogen with a flow rate of 50 mL·min^{-1} in the range from 298 to 1023 K at a heating rate of 10 K·min^{-1}.

Infrared Spectroscopy Measurements. FTIR experiments for liquid samples were performed using a Jasco-4700 instrument (4000−400 cm^{-1} with 32 scans, 4 cm^{-1} resolution; Jasco Company, Tokyo, Japan). Thin film method using salt (KBr) plates was applied by placing 1 drop of the solution on one salt plate. The spectrum from a clean plate was recorded as a background, and analysis of spectra was performed using Spectra Analysis software (Jasco Company, Tokyo, Japan). Spectra of solid samples (substrates) were recorded using dry salt KBr. The materials (1 mg) were compressed with potassium bromide (99 mg) to form a disc. Analysis were performed at 298.15 ± 0.1 K.

Density, Viscosity, and Refractive Index Measurements. The densities of the DES samples were obtained at different temperatures using a digital vibration-tube analyzer (Anton Paar DSA 5000, Austria) with a proportional temperature control that kept the samples at working temperature with an accuracy of ±0.01 K. The calibration was carried out using double-distilled, deionized, and degassed water and dry air at atmospheric pressure (0.1 MPa). The standard uncertainty of the density measurement was better than 0.1 kg·m^{-3}.

The viscosities of the DESs were measured with an LVDV-III Programmable Rheometer (cone-plate viscometer; Brookfield Engineering Laboratory), controlled by a computer. The temperature of the samples was controlled within ±0.01 K using a thermostatic water bath (PolyScience 9106). The display of the viscosimeter was verified with the certified viscosity standard N100 and S3 provided by Cannon at 298.15 ± 0.01 K. The standard uncertainty of viscosity measurement was better than 2%. At least three independent

https://doi.org/10.1021/acssuschemeng.2c06278
ACS Sustainable Chem. Eng. 2023, 11, 4093−4108

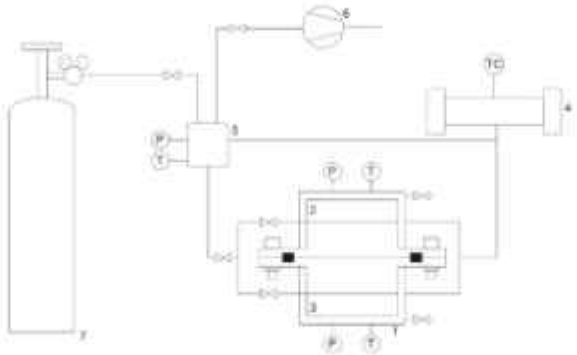

Figure 1. Experimental setup for gas permeation measurements (1, permeation chamber; 2, feed space; 3, permeate space 4, thermostat; 5, intermediate gas tank; 6, vacuum pump; 7, gas tank).

measurements were taken for each sample at each temperature to assure reproducibility of the measurement.

The refractive indices were obtained with an Abbe refractometer (RL-3, Poland) equipped with a thermostat for controlling the cell temperature with an accuracy of ±0.1 K. The standard uncertainty of refractive index measurement on the n_D scale was 0.0003. At least three independent measurements were taken for each sample at each temperature to assure reproducibility of the measurement.

Gas Solubility Measurement. The experimental setup for measuring CO_2 solubility using the isochoric saturation method is presented in Figure 2. The setup included an intermediate gas tank (3) and an equilibrium cell (1) equipped with a pressure sensor and a magnetic stirrer (4). The volume of the cell was 7.8 ± 0.01 cm^3. The individual parts were separated by gas-tight valves, and the system was placed in a thermostated tank (2) controlled by an LS thermostat (PolyScience 9106, Warrington, PA). The experimental uncertainty for the temperature was ±0.1 K.

Prior to the experiment, 1 cm^3 of liquid was placed in the equilibrium cell (1). A vacuum was applied in the system using a vacuum oil pump (5). After that, the intermediate gas tank (3) was filled with the gas (6). When the temperature was stable, the gas was introduced to the cell and initial pressure was recorded. The pressure was recorded continuously with an Aplisens PC-28 transducer with a standard uncertainty of 0.6 kPa, and the experiment was stopped when the equilibrium was reached, i.e., when the pressure in the system did not change for 1 kPa over 24 h. After reaching an equilibrium, another portion of CO_2 was injected into the equilibrium cell from the intermediate gas tank.

Validation of the method was conducted by measuring CO_2 solubility in water at 295.15 K, and the results were compared with the values reported in the literature.[35] The results are presented in Figure S1. A good agreement of data was obtained.

Gas Permeability Measurement. The laboratory setup for permeability measurements is presented in Figure 1 and was constructed in the Department of Process Engineering and Chemical Technology. The main part of the system was a permeation chamber equipped with a water coat (1) and divided into feed (2) and permeate (3) side. Intermediate gas reservoir (5) was placed in a thermostated tank (4) in which the constant temperature was maintained by means of an LS thermostat (PolyScience 9106, Warrington, PA) with an accuracy of ±0.1 K. Additional temperature Pt100 sensors were located in both parts of the membrane cell.

At the start of the experiment, vacuum was applied in the system using a vacuum oil pump (6). Then, gas reservoir (5) was filled with CO_2 or N_2 from the gas tank (7). When the temperature in the system was constant, the gas was delivered into the feed space. The initial gas pressure was about 22 kPa chosen experimentally to prevent from mechanic deformation and degradation of the membrane. The pressure in both chambers was recorded with a frequency of 0.1 Hz.

Theory. In this study, the amount of carbon dioxide dissolved in the DES was calculated by the following equation

$$n = n_0 - n_1 \tag{1}$$

where n_0 is the amount of carbon dioxide introduced to the measurement chamber and n_1 is the amount of CO_2 in the gas phase at equilibrium state.

The amount of CO_2 was obtained from eq 2

$$n_i = \frac{p_i V}{Z_i R T} \tag{2}$$

where V is the volume of the gas phase in the cell in cm^3 (head space volume over DES corresponds to the chamber volume minus the volume of injected DES), p_i is the partial pressure in kPa (the initial or at equilibrium, respectively), R is the universal gas constant in J·mol^{-1}·K^{-1}, T is temperature in K, and Z_i is the compressibility factor, which for ideal gases equals 1.

Since there is a physical absorption of carbon dioxide in DESs containing 1,2-propanediol, the solubility of CO_2 was used to calculate Henry's constant based on mole fraction (H_x) as follows[35]

$$H_x(p, T) \equiv \lim_{x_2 \to 0} \frac{p y_2 \phi_2(p, T, y_2)}{x_2} \tag{3}$$

Due to negligibly small vapor pressures of deep eutectic solvents, y_2 can be simplified to be unity.[35] Additionally, at low CO_2 pressures, the fugacity coefficient of CO_2 is also close to 1;[35] therefore, eq 3 is simplified to

$$H_x(p, T) = \frac{p}{x_2} \tag{4}$$

Thus, in this work, Henry's constant was determined from the slope of the isothermal linear fit of equilibrium pressure versus mole fraction of CO_2.

The gas permeation in DES−SLM was calculated in barrers on the basis of the pressure difference between the feed and permeate side over the selected time period providing that the pressure drop was linear

$$P = 10^{10} \frac{V_p l}{A t (p_{f_2} - p_{f_1})} \tag{5}$$

where l is the thickness of the membrane in cm, A is the membrane area in m^2, t is time in s, V_p is the volume of permeated gas at normal

https://doi.org/10.1021/acssuschemeng.2c06278
ACS Sustainable Chem. Eng. 2023, 11, 4090−4100

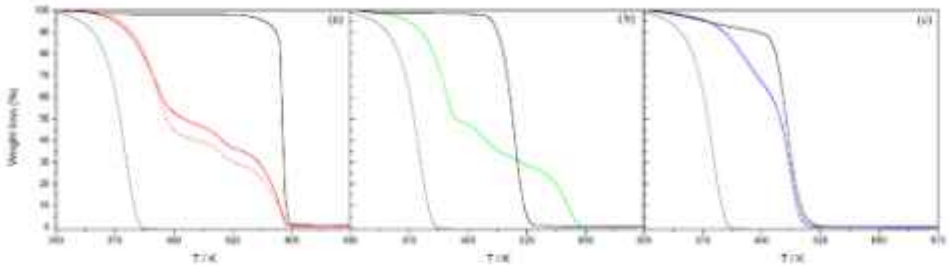

Figure 4. TGA curves obtained by thermogravimetry of DESs: (a) red straight line, ChCl:1,2-propanediol 1:3 (DES-A1); red dashed line, ChCl:1,2-propanediol 1:4 (DES-A2); (b) green straight line, AChCl:1,2-propanediol 1:3 (DES-B1); and (c) blue straight line, TBACl:1,2-propanediol 1:3 (DES-C1); black solid, salt; gray, 1,2-propanediol.

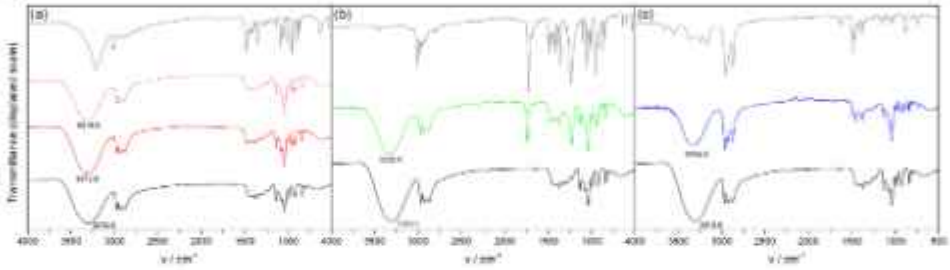

Figure 5. FTIR spectra for DES studied: (a) DES-A1 (red straight line) and DES-A2 (red dashed line), (b) DES-B1 (green straight line) and (c) DES-C1 (blue straight line); black straight line, neat 1,2-propanediol; gray straight line, salts.

conditions in cm^2, $p_{i(f)}$ and $p_{i(p)}$ are the pressure in mmHg of i in feed (f) and permeate (p), respectively.

The ideal CO_2/N_2 selectivity of the CO_2 over N_2 was calculated using the following equation

$$\alpha_{CO_2/N_2} = \frac{P_{CO_2}}{P_{N_2}} \tag{6}$$

where P_{CO_2} and P_{N_2} are the permeability of carbon dioxide and nitrogen, respectively.

RESULTS AND DISCUSSION

Characterization of DESs: Their Thermal Stability, FTIR Spectra, and Physical Properties. The knowledge of the physical properties of solvent, including its thermal stability, is crucial for every industrial and chemical process design, not just for CO_2 capture. Density is essential in many thermodynamic calculations as well as in the design and sizing of process equipment. Viscosity is important because it affects mass transport phenomena and conductivity of ionic fluids, thus affecting their suitability for specific applications. Moreover, it strongly influences the diffusion of dissolved particles in the solvent. Refractive index is an elemental property, which can be used for a component's identification, concentration determination, and purity confirmation.

Figure 4 presents TGA curves, i.e., the weight loss measured in % against temperature, for the studied DESs along with their pure components. As can be seen, for TBAC:1,2-propanediol (DES-C1), the curves consist of two steps: the first shows 1,2-propanediol decomposition and the second corresponds to the degradation of the salt. For acetylcholine chloride- and choline chloride-based DESs, an additional step is observed. The stability of all DESs is in between that of their components, and the order of stability is 1,2-propanediol < DES <salt. However, the complete decomposition of AChCl:1,2-propanediol (DES-B1) occurs at temperature higher than the neat AChCl. For DESs with the same molar ratio of HBA to HBD, the initial decomposition temperature measured as a 10% weight loss ($T_{10\%}$) changes according to the order: TBAC:1,2-propanediol (401.9 K) > ChCl:1,2-propanediol (391.5 K) > AChCl:1,2-propanediol (390.9 K). This sequence is consistent with the results obtained for phosphonium-based DES, showing that the thermal stability of DES increases with increasing length of the alkyl chain length of its components and is higher for systems with stronger hydrogen bond interactions.[36] Since the thermal stability of ChCl:1,2-propanediol (391.5 K) at a molar ratio of HBA to HBD 1:3 is lower than at a molar ratio of 1:4 (396.8 K), it can be suspected that in DES based on choline chloride with a higher content 1,2-propanediol, stronger interactions of hydrogen bonds take place. Summarizing, the obtained results of thermal analysis indicate that the studied DESs are suitable for using in the operating conditions for CO_2 capture.

The FTIR spectra of the studied DESs are presented in Figure 5 together with the spectra of neat 1,2-propanediol, choline chloride, acetylcholine chloride, and tetrabutylammonium chloride.

Regarding choline chloride (Figure 5a), the vibrational bands at 3219 and 3005−3025 cm^{-1} correspond to the

https://doi.org/10.1021/acssuschemeng.2c06278
ACS Sustainable Chem. Eng. 2023, 11, 4093−4108

Table 3. Physical Properties of DESs[a]

DES	T/K	ρ/kg·m^{-3}		η/mPa·s		n_D		f_v/cm^3·mol^{-1}
		Exptl.	Lit.	Exptl.	Lit.	Exptl.	Lit.	
DES-A1 (ChCl-1,2-propanediol 1:3)	293.15	1071.82	1071.82[b], 1073.70[c]	83.79	94.03[b], 89.583[c]	1.4604	1.46137[c]	68.86
	298.15	1068.68	1068.79[b], 1068.62[c], 1069[d]	62.78	72.10[b], 68.432[c], 64.14[d]	1.4592	1.45995[c]	69.16
	303.15	1065.68	1065.71[b], 1065.54[c], 1068[d]	48.12	56.26[b], 53.339[c], 50.22[d]	1.4580	1.45853[c]	69.44
	308.15	1062.61	1062.65[b], 1062.47[c]	37.31	44.30[b], 42.261[c]	1.4565	1.45708[c]	69.71
	313.15	1059.55	1059.60[b], 1059.39[c], 1060[d]	29.17	35.89[b], 33.925[c], 31.92[d]	1.4552	1.45561[c]	70.00
	318.15	1056.48	1056.56[b], 1056.32[c]	23.43	29.13[b], 27.714[c]	1.4541	1.45418[c]	70.28
	323.15	1053.41	1053.48[b], 1053.24[c], 1054[d]	19.20	24.25[b], 22.888[c], 21.61[d]	1.4529	1.45275[c]	70.58
	328.15	1050.34	1050.41[b], 1050.16[c]	15.89	20.01[b], 19.111[c]	1.4516	1.45131[c]	70.85
	333.15	1047.27	1047.35[b], 1047.07[c], 1047[d]	13.37	17.13[b], 16.179[c], 14.92[d]	1.4503	1.45012[c]	71.15
DES-A2 (ChCl-1,2-propanediol 1:4)	293.15	1066.23	1065.56[b]	70.33	80.19[b]	1.4581		62.24
	298.15	1063.08	1062.63[b]	51.12	61.49[b]	1.4546		62.49
	303.15	1059.93	1059.28[b]	38.68	47.74[b]	1.4532		62.70
	308.15	1056.77	1056.12[b]	30.32	37.47[b]	1.4518		62.93
	313.15	1053.61	1053.97[b]	24.67	30.40[b]	1.4501		63.19
	318.15	1050.44	1049.70[b]	20.20	24.70[b]	1.4490		63.42
	323.15	1047.25	1046.63[b]	16.85	20.43[b]	1.4475		63.66
	328.15	1044.08	1043.50[b]	13.76	17.00[b]	1.4459		63.91
	333.15	1040.89	1040.28[b]	11.50	14.43[b]	1.4443		64.16
DES-B1 (AChCl-1,2-propanediol 1:3)	293.15	1083.99		80.69		1.4582		60.78
	298.15	1078.67		65.29		1.4575		61.03
	303.15	1075.37		48.79		1.4561		61.27
	308.15	1071.86		38.18		1.4548		61.51
	313.15	1068.77		29.87		1.4534		61.77
	318.15	1065.47		23.90		1.4520		62.00
	323.15	1061.18		19.05		1.4505		62.26
	328.15	1058.88		17.54		1.4494		62.52
	333.15	1055.59		13.82		1.4478		62.78
DES-C1 (TBAC-1,2-propanediol 1:3)	293.15	975.85		158.59		1.4604		94.26
	298.15	972.59		133.17		1.4588		94.68
	303.15	969.31		83.57		1.4571		95.11
	308.15	966.06		63.41		1.4555		95.54
	313.15	962.80		48.39		1.4540		95.97
	318.15	959.54		37.05		1.4525		96.40
	323.15	956.28		29.48		1.4508		96.84
	328.15	953.03		23.94		1.4492		97.28
	333.15	949.76		19.64		1.4479		97.71

[a]Standard uncertainties are $u(T) = 0.01$ K, $u(p) = 0.001$ MPa, $u(\rho) = 0.1$ kg·m^{-3}, $u(n_D) = 0.0002$, and $u(\eta) = 2\%$. [b]ref 42. [c]ref 41. [d]ref 40. [e]Free volume, f_v, calculated on the basis of experimental values of density and refractive index of DES. The details of the calculations are in the SM.

https://doi.org/10.1021/acssuschemeng.0c09144
ACS Sustainable Chem. Eng. 2021, 9, 4899−4910

presence of a hydroxyl group and an alkyl group, respectively, while the bands at 1205−885 cm^{-1} represent C−N vibrations.[37] Since acetylcholine chloride does not have a OH group, its spectrum (Figure 5b) does not show the vibrational band associated with this group, but it does show a different band at 1731 cm^{-1} characteristic for the C=O stretching vibrations.[38] In the spectrum of tetrabutylammonium chloride, the characteristic bands related to the presence of CH_3 and CH_2 groups were identified at 2958 and 2873 cm^{-1}. Moreover, an additional vibrational band in the range of 3367−3173cm^{-1} was observed, probably due to the water absorbed during the experiment, as TBAC is a highly hygroscopic material.[39] The band in the 1,2-propanediol spectrum represents a typical region of the ν(OH) stretching vibration range, particularly sensitive to hydrogen bonds located at 3314 cm^{-1}.

For the studied DESs, the spectra did not show any changes in the position of the bands and the formation of any new bonds in the relation to the spectra of pure salts. Thus, they confirm the lack of specific chemical interactions between DES components. Almost the only effect in the DES spectrum is the shift of the OH band position to the blue due to the appearance of the new OH-halide hydrogen bonds. The largest shift observed for DES-C1 suggests the strongest interactions between DES components, while the smallest shift obtained for DES-A1 implies the weakest interactions.

The density, viscosity, and refractive index of the deep eutectic solvents studied were measured as a function of temperature in the range of 293.15−333.15 K at ambient pressure, and their values are presented in Table 3 and Figure S2a−c. The literature data only available for choline chloride−1,2-propanediol (DES-A1 and DES-A3) is included in Table 3. As seen, the experimental values of density and refractive index are in good agreement with the values reported by other groups.[40−42] However, in the case of viscosity, there was a significant difference in the data compared to the literature, mainly due to the different water content and the different measurement method. It is worth noting that for the same reasons, the literature data differs remarkably from each other.

For all DESs studied, the density, refractive index, and viscosity decrease with the increase of temperature. Moreover, for the density and the refractive index, a linear relationship with temperature is observed, while the viscosity drops exponentially with temperature, as can be seen in Figure S2.

The fitting parameters of empirical linear equations correlating the effect of temperature on the density and refractive index ($y = a \cdot T + b$), obtained by least-squares analysis, are listed in Table 4. Very low RMSD values and R^2 values close to unity confirm the good linear dependence of these properties on temperature, as can be seen in Figure S2.

Table 5 shows the parameters derived from the experimental dynamic viscosity data that were fitted to the Vogel−Fulcher−Tamman (VFT) equation, which, as known from the literature, describes the viscosity−tempeature relationship better than the Arrhenius equation.[20] The VFT equation is given as

$$\eta = \eta_0 \exp^{b/T - T_0} \tag{7}$$

where η_0, b, and T_0 are the fitting parameters, and T is the temperature in Kelvin.

Since 1,2-propanediol was common to all DESs, differences in the physical properties of the DES are due to the hydrogen bond acceptor and the interaction forces between HBA and glycol.

Table 4. Parameters of the Models of Density and Refractive Index along with Root-Mean-Square Deviations

DES	a	b	RMSD	R^2
		$d/kg\,m^{-3}$		
DES-A1	−0.611	1250.82	0.088	0.9999
DES-A2	−0.633	1252.01	0.021	0.9999
DES-B1	−0.660	1275.42	0.010	1.0000
DES-C1	−0.652	1167.01	0.005	1.0000
		n_D		
DES-A1	−0.00025	1.5343	0.9×10^{-4}	0.9993
DES-A2	−0.00029	1.5416	1.3×10^{-4}	0.9990
DES-B1	−0.00028	1.5410	1.2×10^{-4}	0.9989
DES-C1	−0.00031	1.5558	1.0×10^{-4}	0.9994

Table 5. Fitting Parameters for the Vogel−Fulcher−Tamman (VFT) Equation for Dynamic Viscosity Results Determined within the Temperature Range T = (293.15−333.15) K and P = 0.1 MPa

DES	η_0/mPa·s	b/K	T_0/K	RMSD	R^2
DES-A1	0.0177	1067.4	160.0	0.189	0.9999
DES-A2	0.3210	448.6	211.3	0.316	0.9997
DES-B1	0.3538	445.0	212.8	0.424	0.9997
DES-C1	0.0267	1093.4	167.3	0.412	0.9999

At the fixed temperature and the molar ratio of HBA to HBD, the density of the studied DESs is in the following order: AChCl:P (DES-B1) > ChCl:P (DES-A1) > TBAC:P (DES-C1). The higher density for choline chloride-based DES compared to the density tetrabutylammonium chloride-based DES was also reported for deep eutectic solvents containing p-toluenesulfonic acid as HBD.[43] According to the literature, the density decreases with increasing the length/symmetry of the cation-alkyl chain in DES because the elongation of the alkyl chain length increases the free volume of solvent. This is in line with our results because, as shown in Table 3, the TBAC-based DES has the highest free volume and the lowest AChCl:P (DES-B1).

The size of the solvent has also been found to affect its viscosity, and it has been observed that larger HBD or HBA results in higher DES viscosity.[44] In the present work, this phenomenon is visible in the TBAC:P (DES-C1) viscosity, which shows the highest values among the studied DES, regardless of the temperature. The viscosities of AChCl:P (DES-B1) and ChCl:P (DES-A1) show much lower values, indicating that the alkyl chain length of the salt has a greater effect on DES viscosity than the presence of an additional acetyl group in HBA. Taking into account the amount of 1,2-propanediol, the viscosity decreases when the ratio of HBA and HBD is lower. Obviously, the viscosity values of the studied DESs are also a result of the presence of hydrogen bonds, electrostatic, and van der Waals interactions between the individual components of DESs, which lead to an increase in flow resistance.

With regard to the refractive index of DESs, the order of ChCl:P (DES-A1) > TBAC:P (DES-C1) > AChCl:P (DES-B1) suggests that the ChCl is the most favorable enhancing HBA of refractive index, while AChCl is the lowest. This observation is somewhat surprising as it has been observed that the denser the liquid, the higher the refractive index.[45] Thus,

https://doi.org/10.1021/acssuschemeng.2c06278
ACS Sustainable Chem. Eng. 2023, 11, 4093−4108

many factors must determine the refractive index, not only the free volume as in the case of density, but also, i.e., the electronic polarizability of the DES molecule.

As seen from Table 3 and Figure S2, all physical properties of DESs depend on the HBA:HBD molar ratio. For ChCl-based deep eutectic solvent, both the density, refractive index, and viscosity decrease with the increasing of molar ratio of 1,2-propanediol. Obviously, this is the result of the relation of these properties for DESs and glycol. The densities, refractive indices, and viscosities for ChCl:P (DES-A1-A2) are higher than for neat 1,2-propanediol. Thus, as the amount of glycol in DES increases, the properties, tending to lower properties of pure 1,2-propanediol, decrease.

Solubility of Carbon Dioxide and Henry's Constant. The solubility of CO_2 in the studied deep eutectic solvents was measured in the temperature range of 293.15−313.15 K and pressures of 18−256 kPa. The solubility results at 298.15 K are shown in Figure 6. Table S1 presents the gas equilibrium

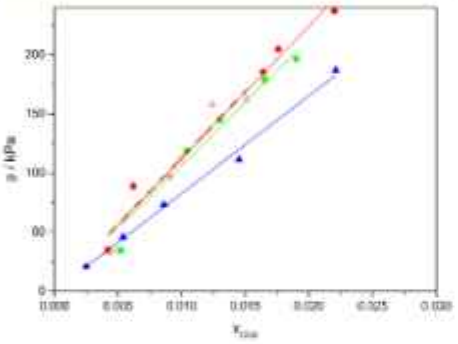

Figure 6. Solubility of carbon dioxide in studied DESs: circle, DES-A1; star, DES-A2; square, DES-B1; triangle, DES-C1; and lines, linear fit.

pressure (P), the liquid phase molality (m_{CO_2}), and the mole fraction of CO_2 (x_{CO_2}). As expected, it was observed that for each DES, the solubility of CO_2 increased with decreasing temperature and increasing pressure.

Literature reports indicate that the absorption of carbon dioxide in DESs based on 1,2-propanediol is purely physical.[60] Thus, the solubility was described in terms of Henry's law (eq 4) and the obtained results are presented in Table 6. Henry's constants for DES-containing choline chloride, i.e., DES-A1 and DES-A2, have already been reported by Chen et al.[60] However, the authors obtained values of 30.68 and 30.59 at 293.15 K, which are about 3 times higher than those obtained in this study. This can result from different DES volumes and the similar equilibration time in both studies.

As the volume of the sample increases, the time needed to reach equilibrium and to ensure the homogeneous saturation of the whole volume of the sample also increases. Higher volume results in the elongation of equilibration period due to longer time needed for gas molecules to diffuse in the whole volume of the liquid and pressure changes become slower with time, from our experience, even barely noticeable in the short time periods. Chen et al. reported the volume of equilibrium

Table 6. Henry's Law Constants (H_x) of CO_2 in the Studied DESs

DES	T/K	H_x/MPa
DES-A1	293.15	10.8 ± 0.36
	298.15	11.2 ± 0.39
	303.15	11.8 ± 0.44
	308.15	12.3 ± 0.51
	313.15	13.3 ± 0.58
DES-A2	293.15	10.7 ± 0.34
	298.15	11.1 ± 0.35
	303.15	11.9 ± 0.37
	308.15	12.8 ± 0.57
	313.15	13.4 ± 0.59
DES-B1	293.15	10.2 ± 0.40
	298.15	10.7 ± 0.40
	303.15	11.3 ± 0.42
	308.15	11.9 ±0.43
	313.15	12.7 ± 0.48
DES-C1	293.15	7.8 ± 0.21
	298.15	8.3 ± 0.18
	303.15	8.8 ± 0.26
	308.15	9.6 ± 0.35
	313.15	10.4 ± 0.31

cell of 141.61 cm^3 and they assumed that the system reached equilibrium when the pressure remained stable for 4 h.[60] From our experience, the time was not enough for the large volume system to ensure homogeneous saturation of the whole liquid column. In our methodology, equilibrium was considered to be reached when the pressure in the system did not change for 1 kPa over 24 h. Thus, a much lower solubility of CO_2 in the cited work may result from too short waiting time for reaching equilibrium. The correctness of our experimental procedure is also confirmed by the validation presented in the Supporting Information.

Comparison of Henry's constants values for DES-A1 and DES-A2 shows the effect of HBA/HBD molar ratio on carbon dioxide solubility in deep eutectic solvents. As can be seen from Table 6, for all temperatures and after consideration of experimental error, Henry's constants are undistinguishable. This indicates a similar solubility of CO_2 in ChCl:1,2-propanediol at a HBA/HBD molar ratio of 1:4 and 1:3.

When DESs with different salts are considered, depending on HBA, the solubility of CO_2 increases in the following order: ChCl:P (DES-A1) < AchCl:P (DES-B1) < TBAC:P (DES-C1) regardless of temperature. The higher CO_2 solubility observed by our group for DES based on acetylcholine chloride than for DES based on choline chloride is consistent with the literature.[17] The results obtained by Liu et al. for guaiacol-based DESs also showed a positive effect of the carboxylic group on the affinity for CO_2 compared to that of the hydroxyl group. The highest solubility of carbon dioxide in DES-containing TBAC seems to be related to the distinctly largest free volume (see Table 3) of this solvent, resulting from longer alkyl chains and greater symmetry of the TBAC molecule compared to the ChCl and ACC molecules.[58,59]

Permeability of Gases in DES-Based SLMs. The permeability of pure gases (CO_2 and N_2) in the synthesized SLMs was studied in the temperature range of 293.15−313.15 K, and the results along with the ideal selectivity α_{CO_2/N_2} are presented in Table 7.

https://doi.org/10.1021/acssuschemeng.2c06278
ACS Sustainable Chem. Eng. 2023, 11, 4093−4100

Table 7. Pure Gas Permeability and Ideal Selectivity

		P/barrer		
DES	T/K	CO_2	N_2	α_{CO_2/N_2}
DES-A1 (ChCl:1,2-propanediol 1:3)	293.15	86 ± 6.4	3 ± 0.3	29 ± 3.0
	298.15	104 ± 7.8	5 ± 0.4	21 ± 2.2
	303.15	117 ± 9.4	6 ± 0.5	19 ± 2.2
	308.15	130 ± 10.7	7 ± 0.5	19 ± 2.0
	313.15	145 ± 11.8	16 ± 1.2	9 ± 1.0
DES-A2 (ChCl:1,2-propanediol 1:4)	293.15	90 ± 6.7	4 ± 0.3	24 ± 2.5
	298.15	112 ± 8.0	5 ± 0.5	22 ± 2.0
	303.15	120 ± 8.5	8 ± 0.6	15 ± 1.3
	308.15	135 ± 10.1	10 ± 0.7	14 ± 1.4
	313.15	149 ± 11.3	23 ± 1.8	6 ± 0.7
DES-B1 (AchCl:1,2-propanediol 1:3)	293.15	117 ± 8.0	4 ± 0.3	29 ± 3.0
	298.15	127 ± 8.9	7 ± 0.5	18 ± 1.8
	303.15	141 ± 9.9	8 ± 0.6	18 ± 1.8
	308.15	134 ± 10.6	8 ± 0.7	19 ± 2.1
	313.15	170 ± 11.0	14 ± 1.1	12 ± 1.2
DES-C1 (TBAC:1,2-propanediol 1:3)	293.15	152 ± 9.3	5 ± 0.4	30 ± 3.1
	298.15	162 ± 10.4	8 ± 0.6	20 ± 2.0
	303.15	191 ± 13.8	14 ± 0.9	14 ± 1.3
	308.15	207 ± 14.6	24 ± 1.6	9 ± 0.8
	313.15	226 ± 17.0	29 ± 1.9	8 ± 0.8

The solution−diffusion theory (SDT) was found to be the most accepted model to explain gas transport through a membrane.[50] According to this theory, gas is first absorbed at the membrane feed side surface, then diffuses through the membrane, and finally is desorbed from the permeate side surface of the membrane. The driving force of this process is the gas chemical potential gradient over the membrane. The separation process depends on both the solubility of the gas in the liquid forming the membrane phase and the viscosity and free volume of the solvent. Both solubility and diffusivity determine permeability and selectivity.

Thus, the higher CO_2 permeability in the DES-based SLMs compared to N_2 (Table 7) is undoubtedly the result of the distinctly higher solubility of carbon dioxide in the studied DESs.

Solubility also determines the order of pure CO_2 permeability, which varies as follows: DES-C1 > DES-B1 > DES-A2 > DES-A1. This factor seems to be stronger than the viscosity effect because DES-C1, despite the highest viscosity, and the same highest diffusion resistance, has the highest permeability. The high permeability of this DES is favored not only by high solubility of CO_2 but also by its large free volume. The largest free volume of DES-C1 can compensate for the diffusion resistance associated with the high viscosity, resulting in the best permeability values. DES-B1, despite higher viscosity and lower free volume than DES-A1 and DES-A2, shows higher values of CO_2 permeability. This suggests a greater influence of the solubility of carbon dioxide in this DES than its properties responsible for diffusion resistance.

The permeability of N_2 is mainly due to the diffusion resistance since the solubility of N_2 in DESs is negligibly small.[51−54] In general, the values of N_2 permeability are the highest for DES-C1-based SLM at all temperatures, while for other DES-based SLMs the values of this parameter are similar, and their order is different from temperature. It seems that the free volume of DESs is mostly responsible for this behavior as its value is highest for DES-C1 and is similar for other DESs.

Effect of Temperature on Permeability of Gases in Synthesized DES-Based SLMs. As shown in Table 7, for all membranes, an increase in temperature results in an increase of the permeability of both carbon dioxide and nitrogen. This phenomenon may be due to the rapid decrease in DES viscosity with increasing temperature. At higher temperatures, the intermolecular interactions in DESs become weaker, resulting in lower diffusion resistance. This increases the mobility of free species in DES and consequently leads to their higher permeability. On the other hand, the solubility of gases decreases with increasing temperature, which would result in a decrease in permeability. However, since the permeability of CO_2 and N_2 increases with the increase of temperature, the solubility effect seems to be much less significant than that related to decreasing viscosity. This conclusion is consistent with the results obtained by other authors for the different DES and IL-based SLMs.[13,54,55,56] This effect is the most easily noticeable for DES-C1. Increase of temperature causes the drop of viscosity and the viscosity decreased at a faster rate for DES-C1, which has the highest viscosity of DESs used in this study. And for that mixture, the increase of N_2 permeability has the highest slope, corresponding to the decrease of viscosity. The permeability of CO_2 increases with temperature at approximately the same rate for all of DESs and it is in agreement with the viscosity and solubility values. Solubility decreases at the same rate for DES-A1, DES-A2, and DES-B1, and the highest decrease in the examined range is observed for DES-C1. The highest decrease of CO_2 solubility combined with the highest viscosity decrease results in similar CO_2 permeability increase rate.

The effect of temperature on the carbon dioxide permeability in the studied DES−SLMs is presented in Figure 7. As can be seen, all DES−SLMs show Arrhenius behavior in terms of CO_2 permeability in the studied temperature range with the coefficient of determination (R^2) close to 0.99. The Arrhenius equation explains the relationship between temperature and permeation using activation energy and is given as

https://doi.org/10.1021/acssuschemeng.2c06278
ACS Sustainable Chem. Eng. 2023, 11, 4093−4108

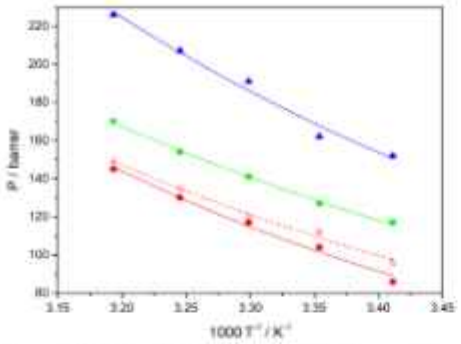

Figure 7. Arrhenius plot of temperature and CO_2 permeability; squares are experimental values, while solid lines are calculated by the Arrhenius equation; circle, DES-A1; star, DES-A2; square, DES-B1; and triangle, DES-C1.

$$P = P_0 e^{-E_a/RT} \tag{8}$$

where P is the permeability of CO_2, P_0 is the pre-exponential coefficient, R is the gas constant, T is the temperature, and E_a is the activation energy.

The activation energies of permeation were found to be 18.85, 16.17, 14.45, and 15.78 kJ·mol^{-1} for DES-A1, DES-A2, DES-B1, and DES-C1, respectively. They are therefore between for the earlier reported SLMs using different commercial polymeric supports based on DESs consisting of choline chloride and alkanoamines or acids and SLMs based on ILs containing acetic anion.[13,15,23,55] According to the literature, this may be due to many reasons, including differences in the viscosity of solvents and the porosity of solid materials in SLM.[13,55]

Selectivity of Studied Membranes. The ideal CO_2/N_2 selectivity values were calculated from eq 6 and are presented in Table 7 and Figure 8. As can be seen from eq 6, the ideal CO_2/N_2 selectivity of membranes is strictly connected to the permeability of pure gases.

Temperature has a great effect on all physical properties of DESs and by that on ideal CO_2/N_2 selectivity. As can be seen from Figure 8, the effect of temperature on α_{CO_2/N_2} is complex. For the ease of discussion, Figure 8 has been divided into four segments. In general, the ideal CO_2/N_2 selectivity decreases with an increase of temperature for all systems studied because the solubility-driven permeability of CO_2 increases at lower rate than the diffusion-driven permeability of N_2. For DES-C1-based SLMs, the ideal CO_2/N_2 selectivity decreases exponentially from segments I–IV, while for DES-A1 and DES-B1 is decreasing exponentially from segments I–III and then drops harshly in segment IV.

In the first segment, α_{CO_2/N_2} order is as follows: DES-B1 > DES-C1 > DES-A1 > DES-A2. The lowest values of α_{CO_2/N_2} for DES-A2 are due to its relatively low permeability of CO_2 and medium permeability of N_2 in comparison to other membranes studied in this work. This can be a combined result of the lowest viscosity of DES-A2 and low free volume values. The similar values of ideal CO_2/N_2 selectivity for DES-B1 and DES-C1 could be due to the compensation of high CO_2 solubility values in DES-C1 with its high viscosity in comparison for DES-B1. The other important factor may be the highest differences in free volume in these two DESs, which have an impact on the permeability of both CO_2 and N_2.

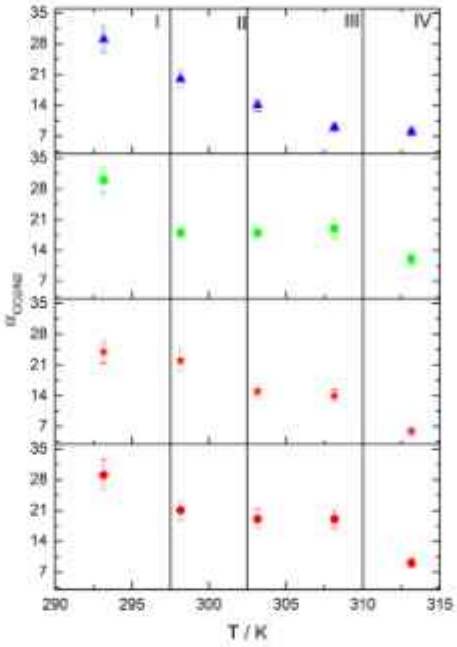

Figure 8. Experimental ideal CO_2/N_2 selectivity values as a function of temperature; circle, DES-A1; star, DES-A2; square, DES-B1; and triangle, DES-C1.

In the second segment, the ideal CO_2/N_2 selectivity values are close for all membranes studied. This is due to a high drop in viscosity for DES-B1 and DES-C1 and a relatively low decrease for DES-A1 and DES-A2. By that, the viscosity values of DES-A2 and DES-B2 are becoming similar to each other, which could explain similar behavior and values of selectivity.

In the third segment, α_{CO_2/N_2} of DES-A1 and DES-B1 is rather stable, whereas that of DES-A2 and DES-C1 is decreasing. The highest ideal CO_2/N_2 selectivity for DES-A1-based SLM is due its lowest CO_2 and N_2 permeability. The lowest values of selectivity obtained for DES-C1-based SLM might be due to the highest free volume values at that range.

In the last segment, α_{CO_2/N_2} order is as follows: DES-B1 > DES-A1 > DES-C2 > DES-A2. The shift between the order of the first two membranes might be due to the fact that both DESs have similar viscosity values at this temperature, but AChCl-based DES has lower free volume values and higher solubility of CO_2. The lowest values of ideal CO_2/N_2 selectivity for the DES-A2 based membrane are due to its lowest viscosity and lowest carbon dioxide solubility.

In general, its seems that the effect of temperature on the ideal CO_2/N_2 selectivity of DES-based SLM is mostly viscosity-driven, as the viscosity of DESs decreased at a higher

https://doi.org/10.1021/acssuschemeng.2c06278
ACS Sustainable Chem. Eng. 2023, 11, 4099−4110

rate than the solubility of CO_2. However, molar volume and CO_2 solubility also affect this parameter, suggesting a complex relationship between temperature and α_{CO_2/N_2}, which implies that all of these parameters must be taken into account when designing new membranes. At the examined range, the highest decrease of selectivity was observed for DES-C1, as both the viscosity and the CO_2 solubility drop were the highest. The lowest selectivity decrease was recorded for DES-B1, though the viscosity drop was comparable to DES-A1 and DES-A2, the CO_2 solubility decreased for most of the DESs studied.

Only a few DES-based supported liquid membranes were reported in the literature. Alkanolamine-based deep eutectic solvents reported by Ishaq et al. were characterized by lower permeabilities of CO_2 and N_2 but higher ideal selectivities than SLMs reported by our group. The higher ideal selectivities were also obtained by Saeed et al.[25] From results obtained by Craveiro *et al.*, in most cases, the values were similar to those reported in this study.[14] Selectivities obtained for ionic liquids are close to values obtained within this study. Scovazzo et al.[17] reported ideal selectivities for SILMs based on $[emim][Tf_2N]$ and $[C_6mim][Tf_2N]$ equal to 23 and 15, respectively. It proves that DES−SLMs can be a "greener" alternative for ionic liquid-based SLMs. It is worth mentioning that supported liquid membranes are not yet more efficient than traditional carbon dioxide removal methods. However, this work shows that DES-based SLMs are a great new research direction for more energy-efficient and less environmentally harmful methods.

CONCLUSIONS

The newly supported liquid membranes were prepared based on deep eutectic solvents composed of 1,2-propanediol combined with choline chloride, acetylcholine chloride, or tetrabutylammonium chloride. The physical properties, namely, thermal stability, density, viscosity, and refractive indices of DESs, were measured. In addition, FTIR spectra were recorded to confirm the formation of DESs. Solubility of carbon dioxide in studied DESs was examined and used for calculations of Henry's constants. The permeability values of pure carbon dioxide and nitrogen in DES-based SLMs were measured, and ideal CO_2/N_2 selectivities were determined.

It was found that both hydrogen bond acceptor type and molar ratio of HBA/HBD affect the physicochemical properties of DESs. The greatest differences were observed for the TBAC-based deep eutectic solvent. It was attributed to the presence of long alkyl chains in the TBAC molecule. It was also established that the type of HBA highly affects carbon dioxide solubility. The highest solubility was observed for TBAC-based DESs, while the lowest was observed for ChCl-based DESs. In addition, the molar ratio of HBA/HBA has a very little effect on CO_2 solubility.

The type of solvent used as well as its physical properties appeared to have a significant effect on the permeability of gases in the synthesized DES-based SLMs and by that on its selectivity. It was concluded that carbon dioxide solubility, free volume, and viscosity of deep eutectic solvents must be taken into account when considering DES potential for membrane separation. It was found that increasing the temperature results in a decrease of the viscosity of DESs at a higher rate than the solubility of CO_2, resulting in a higher rate of N_2 permeability increase over the CO_2 permeability, affecting the values of ideal selectivity. It appears that at lower temperatures the influence of CO_2 solubility predominates, while at higher temperatures the viscosity factor plays a key role in membrane selectivity.

ASSOCIATED CONTENT

Supporting Information

The Supporting Information is available free of charge at https://pubs.acs.org/doi/10.1021/acssuschemeng.2c06278.

Validation of the gas solubility method, fitting of physicochemical parameters, and experimental results of gas solubility (PDF)

(PDF)

(PDF)

AUTHOR INFORMATION

Corresponding Author

Iwona Cichowska-Kopczyńska − *Department of Process Engineering and Chemical Technology, Chemical Faculty, Gdańsk University of Technology, 80-233 Gdańsk, Poland;* orcid.org/0000-0003-3070-9603; Phone: +48583471869; Email: iwona.kopczynska@pg.edu.pl; Fax: +48583472065

Authors

Bartosz Nowosielski − *Department of Physical Chemistry, Chemical Faculty, Gdańsk University of Technology, 80-233 Gdańsk, Poland*

Dorota Warmińska − *Department of Physical Chemistry, Chemical Faculty, Gdańsk University of Technology, 80-233 Gdańsk, Poland*

Complete contact information is available at: https://pubs.acs.org/10.1021/acssuschemeng.2c06278

Notes

The authors declare no competing financial interest.

REFERENCES

(1) Keith, D. W. Why Capture CO2 from the Atmosphere? *Science* **2009**, *325*, 1654−1655.

(2) Song, C.; Liu, Q.; Deng, S.; Li, H.; Kitamura, Y. Cryogenic-Based CO2 Capture Technologies: State-of-the-Art Developments and Current Challenges. *Renewable Sustainable Energy Rev.* **2019**, *101*, 265−278.

(3) Yu, C. H.; Huang, C. H.; Tan, C. S. A Review of CO2 Capture by Absorption and Adsorption. *Aerosol Air Qual. Res.* **2012**, *12*, 745−769.

(4) Kenarsari, S. D.; Yang, D.; Jiang, G.; Zhang, S.; Wang, J.; Russell, A. G.; Wei, Q.; Fan, M. Review of Recent Advances in Carbon Dioxide Separation and Capture. *RSC Adv.* **2013**, *3*, 22739−22773.

(5) Scholes, C. A.; Stevens, G. W.; Kentish, S. E. Membrane Gas Separation Applications in Natural Gas Processing. *Fuel* **2012**, *96*, 15−28.

(6) Grünauer, J.; Shishatskiy, S.; Abetz, C.; Abetz, V.; Filiz, V. Ionic Liquids Supported by Isoporous Membranes for CO2/N2 Gas Separation Applications. *J. Membr. Sci.* **2015**, *494*, 224−233.

(7) Yan, X.; Anguille, S.; Bendahan, M.; Moulin, P. Ionic Liquids Combined with Membrane Separation Processes: A Review. *Sep. Purif. Technol.* **2019**, *222*, 230−253.

(8) Cichowska-Kopczyńska, I.; Aranowski, R. Use of Pyridinium and Pyrrolidinium Ionic Liquids for Removal of Toluene from Gas Streams. *J. Mol. Liq.* **2019**, No. 112091.

(9) Wang, J.; Luo, J.; Feng, S.; Li, H.; Wan, Y.; Zhang, X. Recent Development of Ionic Liquid Membranes. *Green Energy Environ.* **2016**, *1*, 43−61.

(10) Mubashir, M.; D'Angelo, F. N.; Gallucci, F. Recent Advances and Challenges of Deep Eutectic Solvent Based Supported Liquid Membranes. *Sep. Purif. Rev.* **2022**, *51*, 226−244.

(11) Patiño, J.; Gutiérrez, M. C.; Carriazo, D.; Ania, C. O.; Parra, J. B.; Ferrer, M. L.; Monte, F. Del. Deep Eutectic Assisted Synthesis of Carbon Adsorbents Highly Suitable for Low-Pressure Separation of CO 2-CH 4 Gas Mixtures. *Energy Environ. Sci.* **2012**, *5*, 8699−8707.

(12) Jiang, B.; Zhang, N.; Wang, B.; Yang, N.; Huang, Z.; Yang, H.; Shu, Z. Deep Eutectic Solvent as Novel Additive for PES Membrane with Improved Performance. *Sep. Purif. Technol.* **2018**, *194*, 239−248.

(13) Ishaq, M.; Gilani, M. A.; Bilad, M. R.; Faizan, A.; Raja, A. A.; Afzal, Z. M.; Khan, A. L. Exploring the Potential of Highly Selective Alkanolamine Containing Deep Eutectic Solvents Based Supported Liquid Membranes for CO2 Capture. *J. Mol. Liq.* **2021**, *340*, No. 117274.

(14) Craveiro, R.; Neves, L. A.; Duarte, A. R. C.; Paiva, A. Supported Liquid Membranes Based on Deep Eutectic Solvents for Gas Separation Processes. *Sep. Purif. Technol.* **2021**, *254*, No. 117593.

(15) Cichowska-Kopczyńska, I.; Warmińska, D.; Nowosielski, B. Solubility of Carbon Dioxide in Deep Eutectic Solvents Based on 3-Amino-1-Propanol and Tetraalkylammonium Salts at Low Pressure. *Materials* **2021**, *14*, No. 594.

(16) Xu, M.; Dou, H.; Peng, F.; Yang, N.; Xiao, X.; Tantai, X.; Sun, Y.; Jiang, B.; Zhang, L. Ultra-Stable Copper Decorated Deep Eutectic Solvent Based Supported Liquid Membranes for Olefin/Paraffin Separation: In-Depth Study of Carrier Stability. *J. Membr. Sci.* **2022**, *659*, No. 120775.

(17) Seyyed Shahabi, S.; Azizi, N.; Vatanpour, V. Tuning Thin-Film Composite Reverse Osmosis Membranes Using Deep Eutectic Solvents and Ionic Liquids toward Enhanced Water Permeation. *J. Membr. Sci.* **2020**, *610*, No. 118267.

(18) Castro-Muñoz, R.; Galiano, F.; Figoli, A.; Boczkaj, G. Deep Eutectic Solvents − A New Platform in Membrane Fabrication and Membrane-Assisted Technologies. *J. Environ. Chem. Eng.* **2022**, *10*, No. 106414.

(19) Taghizadeh, M.; Taghizadeh, A.; Vatanpour, V.; Ganjali, M. R.; Saeb, M. R. Deep Eutectic Solvents in Membrane Science and Technology: Fundamental, Preparation, Application, and Future Perspective. *Sep. Purif. Technol.* **2021**, *258*, No. 118015.

(20) Marcus, Y. *Deep Eutectic Solvents*; Springer International Publishing, 2019. DOI: 10.1007/978-3-030-00608-2.

(21) Amira, M. N.; Irfan Hatim, M. D.; Jullok, N.; Syahmie Rasidi, M.; Alamery, H. R. Synthesis and Preparation of Asymmetric PVDF-Co-PTFE/DES Supported Membrane for CO2/N2 Separation. *IOP Conf. Ser. Mater. Sci. Eng.* **2018**, *429*, No. 012067.

(22) Ishaq, M.; Gilani, M. A.; Ahmad, F.; Afzal, Z. M.; Arshad, I.; Bilad, M. R.; Ayub, K.; Khan, A. L. Theoretical and Experimental Investigation of CO2 Capture through Choline Chloride Based Supported Deep Eutectic Liquid Membranes. *J. Mol. Liq.* **2021**, *335*, No. 116234.

(23) Ishaq, M.; Gilani, M. A.; Afzal, Z. M.; Bilad, M. R.; Nizami, A. S.; Rehan, M.; Tahir, E.; Khan, A. L. Novel Poly Deep Eutectic Solvents Based Supported Liquid Membranes for CO2 Capture. *Front. Energy Res.* **2020**, *8*, No. 595041.

(24) Saeed, U.; Khan, A. L.; Gilani, M. A.; Aslam, M.; Khan, A. U. CO2 Separation by Supported Liquid Membranes Synthesized with Natural Deep Eutectic Solvents. *Environ. Sci. Pollut. Res.* **2021**, *28*, 33994−34008.

(25) Saeed, U.; Khan, A. L.; Gilani, M. A.; Bilad, M. R.; Khan, A. U. Supported Deep Eutectic Liquid Membranes with Highly Selective Interaction Sites for Efficient CO2 Separation. *J. Mol. Liq.* **2021**, *342*, No. 117509.

(26) Saeed, U.; Khan, A. U.; Khan, A. L.; Gilani, M. A.; Bilad, M. R. Separation of Carbon Dioxide by Potassium Carbonate Based Supported Deep Eutectic Liquid Membranes: Influence of Hydrogen Bond Donor. *J. Membr. Sci. Res.* **2022**, *8*, No. 526587.

(27) Lian, S.; Li, R.; Zhang, Z.; Liu, Q.; Song, C.; Lu, S. Improved CO2 Separation Performance and Interfacial Affinity of Composite Membranes by Incorporating Amino Acid-Based Deep Eutectic Solvents. *Sep. Purif. Technol.* **2021**, *272*, No. 118953.

(28) Castro, A. M. de.; Prasavath, D.; Bevilaqua, J. V.; Portugal, C. A. M.; Neves, L. A.; Crespo, J. G. Role of Water on Deep Eutectic Solvents (DES) Properties and Gas Transport Performance in Biocatalytic Supported DES Membranes. *Sep. Purif. Technol.* **2021**, *255*, No. 117763.

(29) Cichowska-Kopczyńska, I.; Aranowski, R. Effectiveness of Toluene Separation from Gas Phase Using Supported Ammonium Ionic Liquid Membrane. *Chem. Eng. Sci.* **2020**, *219*, No. 115605.

(30) Fortunato, R.; Afonso, C. A. M.; Reis, M. A. M.; Crespo, J. G. Supported Liquid Membranes Using Ionic Liquids: Study of Stability and Transport Mechanisms. *J. Membr. Sci.* **2004**, *242*, 197−209.

(31) Hernández-Fernández, F. J.; de los Ríos, A. P.; Tomás-Alonso, F.; Palacios, J. M.; Víllora, G. Preparation of Supported Ionic Liquid Membranes: Influence of the Ionic Liquid Immobilization Method on Their Operational Stability. *J. Membr. Sci.* **2009**, *341*, 172−177.

(32) Jia, T.; Bi, S.; Wu, J. Solubilities of Carbon Dioxide, Oxygen, and Nitrogen in Aqueous Ethylene Glycol Solution under Low Pressures. *Fluid Phase Equilib.* **2019**, *485*, 16−22.

(33) Prausnitz, J.; Azevedo, E. G.; Lichtenthaler, R. *Molecular Thermodynamics of Fluid-Phase Equilibria*, 2nd ed.; Prentice-Hall Inc.: Englewood Cliffs New Jersey, 1986.

(34) Lu, M.; Han, G.; Jiang, Y.; Zhang, X.; Deng, D.; Ai, N. Solubilities of Carbon Dioxide in the Eutectic Mixture of Levulinic Acid (or Furfuryl Alcohol) and Choline Chloride. *J. Chem. Thermodyn.* **2015**, *88*, 72−77.

(35) Liu, F.; Chen, W.; Mi, J.; Zhang, J. Y.; Kan, X.; Zhong, F. Y.; Huang, K.; Zheng, A. M.; Jiang, L. Thermodynamic and Molecular Insights into the Absorption of H2S, CO2, and CH4 in Choline Chloride plus Urea Mixtures. *AIChE J.* **2019**, *65*, No. e16574.

(36) Ghaedi, H.; Ayoub, M.; Sufian, S.; Lal, B.; Uemura, Y. Thermal Stability and FT-IR Analysis of Phosphonium-Based Deep Eutectic Solvents with Different Hydrogen Bond Donors. *J. Mol. Liq.* **2017**, *242*, 395−403.

(37) Ullah, R.; Atilhan, M.; Anaya, B.; Khraisheh, M.; García, G.; Elkhattat, A.; Tariq, M.; Aparicio, S. A Detailed Study of Cholinium Chloride and Levulinic Acid Deep Eutectic Solvent System for CO2capture via Experimental and Molecular Simulation Approaches. *Phys. Chem. Chem. Phys.* **2015**, *17*, 20941−20960.

(38) Al-Badr, A. A.; El-Obeid, H. A. Acetylcholine Chloride: Physical Profile. *Profiles Drug Subst., Excipients, Relat. Methodol.* **2005**, *31*, 1−19.

(39) Majid, M. F.; Mohd Zaid, H. F.; Kait, C. F.; Ghani, N. A.; Jumbri, K. Mixtures of Tetrabutylammonium Chloride Salt with Different Glycol Structures: Thermal Stability and Functional Groups Characterizations. *J. Mol. Liq.* **2019**, *294*, No. 111588.

(40) Dias, M. C. G. C.; Farias, F. O.; Gaioto, R. C.; da Costa, M. C.; Igarashi-Mafra, L.; Mafra, M. R. The Feasibility of the Alcohol-Based Deep Eutectic Solvents: From Thermophysical Characterization to Application in Active Pharmaceutical Ingredients Systems. *J. Solution Chem.* **2022**, *51*, 577−593.

(41) Vuksanović, J.; Kijevčanin, M. L.; Radović, I. R. Effect of Water Addition on Extraction Ability of Eutectic Solvent Choline Chloride+ 1,2-Propanediol for Separation of Hexane/Heptane+ethanol Systems. *Korean J. Chem. Eng.* **2018**, *35*, 1477−1487.

(42) Gajardo-Parra, N. F.; Cotroneo-Figueroa, V. P.; Aravena, P.; Vesovic, V.; Canales, R. I. Viscosity of Choline Chloride-Based Deep Eutectic Solvents: Experiments and Modeling. *J. Chem. Eng. Data* **2020**, *65*, 5581−5592.

(43) Rodriguez Rodriguez, N.; Machiels, L.; Binnemans, K. P-Toluenesulfonic Acid-Based Deep-Eutectic Solvents for Solubilizing Metal Oxides. *ACS Sustainable Chem. Eng.* **2019**, *7*, 3940−3948.

(44) Abbott, A. P.; Capper, G.; Gray, S. Design of Improved Deep Eutectic Solvents Using Hole Theory. *ChemPhysChem* **2006**, *7*, 803−806.

(45) Ghaedi, H.; Ayoub, M.; Sufian, S.; Lal, B.; Shariff, A. M. Measurement and Correlation of Physicochemical Properties of Phosphonium-Based Deep Eutectic Solvents at Several Temperatures

https://doi.org/10.1021/acssuschemeng.2c06278
ACS Sustainable Chem. Eng. 2023, 11, 4093−4106

(293.15 K−343.15 K) for CO2 Capture. *J. Chem. Thermodyn.* **2017**, *113*, 41−51.

(46) Chen, Y.; Ai, N.; Li, G.; Shan, H.; Cui, Y.; Deng, D. Solubilities of Carbon Dioxide in Eutectic Mixtures of Choline Chloride and Dihydric Alcohols. *J. Chem. Eng. Data* **2014**, *59*, 1247−1253.

(47) Liu, X.; Gao, B.; Jiang, Y.; Ai, N.; Deng, D. Solubilities and Thermodynamic Properties of Carbon Dioxide in Guaiacol-Based Deep Eutectic Solvents. *J. Chem. Eng. Data* **2017**, *62*, 1448−1455.

(48) Zubeir, L. F.; Lacroix, M. H. M.; Kroon, M. C. Low Transition Temperature Mixtures as Innovative and Sustainable CO2 Capture Solvents. *J. Phys. Chem. B* **2014**, *118*, 14429−14441.

(49) Haider, M. B.; Jha, D.; Marriyappan Sivagnanam, B.; Kumar, R. Thermodynamic and Kinetic Studies of CO2 Capture by Glycol and Amine-Based Deep Eutectic Solvents. *J. Chem. Eng. Data* **2018**, *63*, 2671−2680.

(50) Wijmans, J. G.; Baker, R. W. The Solution-Diffusion Model: A Review. *J. Membr. Sci.* **1995**, *107*, 1−21.

(51) Li, Z. L.; Zhong, F. Y.; Huang, J. Y.; Peng, H. L.; Huang, K. Sugar-Based Natural Deep Eutectic Solvents as Potential Absorbents for NH3 Capture at Elevated Temperatures and Reduced Pressures. *J. Mol. Liq.* **2020**, *317*, No. 113992.

(52) Cheng, N.-N.; Li, Z.-L.; Lan, H.-C.; Xu, W.-L.; Jiang, W.-J.; Huang, K.; Peng, H.-L. Deep Eutectic Solvents with Multiple Weak Acid Sites for Highly Efficient, Reversible and Selective Absorption of Ammonia. *Sep. Purif. Technol.* **2021**, *269*, No. 118791.

(53) Jiang, W. J.; Zhang, J. B.; Zou, Y. T.; Peng, H. L.; Huang, K. Manufacturing Acidities of Hydrogen-Bond Donors in Deep Eutectic Solvents for Effective and Reversible NH3Capture. *ACS Sustainable Chem. Eng.* **2020**, *8*, 13408−13417.

(54) Liu, B.; Tian, J. Investigation of Glycolic Acid Natural Deep Eutectic Solvents with Strong Proton Donors for Ammonia Capture and Separation. *Ind. Eng. Chem. Res.* **2021**, *60*, 11600−11610.

(55) Santos, E.; Albo, J.; Irabien, A. Acetate Based Supported Ionic Liquid Membranes (SILMs) for CO2 Separation: Influence of the Temperature. *J. Membr. Sci.* **2014**, *452*, 277−283.

(56) Jindaratsamee, P.; Shimoyama, Y.; Morizaki, H.; Ito, A. Effects of Temperature and Anion Species on CO2 Permeability and CO2/N2 Separation Coefficient through Ionic Liquid Membranes. *J. Chem. Thermodyn.* **2011**, *43*, 311−314.

(57) Scovazzo, P.; Havard, D.; McShea, M.; Mixon, S.; Morgan, D. Long-Term, Continuous Mixed-Gas Dry Fed CO2/CH4 and CO2/N2 Separation Performance and Selectivities for Room Temperature Ionic Liquid Membranes. *J. Membr. Sci.* **2009**, *327*, 41−48.

CO_2 separation using supported deep eutectic liquid membranes based on 1,2-propanediol

4 pages, 2 figures, 1 table

Bartosz Nowosielski[a], Dorota Warmińska[a], Iwona Cichowska-Kopczyńska[b]*

[1] Department of Physical Chemistry, Chemical Faculty, Gdańsk University of Technology, Narutowicza 11/12, 80-233 Gdańsk, POLAND

[2] Department of Process Engineering and Chemical Technology, Chemical Faculty, Gdańsk University of Technology, Narutowicza 11/12, 80-233 Gdańsk, POLAND

*Corresponding author: Tel.:+48583471869; fax:+48583472694,
e-mail address: iwona.kopczynska@ pg.edu.pl

Free volume (f_m) of liquid can be defined as the volume of the total mass, that is not occupied by liquid molecules themselves and hence diffusing molecules can be situated there. Obviously, this property have the great effect on permeability od DES-based SLM. Free volume is defined as:

$$f_m = V_m - R_m \tag{1}$$

where V_m [$cm^3 mol^{-1}$] is molar volume and R_m [$cm^3 mol^{-1}$] is molar refraction. The molar volume can be obtained by Equation (2) while molar refraction from Equation(3).

$$V_m = \frac{M}{\rho} \tag{2}$$

$$R_m = \left(\frac{n^2-1}{n^2+2}\right) V_m \tag{3}$$

Where M is a molar mass of DES [$g\,mol^{-1}$], ρ is a density of DES [$g\,cm^{-3}$], n is refractive index of DES.

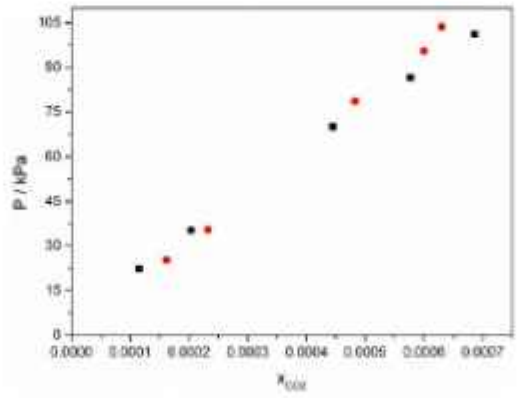

Figure S1 Solubility of CO_2 in water at 293.15 K: • our results, ■ the literature data from ref. [1].

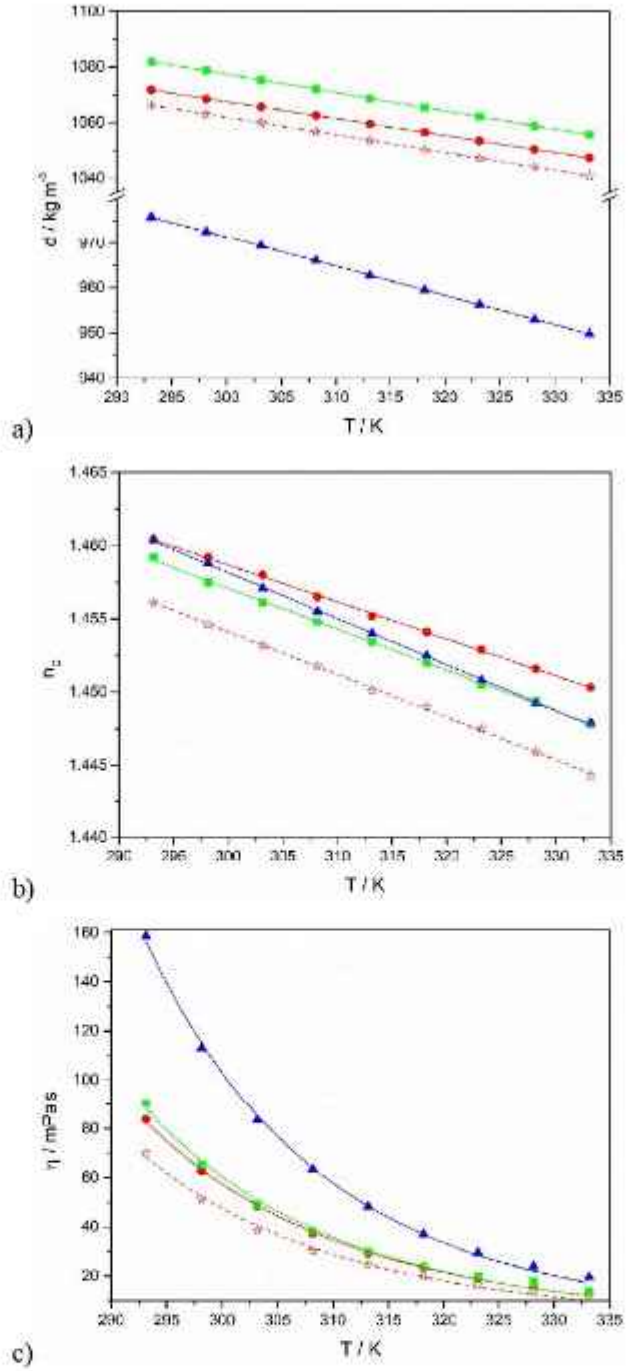

Figure S2 Physical properties of DESs studied as a function of temperature in the range of 293.15–333.15K and at atmospheric pressure: a) density, b) refractive index, c) viscosity, circle – DES-A1; star – DES-A2; square – DES-B1; triangle – DES-C1; solid lines - linear fit for density and refractive index, and Vogel-Fulcher-Tamman equation for viscosity.

Table S1 Experimental CO_2 mole fraction (x_{CO2}) and molality (m_{CO2}) in DESs at temperature (T) and equilibrium pressure (P)

T = 293.15 K			T = 298.15 K			T = 303.15 K			T = 308.15 K			T = 313.15 K		
P / kPa	x_{CO2}	m_{CO2} / mol kg^{-1}	P / kPa	x_{CO2}	m_{CO2} / mol kg^{-1}	P / kPa	x_{CO2}	m_{CO2} / mol kg^{-1}	P / kPa	x_{CO2}	m_{CO2} / mol kg^{-1}	P / kPa	x_{CO2}	m_{CO2} / mol kg^{-1}
DES-A1														
34.02	0.0043	0.0473	35.04	0.0042	0.0463	36.44	0.0041	0.0445	37.94	0.0039	0.0426	39.86	0.0036	0.0398
86.12	0.0064	0.0706	88.83	0.0062	0.0678	91.89	0.0059	0.0643	95.15	0.0055	0.0606	98.59	0.0051	0.0566
180.93	0.0166	0.1848	185.30	0.0164	0.1819	190.01	0.0161	0.1783	195.20	0.0157	0.1739	200.80	0.0152	0.1686
200.00	0.0179	0.1991	204.69	0.0176	0.1962	209.72	0.0173	0.1926	215.48	0.0169	0.1876	221.91	0.0163	0.1813
231.81	0.0223	0.2488	237.18	0.0220	0.2456	243.30	0.0216	0.2408	249.28	0.0212	0.2365	257.05	0.0205	0.2285
DES-A2														
32.37	0.0045	0.0509	33.53	0.0044	0.0494	34.90	0.0042	0.0474	36.57	0.0040	0.0448	38.27	0.0037	0.0422
94.50	0.0093	0.1054	97.10	0.0091	0.1029	100.16	0.0088	0.0994	103.46	0.0084	0.0954	106.66	0.0081	0.0918
108.63	0.0102	0.1159	111.73	0.0099	0.1128	115.01	0.0096	0.1093	118.36	0.0093	0.1058	121.98	0.0090	0.1018
154.47	0.0126	0.1436	158.21	0.0124	0.1409	162.45	0.0120	0.1369	166.93	0.0117	0.1326	171.31	0.0113	0.1286
158.31	0.0154	0.1754	162.45	0.0151	0.1718	166.67	0.0147	0.1681	171.45	0.0143	0.1631	175.98	0.0140	0.1590
DES-B1														
33.37	0.0054	0.0525	34.67	0.0052	0.0509	36.10	0.0050	0.0490	37.79	0.0047	0.0466	56.04	0.0045	0.0440
115.89	0.0107	0.1056	119.11	0.0104	0.1028	122.45	0.0101	0.0997	126.23	0.0097	0.0958	154.93	0.0093	0.0919
141.41	0.0133	0.1312	145.00	0.0130	0.1285	149.01	0.0126	0.1249	153.51	0.0122	0.1204	173.96	0.0117	0.1159
174.46	0.0168	0.1667	178.79	0.0165	0.1636	183.68	0.0161	0.1593	188.55	0.0157	0.1552	215.61	0.0150	0.1485
191.37	0.0194	0.1927	196.42	0.0190	0.1886	201.46	0.0186	0.1846	206.98	0.0181	0.1797	232.21	0.0176	0.1746
DES-C1														
18.77	0.0032	0.0250	20.97	0.0025	0.0195	23.47	0.0017	0.0133	24.83	0.0013	0.0106	26.55	0.0009	0.0069
44.14	0.0057	0.0452	45.80	0.0054	0.0426	47.76	0.0049	0.0392	50.08	0.0044	0.0348	52.83	0.0037	0.0294
70.88	0.0090	0.0721	73.19	0.0086	0.0688	75.76	0.0082	0.0650	78.62	0.0076	0.0604	81.59	0.0070	0.0557
108.67	0.0149	0.1193	111.59	0.0145	0.1162	114.86	0.0140	0.1121	118.83	0.0133	0.1062	123.18	0.0124	0.0994
182.55	0.0225	0.1821	187.03	0.0221	0.1780	191.93	0.0214	0.1729	197.49	0.0206	0.1660	203.02	0.0198	0.1594

[a]Standard uncertainties u are $u(T)$ = 0.10 K, $u(P)$ = 0.6 kPa, $u_r(x)$ = 0.03 and $u_r(m)$ = 0.03.

[1] T. Jia, S. Bi, and J. Wu, "Solubilities of carbon dioxide, oxygen, and nitrogen in aqueous ethylene glycol solution under low pressures," *Fluid Phase Equilib.*, vol. 485, pp. 16–22, Apr. 2019, doi: 10.1016/j.fluid.2018.11.035.

Oświadczenia współautorów publikacji

Oświadczenia autorów, dotyczące opisu udziału i wkładu procentowego udziału w przygotowaniu publikacji naukowej.

Autorzy pracy: Iwona Cichowska-Kopczyńska, Bartosz Nowosielski, Dorota Warmińska

Tytuł pracy: Deep Eutectic Solvents: Properties and Applications in CO_2 Separation

Czasopismo, rok wydania, zeszyt, numer strony, numer doi: MOLECULES Vol. 28 (14) (2023), s.5293, 10.3390/molecules28145293

Lp.	Autor	Opis udziału	Wkład procentowy udziału	Podpis
1	Iwona Cichowska-Kopczyńska	opracowanie koncepcji manuskryptu, edycja manuskryptu, przygotowanie odpowiedzi dla recenzentów	33%	27.11.2024
2	Bartosz Nowosielski	przegląd literaturowy, napisanie części manuskryptu dotyczącej separacji CO_2, przygotowanie odpowiedzi dla recenzentów	34%	27.11.2024
3	Dorota Warmińska	napisanie części manuskryptu dotyczącej właściwości fizycznych DES, edycja manuskryptu, przygotowanie odpowiedzi dla recenzentów	33%	27.11.2024

Oświadczenia autorów, dotyczące opisu udziału i wkładu procentowego udziału w przygotowaniu publikacji naukowej.

Autorzy pracy: Bartosz Nowosielski, Marzena Jamrógiewicz, Justyna Łuczak, Maciej Śmiechowski, Dorota Warmińska

Tytuł pracy: Experimental and predicted physicochemical properties of monopropanolamine-based deep eutectic solvents

Czasopismo, rok wydania, zeszyt, numer strony, numer doi: JOURNAL OF MOLECULAR LIQUIDS -Vol. 309, (2020), s.113110, 10.1016/j.molliq.2020.113110

Lp.	Autor	Opis udziału	Wkład procentowy udziału	Podpis
1	Bartosz Nowosielski	preparatyka DES, wykonanie pomiarów stałych fizycznych rozpuszczalników (d, u i n_D), opracowanie i opis ich wyników, napisanie wstępu do publikacji , przygotowanie odpowiedzi dla recenzenta	20%	27.11.2024
2	Marzena Jamrógiewicz	wykonanie pomiarów DSC i opis ich wyników	20%	27.11.2024
3	Justyna Łuczak	wykonanie pomiarów lepkości i opis ich wyników	20%	
4	Maciej Śmiechowski	wykonanie widm FTIR i opis ich wyników	20%	
5	Dorota Warmińska	opracowanie koncepcji manuskryptu i jego edycja przygotowanie odpowiedzi dla recenzenta	20%	27.11.2024

Oświadczenia autorów, dotyczące opisu udziału i wkładu procentowego udziału w przygotowaniu publikacji naukowej.

Autorzy pracy: Bartosz Nowosielski, Marzena Jamrógiewicz, Justyna Łuczak, Agnieszka Tercjak, Dorota Warmińska

Tytuł pracy: Effect of temperature and composition on physical properties of deep eutectic solvents based on 2-(methylamino)ethanol – measurement and prediction

Czasopismo, rok wydania, zeszyt, numer strony, numer doi: JOURNAL OF MOLECULAR LIQUIDS -Vol. 371, (2023), s.121069, 10.1016/j.molliq.2022.121069

Lp.	Autor	Opis udziału	Wkład procentowy udziału	Podpis
1	Bartosz Nowosielski	opracowanie koncepcji i metodologii, preparatyka DES, wykonanie pomiarów stałych fizycznych analiza wyników, napisanie i edycja manuskryptu, przygotowanie odpowiedzi dla recenzentów	40%	27.11.2024
2	Marzena Jamrógiewicz	nadzór nad wynikami DSC, edycja manuskryptu	10%	27.11.2024
3	Justyna Łuczak	edycja manuskryptu, nadzór nad wynikami lepkości	10%	
4	Agnieszka Tercjak	wykonanie pomiarów TGA	10%	
5	Dorota Warmińska	opracowanie koncepcji, edycja manuskryptu, przygotowanie odpowiedzi dla recenzentów	30%	29.11.2024

Oświadczenia autorów, dotyczące opisu udziału i wkładu procentowego udziału w przygotowaniu publikacji naukowej.

Autorzy pracy: Bartosz Nowosielski, Marzena Jamrógiewicz, Iwona Cichowska-Kopczyńska, Dorota Warmińska

Tytuł pracy: Comprehensive evaluation of physical properties and carbon dioxide capacities of new 2-(butylamino)ethanol -based deep eutectic solvents

Czasopismo, rok wydania, zeszyt, numer strony, numer doi: PURE AND APPLIED CHEMISTRY (2024), 10.1515/pac-2024-0228

Lp.	Autor	Opis udziału	Wkład procentowy udziału	Podpis
1	Bartosz Nowosielski	opracowanie koncepcji manuskryptu, preparatyka DES, wykonanie pomiarów DSC, TGA oraz wyznaczenie stałych fizycznych DES, wykonanie pomiarów absorpcji CO_2 analiza wyników, napisanie i edycja manuskryptu, przygotowanie odpowiedzi dla recenzentów	30%	27.11.2024 Nowosielski
2	Marzena Jamrógiewicz	nadzór nad wynikami DSC, edycja manuskryptu	10%	27.11.2024 Jamrógiewicz
3	Iwona Cichowska-Kopczyńska	opracowanie metodologii pomiarów rozpuszczalności CO_2, edycja manuskryptu, analiza wyników, nadzór nad pracą, przygotowanie odpowiedzi dla recenzentów	30%	27.11.2024 Kopczyńska
4	Dorota Warmińska	opracowanie koncepcji, analiza wyników, edycja manuskryptu, nadzór nad pracą, przygotowanie odpowiedzi dla recenzentów	30%	27.11.2024 Warmińska

Oświadczenia autorów, dotyczące opisu udziału i wkładu procentowego udziału w przygotowaniu publikacji naukowej.

Autorzy pracy: Bartosz Nowosielski, Marzena Jamróglewicz, Justyna Łuczak, Dorota Warmińska

Tytuł pracy: Novel Binary Mixtures of Alkanolamine Based Deep Eutectic Solvents with Water—Thermodynamic Calculation and Correlation of Crucial Physicochemical Properties

Czasopismo, rok wydania, zeszyt, numer strony, numer doi: MOLECULES -Vol. 27 (3) (2022), s.788, 10.3390/molecules27030788

Lp.	Autor	Opis udziału	Wkład procentowy udziału	Podpis
1	Bartosz Nowosielski	preparatyka DES wykonanie pomiarów, opracowanie i opis wyników napisanie i edycja manuskryptu, nadzór nad wynikami, przygotowanie odpowiedzi dla recenzentów	40%	27.11.2024
2	Marzena Jamróglewicz	wyznaczenie pojemności cieplnej DES	10%	27.11.2024
3	Justyna Łuczak	edycja manuskryptu	10%	
4	Dorota Warmińska	opracowanie koncepcji i metodologii, napisanie i edycja manuskryptu, nadzór nad pracą i wynikami, przygotowanie odpowiedzi dla recenzentów	40%	27.11.2024

Oświadczenia autorów, dotyczące opisu udziału i wkładu procentowego udziału w przygotowaniu publikacji naukowej.

Autorzy pracy: Iwona Cichowska-Kopczyńska, Dorota Warmińska, Bartosz Nowosielski

Tytuł pracy: Solubility of Carbon Dioxide in Deep Eutectic Solvents Based on 3-Amino-1-Propanol and Tetraalkylammonium Salts at Low Pressure

Czasopismo, rok wydania, zeszyt, numer strony, numer doi: Materials -Vol. 14(3) (2021), s.594, 10.3390/ma14030594

Lp.	Autor	Opis udziału	Wkład procentowy udziału	Podpis
1	Iwona Cichowska-Kopczyńska	opracowanie metodologii, nadzór nad wynikami, napisanie i edycja manuskryptu, przygotowanie odpowiedzi dla recenzentów	34%	27.11.2024
2	Dorota Warmińska	opracowanie koncepcji, analiza wyników, edycja manuskryptu, przygotowanie odpowiedzi dla recenzentów	33%	27.11.2024
3	Bartosz Nowosielski	wykonanie pomiarów i opracowanie wyników, napisanie wstępu i edycja manuskryptu, przygotowanie odpowiedzi dla recenzentów	33%	27.11.2024

Oświadczenia autorów, dotyczące opisu udziału i wkładu procentowego udziału w przygotowaniu publikacji naukowej.

Autorzy pracy: Bartosz Nowosielski, Iwona Cichowska-Kopczyńska, Dorota Warmińska

Tytuł pracy: CO_2 Separation Using Supported Deep Eutectic Liquid Membranes Based on 1,2-propanediol

Czasopismo, rok wydania, zeszyt, numer strony, numer doi: ACS SUSTAINABLE CHEMISTRY & ENGINEERING -Vol. 11,iss. 10 (2023), s.4093-4105, 10.1021/acssuschemeng.2c06278

Lp.	Autor	Opis udziału	Wkład procentowy udziału	Podpis
1	Bartosz Nowosielski	wykonanie pomiarów i opracowanie wyników, napisanie i edycja manuskryptu, przygotowanie odpowiedzi dla recenzentów	34%	27.11.2024 Nowosielski
2	Iwona Cichowska-Kopczyńska	opracowanie metodologii, edycja manuskryptu, analiza wyników, nadzór nad wynikami, przygotowanie odpowiedzi dla recenzentów	33%	27.11.2024 Kopczyńska
3	Dorota Warmińska	Opracowanie koncepcji i edycja manuskryptu, analiza wyników, nadzór nad pracą, przygotowanie odpowiedzi dla recenzentów	33%	27.11.2024 Warmińska

Załącznik B

Tabela B1 Specyfikacja cieczy głęboko eutektycznych opartych o propano-1,3-diol, użytych do przygotowania SLM.

symbol	HBA	stosunek molowy HBA/HBD	M_{DES} / $g \cdot mol^{-1}$	ułamek molowy HBD	zawartość wody / ppm
DES32	chlorek choliny	1:3,006	91,947	0,7504	0,00207
DES34	chlorek choliny	1:4,030	88,718	0,8012	0,00167
DES35	chlorek acetylocholiny	1:2,985	102,581	0,7491	0,00292
DES36	chlorek tetrabutyloammoniowy	1:3,026	126,219	0,7516	0,00319

Tabela B2 Temperatury rozkładu przy 10% i 90% utracie masy uzyskane przy pomocy techniki TGA dla DES opartych o AP.

DES	$T_{10\%}$ / K	$T_{90\%}$ / K
TBAB/AP 1:4	398,2	508,3
TBAB/AP 1:6	394,0	507,5
TBAB/AP 1:8	387,2	507,3
TEAC/AP 1:4	381,0	560,2
TEAC/AP 1:6	383,7	554,7
TEAC/AP 1:8	358,2	552,3
TBAC/AP 1:4	396,7	500,2
TBAC/AP 1:6	382,3	495,8
TBAC/AP 1:8	374,2	492,5

Tabela B3 Temperatury rozkładu przy 10% i 90% utracie masy uzyskane przy pomocy techniki TGA dla DES opartych o propano-1,3-diol.

DES	$T_{10\%}$ / K	$T_{90\%}$ / K
ChCl/propano-1,3-diol 1:3	451,3	568,8
ChCl/propano-1,3-diol 1:4	444,8	562,8
AcChCl/propano-1,3-diol 1:3	452,8	536,5
TBAC/propano-1,3-diol 1:3	472,8	522,5

Tabela B4 Właściwości fizyczne cieczy głęboko eutektycznych opartych o propano-1,3-diol.

DES	T / K	ρ / kg·m^{-3}		η / mPa·s		n
		eks.	lit.	eks.	lit.	eks.
ChCl/propano-1,3-diol 1:3	293,15	1081,96	1080,91[a], 1081,0[b]	64,43	69,74[a], 69,190[b]	1,4646
	298,15	1079,16	1078,14[a],	49,12	55,75[a], 59,5[c]	1,4630
	303,15	1076,37	1075,34[a], 1075,4[b], 1075,3[d]	40,21	45,40[a], 45,421[b] 40,05[d]	1,4617
	308,15	1073,59	1072,55[a], 1072,5[d]	32,28	37,42[a], 33,17[d]	1,4602
	313,15	1070,82	1069,78[a], 1069,9[b], 1069,7[d]	26,30	31,35[a], 31,389[b], 27,84[d]	1,4588
ChCl/propano-1,3-diol 1:4	293,15	1076,62	1076,27[a]	59,40	61,31[a]	1,4589
	298,15	1073,77	1073,46[a]	48,50	49,49[a] 51,4[c]	1,4575
	303,15	1070,93	1070,62[a], 1070,5[d]	39,02	40,70[a] 34,45[d],	1,4563
	308,15	1068,09	1067,80[a], 1067,6[d]	32,08	33,88[a], 28,87[d]	1,4551
	313,15	1065,25	1064,97[a], 1064,8[d]	26,67	27,31[a], 24,21[d]	1,4540
AChCl/propano-1,3-diol 1:3	293,15	1094,44		83,71		1,4628
	298,15	1091,41		65,81		1,4616
	303,15	1088,38		56,67		1,4603
	308,15	1085,38		47,42		1,4591
	313,15	1082,38		38,06		1,4578
TBAC/propano-1,3-diol 1:3	293,15	986,33		237,42		1,4661
	298,15	983,43		170,75		1,4651
	303,15	980,53		125,95		1,4639
	308,15	977,62		95,04		1,4628
	313,15	974,72		72,71		1,4616

standardowe niepewności wynoszą: $u(T)$ = 0,01 K, $u(p)$= 0,001 MPa, $u(\rho)$ = 0,1 kg·m^{-3}, $u(n_D)$ = 0,0002, $u(\ )$ = 2%, a-ref.[159], b-ref.[46], c-ref[160], d-ref[161]

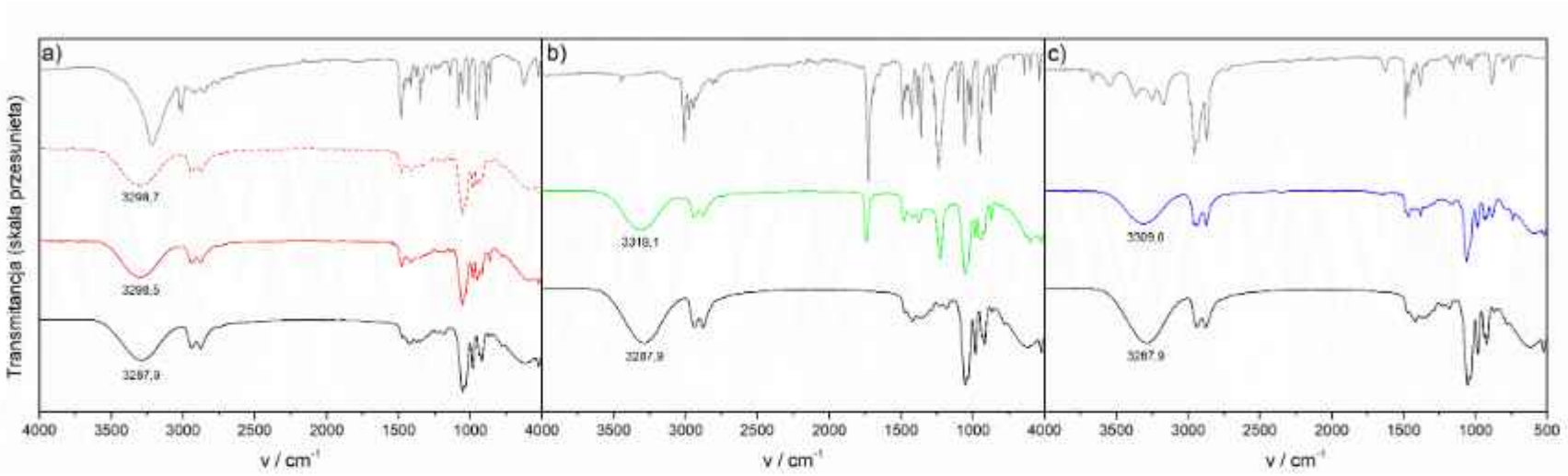

Rysunek B1 Widma FTIR otrzymane dla cieczy opartych o propano-1,3-diol: a) DES32 (czerwona linia) oraz DES33 (czerwona przerywana linia), b) DES34 (zielona linia) i c) DES35 (niebieska linia); czarna linia – propano-1,3-diol, szara linia –sól.

Tabela B5 Wartości %ARD dla modeli służących do przewidywania wartości gęstości użytych dla cieczy opartych o 3-aminopropan-1-ol oraz cieczy zawierających propan-1,2-diol lub propan-1,3-diol.

DES	%ARD[1]	%ARD[2]	%ARD[3]	%ARD[4]	%ARD[5]	%ARD[6]	%ARD[7]
TBAB/AP 1:4	0,62	1,9	7,6	0,31	0,07	1,4	0,35
TBAB/AP 1:6	0,63	1,9	9,0	0,36	0,06	2,7	7,6
TBAB/AP 1:8	0,64	1,8	9,8	0,35	0,03	4,5	16,4
TEAC/AP 1:4	0,90	2,3	8,4	0,34	0,09	3,5	10,2
TEAC/AP 1:6	0,83	2,2	9,8	0,34	0,07	4,3	19,3
TEAC/AP 1:8	0,79	1,0	11,9	0,33	0,05	5,6	29,2
TBAC/AP 1:4	0,68	2,0	13,4	0,39	0,03	5,0	8,1
TBAC/AP 1:6	0,67	2,0	13,8	0,59	0,02	4,9	15,6
TBAC/AP 1:8	0,66	2,0	13,9	0,56	0,03	5,8	23,6
TBAB/BAE 1:6	0,46	1,7	14	3,02	0,09	1,0	7,3
TBAB/BAE 1:8	0,46	1,7	15	3,33	0,15	1,8	12,9
TBAB/BAE 1:10	0,46	1,7	16	3,47	0,22	3,3	20,0
TEAC/BAE 1:6	0,65	2,0	16	3,76	0,12	1,5	15,9
TEAC/BAE 1:8	0,60	1,9	17	3,87	0,16	1,9	21,8
TEAC/BAE 1:10	1,36	0,8	18	3,97	0,22	2,9	28,2
TBAC/BAE 1:6	0,50	1,8	18	3,26	0,18	2,6	13,3
TBAC/BAE 1:8	0,48	1,8	18	3,47	0,23	2,7	18,7
TBAC/BAE 1:10	0,48	1,8	19	3,64	0,27	3,5	24,7
ChCl/propano-1,2-diol 1:3	0,62	1,4	4,9	2,46	0,73	0,3	4,8
ChCl/propano-1,2-diol 1:4	0,60	1,4	6,0	2,30	0,75	0,9	2,3
AcChCl/propano-1,2-diol 1:3	0,54	1,2	2,8	2,00	0,77	1,1	1,1
TBAC/propano-1,2-diol 1:3	0,41	1,2	13	0,71	0,84	2,1	2,3
ChCl/propano-1,3-diol 1:3	0,69	1,5	3,8	3,59	0,65	1,0	0,4
ChCl/propano-1,3-diol 1:4	0,30	1,0	4,8	3,52	0,66	1,5	1,3
AcChCl/propano-1,3-diol 1:3	0,60	1,4	1,5	2,69	0,70	2,2	0,2
TBAC/propano-1,3-diol 1:3	0,51	1,3	11	0,96	0,74	1,9	1,1

1- metoda oparta na równaniu Rackett'a zmodyfikowanego przez Spencer'a i Danner'a[62], 2- metoda oparta na równaniu Rackett'a zmodyfikowanego przez Mjalli[63], 3- metoda oparta na właściwościach krytycznych opracowana przez Haghbakhsh i in.[64], 4- metoda oparta na BGI[69], 5- metoda oparta na MCI[70], 6- metoda oparta na GC opracowana przez Haghbakhsh i in.[66], 7- metoda oparta na AC opracowana przez Haghbakhsh i in.[66].

Tabela B6 Wartości %ARD dla modelu służącego do przewidywania wartości lepkości użytego opracowanego przez Bakhtyari-ego i in.[61] dla cieczy opartych o 3-aminopropan-1-ol oraz cieczy zawierających propano-1,2-diol lub propano-1,3-diol.

DES	%ARD
TBAB/AP 1:4	7,6
TBAB/AP 1:6	6,7
TBAB/AP 1:8	7,0
TEAC/AP 1:4	6,4
TEAC/AP 1:6	6,4
TEAC/AP 1:8	4,3
TBAC/AP 1:4	6,5
TBAC/AP 1:6	6,1
TBAC/AP 1:8	5,8
TBAB/BAE 1:6	16
TBAB/BAE 1:8	18
TBAB/BAE 1:10	14
TEAC/BAE 1:6	10
TEAC/BAE 1:8	9
TEAC/BAE 1:10	12
TBAC/BAE 1:6	17
TBAC/BAE 1:8	16
TBAC/BAE 1:10	14
ChCl/propano-1,2-diol 1:3	2,4
ChCl/propano-1,2-diol 1:4	4,2
AcChCl/propano-1,2-diol 1:3	5,1
TBAC/propano-1,2-diol 1:3	5,2
ChCl/propano-1,3-diol 1:3	1,4
ChCl/propano-1,3-diol 1:4	4,4
AcChCl/propano-1,3-diol 1:3	5,8
TBAC/propano-1,3-diol 1:3	2,9

Tabela B7 Wartości %ARD dla modeli służących do przewidywania wartości współczynnika załamania światła użytych dla cieczy opartych o 3-aminopropan-1-ol oraz cieczy zawierających propano-1,2-diol lub propano-1,3-diol.

DES	%ARD[1]	%ARD[2]	%ARD[3]	%ARD[4]	%ARD[5]
TBAB/AP 1:4	1,8	0,31	-	0,15	0,22
TBAB/AP 1:6	2,0	0,12	-	0,30	0,31
TBAB/AP 1:8	2,1	0,13	-	0,67	0,50
TEAC/AP 1:4	2,0	0,45	1,05	0,41	0,32
TEAC/AP 1:6	2,2	0,13	0,74	0,13	0,54
TEAC/AP 1:8	2,3	0,15	0,56	0,32	0,70
TBAC/AP 1:4	1,6	0,19	1,05	0,25	0,39
TBAC/AP 1:6	1,9	0,12	0,84	0,15	0,62
TBAC/AP 1:8	2,0	0,19	0,73	0,41	0,77
TBAB/BAE 1:6	13	0,59	-	2,8	1,5
TBAB/BAE 1:8	15	0,72	-	3,3	1,8
TBAB/BAE 1:10	16	0,83	-	4,0	2,1
TEAC/BAE 1:6	17	0,53	2,0	2,7	1,7
TEAC/BAE 1:8	18	0,73	1,8	3,2	2,0
TEAC/BAE 1:10	19	0,84	1,7	3,7	2,2
TBAC/BAE 1:6	14	0,74	2,3	2,5	1,7
TBAC/BAE 1:8	15	0,85	2,1	3,0	2,0
TBAC/BAE 1:10	16	0,93	2,0	3,5	2,3
ChCl/propano-1,2-diol 1:3	0,42	0,52	0,29	0,69	1,05
ChCl/propano-1,2-diol 1:4	0,39	0,75	0,62	0,87	1,23
AcChCl/propano-1,2-diol 1:3	1,9	1,05	-	0,34	1,19
TBAC/propano-1,2-diol 1:3	4,7	1,08	0,06	0,32	0,68
ChCl/propano-1,3-diol 1:3	0,86	0,18	0,70	0,45	0,78
ChCl/propano-1,3-diol 1:4	0,69	0,43	1,07	0,81	1,00
AcChCl/propano-1,3-diol 1:3	6,3	0,71	-	0,96	0,90
TBAC/propano-1,3-diol 1:3	0,23	0,60	1,45	0,36	0,22

1- metoda oparta na refrakcji molowej opracowana przez Shabaz'a i in.[67], 2- metoda oparta na właściwościach krytycznych opracowana przez Taherzadeh'a i in.[60], 3- metoda oparta na GC opracowana przez Khajeh'a i in.[68], 4- metoda oparta na GC opracowana przez Haghbakhsh i in.[66], 5- metoda oparta na AC opracowana przez Haghbakhsh i in.[66].

Tabela B8 Wartości liczb koordynacyjnych dla badanych cieczy głęboko eutektycznych opartych o aminoalkohole uzyskane przy pomocy symulacji MD.

Centrum	Powłoka	r_{max} / nm	r_{min} / nm	N_{coord}
		TBAB/AP 1:4		
Br^-	NH	0,250	0,462	3,566
Br^-	OH	0,232	0,344	2,145
Br^-	N^+	0,460	0,776	2,118
		TBAB/AP 1:6		
Br^-	NH	0,250	0,454	3,857
Br^-	OH	0,232	0,344	2,467
Br^-	N^+	0,458	0,768	1,812
		TBAB/AP 1:8		
Br^-	NH	0,252	0,452	3,997
Br^-	OH	0,232	0,338	2,641
Br^-	N^+	0,460	0,788	1,685
		TBAC/AP 1:4		
Cl^-	NH	0,244	0,450	3,432
Cl^-	OH	0,226	0,340	2,265
Cl^-	N^+	0,454	0,772	2,095
		TBAC/AP 1:6		
Cl^-	NH	0,244	0,446	3,710
Cl^-	OH	0,226	0,336	2,626
Cl^-	N^+	0,454	0,782	1,823
		TBAC/AP 1:8		
Cl^-	NH	0,246	0,442	3,840
Cl^-	OH	0,226	0,338	2,820
Cl^-	N^+	0,456	0,768	1,602
		TEAC/AP 1:4		
Cl^-	NH	0,246	0,446	3,583
Cl^-	OH	0,226	0,334	2,299
Cl^-	N^+	0,458	0,746	2,698
		TEAC/AP 1:6		
Cl^-	NH	0,246	0,446	3,978
Cl^-	OH	0,226	0,332	2,677
Cl^-	N^+	0,462	0,766	2,299
		TEAC/AP 1:8		
Cl^-	NH	0,246	0,444	4,112
Cl^-	OH	0,226	0,338	2,866
Cl^-	N^+	0,458	0,768	2,042

c.d. Tabeli B8

TBAB/MAE 1:6				
Br^-	NH	0,244	0,354	0,836
Br^-	OH	0,232	0,340	2,208
Br^-	N^+	0,456	0,760	1,891
TBAB/MAE 1:8				
Br^-	NH	0,244	0,348	0,878
Br^-	OH	0,232	0,340	2,434
Br^-	N^+	0,454	0,742	1,669
TBAB/MAE 1:10				
Br^-	NH	0,244	0,352	0,904
Br^-	OH	0,232	0,342	2,520
Br^-	N^+	0,456	0,776	1,626
TBAC/MAE 1:6				
Cl^-	NH	0,238	0,342	0,884
Cl^-	OH	0,226	0,332	2,369
Cl^-	N^+	0,450	0,752	1,795
TBAC/MAE 1:8				
Cl^-	NH	0,238	0,340	0,890
Cl^-	OH	0,226	0,332	2,616
Cl^-	N^+	0,452	0,756	1,622
TBAC/MAE 1:10				
Cl^-	NH	0,238	0,346	0,891
Cl^-	OH	0,226	0,336	2,758
Cl^-	N^+	0,450	0,768	1,429
TEAC/MAE 1:6				
Cl^-	NH	0,238	0,348	0,856
Cl^-	OH	0,226	0,332	2,475
Cl^-	N^+	0,456	0,740	2,411
TEAC/MAE 1:8				
Cl^-	NH	0,238	0,346	0,891
Cl^-	OH	0,226	0,332	2,599
Cl^-	N^+	0,456	0,742	2,209
TEAC/MAE 1:10				
Cl^-	NH	0,238	0,348	0,934
Cl^-	OH	0,226	0,332	2,790
Cl^-	N^+	0,454	0,746	1,964

c.d. Tabeli B8

TBAB/BAE 1:6				
Br^-	NH	0,244	0,352	1,039
Br^-	OH	0,232	0,338	1,757
Br^-	N^+	0,448	0,758	1,689
TBAB/BAE 1:8				
Br^-	NH	0,244	0,352	1,108
Br^-	OH	0,232	0,336	1,896
Br^-	N^+	0,452	0,756	1,562
TBAB/BAE 1:10				
Br^-	NH	0,246	0,352	1,163
Br^-	OH	0,232	0,336	2,060
Br^-	N^+	0,450	0,776	1,556
TBAC/BAE 1:6				
Cl^-	NH	0,238	0,352	1,025
Cl^-	OH	0,226	0,332	1,953
Cl^-	N^+	0,446	0,748	1,714
TBAC/BAE 1:8				
Cl^-	NH	0,240	0,350	1,054
Cl^-	OH	0,226	0,332	2,232
Cl^-	N^+	0,448	0,754	1,561
TBAC/BAE 1:10				
Cl^-	NH	0,240	0,346	1,138
Cl^-	OH	0,226	0,332	2,281
Cl^-	N^+	0,444	0,762	1,370
TEAC/BAE 1:6				
Cl^-	NH	0,238	0,350	1,103
Cl^-	OH	0,226	0,334	2,035
Cl^-	N^+	0,450	0,698	2,084
TEAC/BAE 1:8				
Cl^-	NH	0,238	0,346	1,111
Cl^-	OH	0,226	0,330	2,195
Cl^-	N^+	0,452	0,730	1,981
TEAC/BAE 1:10				
Cl^-	NH	0,238	0,350	1,139
Cl^-	OH	0,226	0,334	2,277
Cl^-	N^+	0,450	0,636	1,778

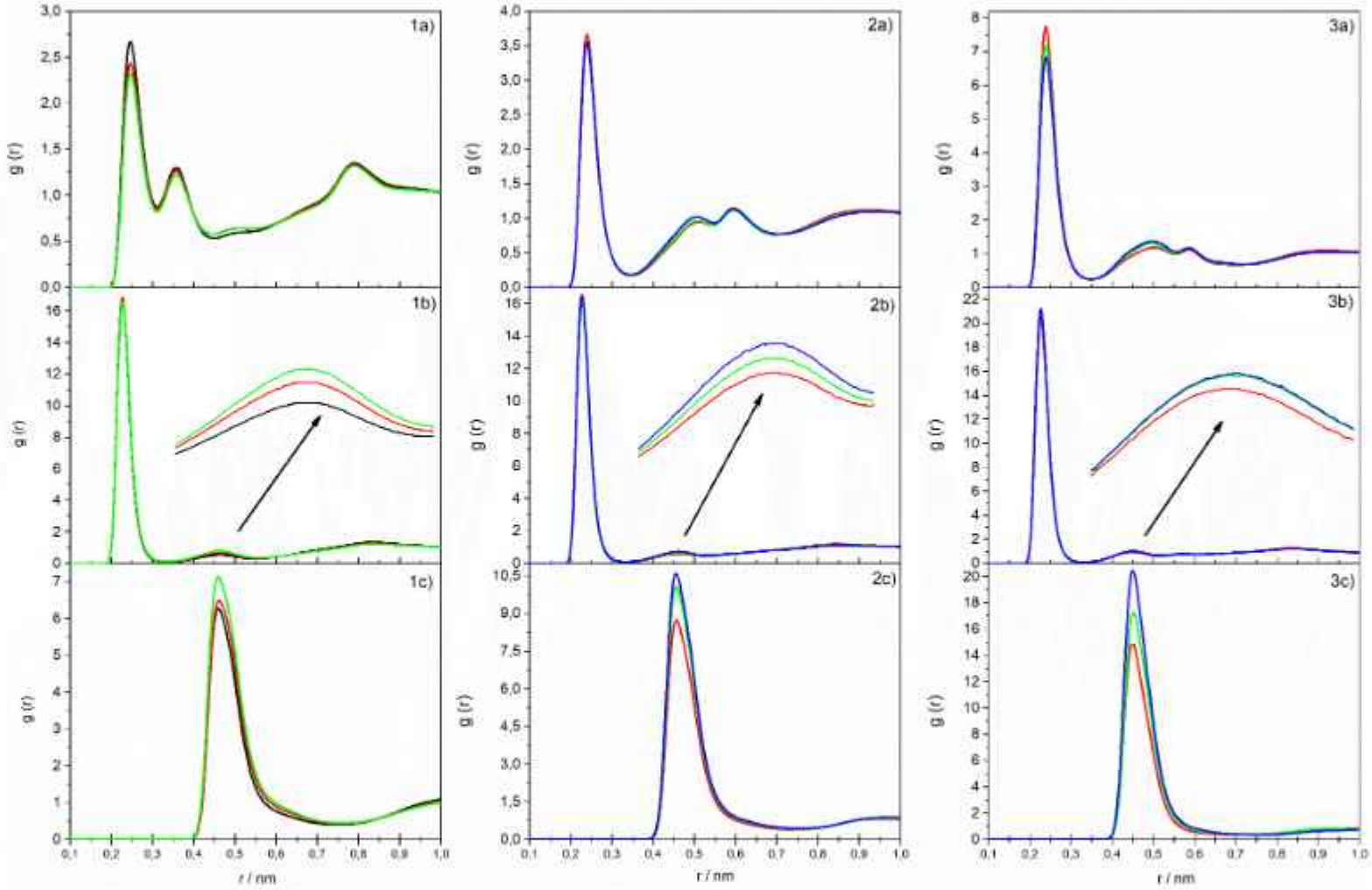

Rysunek B2 Funkcje rozkładu radialnego oparte na środkach rozkładów mas a) $Cl^{-}\cdots H\text{–}N$; b) $Cl^{-}\cdots H\text{–}O$; c) $N^{+}\cdots Cl^{-}$ dla DES opartych o TEAC zawierających 1) AP; 2) MAE; 3) BAE przy ułamkach molowych; czarna linia – 1:4; czerwona linia – 1:6; zielona linia 1:8; niebieska linia - 1:10

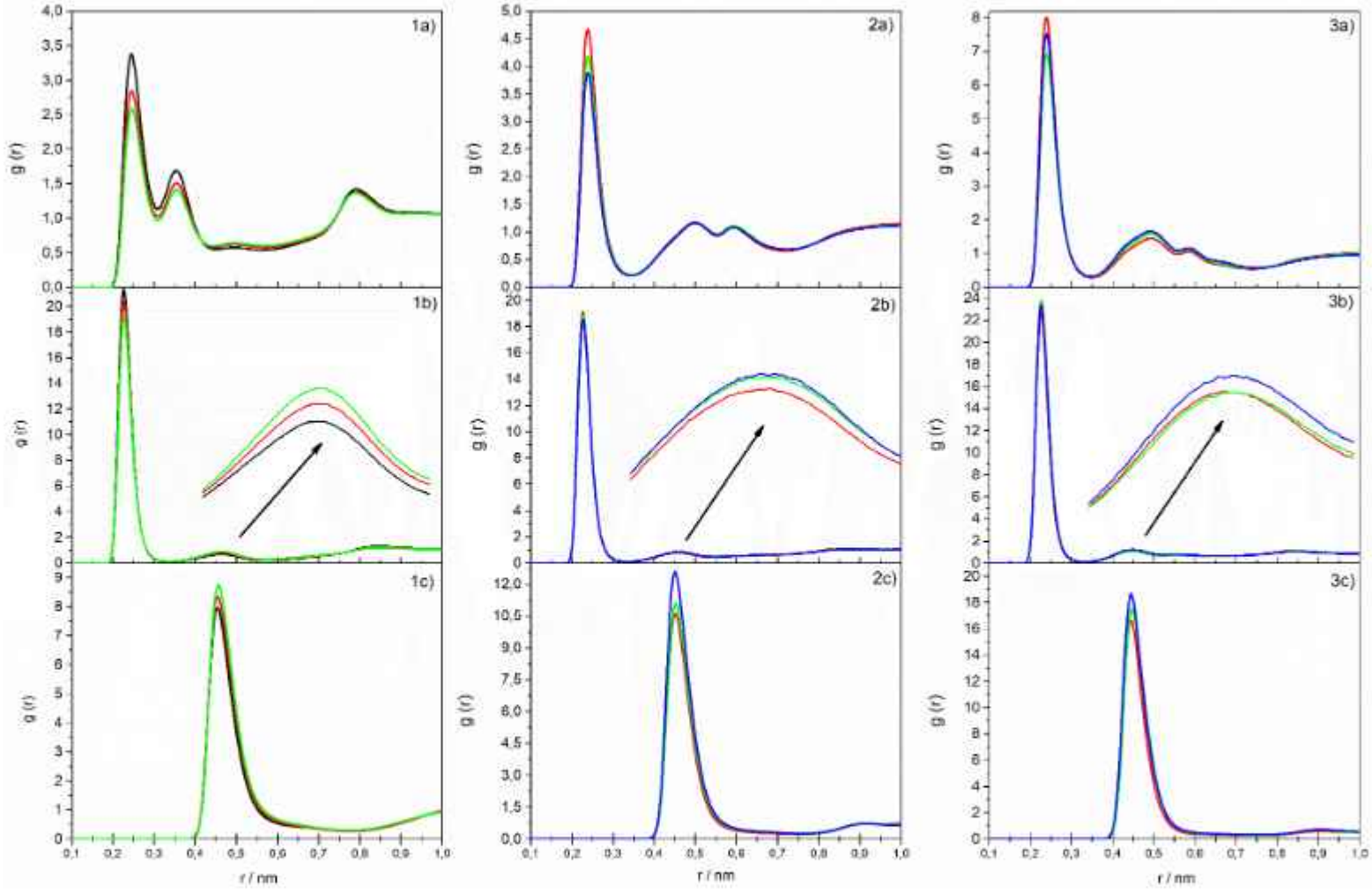

Rysunek B3 Funkcje rozkładu radialnego oparte na środkach rozkładów mas a) $Cl^{-}\cdots H–N$; b) $Cl^{-}\cdots H–O$; c) $N^{+}\cdots Cl^{-}$ dla DES opartych o TBAC zawierających 1) AP; 2) MAE; 3) BAE przy ułamkach molowych; czarna linia – 1:4; czerwona linia – 1:6; zielona linia 1:8; niebieska linia - 1:10

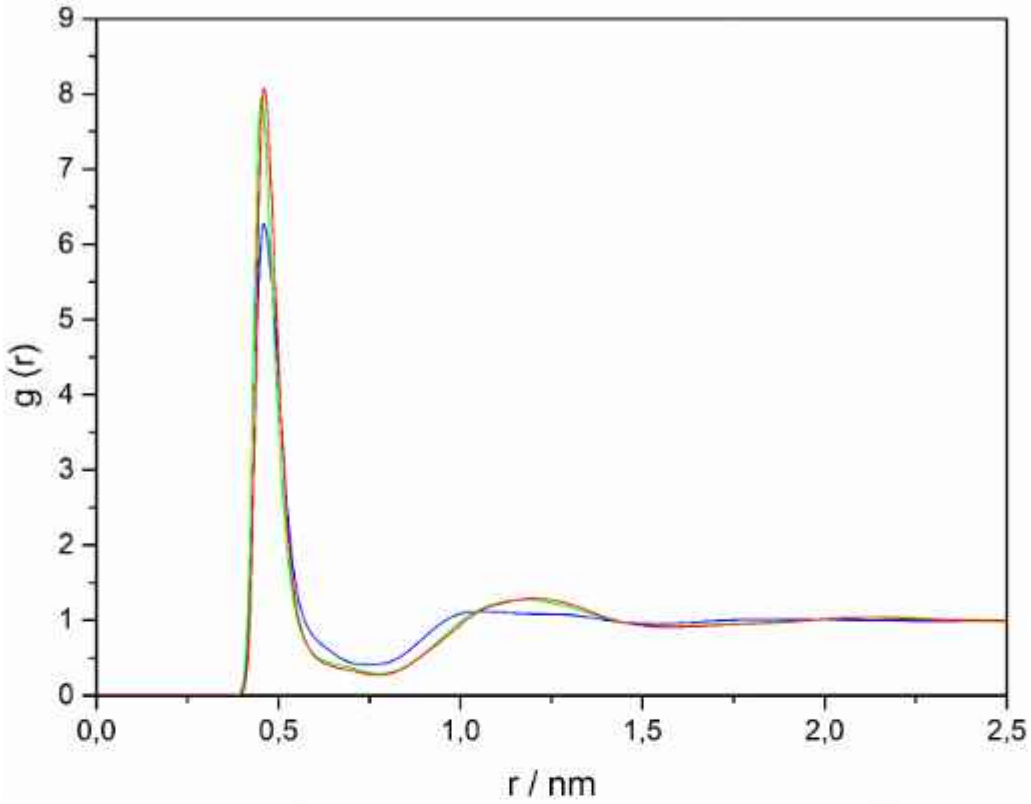

Rysunek B4 Funkcje rozkładu radialnego $N^{+}\cdots X^{-}$ oparte o odległości środków mas cząsteczek dla DES opartych o AP zawierających; czerwona linia – TBAB; zielona linia - TBAC; niebieska linia - TEAC przy stosunku molowym HBA do HBD 1:4.

Tabela B9 Wartości liczb koordynacyjnych dla wodnych roztworów badanych cieczy głęboko eutektycznych uzyskanych przy pomocy symulacji MD.

Centrum	Powłoka	r_{max} / nm	r_{min} / nm	N_{coord}
		TBAB-AP 1:6 + H_2O x_{DES}=0,1		
Br	NH	0,256	0,456	0,982
Br	OH	0,236	0,314	0,188
Br	H_2O	0,228	0,302	6,028
Br	N^+	0,486	0,598	0,151
		TBAB-AP 1:6 + H_2O x_{DES}=0,2		
Br	NH	0,252	0,478	2,145
Br	OH	0,236	0,318	0,421
Br	H_2O	0,226	0,300	5,281
Br	N^+	0,484	0,604	0,399
		TBAB-AP 1:6 + H_2O x_{DES}=0,3		
Br	NH	0,250	0,478	2,866
Br	OH	0,234	0,322	0,672
Br	H_2O	0,228	0,298	4,428
Br	N^+	0,484	0,626	0,737
		TBAB-AP 1:6 + H_2O x_{DES}=0,4		
Br	NH	0,254	0,476	3,249
Br	OH	0,232	0,326	0,969
Br	H_2O	0,228	0,298	3,567
Br	N^+	0,482	0,640	1,044
		TBAB-AP 1:6 + H_2O x_{DES}=0,5		
Br	NH	0,254	0,468	3,402
Br	OH	0,232	0,328	1,227
Br	H_2O	0,226	0,298	2,811
Br	N^+	0,478	0,658	1,269
		TBAB-AP 1:6 + H_2O x_{DES}=0,6		
Br	NH	0,252	0,468	3,632
Br	OH	0,232	0,330	1,553
Br	H_2O	0,226	0,298	2,076
Br	N^+	0,478	0,682	1,443
		TBAB-AP 1:6 + H_2O x_{DES}=0,7		
Br	NH	0,252	0,464	3,625
Br	OH	0,232	0,336	1,832
Br	H_2O	0,226	0,298	1,423
Br	N^+	0,474	0,682	1,565
		TBAB-AP 1:6 + H_2O x_{DES}=0,8		
Br	NH	0,252	0,460	3,681
Br	OH	0,232	0,340	2,035
Br	H_2O	0,226	0,298	0,902
Br	N^+	0,474	0,664	1,611
		TBAB-AP 1:6 + H_2O x_{DES}=0,9		
Br	NH	0,252	0,458	3,761
Br	OH	0,232	0,338	2,296
Br	H_2O	0,226	0,296	0,402
Br	N^+	0,474	0,648	1,586

c.d. Tabeli B9

TBAB-MAE 1:6 + H_2O x_{DES}=0,1				
Br	NH	0,254	0,314	0,078
Br	OH	0,242	0,312	0,135
Br	H_2O	0,228	0,300	6,084
Br	N^+	0,482	0,564	0,112
TBAB-MAE 1:6 + H_2O x_{DES}=0,2				
Br	NH	0,250	0,324	0,153
Br	OH	0,236	0,310	0,300
Br	H_2O	0,228	0,300	5,550
Br	N^+	0,478	0,624	0,388
TBAB-MAE 1:6 + H_2O x_{DES}=0,3				
Br	NH	0,250	0,326	0,267
Br	OH	0,234	0,318	0,397
Br	H_2O	0,228	0,298	4,888
Br	N^+	0,482	0,636	0,728
TBAB-MAE 1:6 + H_2O x_{DES}=0,4				
Br	NH	0,248	0,332	0,350
Br	OH	0,232	0,318	0,697
Br	H_2O	0,228	0,298	4,094
Br	N^+	0,472	0,630	0,931
TBAB-MAE 1:6 + H_2O x_{DES}=0,5				
Br	NH	0,246	0,336	0,463
Br	OH	0,232	0,330	1,049
Br	H_2O	0,228	0,296	3,139
Br	N^+	0,464	0,664	1,278
TBAB-MAE 1:6 + H_2O x_{DES}=0,6				
Br	NH	0,246	0,338	0,598
Br	OH	0,234	0,332	1,277
Br	H_2O	0,228	0,296	2,379
Br	N^+	0,458	0,662	1,403
TBAB-MAE 1:6 + H_2O x_{DES}=0,7				
Br	NH	0,246	0,342	0,725
Br	OH	0,232	0,332	1,556
Br	H_2O	0,228	0,296	1,701
Br	N^+	0,458	0,660	1,459
TBAB-MAE 1:6 + H_2O x_{DES}=0,8				
Br	NH	0,244	0,348	0,792
Br	OH	0,232	0,338	1,843
Br	H_2O	0,226	0,296	1,058
Br	N^+	0,462	0,664	1,567
TBAB-MAE 1:6 + H_2O x_{DES}=0,9				
Br	NH	0,246	0,350	0,939
Br	OH	0,234	0,338	2,023
Br	H_2O	0,228	0,296	0,494
Br	N^+	0,456	0,648	1,570
TBAB-BAE 1:6 + H_2O x_{DES}=0,1				
Br	NH	0,252	0,328	0,024
Br	OH	0,232	0,306	0,015
Br	H_2O	0,226	0,300	6,296
Br	N^+	0,486	0,610	0,163

c.d. Tabeli B9

TBAB-BAE 1:6 + H_2O x_{DES}=0,2				
Br	NH	0,252	0,330	0,065
Br	OH	0,234	0,308	0,131
Br	H_2O	0,226	0,298	5,838
Br	N^+	0,484	0,608	0,386
TBAB-BAE 1:6 + H_2O x_{DES}=0,3				
Br	NH	0,250	0,330	0,121
Br	OH	0,232	0,314	0,256
Br	H_2O	0,228	0,298	5,256
Br	N^+	0,472	0,616	0,656
TBAB-BAE 1:6 + H_2O x_{DES}=0,4				
Br	NH	0,248	0,334	0,222
Br	OH	0,234	0,322	0,413
Br	H_2O	0,228	0,298	4,455
Br	N^+	0,464	0,632	1,071
TBAB-BAE 1:6 + H_2O x_{DES}=0,5				
Br	NH	0,246	0,338	0,326
Br	OH	0,234	0,326	0,580
Br	H_2O	0,226	0,298	3,695
Br	N^+	0,462	0,662	1,382
TBAB-BAE 1:6 + H_2O x_{DES}=0,6				
Br	NH	0,246	0,338	0,459
Br	OH	0,234	0,328	0,782
Br	H_2O	0,226	0,296	2,870
Br	N^+	0,460	0,66	1,530
TBAB-BAE 1:6 + H_2O x_{DES}=0,7				
Br	NH	0,248	0,346	0,649
Br	OH	0,232	0,328	1,058
Br	H_2O	0,226	0,296	2,055
Br	N^+	0,456	0,674	1,621
TBAB-BAE 1:6 + H_2O x_{DES}=0,8				
Br	NH	0,246	0,346	0,802
Br	OH	0,232	0,332	1,330
Br	H_2O	0,226	0,296	1,239
Br	N^+	0,456	0,67	1,632
TBAB-BAE 1:6 + H_2O x_{DES}=0,9				
Br	NH	0,244	0,354	0,929
Br	OH	0,232	0,334	1,491
Br	H_2O	0,226	0,296	0,587
Br	N^+	0,454	0,654	1,698
TBAB + H_2O x_{TBAB}=0,1				
Br	H_2O	0,228	0,300	6,459
Br	N^+	0,490	0,584	0,135

Tabela B10 Eksperymentalna rozpuszczalność CO_2 w cieczach głęboko eutektycznych opartych o propan-1,3-diol, wyrażona jako ułamek molowy (x_{CO2}) oraz molalność (m_{CO2}) w zadanej temperaturze (T) i pod ciśnieniu równowagowym (P).

T = 293,15 K			*T = 298,15 K*			*T = 303,15 K*			*T = 308,15 K*			*T = 313,15 K*		
P / kPa	x_{CO2}	m_{CO2} / mol·kg^{-1}	*P / kPa*	x_{CO2}	m_{CO2} / mol·kg^{-1}	*P / kPa*	x_{CO2}	m_{CO2} / mol·kg^{-1}	*P / kPa*	x_{CO2}	m_{CO2} / mol·kg^{-1}	*P / kPa*	x_{CO2}	m_{CO2} / mol·kg^{-1}
							DES32							
23,79	0,0014	0,0150	25,02	0,0012	0,0126	26,33	0,0009	0,0101	27,76	0,0007	0,0073	29,21	0,0004	0,0045
56,31	0,0038	0,0414	58,13	0,0036	0,0388	60,08	0,0033	0,0360	62,26	0,0030	0,0327	64,32	0,0027	0,0297
116,13	0,0079	0,0868	119,03	0,0077	0,0841	122,09	0,0074	0,0810	125,21	0,0071	0,0779	128,3	0,0068	0,0045
145,28	0,0095	0,1037	149,12	0,0091	0,0997	152,93	0,0087	0,0959	157,12	0,0083	0,0911	161,13	0,0079	0,0870
191,91	0,0129	0,1425	196,58	0,0126	0,1383	201,99	0,0120	0,1322	206,83	0,0116	0,1278	212,02	0,0112	0,1227
							DES33							
33,54	0,0014	0,0153	34,87	0,0012	0,0130	36,45	0,0009	0,0102	37,96	0,0007	0,0076	39,83	0,0004	0,0041
54,60	0,0024	0,0258	56,27	0,0022	0,0237	58,14	0,0019	0,0210	60,16	0,0017	0,0180	62,15	0,0014	0,0152
90,86	0,0041	0,0444	93,45	0,0038	0,0413	96,45	0,0034	0,0372	98,91	0,0032	0,0347	102,02	0,0028	0,0305
125,95	0,0058	0,0635	129,08	0,0055	0,0606	132,51	0,0052	0,0569	136,06	0,0049	0,0531	140,14	0,0044	0,0478
170,13	0,0075	0,0815	174,21	0,0071	0,0781	178,42	0,0068	0,0743	183,67	0,0062	0,0677	187,91	0,0059	0,0641
							DES34							
33,37	0,0013	0,0125	34,67	0,0011	0,0110	36,10	0,0010	0,0094	37,79	0,0007	0,0072	39,58	0,0005	0,0050
78,08	0,0029	0,0282	80,16	0,0027	0,0267	82,52	0,0025	0,0247	84,94	0,0023	0,0226	87,11	0,0021	0,0211
94,12	0,0036	0,0360	96,54	0,0035	0,0344	99,13	0,0033	0,0324	101,79	0,0031	0,0304	104,55	0,0029	0,0283
117,44	0,0047	0,0467	120,08	0,0046	0,0454	123,27	0,0044	0,0431	126,18	0,0042	0,0414	129,30	0,0040	0,0393
192,87	0,0076	0,0756	196,97	0,0075	0,0739	202,21	0,0071	0,0701	206,91	0,0068	0,0674	212,20	0,0064	0,0636
							DES35							
40,32	0,0036	0,0393	41,85	0,0034	0,0368	43,74	0,0031	0,0334	45,80	0,0027	0,0296	48,19	0,0023	0,0250
55,90	0,0051	0,0552	58,20	0,0047	0,0513	60,54	0,0043	0,0473	63,14	0,0039	0,0428	65,89	0,0035	0,0380
76,24	0,0073	0,0799	78,55	0,0070	0,0770	81,30	0,0067	0,0728	84,23	0,0062	0,0683	87,49	0,0058	0,0630
148,71	0,0121	0,1332	152,71	0,0117	0,1289	156,58	0,0114	0,1251	161,53	0,0108	0,1183	165,69	0,0104	0,114
181,24	0,0157	0,1736	186,44	0,0152	0,1673	191,12	0,0148	0,1628	196,99	0,0141	0,1550	201,82	0,0137	0,1504